INSTITUTE OF FUNDAMENTAL TECHNOLOGICAL RESEARCH
POLISH ACADEMY OF SCIENCES

INFLATABLE STRUCTURES FOR ADAPTIVE IMPACT ABSORPTION

Cezary Graczykowski

Doctoral Dissertation
supervised by Prof. Jan Holnicki-Szulc

Warsaw 2011

Acknowledgement

I would like to express gratitude to my supervisor, Professor Jan Holnicki-Szulc, for introducing me to the concept of the adaptive structures, which has significantly changed my comprehension of optimal structural design, and for the support he had provided me during the research work. I also would like to thank my colleague, Dr Piotr Pawłowski, for many inspiring discussions concerning continuum and structural mechanics.

The financial support of Structural Funds in the Operational Programme –Innovative Economy (IE OP) financed from the European Regional Development Fund - Project "Modern material technologies in aerospace industry", Nr POIG.01.01.02-00-015/08-00 and the financial support through the project "Health Monitoring and Lifetime Assessment of Structures" – MONIT –POIG.01.01.02-00-013/08-00 from the EU Structural Funds in Poland is gratefully acknowledged. I would like to express my gratitude to the Polish Ministry of Science and Higher Education for financial support through research grant N N502 3414 36.

Abstract

The doctoral dissertation introduces the concept of Adaptive Inflatable Structures and their application for adaptive absorption of the impact loading. Proposed concept is based on effective use of compressed gas and controlling its pressure during the impact process. Adaptive Inflatable Structures contain sealed air chambers equipped with inflators and controllable exhaust valves which enable flow of the gas between the chambers and outside the structure. Control of internal pressure allows for optimal adjustment of dynamic characteristics of the structure and, as a result, for optimal dissipation of the energy of impact loading.

The thesis constitutes an attempt of elaboration of complete and coherent theory of Adaptive Inflatable Structures. The first part of the thesis concerns development of theoretical models of adaptive inflatable structures which are based on coupling of the equilibrium equations of deformable solid walls and the Navier-Stokes equations describing the fluid. Additionally, the model takes into account controllable valve which enables control of the fluid flow during impact. Simplified models of the inflatable structures are based on the assumption of homogeneity of fluid parameters in particular chambers and analytical description of the fluid flow through controllable valve. Further part of this thesis concerns numerical simulation and control of the simplest inflatable structures - adaptive pneumatic cylinders. For three types of absorbers, simplified mathematical models are used to examine characteristics of the dynamic response, the process of energy dissipation and to analyze mathematical structure of the governing equations. Developed control strategies take into account various operating principles and constraints of the valve and they are aimed at protection of the impacting object and impacted structure. Moreover, the methodology of optimal design of the adaptive pneumatic absorbers is proposed and basic experimental verification is presented. Separate, more complicated model based on methods of computational fluid dynamics is used to simulate dynamic response of the absorber and to control the outflow of the gas in case of impacts with high initial velocity.

The further part of the thesis concerns more complex Adaptive Inflatable Structures of various types, i.e. thin-walled inflatable steel structures, adaptive pneumatic fenders for offshore structures and ‘flow control – based’ airbags. All these structures are analyzed by means of Finite Element Method complemented with simplified equations describing the gas, and with the use of developed strategies of internal pressure control. The concept of multi-chamber barrier is introduced and the algorithms of pressure adjustment in particular chambers aimed at maximization of the load capacity or adaptation to actual dynamic loading are developed. The next analyzed structure is adaptive, torus-shaped pneumatic fender surrounding the offshore wind turbine tower which optimally mitigates dynamic response of the tower and the ship during offshore docking. Furthermore, the system of emergency landing composed of adaptive airbags equipped with controllable valves is proposed and tested by means of several numerical models. In the last chapter of the thesis, sophisticated models which utilize full coupling of the structural dynamics equations and fluid dynamics equations are used for simulation and analysis of the controllability of the valves for inflatable structures. Three methods of modeling of piezoelectric valves are introduced and the strategy of controlling the fluid flow is developed. Two competitive numerical methods are used to conduct simulation of self-closing membrane valve and the strategies of control of the valve opening which utilize various feedback couplings are implemented.

Streszczenie

Rozprawa doktorska przedstawia koncepcję Adaptacyjnych Konstrukcji Pneumatycznych oraz ich zastosowanie do adaptacyjnego rozpraszania energii uderzeń. Zaproponowana koncepcja polega na wykorzystaniu sprężonego gazu oraz sterowaniu jego ciśnieniem w czasie procesu uderzenia. Adaptacyjne Konstrukcje Pneumatyczne składają się z uszczelnionych komór powietrznych wyposażonych w sterowalne inflatory oraz szybkie zawory upustowe umożliwiające przepływ gazu pomiędzy komorami oraz na zewnątrz konstrukcji. Sterowanie ciśnieniem gazu pozwala na optymalne dostosowanie charakterystyki dynamicznej i w efekcie na optymalną dysypację energii uderzenia.

Praca stanowi próbę opracowania kompletnej i spójnej teorii Adaptacyjnych Konstrukcji Pneumatycznych. W pierwszym rozdziale rozprawy opracowane zostały modele teoretyczne oparte na sprzężeniu równań równowagi deformowalnych ścianek konstrukcji i równań Naviera-Stokesa opisujących sprężony gaz. Dodatkowo w modelu uwzględniono sterowalny zawór umożliwiający kontrolowanie przepływu gazu podczas uderzenia. Zaproponowano również modele uproszczone oparte na założeniu jednorodności parametrów gazu w komorach oraz analitycznym opisie przepływu przez zawór. Dalsza część rozprawy dotyczy symulacji i sterowania najprostszych konstrukcji pneumatycznych jakimi są adaptacyjne amortyzatory pneumatyczne. Dla trzech typów absorberów uproszczony model matematyczny wykorzystany jest do zbadania charakterystyki odpowiedzi dynamicznej, procesu dysypacji energii oraz do analizy struktury matematycznej opisujących równań. Zaproponowane strategie sterowania, uwzględniające różne zasady działania i ograniczenia zaworu, mają na celu optymalną ochronę uderzającego i uderzanego obiektu. Przedstawiona jest metodologia optymalnego projektowania adaptacyjnych absorberów pneumatycznych oraz podstawowa weryfikacja eksperymentalna. Ponadto osobny, bardziej złożony model oparty na metodach numerycznej dynamiki płynów wykorzystany jest do symulacji odpowiedzi absorbera oraz sterownia przepływem gazu w przypadku uderzeń z dużymi prędkościami.

Kolejna część rozprawy przedstawia bardziej skomplikowane adaptacyjne konstrukcje pneumatyczne różnych typów, tzn. cienkościenne pompowane konstrukcje stalowe, adaptacyjne odbojniki morskie oraz poduszki powietrzne. Konstrukcje te analizowane są za pomocą Metody Elementów Skończonych sprzężonej z uproszczonymi modelami gazu oraz przy wykorzystaniu opracowanych strategii sterowania ciśnieniem. Zaproponowana jest koncepcja wielokomorowej bariery oraz opracowane są algorytmy zmian ciśnienia gazu w komorach w czasie uderzenia mające na celu maksymalizację nośności lub adaptację do aktualnego obciążenia dynamicznego. Następną analizowaną konstrukcją jest adaptacyjny odbojnik pneumatyczny w kształcie torusa otaczający wieżę morskiej elektrowni wiatrowej, optymalnie łagodzący odpowiedź dynamiczną wieży i statku podczas dokowania. Ponadto przedstawiony jest system adaptacyjnych poduszek powietrznych awaryjnego lądownia wyposażonych w sterowalne zawory, a jego efektywność zweryfikowana jest przy użyciu kilku różnych modeli numerycznych. W ostatnim rozdziale rozprawy modele wykorzystujące pełne sprzężenie równań mechaniki konstrukcji i mechaniki płynów użyte są do symulacji i analizy sterowalności zaworów do konstrukcji pneumatycznych. Zaproponowane są trzy metody modelowania oraz strategia sterowania zaworu piezoelektrycznego. Przy wykorzystaniu dwóch metod numerycznych wykonane zostały symulacje działania samoczynnie zamykającego się zaworu membranowego oraz zaimplementowano strategie sterowania jego otwarciem wykorzystujące różne sprzężenia zwrotne.

CONTENTS

CHAPTER 1 - INTRODUCTION

1.1 Motivation for the research

Motivation for undertaking this research is development of alternative, efficient and robust systems for impact energy dissipation which are required in many branches of contemporary engineering. Considered impact loading may be of various source and nature: it may be exploitive loading resulting from the typical destination of the structure (airplane landing gear), it may occur during emergency situation (car hitting the protective barrier) or it may be caused by harsh environmental conditions. Independently on type of impact loading optimal dissipation of the corresponding impact energy constitutes one of the fundamental problems from the point of view of safety and economy. Application of incorrect or non-optimal solutions inevitably leads to serious damages of impacting objects, resulting threat to life or health or high material costs. Structures currently applied for impact energy dissipation are usually passive systems which are designed for the typical expected or maximal allowable impact energy. However, in many practical cases the characteristics of the impact loading acting on the structure may vary significantly or it may be difficult for precise estimation. Therefore, most of the classical passive energy absorbing structures do not provide optimal protection against wide range of possible impact scenarios.

Recently, the innovative concept of Adaptive Impact Absorption (AIA) [1] which overcomes the disadvantages of passive systems is being extensively developed. The essence of AIA is real-time adaptation of energy absorbing structures to actual impact loading. Application of adaptive systems allows for substantial mitigation of dynamic response and for accommodation to strict contemporary safety requirements. Nowadays, the design and practical realisation of AIA systems is possible and justified due to a broad accessibility and low cost of functional materials and required electronic devices (sensors, actuators and hardware controllers). Adaptive impact absorbing structures are based on miscellaneous adaptation techniques such as application of magneto-rheological fluids, piezoelectric actuators or detachable pyrotechnic connections. However, each of the invented solutions has its disadvantages, e.g. large mass and inertia, long response times or insufficient controllability, which confine the range of their possible applications. Therefore, development of innovative technologies and mechanisms which allow for effective adaptation of the structure to actual impact loading is still desired.

From theoretical perspective most of the adaptive structures are complex systems which require multi-physical modelling involving disciplines like structural mechanics, fluid mechanics, electricity and magnetism. Additionally, simulation of dynamic response of adaptive structures exposed to impact loading requires taking into account large deformations and material nonlinearities. In turn, development of optimal adaptation strategies for various impact scenarios entails application of advanced methods of control theory and complex optimisation algorithms. Despite the intensive development of theory of coupled problems together with corresponding numerical methods on one side and optimisation and control techniques on the other, both topics seem not to be well combined with each other. According to author's opinion, the precise modelling of dynamics and control of impact subjected adaptive structures is not fully recognized in the scientific literature.

The thesis introduces the concept of 'Adaptive Inflatable Structures' equipped with sealed pressure chambers, inflators and fast controllable valves providing the possibility of real-time control of internal pressure and adaptation to actual impact loading. Methods of modelling, development of control strategies and possible applications of Adaptive Inflatable Structures for impact absorption are thoroughly analyzed. According to above discussion the undertaken research seems to be important from both practical and theoretical point of view.

1.2 State of the art

The topic of the thesis explores the intersection of two fields of engineering: Adaptive Impact Absorption and mechanics and applications of inflatable structures. Therefore, the review of a current research and literature will concern both these topics separately (Sec.1.2.1, Sec.1.2.2).

1.2.1 Adaptive Impact Absorption (AIA)

Adaptive Impact Absorption (AIA) [1 2 3 4] is a contemporary scientific and engineering discipline which belongs to a group of 'smart technologies' [1 5 6 7 8 9 10 11] and encompasses the elements of impact mechanics, control theory (including optimisation techniques) and material sciences concerning functional materials. Historically these three general disciplines had contributed the most significantly to the inception of Adaptive Impact Absorption (Fig.1.1) and hence their development will be briefly outlined.

In a field of **impact mechanics** fast progress was observed during last several decades both in analytical and numerical methods of analysis. Classical analytical methods of impact mechanics describe collisions of rigid and deformable objects including collinear and planar impact, local and global effects, discrete and continuum modelling of contact and influence of visco-elastic or plastic material properties, cf. Gryboś [12], Stronge [13]. Other analytical models describe propagation of elastic and plastic waves in bars and beams initiated by longitudinal or transversal impact, cf. Kaliski [14]. The requirement for designing light thin-walled structures being able to dissipate high impact energies, which had arisen in the context of safety of road and rail transportation, gave birth to discipline called 'crashworthiness'. The main achievement of crashworthiness was precise description of plastic folding as an effective mechanism of energy dissipation. Despite many complex phenomena that occur during crushing of thin walled structures (including material and geometrical nonlinearities such as plasticity, hardening, strain rate dependence, buckling and contact) many analytical and semi-empirical solutions were derived thanks to application of simplifying assumptions concerning material models and kinematics of deformation. Analytical solution for axisymetric crushing of the circular tube by Alexander is here a well-known example [15]. Comprehensive approach to mechanics of thin-walled profiles, methods of determination of their folding patterns and estimation of impact absorption capabilities are presented in books by Jones [16] and conference proceedings by Jones and Wierzbicki [17 18 19]. Further research work in crashworthiness was related to mechanics of more complex crashworthy structures such as passenger vehicles, trains and ships [20], as well as other types of loadings like blast and explosion, cf. Bangash [21] . Numerical approach to impact problems was possible thanks to contemporary understanding of structural dynamics [22 23 24] and development of Finite

Element Method as an efficient tool for solving complex problems of nonlinear mechanics [25 26 27 28]. The recent finite element codes dedicated to crashworthiness utilize explicit methods for integrating equation of motion [29 30] which allows to avoid iterative searching of the equilibrium state at each time step of the analysis and to eliminate convergence difficulties encountered in implicit methods of integration. Contemporary explicit FEM codes enable to perform highly nonlinear simulations of complex collision scenarios (involving millions of finite elements) within a reasonable time and to obtain good quantitative correspondence with the experiments. Nonetheless, alternative semi-analytical approaches which substantially simplify the crashworthiness problem and reduce the computational cost are also proposed. The methods which utilize discretisation of the considered structure into so-called super folding elements with prescribed folding patterns were introduced by Abramowicz [31]. Comprehensive theoretical description of mechanics of the impact process including detailed discussion of modern FEM-based computational methods is presented by Laursen [32].

The emphasis should be put on the fact that thin-walled steel profiles considered in classical impact mechanics are passive structures which can not be controlled during the impact process and therefore have no ability of adaptation to actual dynamic loading.

Application of the **control theory** to the mechanical systems initially developed in the field of active damping of vibrations. Basic principles of mechanical control systems were based on concepts applied previously in automatics and electronics. In particular, mechanical control systems took advantage of the concept of 'feedback control' [33] understood as dependence of applied control signal on measured response. Developed control systems utilized feedback to a measured state vector, feedback to a state vector estimated by the 'observer' or they were designed as decentralized systems with feedback to selected part of the system output. The attention was paid to optimal location of sensors and actuators which resulted in wide application of the concepts of observability and controllability [34]. Typically, the control was executed by introducing additional external forces that counteract external excitation in order to mitigate dynamic response of the system. General problem of damping of vibrations was formulated as a problem of 'optimal control' [35] which relies on minimisation of certain functional dependent on both controlled quantities (displacement amplitudes or frequencies) and applied control forces. The following step was development of algorithms of 'robust control' [36] which allow to control systems with disturbances or uncertainties and 'adaptive control' [37] being able to adjust control strategy according to gradual change of system parameters in time. Apart from aforementioned, the separate group of semi-active control strategies can be distinguished [38 39] where the control is executed by changing properties of the selected elements (typically stiffness or damping) instead of introducing additional external forces. Semi-active approach substantially reduces required amount energy and decreases overall cost of control. Semi-active control systems constituted strong inspiration for future systems of Adaptive Impact Absorption.

Practical application of control to large engineering structures was initially focused on flexible structures located at the Earth's orbit [40 41]. In last decades miscellaneous control systems dedicated to mitigation of wind excited vibrations of compliant civil engineering structures including chimneys and guyed masts, bridges and buildings were proposed [42 43 44]. Realisation of control systems was planned to be executed by active cables, tendons or

supports able to generate required control forces depending on actual operating conditions of a structure. During 1990's several successful laboratory tests of control systems were performed including reduction of vibrations of cable-stayed bridge by using tendons equipped with hydraulic cylinders [45]. The most impressive of the contemporary applications of control theory in civil engineering embrace damping of vibrations of large span bridges excited by wind gusts and vibrations of high buildings excited by seismic movements [46].

Independently, the progress in material sciences concerning **functional materials** [47] had enabled the development of extremely fast sensors and actuators which are crucial for realisation of control algorithms, especially in case of structures exposed to impact loading. The functional materials are defined, in general, as materials being able to change their mechanical properties in the presence of non-mechanical field as temperature, electric or magnetic field. Functional materials can be divided into smart solids and smart fluids. The most popular smart solids are:

- piezoelectric materials which deform under applied electrical field [48 49],
- magnetostrictive materials which change geometry under magnetic field,
- magnetorheological elastomers which alter their rheological properties when influenced by magnetic field,
- shape memory alloys which exhibit phase transformation (austenite-martensite) under action of temperature,
- magnetic shape memory alloys which exhibit the above phase change under influence of magnetic field.

The most well-known functional fluids are magneto-rheological fluids and electro-rheological fluids, which change their rheological properties when subjected to magnetic and electric field, respectively. The deformations and forces that can be obtained by using the above materials are strongly limited [50] and therefore they can be used rather in semi-active control strategies to change local properties of elements than as actuators introducing additional external forces to the controlled structure. The other important limitation of functional materials is their time of activation which has to be substantially shorter than the time of controlled impact process.

Application of functional materials is strongly dependent on availability of corresponding control electronics. The development of electronic hardware controllers, especially their miniaturisation and fast operating times were a key matters for Adaptive Impact Absorption. Nowadays, developed AIA control strategies can be relatively easily implemented by means of field-programmable gate arrays (FPGA) which utilise data gathered from sensors to generate control signal in real time [51].

Beside described above three general disciplines, two particular engineering problems had significant contribution to development of Adaptive Impact Absorption: **design of adaptive landing gears** and **design of adaptive truss structures**. The first discipline was focused on application of functional materials and control electronics in design of unidirectional impact absorbers, while the latter one had utilized the optimisation techniques, reanalysis and remodelling methods for initial sizing and development of adaptation strategies for multi-element structures subjected to impact loading. Division of research conducted in the field of AIA and applied methodology into, stated above, two groups remains apparent until now (Fig. 1.1).

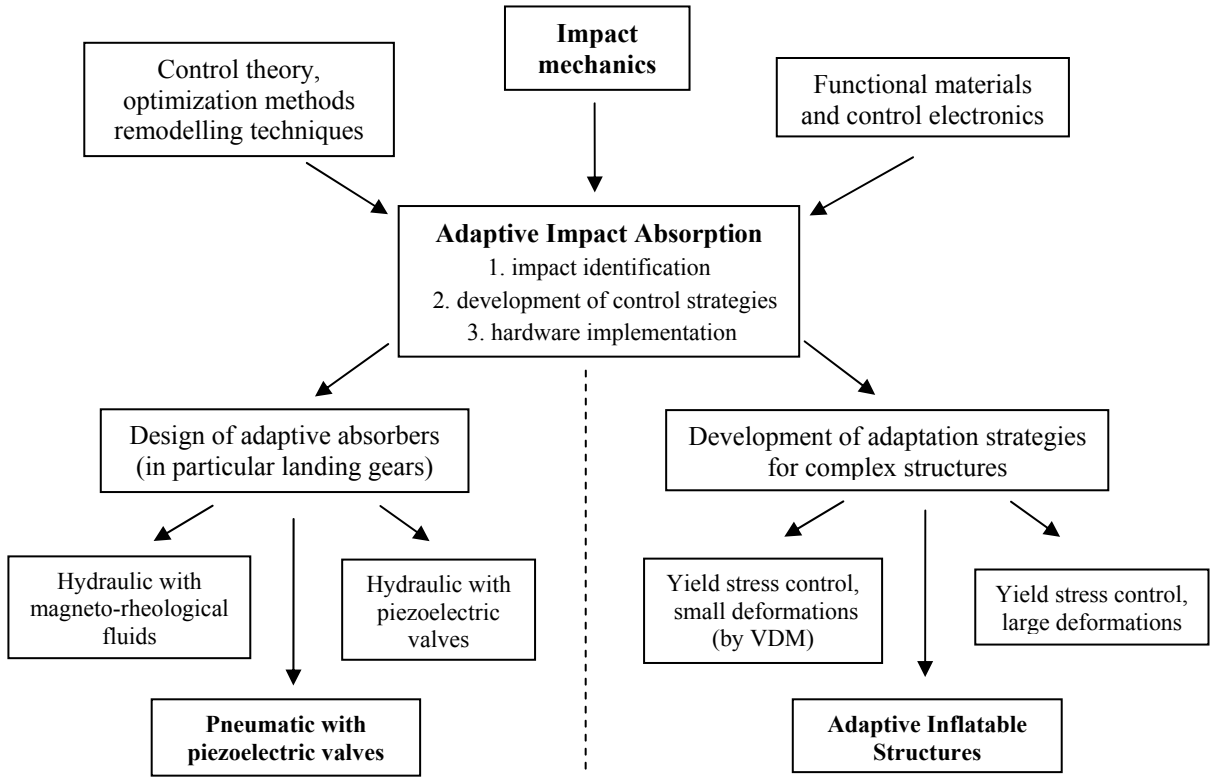

Fig. 1.1 Development of Adaptive Impact Absorption (AIA)

The concepts of active and adaptive **landing gears** were proposed as a response to large changeability of forces acting on the airplane during particular landings. Conventional passive oleo-pneumatic absorbers applied in landing gear contain a gas spring and two oil chambers connected by the orifice with metering pin which modulates orifice area depending on actual position of the piston. Although the oleo-pneumatic landing gear has favourable force-displacement characteristics due to interaction of pneumatic and hydraulic force, it is usually designed for the harshest landing conditions and, consequently, it does not provide optimal reduction of airplane deceleration for the whole range of possible landing scenarios.

Development of active landing gear was initially aimed at reduction of vibrations of the fuselages of supersonic airplanes during take-off and landing [52]. The initial concept had assumed that control of the damping force according to actual landing conditions is achieved by changing hydraulic pressure by means of external reservoirs with hydraulic or pneumatic medium [53]. The satisfactory experimental results were obtained during the 1980's [54] and the concept was applied to several military airplanes during the 1990's [55]. However, due the high power consumption required by designed active systems the further efforts were focused on semi-active solutions, which can be treated as first systems of Adaptive Impact Absorption. Researchers had considered application of electro-rheological or magneto-rheological fluids with apparent viscosity controlled by external electric or magnetic field [56 57] and application of fast servo-valves for controlling flow of the fluid through the orifice during landing [58]. The thorough research concerning both mentioned design options was performed within the European project ADLAND coordinated by IPPT PAN [59], which represents the state of the art in design of adaptive landing gears. Two main options of semi-active control of absorber force were investigated: application of piezoelectric valve for changing size of the internal

orifice and application of magneto-rheological valve for changing local properties of the MR-fluid. In case of magneto-rheological landing gear feedback control system with feedback to difference between obtained and optimal acceleration level was designed and positively validated [60]. Moreover, the potential benefit that can be achieved by using adaptive landing gear during various landing conditions was precisely analysed [61 62]. Finally, the efficiency of adaptive landing gear equipped with piezoelectric valve was presented during full scale field tests performed on middle-size airplane [63 64].

Independently, in the middle of 1990's, application of **topological optimisation** methods to problems of crashworthiness was initiated, which was possible due to the development of homogenisation method and formulation of the problem of optimal material distribution [65 66]. Initially, topology optimisation techniques were used to design structures subjected to large plastic deformations and buckling [67 68 69]. Further, the classical topology optimisation problem of compliance minimisation was reformulated to the problem of energy absorption maximisation and developed approach was applied to optimize crashworthy structures for automotive and railway industry [70 71 72 73]. Different approach was proposed in thesis [74] where topology of the energy absorbing truss structure was modified in order to achieve assumed deceleration of the selected node during the impact process. Since methods based on topology optimisation were focused on designing passive structures able to sustain various impact loadings rather than to adapt to actual impact scenario, typically they are not qualified as systems of adaptive impact absorption.

At the same time, an alternative, innovative approach to optimal design of **truss structures** subjected to impact loading was proposed by Holnicki, Mackiewicz, and Kołakowski [75]. The authors postulated replacing selected passive elements of the considered structure with adaptive elements (‘structural fuses’) with controllable yield stress levels. The general paradigm of **Adaptive Impact Absorption** was formulated as real-time adaptation of energy absorbing structure to actual dynamic loading by changing local mechanical properties of the structural fuses during impact without supplying additional energy to the system.

The concept was initially applied to design of a lattice structure of adaptive barriers [76 77] and adaptive car buffers [78 79 80] with controllable elasto-plastic characteristics subjected to a static loading. Further applications of AIA concerned optimal design of adaptive railway cars [81 82], which was based on preliminary optimisation of elements cross sections and optimal choice of yield stress levels aimed at maximization of energy dissipation. Early adaptation methods assumed identification of impact energy in the initial stage of collision and optimal adjustment of structural fuses’ characteristics which remained constant during the entire impact process. Moreover, it was assumed that deformation of the particular elements is small (in the range of geometrical linearity) which substantially simplified performed analysis and enabled utilisation of Virtual Distortion Method (VDM) [83] as versatile reanalysis and remodelling tool. Precise description of various types of remodelling of truss structures by using VDM (change of elements stiffness, change of nodal mass and yield stress levels) was presented in papers [84 85]. In the following work the authors had formulated and solved the problem of optimal design of adaptive structure subjected to multiple load cases as composed of three stages: optimal distribution of material, optimal choice of structural fuses location, optimal tuning of the yield stress levels [86].

Although the above mentioned papers extensively utilized various methods of reanalysis and optimisation techniques for development of optimal adaptation strategy, the methods of control theory had remained almost completely neglected. In authors opinion, application of the concepts of observability, controllability as well as introduction of feedback control systems and analysis of their general properties would constitute important part of AIA theory of truss structures subjected to small deformations.

The problem of optimal adaptation of **nonlinear truss structures** (including large deformation and contact) was initially solved for a quasi one-dimensional multi-folding structure, where structural fuses with changeable yield stress levels were used to control sequence of the folding mechanism [87 88 63]. The advanced adaptation strategy with continuous change of elements characteristics based on gradients of the objective function (certain deceleration measure or actual energy dissipation) was proposed and tested numerically. Moreover, experimental verification of performance of a single section of multi-folding structure constructed with the use of magneto-rheological dampers was conducted. In the subsequent paper [89] the authors had investigated adaptive bumper to be applied in framework tower, together with an algorithm of adjusting values of initial plastic yield stress levels and procedure of self-repair after impact executed by using the external shaker.

In the following research work the concept of Adaptive Impact Absorption was expanded **beyond the class of truss structures**. Adaptive solution was applied in innovative design of adaptive thin-walled automotive energy absorber where the crushing force was controlled by using stiffening plates connected by detachable pyrotechnic joints. A decrease of crushing stiffness was performed by deflagration of the pyrotechnic material and controlled disconnection of stiffening plates from the main absorber's profile [90 91]. The pyrotechnic device was also proposed to control yield stress levels in elements of truss structure subjected to impact loading and large deformations [92]. The authors developed heuristic algorithm of adaptation which tends to maximise energy dissipation and to prevent destruction of particular elements by changing yield stress levels in neighbouring elements of the greatest influence.

The concept of Adaptive Impact Absorption was also effectively utilised for improvement of safety of wind generators. The first application concerned semi-active control of ice-braking cones which protect offshore wind turbines located in arctic areas. Characteristics of the connection between the cone and the tower was proposed to be adjusted according to actual cone position and ice velocity in order to minimise horizontal loading causing vibration of the structure and to preserve vertical force causing ice crushing [93]. Further research concerned wind turbines with adaptive blade-hub connection realized by magneto-rheological clutch which allows to control force between blade and hub thus protecting wind turbines against severe wind gusts [94].

Apart from the above mentioned development of AIA systems conducted at IPPT PAN, adaptive impact absorbing systems were proposed by other researchers. The most attention was given to the problem of car collisions. The thesis [95] presents the concept of innovative car bumper whose design combines explosive airbag, lattice structure and tubes filled with granular material. Another investigated solution is the use of two controllable hydraulic cylinders located between the bumper and car compartment which extend the crashing distance and allow to and maintain constant deceleration level during collision [96].

The authors of [97] propose adaptive design of the frontal structure of the car based on application of steel cables which counteracts the asymmetry of forces and optimizes energy absorption during collisions with offset. In turn, the paper [98] investigates performance and characteristics of a magneto-rheological damper for controllable automotive bumper, while the paper [99] demonstrates the injury reducing potential of an adaptive system for frontal car collisions by using mathematical model and series of crash tests. In addition, application fluid-impregnated cellular solids was proposed and MR-fluid impregnated automotive whiplash was investigated [100]. Beside automotive applications, the thesis [101] analyses various types of adaptive absorbers including thin-walled profiles with buckling initiators, pressurized tubes with explosives and application of electro-rheological fluids. Moreover, diverse methodologies of controlling the system composed of masses, pneumatic springs and hydraulic dampers aimed at impact mitigation are developed in [102].

Additional important issue strongly related to AIA systems is **impact load identification** which has to be performed during initial milliseconds of impact and decides about the further strategy of structural adaptation. In the most general case the location of impact has to be detected and, moreover, mass and velocity of the impacting object (and expected time-variation of the impact force) has to be identified. The initial velocity of the impacting object, its actual location and impact direction can be usually measured by ultrasonic velocity sensors located on the impacted structure [103]. In case of one-dimensional impact the effective procedures for fast identification of impacting mass and velocity based on application of accelerometers and force sensors can be proposed [104 105]. More detailed classification of identification methods belonging to this group will be presented in Sect. 3.2.

Let us briefly summarise the Adaptive Impact Absorption methodology. AIA is based on the concepts of preliminary impact identification and real-time adaptation of energy absorbing structure to actual dynamic loading. In order to conduct the adaptation process the structure is equipped with embedded system of sensors, hardware controller and dissipaters with controllable mechanical properties (structural fuses) which enable change of global dynamic characteristics of the system. Typically the process is performed by means of purely dissipative devices which require only a small power supply. The following **types of AIA systems** can be distinguished in terms of objectives they execute:

- The case of ideal absorber providing optimal dissipation of exploitive, repetitive impact loading. This type of adaptive structure is used to minimise accelerations or internal forces in selected locations or to reduce impacting object rebound. Such approach is usually applied in case of structures subjected to impact loading characterised by wide range of energies where application of AIA systems provides minimisation of fatigue which has crucial importance for structure service life. Mentioned earlier adaptive landing gear with adjustable damping force can be quoted here as typical example.
- The case of protective structure providing maximal energy dissipation during critical impact loading. That approach is justified when the structure is potentially endangered of unexpected emergency situation (such as collision or blast) or harsh environmental loading. In such situation the desired response of the structure must be qualitatively different than in previously considered case

of exploitive loading. The main objective is either maximisation of energy dissipation or preserving structural integrity. Typical examples of such approach is protection of thin-walled pressure vessels against bullet impact, adaptation of traffic barriers to collision of extremely heavy vehicle, etc.

Another case of AIA systems distinguished by some of the authors [4] corresponds to adaptive structure sustaining impact loading with 'minimal measure of introduced distortions' which corresponds to minimal energy of applied control. According to terminology introduced in [1] the **strategies of adaptation** applied to fulfil above objectives can be divided as follows:

- semi-active strategy of adaptation where mechanical properties of the structural fuses are tuned after impact identification but they remain constant during the whole impact process;
- partially active strategy of adaptation where the characteristics of structural fuses can be modified during impact but only weakening of the characteristics is possible (decrease of yield stress level or opening of the valve);
- fully active strategy of adaptation where characteristics of structural fuses can be arbitrary changed during impact period and both increase and decrease of characteristics is allowable (e.g. closing of the loaded valve or increasing of yield stress level is feasible).

Nevertheless, all above strategies of adaptation can be classified as 'semi-active control strategies' from the point of view of control theory, which leads to discrepancies in terminology used by various authors. Moreover, in some publications, adaptive structures under consideration and applied control strategies are referred to as 'active structures' and 'active control', which may cause confusion in interpretation. In this thesis we will apply the terminology established in [1] and expressions 'semi-/partially/fully active strategy of adaptation', emphasizing the fact that the terms *semi-active* and *active* used in the context of *adaptation* have different meaning than used in the context of *control*.

1.2.2 Pneumatic and inflatable structures and their applications

'Pneumatic structure' is a structure which is utilizes compressed gas. Structures equipped with stiff compartments are usually referred as pneumatic (pneumatic cylinders is a typical example). On the contrary 'inflatable structure' is the pliable-walled structure that can be filled with gas and maintains its size, shape and strength due to internal pressure. The term 'inflatable' comes from the latin word 'inflare' which means to blow into, to pump. Pneumatic and inflatable structures have comprehensive applications in civil engineering, transportation and mechanical engineering.

Applications in architecture and civil engineering

The pioneer of application of large scale pneumatic structures in civil engineering was Walter Bird who had invented domes for radars (so called 'radomes') during World War II [106]. The academic research in this field was commenced by famous architects Otto Frei and Buckminster Fuller [107] who were involved in design and static analysis of inflatable

structures during the 1960's. The popularity of large scale pneumatic civil engineering structures has started after the exhibition Expo'70 [108] held in Osaka where two remarkable structures were presented: the American pavilion by Walter Bird et al [109] and the Fuji Pavilion by Yutaka Murata [110]. Both these structures are typical representations of two main forms applied in contemporary civil engineering: air-supported and air-inflated structures.

Air-supported structures [111 112] are used as large scale roofs which derive their shape and stability from overpressure inside the space they cover. Air-supported structures are usually constructed as double curvature domes (often hemispheres) which provides that the whole envelope surface is evenly pressurized. They are successfully used as light coverings for large objects as stadiums (e.g. BC Place Stadium in Vancouver and Tokyo 'Big-Egg' Dome [110], see Fig.1.2a), warehouses, markets and arrival halls. The value of internal pressure which constitutes the main support to the structure is adjusted to equilibrate self weigh of fabric, wind and possible snow loading and usually equals to several hundred Pascals. Air-supported structures are not strictly air-tight (however they are equipped with air-locks on entrances) and they require continuously working air support system. Most of modern air-supported structures are equipped with loading and deformation sensors which determine both external conditions and actual state of the structure and adjust internal pressure accordingly [110].

In contrast, air-inflated structures [113] are composed of closed sections filled with air (usually cylindrically shaped air-beams) which either form a complete structure or constitute only a framework to which main covering material is attached. Air-inflated elements are typically used to erect structures serving as a permanent or temporary shelters [114] (inflatable pavilions, tents, structures for environmental disasters), coverings (arches and canopies) and structures of other applications as masts, pillars and even footbridges. Recently popular applications of air-inflated structures are inflatable bouncers for children and inflatable street advertisements typically designed as single air filled chamber stabilised by internal and external cables. Regarding environmental engineering, inflatable dam applications include hydropower and water supply, gates for irrigation, tidal waves barriers, raising the crest of an existing dam and ice control on ice-affected waters [115]. Unconventional application of pressure is utilized in vacuum supported (deflated) structures which follow the inversed principle of inflatable structures: they are composed of external airtight membrane and filling material and maintain their shape and strength due to compression evoked by external pressure [116].

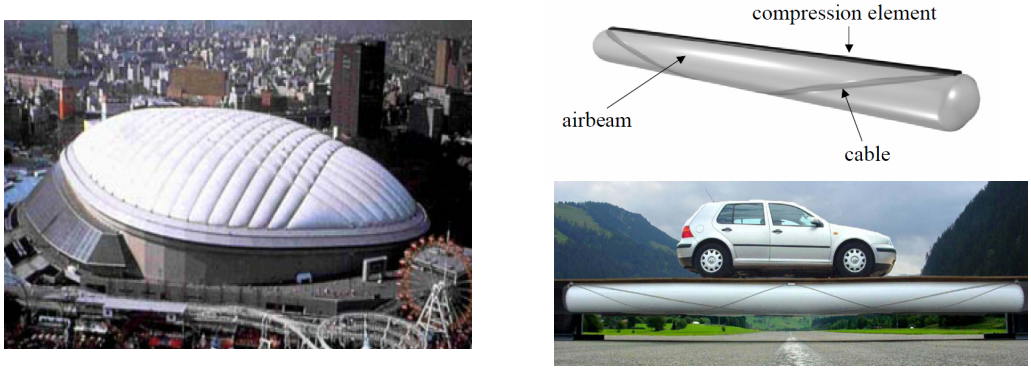

Fig. 1.2. a) Air-supported structure: Tokyo 'Big Egg' dome, b) Tensairity girder by Airlight company

An innovative concept of design air-inflated structures, called Tensairity [117 118] (synergy of tension, air and integrity) enables to construct air-beams intended to sustain large bending forces. Tensaitity beam is constructed of air filled deformable tube, stiff rod located on its top and external cables spiralled around the tube, cf. Fig 1.2b. Compressive forces generated during bending are sustained by the stiff rod, while tensile forces are sustained by external cables. Compressed air does not carry any load itself but prestresses the external cables and stabilises compressed rod element against buckling. As a result, load bearing capacity of the tensairity air-beam is several times larger than in case of traditional air-beam and in certain situations it may supersede steel beams in design of large span roofs, light weight bridges or pillars [119]. Successfully completed Tensairity projects include roof of car park in Montreaux and a bridge for skiers in Alps [120].

The history of evolution of architectural concepts concerning inflatable structures and their applications in civil engineering can be found in [121], a huge collection of inflatable engineering structures is reported by Tensinet Association [110], whereas the recent advances in this field are collected in books [122] and [123].

Applications in road, aeronautical and waterborne transportation

The most common application of inflatable structures in road transportation, and probably the most appreciated application of inflatable structure in general, is a pneumatic tire. It constitutes successful implementation of toroidal shape, being together with sphere and cylinder, the third main shape of inflatable structure. Since invention by Thomson at 1846 the pneumatic tires became commonly used in various types of vehicles from trolleys to passenger aeroplanes and more then one billion of them is produced annually.

The first prominent application of inflatable structure in aeronautics was hot-air balloon by Montgolfier brothers [124] and hydrogen balloon by Jacques Charles, both invented in 1783 and both controlled by gas pressure. The following invention was an airship - lighter than air flying object usually filled with helium and constructed either as non-rigid structure (blimp) or with internal skeleton (zeppelin). After several serious crashes during 20th century, including the most well known crash of Hindenburg in 1937 [125 126], airships were withdrawn from massive commercial transportation and currently they are used mainly for advertisement and observation purposes.

In the later years designers had concentrated on smaller inflatable flying objects: single person and unmanned aerials vehicles. During the 1950's the Goodyear company has constructed 'inflatoplane' [127 128 129] - regular engine airplane made of inflated rubber envelope, however the project was cancelled soon afterwards by the US Army because of low military importance. An extraordinary inflatable aerial vehicles being hybrid between aircraft and airship, called Stingray, was designed by 'Prospective Concepts' [130] company, cf. Fig 3a. One of the first Unmanned Aerial Vehicles equipped with inflatable wings was Dryden I2000 [131], a gun lunched observation vehicle developed by NASA researchers. The following innovative concept related to UAVs was morphing inflatable wing which can alter shape depending on actual conditions of the flight [132 133 134]. Change of wing shape was performed by controlling pressure in selected chambers of the wing or, alternatively, by external actuators such as shape memory alloy wires or piezo-fiber composites, cf. Fig. 3b. The

combination of pneumatic technology and morphing concept causes that change of the wing shape can be significant and the wing can adapt to substantially different flight regimes. Due to lightness, deployability and low cost of transportation to Earth's orbit, inflatable structures are frequently used in space exploration as inflatable antennas, reflectors, solar arrays and solar sails [135 136] as well as elements of space stations [137 138].

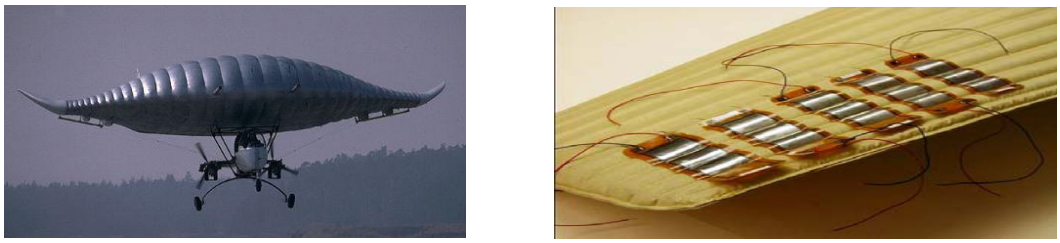

Fig.1.3. a) Stingray air vehicle, b) Morphing adaptive airfoil controlled by piezoelectric actuators

Applications of inflatable structures in waterborne transport include (flexible and rigid-hulled) inflatable boats, catamarans and kayaks but also rescue systems such as inflatable lifejackets, life rafts and traps used in ships and airplanes. Recently introduced 'Kafloat' system [139] is based on application of external airbags to increase ship load displacement and to prevent ship sinking in emergency situations.

Applications in mechanical engineering

Pneumatic structures are commonly used in mechanical engineering, in particular as pneumatic cylinders being parts of the machines or engines which convert internal energy of compressed gas into kinetic energy of piston motion. In industrial automation pneumatic structures are used mainly as actuators and switches. Other mechanical applications are pneumatic drills, nail-guns, compressed-air engines and pneumatic brakes [140] .

Applications of inflatable structures for impact absorption

Pneumatic and inflatable structures are also widely applied for protection against single or cyclic impact loadings. Devices based on pneumatic principles are nowadays utilised as energy absorbers in land and water transport, aeronautics and astronautics.

- In road transport protection against impact is mainly related to providing safety of passengers during collisions by means of system of internal airbags. Contemporary airbag systems are equipped with sensors identifying severity of collision (accelerometers, wheel speed sensor, gyroscopes) and sensors identifying the occupant (his presence, weight, seat-belt usage and approximate position). Airbag control unit utilizes data from sensors to initiate deployment of the particular airbags and to adjust strength of their inflation. Thanks to application of fast gas generators airbags become fully inflated after 40-50ms of impact, usually before contact with the occupant. During occupant collision and corresponding compression of the airbag, pressure is released by vent holes in airbag fabric. Airbag allows to spread the force acting on occupant during impact and prevent him from striking interior body of the car. Miscellaneous types of airbags applied in passenger cars include frontal airbag, side airbag, side curtain, knee airbag, rear curtain airbag, child airbag, etc [141 142].

Preliminary test were made in order to introduce frontal external airbags protecting pedestrians in case being impacted by passenger car [143] and an external airbag installed in the front of train to protect the vehicle located on a train passage [144].

- Airbags are also used to protect vulnerable road users as motorcyclists and bikers. Airbags deployed between the rider's seat and the steering handlebar were recently introduced to several types of motorcycles. Another type of protection are personal airbags being part of the motorcyclists suits (for instance inflatable protective collars activated during accident [145]) or prototype inflatable helmets for bikers. Permanently inflated pneumatic barriers are used on a speedway tracks to protect competitors in case of falling out of the route.
- Adaptive pneumatic devices are used in construction of modern car suspension systems, for instance 'Audi Adaptive Air Suspension' adjusts pressure inside pneumatic cylinders depending on type of road surface and dynamics of driving [146].
- In aviation external airbags are applied during landing on water (Polish helicopter Anakonda [147]) and, experimentally, as emergency system improving safety of passengers and integrity of the helicopter chassis during harsh landing (the system REAPS developed by Rafael company [148 149]). Application of airbags for protection of the helicopter or airplane pilot during landing under extreme conditions is also known. Airbags applied in astronautics are designed as completely closed (non-vented airbags) or they include the possibility of gas outflow through the pores of the airbag fabric (vented airbags). In space exploration multi-chamber airbags are used during unmanned landings when conditions concerning the target surface or the lading kinematics are not fully determined. Both in case of landing on a target planet and return landing on Earth airbags are used in conjunction with the other systems as parachutes or reverse engines (e.g. in Mars Pathfinder [150 151]). Moreover, special type of flat but large-surface multi-chamber pneumatic structures are used as a protection against space debris [152].
- Maritime applications of inflatable structures include inflatable fenders for ship docking in ports and harbours. Large scale Yokohama-type fenders constructed as inflated rubber cylinders (of diameter up to 6 meters) surrounded by chain tyre net are used for docking of oil-tankers, container-vessels and barges. Another application are floating on water inflatable barriers which serve for protection of ships or strategic objects against terrorist attacks.

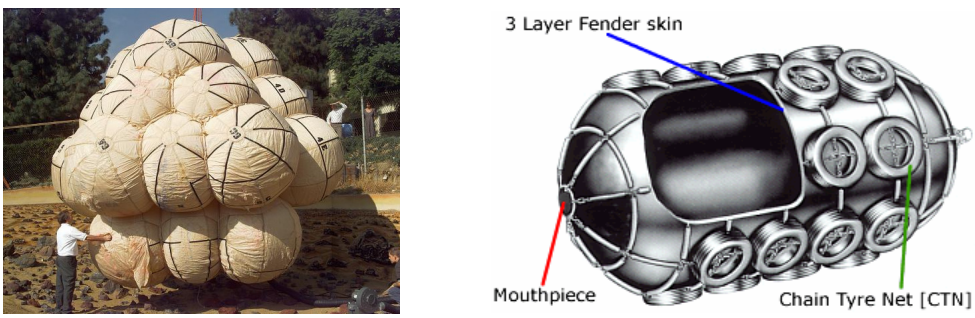

Fig. 1.4. a) Airbags used in 'Mars Pathfinder' , b) Yokohama inflatable fender

- Pneumatic devices are also used by fire-brigades to protect people jumping from burning buildings. Typical device belonging to this group is 'skokochron' produced by Polish company Moratex. [153]
- Common applications are inflatable packaging made of foil with small inflatable cells [154] for protecting fragile objects during transportation and sport shoes with inflatable sole providing protection during jumping or running.

Recent stage of development, functionality and modelling methods of particular types of inflatable structures will be described in the appropriate following chapters. The emphasis should be put on a fact that design of above systems enables adjustment of initial pressure only. During the impact process the above devices remain completely passive since change of internal pressure is by no means controlled. Therefore, the process of energy dissipation is definitely not optimal and it is expected that considerable improvement can be still obtained.

1.3. Thesis objectives and itinerary

The main objective of the thesis is elaboration and verification of the concept of pneumatics-based structures serving for Adaptive Impact Absorption. The thesis introduces the idea of **Adaptive Inflatable Structures** (Adaptacyjne Konstrukcje Pneumatyczne), which are rigid or deformable structures containing sealed chambers filled with compressed gas and additionally equipped with inflators and controllable **high performance valves**. Such valves enable control of the gas flow between the chambers and outside the structure during the impact period. Consequently, change of pressure in different parts of the structure can be controlled and dynamic characteristics of the structure can be optimally adjusted to a actual impact loading. This, in turn, allows for optimal dissipation of the impact energy and mitigation of dynamic response of both protected structure and impacting object.

Particular goals can be divided into three groups related to:

1. formulation of mathematical models describing Adaptive Inflatable Structures and their numerical implementation;
2. development of control algorithms (strategies of inflation and pressure release) aimed at optimal mitigation of the impact loading;
3. elaboration of concepts of engineering structures which utilize the above paradigm and numerical simulation of their effectiveness.

In regard to the first objective, modelling of inflatable structures subjected to impact loading involves coupling between large deformation of the solid body and forces exerted by flow of the compressible fluid. Therefore, modelling of inflatable structures belongs to the most sophisticated type of Fluid-Structure Interaction (FSI) problems. An additional element of the model, which is entirely novel in comparison to classical FSI problem, is the controllable valve whose opening can be changed during the impact period – arbitrarily or according to actual results of the analysis. Consequently, the first objective of the thesis is formulation of mathematical models of Adaptive Inflatable Structures exposed to impact loading, based on coupling of nonlinear solid mechanics equations and Navier-Stokes equations, which take into account the controllable valve with actively altered opening and

the influence of controlled fluid outflow on simulated dynamic response. The following objective is development of simplified models (which are valid for certain types of inflatable structures and loading conditions) including fundamental model based on assumption of uniform distribution of pressure inside chambers and analytical description of the gas flow through controllable valve. An additional task is implementation of developed theoretical models, which will be achieved with the use of commercial Computational Solid Mechanics and Computational Fluid Dynamics software and by utilizing user subroutines to model active operation of the valve. The simplified models of AIS will be implemented within purely mechanical codes or programmed from scratch by using mathematical software.

The second group of objectives is related to optimal design and control of Adaptive Inflatable Structures. In the most general case, optimal geometry of inflatable structure has to be selected, division into several separate pressure chambers has to be performed and initial pressure inside each chamber has to be adjusted. The subsequent task is development of algorithms for optimal control of inflatable structure during impact. Miscellaneous strategies providing optimal release of gas from the chambers and optimal change of pressure in particular parts of the structure during impact will be proposed. The strategies will depend on characteristics of the impact loading, e.g. mass and velocity of the hitting object, and they will be aimed either at optimal adaptation of the structure to actual impact scenario (mitigation of accelerations, internal forces or rebound) or maximisation of load-bearing capacity. The main difficulty related to development of control strategies is high complexity and nonlinearity of considered systems combined with various operating principles and limitations of the valves. The control algorithms will be incorporated to commercial software or included into own-developed codes. The overall result of the first and the second objective will be complete software for simulation, optimisation and control of various types of Adaptive Inflatable Structures subjected to impact loading.

The following, third objective of the thesis is proposition and elaboration of concepts of innovative adaptive impact absorbing structures based on the idea of real-time control of internal pressure. Three main types of adaptive inflatable structures will be presented and verified: the simplest pneumatic structures - adaptive pneumatic cylinders, inflatable road barriers divided into pressurised chambers and, finally, adaptive ‘flow control - based’ airbags for two applications: protection of offshore structures and providing safety of emergency landing. Conducted simulations take into account various design of inflatable structures and various parameters of the applied dynamic loading. For each structure appropriate geometry and division into pressurized chambers will be determined and optimal strategy of pressure control will be developed. Methods and objectives of control will depend on type of considered structure and its intended application. The subsequent task is oriented towards methods of realization and control of gas flows of high intensity. Two concepts of high speed and stroke valves will be analysed and possibilities of controlling the gas flow will be verified.

Thesis is composed of introduction, six main chapters and final remarks:

Chapter 1 ‘Introduction’ presents motivation for undertaken research, review of literature concerning Adaptive Impact Absorption, state of the art applications of inflatable structures and defines thesis scope and objectives.

Chapter 2 'The concept and modelling of Adaptive Inflatable Structures' introduces the idea of Adaptive Inflatable Structures and the concept of internal pressure control as an efficient method of adaptation to impact loading. Three mathematical models of Adaptive Inflatable Structures are described. Initially, the most direct and exact model based on coupling of nonlinear structural mechanics equations and Navier-Stokes equations describing the gas (Fluid-Structure Interaction approach) is precisely derived. Further, two simplified models are introduced: model based on homogeneity of gas parameters inside each chamber (Uniform Pressure Method) and hybrid model based on decomposition of the problem into two parts modelled by FSI- and UPM-based approaches. Each model incorporates the controllable valve with actively changed opening, which is the core element of Adaptive Inflatable Structure. At the end of the chapter, general formulations of possible control problems are derived and compared against each other.

Chapter 3 'Adaptive pneumatic cylinders' is devoted to the simplest type of adaptive pneumatic structures - cylinders equipped with controllable valves. The first part of the chapter utilizes modelling by Uniform Pressure Method to investigate basic dynamic characteristics of three types of adaptive pneumatic cylinders and to describe their capabilities of impact energy dissipation. The second part of the chapter is aimed at development of valve opening strategies which provide optimal adaptation for various impact scenarios. Above control strategies include diverse control objectives and they take into account limitations of valve operation. Moreover, the methodology of optimal design of adaptive pneumatic cylinders is briefly outlined and utilized for design of adaptive pneumatic landing gear. Finally, developed models and control strategies are compared with the experiment.

Chapter 4 'CFD models of adaptive pneumatic cylinders' is dedicated to modelling of adaptive pneumatic cylinders with the use of methods of Computational Fluid Dynamics. Initial part of the chapter concerns two-dimensional simulation of the single chamber cylinder by means of Navier-Stokes equations coupled with equation governing dynamics of the piston. The influence of the valve opening on dynamic response of the system is investigated and two control strategies (corresponding to different models of the valve) aimed at maintaining constant piston acceleration are developed. In a further sections various options of CFD-based modelling of double chamber system are presented and application of hybrid approach for simulation of pneumatic cylinders is discussed. The chapter finishes with control of one dimensional pneumatic system with a point mass and a moving boundary.

Chapter 5 'Crashworthiness of Adaptive Inflatable Structures' concerns dynamics and control of aluminium and steel air-filled structures subjected to impact loading. In the first part the influence of internal pressure on static and dynamic characteristics of thin-walled structures is analysed on the basis of elementary experiment with aluminium can and numerical simulations of several types of pressurized structures. The following part of the chapter focuses on precise examination of two-dimensional model of adaptive inflatable barrier divided into several sealed chambers equipped with controllable valves. Adjustment of pressure inside chambers is initially aimed at maximal increase of global load-bearing capacity of the structure. Further control strategies concern optimal reduction of deceleration, minimisation of required inflation and obtaining desired final deformation of the structure.

Chapter 6 ‘Adaptive flow control - based airbags’ is devoted to the concept of airbags which are additionally equipped with controllable high performance valves. Two particular problems are modelled numerically: docking of the ship to the offshore wind turbine tower and the process of emergency landing. In the first case the objective is to propose adaptive pneumatic structure protecting both the ship (by reducing its deceleration and rebound) and the wind turbine tower (by mitigating its vibrations and local stresses in tower wall). The problem of emergency landing is considered subsequently for rigid two-dimensional landing object, for two-dimensional compliant object and, finally, for three dimensional object. Developed strategies for controlling gas outflow are oriented towards stabilization of the landing object during touchdown and towards simultaneous decrease of its linear and angular deceleration.

Chapter 7 ‘Controllable high performance valves’ presents methods of modelling, simulation and control of high speed and stroke valves for Adaptive Inflatable Structures. Numerical simulation of controllable valves is performed with the use of FSI-based model since precise analysis of the valve flow requires Navier-Stokes equations, while the analysis of controllability requires precise model of the solid part of the valve. In the first section three approaches to modelling piezoelectric valve are proposed and algorithm for obtaining desired mass flow rate of gas is developed. The second section concerns simulation and control of self-closing membrane valve based on controllable deformation of thin membrane under pressure of the flowing gas. Non-trivial analysis of controllability of the membrane valve is performed by means of additional coupling of arbitrary (non-boundary) quantities of fluid and solid domain and by implementation of cross-domain feedback control algorithm.

Chapter 8 ‘Final Remarks’ concludes the whole thesis, recalls its original achievements, presents open lines of research and further steps planned by the author.

Additional comments of thesis composition

Although the thesis is heterogonous in nature and variety of topics is covered by subsequent chapters, the coherent composition is predetermined by the arrangement of applied methods of inflatable structure modelling. As it was pointed out, the simulation of inflatable structures inherently requires coupling of solid and fluid mechanics. Solid part can be modelled as:

- general problem of computational solid mechanics (CSM) - initial boundary value problem (IBVP) described by partial differential equations (PDEs) or
- rigid body dynamics (RBD) - initial value problem (IVP) described by ordinary differential equations (ODEs)

Similarly, fluid part can be modelled:

- as general problem of computational fluid mechanics (CFD) – (IBVP) described by (PDEs) or
- by simplified approach based on uniform pressure method (UPM) and analytical definition of the valve flow – (IVP) described by (ODEs)

Consequently, four possible combinations of the above approaches can be distinguished, see Fig. 1.5 and Fig. 1.6. The thesis starts with theoretical part (Chapter 2) where the most general model of inflatable structure (‘CSM+CFD’) is derived and further is simplified. Composition of the subsequent part of the thesis, where particular engineering problems are considered, is

reverse. The first type of analyzed structures are adaptive pneumatic cylinders (Chapter 3) modelled by the simplest proposed approach being combination of rigid body dynamics and uniform pressure method ('RBD+UPM'). In Chapter 4 concerning cylinders subjected to impacts of high initial velocities, more precise modelling of the fluid is required so the uniform pressure method is replaced by Navier-Stokes equations and the approach 'RBD+CFD' is applied.

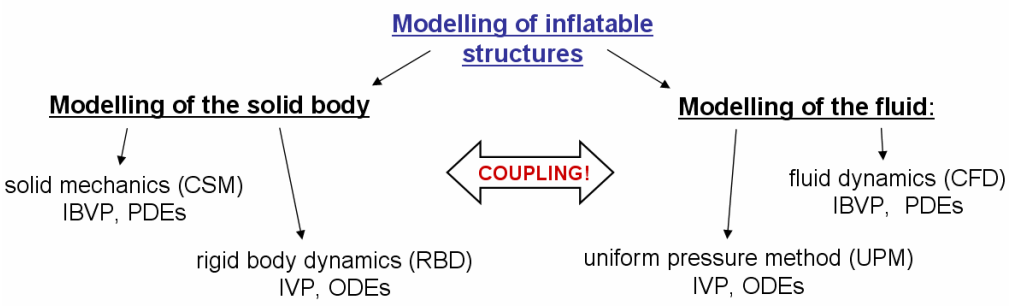

Fig. 1.5. Inflatable structures modelling methods

Simulation of inflatable thin-walled structures and 'flow-control based airbags' in Chapter 5 and Chapter 6 requires considering problem of solid mechanics (with simplification to shells and membranes structures, respectively), however (after the inflation stage) simplified modelling of the fluid can be utilized ('CSM+UPM'). Eventually, the exact modelling of the controllable valves in Chapter 7 requires precise approach to modelling of both solid and fluid part of the problem ('CSM+CFD').

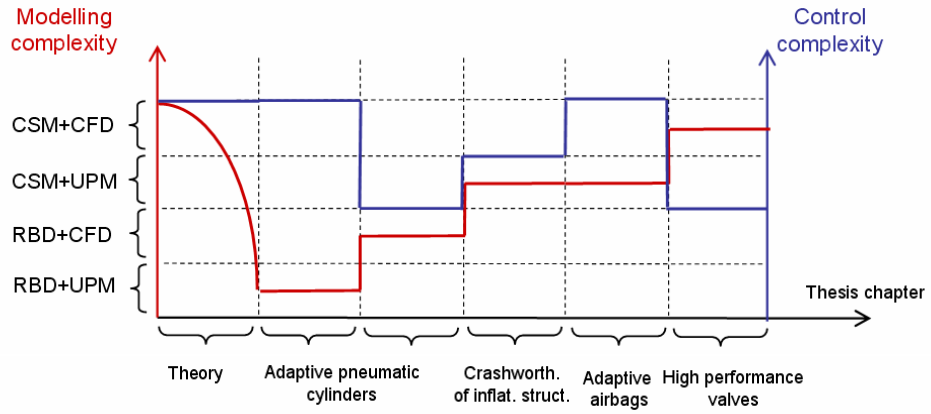

Fig. 1.6. Modelling complexity and control complexity in subsequent chapters of the thesis

Applied method of modelling and its complexity is strongly related to the complexity of applied control algorithms. The most advanced and precise control strategies can be applied for simplified models based on uniform pressure method (subsequently for: pneumatic cylinders, inflatable barriers and adaptive airbags). Modelling of the fluid part of the problem by CFD methods substantially complicates simulation of the dynamic process and therefore enforces application of the simpler, more approximate control algorithms. Change of modelling and control complexity in subsequent chapters of the thesis is presented in Fig. 1.6.

CHAPTER 2 - THE CONCEPT AND MODELLING OF ADAPTIVE INFLATABLE STRUCTURES

2.1 The concept of Adaptive Inflatable Structures

Adaptive Inflatable Structures are designed as one of the special technologies for Adaptive Impact Absorption. The proposed concept is based on application of compressed gas and its controlled migration and release as an effective methodology allowing for adaptation of energy absorbing structure to actual impact loading. AIS are structures containing sealed chambers filled with compressed gas, whose pressure can be adjusted during the impact process. Pressure adjustment relies on appropriate initial inflation of particular chambers and control of the gas flow between the chambers and outside the structure. Real-time control of actual value of pressure in different parts of the structure enables adaptation to dynamic loading of various energy, amplitude and location.

The form and shape of Adaptive Inflatable Structure depends on its particular application [155]. The inflated structure may act uni-directionally (as cylinder enclosed by piston), it may be a thin-walled steel structure or it may be completely deformable cushion made of rubber or fabric. Moreover, AIS may constitute an independent system, it may be attached to impacting object or, alternatively, to protected structure. General term 'Adaptive Inflatable Structure' comprises all systems analysed in further chapters of this thesis: adaptive pneumatic cylinders, inflatable road barriers and 'flow controlled - based' airbags in the form of torus-shaped pneumatic fenders and external cushions for emergency landing, see Fig. 2.1. Design of AIS for a particular application involves finding optimal dimensions and geometry of inflatable structure, design of the external walls which will sustain internal overpressure and proper division into pressurized chambers.

The preliminary procedure, which precedes absorption of the impact loading, is impact identification. The identification procedure should be performed in the initial stage of impact in order to provide data for development of the optimal adaptation strategy. Initial velocity of the hitting object, its actual location and impact direction can be identified before collision by means of system of ultrasonic sensors located on a structure. Identification of impacting object mass and its basic mechanical properties requires utilisation of initial response of inflatable structures such as pressure or stress measurement or, alternatively, application of additional sensors located in the impact zone (cf. Sect.3.2.1). Hereinafter, it will be assumed that the impact scenario is either known or it can be identified during initial milliseconds of the process and thus full data concerning impact scenario is available for development of the adaptation strategy. Moreover, in particular simple cases (e.g. pneumatic cylinders, Sect. 3.2.2) the control strategy effectively utilizes actual response of the inflatable structure and it does not require separate preliminary procedure for identification of impact parameters.

The process of inflation and operating pressures of Adaptive Inflatable Structures also depend on their type and practical application. Particular types of pneumatic structures, such as adaptive pneumatic cylinders or inflatable fenders can be permanently inflated with pressure which enables adaptation to typical expected impacts. On the contrary, other structures such as emergency airbags or road barriers are inflated only when the collision is expected. Due to required short operation times fast gas generators based on deflagration of

pyrotechnic material are planned to be used. The value of initial pressure and its diversification between particular chambers of inflatable structure is determined on the basis of identified impact scenario and according to assumed control objective. The main function of initial internal pressure is to adjust initial compliance of the inflatable structure to actual loading conditions. Division of the inflatable structure into separate chambers significantly improves its adaptability since it enables independent adjustment of initial pressure in different locations and allows to obtain diverse initial mechanical properties. On the other hand, the method requires plenty of inflators to fully exploit its potential.

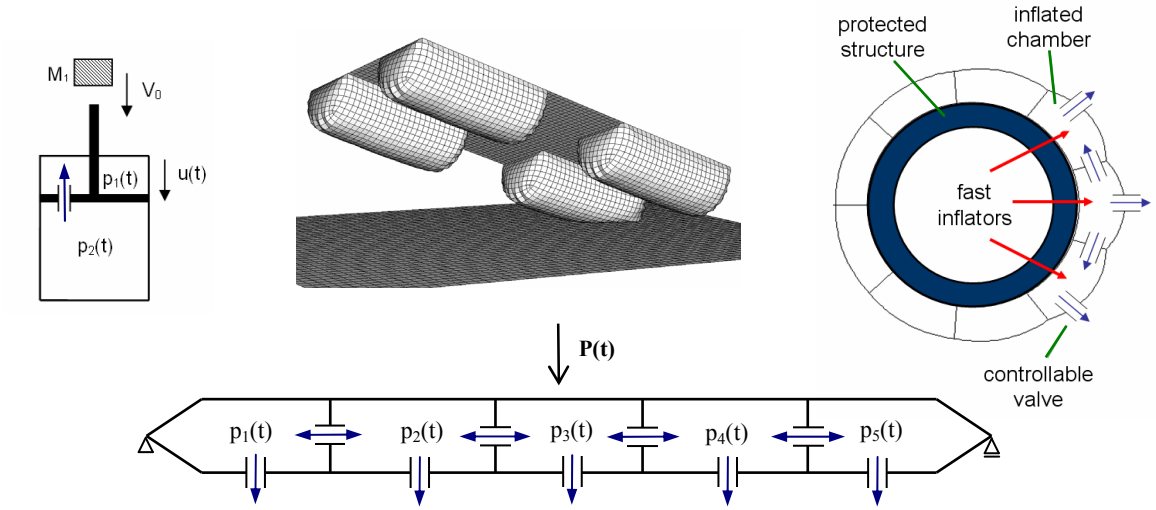

Fig. 2.1. Adaptive Inflatable Structures: a) adaptive pneumatic cylinders, b) emergency flow control - based airbags, c) inflatable fenders, d) adaptive inflatable barrier

During collision with external object control of internal pressure is executed by controllable high performance valves. Such valves are mounted both in internal partitions and external walls of the inflatable structure and they enable control of gas flow between internal chambers and outside the structure during the impact period. In this manner, change of pressure in different parts of the structure can be controlled and actual stiffness and global dynamic characteristics of the structure can be adjusted in real-time during subsequent stages of impact. Control of internal pressure allows for substantial improvement of the process of energy dissipation and for optimal reception of impact, i.e. for mitigation of the dynamic response of hitting object and impacted structure. Hitting object can be stopped by using the whole admissible braking distance, its deceleration can be significantly reduced and its possible rebound can be mitigated. Simultaneously, forces transmitted to impacted structure causing its excessive vibration or local stresses can be minimised.

On the other hand, application of inflatable technology with fast gas generators and controllable valves allows for adaptation to critical impact (of energy substantially higher than expected) where maximisation of impact energy dissipation and preserving system integrity are the crucial objectives.

2.2 FSI model of inflatable structure subjected to an impact load

Modelling of inflatable structure subjected to impact loading requires considering the interaction between its walls and fluid enclosed inside. Applied external loading causes large

deformation of the structure and change of volume of the internal chambers, which affects gas pressure and enforces its flow. Forces exerted by the compressed gas affect, in turn, deformation of the solid walls and their state of stress.

The most precise method of analysing the above coupled problem is the so-called Fluid-Structure Interaction (FSI) [156 157 158 159] where both solid and fluid domains are described by mechanical and thermodynamic conservation laws and moreover appropriate coupling conditions at the interface between domains are taken into account. In the FSI approach all quantities of interest (solid density, displacement and temperature; fluid density, velocity and temperature) are assumed to vary in time and space and their rates of change in time and space are related to each other by system of coupled nonlinear partial differential equations. The FSI approach is commonly used in modelling of automotive airbags especially airbag deployment and out-of-position airbag-occupant collisions [160], advanced design methods of lightweight structures [161 162], modelling of biomechanical problems such as flow of blood through ventricles [163 164] and flow of air in trachea and lungs [165].

In case of modelling of inflatable structure subjected to impact loading the equations describing solid wall have to account for large displacements causing geometrical nonlinearities, large strains causing nonlinearities of constitutive relations and solid compressibility. On the other hand, Navier-Stokes equations describing the fluid have to include effects related to fluid compressibility and viscosity, conductive and convective heat transfer and the influence of structure deformation and controllable valves on the fluid flow.

2.2.1 Continuum kinematics and balance laws

Analysis of fluid-structure interaction problems involving large deformations is challenging due to a necessity of describing deforming continuum composed of solid body and fluid. Proper analysis of system kinematics requires using both Lagrangian and Eulerian descriptions or some kind of mixed formulation.

Eulerian (spatial) approach is typically used in fluid mechanics where flow of the fluid in fixed spatial region is analyzed. In the Eulerian approach material particles can freely enter or leave considered spatial region, but shape of this region typically remains unchanged. The main problem addressed is observation of the fluid velocity at fixed point of the spatial region. This goal is achieved by using velocity vector being the fundamental quantity describing the fluid flow. On the other hand, Lagrangian (material) approach is typically used for description of deforming solid body where fixed set of material particles is analyzed. In the Lagrangian approach the shape of the considered domain changes as body deforms. The main problem addressed is tracking of material particles and it is executed by using displacement vector which indicates displacement of each particle from the referential state.

In case of FSI problems the solid kinematics is usually described in Lagrangian approach as in classical solid mechanics. However, the flow of the fluid takes place in a domain which changes its shape as solid body deforms and therefore the classical Eulerian approach cannot be directly applied. Instead, the so-called Arbitrary Lagrangian Eulerian (ALE) description is often used. In this approach the main quantity describing the fluid flow is still the velocity vector, but an additional displacement field which describes the change of shape of the fluid domain is introduced into the formulation. Since deformation of the fluid

domain is established only at the fluid-solid interface, the additional displacement field can be introduced in an 'arbitrary way' and it is usually not related to the actual fluid velocity. The purpose of introducing this additional displacement field is to provide a transformation of changing in time fluid domain into a domain which is fixed in a new reference system.

For the sake of coherence the description of continuum kinematics and derivation of balance laws in the Arbitrary Lagrangian-Eulerian frame of reference will be briefly presented. The derivation is based on classical continuum mechanics books [166 167 168 169], publications and papers dedicated to ALE approach, including [170] and [171], however it involves elements of original reasoning by the author.

Let us denote $\Omega_{\mathbf{X}}$ the material domain consisting of material particles $\mathbf{X}$ and $\Omega_{\mathbf{x}}$ the spatial domain consisting of spatial points $\mathbf{x}$. Moreover, we will introduce coordinate system $\mathbf{X}$ which is permanently connected to material particles. In Lagrangian description we follow continuum particles in their motion. The motion of the particles is described by the mapping φ which relates material coordinates to the spatial ones, Fig. 2.2:

$$\varphi : \Omega_{\mathbf{X}} \times [0,T] \to \Omega_{\mathbf{x}} \times [0,T] \qquad (2.2.1)$$
$$\mathbf{x} = \varphi(\mathbf{X}, t)$$

and thus allows to identify location of each particle during the process. The mapping reverse to (2.2.1), called the Eulerian description, takes the form:

$$\varphi^{-1} : \Omega_{\mathbf{x}} \times [0,T] \to \Omega_{\mathbf{X}} \times [0,T] \qquad (2.2.2)$$
$$\mathbf{X} = \varphi^{-1}(\mathbf{x}, t)$$

and allows to identify particles on the basis of their actual location $\mathbf{x}$. Consequently, in the context of velocity, in Lagrangian formulation the velocity of a certain particle is observed, while in Eulerian formulation the velocity at certain point in space is observed.

In ALE approach, besides the classical domains $\Omega_{\mathbf{X}}$ and $\Omega_{\mathbf{x}}$, an additional referential domain Ω_{χ} has to be introduced. Main feature of the referential domain Ω_{χ} is the fact that it can be arbitrarily moved during the process of body deformation. In particular, it can follow material particles or it may stay fixed in space. Therefore, the description of motion by means of referential domain Ω_{χ} is a generalisation of the classical Eulerian and Lagrangian formulations. The motion of the referential domain in space is described by the mapping Φ:

$$\Phi : \Omega_{\chi} \times [0,T] \to \Omega_{\mathbf{x}} \times [0,T] \qquad (2.2.3)$$
$$\mathbf{x} = \Phi(\boldsymbol{\chi}, t)$$

while the mapping Ψ describes the motion of the referential domain in material domain:

$$\Psi : \Omega_{\chi} \times [0,T] \to \Omega_{\mathbf{X}} \times [0,T] \qquad (2.2.4)$$
$$\mathbf{X} = \Psi(\boldsymbol{\chi}, t)$$

In turn, motion of the material in referential domain is described by mapping the Ψ^{-1}. In case when $\Phi = \mathbf{I}$ we obtain $\boldsymbol{\chi} = \mathbf{x}$, the reference domain does not move in space and the Eulerian formulation is recovered. By contrast, when $\Psi = \mathbf{I}$ we have $\boldsymbol{\chi} = \mathbf{X}$, the reference domain moves with the material and the Lagrangian formulation is regained.

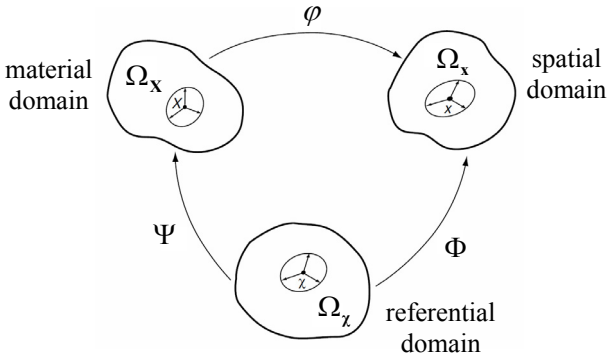

Fig. 2.2. Relations between three considered types of kinematic descriptions

In general, separate notations will be used for description of an arbitrary (scalar, vector or tensor) field f in Lagrangian, Eulerian and ALE approaches. In **Lagrangian** description, based on mapping φ, the field f is defined as a function of material point $\mathbf{X}$:

$$f(\mathbf{X},t):\Omega_{\mathbf{X}}\times[0,T]\to\mathbf{Y} \tag{2.2.5}$$

The derivatives of the field f over time t and material coordinate $\mathbf{X}$ are expressed as follows:

$$\frac{\partial f(\mathbf{X},t)}{\partial t}=\left.\frac{\partial f}{\partial t}\right|_{\mathbf{X}}=\frac{Df}{Dt},\quad \frac{\partial f(\mathbf{X},t)}{\partial \mathbf{X}}=\nabla_{\mathbf{X}}f,\quad \mathrm{tr}\nabla_{\mathbf{X}}f=\mathrm{Div}(f), \tag{2.2.6}$$

In particular, the Lagrangian displacement and material velocity are defined as:

$$\mathbf{u},\mathbf{v}:\Omega_{\mathbf{X}}\to\Omega_{\mathbf{x}},\quad \mathbf{u}(\mathbf{X},t)=\mathbf{x}(\mathbf{X},t)-\mathbf{X},\quad \mathbf{v}(\mathbf{X},t)=\left.\frac{\partial \mathbf{x}}{\partial t}\right|_{\mathbf{X}} \tag{2.2.7}$$

and $\mathbf{v}(\mathbf{X},t)$ indicates velocity of each particle in space. Moreover, Lagrangian gradient of deformation and gradient of displacement take the following forms:

$$\mathbf{F}=\frac{\partial \mathbf{x}}{\partial \mathbf{X}},\qquad \mathbf{Y}=\frac{\partial \mathbf{u}}{\partial \mathbf{X}}=\mathbf{F}-\mathbf{I} \tag{2.2.8}$$

Finally, the Green-Lagrange strain tensor related to the initial configuration reads:

$$\mathbf{L}=\tfrac{1}{2}\left(\mathbf{F}^{\mathbf{T}}\mathbf{F}-\mathbf{I}\right)=\tfrac{1}{2}(\mathbf{Y}+\mathbf{Y}^{\mathbf{T}}+\mathbf{Y}^{\mathbf{T}}\mathbf{Y}) \tag{2.2.9}$$

In **Eulerian** description, based on mapping φ^{-1}, the field f is defined as a function of spatial position $\mathbf{x}$:

$$f(\mathbf{x},t):\Omega_{\mathbf{x}}\times[0,T]\to\mathbf{Y} \tag{2.2.10}$$

The derivatives of the field f over time and spatial coordinate $\mathbf{x}$ are expressed as:

$$\frac{\partial f(\mathbf{x},t)}{\partial t}=\left.\frac{\partial f}{\partial t}\right|_{\mathbf{x}}=\frac{\partial f}{\partial t},\quad \frac{\partial f(\mathbf{x},t)}{\partial \mathbf{x}}=\nabla f,\quad \mathrm{tr}\nabla f=\mathrm{div}(f) \tag{2.2.11}$$

In an Eulerian description the displacement field $\overline{\mathbf{u}}$ and velocity field $\overline{\mathbf{v}}$ are defined as equivalent to the Lagrangian ones (but expressed in terms of different coordinates):

$$\overline{\mathbf{u}}:\Omega_{\mathbf{x}}\to\Omega_{\mathbf{x}},\quad \overline{\mathbf{u}}(\mathbf{x},t)=\mathbf{x}-\mathbf{X}(\mathbf{x},t) \tag{2.2.12}$$

$$\overline{\mathbf{v}}:\Omega_{\mathbf{x}}\to\Omega_{\mathbf{x}},\quad \overline{\mathbf{v}}(\mathbf{x},t)=\mathbf{v}(\mathbf{X},t)\ \text{ where: }\ \mathbf{X}=\mathbf{x}-\overline{\mathbf{u}}(\mathbf{x},t)$$

The above fields denote displacement and velocity of the material particle which is located at

spatial point **x** at considered time instant. The Eulerian displacement $\overline{\mathbf{u}}$ can be used to define Eulerian gradient of deformation and gradient of displacement:

$$\mathbf{H} = \frac{\partial \mathbf{X}}{\partial \mathbf{x}}, \quad \mathbf{K} = \frac{\partial \mathbf{u}}{\partial \mathbf{x}} = \mathbf{I} - \mathbf{H} \tag{2.2.13}$$

Finally, the Almansi strain tensor related to actual configuration reads:

$$\mathbf{E} = \tfrac{1}{2}\left(\mathbf{I} - \mathbf{H}^{\mathrm{T}}\mathbf{H}\right) = \tfrac{1}{2}(\mathbf{K} + \mathbf{K}^{\mathrm{T}} - \mathbf{K}^{\mathrm{T}}\mathbf{K}) \tag{2.2.14}$$

In **ALE** description, based on mappings Φ and Ψ, an arbitrary field f will be defined in referential domain as a function of referential coordinate $\boldsymbol{\chi}$:

$$f(\boldsymbol{\chi}, t) : \Omega_{\chi} \times [0, T] \to \mathbf{Y} \tag{2.2.15}$$

The derivatives of the field f over time t and referential coordinate $\boldsymbol{\chi}$ can be expressed as:

$$\frac{\partial f(\boldsymbol{\chi}, t)}{\partial t} = \left.\frac{\partial f}{\partial t}\right|_{\chi} = \frac{\overline{D} f}{\overline{D} t}, \quad \frac{\partial f}{\partial \boldsymbol{\chi}} = \nabla_{\chi} f, \quad \mathrm{tr}\nabla_{\chi} f = \overline{\mathrm{Div}}(f), \tag{2.2.16}$$

The displacement and velocity of the referential domain in space will be defined on the basis of the mapping Φ:

$$\hat{\mathbf{u}}, \hat{\mathbf{v}} : \Omega_{\chi} \to \Omega_{\mathrm{x}}, \quad \hat{\mathbf{u}}(\boldsymbol{\chi}, t) = \mathbf{x}(\boldsymbol{\chi}, t) - \boldsymbol{\chi}, \quad \hat{\mathbf{v}}(\boldsymbol{\chi}, t) = \left.\frac{\partial \mathbf{x}}{\partial t}\right|_{\chi} \tag{2.2.17a}$$

Further we will follow the derivation conducted for Lagrangian and Eulerian descriptions, however we will replace spatial domain with the referential one. Definitions of the displacement and velocity of particles in referential domain will be based on mapping Ψ^{-1}:

$$\breve{\mathbf{u}}, \mathbf{w} : \Omega_{\mathrm{X}} \to \Omega_{\chi}, \quad \breve{\mathbf{u}}(\mathbf{X}, t) = \boldsymbol{\chi}(\mathbf{X}, t) - \mathbf{X}, \quad \mathbf{w}(\mathbf{X}, t) = \left.\frac{\partial \boldsymbol{\chi}}{\partial t}\right|_{\mathrm{X}} \tag{2.2.17b}$$

and further both fields will be expressed in terms of referential coordinates:

$$\breve{\mathbf{u}}^{*} : \Omega_{\chi} \to \Omega_{\chi}, \quad \breve{\mathbf{u}}^{*}(\boldsymbol{\chi}, t) = \boldsymbol{\chi} - \mathbf{X}(\boldsymbol{\chi}, t) \tag{2.2.17c}$$

$$\mathbf{w}^{*} : \Omega_{\chi} \to \Omega_{\chi}, \quad \mathbf{w}^{*}(\boldsymbol{\chi}, t) = \mathbf{w}(\mathbf{X}, t) \quad \text{where: } \mathbf{X} = \boldsymbol{\chi} - \breve{\mathbf{u}}^{*}(\boldsymbol{\chi}, t)$$

The introduced quantities denote referential displacement and referential velocity of the particle located at referential point $\boldsymbol{\chi}$ at considered time instant. The definitions of displacements $\hat{\mathbf{u}}(\boldsymbol{\chi}, t)$, $\breve{\mathbf{u}}^{*}(\boldsymbol{\chi}, t)$ allow to define two ALE gradients, based on the mappings Φ and Ψ:

$$\mathbf{F}_{\chi} = \frac{\partial \mathbf{x}(\boldsymbol{\chi}, t)}{\partial \boldsymbol{\chi}}, \qquad \mathbf{H}_{\chi} = \frac{\partial \mathbf{X}(\boldsymbol{\chi}, t)}{\partial \boldsymbol{\chi}} \tag{2.2.18}$$

The transformation similar as for referential velocity **w** can be applied for spatial velocity **v**:

$$\overline{\overline{\mathbf{v}}} : \Omega_{\chi} \to \Omega_{\mathrm{x}}, \quad \overline{\overline{\mathbf{v}}}(\boldsymbol{\chi}, t) = \mathbf{v}(\mathbf{X}, t) \quad \text{where: } \mathbf{X} = \boldsymbol{\chi} - \breve{\mathbf{u}}^{*}(\boldsymbol{\chi}, t) \tag{2.2.19}$$

Let us note that the quantities $\mathbf{v}, \overline{\mathbf{v}}, \overline{\overline{\mathbf{v}}}$ denote the same physical field (particles velocity in space) described in various coordinate systems. These quantities will be used in Lagrangian, Eulerian and ALE form of the governing equations. The over-bars will be further omitted.

Taking into account the definition of material velocity in space (Eq. 2.2.7) and the definition of referential domain velocity in space (Eq. 2.2.17a) we can define the convective velocity:

$$\mathbf{c} = \mathbf{v}(\mathbf{X},t) - \hat{\mathbf{v}}(\boldsymbol{\chi},t) = \left.\frac{\partial \mathbf{x}}{\partial t}\right|_{\mathbf{X}} - \left.\frac{\partial \mathbf{x}}{\partial t}\right|_{\boldsymbol{\chi}} \tag{2.2.20}$$

This fundamental quantity of the ALE approach indicates relative velocity between the material and referential domains, as seen from spatial domain. The convective velocity **c** is not equivalent to velocity of material in referential domain **w** and both velocities are equal only in case when motion of the referential domain is purely translational.

In the following step, the dependencies between time and space derivatives in three considered domains will be derived. Since the Lagrangian and Eulerian descriptions are connected by an obvious relation:

$$f(\mathbf{X},t) = f(\mathbf{x},t) \tag{2.2.21a}$$

the material derivative can be expressed by the Eulerian derivative as follows:

$$\frac{Df}{Dt} = \frac{\partial f}{\partial t} + \nabla f \cdot \left.\frac{\partial \mathbf{x}}{\partial t}\right|_{\mathbf{X}} = \frac{\partial f}{\partial t} + (\mathbf{v}\cdot\nabla) f \tag{2.2.21b}$$

which is, in fact, a well-known definition of the material derivative. Similarly, referential and Eulerian descriptions are connected by the relation:

$$f(\boldsymbol{\chi},t) = f(\mathbf{x},t) \tag{2.2.22a}$$

which leads to the following equality:

$$\frac{\overline{D}f}{\overline{D}t} = \frac{\partial f}{\partial t} + \nabla f \cdot \left.\frac{\partial \mathbf{x}}{\partial t}\right|_{\boldsymbol{\chi}} = \frac{\partial f}{\partial t} + (\hat{\mathbf{v}}\cdot\nabla) f \tag{2.2.22b}$$

The dependence between material and referential time derivatives can be derived either by using analogous methodology or by combining Eq. 2.2.21b and Eq. 2.2.22b, which yields:

$$\frac{Df}{Dt} = \frac{\overline{D}f}{\overline{D}t} + (\mathbf{w}\cdot\nabla_{\boldsymbol{\chi}}) f \quad \text{and} \quad \frac{Df}{Dt} = \frac{\overline{D}f}{\overline{D}t} + \nabla f \cdot (\mathbf{v} - \hat{\mathbf{v}}) = \frac{\overline{D}f}{\overline{D}t} + (\mathbf{c}\cdot\nabla) f \tag{2.2.23}$$

The second formulae is known as fundamental ALE equation. The relation between gradients and divergences of an arbitrary quantity f in ALE and Eulerian descriptions is expressed by means of gradient $\mathbf{F}_{\boldsymbol{\chi}}$ and its determinant $J_{\boldsymbol{\chi}} = \det(\mathbf{F}_{\boldsymbol{\chi}})$ [166 168]:

$$\nabla_{\boldsymbol{\chi}} f = \mathbf{F}_{\boldsymbol{\chi}}^{\mathrm{T}} (\nabla f), \qquad \nabla_{\boldsymbol{\chi}} \cdot f = J_{\boldsymbol{\chi}} \nabla \cdot \left(J_{\boldsymbol{\chi}}^{-1} \mathbf{F}_{\boldsymbol{\chi}} f \right) \tag{2.2.24}$$

Finally, the correspondence between volume and line integrals in Eulerian (l.h.s.) and referential (r.h.s.) description is the following:

$$\int_{\Omega_t} f dv = \int_{\Omega} f J_{\boldsymbol{\chi}} dV, \qquad \int_{\Omega_t} f \mathbf{da} = \int_{\Omega} f J_{\boldsymbol{\chi}} \mathbf{F}_{\boldsymbol{\chi}}^{-\mathrm{T}} \mathbf{dA} \tag{2.2.25}$$

Typically, the **conservation laws** are derived by using Eulerian formulation where a fixed region of space is considered or, alternatively, by using Lagrangian formulation where a fixed set of particles is analysed. In such a case the Eulerian and Lagrangian coordinates and differential operators are used, respectively. Here, the balance equations will be derived by

using the Arbitrary Lagrangian-Eulerian approach and the referential domain which is moving in space independently of the material. The equations in ALE form constitute convenient generalisation of the Eulerian and Lagrangian balance equations and they are crucial for a proper formulation of the FSI problem required for modelling of inflatable structures.

The integral ALE form of the conservation law for the region Ω_t with outward normal $\mathbf{n}_t$ moving in space with velocity $\hat{\mathbf{v}}$ reads:

$$\left.\frac{\partial}{\partial t}\right|_{\chi} \int_{\Omega_t} f dv + \int_{\partial\Omega_t} f(\mathbf{v}-\hat{\mathbf{v}})\cdot\mathbf{n}_t da = X \tag{2.2.26}$$

where the first integral indicates change of the considered quantity within referential domain and the second integral indicates transfer of the considered quantity through the boundary of the referential domain. The right-hand side X indicates internal and external factors enforcing change of the considered quantity. Let us note here that classical form of the conservation law (expressed simply as the material derivative of an integral of the considered quantity) can be obtained from Eq. 2.2.26 by introducing $\boldsymbol{\chi} = \mathbf{X}$ and $\hat{\mathbf{v}} = \mathbf{v}$.

Derivation of local referential forms of conservation laws will be performed in two distinct ways. The first method is based on a direct calculation of the referential time derivative of the first integral in Eq. 2.2.26. Since this integral is defined over a domain which changes in time it has to be calculated according to the formulae [170]:

$$\left.\frac{\partial}{\partial t}\right|_{\chi} \int_{\Omega_t} f(\mathbf{x},t) dv = \int_{\Omega_t} \left.\frac{\partial f}{\partial t}\right|_{\mathbf{x}} dv + \int_{\Omega_t} \nabla\cdot(f\hat{\mathbf{v}}) dv \tag{2.2.27a}$$

$$\text{or} \quad \left.\frac{\partial}{\partial t}\right|_{\chi} \int_{\Omega_t} f(\mathbf{x},t) dv = \int_{\Omega_t} \left.\frac{\partial f}{\partial t}\right|_{\chi} dv + \int_{\Omega_t} f(\nabla\cdot\hat{\mathbf{v}}) dv \tag{2.2.27b}$$

which are generalisations of analogous formulae for material derivative of an integral. Application of Eq. 2.2.27b in the integral conservation law (Eq. 2.2.26) leads to 'referential quasi-Eulerian' form of the balance equations where the left-hand side is expressed by referential time derivative and Eulerian gradients of quantity of interest. The second method of derivation of local referential forms of conservation laws is based on transformation of considered domain which changes in time into a domain which is fixed in the referential coordinate system. This method leads to balance equations expressed entirely in terms of referential coordinates and referential differential operators.

In particular , the integral ALE form of the **continuity equation** for an arbitrary region Ω_t moving independently in space with the velocity $\hat{\mathbf{v}}$ reads:

$$\left.\frac{\partial}{\partial t}\right|_{\chi} \int_{\Omega_t} \rho dv + \int_{\partial\Omega_t} \rho(\mathbf{v}-\hat{\mathbf{v}})\cdot\mathbf{n}_t da = 0 \tag{2.2.28}$$

By applying Eq. (2.2.27b) to volume integral and the Gauss-Ostrogradski theorem to surface integral and by taking advantage of discretion of choice of Ω_t we obtain local 'referential quasi-Eulerian' form of the continuity equation:

$$\left.\frac{\partial \rho}{\partial t}\right|_{\chi} + \rho(\nabla\cdot\hat{\mathbf{v}}) + \nabla\cdot(\rho\mathbf{c}) = 0 \tag{2.2.29a}$$

which by simple manipulations can be transformed into the form:

$$\left.\frac{\partial \rho}{\partial t}\right|_{\chi} + \nabla\rho \cdot \mathbf{c} + \rho(\nabla \cdot \mathbf{v}) = 0 \tag{2.2.29b}$$

Two initial terms of Eq. 2.2.29b denote material derivative of density (cf. Eq. 2.2.23) which indicates that 'referential quasi-Eulerian' form of continuity equation is fully equivalent to classical 'Lagrangian quasi-Eulerian' form. Moreover, the classical formulations can be recovered by considering two special cases of ALE formulation: referential domain moving together with the material and referential domain fixed in space. In the first case, substitution:

$$\boldsymbol{\chi} = \mathbf{X}, \quad \hat{\mathbf{v}} = \mathbf{v}, \quad \mathbf{c} = 0 \tag{2.2.30}$$

into Eqs. 2.2.29 leads to Lagrangian quasi-Eulerian form of the continuity equation:

$$\frac{D\rho}{Dt} + \rho(\nabla \cdot \mathbf{v}) = 0 \tag{2.2.31}$$

while in the second case the substitution:

$$\boldsymbol{\chi} = \mathbf{x}, \quad \hat{\mathbf{v}} = 0, \quad \mathbf{c} = \mathbf{v} \tag{2.2.32}$$

into Eqs. 2.2.29 leads to purely Eulerian form of continuity equation:

$$\frac{\partial \rho}{\partial t} + \nabla\rho \cdot \mathbf{v} = -\rho(\nabla \cdot \mathbf{v}) \tag{2.2.33}$$

By using the second introduced method, i.e. by transforming Eq. 2.2.28 into a reference domain we arrive at:

$$\left.\frac{\partial}{\partial t}\right|_{\chi} \int_{\Omega} J_{\chi}\rho dV + \int_{\partial\Omega} \rho J_{\chi}(\mathbf{v} - \hat{\mathbf{v}})\mathbf{F}_{\chi}^{-\mathrm{T}}\mathbf{n} dA = 0 \tag{2.2.34}$$

Since the integration is performed over fixed domain the time derivative of the volume integral can be calculated directly in order to obtain local 'referential form':

$$\left.\frac{\partial (J_{\chi}\rho)}{\partial t}\right|_{\chi} + \nabla_{\chi} \cdot \left[\rho J_{\chi}(\mathbf{v} - \hat{\mathbf{v}})\mathbf{F}_{\chi}^{-\mathrm{T}}\right] = 0 \tag{2.2.35}$$

The equations (2.2.35) and (2.2.29) are fully equivalent which can be proved by using identities related to differentiation of the quantities J_{χ} and $\mathbf{F}_{\chi}$: [171]

$$\left.\frac{\partial J_{\chi}}{\partial t}\right|_{\chi} = J_{\chi}(\nabla \cdot \hat{\mathbf{v}}), \quad \left.\frac{\partial \mathbf{F}_{\chi}}{\partial t}\right|_{\chi} = \nabla_{\chi}\hat{\mathbf{v}}, \quad \nabla_{\chi} \cdot (J_{\chi}\mathbf{F}_{\chi}^{-\mathrm{T}}) = 0\,, \tag{2.2.36}$$

or by using the rules of gradients and divergence transformation (Eq. 2.2.24). When referential domain is moving together with the material, i.e.:

$$\boldsymbol{\chi} = \mathbf{X}, \quad \mathbf{F}_{\chi} = \mathbf{F}, \quad J_{\chi} = J = \det(\mathbf{F}), \quad \hat{\mathbf{v}} = \mathbf{v} \tag{2.2.37}$$

Eq. 2.2.35 reduces to the Lagrangian form of the continuity equation:

$$\frac{D}{Dt}(\rho J) = 0 \tag{2.2.38}$$

On the contrary, in case when referential domain is fixed in space, i.e.:

$$\boldsymbol{\chi} = \mathbf{x}, \quad \mathbf{F}_{\chi} = \mathbf{I}, \quad J_{\chi} = 1, \quad \hat{\mathbf{v}} = 0 \tag{2.2.39}$$

Eq. 2.2.35 reduces to the Eulerian form:

$$\frac{\partial \rho}{\partial t} + \nabla \cdot (\rho \mathbf{v}) = 0 \tag{2.2.40}$$

which is obviously fully equivalent to the Eq. 2.2.33.

Derivation of equations describing **balance of linear momentum** requires introduction of Cauchy stress tensor $\boldsymbol{\sigma}$ which is related to actual configuration and which represents surface forces per unit area of deformed body. Let us also introduce two tensors describing state of stress related to initial configuration. The first (unsymmetric) and the second (symmetric) Piola-Kirchhoff stress tensors:

$$\mathbf{T}^{(1)} = J\boldsymbol{\sigma}\mathbf{F}^{-\mathrm{T}}, \quad \mathbf{T}^{(2)} = \mathbf{F}^{-1}J\boldsymbol{\sigma}\mathbf{F}^{-\mathrm{T}} \tag{2.2.41}$$

Integral ALE form of balance of momentum written for the region Ω_t moving independently in space with the velocity $\hat{\mathbf{v}}$ reads:

$$\left.\frac{\partial}{\partial t}\right|_{\chi} \int_{\Omega t} \rho \mathbf{v} dv + \int_{\partial \Omega t} \rho \mathbf{v} \otimes (\mathbf{v} - \hat{\mathbf{v}}) \mathbf{n}_t da = \int_{\partial \Omega t} (\boldsymbol{\sigma} \mathbf{n}_t) da + \int_{\Omega t} (\rho \mathbf{f}) dv \tag{2.2.42}$$

Similarly as previously, 'referential quasi-Eulerian' form is obtained by direct calculation of referential derivative according to Eq. 2.2.27b and by using Gauss-Ostrogradski theorem:

$$\left.\frac{\partial \rho \mathbf{v}}{\partial t}\right|_{\chi} + \rho \mathbf{v}(\nabla \cdot \hat{\mathbf{v}}) + \nabla \cdot (\rho \mathbf{v} \otimes \mathbf{c}) = \nabla \cdot \boldsymbol{\sigma}^{\mathrm{T}} + \rho \mathbf{f} \tag{2.2.43a}$$

Calculation of the divergence of the tensor product leads to alternative form:

$$\left.\frac{\partial \rho \mathbf{v}}{\partial t}\right|_{\chi} + \nabla(\rho \mathbf{v}) \mathbf{c} + \rho \mathbf{v}(\nabla \cdot \mathbf{v}) = \nabla \cdot \boldsymbol{\sigma}^{\mathrm{T}} + \rho \mathbf{f} \tag{2.2.43b}$$

Moreover, by combining above equation with the continuity equation (2.2.29b) one gets:

$$\rho \left(\left.\frac{\partial \mathbf{v}}{\partial t}\right|_{\chi} + (\nabla \mathbf{v}) \mathbf{c} \right) = \nabla \cdot \boldsymbol{\sigma}^{\mathrm{T}} + \rho \mathbf{f} \tag{2.2.43c}$$

Again we notice that two initial terms of Eq. 2.2.43b and Eq. 2.2.43c indicate material derivative (of the quantity $\rho \mathbf{v}$ and $\mathbf{v}$, respectively) which reveals that 'referential quasi-Eulerian' forms of momentum equations are equivalent to 'Lagrangian quasi-Eulerian' forms. Similarly as previously, the classical formulations are also recovered by considering special cases of referential domain movement. When the referential domain is moving with the material substitution (2.2.30) into Eq. (2.2.43b,c) leads to 'Lagrangian quasi-Eulerian' forms:

$$\frac{D(\rho \mathbf{v})}{Dt} + \rho \mathbf{v}(\nabla \cdot \mathbf{v}) = \nabla \cdot \boldsymbol{\sigma}^{\mathrm{T}} + \rho \mathbf{f} \tag{2.2.44a}$$

$$\text{and} \quad \rho \frac{D\mathbf{v}}{Dt} = \nabla \cdot \boldsymbol{\sigma}^{\mathrm{T}} + \rho \mathbf{f} \tag{2.2.44b}$$

On the contrary, when the referential domain fixed in space substitution (2.2.32) leads to Eulerian forms:

$$\frac{\partial \rho \mathbf{v}}{\partial t} + \nabla \cdot (\rho \mathbf{v} \otimes \mathbf{v}) = \nabla \cdot \boldsymbol{\sigma}^{\mathrm{T}} + \rho \mathbf{f} \tag{2.2.45a}$$

$$\text{and} \quad \rho \left(\frac{\partial \mathbf{v}}{\partial t} + (\nabla \mathbf{v}) \mathbf{v} \right) = \nabla \cdot \boldsymbol{\sigma}^{\mathrm{T}} + \rho \mathbf{f} \tag{2.2.45b}$$

In turn, the method based on transformation of Eq. (2.2.42) into referential domain allows to obtain the equation:

$$\left. \frac{\partial}{\partial t} \right|_{\chi} \int_{\Omega} J_{\chi} \rho \mathbf{v} dV + \int_{\partial \Omega} \rho J_{\chi} \mathbf{v} \otimes (\mathbf{v} - \hat{\mathbf{v}}) \mathbf{F}_{\chi}^{-\mathrm{T}} \mathbf{n} dA = \int_{\partial \Omega} \left(J_{\chi} \boldsymbol{\sigma} \mathbf{F}_{\chi}^{-\mathrm{T}} \right) \mathbf{n} da + \int_{\Omega} (\rho J_{\chi} \mathbf{f}) dv \tag{2.2.46}$$

which can be transformed into a local referential form:

$$\left. \frac{\partial (\rho J_{\chi} \mathbf{v})}{\partial t} \right|_{\chi} + \nabla_{\chi} \cdot \left[\rho J_{\chi} \mathbf{v} \otimes (\mathbf{v} - \hat{\mathbf{v}}) \mathbf{F}_{\chi}^{-\mathrm{T}} \right] = \nabla_{\chi} \cdot \left[J_{\chi} \boldsymbol{\sigma}^{\mathrm{T}} \mathbf{F}_{\chi}^{-\mathrm{T}} \right] + \rho J_{\chi} \mathbf{f} \tag{2.2.47a}$$

and by using continuity equation (2.2.35) to the alternative referential form :

$$\rho J_{\chi} \left. \frac{\partial \mathbf{v}}{\partial t} \right|_{\chi} + \left[\rho J_{\chi} (\mathbf{v} - \hat{\mathbf{v}}) \mathbf{F}_{\chi}^{-\mathrm{T}} \right] \nabla_{\chi} \mathbf{v} = \nabla_{\chi} \cdot \left[J_{\chi} \boldsymbol{\sigma}^{\mathrm{T}} \mathbf{F}_{\chi}^{-\mathrm{T}} \right] + \rho J_{\chi} \mathbf{f} \tag{2.2.47b}$$

The proof of equivalence of above purely referential forms (2.2.47) with referential quasi-Eulerian forms (2.2.43) can be conducted with the use of identities (2.2.36) and rules of referential derivatives transformation (2.2.24). In case when the domain Ω_t is moving together with the material the equations (2.2.47) reduce to the Lagrangian forms:

$$\frac{D}{Dt}(\rho J \mathbf{v}) = \mathrm{Div}(J \boldsymbol{\sigma}^{\mathrm{T}} \mathbf{F}^{-\mathrm{T}}) + \rho J \mathbf{f} \tag{2.2.48}$$

$$\text{and} \quad \rho J \frac{D \mathbf{v}}{Dt} = \mathrm{Div}(J \boldsymbol{\sigma}^{\mathrm{T}} \mathbf{F}^{-\mathrm{T}}) + \rho J \mathbf{f}$$

By using the identities between Cauchy and Piola-Kirchhoff stress tensors:

$$\mathrm{Div}(J \boldsymbol{\sigma}^{\mathrm{T}} \mathbf{F}^{-\mathrm{T}}) = \mathrm{Div}(\mathbf{T}^{(1)}), \quad \mathrm{Div}(J \boldsymbol{\sigma}^{\mathrm{T}} \mathbf{F}^{-\mathrm{T}}) = \mathrm{Div}(\mathbf{F} \mathbf{T}^{(2)}) \tag{2.2.49}$$

the above momentum balances can be written in terms of the first and second Piola-Kirchhoff stress tensors. In case when the domain Ω_t is fixed in space the referential forms of the momentum conservation equation (2.2.47) reduce to purely Eulerian forms (2.2.45).

The balance of angular momentum derived under assumption that there are no sources of angular momentum leads to the symmetry of Cauchy stress tensor:

$$\boldsymbol{\sigma} = \boldsymbol{\sigma}^{\mathrm{T}} \quad \text{or} \quad \mathbf{T}^{(1)\mathrm{T}} \mathbf{F}^{\mathrm{T}} = \mathbf{T}^{(1)} \mathbf{F} \tag{2.2.50}$$

Finally, integral ALE form of **balance of total energy** written for the region Ω_t moving independently in space with the velocity $\hat{\mathbf{v}}$ reads:

$$\left. \frac{\partial}{\partial t} \right|_{\chi} \int_{\Omega_t} \rho E dv + \int_{\partial \Omega_t} \rho E (\mathbf{v} - \hat{\mathbf{v}}) \cdot \mathbf{n}_t da = \int_{\partial \Omega_t} \left(-(\mathbf{q} \cdot \mathbf{n}_t) + (\boldsymbol{\sigma} \mathbf{n}_t) \cdot \mathbf{v} \right) da + \int_{\Omega t} (\rho \mathbf{f} \cdot \mathbf{v} + \rho h) dv \tag{2.2.51}$$

where total specific energy is defined as a sum of specific internal energy and specific kinetic energy as

$$E = e + \tfrac{1}{2}\mathbf{v}\cdot\mathbf{v} \tag{2.2.52}$$

and moreover **q** indicates heat flux, **f** indicates body forces and *h* denotes internal sources of energy. By calculating referential time derivative from integral in equation of total energy balance (2.2.51) we obtain referential quasi-Eulerian form:

$$\left.\frac{\partial(\rho E)}{\partial t}\right|_{\chi} + \rho E\left(\nabla\cdot\hat{\mathbf{v}}\right) + \nabla\cdot(\rho E\mathbf{c}) = -\nabla\cdot\mathbf{q} + \nabla\cdot(\boldsymbol{\sigma}\mathbf{v}) + \rho\mathbf{f}\cdot\mathbf{v} + \rho h \tag{2.2.53a}$$

which after simple manipulations gives:

$$\left.\frac{\partial(\rho E)}{\partial t}\right|_{\chi} + \nabla\left(\rho E\right)\cdot\mathbf{c} + \rho E(\nabla\cdot\mathbf{v}) = -\nabla\cdot\mathbf{q} + \nabla\cdot(\boldsymbol{\sigma}\mathbf{v}) + \rho\mathbf{f}\cdot\mathbf{v} + \rho h \tag{2.2.53b}$$

Introduction of the continuity equation (2.2.29a) into the above yields:

$$\rho\left(\left.\frac{\partial E}{\partial t}\right|_{\chi} + \nabla E\cdot\mathbf{c}\right) = -\nabla\cdot\mathbf{q} + \nabla\cdot(\boldsymbol{\sigma}\mathbf{v}) + \rho\mathbf{f}\cdot\mathbf{v} + \rho h \tag{2.2.53c}$$

Similarly as in case of continuity and momentum equations, above equations are equivalent to Lagrangian quasi-Eulerian forms:

$$\frac{D(\rho E)}{Dt} + \rho E(\nabla\cdot\mathbf{v}) = -\nabla\cdot\mathbf{q} + \nabla\cdot(\boldsymbol{\sigma}\mathbf{v}) + \rho\mathbf{f}\cdot\mathbf{v} + \rho h \tag{2.2.54b}$$

$$\text{and}\quad \rho\frac{DE}{Dt} = -\nabla\cdot\mathbf{q} + \nabla\cdot(\boldsymbol{\sigma}\mathbf{v}) + \rho\mathbf{f}\cdot\mathbf{v} + \rho h \tag{2.2.54c}$$

as well as to purely Eulerian forms:

$$\frac{\partial(\rho E)}{\partial t} + \nabla\left(\rho E\right)\cdot\mathbf{v} + \rho E(\nabla\cdot\mathbf{v}) = -\nabla\cdot\mathbf{q} + \nabla\cdot(\boldsymbol{\sigma}\mathbf{v}) + \rho\mathbf{f}\cdot\mathbf{v} + \rho h \tag{2.2.55b}$$

$$\text{and}\quad \rho\left(\frac{\partial E}{\partial t} + \nabla E\cdot\mathbf{v}\right) = -\nabla\cdot\mathbf{q} + \nabla\cdot(\boldsymbol{\sigma}\mathbf{v}) + \rho\mathbf{f}\cdot\mathbf{v} + \rho h \tag{2.2.55c}$$

The method based on transformation to a referential domain leads to integral form:

$$\begin{aligned}\left.\frac{\partial}{\partial t}\right|_{\chi}\int_{\Omega}\rho E J_{\chi}dV + \int_{\partial\Omega}\rho E J_{\chi}(\mathbf{v}-\hat{\mathbf{v}})\cdot\mathbf{F}_{\chi}^{-\mathrm{T}}\mathbf{n}dA = \\ = \int_{\partial\Omega}\left(-(J_{\chi}\mathbf{q}\cdot\mathbf{F}_{\chi}^{-\mathrm{T}}\mathbf{n}) + J_{\chi}(\boldsymbol{\sigma}\mathbf{n})\cdot\mathbf{F}_{\chi}^{-\mathrm{T}}\mathbf{v}\right)da + \int_{\Omega}(\rho J_{\chi}\mathbf{f}\cdot\mathbf{v} + \rho J_{\chi}h)dv\end{aligned} \tag{2.2.56}$$

and local referential form:

$$\begin{aligned}\left.\frac{\partial(\rho J_{\chi}E)}{\partial t}\right|_{\chi} + \nabla_{\chi}\cdot\left[J_{\chi}\rho E(\mathbf{v}-\hat{\mathbf{v}})\mathbf{F}_{\chi}^{-\mathrm{T}}\right] = \\ = -\nabla_{\chi}\cdot\left[J_{\chi}\mathbf{q}\mathbf{F}_{\chi}^{-\mathrm{T}}\right] + \nabla_{\chi}\cdot\left[J_{\chi}(\boldsymbol{\sigma}\mathbf{v})\mathbf{F}_{\chi}^{-\mathrm{T}}\right] + \rho J_{\chi}\mathbf{f}\cdot\mathbf{v} + \rho J_{\chi}h\end{aligned} \tag{2.2.57a}$$

which by can be transformed by using the continuity equation (Eq. 2.2.35):

$$\rho J_\chi \left.\frac{\partial E}{\partial t}\right|_\chi + \left[(\rho J_\chi (\mathbf{v}-\hat{\mathbf{v}})\mathbf{F}_\chi^{-\mathrm{T}})\right]\cdot\nabla_\chi E = \\ = -\nabla_\chi\cdot\left[J_\chi \mathbf{q}\mathbf{F}_\chi^{-\mathrm{T}}\right] + \nabla_\chi\cdot\left[J_\chi(\boldsymbol{\sigma}\mathbf{v})\mathbf{F}_\chi^{-\mathrm{T}}\right] + \rho J_\chi \mathbf{f}\cdot\mathbf{v} + \rho J_\chi h \tag{2.2.57b}$$

In purely Lagrangian description the above equation can be written as:

$$\frac{D}{Dt}(\rho J E) = -\mathrm{Div}(J\mathbf{q}\mathbf{F}^{-\mathrm{T}}) + \mathrm{Div}(J(\boldsymbol{\sigma}\mathbf{v})\mathbf{F}^{-\mathrm{T}}) + \rho J\mathbf{f}\cdot\mathbf{v} + \rho J h \tag{2.2.58a}$$

$$\text{and } \rho J\frac{DE}{Dt} = -\mathrm{Div}(J\mathbf{q}\mathbf{F}^{-\mathrm{T}}) + \mathrm{Div}(J(\boldsymbol{\sigma}\mathbf{v})\mathbf{F}^{-\mathrm{T}}) + \rho J\mathbf{f}\cdot\mathbf{v} + \rho J h \tag{2.2.58b}$$

Alternatively, the energy balance can be formulated separately for internal and kinetic energy. By multiplication of the equilibrium equation (2.2.44c) by material velocity **v** the kinetic energy is obtained:

$$\rho\frac{D\mathbf{v}}{Dt}\mathbf{v} = \rho\frac{D}{Dt}\left(\tfrac{1}{2}\mathbf{v}\cdot\mathbf{v}\right) = \mathbf{v}\cdot(\nabla\cdot\boldsymbol{\sigma}) + \rho\mathbf{f}\cdot\mathbf{v} \tag{2.2.59}$$

Subtracting kinetic energy (2.2.59) from total energy balance (2.2.54) yields:

$$\rho\frac{De}{Dt} = -\nabla\cdot\mathbf{q} + \rho h + [\nabla\cdot(\boldsymbol{\sigma}\mathbf{v}) - \mathbf{v}\cdot(\nabla\cdot\boldsymbol{\sigma})] = -\nabla\cdot\mathbf{q} + \rho h + \Theta \tag{2.2.60}$$

where the last term Θ indicates work done by stress which changes internal energy and which can be expressed as:

$$\Theta = \boldsymbol{\sigma}\cdot(\nabla\mathbf{v})^T = \mathrm{tr}(\boldsymbol{\sigma}(\nabla\mathbf{v})^T) \tag{2.2.61}$$

The formula (6.2.60) can be further specified by decomposition of the velocity gradient $\nabla\mathbf{v}$ into strain rate tensor **D** (symmetric part of the Eulerian velocity gradient) and tensor of spin **W** (asymmetric part of the Eulerian velocity gradient):

$$\rho\frac{De}{Dt} = -\nabla\cdot\mathbf{q} + \rho h + \boldsymbol{\sigma}\cdot\mathbf{D} \tag{2.2.62}$$

In a special case of Newtonian fluid with stress tensor dependent on pressure and viscosity the formula (2.2.62) can be written in the form:

$$\rho\frac{De}{Dt} = -\nabla\cdot\mathbf{q} + \rho h - p(\nabla\cdot\mathbf{v}) + \boldsymbol{\sigma}^*\cdot(\nabla\mathbf{v})^T \tag{2.2.63}$$

where p indicates pressure and $\boldsymbol{\sigma}^*$ indicates part of the stress tensor related to fluid viscosity. The above equation can be easily transformed into referential quasi-Eulerian form by expressing material derivative of internal energy by the referential one, according to Eq. 2.2.23b. Let us further introduce standard thermodynamic energy balance expressed in terms of specific entropy s:

$$T\frac{Ds}{Dt} = \frac{De}{Dt} + p\frac{D}{Dt}\left(\frac{1}{\rho}\right) \tag{2.2.64a}$$

which can be transformed to the form:

$$T\frac{Ds}{Dt}=\frac{De}{Dt}-\frac{p}{\rho^2}\frac{D\rho}{Dt} \tag{2.2.64b}$$

and further by using the continuity equation (2.2.31):

$$\rho T\frac{Ds}{Dt}=\rho\frac{De}{Dt}+p(\nabla\cdot\mathbf{v}) \tag{2.2.64c}$$

The above formula allows to identify term $p(\nabla\cdot\mathbf{v})$ which indicates work done by fluid pressure on change of fluid volume which is reversible and indicates difference between work which changes internal energy and work which changes fluid entropy (cf. Eq. 2.2.63 and Eq. 2.2.65). Finally, change of entropy is governed by the equation:

$$\rho T\frac{Ds}{Dt}=-\nabla\cdot\mathbf{q}+\rho h+\boldsymbol{\sigma}^{*}\cdot(\nabla\mathbf{v})^{T} \tag{2.2.65}$$

Moreover, the introduced conservation laws has to be complemented with **Clausius-Duhem entropy inequality** [172] (the second law of thermodynamics) which states that for any feasible process the entropy of the system and surroundings can not decrease:

$$\rho\frac{Ds}{Dt}+\nabla\cdot\left(\frac{\mathbf{q}}{T}\right)-\frac{\rho h}{T}\geq 0 \tag{2.2.66}$$

by combining the above equation with equation governing change of internal energy (2.2.62) we obtain function $\mathcal{D}$ which describes dissipation and which has to be positive during the whole process:

$$\mathcal{D}=\rho\left(T\frac{Ds}{Dt}-\frac{De}{Dt}\right)+\boldsymbol{\sigma}\cdot\mathbf{D}-\frac{\mathbf{q}\cdot\nabla T}{T}\geq 0 \tag{2.2.67}$$

The next step in formulation of mathematical model of fluid structure interaction problem is definition of **constitutive relations** which connect state of deformation with corresponding state of stress. Constitutive relations will be presented separately for the continuum composed of solid and fluid.

Solids involved in considered Fluid-Structure Interaction problems will be made materials of miscellaneous mechanical characteristics depending on application of considered inflatable structure, such as metals characterized by various types of plasticity, fabrics with strong orthotropic properties or rubber. However, for the sake of simplicity, only general form of the constitutive relations for hypo-elastic and hyper-elastic material will be briefly discussed. For hypo-elastic material constitutive relation links arbitrary objective stress rate $\boldsymbol{\sigma}^{\circ}$ (e.g. Truesdell, Green-Naghdi or Jaumann rate [173]) with strain rate tensor **D**:

$$\boldsymbol{\sigma}^{\circ}=f(\boldsymbol{\sigma},\mathbf{D}) \tag{2.2.67}$$

In many practical cases linear relation between $\boldsymbol{\sigma}^{\circ}$ and **D** can be assumed. One of the most often used objective stress rates is Jaumann rate which eliminates the influence of rotations from the constitutive relations:

$$\boldsymbol{\sigma}^{\nabla}=\dot{\boldsymbol{\sigma}}-\mathbf{W}\cdot\boldsymbol{\sigma}+\boldsymbol{\sigma}\cdot\mathbf{W} \tag{2.2.68}$$

where **W** is the spin tensor (asymmetric part of the velocity gradient). In case of hyper-elastic materials the stress tensor is defined as derivative of elastic potential which indicates density of internal energy and which is expressed by deformation gradient **F** or Green-Lagrange strain tensor **L**:

$$\mathbf{P}(\mathbf{X},t) = \frac{\partial W(\mathbf{X},\mathbf{F}(\mathbf{X},t))}{\partial \mathbf{F}} \tag{2.2.69}$$

Let us also consider simple particular case of Saint-Venant-Kirchhoff material for which state of strain can be described by Green-Lagrange tensor **L** corresponding to initial configuration:

$$\boldsymbol{\varepsilon}_\mathbf{s} = \mathbf{L} = \tfrac{1}{2}(\mathbf{F}^\mathbf{T}\mathbf{F} - \mathbf{I}) = \tfrac{1}{2}(\nabla\mathbf{u} + (\nabla\mathbf{u})^\mathbf{T} + (\nabla\mathbf{u})^\mathbf{T}\nabla\mathbf{u}) \tag{2.2.70}$$

and constitutive relation defines second Piola-Kirchhoff stress tensor $\mathbf{T}^{(2)}$ by means of Lame coefficients μ and λ, according to the equation:

$$\mathbf{T}^{(2)} = 2\mu\boldsymbol{\varepsilon}_\mathbf{S} + \lambda\mathrm{tr}(\boldsymbol{\varepsilon}_\mathbf{S})\mathbf{I} \tag{2.2.71}$$

Lame constants are related to Young modulus E and Poisson coefficient ν by the formulae:

$$\mu = \frac{E}{2(1+\nu)}, \quad \lambda = \frac{\nu E}{(1+\nu)(1-2\nu)} \tag{2.2.72}$$

By introducing Eq. 2.2.70 into the constitutive relation (2.2.71) the second Piola-Kirchhoff stress tensor can be expressed in terms of solid displacement:

$$\mathbf{T}^{(2)} = \mu(\nabla\mathbf{u} + (\nabla\mathbf{u})^\mathbf{T} + (\nabla\mathbf{u})^\mathbf{T}\nabla\mathbf{u}) + \lambda[(\nabla\cdot\mathbf{u})\mathbf{I} + \tfrac{1}{2}\mathrm{tr}((\nabla\mathbf{u})^\mathbf{T}\nabla\mathbf{u})] \tag{2.2.73}$$

Further, general form of the equation of momentum balance can be derived:

$$\rho\frac{D^2\mathbf{u}}{Dt^2} = (\lambda+\mu)\nabla(\nabla\cdot\mathbf{u}) + \mu\Delta\mathbf{u} + \mu\nabla\cdot((\nabla\mathbf{u})^\mathbf{T}\nabla\mathbf{u}) + \tfrac{\lambda}{2}\nabla\cdot[\mathrm{tr}((\nabla\mathbf{u})^\mathbf{T}\nabla\mathbf{u})] + \rho\mathbf{f} \tag{2.2.74}$$

By applying the assumption of small displacements (and thus reducing material derivative to time derivative) and neglecting nonlinear terms depending on product of displacement gradient, the well known equilibrium equation of linear theory of elasticity is obtained [[174]]:

$$\rho\frac{\partial^2\mathbf{u}}{\partial t^2} = (\lambda+\mu)\nabla(\nabla\cdot\mathbf{u}) + \mu\Delta\mathbf{u} + \rho\mathbf{f} \tag{2.2.75}$$

Fluids involved in considered Fluid-Structure Interaction problem are in general gases which are Newtonian fluids characterised by compressibility and viscosity. For Newtonian fluids [[175] [176]] the main kinematic quantity is the strain rate tensor $\dot{\boldsymbol{\varepsilon}}_\mathbf{f}$ defined as:

$$\dot{\boldsymbol{\varepsilon}}_\mathbf{f} = \mathbf{D} = \tfrac{1}{2}(\nabla\mathbf{v} + (\nabla\mathbf{v})^\mathbf{T}) \tag{2.2.76}$$

The stress tensor $\boldsymbol{\sigma}_\mathbf{f}$ depends separately on deviatoric part of the strain rate tensor $\mathbf{D}'$, its spherical part $\mathbf{S}$ and fluid pressure p:

$$\boldsymbol{\sigma}_\mathbf{f} = \boldsymbol{\tau} - p\mathbf{I} = 2\mu\mathbf{D}' + \mu_b\mathbf{S} - p\mathbf{I} \tag{2.2.77}$$

$$\boldsymbol{\sigma}_\mathbf{f} = 2\mu[\mathbf{D} - \tfrac{1}{3}\mathrm{tr}(\mathbf{D})\mathbf{I}] + \mu_b\mathrm{tr}(\mathbf{D})\mathbf{I} - p\mathbf{I} \tag{2.2.78}$$

where μ is the dynamic viscosity, μ_b is bulk viscosity. Above constitutive equation can be also written in alternative form:

$$\boldsymbol{\sigma}_{\mathbf{f}} = 2\mu\mathbf{D} + \lambda \mathrm{tr}(\mathbf{D})\mathbf{I} - p\mathbf{I} \tag{2.2.79}$$

where the secondary viscosity λ is related to dynamic viscosity μ and bulk viscosity μ_b by the relation: $\lambda = \mu_b - \frac{2}{3}\mu$. Bulk viscosity μ_b is often neglected and such assumption will be also employed herein. Equation (2.2.79) can be also expressed in terms of fluid velocity:

$$\boldsymbol{\sigma}_{\mathbf{f}} = \mu(\nabla\mathbf{v} + (\nabla\mathbf{v})^{\mathrm{T}}) + \lambda(\nabla\cdot\mathbf{v})\mathbf{I} - p\mathbf{I} \tag{2.2.80}$$

Introduced constitutive relations can be used to derive momentum and energy equations in terms of kinematic quantities. For Newtonian fluid, the momentum equation can be initially expressed in terms of pressure and deviatoric part of the stress tensor:

$$\rho\frac{D\mathbf{v}}{Dt} = -\nabla p + 2\mu\nabla\cdot\mathbf{D}' + \rho\mathbf{f} \tag{2.2.81}$$

and further in terms of fluid velocity:

$$\rho\frac{D\mathbf{v}}{Dt} = -\nabla p + (\lambda+\mu)\nabla(\nabla\cdot\mathbf{v}) + \mu\Delta\mathbf{v} + \rho\mathbf{f} \tag{2.2.82}$$

Energy equation expressed in terms of pressure and deviatoric part of stress tensor reads :

$$\rho\frac{D}{Dt}(e + \tfrac{1}{2}\mathbf{v}\cdot\mathbf{v}) = -\nabla\cdot\mathbf{q} - \nabla p\cdot\mathbf{v} - p(\nabla\cdot\mathbf{v}) + 2\mu[\nabla\cdot(\mathbf{D}'\mathbf{v})] + \rho\mathbf{f}\cdot\mathbf{v} + \rho h \tag{2.2.83}$$

while in terms of fluid velocity it takes the form:

$$\begin{aligned}&\rho\frac{D}{Dt}(e + \tfrac{1}{2}\mathbf{v}\cdot\mathbf{v}) = \\ &= -\nabla\cdot\mathbf{q} - \nabla p\cdot\mathbf{v} - p(\nabla\cdot\mathbf{v}) + \nabla\cdot[(\mu(\nabla\mathbf{v} + (\nabla\mathbf{v})^{\mathrm{T}}) + \lambda(\nabla\cdot\mathbf{v})\mathbf{I})\cdot\mathbf{v}] + \rho\mathbf{f}\cdot\mathbf{v} + \rho h\end{aligned} \tag{2.2.84}$$

Kinematic part of energy balance reads:

$$\rho\frac{D\mathbf{v}}{Dt}\mathbf{v} = \rho\frac{D}{Dt}\left(\tfrac{1}{2}\mathbf{v}\cdot\mathbf{v}\right) = -\nabla p\cdot\mathbf{v} + 2\mu\mathbf{v}\cdot\nabla\cdot\mathbf{D}' + \rho\mathbf{f}\cdot\mathbf{v} \tag{2.2.85}$$

while thermal part assumes the form:

$$\begin{aligned}\rho\frac{De}{Dt} &= -\nabla\cdot\mathbf{q} + \rho h - p(\nabla\cdot\mathbf{v}) + 2\mu[\nabla\cdot(\mathbf{D}'\mathbf{v}) - \mathbf{v}\cdot(\nabla\cdot\mathbf{D}')] = \\ &= -\nabla\cdot\mathbf{q} + \rho h - p(\nabla\cdot\mathbf{v}) + 2\mu\,\mathrm{tr}[(\mathbf{D}')^2]\end{aligned} \tag{2.2.86}$$

Moreover, derived system of equations has to be complemented with definitions of gas pressure, gas internal energy and Fourier's law of heat conduction. Gas pressure depends on gas density, gas constant and gas temperature according to ideal gas law:

$$p = \rho R T \tag{2.2.87}$$

where gas constant R is related to the universal gas constant $\overline{R}$ and molecular weight MW by the formula: $R = \overline{R}/MW$. Gas internal energy e depends on gas specific heat at constant volume c_V and gas temperature T:

$$e = c_V T \tag{2.2.88}$$

Finally, the Fourier's law of Heat Conduction states that heat flux depends on thermal conductivity and temperature gradient:

$$\mathbf{q} = -k\nabla T \tag{2.2.89}$$

Another possibility is applying the Cataneo relation which is generalisation of Fourier's law for non-equilibrium systems [177]:

$$\frac{\partial \mathbf{q}}{\partial t} = -\frac{\mathbf{q} + k\nabla T}{\tau_{\mathbf{q}}} \tag{2.2.90}$$

and which introduces additional conservative term into heat transfer equation and changes its type from parabolic to hyperbolic [178].

2.2.2 Passive inflatable structure

In this section basic theoretical model of passive inflatable structure will be defined as composed of deformable solid body and single internal chamber filled with compressible fluid. Basic feature of passive inflatable structure is the lack of inflator and controllable gas exhaust. Two basic types of passive inflatable structure may be distinguished:

- the one that is completely closed thereby excluding escape of gas (Fig. 2.3) or
- the one that contains orifice of a constant diameter allowing outflow of gas to environment (Fig. 2.4).

Modelling of passive inflatable structure will be considered as a preliminary step before modelling adaptive inflatable structure equipped with controllable valve.

The elementary FSI model of closed inflatable structure is composed of external domain $\Omega_S(t)$ occupied by solid body and located inside domain $\Omega_F(t)$ occupied by fluid, see Fig 2.3. Internal part of the solid boundary $\Gamma_{FS} = \Omega_S \cap \Omega_F$ constitutes fluid-solid interface where solid body interacts with internal fluid. It is assumed that no additional mechanical boundary conditions are applied at fluid-solid interface. External boundary of the solid region comprises Dirichlet part $\Gamma_{\mathbf{u}} = \Gamma_{fix}$ which is usually fixed in space and Neumann part $\Gamma_{\boldsymbol{\sigma}}$ where stress boundary conditions can be imposed. Neumann part of the boundary contains part Γ_{imp} where external force modelling impact is applied. During impact the solid body deforms under applied external loading and thus geometry of both solid and fluid domains changes.

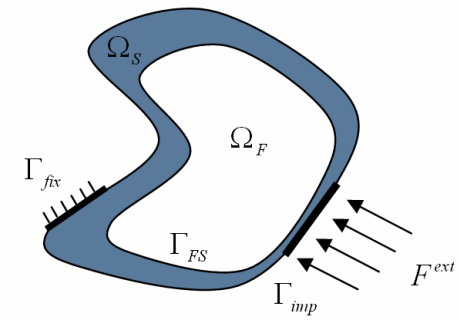

Fig. 2.3 FSI model of a closed inflatable structure with impact modelled as an external loading

The FSI model of inflatable structure equipped with orifice of a constant diameter is composed of domain $\Omega_F(t)$ occupied by fluid and internal solid domain $\Omega_S(t)$ totally immersed in fluid, see Fig 2.4. Let $\Gamma = \Omega_S \cap \Omega_F$ be a common interface between solid and fluid domains located both inside and outside the solid body. The boundary $\Gamma = \Gamma_{fix} \cup \Gamma_{FS}$ is composed of two separate parts: Γ_{fix} which is fixed in space and part Γ_{FS} which constitutes fluid-solid interface. In general, external loading can be applied at arbitrary part of fluid-solid interface Γ_{FS}, but in considered case the non-zero external force modelling impact is applied only at part denoted as Γ_{imp}. Moreover, Γ_{ext} constitutes external boundary of the fluid region where external boundary conditions are prescribed.

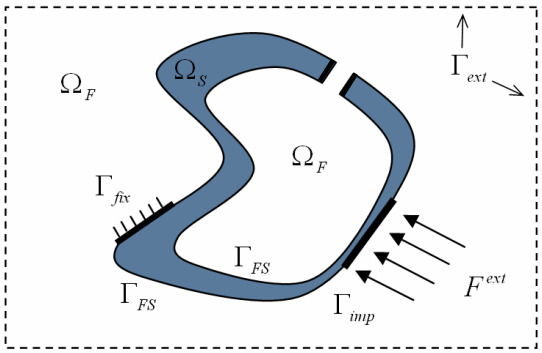

Fig. 2.4 FSI model of passive inflatable structure with orifice of a constant diameter

Two combined, not purely Lagrangian or Eulerian, descriptions of continuum kinematics and two arising from them numerical methods are used to handle FSI problems of the considered type [179 180]:

1. Conforming boundary methods (mainly Arbitrary Lagrangian Eulerian approach) [181 182]: Lagrangian description of the solid body, Arbitrary Lagrangian-Eulerian description of the fluid in deforming fluid domain and fluid-solid interface located between the domains, Fig. 2.5a
2. Fixed grid methods (mainly Coupled Eulerian-Lagrangain approach) [183 184]: Lagrangian description of the solid body, Eulerian 'background' fluid domain and fluid-solid interface defined inside Eulerian domain, Fig. 2.5b.

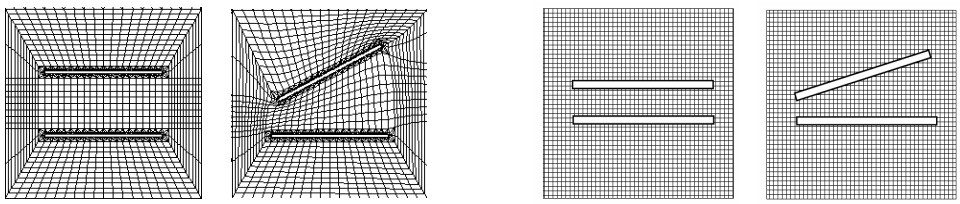

Fig. 2.5 Comparison of 'conforming boundary method' and 'fixed grid methods' for modelling of fluid-structure interaction problems

Both above methods are well suited for modelling of Adaptive Inflatable Structures and thus both of them will be described and used in further parts of this thesis. In both methods, deformation of a solid body is described in classical Lagrangian manner and it is used either to determine actual shape of the fluid domain (in ALE) or to determine actual area occupied by fluid (in CEL). Therefore, the difference between two methods relies on various

description of the fluid flow within changing in time domain and appropriate handling of the mechanical and thermal coupling between fluid and solid body.

Conforming boundary method (ALE approach):

Conforming boundary method will be used to formulate initial boundary value problem describing passive inflatable structure with the orifice (Fig. 2.4) subjected to impact loading.

Let us start with the definitions of required displacement and velocity fields. Deformation of the solid body can be described in a classical way by Lagrangian approach:

$$\mathbf{u}_{\mathrm{S}}(\mathbf{X},t):\Omega_{\mathbf{X}}^{\mathrm{S}}\times[0,T]\rightarrow\Omega_{\mathbf{x}}(t)\times[0,T] \tag{2.2.91}$$

$$\mathbf{u}_{\mathrm{S}}(\mathbf{X},t)=\mathbf{x}_{\mathrm{S}}(\mathbf{X},t)-\mathbf{X},\qquad \mathbf{v}_{\mathrm{S}}(\mathbf{X},t)=\frac{\partial\mathbf{x}_{\mathrm{S}}(\mathbf{X},t)}{\partial t}$$

Since the fluid will be described in the referential coordinate system, the fields describing deformation of solid will be artificially transformed into referential coordinate system whose movement coincides with movement of the material ($\boldsymbol{\chi}=\mathbf{X}$):

$$\overline{\overline{\mathbf{u}}}_{\mathrm{S}}(\boldsymbol{\chi},t):\Omega_{\boldsymbol{\chi}}^{\mathrm{S}}\times[0,T]\rightarrow\Omega_{\mathbf{x}}(t)\times[0,T] \tag{2.2.92}$$

$$\overline{\overline{\mathbf{u}}}_{\mathrm{S}}(\boldsymbol{\chi},t)=\mathbf{u}_{\mathrm{S}}(\mathbf{X},t),\qquad \overline{\overline{\mathbf{v}}}_{\mathrm{S}}(\boldsymbol{\chi},t)=\mathbf{v}_{\mathrm{S}}(\mathbf{X},t)\quad\text{where:}\quad\mathbf{X}=\boldsymbol{\chi}$$

Definition of the fluid velocity field starts with definition of Lagrangian displacement and velocity fields:

$$\mathbf{u}_{\mathrm{f}}(\mathbf{X},t):\Omega_{\mathbf{X}}^{\mathrm{f}}\times[0,T]\rightarrow\Omega_{\mathbf{x}}(t)\times[0,T] \tag{2.2.93}$$

$$\mathbf{u}_{\mathrm{f}}(\mathbf{X},t):\mathbf{x}_{\mathrm{f}}(\mathbf{X},t)-\mathbf{X},\qquad \mathbf{v}_{\mathrm{f}}(\mathbf{X},t)=\frac{\partial\mathbf{x}_{\mathrm{f}}(\mathbf{X},t)}{\partial t}$$

Definition of the Eulerian fluid velocity $\overline{\mathbf{v}}_{\mathrm{f}}(\mathbf{x},t)$ utilizes transformation of the Lagrangian velocity to spatial coordinate system (cf. Eq. 2.2.12). The Eulerian velocity field is defined in a spatial domain $\Omega_{\mathbf{x}}^{\mathrm{f}}(t)$ which changes during the process due to deformation of solid.

$$\overline{\mathbf{v}}_{\mathrm{f}}(\mathbf{x},t):\Omega_{\mathbf{x}}^{\mathrm{f}}(t)\times[0,T]\rightarrow\Omega_{\mathbf{x}}^{\mathrm{f}}(t)\times[0,T],\qquad \overline{\mathbf{v}}_{\mathrm{f}}(\mathbf{x},t)=\mathbf{v}_{\mathrm{f}}(\mathbf{X},t),\quad \mathbf{X}=\mathbf{x}-\overline{\mathbf{u}}_{\mathrm{f}}(\mathbf{x},t) \tag{2.2.94a}$$

By contrast, ALE approach utilizes transformation of the Lagrangian fields to the referential coordinate system which itself deforms during the process (cf. Eq. 2.2.19):

$$\overline{\overline{\mathbf{v}}}_{\mathrm{f}}(\boldsymbol{\chi},t):\Omega_{\boldsymbol{\chi}}^{\mathrm{f}}\times[0,T]\rightarrow\Omega_{\mathbf{x}}^{\mathrm{f}}(t)\times[0,T],\qquad \overline{\overline{\mathbf{v}}}_{\mathrm{f}}(\boldsymbol{\chi},t)=\mathbf{v}_{\mathrm{f}}(\mathbf{X},t),\quad \mathbf{X}=\boldsymbol{\chi}-\breve{\mathbf{u}}_{\mathrm{f}}^{*}(\boldsymbol{\chi},t) \tag{2.2.94b}$$

Finally, arbitrary deformation of referential coordinate system in space has to be defined by means of mapping Φ (see Fig. 2.2):

$$\hat{\mathbf{u}}_{\mathrm{f}}(\boldsymbol{\chi},t):\Omega_{\boldsymbol{\chi}}^{\mathrm{f}}\times[0,T]\rightarrow\Omega_{\mathbf{x}}^{\mathrm{f}}(t)\times[0,T] \tag{2.2.95}$$

$$\hat{\mathbf{u}}_{\mathrm{f}}(\boldsymbol{\chi},t)=\mathbf{x}(\boldsymbol{\chi},t)-\boldsymbol{\chi}$$

The mapping $\hat{\mathbf{u}}_{\mathrm{f}}$ is not known by default and it can be chosen as a solution of an arbitrary initial-boundary value problem satisfying Dirichlet boundary condition enforced by displacement of the solid body at fluid-solid interface. Finally, the kinematics of the system is described by the quantities $\hat{\mathbf{u}}_{\mathrm{f}},\overline{\overline{\mathbf{v}}}_{\mathrm{S}},\overline{\overline{\mathbf{v}}}_{\mathrm{f}}$ all expressed in terms of referential coordinates $\boldsymbol{\chi}$.

The system of equations governing considered FSI problem is in general composed of conservation equations (continuity equation, balance of momentum and total energy) derived in Sec.2.2.1 formulated for both solid and fluid domain. The ALE form of the equilibrium equations for a solid body (here equivalent to Lagrange form, $\boldsymbol{\chi} = \mathbf{X}$) reads, cf. Sect. 2.2.1:

$$\left.\frac{\partial(\rho_{\mathbf{S}} J)}{\partial t}\right|_{\chi} = 0 \qquad \text{in } \Omega_S \tag{2.2.96}$$

$$\left.\frac{\partial(J\rho_{\mathbf{S}}\mathbf{v}_{\mathbf{S}})}{\partial t}\right|_{\chi} = \nabla_{\chi}\cdot(J\boldsymbol{\sigma}_{\mathbf{S}}{}^{\mathrm{T}}\mathbf{F}^{-\mathrm{T}}) + \rho_{\mathbf{S}} J_{\chi}\mathbf{f} \tag{2.2.97}$$

$$\left.\frac{\partial(J\rho_{\mathbf{S}}E_S)}{\partial t}\right|_{\chi} = -\nabla_{\chi}\cdot(J\mathbf{q}_{\mathbf{S}}\mathbf{F}^{-\mathrm{T}}) + \nabla_{\chi}\cdot(J(\boldsymbol{\sigma}_{\mathbf{S}}\mathbf{v}_{\mathbf{S}})\mathbf{F}^{-\mathrm{T}}) + \rho_{\mathbf{S}} J\mathbf{f}\cdot\mathbf{v}_{\mathbf{S}} + \rho_{\mathbf{S}} J h \tag{2.2.98}$$

The ALE form of the Navier-Stokes equations for the fluid is the following, cf. Sect. 2.2.1:

$$\left.\frac{\partial(J_{\chi}\rho_{\mathbf{f}})}{\partial t}\right|_{\chi} + \nabla_{\chi}\cdot\left[\rho_{\mathbf{f}} J_{\chi}\left(\mathbf{v}_{\mathbf{f}} - \frac{\partial\hat{\mathbf{u}}_{\mathbf{f}}}{\partial t}\right)\mathbf{F}_{\chi}^{-\mathrm{T}}\right] = 0 \qquad \text{in } \Omega_f \tag{2.2.99}$$

$$\left.\frac{\partial(\rho_{\mathbf{f}} J_{\chi}\mathbf{v}_{\mathbf{f}})}{\partial t}\right|_{\chi} + \nabla_{\chi}\cdot\left[\rho_{\mathbf{f}} J_{\chi}\mathbf{v}_{\mathbf{f}}\otimes\left(\mathbf{v}_{\mathbf{f}} - \frac{\partial\hat{\mathbf{u}}_{\mathbf{f}}}{\partial t}\right)\mathbf{F}_{\chi}^{-\mathrm{T}}\right] = \nabla_{\chi}\cdot\left[J_{\chi}\boldsymbol{\sigma}_{\mathbf{f}}{}^{\mathrm{T}}\mathbf{F}_{\chi}^{-\mathrm{T}}\right] + \rho_{\mathbf{f}} J_{\chi}\mathbf{f} \tag{2.2.100}$$

$$\begin{aligned}\left.\frac{\partial(\rho_{\mathbf{f}} J_{\chi}E_f)}{\partial t}\right|_{\chi} + \nabla_{\chi}\cdot\left[\rho_{\mathbf{f}} J_{\chi}E_f\left(\mathbf{v}_{\mathbf{f}} - \frac{\partial\hat{\mathbf{u}}_{\mathbf{f}}}{\partial t}\right)\mathbf{F}_{\chi}^{-\mathrm{T}}\right] = \\ = -\nabla_{\chi}\cdot\left[J_{\chi}\mathbf{q}_{\mathbf{f}}\mathbf{F}_{\chi}^{-\mathrm{T}}\right] + \nabla_{\chi}\cdot\left[J_{\chi}(\boldsymbol{\sigma}_{\mathbf{f}}\mathbf{v}_{\mathbf{f}})\mathbf{F}_{\chi}^{-\mathrm{T}}\right] + \rho_{\mathbf{f}} J_{\chi}\mathbf{f}\cdot\mathbf{v}_{\mathbf{f}} + \rho_{\mathbf{f}} J_{\chi} h\end{aligned} \tag{2.2.101}$$

In above equations all quantities are expressed in terms of referential coordinates and double overbars and the arguments of the quantities $\overline{\overline{\mathbf{v}}}_{\mathbf{s/f}}(\boldsymbol{\chi},t)$ are omitted in order to ease notation. Finally, the system of differential equations is complemented by an arbitrary equation governing mesh deformation inside fluid domain whose general form reads:

$$\frac{\partial\hat{\mathbf{u}}_{\mathbf{f}}}{\partial t} = \mathbf{D}(\hat{\mathbf{u}}_{\mathbf{f}}) \quad \text{in } \Omega_f \tag{2.2.102}$$

where **D** is an arbitrary differential operator. Set of PDEs presented above describes both closed inflatable structure (Fig. 2.3) and inflatable structure with the orifice (Fig. 2.4). However, boundary and coupling conditions presented below describe only the latter case.

Boundary conditions concerning solid are defined at fixed part of the boundary Γ_{fix} and at the part of boundary where impact is applied Γ_{imp}:

$$\mathbf{v}_{\mathbf{S}} = \mathbf{0} \quad \text{on } \Gamma_{fix} \quad \text{and} \quad \boldsymbol{\sigma}_{\mathbf{S}}\mathbf{n} = \mathbf{F}^{ext} \quad \text{on } \Gamma_{imp} \tag{2.2.103}$$

Boundary conditions for the fluid are also defined at fixed part of the boundary Γ_{fix}:

$$\mathbf{v}_{\mathbf{f}} = \mathbf{0} \quad \text{on } \Gamma_{fix} \tag{2.2.104}$$

and at external boundary of the fluid domain Γ_{ext} (here defined in theoretical, the most general form):

$$\rho_{\mathbf{f}} = \widetilde{\rho}_{\mathbf{f}} \quad \text{on} \quad \Gamma_{ext} \tag{2.2.104b}$$

$$\mathbf{v}_{\mathbf{f}} = \widetilde{\mathbf{v}}_{\mathbf{f}} \quad \text{or} \quad \boldsymbol{\sigma}_{\mathbf{f}}\mathbf{n} = \widetilde{\mathbf{t}} \quad \text{on} \ \Gamma_{ext} \tag{2.2.104c}$$

$$T_{\mathbf{f}} = \widetilde{T}_{\mathbf{f}} \quad \text{or} \quad -\mathbf{q}_{\mathbf{f}} \cdot \mathbf{n} = \widetilde{q}_f \quad \text{on} \ \Gamma_{ext} \tag{2.2.104d}$$

Coupling conditions defined on a fluid-solid interface concern both mechanical part:

$$\boldsymbol{\sigma}_{\mathbf{S}}\mathbf{n} = \boldsymbol{\sigma}_{\mathbf{f}}\mathbf{n} + \mathbf{F}^{ext} \ \text{ and } \ \mathbf{v}_{\mathbf{f}} = \mathbf{v}_{\mathbf{S}} \quad \text{on} \ \Gamma_{FS} \tag{2.2.105a}$$

and thermal part of the problem:

$$T_{\mathbf{S}} = T_{\mathbf{f}} \quad \text{and} \quad \mathbf{q}_{\mathbf{S}} \cdot \mathbf{n} = \mathbf{q}_{\mathbf{f}} \cdot \mathbf{n} \quad \text{on} \ \Gamma_{FS} \cup \Gamma_{fix} \tag{2.2.105b}$$

where $\mathbf{q}_{\mathbf{S}}, \mathbf{q}_{\mathbf{f}}$ are heat fluxes inside solid and fluid domains. Moreover coupling / boundary conditions for the field $\hat{\mathbf{u}}_{\mathbf{f}}$ defining deformation of the referential coordinate system read:

$$\hat{\mathbf{u}}_{\mathbf{f}} = \mathbf{u}_{\mathbf{S}} \quad \text{on} \ \Gamma_{FS} \quad \text{and} \quad \hat{\mathbf{u}}_{\mathbf{f}} = 0 \quad \text{on} \ \Gamma_{ext} \tag{2.2.106}$$

and causes that fluid mesh is moved in a Lagrangian manner at fluid-solid interface.

Finally, initial conditions concern solid quantities, fluid quantities and displacement of the referential coordinate system and they are defined as:

$$\begin{gathered} \rho_{\mathbf{S}}(0) = \widetilde{\rho}_{\mathbf{S}}, \quad \mathbf{v}_{\mathbf{S}}(0) = 0, \quad T_{\mathbf{S}}(0) = \widetilde{T}_{\mathbf{S}} \\ \rho_{\mathbf{f}}(0) = \widetilde{\rho}_{\mathbf{f}}, \quad \mathbf{v}_{\mathbf{f}}(0) = 0, \quad T_{\mathbf{f}}(0) = \widetilde{T}_{\mathbf{f}} \\ \hat{\mathbf{u}}_{\mathbf{f}}(0) = \widetilde{\mathbf{u}}_{\mathbf{f}} \end{gathered} \tag{2.2.107}$$

The basic disadvantage of the ALE approach is that initial topology of the system has to be preserved, i.e., the fluid region can not disappear or split into several separate regions. For the same reason handling contact between two solid bodies is difficult due to permanent presence of fluid layer between two approaching solid bodies. Other drawback of ALE approach is that large deformation of the solid body may cause strong distortion of the referential coordinate system (and corresponding computational mesh). This may cause inaccuracies in the numerical solution and re-meshing of the fluid domain may be required.

Resulting system of nonlinear partial differential equations is fairly complicated and obtaining numerical solution may be challenging, especially for complex geometries. Such a complicated model is not required for most structures considered in further parts of the thesis. However, the above general and precise model constitutes a good basis for deriving simplified models based on numerous assumptions concerning solid and fluid.

Fixed grid methods:

In contrast to the approach presented above, in methods belonging to the class of 'fix (background) grid methods' (also called non-boundary-fitting methods) the solid body is immersed in stationary fluid domain.

Historically, the first method utilizing 'fixed background grid' was 'Immersed Boundary Method' proposed by Peskin [185]. In IBM the set of solid boundary points connected by elastic law was immersed in fluid domain described by finite difference grid.

The interaction between fluid and solid was performed by applying additional forces to the fluid at the location of solid points which introduces coupling locally at a given point. The proposed methodology was further developed as 'Extended Immersed Boundary Method, EIBM', which utilizes finite element grid for solid and finite difference grid for a fluid [186] and as 'Immersed Finite Element Method, IFEM', which utilizes finite elements for both fluid and solid [187]. In both above methods deformation of the structure is calculated by interpolating fluid forces into the Lagrangian solid nodes. Further, computed elastic forces from solid body are transferred back to the fluid and, as a result, fluid momentum equation contains additional force terms caused by coupling with solid.

In method called 'Distributed Lagrange Multiplier / Fictitious Domain (DLM/FD)' coupling between fluid and rigid body is performed by using distributed Lagrange multipliers at the fluid-solid interface in the weak (integral) form of the governing equations [188]. Moreover, the 'Immersed Continuum Method' [189] is aimed at handling problems which involve coupling of compressible solid body and compressible fluid. Apart from the above classical fixed grid approaches, application of combined Chimera-like algorithms and XFEM-based approaches for solving FSI problems defined on fixed grids was proposed [190 191].

In considered herein 'fixed grid method' balance equations for solid and fluid part of the problem are formulated in classical Lagrangian and Eulerian approaches, respectively. Equations describing the solid part of general FSI problem in Lagrange description take the following form, cf. Sect. 2.2.1:

$$\frac{D}{Dt}(\rho_{\mathbf{S}} J) = 0 \qquad \text{in } \Omega_S \tag{2.2.108}$$

$$\rho_{\mathbf{S}} J \frac{D\mathbf{v}_{\mathbf{S}}}{Dt} = \nabla_{\mathbf{X}} \cdot (J\boldsymbol{\sigma}_{\mathbf{S}}{}^{\mathrm{T}}\mathbf{F}^{-\mathrm{T}}) + \rho_{\mathbf{S}} J\mathbf{f} \tag{2.2.109}$$

$$\rho_{\mathbf{S}} J \frac{DE_S}{Dt} = -\nabla_{\mathbf{X}} \cdot (J\mathbf{q}_{\mathbf{S}}\mathbf{F}^{-\mathrm{T}}) + \nabla_{\mathbf{X}} \cdot (J(\boldsymbol{\sigma}_{\mathbf{S}}\mathbf{v}_{\mathbf{S}})\mathbf{F}^{-\mathrm{T}}) + \rho_{\mathbf{S}} J\mathbf{f} \cdot \mathbf{v}_{\mathbf{S}} + \rho_{\mathbf{S}} Jh \tag{2.2.110}$$

The conservation equations describing fluid part of the problem in the Eulerian frame of reference read:

$$\frac{\partial \rho_f}{\partial t} + \nabla \rho_f \cdot \mathbf{v}_{\mathbf{f}} = -\rho_f (\nabla \cdot \mathbf{v}_{\mathbf{f}}) \qquad \text{in } \Omega_f \tag{2.2.111}$$

$$\rho_F \frac{\partial \mathbf{v}_{\mathbf{f}}}{\partial t} + \rho_f (\nabla \mathbf{v}_{\mathbf{f}})\mathbf{v}_{\mathbf{f}} = \nabla \cdot \boldsymbol{\sigma}_{\mathbf{f}}{}^{\mathrm{T}} + \rho_f \mathbf{f} \tag{2.2.112}$$

$$\rho_f \frac{\partial E_f}{\partial t} + \rho_f \nabla E_f \cdot \mathbf{v}_f = -\nabla \cdot \mathbf{q}_{\mathbf{f}} + \nabla \cdot (\boldsymbol{\sigma}_{\mathbf{f}} \mathbf{v}_{\mathbf{f}}) + \rho_f \mathbf{f} \cdot \mathbf{v}_{\mathbf{f}} + \rho_f h \tag{2.2.113}$$

Due to the form of governing equations the method is also called 'Coupled Lagrangian-Eulerian approach'. Boundary, coupling and initial conditions for solid domain and fluid domain are defined in a similar way as in case of ALE approach.

Most of the fixed grid methods utilise, in some extend, the Volume of Fluid (VOF) method [192] which handles problems where only part of Eulerian region is physically

occupied by fluid. The Volume of Fluid method is used for tracking change of fluid-solid interface during solid movement and deformation. The basic quantity in the VOF method in a scalar fraction function $C \in \langle 0,1 \rangle$ which is defined as an integral of fluid characteristic value inside a control volume and describes presence of the fluid in certain region. The equation governing the fraction function reads:

$$\frac{\partial C}{\partial t} + \nabla C \cdot \mathbf{v}_f = 0 \tag{2.2.114}$$

The geometrical compatibility between fluid and solid region is provided not only by the VOF method, but also by kinematic coupling conditions defined at fluid-solid interface which take into account relative motion of fluid and solid.

Basic drawback of the 'fixed grid method' is reduced accuracy at the vicinity of the fluid-solid interface caused by interpolation errors. Accordingly, the discretisation of the fluid domain has to be relatively dense in order to avoid 'leakages' of the fluid into or across solid body (the latter case may occur when thin solid elements or membrane elements are used). The problem could be partially avoided by adaptive remeshing of the Eulerian mesh located at the vicinity of the interface during the numerical analysis.

On the other hand, 'fixed grid' approach is well suited for modelling systems subjected to large deformations and topology changes due to application of Volume of Fluid method. In particular, the impact process does not have to be modelled in a simplified way by application of Neumann boundary condition but it can be formulated as a contact problem. In this case impacting object is modelled as additional solid or rigid body (defined by shape, mass and moments of inertia) moving towards inflatable structure with prescribed initial velocity, Fig. 2.6. When hitting object approaches inflatable structure, part of fluid-solid interface can be changed into contact region where coupling conditions between inflatable structure and impacting object can be formulated. In general, these coupling conditions may concern both mechanical and thermal part of the problem. Mechanical contact conditions can be formulated in a classical way by using penalty function or Lagrange multipliers.

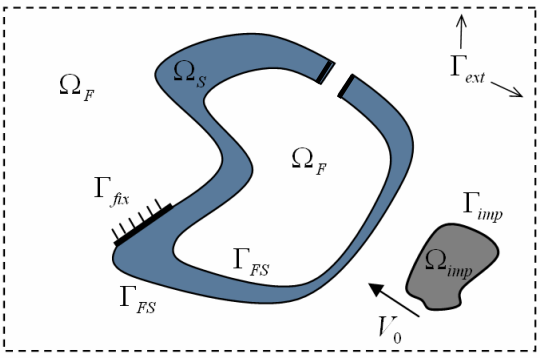

Fig. 2.6 FSI model of passive inflatable structure with impact modelled as a contact problem

Beside 'conforming boundary methods' and 'fixed grid methods', in some special cases uniform description of the whole considered domain can be applied, i.e.:

1. Lagrangian description of both fluid and solid domain
2. Eulerian description of both fluid and solid domain.

Lagrangian method

In this method the Lagrangian approach is used for description of kinematics of both solid and fluid. As it was previously discussed, in Lagrangian approach a given set of particles has to be observed during the whole period of analysis. Therefore, the Lagrangian method is well suited only for modelling of inflatable structure which constitutes a closed system (i.e. does not contain any inflator or valve) and all fluid particles remain inside solid compartment during the entire analysis. From mathematical point of view the Lagrangian approach can be applied for problems where the only conditions applied at external boundary of the fluid region are classical coupling conditions with the solid body, while typical inlet and outlet boundary conditions does not occur. In described systems the mixing of the gas is not as intensive as in systems with inlet and outlet and, as a consequence, motion of all particles can be followed by the Lagrangain mesh.

The disadvantage of purely Lagrangian approach is that the fluid mechanics problem for which the most common and intuitive approach is Eulerian one, has to be solved in Lagrangian manner. Moreover, most fluid mechanics codes use Eulerian description of fluid kinematics not the Lagrangian one. However, a clear advantage of the approach is using only one, well-established kinematical description for the whole FSI problem.

Eulerian method

In Eulerian method both fluid and solid are considered in Eulerian frame of reference. In this approach there are no separate meshes for the solid and fluid domain but there is a single stationary mesh occupied partially by fluid and solid. When solid body is moving or deforming, the particular regions of the Eulerian domain change from solid regions to fluid regions and vice versa.

Eulerian method does not involve limitations of allowable change of system topology, as it occurs in the Lagrangian method. However, a major disadvantage of the method is the necessity of solving solid mechanics problem in Eulerian frame of reference, while the typical approach is the Lagrangian one. Moreover, discretisation of the domain has to be fine enough to precisely handle change of shape of fluid and solid body. The typical example of application of Eulerian method is deformation of a cantilever beam immersed in incompressible fluid, cf. Ref. [193 194].

Numerical methods for simulation of inflatable structures

Two main methods used to obtain numerical solutions of FSI problems are the so-called [195 196]:

- monolithic approach and
- partitioned approach.

In monolithic approach [197 198] the whole system of equations is discretised and solved simultaneously by using single numerical code. The advantage of this method is that interface between fluid and solid is included into the numerical procedure in natural way and it does not require any separate treatment. However, the strong disadvantage of the monolithic approach is that the same solver has to be used for both fluid and solid part of the problem

where equations of a different type are defined. Therefore, the choice of the numerical method has to be a compromise between optimal performance in fluid and solid domains. In monolithic approach classical Newton-Raphson method is used, as well as space-time techniques as proposed in [199].

On the contrary, partitioned approach [200 201] assumes application of two distinct solvers for solid and fluid part of the problem. Solid mechanics is solved by using CSM software typically based on Finite Element Method and fluid mechanics is solved by CFD software typically based on Finite Volume Method or more rarely on Finite Difference Method. The main advantage of the partitioned approach is application of specialised solvers, optimally suited for two problems of a different nature. On the other hand, a strong disadvantage of the partitioned approach is the requirement of introducing additional numerical procedure for handling coupling conditions between fluid and solid domains. Such an additional procedure includes exchange of data between two solvers and obtaining convergent solution at the interface. The coupling procedures can be divided, in general, into weak and strong. In weak coupling procedures the condition of equilibrium of the solid-fluid interface is not exactly fulfilled at every single time step of the numerical solution (similarly as in explicit methods of integration). Such methods are typically applied in problems involving small structural displacements such as aeroelasticity [202]. On a contrary, strong coupling is required in problems with large deformation and strong interaction involving both displacements and forces at the interface. Strong coupling of the partitioned solvers can be achieved by using both conforming boundary and fixed grid methods.

From the numerical point of view the coupling can be treated as a root finding problem or fixed point problem. Therefore, both Newton-Raphson methods and fixed point (Gauss-Seidel) iterations can be used for obtaining numerical solution. Strong coupling of partitioned solvers is usually achieved by using exact or approximate Jacobians, however both approaches require using open (not black-box) fluid and solid solvers [201 203 204]. Other methods utilize reduced model of fluid and solid problems which is based on information collected during coupling iterations and sensitivity analysis techniques [205]. Fixed point iterations require using iteratively staggered coupling algorithms in which fluid and solid problems are solved until the convergence is reached. In case of slow convergence the methods of problem relaxation (as steepest descent relaxation or Aitken method) are used to facilitate obtaining solution [206].

2.2.3 Adaptive Inflatable Structure with controllable valve

Adaptive Inflatable Structure, being the main subject of this thesis, differs from the passive inflatable structure described in Sec. 2.2.2 in two aspects:

- at first, it contains an controllable inflator which serves for inflating the structure to appropriate initial pressure
- at second, it contains controllable valve that enables controlled outflow of the fluid during the impact process

In general, inflation can be executed by external compressor or by deflagration of pyrotechnic material. However, in this section it will be assumed that inflatable structure is preliminarily

inflated to appropriate initial pressure and we will concentrate on adaptation performed during impact by controlled gas release. Consequently, the attention will be focused on possibilities of modelling of the controllable valve.

Model 1 (boundary condition control)

The simplest model of Adaptive Inflatable Structure is based on a fundamental model of a passive inflatable structure which consists of external solid wall and fluid region enclosed inside, which was introduced in Fig. 2.3. Similarly like in case of passive inflatable structure external fluid is not modelled due to assumed small influence on overall response of inflatable structure. Both solid body and internal fluid are described by previously derived conservation laws (e.g. Eq.2.2.96-2.2.102) complemented by constitutive relations, internal energy definition, ideal gas law and Fourier's law of heat conduction. Moreover, initial, boundary and coupling conditions between fluid and solid body has to be defined.

An additional element of the introduced numerical model of Adaptive Inflatable Structure is a controllable valve, modelled here as additional boundary condition for the fluid. In proposed model the common boundary of fluid and solid region Γ consists of two parts: the part Γ_{FS} which constitutes typical fluid-solid interface and the part Γ_V which constitutes the valve: $\Gamma = \Gamma_{FS} + \Gamma_V$, see Fig. 2.7.

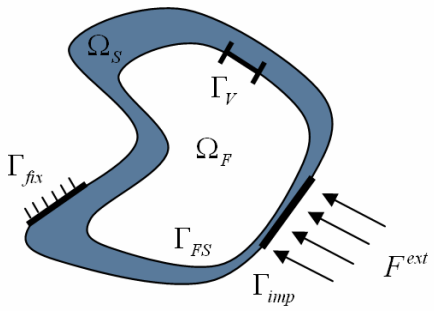

Fig. 2.7. FSI model of Adaptive Inflatable Structure with controllable valve modelled by additional boundary condition for the fluid

At fluid-solid interface Γ_{FS} typical coupling conditions concerning solid and fluid velocities, stresses, heat flux and temperature are defined:

$$\boldsymbol{\sigma}_{\mathbf{S}}\mathbf{n} = \boldsymbol{\sigma}_{\mathbf{f}}\mathbf{n} \quad \text{and} \quad \mathbf{v}_{\mathbf{f}} = \mathbf{v}_{\mathbf{S}} \quad \text{on} \quad \Gamma_{FS} \tag{2.2.115a}$$

$$T_S = T_f \quad \text{and} \quad \mathbf{q}_{\mathbf{S}} \cdot \mathbf{n} = \mathbf{q}_{\mathbf{f}} \cdot \mathbf{n} \quad \text{on} \quad \Gamma_{FS} \tag{2.2.115b}$$

At the part of the boundary Γ_V, which is relatively small in comparison to the whole interface and which models in an approximate way an open valve, boundary conditions for both fluid and solid domain have to be formulated. Boundary conditions for the fluid define either external environment of the inflatable structure (external pressure) or they directly define conditions of the fluid outflow (outflow velocity or mass flow rate of gas):

$$\boldsymbol{\sigma}_{\mathbf{f}}\mathbf{n} = -\tilde{p}\mathbf{n} \quad \text{or} \quad \mathbf{v}_{\mathbf{f}} = \tilde{\mathbf{v}}_{\mathbf{f}} \quad \text{or} \quad \dot{m} = \tilde{q}_V \quad \text{on } \Gamma_V \tag{2.2.116}$$

$$T_{\mathbf{f}} = \tilde{T}_{\mathbf{f}} \quad \text{on } \Gamma_V \text{ (for the 'opening' b.c. only)}$$

Boundary conditions imposed on the solid body at the location of the valve are in a way artificial (since presence of the solid body in considered region is also artificial) and they can be defined as extrapolation of coupling conditions imposed at the other parts of the boundary Γ_{FS}. These conditions, however, do not significantly influence global response of the solid body due to small area of the valve region and, typically applied, large stiffness of the material located in the adjacent solid region. For the latter reason dimensions of the 'valve' part of the boundary (Γ_V) do not change during deformation of the inflatable structure which occurs under action of external loading.

The main idea behind the proposed theoretical model of Adaptive Inflatable Structure is that introduced fluid boundary condition can be controlled during the analysis. In general, division into the 'fluid-solid interface' and 'valve' part of the boundary, as well as value of imposed boundary conditions (2.2.116) can be arbitrarily changed. Therefore, control of the gas flow can be performed in three manners:

1. by applying on/off control, i.e. changing boundary conditions imposed at Γ_V from 'valve' conditions (2.2.116) to 'fluid-solid interface' conditions (2.2.115),
2. by changing value of fluid boundary condition imposed at Γ_V (change of external pressure; velocity or mass flow rate of fluid at outlet),
3. by changing size of the outlet (length/ area of Γ_V) during the numerical analysis.

Application of on/off control strategy introduces harsh discontinuities in the global numerical solution and therefore, some kind of smoothing procedure has to be applied, e.g. boundary condition has to be changed from the 'fsi-type' to 'valve-type' in a continuous way. The second of the above options (change of fluid boundary condition value) will be applied for control of piston deceleration in adaptive pneumatic cylinder (cf. Chapter 4).

Model 2 (orifice width control)

More precise FSI model of Adaptive Inflatable Structure is based on the model of passive inflatable structure introduced in Fig. 2.4. The model is composed of almost-closed solid domain Ω_S and located inside fluid domain Ω_F, cf. Fig 2.8. The model is, in general, described by equations (2.2.96 - 2.2.102) or (2.2.108 - 2.2.113) depending on a kinematical approach which is applied. Moreover, typical initial and boundary conditions for fluid and solid domain have to be assumed and coupling conditions on the fluid-solid interface Γ_{FS} have to be formulated.

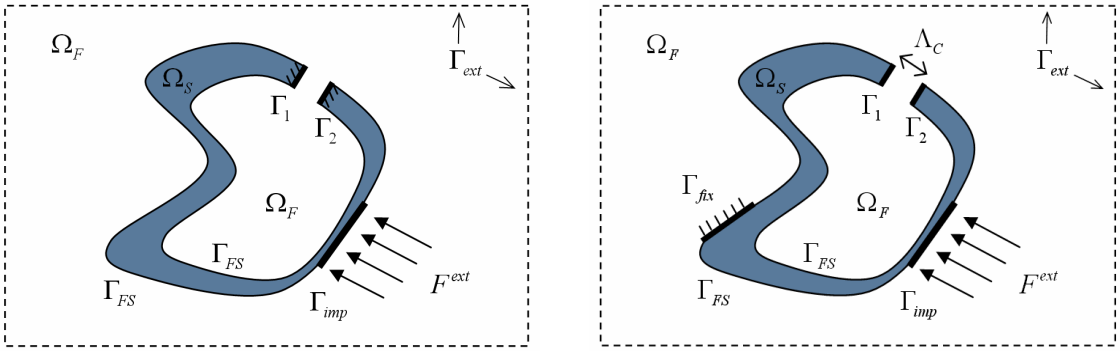

Fig. 2.8. FSI model of Adaptive Inflatable Structure with controllable orifice

Two cases of the Adaptive Inflatable Structure have to be considered separately: when the orifice is fixed in space (Fig. 2.8a) and when the orifice can move freely inside fluid domain (Fig. 2.8b). In the first case, size of the orifice and therefore conditions of the gas outflow can be changed by imposing arbitrary displacement of the fixed parts of the boundary $\Gamma_1(t)$ or $\Gamma_2(t)$. In case of three-dimensional systems boundary of the orifice constitutes a single surface and therefore location of a single boundary has to be altered. Both in case of two and three-dimensional model, the disadvantage of the method is that altering of the orifice width introduces additional, non-physical stresses into the solid body.

In case when the orifice is not fixed in space, displacement of its boundaries can not be directly prescribed since movement of the whole inflatable structure is not known a priori. Therefore, an additional function Λ_C defining actual shape of the orifice (or mutual location of its edges in two dimensional case) has to be introduced and modified during the analysis to control conditions of gas exhaust. Change of the orifice width will be used as alternative option for controlling deceleration of the piston in pneumatic cylinder (cf. Chapter 4).

Model 3 (valve head control)

Another model of Adaptive Inflatable Structure contains more sophisticated model of the valve composed of two elements: an orifice of a constant width and a controllable valve head. In comparison to previously considered model (Fig. 2.8), an additional element is a control region Ω_C with the boundary Γ_C which models the valve head. The control region can be located inside or outside inflatable structure or inside the orifice. The only requirement for the control region Ω_C is that it should be fully surrounded by the fluid domain and that it influences the flow of the gas through the orifice.

Let us initially consider the situation when edges of the orifice are fixed in space, see Fig. 2.9. In such a case, formulation of the mathematical model is easier since fixed position of the control region corresponds to constant opening of the valve. The control region itself can be modelled in two manners:

- as an internal void (region not filled with fluid or solid) located inside fluid domain,
- as an additional solid domain made of functional material.

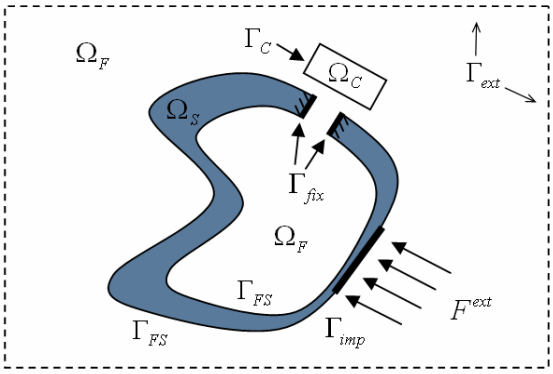

Fig. 2.9. FSI model of Adaptive Inflatable Structure with orifice fixed in space and controllable valve head

When Ω_C is modelled as internal void its contribution to mathematical model is modification of shape of the fluid domain and introduction of additional boundary conditions on fluid

velocity at the boundary Γ_C. If region Ω_C remains fixed the conditions of the fluid flow remain unaltered. Control of the valve relies on direct change of location or shape of the void region Ω_C by modifying shape of its boundary Γ_C, which locally modifies shape of the fluid domain and conditions of the fluid flow. The method based on change of position of the void region will be applied for the control of the mass flow rate through the piezoelectric valve and control of the membrane valve in Chapter 7.

Alternatively, the control region Ω_C can be modelled as a solid domain composed of functional material (such as piezoelectric or magneto-strictive material) which allows to control its actual shape or location. Presence of the additional control domain substantially complicates mathematical model of Adaptive Inflatable Structure. In general, equilibrium equations formulated inside control domain couple applied external excitation (such as electric field) with state of deformation and stress inside a control domain. The coupling conditions between control domain and fluid domain are formulated in the same way as between solid and fluid domains. As a result, applied external excitation allows to govern deformation of the solid domain Ω_C and to control flow of the fluid and pressure inside inflatable structure. Simplified version of the method will be used for controlling closing of the membrane valve in Chapter 7.

In case when the orifice is not fixed (Fig. 2.10a), it moves inside fluid domain due to global deformation of the inflatable structure. Accordingly, fixed position of the valve head does not provide constant valve opening. Therefore, an additional initial task is to provide constant position of the valve relative to orifice in case when no control is applied. When control region is modelled as internal void, the above task can be attained by introduction of additional procedure which provides rigid motions of the valve head corresponding to change of position of the orifice (Fig. 2.10a). In the second case, when control region is modelled as an additional solid domain, it may be attached to the solid region adjacent to the orifice (Fig. 2.10b). Moreover, appropriately large stiffness of both the valve head and the region in the vicinity of the orifice has to be provided to couple displacement of the orifice with displacement of the valve head.

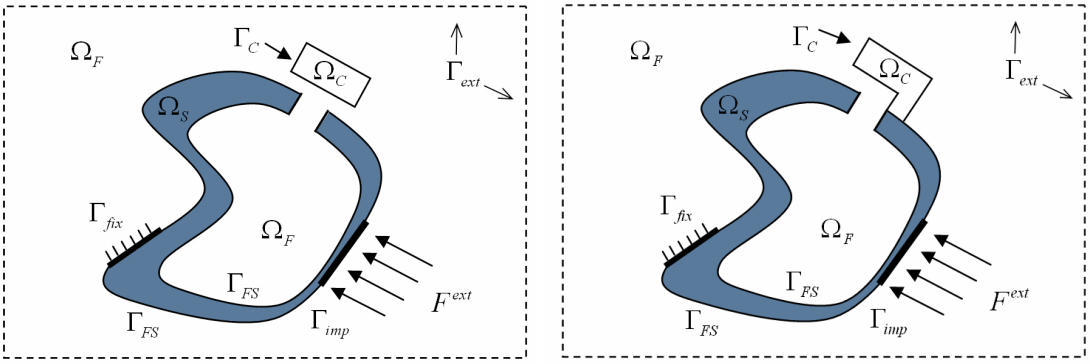

Fig. 2.10. FSI model of Adaptive Inflatable Structure with moving orifice: a) valve head modelled as internal void in fluid domain, b) valve head modelled as an additional solid domain

The above models of Adaptive Inflatable Structures with controllable valve are based on a models of passive inflatable structures described in Sec. (2.2.2) and thus they are based on a full system of conservation equations for both solid and fluid part of the problem. However, considering such complicated model involving laws of conservation of mass,

momentum and energy is not required for all types of Adaptive Inflatable Structures and numerous simplifying assumptions can be introduced.

Possible simplifications of FSI model of Adaptive Inflatable Structure include:

1. Assumption of the incompressibility of the solid body. Solid incompressibility will often directly result from the assumed constitutive relation (elastic deformations typically cause small changes in volume and standard models of plasticity are volume-preserving). Consequently, the continuity equation does not have to be considered.
2. Decoupling of mechanical and thermal equations of the solid body. When constitutive relation for the solid does not involve temperature dependence mechanical and thermal equations within solid domain are not directly coupled. Nevertheless, both equations are still coupled with each other by the boundary terms at the interface with the fluid.
3. Assumption of the inviscid flow of gas. For relatively high Reynolds numbers (high ratio of inertial to viscous terms in Navier-Stokes equations) the viscous forces can be totally neglected. In such a case, the second N-S equation reduces to Euler equation with variable density. The assumption of inviscid flow can also be applied for the flows with high Mach numbers regardless on the Reynolds number value [207].
4. Neglecting heat transfer inside fluid domain. This assumption is often considered simultaneously with the previous one since the same molecular mechanism is responsible for viscosity and heat transfer. When both these quantities are neglected the third Navier Stokes equation (energy conservation) is reduced to a simple form:

$$\frac{D}{Dt}\left(\ln\frac{p}{\rho^{\kappa}}\right)=0 \tag{2.2.117}$$

   which indicates that isentropic conditions are fulfilled along the streamlines. Consequently, corresponding boundary conditions are simplified.
5. Assumption of incompressible flow of the gas. Despite the fact that the gas that fills the inflatable structure is a highly compressible medium, the flow of gas with low Mach number can be treated as incompressible. The assumption of incompressibility can be applied only for the analysis of the gas flow in the valve region, but not for the whole inflatable structure which is being strongly compressed. When assumption of incompressibility is applied, equations of fluid continuity and momentum conservation are decoupled from the energy equation.
6. Simplification to acoustic equations [208]. Finally, when the assumption of small pressure variation together with the assumptions of incompressibility and constant temperature is applied, the Navier-Stokes equations can be simplified to Lighthill equation frequently used in acoustics. The next step of simplification is a reduction to Burger's equation and finally to wave equation.

2.3 Uniform Pressure Method

Despite a huge variety of introduced FSI-based models and their possible simplifications, the approach based on coupling of partial differential equation describing the conservation laws

remains complex and obtaining numerical solution may be difficult or time consuming. On the other hand, in the considered problems of impact absorption, fluid part of the analysis is used to compute global forces acting on the walls of inflatable structure and the exact space variation of fluid velocity in particular parts of the structure is often not of primary interest. Moreover, the impacting object velocity is usually much lower than speed of propagation of pressure impulse so it is expected that pressure distribution becomes uniform relatively fast in comparison to total duration of impact process.

According to the above discussion, a convenient model of inflatable structure may be obtained by applying the so-called Uniform Pressure Method (UPM) which assumes that gas is uniformly distributed inside each chamber [209 210], i.e.:

$$p(x,y,z,t) = p(t),\ \ \rho(x,y,z,t) = \rho(t),\ \ T(x,y,z,t) = T(t) \tag{2.3.1}$$

and consequently, that walls of the chambers are subjected to uniform pressure. The straightforward consequence of this assumption is that the quantity defining velocity of the fluid in each point of the fluid region is no longer defined. Accordingly, the influence of the fluid viscosity on the internal fluid stresses is neglected and fluid stress tensor is composed of spherical part only. However, fluid viscosity can be taken into account in the analytic equations describing flow of the gas between the chambers.

The conditions restricting application of UPM should be defined basing on relaxation time (i.e. time period when space variation of considered quantity drops below an arbitrary threshold) [211] which depends, in general, on both conduction and convection - based phenomena. Convection processes depend, however, on medium velocity which is not known a priori as being one of the main unknowns in Navier-Stokes equations. Nevertheless, an attempt of rough estimation of pressure and temperature relaxation times will be conducted.

Assessment of pressure relaxation time t_R^p will be based on time of propagation of infinitesimal pressure impulse Δt^p which is defined as:

$$\Delta t^p = \frac{h_0}{\sqrt{\kappa R T}} \tag{2.3.2}$$

and for approximate chamber length $h_0 = 1m$ and range of temperatures T=273-400K equals 2.5-3ms. Therefore, pressure relaxation time t_R^p which depends on time Δt^p, overall damping of the medium and wave interference effects is expected to be in the range of several up to a dozen milliseconds.

The above method can not be applied for the temperature since classical conductive heat transfer is described by parabolic equation in which the speed of impulse propagation is infinite. On the other hand, considering one dimensional problem in which the temperature is applied at one of the boundaries:

$$\frac{\partial T}{\partial t} = k\frac{\partial^2 T}{\partial x^2},\quad T(0,t) = \widetilde{T},\quad \frac{\partial T}{\partial x}(h_0,t) = 0,\quad \text{IC}: T(x,0) = T_0 \tag{2.3.3a}$$

and calculating time when temperature at the opposite boundary achieves the value of imposed temperature with assumed accuracy (for instance of 5%):

$$t_R^T = t \quad \text{such} \quad \text{that} \quad T(h_0,t) = T_0 + 0.95(\widetilde{T} - T_0) \tag{2.3.3b}$$

leads to the result in the range of dozens of seconds due to low thermal conductivity of gas. However, the above situation concerns equalisation of the temperature when the fluid remains immobile. In real situation, the temperature equalisation strongly depends on convective processes as mixing of the fluid within a single chamber. In considered situation, when transfer of the fluid between the chambers occurs, the mixing of the fluid is expected to be intensive and therefore the assumption of temperature uniformity can roughly considered as justified.

According to above argumentation, the Uniform Pressure Method can be used as an approximate tool for modelling inflatable structures subjected to impact loads of moderate velocities, however, the results should be considered deliberately. The UPM-based approach will be applied when the impact time is substantially longer than estimated time of pressure relaxation i.e. when the impact lasts for at least 30-50 ms. The method will be used for modelling selected cases of impacts against adaptive pneumatic cylinders, inflatable road barriers and adaptive airbags after the inflation stage.

Model formulation

The UPM-based model of adaptive inflatable structure is much easier to formulate and solve due to the fact that separate kinematic description of solid and fluid is not required. The whole inflatable structure can be modelled in Lagrangian frame of reference since partial differential equations are formulated exclusively for the solid body (cf. Fig. 2.11).

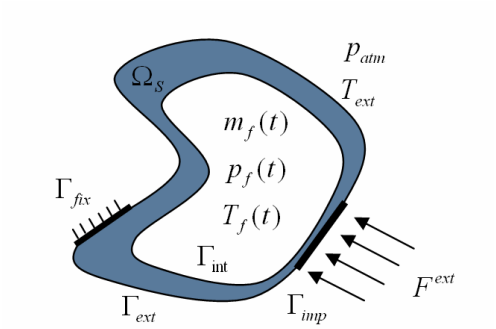

Fig. 2.11. 'Uniform Pressure Method' – based model of Adaptive Inflatable Structure

In a classical problem of structural mechanics, in case when the material properties are independent of temperature, the continuity and momentum equations constitute a closed system and they can be solved independently from the energy equation. This is, however, not the case in coupled system based on Uniform Pressure Method since actual temperature of solid body is required to compute heat flux between fluid and solid which influences gas temperature, its pressure and, in effect, forces exerted on solid and its deformation. Equations governing response of solid part of inflatable structure are exactly the same as in case of FSI-based model derived in Sec.2.2 (they are recalled here for the sake of the model completeness):

$$\frac{D}{Dt}(\rho_S J) = 0 \qquad \text{in } \Omega_S \tag{2.3.4}$$

$$\frac{D}{Dt}(\rho_S J \mathbf{v_S}) = Div(J\boldsymbol{\sigma}_\mathbf{S}{}^{\mathbf{T}}\mathbf{F}^{-\mathbf{T}}) + \rho_S J\mathbf{f} \tag{2.3.5}$$

$$\frac{D}{Dt}(\rho_S J E_S) = -\mathrm{Div}(J\mathbf{q_S}\mathbf{F}^{-\mathrm{T}}) + \mathrm{Div}(J\boldsymbol{\sigma}_S\mathbf{F}^{-\mathrm{T}}\mathbf{v_S}) + \rho_S J\mathbf{f}\cdot\mathbf{v_S} + \rho_S J h \tag{2.3.6}$$

Fluid part of the system is described by ordinary differential equation governing change of internal gas energy (the first law of thermodynamics for an open system), ordinary differential equation defining outflow and inflow of the gas (the flow equation) and algebraic relation between fluid parameters (ideal gas law). The first law of thermodynamics can be derived from the corresponding partial differential equation governing energy balance (e.g. Eq. 2.2.113) by performing integration over gas volume. This equation couples heat transferred to the gas dQ, enthalpy of the gas added to (removed from) the system $dm_{in}\overline{H}_{in}$ ($dm_{out}\overline{H}_{out}$), change of gas internal energy $d(m\overline{U})$ and the work done by gas dW [212 213 214]:

$$\frac{dQ}{dt} + \sum\frac{dm_{in}}{dt}\overline{H}_{in} - \sum\frac{dm_{out}}{dt}\overline{H}_{out} = \frac{d(m\overline{U})}{dt} + \frac{dW}{dt} \qquad \text{in } \Omega_f \tag{2.3.7}$$

Specific enthalpy of the gas added and removed from the system is defined as:

$$\overline{H}_{in}(t) = c_p T_{in}(t)\,; \qquad \overline{H}_{out}(t) = c_p T_f(t) \tag{2.3.8}$$

while specific gas energy and work done by gas reads:

$$\overline{U}(t) = c_V T_f\,, \quad dW = pdV \tag{2.3.9}$$

The ideal gas law is now applied for the whole volume of fluid occupying each cavity (not for certain point in space as in FSI model). Therefore, four parameters defining fluid cavity are not independent but connected by analytical formula:

$$pV = mRT \tag{2.3.10}$$

Absolute pressure p is defined as $p = \tilde{p} + p_A$ where $\tilde{p}$ is a gauge pressure and p_A is an ambient pressure, the absolute temperature is defined as $T = \tilde{T} - T_Z$ where $\tilde{T}$ is current temperature on the Celsius scale and T_Z is absolute zero temperature. Moreover, the equation governing gas inflow and outflow will be temporarily omitted and it will be assumed that change of mass of the gas inside inflatable structure is arbitrarily defined.

The conditions which couple solid region described by partial differential equations and fluid region described by ordinary differential equation concern both mechanical and thermal part of the problem:

$$\boldsymbol{\sigma}_\mathbf{S}\mathbf{n} = -p\mathbf{n} \ \text{ on } \ \Gamma_{\text{int}} \quad \text{and} \quad V = \int d\Omega_f \tag{2.3.11}$$

$$T_S = T_f \ \text{ on } \ \Gamma_{\text{int}} \quad \text{and} \quad \int(\mathbf{q_S}\cdot\mathbf{n})\mathrm{d}\Gamma_{\text{int}} = \dot{Q} \tag{2.3.12}$$

or

$$-\mathbf{q_S}\cdot\mathbf{n} = h(T_f - T_S) \quad \text{and} \quad \int(\mathbf{q_S}\cdot\mathbf{n})d\Gamma_{\text{int}} = \dot{Q} \quad \text{on } \ \Gamma_{\text{int}}$$

The first mechanical coupling condition provides that gas pressure is applied as an external loading to the solid body (it is imposed as Neumann b.c.). Displacement coupling condition is satisfied in an integral sense, i.e. total deformation of the interior boundary of the solid domain influences actual volume of the fluid cavity. The first option for defining thermal coupling condition assumes that only conductive heat transfer occurs and provides that

temperatures of fluid and solid are equal. In contrast, the second option of thermal boundary conditions assumes that only convective heat transfer occurs and provides that flux of heat to the solid depends on local temperature difference. In both cases, heat flux that occurs along the boundary of the solid body is integrated in order to compute total heat flux to the fluid. Concluding, the quantities that are transferred from fluid to solid body region are pressure and temperature (or in the second option heat flux) and quantities that are transferred, in integral sense, from solid body to the fluid are: total change of volume and total heat flux.

Boundary conditions for the solid body concern mechanical as well as thermal loads applied both at the external part of the solid body:

$$\mathbf{u_S} = \mathbf{0} \ \text{ on } \ \Gamma_{fix}, \quad \boldsymbol{\sigma_S}\mathbf{n} = -p\mathbf{n} \ \text{ on } \ \Gamma_{ext}, \quad \boldsymbol{\sigma_S}\mathbf{n} = \mathbf{F}^{ext} \ \text{ on } \ \Gamma_{imp} \tag{2.3.13}$$

$$T_S = T_{ext} \quad \text{or} \quad -\mathbf{q_S}\cdot\mathbf{n} = h(T_{ext} - T_S) \quad \text{on } \ \Gamma_{ext} \tag{2.3.14}$$

Finally, initial conditions for solid domain are the following:

$$\rho_S(0) = \widetilde{\rho}_S, \quad \mathbf{v_S}(0) = 0, \quad T_S(0) = \widetilde{T}_S \tag{2.3.15}$$

Initial conditions for the fluid are formulated by defining two out of three quantities appearing in ideal gas law, for instance, initial pressure and temperature $p(0) = p_0$, $T(0) = T_0$. Equations (2.3.4-2.3.15) formulate a closed system of equations and they completely describe impact subjected inflatable structure in case when mass of the fluid is constant or its change in time is arbitrarily defined.

An additional assumptions will be made in order to simplify system of partial differential equations governing the response of the solid body. The first assumption is that during deformation of the inflatable structure the density of solid does not change, which allows to neglect the continuity equation. The second simplification is superseding the energy conservation law by Newton's law of cooling (2.3.18) which governs transfer of heat to the fluid. Under the above assumptions system of equations describing inflatable structure reads:

$$\frac{D}{Dt}(\rho_S J\mathbf{v}) = \mathrm{Div}(J\boldsymbol{\sigma_S}^{\mathrm{T}}\mathbf{F}^{-\mathrm{T}}) + \rho_S J\mathbf{f} \qquad \text{in } \Omega_S \tag{2.3.16}$$

$$\dot{Q} + \sum \dot{m}_{in}\overline{H}_{in} - \sum \dot{m}_{out}\overline{H}_{out} = \dot{U} + \dot{W} \qquad \text{in } \Omega_f \tag{2.3.17}$$

and additionally:

$$\frac{dQ}{dt} = \lambda A(T_{ext} - T) \tag{2.3.18}$$

where λ is mean heat conductivity coefficient of the chamber walls and A is total area of the chamber walls through which heat transfer to the considered chamber occurs. The above system of equation has to be complemented with ideal gas law in the form (2.3.10). Boundary and coupling conditions concern only mechanical part of the problem and they are defined by equations (2.3.11) and (2.3.13), respectively. Finally initial conditions are formulated for solid velocity and two selected parameters of the fluid.

As a next step, several special cases of simplified energy balance will be considered. If the wall of the cavity is perfect insulator ($\lambda = 0$) or when the process is very fast, no heat

transfer through the chamber wall occurs ($dQ = 0$) and process can be treated as adiabatic. In case of adiabatic process with inflow of the gas to considered chamber (mass flow rate $\dot{m}$, temperature T_{in}) the energy balance (Eq. 2.3.17) can be written in three equivalent forms:

$$\frac{\dot{T}}{T} = \left(\frac{T_{in}}{T} - 1\right)\frac{\dot{m}}{m} + \left(1 - \frac{1}{\kappa}\right)\frac{\dot{p}}{p} \tag{2.3.19}$$

$$\frac{\dot{T}}{T} = \left(\kappa\frac{T_{in}}{T} - 1\right)\frac{\dot{m}}{m} - (\kappa - 1)\frac{\dot{V}}{V} \tag{a,b,c}$$

$$\frac{\dot{p}}{p} = \kappa\frac{\dot{m}RT_{in}(t)}{pV} - \kappa\frac{\dot{V}}{V}$$

In case of adiabatic process in which only outflow of the gas occurs differential equation (2.3.17) can be solved analytically to obtain:

$$\frac{T}{T_0} = \left(\frac{m_0}{V_0}\frac{V}{m}\right)^{1-\kappa}, \quad \frac{p}{p_0} = \left(\frac{m_0}{V_0}\frac{V}{m}\right)^{-\kappa}, \quad \frac{T}{T_0} = \left(\frac{p_0}{p}\right)^{\frac{1}{\kappa}-1} \tag{2.3.20}$$

(a,b,c)

where κ is an adiabatic exponent defined as ratio of constant pressure heat capacity c_p and constant volume heat capacity c_V and for the air $\kappa = 1.4$. Finally, when no flow of the gas occurs (i.e. mass of the gas in the cavity remains constant) we obtain well-known equations:

$$T = T_0\left(V/V_0\right)^{1-\kappa} \quad , \quad pV^{\kappa} = p_0V_0^{\kappa}. \tag{2.3.21}$$

Obviously, under the assumption of an isothermal process or arbitrarily defined change of temperature the temperature T is not an additional unknown of the problem and therefore equations (2.3.17-2.3.21) are not required to describe the response of the inflatable structure.

Hitherto, change of mass of the fluid inside inflatable structure was assumed to be arbitrarily defined. Since control of the gas migration and gas outflow is a key issue for inflatable structures operation it will be subjected to a more precise analysis. In general, change of fluid mass inside each chamber is described by equation:

$$m(t) = m_0 + \int_0^t q(\bar{t})d\bar{t} = m_0 + \int_0^t q_{in}(\bar{t}) - \int_0^t q_{out}(\bar{t}) \tag{2.3.22}$$

where q_{in} is the mass flow rate into the cavity, q_{out} is the mass flow rate outside the cavity and direction of the flow depends on the sign of pressure difference between the cavities. In general two types of fluid exchange will be modelled: inflation of the pneumatic structure which usually takes place before expected impact and controlled gas migration or release which is executed during collision.

Inflation of pneumatic structure will be described by two methods that are common in literature, by using tank test data and by using dual pressure method [215 216] . In the tank test method the particular inflator is discharged into closed fixed-volume tank and time history of pressure change inside the tank is measured. The inflator mass flow rate can be calculated from adiabatic energy balance by utilising measured inflator temperature and tank pressure according to the formula:

$$q(t) = \frac{\dot{p}_{\text{tank}} V_{\text{tank}}}{\kappa R (T_{\text{inflat.}} - T_Z)} \tag{2.3.23}$$

In dual pressure method calculation of mass flow rate is based on measurement of pressure inside inflator and pressure tank. Moreover, the assumption of isentropic flow between the inflator and tank is assumed, which leads to the alternative definition of mass flow rate of gas from the inflator:

$$q(t) = \frac{\kappa (CAC_{\text{tank}} p_{\text{inflat.}})^2}{\dot{p}_{\text{tank}} V_{\text{tank}}} \tag{2.3.24}$$

where C is a discharged coefficient, A is an orifice area and coefficient C_{tank} is determined by taking into account the assumption of chocked or sonic flow:

$$C_{\text{tank}} = \left(\frac{2}{\kappa + 1} \right)^{\frac{1}{\kappa - 1}} \sqrt{\frac{2\kappa}{\kappa + 1}} \tag{2.3.25}$$

Regarding gas migration and release, two main cases will be modelled: leakage of gas through pores of fabric which occurs for instance in automotive airbags and flow of the gas through controllable valves. Applied model of a fabric leakage assumes that mass flow rate of gas depends on two parameters: density of the gas inside airbag and pressure difference between and airbag and its environment [217]

$$|q(t)| = CA\sqrt{2\rho|\Delta p|} \tag{2.3.26}$$

where C is the discharge coefficient and A is the total area where the fabric leakage occurs.

Two fundamental models of the gas flow will be considered and applied in further modelling [218]. The most simplified model of the gas flow assumes that the mass flow rate of gas q is related to pressure difference Δp by the formula:

$$\Delta p(t) = C_V q(t) + C_H q(t)|q(t)| \tag{2.3.27}$$

where $\Delta p(t) = p(t) - p_{out}$; C_V and C_H are viscous and hydrodynamic resistance coefficients. Both these coefficients are assumed to depend on actual valve opening and they can be found experimentally for a particular type of valve. The Eq. 2.3.27 with constant values of coefficient C_V and C_H allow to model passive inflatable structure with constant valve opening. On a contrary, when the values of the resistance coefficients can be arbitrarily changed during the numerical analysis adaptive inflatable structure with controllable valve can be simulated.

Alternatively, flow of the gas through the orifice can be described by more precise Saint-Venant model [217] which assumes that flow is blocked at critical velocity. In a such case mass flow rate of gas is defined as:

$$|q(t)| = CA \frac{p_e}{\sqrt{R(T - T_Z)}} \sqrt{\frac{2\kappa}{\kappa - 1} \left(\left(\frac{p_{or}}{p_e} \right)^{\frac{2}{\kappa}} - \left(\frac{p_{or}}{p_e} \right)^{\frac{\kappa + 1}{\kappa}} \right)} \tag{2.3.28}$$

where C is the discharge coefficient, A is the orifice area, p_e is the absolute pressure in the upstream fluid cavity, p_{or} is the absolute pressure in the orifice defined as:

$$p_{or} = p_a \quad \text{if} \quad p_a \geq p_c \tag{2.3.29}$$
$$p_{or} = p_a \quad \text{if} \quad p_a < p_c$$

where p_a is equal to the ambient pressure or the downstream cavity pressure. The critical pressure p_c at which chocked or sonic flow occurs equals:

$$p_c = p_e \left(\frac{2}{\kappa + 1} \right)^{\frac{\kappa}{\kappa - 1}} \tag{2.3.30}$$

The conditions (2.3.29) indicate that when absolute pressure in the upstream cavity is adequately large the mass flow rate depends only on the parameters of the upstream cavity:

$$|q(t)| = CA \frac{p_e}{\sqrt{RT}} \left(\frac{2}{\kappa + 1} \right)^{\frac{1}{\kappa + 1}} \sqrt{\frac{2\kappa}{\kappa - 1}} \tag{2.3.31}$$

In case of model of the flow based on Saint-Venant formula, controllability of the valve is achieved by altering coefficient A indicating area of the orifice.

The above equations defining inflow / outflow of the fluid should be further incorporated into systems of equations (2.3.4 - 2.3.15) or alternatively (2.3.16 - 2.3.18). As a result, classical problem of solid mechanics is complemented with three additional equations, namely: fluid energy balance, ideal gas law and equation defining fluid exchange. Since three additional unknowns related to fluid are introduced (fluid mass, pressure and temperature), the above equations constitute a closed system which allows to compute response of impact subjected inflatable structure in case when valve opening is predefined.

Two additional quantities which are especially important for overall properties of the inflatable structure have to be defined: gas entropy and gas exergy. Entropy can be considered as a measure of reversibility of the thermodynamical process [219]. General relation between change of entropy S, heat transferred to the system dQ and submitted specific entropy s_i reads:

$$dS \geq \frac{dQ}{T} + \sum_i m_i ds_i \tag{2.3.32}$$

and the equality holds for the reversible process only. Moreover, in case of reversible process in which mass of the gas remains constant, entropy of the gas can be calculated as:

$$S = S_0 + mc_V \ln T + mR \ln V \quad \text{or} \quad S = S_0 + mc_p \ln T - mR \ln p \tag{2.3.33}$$

and it can be determined with respect to a reference value S_0. For adiabatic process the formula defining change of specific entropy s simplifies to the form:

$$s = s_0 + c_V \ln \left(\frac{p}{\rho^\kappa} \right) \tag{2.3.34}$$

and entropy remains constant. In case of inflatable structure where mass of the gas inside particular chambers is not constant the following definition of the entropy can be derived:

$$S = S_0 + mc_V \ln T + mR \ln \frac{V}{m} \tag{2.3.35}$$

The exergy of gas enclosed in a single pressure chamber will be defined as 'useful' part of gas internal energy, i.e. the energy which can be changed into mechanical work [220]. Exergy of certain volume of gas X^{gas} equals to work that can be done by gas during transition from 'actual state' $(\bar{t},\overline{V},\overline{T},\overline{m})$ to a 'referential state' in which mechanical energy of the impacting object is the largest $(t^{ref},V^{ref},T^{ref},\overline{m})$ in a process without intended dissipation, i.e. without dissipation caused by gas release. The value of exergy depends on change of internal gas energy ΔU_{act}^{ref} and transfer of heat ΔQ_{act}^{ref} during the process of transition between two considered states:

$$X^{gas} = W_{act}^{ref} = -\Delta U_{act}^{ref} + \Delta Q_{act}^{ref} \tag{2.3.36a}$$

By using ideal gas law and by performing integration by parts (cf. Eq. 3.1.25e) we obtain general definition of gas exergy:

$$X^{gas}(\bar{t}) = \int_{\overline{V}}^{V^{ref}} pdV = \int_{\bar{t}}^{t^{ref}} \overline{m}RT\frac{\dot{V}}{V}\,dt = \overline{m}R\overline{T}\ln\left(\frac{V^{ref}}{\overline{V}}\right) - \overline{m}R\int_{\bar{t}}^{t^{ref}} \dot{T}\ln\left(\frac{V}{V^{ref}}\right)dt \tag{2.3.36b}$$

The actual value of gas exergy defines maximal work that will be done by gas if gas release will not be further performed. The formula 2.3.36b can be specified to the case of adiabatic and isothermal system and expressed as simple formulae:

$$X^{gas} = \frac{\overline{m}R\overline{T}}{1-\kappa}\left(\left(\frac{V^{ref}}{\overline{V}}\right)^{1-\kappa} - 1\right), \qquad X^{gas} = \overline{m}RT_0\ln\left(\frac{V^{ref}}{\overline{V}}\right) \tag{2.3.36c}$$

The remaining part of the energy which can not be transferred into mechanical energy will be called an 'anergy'. During the process without release of gas the exergy is entirely converted into mechanical energy. In contrast, when gas is released from the pressure chamber to environment both exergy and anergy of the gas decrease.

The exergy can be defined not only for gas enclosed inside single chamber, but also for the entire inflatable structure. Definition of inflatable structure exergy depends on type of pneumatic system considered (cf. Ch. 3.1.1-3.1.3 concerning various types of pneumatic cylinders). Change of exergy of the inflatable structure is caused either by release of gas to environment or by transfer of gas between the chambers. Since in the latter case total internal energy of the gas enclosed inside chambers remains constant, it can not be used as a quantitative measure of impact energy dissipation. In contrast, tracking of changes of exergy during the process allows to calculate the amount of energy that will be transferred back to the impacting object and the amount of energy that was already dissipated by controlled transfer of gas between the chambers.

Multi-chamber systems

Previously considered theoretical model of inflatable structure (depicted in Fig. 2.11 and described by Eq. 2.3.4-2.3.36) was composed of a single air chamber. However, optimal reception of the various impact loadings requires design of more complex inflatable structures being multi-chamber systems and containing many controllable valves. Therefore, the following task is to derive matrix-based method describing dynamics of inflatable structure composed of finite number of air chambers and controllable valves located between them.

Let us consider system containing i chambers, k internal and external walls allowing for heat transfer between chambers and equipped with j valves serving for gas migration and outflow (mass and enthalpy exchange). Heat transfer occurs only between chambers of inflatable structure which are adjacent to each other. In contrast, flow of the gas may occur between arbitrarily selected chambers, i.e. arbitrary chambers may be connected by links equipped with valves. Therefore, in general, number of both connections is not equal: $j \neq k$.

Description of multi-chamber adaptive inflatable structure as a set of chambers and connections between them allows to define the whole system as oriented graph. Let us denote gas pressure, gas temperature, mass of the gas in a single chamber and chamber volume by vectors $\mathbf{p,T,m,V}$ with components p_i, T_i, m_i, V_i. Pressure and temperature vectors expanded by the component indicating external pressure and external temperature will be represented by vectors $\mathbf{p}^{\exp}$ and $\mathbf{T}^{\exp}$, each of dimension $i+1$. Connections between the chambers indicating the possibility of mass and heat exchange are defined by allocation matrices $\mathbf{L_{i,j}}$ and $\widetilde{\mathbf{L}}_{\mathbf{i,k}}$, respectively. Each column of the allocation matrix contains two nonzero elements (-1 and 1) at rows representing connected chambers. Moreover, $\mathbf{L}^{\exp}_{\mathbf{i+1,j}}$ and $\widetilde{\mathbf{L}}^{\exp}_{\mathbf{i+1,k}}$ denotes expanded allocation matrices in which the last row corresponds to external environment. Allocation matrices fully define topology of the system and thus they can be effectively utilized in formulating equations governing pneumatic part of the problem.

Dynamics of multi-chamber inflatable structure will be described in Finite Element Method notation. General form of finite element nonlinear equation of motion reads:

$$\mathbf{M}\ddot{\mathbf{u}} + \mathbf{C}\dot{\mathbf{u}} + \mathbf{K}(\mathbf{u})\mathbf{u} = \mathbf{F}(\mathbf{p}^{\exp}, \mathbf{u}) + \mathbf{F_I} \qquad (2.3.37)$$

$$\mathbf{u}(0) = \mathbf{u}_0 \,,\ \dot{\mathbf{u}}(0) = \mathbf{V}_0$$

where the matrices **M,C,K** indicate mass, damping and stiffness matrices of the solid body, respectively and **u** denotes vector of degrees of freedom. Initial conditions are imposed on both initial displacements and velocities of inflatable structure. Impact loading can be modelled by right-hand side force vector $\mathbf{F_I}$, by initial conditions or by contact defined between the inflatable structure and other object. Moreover, vector $\mathbf{F}(\mathbf{p}^{ext}, \mathbf{u})$ represents forces exerted by fluid on solid walls of inflatable structure and therefore provides mechanical coupling between solid and fluid. The interaction of the structure and fluid during large deformation can be correctly taken into account only by assembling equilibrium equations in actual configuration so equation of motion has to be considered in nonlinear form.

Balance of mass of fluid in each chamber can be expressed by using allocation matrix $\mathbf{L_{i,j}}$, vector indicating mass flow rate between the chambers **q** and vector indicating inflow rate from inflators $\mathbf{q}^{\inf}$:

$$\dot{\mathbf{m}} - \mathbf{L}\mathbf{q} = \mathbf{q}^{\inf} \quad \text{or} \quad \dot{m}_i - L_{ij} q_j = q_i^{\inf} \qquad (2.3.38)$$

Pressure differences between connected cavities and between selected cavities and environment $\Delta\mathbf{p}$ are defined as:

$$(\mathbf{L}^{\exp})^{\mathrm{T}} \mathbf{p}^{\exp} = \Delta\mathbf{p} \quad \text{or} \quad L^{\exp}_{ji} p_i^{\exp} = \Delta p_j \qquad (2.3.39)$$

For the sake of simplicity, the most basic, proportional relation between mass flow rate of gas

$\mathbf{q}$ and pressure difference $\Delta\mathbf{p}$ will be assumed (cf. Eq. 2.3.27):

$$\mathbf{q} = \frac{\Delta\mathbf{p}}{\mathbf{C}} \quad \text{or} \quad q_j = \frac{\Delta p_j}{C_j} \tag{2.3.40}$$

Finally ideal gas law for each cavity is expressed in a classical way as:

$$\mathbf{pV} = \mathbf{m}R\mathbf{T} \quad \text{or} \quad p_i V_i = m_i R T_i \tag{2.3.41}$$

Equation (2.3.38-2.3.41) can be rearranged to a single equation which involves gas pressures, temperatures and chamber volumes:

$$\frac{d\left(\frac{\mathbf{pV}}{R\mathbf{T}}\right)}{dt} - \frac{\mathbf{L}(\mathbf{L}^{\exp})^{\mathbf{T}}}{\mathbf{C}}\mathbf{p}^{\exp} = \mathbf{q}^{\inf} \quad \text{or} \quad \frac{d\left(\frac{p_i V_i}{R T_i}\right)}{dt} - \frac{L_{ij}L_{ji}^{\exp}}{C_j}p_i^{\exp} = q_i^{\inf} \tag{2.3.42}$$

In a special case when temperature of gas in all chambers remains constant equation (2.3.42) can be rearranged to a form:

$$\left(\frac{\dot{\mathbf{p}}\mathbf{V} + \mathbf{p}\dot{\mathbf{V}}}{R\mathbf{T}}\right) - \frac{\mathbf{L}(\mathbf{L}^{\exp})^{\mathbf{T}}}{\mathbf{C}}\mathbf{p}^{\exp} = \mathbf{q}^{\inf} \quad \text{or} \quad \frac{\dot{p}_i V_i + p_i \dot{V}_i}{R T_i} - \frac{L_{ij}L_{ji}^{\exp}}{C_j}p_i^{\exp} = q_i^{\inf} \tag{2.3.43}$$

where the only unknown quantities are pressures inside chambers and chambers volumes. However, volume of each chamber can be expressed in terms of inflatable structure deformation so it does not constitute an independent unknown. Multi-chamber inflatable structure under isothermal conditions is described by finite element equation of motion (2.3.37) and i additional equations (2.3.43) containing i pressures as additional unknowns.

In a more general model, change of gas temperature inside each cavity has to be considered. Equation of energy balance reads:

$$\dot{\mathbf{Q}} + \dot{\hat{\mathbf{H}}} = \dot{\mathbf{U}} + \dot{\mathbf{W}} \quad \text{or} \quad \dot{Q}_i + \dot{\hat{H}}_i = \dot{U}_i + \dot{W}_i \tag{2.3.44}$$

and it involves energy transferred in the form of heat $\mathbf{Q}$, energy transferred in the form mass (enthalpy) $\hat{\mathbf{H}}$, change of internal energy $\mathbf{U}$ and work done by gas $\mathbf{W}$ (cf. Eq. 2.3.7). Equation governing balance of heat transferred to each chamber has similar structure to previously derived equation governing balance of fluid mass but it is expressed in terms of allocation matrix $\widetilde{\mathbf{L}}$ and vector $\widetilde{\mathbf{q}}$ indicating heat flux between the chambers:

$$\dot{\mathbf{Q}} - \widetilde{\mathbf{L}}\widetilde{\mathbf{q}} = 0 \quad \text{or} \quad \dot{Q}_i - \widetilde{L}_{ik}\widetilde{q}_k = 0 \tag{2.3.45}$$

Temperature differences between adjacent cavities can be expressed as:

$$(\widetilde{\mathbf{L}}^{\exp})^{\mathbf{T}}\mathbf{T}^{\exp} = \Delta\mathbf{T} \quad \text{or} \quad \widetilde{L}_{ki}^{\exp}T_i^{\exp} = \Delta T_k \tag{2.3.46}$$

Heat flux between the cavities $\widetilde{\mathbf{q}}$ is proportional to corresponding temperature difference $\Delta\mathbf{T}$ (cf. Eq. 2.3.18):

$$\widetilde{\mathbf{q}} = (\mathbf{A}\boldsymbol{\lambda})\Delta\mathbf{T} \quad \text{or} \quad \widetilde{q}_k = (A\lambda)_k \Delta T_k \tag{2.3.47}$$

where the term $\mathbf{A}\boldsymbol{\lambda}$ indicates product of area of the wall separating the cavities and heat conductivity coefficient. Finally, balance of heat transferred to each cavity reads:

$$\dot{\mathbf{Q}} = \widetilde{\mathbf{L}}(\mathbf{A}\boldsymbol{\lambda})(\widetilde{\mathbf{L}}^{ext})^{\mathrm{T}}\mathbf{T}^{ext} \quad \text{or} \quad \dot{Q}_i = \widetilde{L}_{ik}(A\lambda)_k \widetilde{L}^{ext}_{ki} T_i^{ext} \tag{2.3.48}$$

Equation defining balance of energy transferred by mass exchange (the balance of enthalpy) is similar to balance of fluid mass:

$$\dot{\hat{\mathbf{H}}} - \mathbf{L}\hat{\mathbf{q}} = \hat{\mathbf{q}}^{\inf} \quad \text{or} \quad \dot{\hat{H}}_i - L_{ij}\hat{q}_j = \hat{q}_i^{\inf} \tag{2.3.49}$$

where $\hat{\mathbf{q}}^{\inf}$ indicates flux of enthalpy between the chambers and $\hat{\mathbf{q}}^{\inf}$ represents enthalpy submitted by inflators. Similarly to mass flow rate of gas, flux of enthalpy is proportional to pressure difference. Moreover, it depends on specific heat at constant pressure and temperature of the flowing gas:

$$\hat{\mathbf{q}} = \frac{\Delta\mathbf{p}}{\mathbf{C}} c_p \mathbf{T}^* \quad \text{or} \quad \hat{q}_k = \frac{\Delta p_j}{C_j} c_p T_j^* \tag{2.3.50}$$

The quantity T_j^* indicates temperature in the upstream cavity which is defined as:

$$T_j^* = T_{i_1} \quad \text{when} \quad p_{i_1} \geq p_{i_2}, \quad T_j^* = T_{i_2} \quad \text{when} \quad p_{i_1} < p_{i_2} \tag{2.3.51}$$

where: i_1 indicates inflow chamber: $i_1 = i$ such that $L_{ij}^{ext} = 1$

i_2 indicates outflow chamber: $i_2 = i$ such that $L_{ij}^{ext} = -1$

Finally, balance of enthalpy for each cavity reads:

$$\dot{\hat{\mathbf{H}}} = \mathbf{L}\frac{\mathbf{p}^{ext}}{\mathbf{C}}(\mathbf{L}^{ext})^{\mathrm{T}} c_p \mathbf{T}^* + \hat{\mathbf{q}}^{\inf} \quad \text{or} \quad \dot{\hat{H}}_i = L_{ij}\frac{p_i^{ext}}{C_j} L_{ji}^{ext} c_p T_i^* + \hat{q}_i^{\inf} \tag{2.3.52}$$

By introducing the above derived balances of heat and enthalpy into global energy balance for each cavity (2.3.44) and combining it with ideal gas law, we obtain single equation expressed in terms of gas pressure, gas temperature and cavity volumes:

$$\widetilde{\mathbf{L}}(\mathbf{A}\boldsymbol{\lambda})(\widetilde{\mathbf{L}}^{ext})^{\mathrm{T}}\mathbf{T}^{ext} + \mathbf{L}\frac{\mathbf{p}^{ext}}{\mathbf{C}}(\mathbf{L}^{ext})^{\mathrm{T}} c_p \mathbf{T}^* = \frac{d\left(\frac{\mathbf{pV}}{R\mathbf{T}}\right)}{dt} c_V \mathbf{T} + \frac{\mathbf{pV}}{R\mathbf{T}} c_V \dot{\mathbf{T}} + \mathbf{p}\dot{\mathbf{V}} \tag{2.3.53a}$$

or in index form:

$$\widetilde{L}_{i,k}(A\lambda)_j \widetilde{L}^{ext}_{k,i} T_i^{ext} + L_{ij}\frac{p_j^{ext}}{C_j} L_{ji}^{ext} c_p T_{i^*} = \frac{d\left(\frac{p_i V_i}{RT_i}\right)}{dt} c_V T_i + \frac{p_i V_i}{RT_i} c_V \dot{T}_i + p_i \dot{V}_i \tag{2.3.53b}$$

Ultimately, the mathematical model of multi-chamber inflatable structure in UPM-based approach is described by standard equilibrium equations (in direct PDE form Eq. 2.3.16 or FEM formulation Eq. 2.3.37) and additionally by equation (2.3.42) defining global balance of mass transfer between the chambers and equation (2.3.53) defining global balance of internal energy.

2.4 Hybrid approach

Method based on modelling gas by Navier-Stokes equations and Uniform Pressure Method represent two opposite approaches to modelling Adaptive Inflatable Structures with controllable valves. Both these methods involve certain disadvantages when they are used for simulation and development of control strategies for inflatable structures.

The FSI - based methods, both in case of ALE approach and fixed grid approach, often become numerically expensive since large fluid regions has to be discretized and fine fluid mesh has to be used in the vicinity of the interfaces to provide proper coupling between fluid and solid. Moreover, results obtained from the FSI methods may not be accurate due to nonlinearities in Navier-Stokes equations or inexactness of coupling procedures which may arise in case of strong deformation of the solid body. On a contrary, UPM-based approach is much simpler and less numerically expensive. In general, a strong disadvantage of this method is very rough modelling of the phenomena which occur in fluid. Moreover, flow of fluid through controllable valve is described analytically which often requires preliminary experimental testing of the valve. In addition, analytical model does not always precisely describe dynamics of the flow through controllable valve with actively changed opening, which is especially important in considered problem of real-time adaptation to event of a short duration.

An alternative method of modelling Adaptive Inflatable Structures, which helps to eliminate some drawbacks of FSI and UPM methods, is a 'hybrid approach' where substantial part of inflatable structure is modelled in a simplified way by UPM method but the valve region is modelled more precisely by using FSI approach. Proposed hybrid method allows to avoid solving Navier-Stokes equation in substantial part of inflatable structure where, in many practical cases, pressure distribution is almost uniform. Furthermore, it helps to avoid dealing with complex fluid-solid coupling conditions, handling large deformations and solid-solid contact within FSI problem. On the other hand, this method enables precise modelling of dynamics of the flow through controllable valve without performing preliminary experimental tests. Proposed 'hybrid approach' of modelling inflatable structures can be classified as multi-scale modelling due to applied various scales of fluid modelling.

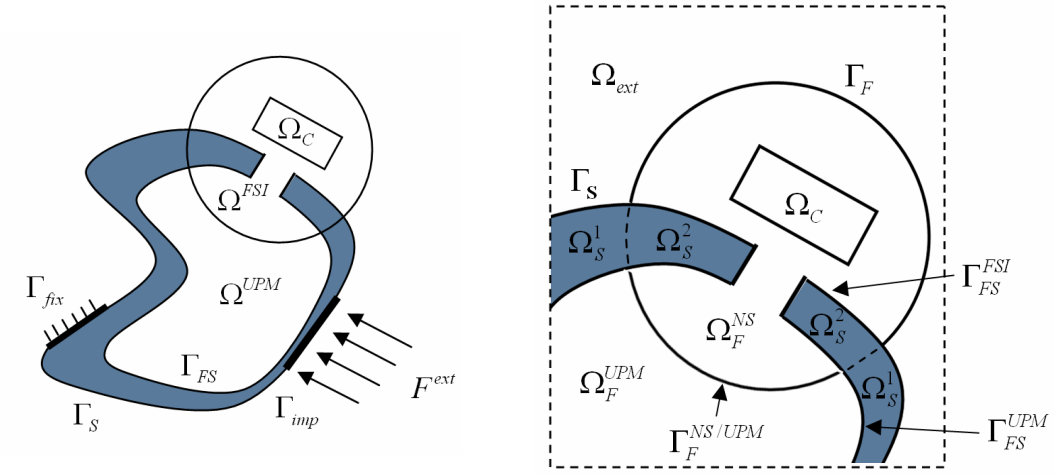

Fig. 2.12. Hybrid model of Adaptive Inflatable Structure with controllable valve: a) division into FSI and UPM regions, b) close-up of the valve region.

The essence of the 'hybrid method' is division of the considered domain into two separate regions: the main region Ω^{UPM} modelled by UPM approach and the region around the valve Ω^{FSI} modelled by full FSI approach, Fig. 2.12a. The fluid region consists of part modelled with the assumption of homogeneity of gas parameters and part modelled by Navier-Stokes equations $\Omega_F = \Omega_F^{UPM} \cup \Omega_F^{NS}$ separated by the interface $\Gamma_F^{NS/UPM}$. The solid part is composed of two regions $\Omega_S = \Omega_S^1 \cup \Omega_S^2$ modelled by exactly the same set of governing equations. Consequently, fluid-solid interface $\Gamma_{FS} = \Gamma_{FS}^{UPM} \cup \Gamma_{FS}^{FSI}$ is composed of two distinct parts located in regions modelled by two approaches: $\Gamma_{FS}^{UPM} = \Omega_F^{UPM} \cap \Omega_S^1$, $\Gamma_{FS}^{FSI} = \Omega_F^{NS} \cap \Omega_S^2$. Additionally, the model contains control domain Ω_C which is now fully enclosed within FSI region.

Division into FSI and UPM regions is much more distinct in fluid domain since the method of fluid modelling changes drastically: from Navier-Stokes equations to a simple method based on uniformity of gas parameters. In region Ω_F^{NS} both conforming boundary methods (such as ALE) and fixed grid methods (such as CEL) can be applied. Here, fixed grid approach is proposed to be used and therefore in corresponding numerical method the whole region that can be occupied by fluid has to be discretized, however Navier-Stokes equations has to be solved only in the region Ω_F^{NS}. Moreover, an additional procedure for tracking position of the region Ω_F^{NS}, which changes during inflatable structure deformation, has to be introduced. Equations describing fluid located inside domain Ω_F^{NS} defined in Eulerian frame of reference read:

$$\frac{\partial \rho_F}{\partial t} + \nabla \rho_F \cdot \mathbf{v}_F = -\rho_F (\nabla \cdot \mathbf{v}_F) \qquad \text{in } \Omega_F^{NS} \tag{2.4.1}$$

$$\rho_F \frac{\partial \mathbf{v}_F}{\partial t} + \rho_F (\nabla \mathbf{v}_F)\mathbf{v}_F = \nabla \cdot \boldsymbol{\sigma}_F{}^{\mathrm{T}} + \rho_F \mathbf{f} \tag{2.4.2}$$

$$\rho_f \frac{\partial E_f}{\partial t} + \rho_f \nabla E_f \cdot \mathbf{v}_f = -\nabla \cdot \mathbf{q}_F + \nabla \cdot (\boldsymbol{\sigma}_F \mathbf{v}_F) + \rho_F \mathbf{f} \cdot \mathbf{v}_F + \rho_F h \tag{2.4.3}$$

Behaviour of the fluid located inside domain Ω_F^{UPM} is governed by a simple differential equation of energy balance and ideal gas law:

$$\dot{Q}_1 + \sum \dot{m}_f^{UPM} \overline{H} = \dot{U} + \dot{W} \qquad \text{in } \Omega_F^{UPM} \tag{2.4.4}$$

$$p_f^{UPM} V_f^{UPM} = m_f^{UPM} R T_f^{UPM}$$

where $\dot{Q}_1$ indicate heat transfer through interface Γ_{FS}^{UPM} and $\dot{m}_f^{UPM} \overline{H}$ indicates transfer of enthalpy through interface $\Gamma_F^{NS/UPM}$, respectively. By contrast, solid body is modelled by complete balance equations in Lagrangian frame of reference in both solid domains Ω_S^1, Ω_S^2:

$$\frac{D}{Dt}(\rho_{\mathbf{S}} J) = 0 \qquad \text{in } \Omega_S \tag{2.4.5}$$

$$\rho_{\mathbf{S}} J \frac{D\mathbf{v}_{\mathbf{S}}}{Dt} = \nabla_{\mathbf{X}} \cdot (J \boldsymbol{\sigma}_{\mathbf{S}}{}^{\mathrm{T}} \mathbf{F}^{-\mathrm{T}}) + \rho_{\mathbf{S}} J \mathbf{f} \tag{2.4.6}$$

$$\rho_{\mathbf{S}} J \frac{DE_S}{Dt} = -\nabla_{\mathbf{X}} \cdot (J \mathbf{q}_{\mathbf{S}} \mathbf{F}^{-\mathrm{T}}) + \nabla_{\mathbf{X}} \cdot (J \boldsymbol{\sigma}_{\mathbf{S}} \mathbf{F}^{-\mathrm{T}} \mathbf{v}_{\mathbf{S}}) + \rho_{\mathbf{S}} J \mathbf{f} \cdot \mathbf{v}_{\mathbf{S}} + \rho_{\mathbf{S}} J h \tag{2.4.7}$$

Division of the solid domain into two parts is reflected only in conditions imposed on its boundary. Mechanical and thermal coupling conditions between solid and fluid formulated on FSI part of the fluid-solid interface Γ_{FS}^{FSI} read:

$$\boldsymbol{\sigma}_{\mathbf{S}}\mathbf{n} = \boldsymbol{\sigma}_{\mathbf{f}}\mathbf{n} \quad \text{and} \quad \mathbf{v}_{\mathbf{f}} = \mathbf{v}_{\mathbf{S}} \quad \text{on} \quad \Gamma_{FS}^{FSI} \tag{2.4.8}$$

$$T_S = T_f \quad \text{and} \quad \mathbf{q}_{\mathbf{S}} \cdot \mathbf{n} = \mathbf{q}_{\mathbf{f}} \cdot \mathbf{n} \quad \text{on} \quad \Gamma_{FS}^{FSI}$$

and on UPM part of the fluid-solid interface Γ_{FS}^{UPM}, cf. Eq. 2.3.11 and Eq. 2.3.12

$$\boldsymbol{\sigma}_{\mathbf{S}}\mathbf{n} = -p_f^{UPM}\mathbf{n} \ \text{ on } \ \Gamma_{FS}^{UPM} \quad \text{and} \quad V_f^{UPM} = \int d\Omega_f^{UPM} \tag{2.4.9}$$

$$T_S = T_f^{UPM} \quad \text{and} \quad \int (\mathbf{q}_{\mathbf{S}} \cdot \mathbf{n}) d\Gamma_{FS}^{UPM} = \dot{Q}_1 \quad \text{on} \quad \Gamma_{FS}^{UPM}$$

or

$$-\mathbf{q}_{\mathbf{S}} \cdot \mathbf{n} = h(T_f^{UPM} - T_S) \quad \text{and} \quad \int (\mathbf{q}_{\mathbf{S}} \cdot \mathbf{n}) d\Gamma_{FS}^{UPM} = \dot{Q}_1 \quad \text{on} \quad \Gamma_{FS}^{UPM}$$

Moreover, at the interface between NS and UPM-modelled fluid region $\Gamma_F^{NS/UPM}$ (which typically constitutes inlet for the region Ω_f^{NS}) the coupling conditions has to be formulated:

$$\boldsymbol{\sigma}_{\mathbf{f}}\mathbf{n} = -p_f^{UPM}\mathbf{n} \quad \text{on} \quad \Gamma_F^{NS/UPM} \tag{2.4.10}$$

$$\int (\mathbf{v}_{\mathbf{f}} \cdot \mathbf{n}) \rho_f d\Gamma_F^{NS/UPM} = \dot{m}_f^{UPM} \ \text{ on } \ \Gamma_F^{NS/UPM}$$

$$T_f = T_f^{UPM} \quad \text{and} \quad \int \left((\mathbf{v}_{\mathbf{f}} \cdot \mathbf{n}) \rho_f \right) c_p T_f d\Gamma_F^{NS/UPM} = \sum \dot{m}_f^{UPM} \overline{H} \ \text{ on } \ \Gamma_F^{NS/UPM}$$

The first, mechanical coupling condition states that actual pressure of the gas modelled by UPM approach is applied as a boundary condition to domain modelled by Navier-Stokes equations. The second condition provides that mass flow rate at the boundary $\Gamma_F^{NS/UPM}$ equals to change of fluid mass inside the structure. Finally, the third, thermal coupling condition provides equality of temperatures of gas at the boundary. Combination of the second and third condition leads to conservation of the enthalpy flux between two considered regions. Boundary conditions are formulated both for the solid domain at its external boundary:

$$\mathbf{u}_{\mathbf{S}} = \mathbf{0} \ \text{ on } \ \Gamma_{fix}, \quad \boldsymbol{\sigma}_{\mathbf{S}}\mathbf{n} = -p_{ext}\mathbf{n} \ \text{ on } \ \Gamma_{\mathbf{S}}, \quad \boldsymbol{\sigma}_{\mathbf{S}}\mathbf{n} = \mathbf{F}^{ext} \ \text{ on } \ \Gamma_{imp} \tag{2.4.12}$$

$$T_S = T_{ext} \quad \text{or} \quad -\mathbf{q}_{\mathbf{S}} \cdot \mathbf{n} = h(T_{ext} - T_S) \quad \text{on} \quad \Gamma_S$$

and for FSI part of the fluid domain ('opening' boundary conditions):

$$\boldsymbol{\sigma}_{\mathbf{F}}\mathbf{n} = -p_{ext}\mathbf{n} \ \text{ on } \ \Gamma_F, \quad T_S = T_{ext} \ \text{ on } \ \Gamma_F \tag{2.4.13}$$

Finally, the model has to be complemented with appropriate coupling conditions between the fluid and control domain.

2.5 Formulation of the control problems

Previous sections of this chapter were focused on various methods of modelling Adaptive Inflatable Structure equipped with controllable valve. Several possibilities of modelling controllable valve with arbitrarily changed opening were introduced, however no prerequisites

or clues for optimal strategy of valve opening were given. Since the goal of introducing controllable valves is adaptation to actual dynamic loading, the next step in the development of theory of AIS is the choice of objectives that should be fulfilled by internal pressure control and formulation of the corresponding control problems. Finding solution of formulated problems, i.e. development of optimal strategies of internal pressure control is the main challenge related to adaptive inflatable structures. Since the above task can not be performed on a current high level of generality, it will be performed for particular types of inflatable structures considered in further chapters of this thesis.

Although problems of optimisation and control of solid structures and control of the fluid flow are widely covered by scientific literature, the research on control of fluid-structure interaction problems is not that well developed. Theoretical aspects of controllability of basic FSI problems concerning both compressible and incompressible fluids were analyzed in mathematical papers, e.g. [221]. Application of sensitivity and optimisation techniques for aerospace and aeroelesticity problems (limited to small deformation of the solid body) were discussed in early papers [222], while theoretical background for gradient-based shaped optimisation of strongly coupled stationary fluid-structure interaction was described in paper [223]. Moreover, authors of [224] proposed application of optimisation methods instead of Newton-Raphson algorithms for efficient solution of FSI problems. Practical problems were considered in paper [225] where physical programming was applied for optimisation of large scale rigidified inflatable structures and in paper [226] where authors consider problem of optimal design of containers that minimises sloshing in case when container is subjected to impact loading. Recently published papers concern combination of the partitioned FSI solver with the optimisation procedures (for instance with the use of NURBS surfaces) [227 228] and shape optimisation of lightweight structures subjected to fluid flow [229 230].

Classification of control problems related to impact absorption

Control problems related Adaptive Impact Absorption correspond either to objective of optimal reception of the exploitive impact loading or to objective of optimal protection against critical impact. In case of exploitive loading the control problems are defined by assuming arbitrary impact scenario and by formulating objectives aimed at mitigation of dynamic response of hitting object or impacted structure. Control problems related to protection of hitting object include:

1. minimisation of maximal value of hitting object deceleration during impact,
2. minimisation of hitting object kinetic energy after impact.

Let us assume two control variables: p_0 indicating initial pressure inside single-chamber inflatable structure and $C(t)$ indicating valve opening which can be arbitrarily changed during the numerical analysis. The first control problem can be mathematically formulated in two manners. The first formulation reads:

$$\text{Find } p_0, C(t) \text{ such that } E_k(t) \cong 0 \text{ for } t > t_{stop} \text{ and } J_1 = \max_t \left|\ddot{u}(t)\right| \text{ is minimal} \qquad \text{(2.5.1a)}$$
$$\text{subject to: } p_0 \in \left\langle p_{\min}, p_{\max} \right\rangle$$

In the above formulation, the control problem is supplemented with an additional condition which indicates that the whole kinetic energy of impacting object E_k has to be dissipated

(E_k is close to zero after time instant when hitting object drops to zero t_{stop}). This conditions automatically excludes solutions with total penetration of the impacted structure or rebound of the hitting object. Alternatively, the additional condition can be expressed in terms of exergy of inflatable structure X which must be equal zero at time t_{stop} or actual energy dissipation D which must be equal to sum of initial kinetic and potential energy of the impacting object:

$$E_k(t) \cong 0 \text{ for } t > t_{stop} \quad \Leftrightarrow \quad X(t_{stop}) \cong 0 \quad \Leftrightarrow \quad D = E_k(t_0) + \Delta E_p \tag{2.5.1b}$$

Formulation (2.5.1) is intuitive and often applied in AIA problems. However, dissipation of the whole kinetic energy of the hitting object is not always possible, for instance, when strict constraints concerning valve opening are imposed. Therefore, the condition of energy dissipation can be omitted and the control problem can be defined as:

$$\begin{aligned} &\text{Find } p_0, C(t) \text{ such that } J_2 = \max_t \left|\ddot{u}(t)\right| \text{ is minimal} \\ &\text{subject to: } p_0 \in \langle p_{\min}, p_{\max} \rangle, \quad C(t) \in \langle C_{\min}, C_{\max} \rangle, \quad \frac{dC(t)}{dt} < \widetilde{C}_{\max} \end{aligned} \tag{2.5.2}$$

Within this formulation the conditions excluding total penetration of the impacted structure and rebound of the hitting object have to be introduced in an artificial way, for instance by locating stiff delimiter behind inflatable structure (mathematically equivalent to Lagrange multiplier). Since contact with the delimiter will cause large value of deceleration, the control algorithm will tend to dissipate the whole impact energy by using the inflatable structure. If fulfilment of this objective is not possible (e.g. due to control constraints) the algorithm will tend to maximise velocity reduction and energy dissipation caused by inflatable structure.

The second of mentioned control problems, the minimisation of hitting object kinetic energy after impact, can be formulated as follows:

$$\begin{aligned} &\text{Find } p_0, C(t) \text{ such that } J_3 = E_k(t_{end}) \text{ is minimal} \\ &\text{subject to: } p_0 \in \langle p_{\min}, p_{\max} \rangle, \quad C(t) \in \langle C_{\min}, C_{\max} \rangle, \quad \frac{dC(t)}{dt} < \widetilde{C}_{\max} \end{aligned} \tag{2.5.3}$$

This control objective can be also understood as maximisation of dissipated kinetic energy of the hitting object or minimisation of its final velocity. The above formulation of the control problem covers both the case when initial velocity of the hitting object is not reduced to zero (i.e. when penetration occurs) or when velocity drops below zero (i.e. when the rebound occurs). Since the objective is formulated only at final time instant of the process t_{end}, it is expected that the solution will not be unique but rather class of functions $C(t)$ will be determined. Control problems (2.5.2) and (2.5.3) can be considered together as a joint problem of minimisation of final value of kinetic energy and maximal value of deceleration:

$$\begin{aligned} &\text{Find } p_0, C(t) \text{ such that } J_4 = E_k(t_{end}) + \max_t \left|\ddot{u}(t)\right| \text{ is minimal} \\ &\text{subject to: } p_0 \in \langle p_{\min}, p_{\max} \rangle, \quad C(t) \in \langle C_{\min}, C_{\max} \rangle, \quad \frac{dC(t)}{dt} < \widetilde{C}_{\max} \end{aligned} \tag{2.5.4}$$

Obviously appropriate weighting coefficients related to final kinetic energy and maximal acceleration can be applied. Let us note that the above formulation is partially equivalent to formulation (2.5.2) in case when the latter one involves application of described additional delimiter (Lagrange multiplier).

In turn, the control problems dedicated to optimal protection of impacted structure involve:

1. minimisation of maximal value of internal pressure inside inflatable structure or pressure impulse transferred to protected structure,
2. minimisation of internal forces arising in solid walls of inflatable structure or its deformation.

Both problems can be defined in a straightforward way. The first problem reads:

$$\begin{aligned} &\text{Find } C(t) \text{ such that } J_5 = \max_t p(t) \text{ or } J_6 = \int_{t_0}^{t_{end}} \left[p(t)A\right]dt \text{ is minimal} \\ &\text{subject to: } p_0 \in \langle p_{\min}, p_{\max} \rangle, \quad C(t) \in \langle C_{\min}, C_{\max} \rangle, \quad \frac{dC(t)}{dt} < \widetilde{C}_{\max} \end{aligned} \tag{2.5.5}$$

Minimisation of internal pressure is related to limitation of the possibility of bursting of the inflatable structure, while minimisation of pressure impulse is associated with minimisation of the vibrations of structure protected by inflatable system (cf. Chapter 6.1). The second problem can be written in a simple form:

$$\begin{aligned} &\text{Find } C(t) \text{ such that } J_6 = \max_t \left|\boldsymbol{\sigma}(t)\right| \text{ or } J_7 = \max_t \left|\boldsymbol{\varepsilon}(t)\right| \text{ is minimal} \\ &\text{subject to: } p_0 \in \langle p_{\min}, p_{\max} \rangle, \quad C(t) \in \langle C_{\min}, C_{\max} \rangle, \quad \frac{dC(t)}{dt} < \widetilde{C}_{\max} \end{aligned} \tag{2.5.6}$$

The above formulation directly pertains to stresses and strains generated in solid walls of inflatable structure during impact, which influence inflatable structure's durability and fatigue. Applied norm of the stress or strain tensor depends on particular type of inflatable structure under consideration.

Another group of control problems is aimed at optimal protection against critical impact. In this case the impact scenario is not preliminarily assumed and the control problem is aimed at finding the strategy of adaptation for which the load capacity of the inflatable structure, defined as the highest allowable initial energy of the impacting object, is maximal. The highest allowable energy of the impacting object is the energy for which the response of the system remains acceptable, i.e. arbitrary conditions imposed on response of hitting object and impacted structure are not violated. Consequently, the constraints of the corresponding control problem can be imposed on selected variables being minimised in the control problems (2.5.1-2.5.6) and additionally on control variables p_0 and $C(t)$. Mathematical formulation of such control problem reads:

$$\begin{aligned} &\text{Find } C(t) \text{ such that } E_k(t_0) \text{ is maximal} \\ &\text{subject to: } \max_t \left|\ddot{u}(t)\right| < f_1, \quad E_k(t_{end}) < f_2 \\ &\max_t p(t) < f_3, \quad \int_0^{t_{end}} p(t)dt < f_4, \quad \max_t \left|\boldsymbol{\sigma}(t)\right| < f_5, \quad \max_t \left|\boldsymbol{\varepsilon}(t)\right| < f_6 \\ &p_0 \in \langle p_{\min}, p_{\max} \rangle, \quad C(t) \in \langle C_{\min}, C_{\max} \rangle, \quad \frac{dC(t)}{dt} < \widetilde{C}_{\max} \end{aligned} \tag{2.5.7}$$

Three groups of constraints concern subsequently: response of the hitting object, response of the inflatable structure and limitations of the impact absorbing system. The above control problem is ambiguous since response of inflatable structure differs for impacts of the same energy but various mass and velocity. Thus, one of this parameters has to be assumed a priori.

Precise formulation of the control problem depends on the type of inflatable structure, its application and type of applied impact loading. The control problems concerning particular inflatable structures and control objectives will be precisely defined in subsequent chapters.

Furthermore, the intrinsic difference between control of the pneumatic systems modelled by means of FSI-based and UPM-based approach has to be distinguished. In a simplified UPM model of Adaptive Inflatable Structure actual value of the flow resistance coefficient $C(t)$ or actual area of the orifice $A(t)$ are used as control functions. By contrast, in full FSI model actual size or value of fluid boundary condition (Γ_V), actual location of the orifice edges or width of the orifice $(\Gamma_{1/2}, \Lambda_C)$, location or shape of void control domain Γ_C or general properties of control region Ω_C modelling the valve head can be treated as an external control (cf. Sec. 2.2.3). Therefore, possible formulations of the control problem defined within FSI approach read:

$$\begin{array}{llll} 1.\ \text{Find} & \Gamma_V(t) \in \Gamma_V^{adm} & & \\ 2.\ \text{Find} & \Gamma_{1/2}(t) \in \Gamma_{1/2}^{adm} & & \\ 3.\ \text{Find} & \Lambda_C(t) \in \Lambda_C^{adm} & \text{such that} & \begin{array}{l} J_1, J_2, J_3, J_4, J_5, J_6 \\ E_k(t_0) \end{array} \quad \text{is minimal} \\ 4.\ \text{Find} & \Gamma_C(t) \in \Gamma_C^{adm} & & \\ 5.\ \text{Find} & \Omega_C(t) \in \Omega_C^{adm} & & \end{array} \tag{2.5.8}$$

where Γ_V^{adm} defines allowable size of outlet or value of fluid boundary condition, $\Gamma_{1/2}^{adm}$ and Λ_C^{adm} define admissible width and shape of the orifice. Similarly Γ_C^{adm} determines admissible locations of the void domain Ω_C, for example it confines its movement to a rigid body motions. Finally, Ω_C^{adm} defines allowable features of the control region, i.e. defines type of governing equations, values of their parameters and range of allowable external excitation.

Let us note that FSI control variables $\Gamma_V(t),...,\Omega_C(t)$ and UPM control variables $C(t), A(t)$ influence corresponding numerical models in a completely different manner. Variables $\Gamma_V(t),...,\Omega_C(t)$ primarily influence geometry of the FSI model and alter shape of the fluid domain where PDEs describing fluid flow are defined. By contrast, functions $C_V(t)$ and $A(t)$ are simply time-dependent coefficients in one of the ODEs defining UPM model. Due to complexity and high computational cost of modelling and control by means of FSI-based method, it will not be applied for all considered types of inflatable structures but only for pneumatic cylinders subjected to impacts of high initial velocities and two types of controllable valves.

Methodology of solving control problems

The next issue that has to be considered is the choice of methodology for solving formulated control problems related to impact absorption. Theoretically, two main groups of methods can be distinguished. One group of methods of finding control function $C(t)$ is based on optimisation techniques [231]. In the most basic approach function $C(t)$ can be represented as a polynomial and coefficients of this polynomial can be treated as unknowns in constrained optimisation problem. In other approach control function $C(t)$ can be represented by step function or piecewise linear function and its values at arbitrary time instances can be treated as optimisation variables. Since classical gradient-based methods are expected not to be always efficient (as prone to find local minima) the solution of the selected optimisation

problems requires application of genetic algorithms and direct-search methods.

Another group of methods is based on a control theory [232]. As it will be shown, some of general control problems can be transformed into control problems with predefined output (problems of regulation) which are well recognized within control theory. Unfortunately, typical in this case methods based on Laplace transform can not be applied due to nonlinearities arising in equations governing even the simplest inflatable structures. In more general case, the problem of adaptation to impact loading can be formulated as problem of 'optimal control' i.e. minimisation of a certain functional which depends on both controlled quantity (system response) and applied control. However, this dependence is usually not defined analytically or even explicitly since minimized functional depends on numerical solution of nonlinear differential equations. This causes that application of typical methods of 'optimal control theory' based on both Bellman's dynamic programming and Pontryagin's minimum principle is strongly aggravated and often impossible.

Methods applied in this thesis for development of control strategies aimed at adaptation of inflatable structure to actual dynamic loading will be based on combination of techniques gathered from optimisation and control theory. Moreover, in many cases, particular phenomenon dominating in the considered process can be distinguished, which allows to propose heuristic algorithms of adaptation. These algorithms can further tested by means of developed numerical models and selected algorithm can be precisely tuned by means of optimisation procedures.

Numerical implementation of developed models

The final matter is the choice of software for implementation of the proposed numerical models of various types of Adaptive Inflatable Structures and software for implementation and development of control strategies. Simulation of AIS was performed by in-house codes written by author, by commercial FEM and CFD software or combination of both. Implementation of adaptation procedures is based, in most cases, on feedback control loop and therefore it requires additional procedures for coupling arbitrary results of the numerical simulation with certain input data. Adaptation procedures were implemented in two manners:

- by means of internal subroutines of applied commercial software
- by means of external programme which controlled the proceeding of the simulation.

In case of simplified models of pneumatic cylinders where mechanical part is reduced to rigid body mechanics and gas is modelled by UPM approach, governing equations (ODEs) and adaptation strategies can be relatively easily programmed by using purely mathematical software. Herein, MAPLE software was used for numerical simulation, while adaptation algorithms were implemented either by internal procedures of MAPLE or by external connection with MATLAB. In case of fully deformable inflatable structure, when finite element modelling of the solid body was required, commercial implicit and explicit Finite Element Method software was used (ABAQUS and ANSYS). In the first attempt, the control algorithms were programmed internally by means of FORTRAN subroutines executed on each step of the analysis. An alternative, more comprehensive method of implementing control algorithm was based on controlling subsequent steps of FEM simulation and changing model parameters from external code developed in MATLAB.

Model	Solid modelling	Fluid modelling	Numerical method	Modelling software	Control software
Pneumatic cylinder UPM	RBM	UPM	Runge-Kutta Newton-Raph.	Maple ABAQUS	Maple / Matlab Fortran / Matlab
Pneumatic cylinder FSI	RBM	CFD	FVM	CFX	CEL + Matlab
Inflatable barrier	CSM	UPM	Implicit FEM Explicit FEM	ANSYS ABAQUS-XPL	Matlab
Adaptive airbags	RBM CSM	UPM	Runge-Kutta Implicit FEM Explicit FEM	Maple ABAQUS-STD ABAQUS-XPL	Maple Fortran Matlab
Valve CFD	RBM	CFD	FVM	CFX	CEL + Matlab
Valve FSI	CSM	CFD	FEM FEM + FVM	ABAQUS-XPL ANSYS +CFX	- CEL + Matlab

Table 1. Numerical methods and software used for modelling and control of various types of AIS

In cases when fluid was modelled by Navier-Stokes equations the specialised commercial CFD software ANSYS CFX, which utilizes Finite Volume Method and supports problems with moving boundaries, was applied. Coupling of the fluid dynamics and rigid body dynamics in simulation of pneumatic cylinder and piezoelectric valve was achieved by programming additional mechanical equations in CFX Expression Language (CEL). Furthermore, when the modelling required considering strong interaction between fluid and deforming solid body (full FSI problem) the coupling of ANSYS Mechanical and ANSYS CFX was used. Both in case of pneumatic cylinders and controllable valves adaptation algorithms were implemented by combination of CEL functions and external procedures launched from MATLAB. All methods applied in further simulations are collected in Table 1.

Summary of Chapter 2

The chapter presents development of the theoretical models of Adaptive Inflatable Structures and serves as a background for the considerations in the following chapters. The complexity of the models results from interaction of the strongly deforming solid and internal fluid. Initially, kinematics of the system is described with the use of referential deforming domain (ALE approach). The conservation equations are derived in ALE forms and further reduced to classical Eulerian and Lagrangian forms. Two basic models of inflatable structures are based on 'conforming boundary' and 'fixed grid' approach. The model of AIS is additionally enriched with a novel element - a controllable valve which allows controlling fluid outflow. In turn, simplified model of inflatable structure utilizes uniform distribution of gas pressure within a single chamber and analytical description of the gas flow. The last model is generalized in order to describe multi-chamber systems. Moreover, both derived models are combined in a hybrid approach where fluid is modelled precisely only in the valve region.

Finally, the control problems related to optimal impact absorption are formulated and methods of implementation of the developed models are proposed. The chapter shows multi-physical nature and sophisticated mathematical description of the problem of inflatable structures subjected to impact loading and reveals the challenges expected in further analysis.

CHAPTER 3 - ADAPTIVE PNEUMATIC CYLINDERS

The following part of the thesis (Chapter 3 and Chapter 4) is dedicated to precise analysis of methods of *modelling* and *control* of the simplest type of Adaptive Inflatable Structures - the adaptive pneumatic cylinders. As it will be proved in the following sections, adaptive pneumatic cylinders of various design can be successfully applied as simple energy dissipating devices with controllable characteristics. Preliminary adjustment of initial pressure and real-time control of valve opening providing appropriate conditions of gas migration enable adaptation of pneumatic absorbers to various impact scenarios. Adaptive pneumatic cylinders can be used as stand-alone devices serving for protection against impacts of external objects or, alternatively, they can be applied as landing gears for small airplanes or unmanned aerial vehicles.

Adaptive pneumatic cylinders were chosen as the first type of analysed inflatable structure because their analysis is substantially simplified due to the following reasons:

- equations governing the solid part are reduced to equation of motion of the piston and possibly heat transfer equation,
- deformation of the system is unidirectional,
- coupling conditions between solid body and a fluid are adequately simplified,
- the system contains only one or two pressure chambers and one controllable valve.

In Chapter 3 the Uniform Pressure Method (UPM) is utilized as a main tool for predicting dynamic response of pneumatic cylinders subjected to impact loading. Three types of pneumatic absorbers are introduced, i.e. absorber with exhaust to environment, with accumulator and with valve between the chambers. Next, the corresponding numerical models are developed. For each type of pneumatic absorber its dynamic characteristics is investigated and mechanism of energy dissipation is precisely analysed. Proposed numerical models are used to develop miscellaneous control strategies aimed mainly at minimisation of hitting object deceleration but also at reduction of rebound, minimisation of internal pressure and maximisation of the allowable impact energy. The chapter accomplishes with introduction of the methodology of optimal design of adaptive pneumatic cylinders and the experiment confirming their advantages over the passive ones.

The concept of purely pneumatic shock absorbers composed of two chambers separated by the piston was proposed e.g. in patents [233 234 235]. Two first patents include the idea of variable or controlled connection between the chambers, however neither the concept nor the methodology of real time control of the gas flow during impact is proposed. A brief review of devices utilizing air damping as well as investigation of the influence of additional external chamber on the operation of the air spring was presented in paper [236]. The concepts of gas absorbers with controlled release to the environment [237] and with controlled communication between the chambers [238] were initially studied to be applied for efficient damping of vibrations. Moreover, application of controllable pneumatic absorbers for mitigating dynamic response of the buildings in seismic conditions was proposed in [239]. On the other hand, the paper [240] describes application of valve based on piezoelectric stack and displacement amplifier for real-time control of the fluid flow between two chambers of the hydraulic adaptive absorber.

The first attempts of application of adaptive pneumatic absorber equipped with piezoelectric valve and accumulation tank performed at IPPT PAN were oriented towards development of systems for real-time mitigation of wind gusts [241]. The concept of adaptive pneumatic absorber was further generalized to various design options and patented [242]. The preliminary research on double chamber adaptive pneumatic absorber with controlled flow of the gas between the chambers [243 244] had led to its final application as landing gear for the small airplane [245 246].

Simplified modelling of pneumatic absorbers with constant and variable mass of the gas inside chambers was described in paper [247], however only selected cases were analysed and mathematical features of the model were not deeply studied. Modelling of pneumatic devices was also conducted to simulate dynamic characteristics of pneumatic vibration isolators, e.g. in [248] and [249] where models in frequency domain were proposed. In many papers the control procedures were developed in order to obtain desired characteristics of pneumatic actuators. Development of feedback controller with saturation, together with detailed mathematical analysis was presented in [250], while the control strategy aimed at saving energy submitted to pneumatic actuator based on application of inter-chamber valve was proposed in [251]. Moreover, the authors of [252] describe unconventional acceleration-feedback control system with time-delay minimisation for pneumatic actuator and prove its advantages over classical PID controller. Various aspects of design and control of the pneumatic generators including nonlinearity compensation are discussed in [253 254 255].

3.1 Modelling and basic features of pneumatic cylinders

The chapter concerns modelling of impact scenarios for which distribution of gas parameters (especially gas pressure) in considered gas volume becomes uniform relatively fast in comparison to total period of impact and, consequently, the Uniform Pressure Method can be applied. General conditions allowing for reduction of FSI-based model into UPM-based model were already described in Section 2.3 where the Uniform Pressure Method was introduced. In case of pneumatic cylinders, conditions of model simplification have to be considered for the dominating dimension, i.e. for cylinder length. It was estimated that for the analyzed pneumatic cylinders which length equals 10 to 30 cm the Uniform Pressure Method can be applied with acceptable precision when impact velocity is lower than 10m/s.

In terms of spatial dimensionality the UPM model of adaptive pneumatic cylinders can be considered as one-dimensional from the point of view of piston dynamics and zer-dimensional from the point of view of fluid mechanics. Two-dimensional figures of the cylinders are used only for the sake of clarity. The UPM models of pneumatic cylinders subjected to impact loading will be analysed as systems with two mechanical degrees of freedom (displacement of the hitting object and the piston) or, alternatively, as systems with one mechanical degree of freedom when motion of both objects is assumed to be identical.

In general, adaptive pneumatic cylinders can be designed in three main configurations, Fig. 3.1.1. In the simplest type of pneumatic absorber, gas is released in controllable way directly to environment, Fig. 3.1.1a. Although this type of absorber is the most elementary, it will be analyzed in the most precise manner since it can be treated as a basis for development

of models of more sophisticated adaptive inflatable structures such as adaptive airbags. Alternatively, the gas can be transferred into the fixed-volume chamber adjacent to the cylinder (Fig. 3.2.1b) which serves as an accumulator and allows for storage of compressed gas for future usage. In the third option, flow of the gas between two chambers located on both sides of the piston is controlled (Fig. 3.2.1c). For the sake of completeness the numerical models for the three mentioned systems were developed, verified and compared against each other.

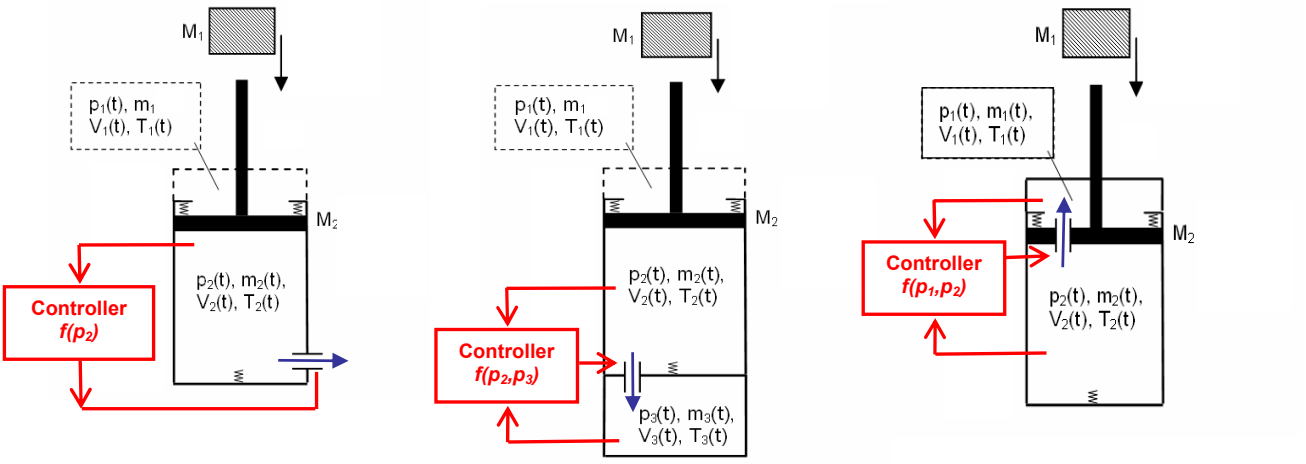

Fig.3.1.1 Various options for design of adaptive pneumatic cylinders

3.1.1 Absorber with exhaust to environment

Numerical model of the adaptive pneumatic cylinder can be obtained from general UPM-based model of adaptive inflatable structure (cf. Chapter 2) by reducing solid body mechanics into rigid motion of the piston. Alternatively, the model can be derived by reducing Navier-Stokes equation, occurring in CFD model of pneumatic cylinder (cf. Chapter 4), to global (integral) balance of gas internal energy in each chamber, equation of the gas state and analytical description of the gas flow through controllable valve.

The simplest pneumatic absorber presented in Fig. 3.1.1a consists of the single air chamber and controllable valve providing communication with the environment. The upper chamber which remains closed will be considered as optional since it plays only a subsidiary role in the process of energy dissipation. Consequently, the systems with and without upper chamber will be considered in parallel. The model is described by equations of motion of the falling mass and the piston, by the balance of gas internal energy which takes into account gas outflow and transfer of heat through cylinder walls, by the equation of the gas flow and, finally, by ideal gas law. Mechanical part of the model reads, cf. Fig. 3.1.2a:

$$M_1 \frac{d^2 u_1}{dt^2} - M_1 g + F_C = 0 \tag{3.1.1}$$

$$M_2 \frac{d^2 u_2}{dt^2} - M_2 g + F_P - F_C - F_D{}^{TOP} + F_D{}^{BOT} + F_{fr} = 0 \tag{3.1.2}$$

where M_1 and M_2 indicate mass of the falling object and mass of the piston, respectively. Equation of motion of the falling mass contains classical terms resulting from inertia and

gravity force, and contact force F_C which arises during collision of the falling mass with the piston rod. Definition of the contact force depends on a type of the contact element located between two colliding bodies. In considered model the contact force F_C is defined as:

$$F_C = F_C^* \quad \text{if} \quad u_1 - u_2 - d_0 \geq 0 \quad \text{and} \quad F_C^* \geq 0; \qquad F_C = 0 \quad \text{otherwise} \tag{3.1.3}$$
$$F_C^* = k(u_1 - u_2 - d_0)^n + c(u_1 - u_2 - d_0)(\dot{u}_1 - \dot{u}_2)$$

where k, c, n are constant coefficients and d_0 is initial distance between the falling mass and the piston rod. The damping term of the contact force depends not only on relative velocity of the colliding bodies, but also on deformation of the contact element. This approach allows to avoid jump of contact force at the time instant of collision, which occurs when classical model with viscous damping is used. The above model enables to obtain characteristic change of contact force with clear distinction of two stages of the process (cf. Fig. 3.1.2).

The main term of equation of piston motion is the pneumatic force F_P which for a single-chamber absorber is defined as a difference of internal cylinder pressure and external ambient pressure, multiplied by the total area of the piston A_2 (Fig. 3.1.2a):

$$F_P = (p_2 - p_A)A_2 \tag{3.1.4a}$$

Although the attention will be paid to the system with single chamber, the model can be easily modified to describe double-chamber system containing upper closed chamber located above the piston. In such a case, global pneumatic force is defined as a difference of pneumatic forces acting on both sides of the piston (pressures multiplied by area of the piston inside lower and upper chamber, A_2 and A_1, respectively) and, moreover, it takes into account the ambient pressure which acts on the cross-sectional area of the piston rod:

$$F_P = p_2 A_2 - p_1 A_1 - p_A(A_2 - A_1) \qquad \text{if upper chamber exists} \tag{3.1.4b}$$

Top delimiting force F_D^{TOP} confines upward movement of the cylinder piston to the maximal length of the cylinder. Moreover, when initial pressure is substantially higher than ambient pressure, top delimiting force contributes to the equilibrium of the piston at the initial configuration (before impact of the external object). On the contrary, the bottom delimiting force F_D^{BOT} is activated at final part of the stroke to protect the piston against hitting bottom of the cylinder. Delimiting forces are defined as:

$$F_D^{TOP} = -k_D(u_2 - u_2^{\min}) \quad \text{if} \quad u_2 < u_2^{\min} \quad \text{and} \quad F_D^{TOP} = 0 \quad \text{if} \quad u_2 \geq u_2^{\min} \tag{3.1.5}$$
$$F_D^{BOT} = k_D(u_2 - u_2^{\max}) \quad \text{if} \quad u_2 > u_2^{\max} \quad \text{and} \quad F_D^{BOT} = 0 \quad \text{if} \quad u_2 \leq u_2^{\max}$$

In mathematical sense delimiting forces allow to avoid oddity which occurs when piston reaches external positions in the cylinder. In addition, equation of piston motion contains force F_{fr} indicating friction which occurs between piston and cylinder walls. In static case when external forces F^{ext} acting on the piston are below level of critical friction force F_{fric}^{crit}, the force F_{fr} provides equilibrium of the piston. In case when the piston is in motion, the friction force may, in general, depend on piston velocity, actual position of the piston and actual value of cylinder pressure. However in considered model, friction is defined in a simplified way as Coulomb friction or velocity dependant friction:

$$F_{fr} = \mp F^{ext} \quad \text{if} \quad \left|F^{ext}\right| \le F_{fric}^{crit} \tag{3.1.6}$$

$$\left\{F_{fr} = c_{fr}\frac{du_2}{dt}\right\} \text{ or } \left\{F_{fr} = F \text{ if } \frac{du_2}{dt} \ge 0 \text{ and } F_{fr} = -F \text{ if } \frac{du_2}{dt} < 0\right\}$$

The following equations describing adaptive pneumatic cylinder are exactly the same as in case of any structure described by the Uniform Pressure Method. Nevertheless, they will be briefly recalled and specified to the case of considered pneumatic cylinder. Gas filling both cavities is described by the ideal gas law in its classical form:

$$p_1V_1 = m_1RT_1 \quad \text{where } V_1 = A_1(h_{01} + u_2) \quad \text{if upper chamber exists} \tag{3.1.7}$$

$$p_2V_2 = m_2RT_2 \quad \text{where } V_2 = A_2(h_{02} - u_2)$$

More complicated types of equations of gas state can be easily incorporated into the model. It will be arbitrarily assumed that gas satisfies the above equations in the whole range of operation (pressures and temperatures), i.e. no phase transitions occurs.

Controllable outflow of the gas is in general defined by the equation:

$$\dot{m}_2 = f(p_2, T_2, p_A, C(t)) \tag{3.1.8a}$$

which indicates dependence of the mass flow rate of gas on pressure and temperature of the gas inside cylinder, external (ambient) pressure and time-dependent parameter defining opening of the valve $C(t)$. The above equation will be often assumed in a simple form which relates mass flow rate to pressure difference by resistance coefficients $C_V(t)$ and $C_H(t)$:

$$\Delta p = p_2 - p_A = -C_V(t)\dot{m}_2 - C_H(t)\dot{m}_2\left|\dot{m}_2\right| \tag{3.1.8b}$$

Such a simple model is applied because at this stage of considerations the type, construction and precise geometry of the valve are not known. Although this simple model neglects many sophisticated phenomena related to flow of the fluid (including blocking of the outflow velocity at certain pressure ratio), it can be successfully used for investigating the basic dynamic characteristics of adaptive pneumatic cylinders. For more precise considerations the Saint-Venant model of the flow (Eq. 2.3.28) should be applied, or properties of the flow through a particular valve should be determined experimentally.

Energy conservation law is considered in a full form involving gas internal energy U, global work done by gas W, energy transferred to the system in the form of heat Q, and enthalpy of added/removed gas (H_{in}, H_{out}):

$$dQ + dm_{in}\overline{H}_{in} - dm_{out}\overline{H}_{out} = d(m\overline{U}) + dW \tag{3.1.9}$$

where specific gas enthalpy, specific gas energy and work done by gas are defined as:

$$\overline{H}_{in} = c_pT_{in}; \quad \overline{H}_{out} = c_pT; \quad \overline{U} = c_VT \; ; \quad dW = pdV \tag{3.1.10}$$

Since analyzed cylinder contains only one valve, only one enthalpy term is active at the particular time instant of the process. In a typical case when gas is released from the cylinder ($p_2 > p_A$), Eq. 3.1.9 contains only the term indicating enthalpy of the gas removed from the cylinder. By contrast, the term related to added enthalpy is present only in case when gas from

the environment is entering the cylinder ($p_2<p_A$). Flow of heat across cylinder walls is described by Newton's law of cooling:

$$\frac{dQ}{dt} = \lambda A_W(u_2)(T_{ext} - T) \tag{3.1.11}$$

where λ indicates mean heat conductivity coefficient and A_W indicates area of the cylinder wall through which heat transfer occurs, which depends on actual position of the piston. If upper chamber of the cylinder is also considered, the corresponding energy conservation law is very similar, however it does not contain any enthalpy terms because the chamber contains fixed amount of gas.

Initial conditions are imposed on initial position and the velocity of falling object and the piston and initial parameters of the gas inside the cylinder (two parameters are independent):

$$u_1(0) = u_1^0, \quad \frac{du_1}{dt}(0) = V_1^0, \quad u_2(0) = u_2^0, \quad \frac{du_2}{dt}(0) = 0, \quad p(0) = p_{02}, \quad T(0) = T_{02} \tag{3.1.12}$$

Static equilibrium of the piston in the initial state is usually provided either by friction force or delimiting force. Equations (3.1.1-3.1.12) together with the definition of time variation of the flow resistance coefficients fully define the problem of impact subjected pneumatic cylinder with exhaust to environment. The model of the system equipped with upper closed chamber can be obtained in straightforward way by describing the upper chamber by equations (3.1.4b, 3.1.7b, and 3.1.9-3.1.11).

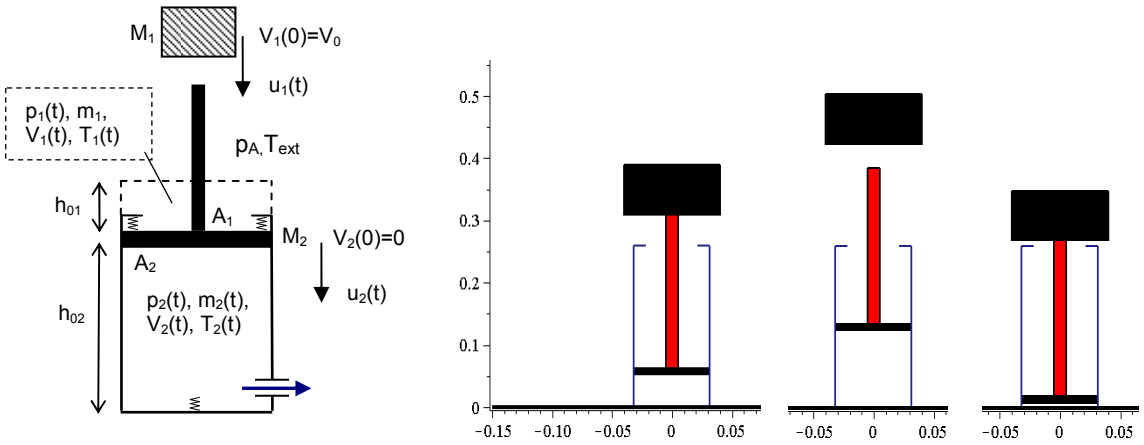

Fig.3.1.2a Pneumatic cylinder with exhaust to environment: a) scheme of the system, b) simulation conducted in MAPLE software (t=0.13s, t=0.29s, t=0.58s, cf. Fig. 3.1.2b)

The resulting system of differential algebraic equations can be easily transformed into system of four differential equations by incorporating the ideal gas law into other equations. The main variables of the problem and the corresponding initial conditions can be chosen arbitrarily among u_1, u_2, m_2, p_2 and T_2. The resulting system of equations was implemented in mathematical software MAPLE, and the fourth order Runge-Kutta method was used for obtaining numerical solution. Exemplary response of the pneumatic absorber with adiabatic walls, constant valve opening (Eq. 3.1.8b with $C_V \neq 0$ and $C_H = 0$) and with neglected friction force is presented in Fig. 3.1.2b and Fig. 3.1.2c.

The response of the pneumatic system can be divided into two parts: the local response and the global response. The main phenomenon that can be classified as 'local' is bouncing of the piston from the falling mass which occurs at the very beginning of the impact process. Therefore, contact force and piston kinematics can be classified as ‘local quantities’. On the contrary, the main global process is a change of force generated by the absorber which causes stopping of the impacting object. Consequently, mass kinematics, pressure values and energy dissipation can be classified as ‘global quantities’. Characteristic property of the system is that it can be divided into two phases which can be distinguished on the basis of local quantities (cf. Fig. 3.1.2b):

- the first stage when the piston bounces from the falling mass and large oscillations of the contact force occurs,
- the second stage of impact which is more stationary since falling mass is moving together with the piston (until rebound of the falling object occurs).

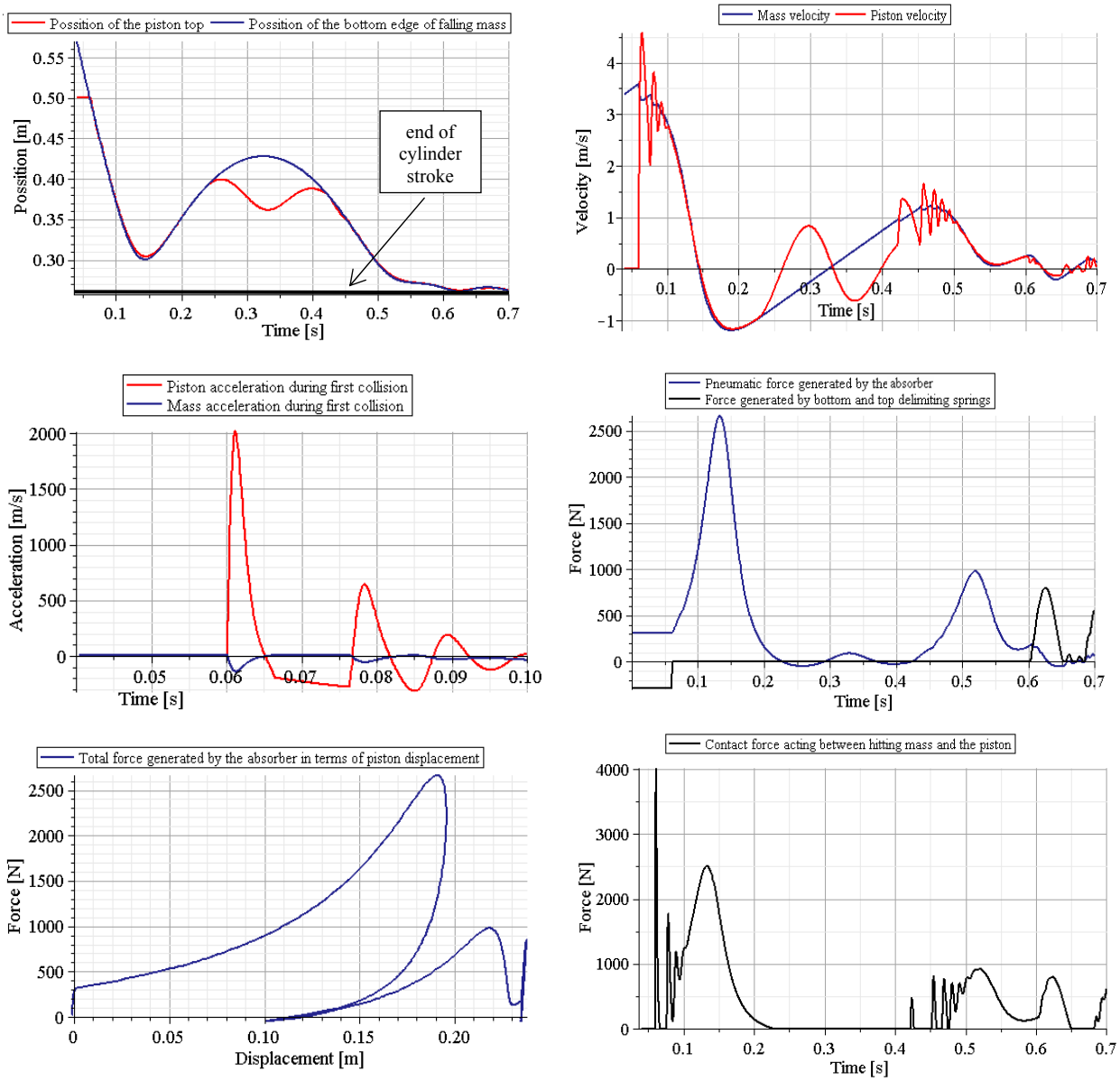

Fig.3.1.2b Results of the analysis (mechanical part): a, b, c) kinematics of the system; d, e) force generated by the absorber, f) contact force between falling mass and piston rod

The phenomena occurring during the first stage of impact are the straightforward consequence of low value of force generated by the absorber at the beginning of the process (which is approximately proportional to initial pressure). Initial rebounds of the piston are clearly seen both in variation of contact force and in kinematics of the system. This phenomenon does not occur in typical hydraulic absorbers where force generated at the beginning of the impact process is high as dependent on velocity of the impacting object.

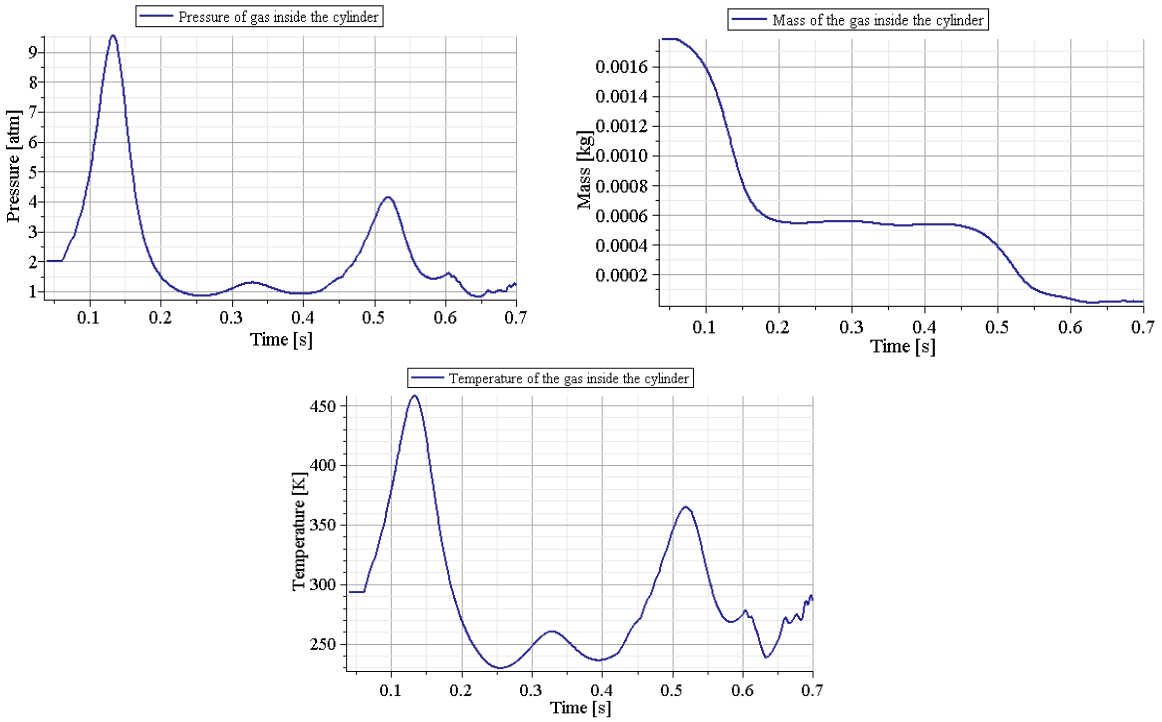

Fig.3.1.2c. Results of the analysis (thermodynamic part): a) pressure inside the cylinder, b) mass of the gas inside the cylinder, c) temperature of the gas inside the cylinder

During the whole impact process pressure inside cylinder and pneumatic force generated by the absorber are affected by two main counteracting processes, i.e. compression of the cylinder by movement of the piston and release of gas through the valve. At the beginning of impact the effect of chamber compression is intensive due to high piston velocity and the effect of gas release is weak due to low pressure difference between cylinder and environment. Consequently, pressure inside cylinder and pneumatic force acting on the piston are increasing. As the impact proceeds, the intensity of both processes tends to equalise, and pneumatic force reaches its maximum. In the subsequent short part of the process pneumatic force decreases since effect of gas release prevails over the process of chamber compression.

In considered case the valve opening is (purposefully) not sufficient for total reduction of pressure inside cylinder, and backward movement of the piston occurs. During this stage reduction of pressure is caused by both chamber expansion and gas release. At the time of 0,24s the impacting object rebounds from the piston and further it is subjected only to gravitational force. After subsequent contact with the piston (at time of 0,42s) the process of cylinder compression repeats, however due to lower velocity of the impacting object, smaller value of maximal pressure is obtained. In this case pressure can be reduced to ambient

pressure without backward movement of the piston. Impacting mass moves together with the piston until the bottom of the cylinder is reached.

Let us start investigation of the **dissipative properties of the pneumatic system** with mathematical analysis of the governing equations based on general theory of dynamical systems. In this approach the main utilized quantity will be kinetic energy of the impacting object and potential energy of the gas spring, while the usage of thermodynamic quantities will be limited to required minimum. Temporarily, we will consider one degree of freedom model of pneumatic absorber which is located horizontally and generates exclusively pneumatic force. Although such a system is not fully equivalent to the original one, it provides basic insight on properties of single chamber pneumatic cylinders with variable mass of gas. Introduced system is described by equation of impacting mass motion, balance of internal gas energy and ideal gas law (already introduced into other equations):

$$M\ddot{u} + \left(\frac{mRT}{(h_0 - u)A} - p_A \right) A = 0 \tag{3.1.13a}$$

$$\lambda A_W(u)(T_{ext} - T) + \dot{m}c_p T + \dot{m}c_p T_{in} = \dot{m}c_V T + mc_V \dot{T} - \frac{mRT}{h_0 - u}\dot{u} \tag{3.1.13b}$$

$$\text{IC: } u(0) = u_0,\ \dot{u}(0) = V_0,\ T(0) = T_0 = T_{ext} \tag{3.1.13c}$$

Since the cylinder contains one valve the enthalpy terms in Eq. 3.1.13b (the 2nd and 3rd one) should be considered interchangeably. The inflow/outflow of the gas from the cylinder is assumed to be predefined and thus equation defining mass exchange is purposefully not considered. Let us analyse more precisely the general formula defining pneumatic force generated by the absorber, which determines its global characteristics:

$$F_p(u,t) = \left(\frac{m(t)RT(t)}{(h_0 - u)A} - p_A \right) A \tag{3.1.14a}$$

At the first sight, the Eq.3.1.14a reveals that from the mechanical point of view the system is characterized by variable in time nonlinear stiffness which depends on two parameters: mass of the gas and temperature of the gas inside cylinder. However, the above statement holds true only when equation of motion (3.1.13a) is analyzed individually and mass and temperature of the gas are treated as two independent parameters. In the problem considered the temperature of gas is not an independent, externally controlled quantity but it is governed by Eq. 3.1.13b and depends on displacement of the piston, mass of the gas inside cylinder and time. Thus, more precise definition of the pneumatic force reads:

$$F_p(u,t) = \left(\frac{m(t)RT(u,m,t)}{(h_0 - u)A} - p_A \right) A \tag{3.1.14b}$$

Due to presence of time-dependent coefficients the considered system is non-conservative.

Total mechanical energy of the analyzed system is composed of kinetic energy of the impacting mass and potential energy of the pneumatic system. Since the system is non-conservative, the potential energy can be defined only for the alternate system which is equivalent to the primal one at considered time instant and which, moreover, is conservative.

Here, the potential energy will be defined as work that can be done by alternate conservative system with time-independent parameters (i.e. actual mass of the gas and gas temperature dependent exclusively on piston displacement) during transition from actual state ($\overline{u},\overline{m},\overline{p}$) to state of static equilibrium with the environment ($u_{eq}, m_{eq}=\overline{m}, p_{eq}=p_A$):

$$E_p(\overline{u}) = -\int_{\overline{u}}^{u_{eq}} \widetilde{F}_p(u)du = -\int_{\overline{u}}^{u_{eq}} \left(\frac{\overline{m}R\widetilde{T}(u)}{(h_0-u)A} - p_A \right) A du \tag{3.1.14c}$$

For isothermal and adiabatic systems (defined by heat transfer coefficient $\lambda \to \infty$ and $\lambda = 0$, respectively) the function describing change of temperature in terms of piston displacement $\widetilde{T}(u)$ is obtained from Eq. 3.1.13b by setting $\dot{m}=0$. Resulting change of temperature equals:

$$\widetilde{T}(u) = T_0 \quad \text{or} \quad \widetilde{T}(u) = \overline{T}\left(\frac{h_0-u}{h_0-\overline{u}} \right)^{1-\kappa} \tag{3.1.14d}$$

and substituted to definition of the potential energy Eqs. 3.1.14c leads to classical formulae defining work of gas under isothermal and adiabatic conditions. For the system with general model of heat transfer through cylinder walls, the only value of λ which provides that the alternate system is conservative is $\lambda = 0$ and, consequently, definition of the potential energy utilizes function of temperature change defined by Eq. 3.1.14d$_2$.

Mechanical energy of the considered pneumatic system remains constant when the explicit dependence of pneumatic force on time in Eq. 3.1.14b vanishes, i.e. when:

$$F_p(u) = \left(\frac{m_0 R T_0}{(h_0-u)A} - p_A \right) A \quad \text{or} \quad F_p(u) = \left(\frac{m_0 R T(u)}{(h_0-u)A} - p_A \right) A \tag{3.1.14e}$$

The above conditions are fulfilled for isothermal and adiabatic systems with constant mass of gas where during the entire process change of temperature is defined by Eqs. 3.1.14d . In above case two terms resulting from integration of equation of motion (3.1.13a) over displacement denote change of kinetic and potential energy and consequently total mechanical energy is constant during the process.

By contrast, in case of system described by general form of Eq.3.1.13b, the total mechanical energy is not conserved since mass and temperature of gas change in terms time. Two mechanisms which typically occur during impact are:

1. exchange of energy with the environment in the form of heat which changes temperature of gas inside cylinder,
2. exchange of energy with the environment in the form of enthalpy which changes mass of the gas inside cylinder and simultaneously changes its temperature.

Let us initially focus on the first case when mass of the gas remains constant and the only mechanism of energy exchange is heat transfer through cylinder walls. In such situation the pneumatic force generated by the absorber is described by the equation:

$$F_p(u,t) = \left(\frac{m_0 R T(u,t)}{(h_0-u)A} - p_A \right) A \tag{3.1.14f}$$

Mechanical energy of the system is dissipated when heat transfer through cylinder walls causes decrease of absolute value of total pneumatic force acting on the mass $F_p(u)$. Taking

into account reduced form of the energy balance ($\Delta Q = \Delta U$) and definition of heat transfer (Eq. 3.1.11) we conclude that energy dissipation occurs in two cases: i) $p > p_A$ and $T > T_{ext}$, ii) $p < p_A$ and $T < T_{ext}$. In other possible combinations of temperature and pressure, which may occur during oscillatory movement of the piston, mechanical energy increases. Since the occurrence of the first situation prevails over the second one, the process is dissipative and leads to damping of the piston movement. It is worth noticing that there is no direct relation between change of internal gas energy and change of mechanical energy of the system.

In the following step the function $T(u,t)$ will be determined. In considered case the equation of energy balance (Eq. 3.1.13b) takes the form:

$$\lambda A_W(u)(T_{ext} - T) = m_0 c_V \dot{T} - \frac{m_0 RT}{h_0 - u}\dot{u}A \tag{3.1.14g}$$

General analytical solution of the above equation for the function $T(t)$ reads:

$$T(u,t) = f\left(\int_0^t u(\bar{t})d\bar{t}, u(t), \lambda, t\right) \tag{3.1.14h}$$

which indicates that pneumatic force can be written in the form:

$$F_p(u,t) = \left(\frac{m_0 R}{(h_0 - u)A} f\left(\int_0^t u(\bar{t})d\bar{t}, u(t), \lambda, t\right) - p_A\right)A \tag{3.1.14i}$$

The above formula reveals the non-locality of the pneumatic force in terms of piston displacement. Pneumatic force at certain time instant is not expressed exclusively in terms of actual position of the piston but instead it depends on integral of piston displacement over time and hence it depends on time history of the process.

In extreme cases of isothermal and adiabatic systems the definition of the pneumatic force (3.1.14i) can be written in a concise form:

$$F_p(u) = \left(p_0\left(\frac{h_0 - u_0}{h_0 - u}\right)^{\kappa} - p_A\right)A \tag{3.1.14j}$$

with $\kappa = 1$ and $\kappa = 1.4$, respectively. The above result indicates that in two extreme cases of heat transfer the pneumatic system with closed valve is conservative and pneumatic force depends exclusively on piston displacement. In both cases system characteristics can be considered as non-linear elastic.

In the second case the dissipation occurs only due to exchange of gas with the environment the pneumatic force is defined as:

$$F_p(u,m) = \left(\frac{m(t)RT(u,m)}{(h_0 - u)A} - p_A\right)A \tag{3.1.14k}$$

Taking into account reduced form of the energy balance ($\Delta H = \Delta U$) and dependence of the direction of the gas flow on the actual pressure difference between cylinder and environment it can be concluded that dissipation of mechanical energy occurs during the whole considered process, both when $p > p_A$ and $p < p_A$. Again, change of mechanical energy of the system is substantially different that change of internal gas energy which conversely decreases and increases in two mentioned cases, respectively.

In the following step of the analysis the function $T(u,m)$ can be determined from the internal energy balance. The cases of gas inflow and outflow have to be considered separately. In case of adiabatic process with outflow only, gas temperature is defined explicitly in terms of actual mass of the gas and volume of the chamber by Eq. 2.3.20b. The definition of the pneumatic force (Eq. 3.1.14k) simplifies to the form:

$$F_p(u,m)=\left(C\left(\frac{m(t)}{(h_0-u)A}\right)^{\kappa}-p_A\right)A \quad \text{where} \quad C=p_0\left(\frac{V_0}{m_0}\right)^{\kappa}=RT_0\left(\frac{m_0}{V_0}\right)^{1-\kappa} \tag{3.1.14l}$$

By contrast, for adiabatic process with inflow of the gas from the environment gas temperature has to be determined by integration of the Eq. (2.3.19b) and equals:

$$T(u,m)=\frac{1}{m(t)}\left(\kappa T_A\int_0^t\left[(h_0-u)A\right]^{\kappa-1}\dot{m}(\bar{t})d\bar{t}+\frac{T_0m_0}{(h_0A)^{1-\kappa}}\right)\left[(h_0-u)A\right]^{1-\kappa} \tag{3.1.14m}$$

Substitution of the above temperature to Eq. 3.1.14k yields:

$$F_p(u,m)=\left(\left(\kappa RT_A\int_0^t\left[(h_0-u)A\right]^{\kappa-1}\dot{m}(\bar{t})d\bar{t}+\frac{p_0}{(h_0A)^{-\kappa}}\right)\left[(h_0-u)A\right]^{-\kappa}-p_A\right)A \tag{3.1.14n}$$

Finally for isothermal process with outflow or inflow of gas (where transfer of heat occurs, however does not cause dissipation of mechanical energy) the pneumatic force equals:

$$F_p(u,m)=\left(\frac{m(t)RT_0}{(h_0-u)A}-p_A\right)A \tag{3.1.14o}$$

In case of adiabatic process with outflow only (3.1.14l) and in case of isothermal process (3.1.14o), variation of the pneumatic force in time is expressed exclusively in terms of actual mass of the gas inside the cylinder. By contrast, Eq. 3.1.14n reveals the time non-locality of the pneumatic force in terms of mass of the gas and piston displacement which indicates that pneumatic force depends on the whole time-history of the process.

In the extreme case when valve is closed and mass of the gas remains constant, both adiabatic and isothermal system can be treated as systems with constant nonlinear stiffness which are conservative and no dissipation of mechanical energy takes place. By contrast, when the valve is fully open, no force is generated by the absorber. For two mentioned above extreme cases of the valve opening the pneumatic force equals:

$$F_p^{\max}(u)=\left(C\left(\frac{m_0}{(h_0-u)A}\right)^{\kappa}-p_A\right)A, \qquad F_p^{\min}(u)=0 \tag{3.1.14p}$$

All characteristics of the absorber which can be obtained for intermediate valve opening are located between two above functions. Although for the extreme valve positions the dissipation of the energy does not occur, the system with any intermediate valve opening is dissipative.

Let us further come back to original system of the equations governing 2DOF model (Eq. 3.1.1, Eq. 3.1.2) to derive **global balance of the system energy.** In all above equations the indices '2' related to thermodynamic quantities will be omitted in order to simplify

notation. By integrating equation of mass motion over displacement u_1 and equation of piston motion over displacement u_2 we obtain:

$$\int_{u_1^0}^{u_1} M_1 \frac{d^2\overline{u_1}}{dt^2}\, d\overline{u_1} - \int_{u_1^0}^{u_1} M_1 g\, d\overline{u_1} + \int_{u_1^0}^{u_1} F_C\, d\overline{u_1} = 0 \tag{3.1.15a}$$

$$\begin{aligned}\int_{u_2^0}^{u_2} M_2 \frac{d^2\overline{u_2}}{dt^2}\, d\overline{u_2} - \int_{u_2^0}^{u_2} M_2 g d\overline{u_2} + \int_{u_2^0}^{u_2} (p - p_A) A d\overline{u_2} - \int_{u_2^0}^{u_2} F_C d\overline{u_2} + \\ - \int_{u_2^0}^{u_2} F_D^{TOP} d\overline{u_2} + \int_{u_2^0}^{u_2} F_D^{BOT} d\overline{u_2} + \int_{u_2^0}^{u_2} F_{fr} d\overline{u_2} = 0\end{aligned} \tag{3.1.15b}$$

The above energy balance can be written in an equivalent form:

$$\Delta E_k^1 + \Delta E_p^1 - W_C^1 = 0 \tag{3.1.15c}$$

$$\Delta E_k^2 + \Delta E_p^2 - W_{Fp} - W_C^2 - W_D^{TOP} - W_D^{BOT} - W_{fr} = 0 \tag{3.1.15d}$$

where $\Delta E_k^{1(2)}$ and $\Delta E_p^{1(2)}$ indicate changes of kinetic and potential energy of the falling mass and the piston, W_C^1 denotes work done by contact force on mass displacement and W_C^2 denotes work done by contact force on piston displacement:

$$W_C^1 = -\int_{u_1^0}^{u_1} F_C\, d\overline{u_1}, \qquad W_C^2 = \int_{u_2^0}^{u_2} F_C\, d\overline{u_2} \tag{3.1.16}$$

In considered problems the work W_C^1 is usually large since it corresponds to change of energy of the falling object. The term W_{Fp} indicates work done by total pneumatic force on piston displacement:

$$W_{Fp} = -\int_{u_2^0}^{u_2} (p - p_A)\, A d\overline{u_2} = \int_{V_0}^{V} (p - p_A)\, d\overline{V} = W + W_{pA} \tag{3.1.17}$$

Moreover, W_D^{TOP}, W_D^{BOT} and W_{fr} denotes work done by the top delimiting force, bottom delimiting force and friction force, respectively. The friction force will be usually assumed as relatively small or it will be completely neglected in order to focus on the 'pneumatic part' of the process. Summation of both energy conservation equations gives:

$$\Delta E_k^1 + \Delta E_p^1 + \Delta E_k^2 + \Delta E_p^2 - W_{Fp} - W_C - W_D^{TOP} - W_D^{BOT} - W_{fr} = 0 \tag{3.1.18}$$

where ΔE_k and ΔE_p denote changes of the kinetic and the potential energy of the system, while W_C indicates work done by the contact force on difference of both objects displacements:

$$W_C = W_C^1 + W_C^2 = \int_{u_2^0}^{u_2} F_C\, d\overline{u_2} - \int_{u_1^0}^{u_1} F_C\, d\overline{u_1} \tag{3.1.19}$$

Alternatively, mechanical part of the problem can be simplified by reducing the falling mass and the piston to a single degree of freedom and by assuming their common displacements during the impact process (delimiting forces are also neglected):

$$M\frac{d^2u}{dt^2} - Mg + (p - p_A)A + F_{Fr} = 0 \tag{3.1.20a}$$

In above equation M is sum of mass of the falling object and the piston and, moreover, initial velocity should be assumed as velocity resulting from inelastic collision of falling mass and piston. The above approach is especially justified for modelling the second part of the process which occurs after initial rebounds of the piston. Integration of the equation of motion (3.1.20a) leads to a very simple and intuitive form of the energy balance:

$$\int_{u_0}^{u} M\frac{d^2\bar{u}}{dt^2}\,d\bar{u} - \int_{u_0}^{u} Mg\,d\bar{u} + \int_{u_0}^{u}(p - p_A)A\,d\bar{u} + \int_{u_0}^{u} F_{fr}\,d\bar{u} = 0 \tag{3.1.20b}$$

which indicates that kinetic and potential energy of the falling object is changed into work done by gas and friction force:

$$\Delta E_k + \Delta E_p - W_{Fp} - W_{fr} = 0 \tag{3.1.20c}$$

Work done by total pneumatic force on piston displacement can be calculated from Eq.3.1.17 by changing integral over volume into time integral and by applying ideal gas law:

$$W_{Fp} = \int_{t_0}^{t} p\frac{dV(m,R,T,p)}{dt}dt - p_A\left(V - V_0\right) \tag{3.1.21a}$$

which after simple manipulations, adding and subtracting arbitrary term $\int_{t_0}^{t}\dot{m}c_pT_{in}dt$ yields:

$$W_{Fp} = -\int_{t_0}^{t}(\dot{m}c_VT + mc_V\dot{T})dt + \int_{t_0}^{t}\dot{m}c_pT_{in}dt + \int_{t_0}^{t}\left(-\dot{m}c_p(T_{in} - T) - \frac{\dot{p}}{p}mRT + mc_p\dot{T}\right)dt - p_A\left(V - V_0\right) \tag{3.1.21b}$$

where T_{in} indicates temperature of the gas entering the fluid cavity. In case when only outflow of the fluid occurs (and in an arbitrary case when gas entering the cylinder has the same temperature as gas inside the cylinder, i.e. $T_{in} = T$), the above formula simplifies to the form:

$$W_{Fp} = -\int_{t_0}^{t}(\dot{m}c_VT + mc_V\dot{T})dt + \int_{t_0}^{t}\dot{m}c_pTdt + \int_{t_0}^{t}\left(-\frac{\dot{p}}{p}mRT + mc_p\dot{T}\right)dt - p_A\left(V - V_0\right) \tag{3.1.21c}$$

Four terms occurring in the equations (3.1.21b and 3.1.21c) indicate change of gas internal energy $-\Delta U$, enthalpy of the gas added (removed) from the system ΔH, energy transferred to the system in the form of heat ΔQ and work done by ambient pressure W_{pA}:

$$W_{Fp} = -\Delta U + \Delta H + \Delta Q + W_{pA} \tag{3.1.22a}$$

The above equation is obviously in agreement with the energy balance (Eq. 3.1.9). The Eq. 3.1.22a can also be expressed in an alternative form which utilizes work done on gas $L = -W$, dissipation of internal energy by change of enthalpy D_H and by heat transfer D_Q:

$$L = \Delta U + \left(D_H + D_Q\right) \tag{3.1.22b}$$

By introducing (Eq. 3.1.22a) into global energy balance (Eq. 3.1.20c) we obtain:

$$\Delta E_k + \Delta E_p - W_{pA} = -\left(\Delta U + D_H + D_Q + D_{fr}\right) \tag{3.1.23a}$$

The above equation clearly explains transformation of the energy introduced to the system. In typical process of impact absorption, decrease of mechanical energy of the falling object and work done by external pressure occurs at expense of increase of internal gas energy, energy released from the system in the form of gas enthalpy, energy transferred to the environment in the form of heat, and work done by friction force. From thermodynamic point of view the following processes causing energy dissipation occur simultaneously during piston motion:

- kinetic energy of the falling object is changed into gas internal energy,
- internal gas energy is reduced by transport of gas from the cylinder to the environment (change of internal energy by exchange of enthalpy),
- internal gas energy is reduced by transport of heat from the cylinder to the environment (change of internal energy by heat transfer).

Due to the fact that the whole system is considered in the context of impact absorption, actual value of total energy (sum of mechanical energy of the hitting object and internal energy of gas) is one of the main quantities of interest. Its actual change can be calculated as:

$$\Delta E = \Delta E_k + \Delta E_p + \Delta U = W_{pA} - D_H - D_Q - D_{fr} \tag{3.1.23b}$$

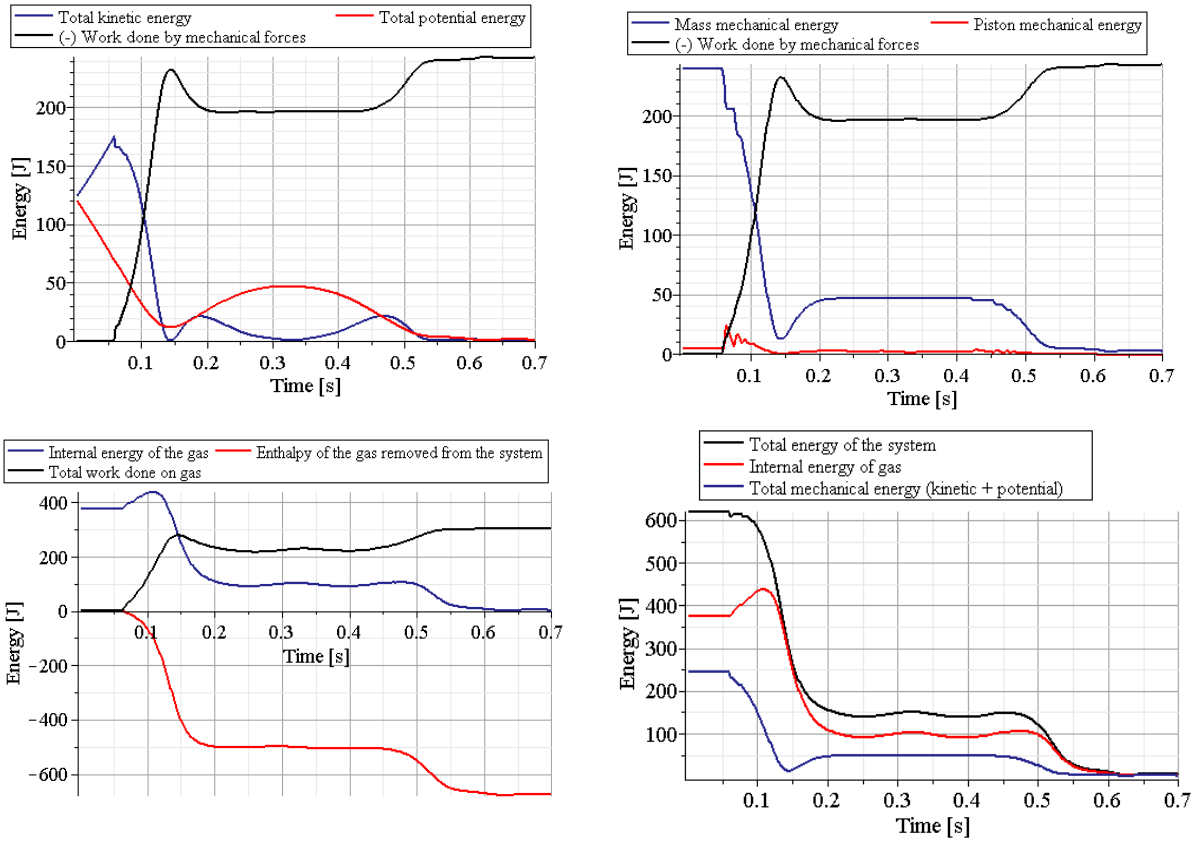

Fig.3.1.3a Analysis of changes of the system energy: a),b) mechanical energy balance (Eq.3.1.18), c) balance of gas internal energy (Eq.3.1.22b), d) dissipation of system energy (Eq.3.1.23a,b)

Although, the Eqs. (3.1.23) and (3.1.24) elucidate balance of kinetic and potential energy of both masses as well as balance of internal gas energy and balance of total system

energy, they do indicate what part of the mechanical energy of the impacting object has been irreversibly changed into other forms of the energy and what part is gathered in compressed gas and will be transferred back to the impacting object.

To resolve this problem we will introduce the quantity X which will be defined as mechanical work that can be done by the absorber during transition from the actual state $(\bar{t},\bar{V},\bar{T},\bar{m})$ to the 'referential state' $(t^{ref},V^{ref},T^{ref},\bar{m})$ in a 'process without intended dissipation'. The 'referential state' is defined as state encountered during rebound stage of impact in which total energy of the hitting object achieves its maximal value. By analyzing equation governing balance of mechanical energy of the impacting object (Eq. 3.1.15) in the form:

$$\Delta E_k + \Delta E_p + \int F_C \dot{u}_1 dt = 0 \tag{3.1.24}$$

we conclude that mechanical energy of the impacting object decreases when the mass moves downward (during forward-stroke) and increases when the mass moves up (during backstroke). Maximal value of mechanical energy is achieved in two cases:

1. when the impacting object rebounds from the piston and contact force completely vanishes: $F_C = 0$,
2. when velocity of the impacting object drops to zero without separating from the piston: $\dot{u}_1 = 0$.

In general, the first condition is encountered during strong rebounds. It occurs either in the middle of the cylinder stroke or when the piston reaches the upper delimiting spring and in both cases it is manifested by separation of the impacting object from the piston. Since the contact spring is short and stiff, the precise condition $F_C = 0$ is equivalent to decrease of total force generated by the absorber to zero and thus the 'referential state' is state of static equilibrium of the piston. In turn, the second condition $\dot{u}_1 = 0$ corresponds to the situation when the gravitational force acting on the impacting object causes that static equilibrium of the piston can not be reached. The second condition becomes valid during slight rebound when both objects are not separated from each other or at the end of the impact process when the mass is stopped. Regardless of the condition satisfied, the 'referential state' will be denoted as $(t^{eq},V^{eq},T^{eq},\bar{m})$.

The ‘process without intended dissipation’ is the process which does not involve purposeful dissipation of the energy (controlled exchange of gas with the environment is not performed) but involves change of system energy caused by transfer of heat to the environment through cylinder walls (which can not be avoided and thus has to be taken into account). Introduced quantity depends, in general, on the process of transition between mentioned two states which is predetermined by parameters and actual state of the system including mass of the impacting object and its actual velocity.

General definition of the quantity X, i.e. work that can be done by pneumatic system during transition $\left(\bar{t} \to t^{eq}\right)$ reads:

$$X(\bar{t}) = W_{Fp}\left(\bar{t} \to t^{eq}\right) = -L_{Fp}\left(\bar{t} \to t^{eq}\right) \tag{3.1.25a}$$

where W_{Fp} indicates work done by pneumatic system and L_{Fp} indicates work done on pneumatic system. The above formula can be specified to the form:

$$X(\bar{t}) = \int_{\bar{t}}^{t^{eq}} \left(p(\overline{m},V,T) - p_A\right)\dot{V}dt = -\int_{\bar{t}}^{t^{eq}} \left(p(\overline{m},u,T) - p_A\right)A\dot{u}dt \tag{3.1.25b}$$

In above formula $\overline{m}$ denotes constant mass of the gas, while T denotes temperature which changes due to heat transfer. The introduced quantity X allows to identify the amount of mechanical energy that can be transferred to the impacting object during the remaining part of the process if intended dissipation will not be further performed. Thus, for system with heat transfer through external walls it constitutes better measure of work performance ability than potential energy introduced in Eq. 3.1.14c. Since X is defined as a 'useful part' of gas energy, i.e. the energy that can be changed into mechanical work it can be referred to as exergy.

Exergy X allows to define total useful energy of the system E^* (as sum of actual mechanical energy and exergy):

$$E^*(\bar{t}) = E_k(\bar{t}) + E_p(\bar{t}) + X(\bar{t}) \tag{3.1.25c}$$

and, by subtracting dissipation by friction $D_{fr}^{t\to t^{eq}}$, the maximal expected value of mechanical energy of the impacting object at subsequent referential state E_{mech}^{eq}:

$$E_{mech}^{eq}(t^{eq}) = E_k(\bar{t}) + E_p(\bar{t}) + X(\bar{t}) - D_{fr}^{t\to t^{eq}} \tag{3.1.25d}$$

Further, exergy can be expressed in terms of gas volume and temperature. By using ideal gas law, and by introducing non-dimensional variable $\xi = V/V_{eq}$ we obtain:

$$X(\bar{t}) = \int_{t}^{t^{eq}} \overline{m}RT\frac{\dot{V}}{V}dt - p_A\left(V^{eq} - \overline{V}\right) = \int_{\bar{t}}^{t^{eq}} \overline{m}RT[\ln(\xi)]'dt - p_A\left(V^{eq} - \overline{V}\right) \tag{3.1.25e}$$

By performing integration by parts and simple manipulations we get the formula:

$$X(\bar{t}) = \overline{m}R\overline{T}\ln\left(\frac{V^{eq}}{\overline{V}}\right) - \int_{\bar{t}}^{t^{eq}} \overline{m}R\dot{T}\ln\left(\frac{V}{V^{eq}}\right)dt - p_A\left(V^{eq} - \overline{V}\right) \tag{3.1.25f}$$

The above defined exergy depends not only on actual and referential state of the system but also on the process of transition between them. Thus, computation of the quantity X at time instant $\bar{t}$ requires preliminary solution of the governing equations in the time period $(\bar{t}, t_{eq})$ with the assumption of constant mass of the gas inside cylinder.

On the contrary, in case of adiabatic process, work done during transition from actual state to the referential state in a process without intended dissipation (which is in this case process without any dissipation) is path-independent. Therefore, exergy depends exclusively on initial and referential state of the system and it is defined as:

$$X = \int_{\bar{t}}^{t^{eq}} \left(\frac{\overline{m}RT(V)}{V} - p_A\right)\frac{dV}{dt}dt = \int_{\overline{V}}^{V^{eq}} \left(\frac{\overline{m}RT(V)}{V} - p_A\right)dV \tag{3.1.26a}$$

By introducing change of temperature during the adiabatic process with constant mass of gas (2.3.21a) we obtain: (the overbars denoting actual state are omitted)

$$X = \frac{mRT}{1-\kappa}\left(\left(\frac{V^{eq}}{V}\right)^{1-\kappa} - 1\right) - p_A\left(V^{eq} - V\right) = mc_V T - mc_V T^{eq} - p_A\left(V^{eq} - V\right) \tag{3.1.26b}$$

Total exergy of the pneumatic system X can be decomposed into specific exergy X^S (related to the gas inside the cylinder) and exergy of the environment X^{env} :

$$X = X^S + X^{env} \tag{3.1.27a}$$

Adiabatic specific exergy assumes positive values when pressure inside the cylinder is larger than external pressure and negative values when pressure inside the cylinder is lower than external pressure. Sign of the exergy of the environment is always opposite to the sign of the specific exergy. Due to the fact that the term corresponding to higher pressure prevails, the total adiabatic exergy is always non-negative. Specific exergy for the adiabatic system has especially simple interpretation since it equals to change of the gas internal energy during transition from the actual state into the state of mechanical equilibrium. The remaining part of gas internal energy (called an anergy A) equals the internal gas energy in the state of mechanical equilibrium with the environment. Thus, internal energy can be decomposed as:

$$U = X^S + A = \left(U - U^{eq}\right) + U^{eq} \tag{3.1.27b}$$

During adiabatic expansion gas exergy decreases (at the expense of work done by gas), its anergy remains constant and, as a result, the internal energy of the gas decreases.

In case of isothermal process work done by pneumatic system also depends exclusively on initial and final state of the system. The formula defining actual exergy of the system takes the form:

$$X = \int_{V}^{V^{eq}} \left(\frac{mRT_0}{V} - p_A \right) dV = mRT_0 \ln\left(\frac{V^{eq}}{V} \right) - p_A\left(V^{eq} - V\right) \tag{3.1.28a}$$

In isothermal system specific exergy equals the heat which can be gathered from the environment in order to perform transition from the actual to equilibrium state. Anergy of the gas equals the difference of its initial energy and the heat transferred from the environment. Internal gas energy can be written as:

$$U = X^S + A = \Delta Q^{V \to V^{eq}} + \left(U - \Delta Q^{V \to V^{eq}}\right) \tag{3.1.28b}$$

During gas expansion, exergy of the gas decreases, but anergy of the gas raises and therefore global internal energy remains constant. Definitions of adiabatic and isothermal exergy (Eq.3.1.26a,b; Eq.3.1.28a) are equivalent to definition of potential energy of pneumatic system (Eq. 3.1.14c), however they may differ with definition of assumed referential state.

Assuming that initial state of the system is not necessarily an equilibrium state we can calculate initial exergy of the system as work that can be done by absorber between the initial state at time t_0 and the corresponding referential state attained at time t_0^{eq} :

$$X_0 = m_0 R T_0 \ln\left(\frac{V_0^{eq}}{V_0} \right) - \int_{t_0}^{t_0^{eq}} m_0 R \dot{T} \ln\left(\frac{V}{V_0^{eq}} \right) dt - p_A\left(V_0^{eq} - V_0\right) \tag{3.1.29a}$$

In case when initial state of the system is a state of static equilibrium the initial exergy X_0 is negative and indicates dissipation of mechanical energy of the impacting object which occurs between initial state and the referential state exclusively due to heat transfer. In case of adiabatic process the corresponding formula takes the form:

$$X_0 = \frac{m_0 R T_0}{1-\kappa}\left(\left(\frac{V_0^{eq}}{V_0}\right)^{1-\kappa} - 1\right) - p_A\left(V_0^{eq} - V_0\right) = mc_V T_0 - mc_V T_0^{eq} - p_A\left(V^{eq} - V\right) \tag{3.1.29b}$$

and in case of isothermal process, it reads:

$$X_0 = m_0 R T_0 \ln\left(\frac{V_0^{eq}}{V_0}\right) - p_A\left(V_0^{eq} - V_0\right) \tag{3.1.29c}$$

For isothermal and adiabatic system initial exergy denotes initial potential energy of the gas spring and it equals zero when the initial state is state of static equilibrium.

The knowledge of actual and initial exergy allow to compute change of exergy during the process $\Delta X = X - X_0$:

$$\Delta X = mRT \ln\left(\frac{V^{eq}}{V}\right) - m_0 R T_0 \ln\left(\frac{V_0^{eq}}{V_0}\right) - \int_t^{t^{eq}} mR\dot{T} \ln\left(\frac{V}{V^{eq}}\right) dt + \int_{t_0}^{t_0^{eq}} m_0 R\dot{T} \ln\left(\frac{V}{V_0^{eq}}\right) dt \tag{3.1.30a}$$
$$- p_A\left(V^{eq} - V_0^{eq}\right) + p_A\left(V - V_0\right)$$

In case of adiabatic process the corresponding formula takes the form:

$$\Delta X = \frac{mRT}{1-\kappa}\left(\left(\frac{V^{eq}}{V}\right)^{1-\kappa} - 1\right) - \frac{m_0 R T_0}{1-\kappa}\left(\left(\frac{V_0^{eq}}{V_0}\right)^{1-\kappa} - 1\right) - p_A\left(V^{eq} - V_0^{eq}\right) + p_A\left(V - V_0\right)$$
$$= mc_V T - mc_V T^{eq} - m_0 c_V T_0 + m_0 c_V T_0^{eq} - p_A\left(V^{eq} - V_0^{eq}\right) + p_A\left(V - V_0\right) \tag{3.1.30b}$$

and in case of isothermal process:

$$\Delta X = mRT_0 \ln\left(\frac{V^{eq}}{V}\right) - m_0 R T_0 \ln\left(\frac{V_0^{eq}}{V_0}\right) - p_A\left(V^{eq} - V_0^{eq}\right) + p_A\left(V - V_0\right) \tag{3.1.30c}$$

Similar formulae can be derived for two arbitrary states of the system during the process. and they allow to investigate change of system exergy caused by change of mass of the gas. The analysis of adiabatic and isothermal systems during simple process which relies on change of the amount of gas without changing actual cylinder volume allows to distinguish four cases:

- removing gas from the cylinder where $p > p_A$: decrease of system exergy
- adding gas to the cylinder where $p > p_A$: increase of system exergy
- removing gas from the cylinder where $p < p_A$: increase of system exergy
- adding gas to the cylinder where $p < p_A$: decrease of system exergy

The above conclusions are in agreement with considerations related to potential energy of the pneumatic system. In two initial cases, where pressure inside cylinder is higher than atmospheric pressure $\left(p > p_A\right)$ change of system exergy is associated with change of specific exergy of gas inside cylinder. Moreover, decrease (increase) of exergy corresponds with decrease (increase) of gas internal energy. When initial pressure is lower than atmospheric pressure $\left(p < p_A\right)$, the effect is reversed. Change of positive exergy of the environment has larger absolute value than change of negative specific exergy and it overrules change of total exergy. In this case change of system exergy is opposite to change of gas internal energy. Let us note that in considered system natural (spontaneous) processes such as removing gas from

cylinder where $p > p_A$, and adding gas to cylinder where $p < p_A$ always lead to decrease of system exergy.

Finally, work done by pneumatic system during transition from the initial state at time instant t_0 to actual state at time t can be calculated as:

$$W_{Fp} = -L_{Fp} = \int_{t_0}^{t} \left(p(m,V,T) - p_A\right)\dot{V}dt \tag{3.1.31a}$$

The intrinsic difference is that now general process with gas outflow is considered $(m \neq const)$ and, consequently, the following formulae have more complicated form. By using ideal gas law the work done by pneumatic system can be expressed as:

$$W_{Fp} = \int_{t_0}^{t} mRT\frac{\dot{V}}{V}dt - p_A\left(V - V_0\right) \tag{3.1.31b}$$

Similarly to previous case, by using non-dimensional variable $\xi = V/V_0$, and by performing integration by parts and simple manipulations, we obtain general formula:

$$W_{Fp} = mRT\ln\left(\frac{V}{V_0}\right) - \int_{t_0}^{t}\left(\dot{m}RT + mR\dot{T}\right)\ln\left(\frac{V}{V_0}\right)dt - p_A\left(V - V_0\right) \tag{3.1.32a}$$

which, in case of adiabatic process with outflow only, takes the form:

$$W_{Fp} = \frac{mRT_0}{1-\kappa}\left(\left(\frac{m}{m_0}\right)^{\kappa}\left(\frac{V}{V_0}\right)^{1-\kappa} - 1\right) - \int_{t_0}^{t} C\frac{d(m^{\kappa})}{dt}\frac{V^{1-\kappa}}{1-\kappa}dt - p_A\left(V - V_0\right) = \tag{3.1.32b}$$

$$- mc_V T + mc_V T_0 - \int_{t_0}^{t} p_0\left(\frac{V_0}{m_0}\right)^{\kappa}\frac{d(m^{\kappa})}{dt}\frac{V^{1-\kappa}}{1-\kappa}dt - p_A\left(V - V_0\right)$$

where constant C is defined by Eq. 3.1.14l. Finally, in case of isothermal process Eq. 3.1.32a simplifies to:

$$W_{Fp} = mRT_0\ln\left(\frac{V}{V_0}\right) - \int_{t_0}^{t}\dot{m}RT\ln\left(\frac{V}{V_0}\right)dt - p_A\left(V^{eq} - V_0^{eq}\right) \tag{3.1.32c}$$

The above introduced quantities allow to define two measures of pneumatic dissipation at arbitrary time instant t. The first one, D_1, denotes pneumatic dissipation of mechanical energy of the impacting object and it is calculated as difference between work done on pneumatic system L_{Fp} at time period (t_0, t) and actual exergy X denoting energy that could be retrieved from pneumatic system at time period (t, t^{eq}):

$$D_1(t) = L_{Fp}(t) - X(t) \tag{3.1.33}$$

According to the above definition D_1 denotes sum of total pneumatic dissipation (intentional by gas release and spontaneous by heat transfer) before time t and spontaneous dissipation until the referential state indicating maximal energy of the impacting object is reached.

The second proposed measure of dissipation, D_2, denotes pneumatic dissipation of total useful energy of the system understood as sum of mechanical energy of the impacting

object and exergy of the pneumatic system (cf. Eq.3.1.25c). Thus, it involves both change of mechanical energy of the impacting object caused by pneumatic force L_{Fp} and change of exergy between actual and initial time instant of the process $\Delta X = X - X_0$:

$$D_2(t) = L_{Fp}(t) - \Delta X(t) = (L_{Fp}(t) - X(t)) + X_0 \tag{3.1.34}$$

In comparison to previous measure of dissipation, D_2 additionally contains initial exergy X_0 which accounts for initial useful energy gathered in gas spring and dissipation which occurs in a closed system due to heat exchange. When X_0 is negative, as for system in initial equilibrium but with heat exchange, the quantity D_2 can be interpreted as difference of pneumatic dissipation of mechanical energy in system with and without gas release.

For isothermal and adiabatic systems pneumatic dissipation D_2 can be decomposed into dissipation of the specific exergy and dissipation of the exergy of the environment:

$$D_2 = D_{X^S} + D_{X^{env}} \tag{3.1.35}$$

Dissipation of internal energy D_U and dissipation of the specific exergy D_{X^S} allows to calculate dissipation of the anergy D_A:

$$D_A = D_U - D_{X^S} = \left(D_H + D_Q\right) - D_{X^S} \tag{3.1.36}$$

where D_H indicates dissipation of internal energy by change of mass of the gas, and D_Q indicates dissipation of internal energy by transfer of heat to environment.

By combining equation defining pneumatic dissipation of useful energy (3.1.34) with approximate balance of global energy (3.1.20c) we obtain total change of useful energy ΔE^*:

$$\Delta E^* = \Delta E_k + \Delta E_p + \Delta X = -D_2 - D_{fr} + W_C + W_D^{TOP} + W_D^{BOT} \tag{3.1.37}$$

The above formula clearly indicates that change of useful energy of the system is caused by pneumatic dissipation D_2, direct dissipation of the mechanical energy by friction force D_{fr} and by action of the contact and delimiting forces. Change of the useful energy is substantially different than the change of total energy of the system (Eq. 3.1.23b). In considered problem of adaptive impact absorption, dissipation of useful energy (3.1.37) is more important than dissipation of total energy (3.1.23b) since it directly corresponds to change energy of the impacting object.

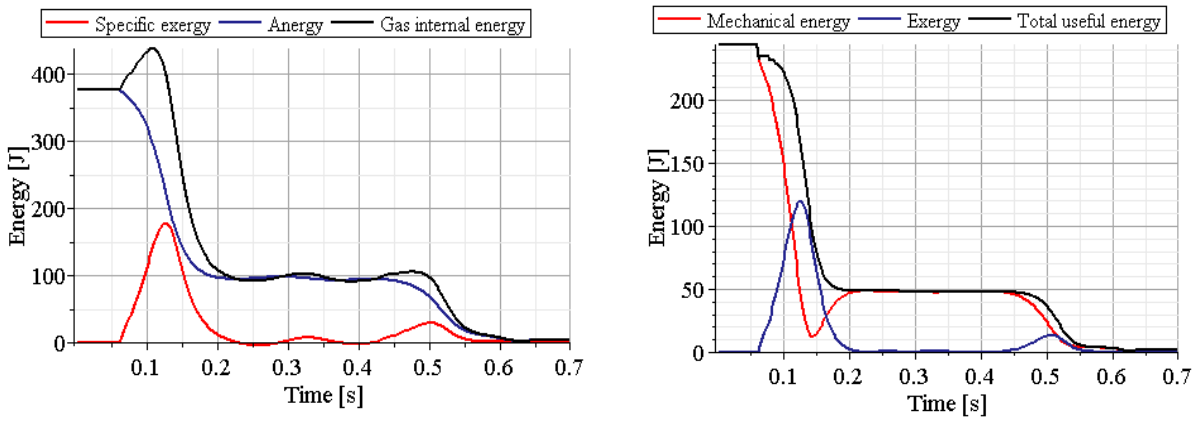

Fig.3.1.3b Analysis based on notions of exergy and anergy: a) division of internal energy into specific exergy and anergy, b) change of mechanical energy, exergy and total useful energy of the system

The figure 3.1.3b corresponds to main numerical example concerning single chamber absorber subjected to impact loading. Since the piston is initially in equilibrium initial exergy equals zero and both measures of dissipation D_1 and D_2 are equivalent and equal to pneumatic dissipation of useful energy. The plot of useful energy in Fig. 3.1.2b$_2$ should be confronted with plot of total energy in Fig. 3.1.2a$_4$. While total energy has no direct correlation with impact absorption, the useful energy indicates what will be the value of impacting object energy if intended dissipation will not be further performed.

Mathematical structure of the system of equations governing a single chamber pneumatic cylinder can be also investigated by using simplified 1DOF model which involves only pneumatic force and assumes isothermal conditions and gas exchange described by the (Eq. 3.1.8b) with $C_V = const.$ and $C_H = 0$:

$$M\ddot{u} + (p - p_A)A = 0 \tag{3.1.38a}$$

$$pA(h_0 - u) = mRT_0, \qquad p - p_A = -C_V\dot{m}$$

$$\text{IC: } u(0) = 0, \dot{u}(0) = V_0, m(0) = m_0$$

By combing ideal gas law with the equation describing the gas flow we obtain a single ODE:

$$C_V\dot{m} + \frac{mRT_0}{A(h_0 - u)} - p_A = 0 \tag{3.1.38b}$$

which can be solved analytically to obtain actual mass of the gas in the cylinder and further, by using ideal gas law, to obtain force exerted on the piston. Equation of mass motion expressed in terms of piston displacement and flow resistance coefficient reads:

$$M\ddot{u} + \frac{\left[\left(\frac{p_A}{C_V}\int_0^t e^{\frac{RT_0}{C_V}\int_0^t \frac{1}{A(h_0-u(t)}dt} dt + m_0\right)e^{\frac{RT_0}{C_V}\int_0^t \frac{1}{A(h_0-u(t)}dt}\right]RT_0}{A(h_0 - u(t))}A - p_A A = 0 \tag{3.1.38c}$$

which can be written in the short form as:

$$M\ddot{u} + f_3\left(\int_0^t f_2\left(\int_0^t f_1(u)dt, C_V\right), \int_0^t f_1(u)dt,\ u,\ C_V\right)A - p_A A = 0 \tag{3.1.38d}$$

Eq. 3.1.38c,d reveal complicated form of the equation governing mass motion. According to these equations pneumatic force generated by the absorber depends not only on the actual piston displacement but also on the time history of piston displacement and time history of valve opening. As a consequence of displacement history dependence, the response of the pneumatic system is substantially different for slow and fast impacts of the same kinetic energy (Fig. 3.1.4a, b).

Alternatively, single equation of mass motion can be written in the form which is void of multiple time integrals. Integration of equation of mass motion (3.1.38a$_1$) and equation of gas flow (3.1.38a$_3$) over time allows to determine actual mass of the gas inside cylinder in terms of difference of actual and initial velocity of the mass:

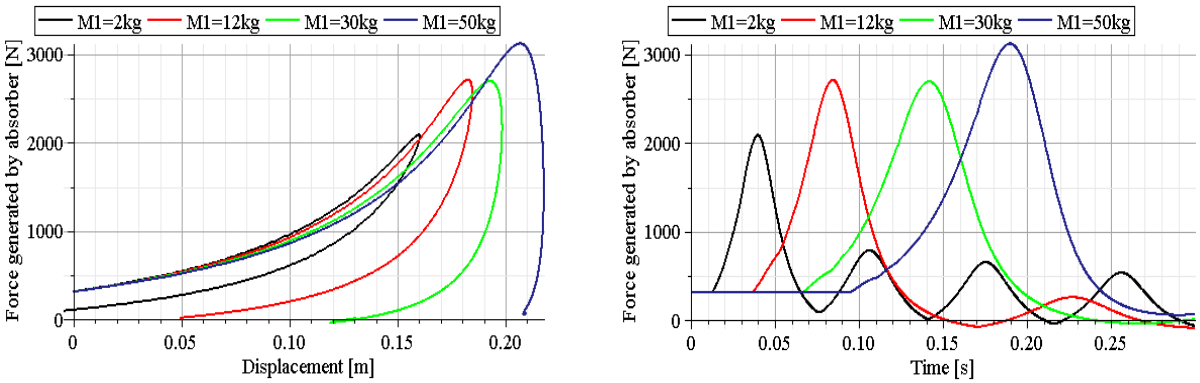

Fig. 3.1.4: Influence of mass of the falling object and its velocity on dynamic response of the system: a) force generated by the absorber in terms of piston displacement, b) force generated by the absorber in terms time. In all cases impact energy is equal.

$$m = \frac{M}{C_V A}\left(\dot{u} - \dot{u}(0)\right) + m_0 \tag{3.1.39a}$$

By combining above definition with ideal gas law and equation of mass motion we obtain:

$$M\ddot{u} - \frac{MRT_0}{C_V A}\frac{\dot{u}}{h_0 - u} - \frac{MRT_0}{C_V A}\frac{V_0}{h_0 - u} + \frac{m_0 RT_0}{h_0 - u} - p_A A = 0 \tag{3.1.39b}$$

The above second order equation contains terms dependent on actual displacement and velocity of the impacting object which additionally depend on mass of the impacting object and its initial velocity. Subsequent terms of the above equations of motion can be identified as: mass-dependant damping term, nonlinear stiffness term dependent on initial momentum, and classical nonlinear stiffness term.

Moreover, Eq. (3.1.39b) can be differentiated over time in order to eliminate of terms dependent on initial conditions, which leads to a nonlinear equation of the third order:

$$M\dddot{u} - \frac{M\,\ddot{u}\left(h_0 - u\right)}{\dot{u}} - \frac{M\,\ddot{u}RT_0}{C_V A\dot{u}} - p_A A = 0 \tag{3.1.40}$$

The above equation has to be complemented with the appropriate initial conditions imposed on the second derivative of the piston displacement. The form of the equation once again confirms sophisticated mathematical description of the mechanism of energy dissipation. The equation does not contain any term which depends exclusively on mass displacement or velocity, but instead, it contains two terms being combinations of displacement derivatives of a different order. In case when the valve is closed ($C_V \to \infty$) the third term of the equation vanishes and the second one indicates force exerted on piston by gas in cylinder chamber. On the contrary, when no flow resistance occurs ($C_V \to 0$) only the third term, which involves piston inertia, remains present at the l.h.s. of the Eq. 3.1.40, which indicates that no force is exerted on piston.

The developed numerical model allows to investigate the **sensitivity of the dynamic response** of the proposed pneumatic system to the following parameters:

- valve opening characterised by viscous resistance coefficient,
- initial pressure inside cylinder ,
- friction between piston and cylinder walls,
- mass of the piston,
- properties of contact material.

Global dynamic response of the system, i.e., time history of pneumatic force and mass acceleration, maximal pressure of gas and total energy dissipation, are all influenced by three initial of these parameters (valve opening, initial pressure and piston friction). On the contrary, local dynamic response (contact force and piston acceleration) depends on all mentioned parameters except valve opening which does not influence initial stage of the process.

Initially, the influence of constant valve opening will be examined. Valve opening changes pneumatic characteristics of the pneumatic cylinder from purely elastic (displacement -dependant with no energy dissipation) into the dissipative one, cf. Fig. 3.1.4. The largest energy dissipation occurs for one of the intermediate valve openings. In case when the valve opening is too large, value of internal cylinder pressure is not able to stop falling mass, and it finally collides against cylinder bottom. In an extreme case of valve opening tending to infinity (and corresponding flow resistance coefficient tending to zero) mass velocity is not altered during cylinder compression. Let us note that purely pneumatic system with constant valve opening allows for permanent stopping of the impacting object only in case of absence of gravitational force (when it is located horizontally). In case when pneumatic cylinder is located vertically, the falling mass can be stopped at particular time instant but further it continues its motion due to gravitational forces.

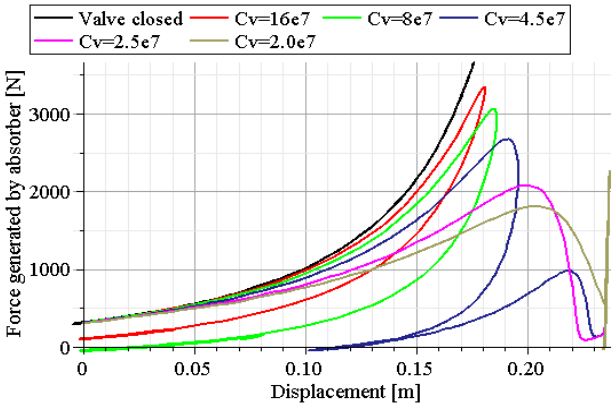

Fig.3.1.5a Influence of valve opening (represented by resistance coefficient [Pa/(kg/s)]) on pneumatic force generated by the absorber and piston displacement. In all cases impact loading is the same.

The easiest method for estimating the influence of initial pressure is a comparison of force generated by the absorber in terms of absorber stroke for various valve openings. The analysis was performed for the basic case of closed valve (Fig. 3.1.5a) and arbitrarily assumed opening of the valve (Fig. 3.1.5b). The second plot indicates strong beneficial influence of initial pressure on amount of dissipated energy. Let us note that the lowest, among maximal values of force, is obtained for intermediate value of initial pressure.

The more precise estimation of influence of initial pressure can be performed by the following methods:

- for various initial pressures constant valve opening is adjusted to obtain maximal allowable stroke and maximal force generated by the absorber is compared,
- for various initial pressures constant valve opening is adjusted to obtain maximal allowable value of force and utilized stroke of the absorber is compared.

In each of the above methods valve opening remains constant during the process, however it is adjusted to assumed impact parameters and particular initial pressure. Precise methods of choice of optimal initial pressure and valve opening for semi-active system (system with constant valve opening), together with quantitative results, will be presented in section dedicated to semi-active adaptation of pneumatic cylinders.

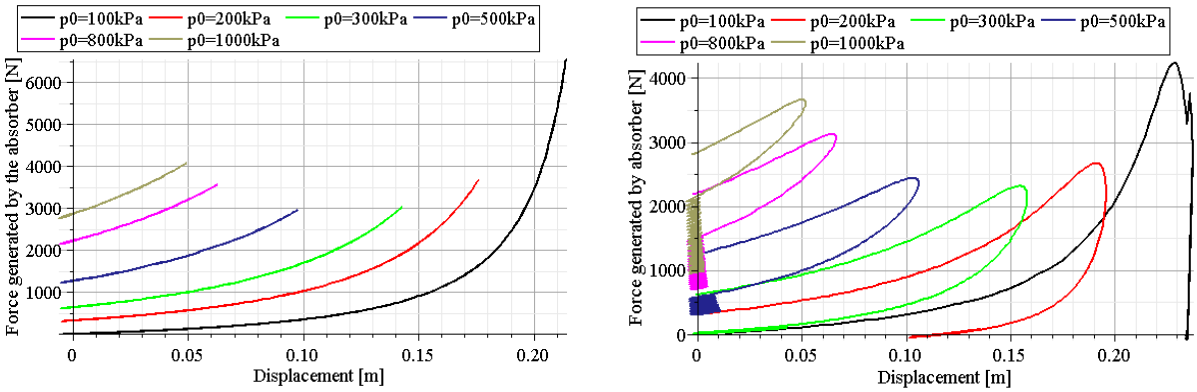

Fig.3.1.5b Influence of initial pressure on force generated by the absorber and maximal absorber stroke: a) valve closed, b) valve partially open (C_v=4,5e7 Pa/(kg/s)).

Although local response of the pneumatic system is not strongly related to global response, it is important for the process of impact identification which is preliminary stage of the process of adaptive impact absorption. Change of initial pressure substantially changes the first stage of impact ('peaks stage'). Along with increase of initial pressure the time interval between initial peaks is decreasing. When initial pressure is large, contact force between the peaks is not reduced to zero which means that piston and falling mass are not separated from each other during the process, Fig. 3.1.6a. The increase of piston mass evokes the opposite effect, i.e. causes that the initial peaks of the contact force tend to be more distinct and separated from each other (cf. Fig.3.1.6b). Due to the fact that more energy is dissipated in the initial stage of impact the maximal value of force during the second stage of impact is reduced.

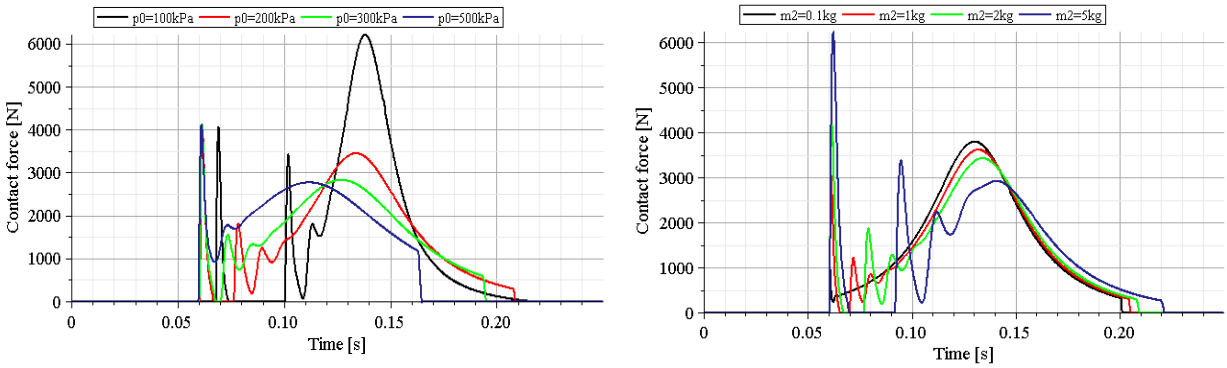

Fig.3.1.6. Change of contact force between mass and piston during impact for various: a) initial pressure inside the cylinder; b) mass of the piston

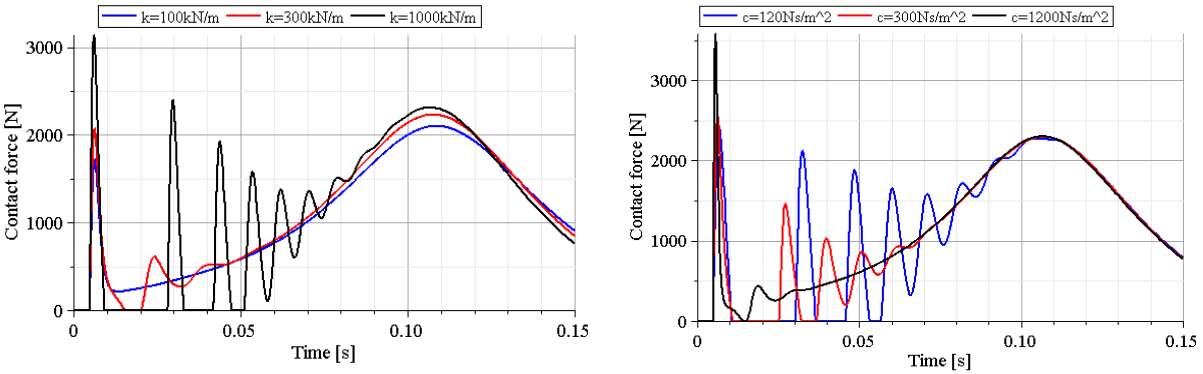

Fig.3.1.6. Change of contact force between mass and piston during impact for various: c) stiffness of the contact element, d) damping of the contact element

The influence of stiffness and damping of the contact element is especially clearly manifested in the first stage of the impact process. Increase of the stiffness coefficient (which increases the ratio of the stiffness term to the damping term) causes growth of the magnitude of the first peak and increase of number of rebounds (Fig. 3.1.6c). On the other hand, it slightly raises maximal value of force during the second stage of impact. The increase of the damping coefficient decreases the ratio of the stiffness term to the damping term. Therefore, increase of damping causes similar effect as decrease of stiffness (Fig. 3.1.6d).

3.1.2 Absorber with accumulator

Adaptive pneumatic cylinder, in which gas is released into additional chamber of constant volume (Fig. 3.1.7a) is more complex for numerical analysis because an additional gas chamber, where inflow of the gas occurs, has to be considered. Equations governing motion of the impacting object and the piston are exactly the same as for previously analyzed absorber with exhaust to environment:

$$M_1 \frac{d^2 u_1}{dt^2} - M_1 g + F_C = 0 \tag{3.1.41}$$

$$M_2 \frac{d^2 u_2}{dt^2} - M_2 g + F_P - F_C - F_D{}^{TOP} + F_D{}^{BOT} + F_{Fr} = 0 \tag{3.1.42}$$

Definition of the pneumatic force depends on whether cylinder contains negative chamber located above the piston:

$$F_P = (p_2 - p_A)A_2 \tag{3.1.43}$$

$$\text{or } F_P = p_2 A_2 - p_1 A_1 - p_A (A_2 - A_1) \text{ if upper chamber exists} \tag{3.1.44}$$

Contact, delimiting and friction forces are defined by equations (3.1.3), (3.1.5) and (3.1.6), respectively. Gas filling each chamber of the system is described by ideal gas law:

$$p_1 V_1 = m_1 R T_1 \quad \text{where} \quad V_1 = A_1 (h_{01} + u_2) \quad \text{if upper chamber exists} \tag{3.1.45}$$

$$p_2 V_2 = m_2 R T_2 \quad \text{where} \quad V_2 = A_2 (h_{02} - u_2)$$

$$p_3 V_3 = (m_t - m_2) R T_3 \quad \text{where} \quad V_3 = const., \quad m_t = m_2 + m_3 = const.$$

where volume of the lower (and possibly the upper) chamber of the system depends on actual location of the piston, but volume of the accumulator remains constant during the process. Mass flow rate of the fluid depends on actual pressure difference between lower cylinder chamber and the accumulator, as well as, on the value of resistance coefficients:

$$p_2 - p_3 = -C_V(t)\dot{m}_2 - C_H(t)\dot{m}_2|\dot{m}_2| \tag{3.1.46}$$

Balance of internal gas energy has to be considered for all chambers of the system including the accumulator. For each chamber the law of the energy conservation is defined by the same general equation:

$$dQ + dm_{in}\overline{H}_{in} - dm_{out}\overline{H}_{out} = d(m\overline{U}) + dW \tag{3.1.47}$$

The form of enthalpy term depends on actual sign of the pressure difference and resulting direction of the flow. The energy conservation law is considered in a full form only for the lower chamber of the absorber. Energy balance for the accumulator does not contain term denoting work of gas since volume of the accumulator remains constant. Moreover, the enthalpy terms can be omitted in the equation describing additional upper chamber.

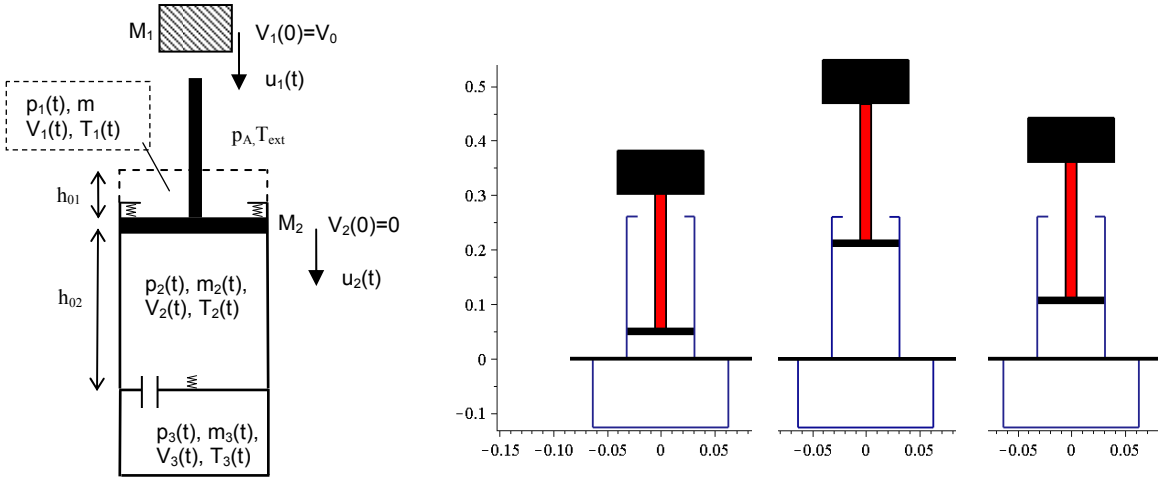

Fig.3.1.7a. Pneumatic cylinder with accumulator: a) scheme of the system, b) simulation conducted in MAPLE software (t=0.145s, t=0.36s, t=1s, cf. Fig. 3.1.7b)

The above system of equations has to be complemented with the initial conditions imposed on initial position and velocity of the falling object and the piston, parameters of gas inside the cylinder and parameters of gas inside the accumulator. The response of the system equipped with accumulator qualitatively resembles response of the system with single air chamber, cf. Fig. 3.1.7b and Fig. 3.1.2b. Geometry of the system, as well as impact parameters and simplifying assumptions, are exactly the same as in case of cylinder with exhaust to environment, so the results can be directly compared.

The impact process can be divided into two stages defined on the basis of the contact force and characterised by different kinematics of the piston. Nevertheless, for the same initial pressure and the same valve opening release of pressure from the main cylinder chamber is less effective due to simultaneous increase of pressure inside the accumulator, cf. Fig. 3.1.7c. Therefore, maximal compression of the absorber is slightly smaller than in case of cylinder with exhaust to environment and higher rebound of the piston occurs.

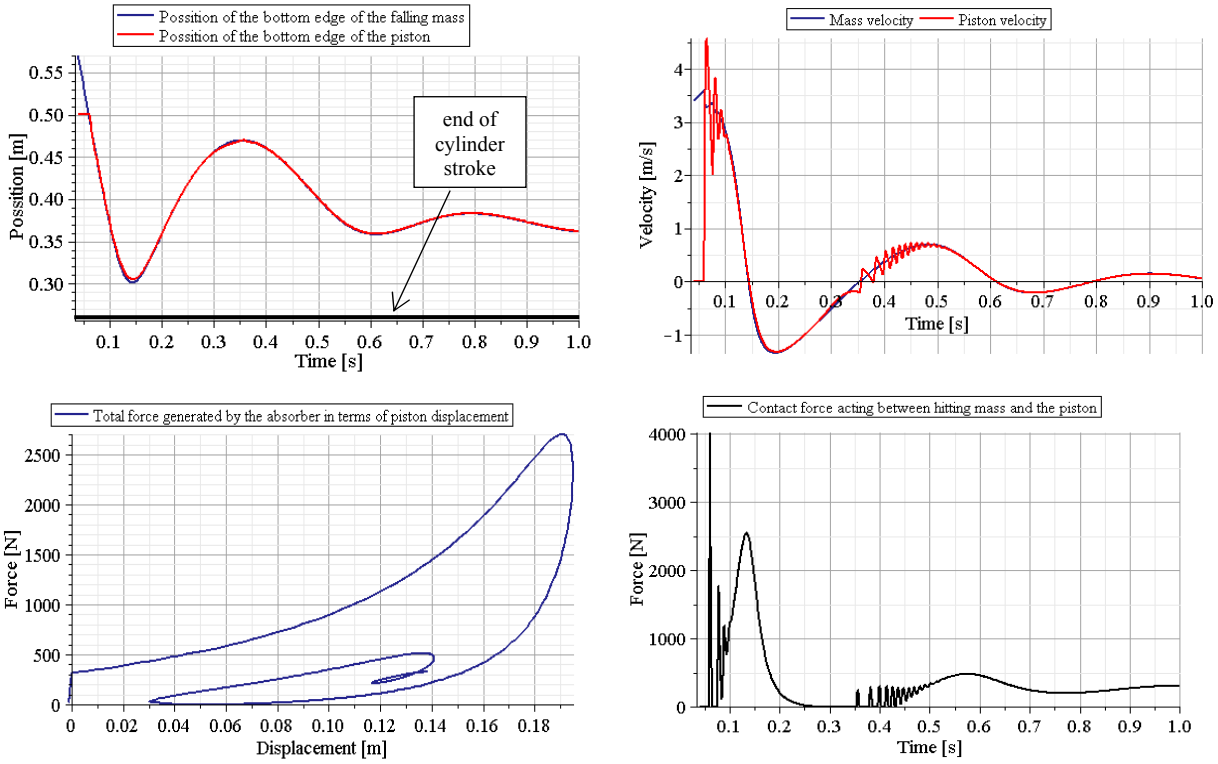

Fig.3.1.7b: Results of the analysis (mechanical part): a), b) kinematics of the system; c) force generated by the absorber, d) contact force between falling mass and piston rod

Due to inflow of the gas from the additional chamber during backstroke the process of stopping of the piston occurs gradually and only small rebound of the impacting object is observed (cf. plot of the contact force, Fig.3.1.7b$_4$). The inflow of the gas from the accumulator during rebound stage of impact causes characteristic loop at the corresponding part of the plot of pneumatic force in terms of piston displacement (cf. Fig.3.1.7b$_3$).

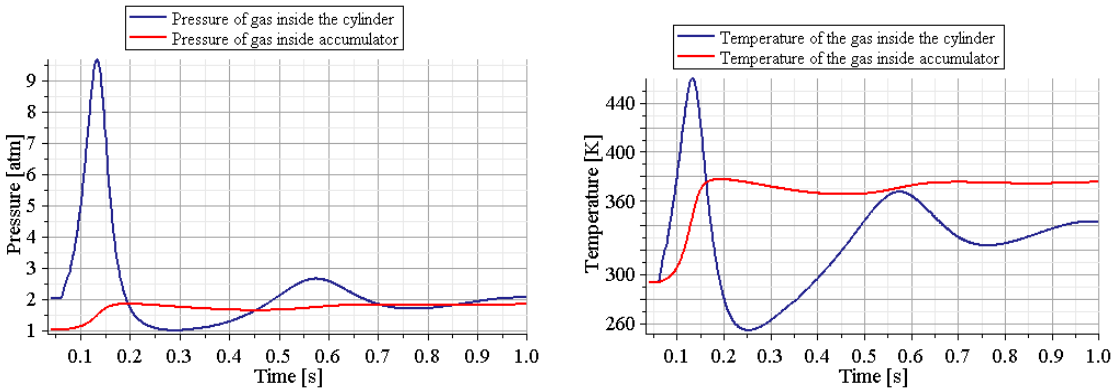

Fig.3.1.7c Results of the analysis (thermodynamic part): a) pressure of the gas inside cylinder and accumulator, b) temperature of the gas inside cylinder and accumulator

Let us analyse the **dissipative properties** of the pneumatic absorber from the point of view of theory of dynamical systems. Pneumatic force is defined by the formula:

$$F_p(u_2,t)=\left(\frac{m_2(t)RT_2(t)}{(h_0-u_2)A}-p_A\right)A \quad \text{or} \quad F_p(u_2,t)=\left(\frac{m_2(t)RT_2(u_2,m,t)}{(h_0-u_2)A}-p_A\right)A \qquad (3.1.48a)$$

which is exactly the same as in case of single chamber absorber with exhaust to environment. Consequently, the system possess most of the features of the system with exhaust to environment described by Eqs. 3.1.14. Two processes which cause change of system mechanical energy are: i) exchange of heat with the environment which changes gas temperature and ii) exchange of enthalpy with the additional tank which changes mass of the gas and its temperature. The first process proceeds similarly as in case of cylinder with exhaust to environment and thus does not have to be considered separately.

In the second dissipative process the exchange of gas between cylinder and accumulator depends on actual sign of pressure difference. However, as it was deduced for single chamber absorber, the dissipation of mechanical energy occurs in two cases: i) outflow of the gas from the cylinder when $p_2 > p_A$ and ii) inflow of the gas to the cylinder when $p_2 < p_A$. Comparison of the above conditions concerning exchange of gas and change of mechanical energy leads to conclusion that in considered system, in contrast to absorber with release to environment, dissipation of mechanical energy due to gas transfer is not permanent.

In case of adiabatic process with transfer of gas from cylinder to accumulator the change of gas temperature inside cylinder can be expressed analytically in terms of mass of the gas and piston displacement on the basis of the corresponding equation of internal energy balance. As a result, definition of the pneumatic force (Eq. 3.1.48a) simplifies to the form:

$$F_p(u_2) = \left(C\left(\frac{m_2(t)}{(h_{02} - u_2)A_2} \right)^{\kappa} - p_A \right) A_2, \qquad C = p_{02}\left(\frac{V_{02}}{m_{02}} \right)^{\kappa} = RT_{02}\left(\frac{m_{02}}{V_{02}} \right)^{1-\kappa} \tag{3.1.48b}$$

(where index '02' indicates initial parameters of gas in the lower chamber of the absorber) and system is characterized by variable in time nonlinear stiffness. However, in case when gas is transferred from the accumulator to the cylinder the calculation of gas temperature inside cylinder based on internal energy balance reveals the non-locality of the pneumatic force in terms of piston displacement and mass of the gas:

$$F_p(u_2) = \left(\left(\kappa R \int_0^t \left[(h_{02} - u_2)A_2 \right]^{\kappa - 1} \dot{m}_2(t) T_3(t) dt + \frac{p_{02}}{\left(h_{02} A_2 \right)^{-\kappa}} \right) \left[(h_{02} - u_2)A_2 \right]^{-\kappa} - p_A \right) A_2 \tag{3.1.48c}$$

In above formula $T_3(t)$ indicates temperature of gas in the accumulator which is not known a priori and also depends on time history of the process. Maximal value of pneumatic force $F_p^{\max}$ is obtained when the valve between the chambers remains closed. By contrast, minimal value of pneumatic force $F_p^{\min}$ is obtained when valve opening is large enough so that the resistance coefficient can be neglected and lower chamber together with accumulator can be treated as a single chamber of larger volume. In both these cases the system can be considered as pneumatic spring of a constant stiffness where energy dissipation does not occur:

$$F_p^{\max}(u_2) = \left(C\left(\frac{m_{02}}{(h_{02} - u_2)A_2} \right)^{\kappa} - p_A \right) A_2, \qquad C = RT_{02}\left(\frac{m_{02}}{V_{02}} \right)^{1-\kappa} \tag{3.1.48d}$$

$$F_p^{\min}(u_2) = \left(C\left(\frac{m_t}{(h_{02} - u_2)A_2 + V_3} \right)^{\kappa} - p_A \right) A_2, \qquad C = RT_{02}\left(\frac{m_t}{V_{02} + V_3} \right)^{1-\kappa} \tag{3.1.48e}$$

where $\kappa = 1{,}4$ in case of adiabatic process, and $\kappa = 1$ in case of isothermal one. All other characteristics of the pneumatic absorber that can be obtained for intermediate valve openings are located between curves described by Eq. 3.1.48d and 3.1.48e. The discrepancy with zero minimal force obtained for system with exhaust to environment mathematically arises from the fact that pressure difference, which occurs in the flow equation, is different than pressure difference occurring in the equation of piston motion.

Equations governing **global balance of system energy** can be obtained directly by integration of equations of motion over displacement of the impacting object and over displacement of the piston. Therefore, the equations of energy balance for both masses and global mechanical energy balance are identical as in case of single chamber cylinder (cf. Eq. 3.1.15 and Eq. 3.1.18). Equations of internal energy balance for both chambers read:

$$\Delta Q_2 + \Delta H_2 = \Delta U_2 + W \tag{3.1.49a}$$

and

$$\Delta Q_3 + \Delta H_3 = \Delta U_3 \quad \text{or} \quad \Delta Q_3 - \Delta H_2 = \Delta U_3 \tag{3.1.49b}$$

Sum of both above equations gives global internal energy balance:

$$\Delta U_2 + \Delta U_3 = \Delta Q_2 + \Delta Q_3 - W \tag{3.1.49c}$$

Global balance of energy for the cylinder can be derived by combining internal energy balance for the lower chamber (3.1.49a) with simplified mechanical energy balance (3.1.20c). The first form of this equation reads:

$$\Delta E_k + \Delta E_p - W_{pA} = -(\Delta U_2 + D_{H2} + D_{Q2} + D_{fr}) \tag{3.1.49d}$$

and defines change of mechanical energy of the system. The alternative form, i.e.:

$$\Delta E_k + \Delta E_p + \Delta U_2 = W_{pA} - (D_{H2} + D_{Q2} + D_{fr}) \tag{3.1.49e}$$

defines change of total energy of the cylinder (sum of mechanical energy and internal energy of gas enclosed in the cylinder). Moreover, global balance of energy for the whole system can be derived by combining global internal energy balance (Eq. 3.1.49c) with simplified mechanical energy balance (Eq. 3.1.20c):

$$\Delta E_k + \Delta E_p - W_{pA} = -(\Delta U_2 + \Delta U_3 + D_{Q2} + D_{Q3} + D_{fr}) \tag{3.1.49f}$$

which is obviously equivalent to (Eq. 3.1.49d) . An alternative form reads:

$$\Delta E_k + \Delta E_p + \Delta U_2 + \Delta U_3 = W_{pA} - (D_{Q2} + D_{Q3} + D_{fr}) \tag{3.1.49g}$$

and defines change of total energy of the system (sum of mechanical energy and internal energy of gas enclosed in the cylinder and in the accumulator).

The process of energy dissipation can be considered either for the gas contained inside the cylinder only or, alternatively, for the gas occupying whole pneumatic system (cylinder and accumulator). In the first case (Eq. 3.1.49d,e), the mechanism of energy dissipation can be viewed as similar to the mechanism occurring in case of cylinder with exhaust to environment. The following processes causing energy dissipation occur simultaneously during impact:

- kinetic energy of the impacting body is changed into gas internal energy,
- energy is transferred from the system into environment in the form of heat,
- flow of the gas from main cylinder chamber to accumulator occurs.

The last of the aforementioned process decreases internal energy of the gas contained inside cylinder and consequently decreases its ability to perform mechanical work. Thus the process of energy dissipation is in principle similar to release of pressure to the environment. The intrinsic difference between two systems is revealed by balance of global energy (Eq. 3.1.49f,g) which indicates that the process of release of gas to the accumulator does not change total internal energy of gas inside the system. Although global internal energy of the system remains constant, smaller part of internal energy can be changed into mechanical work.

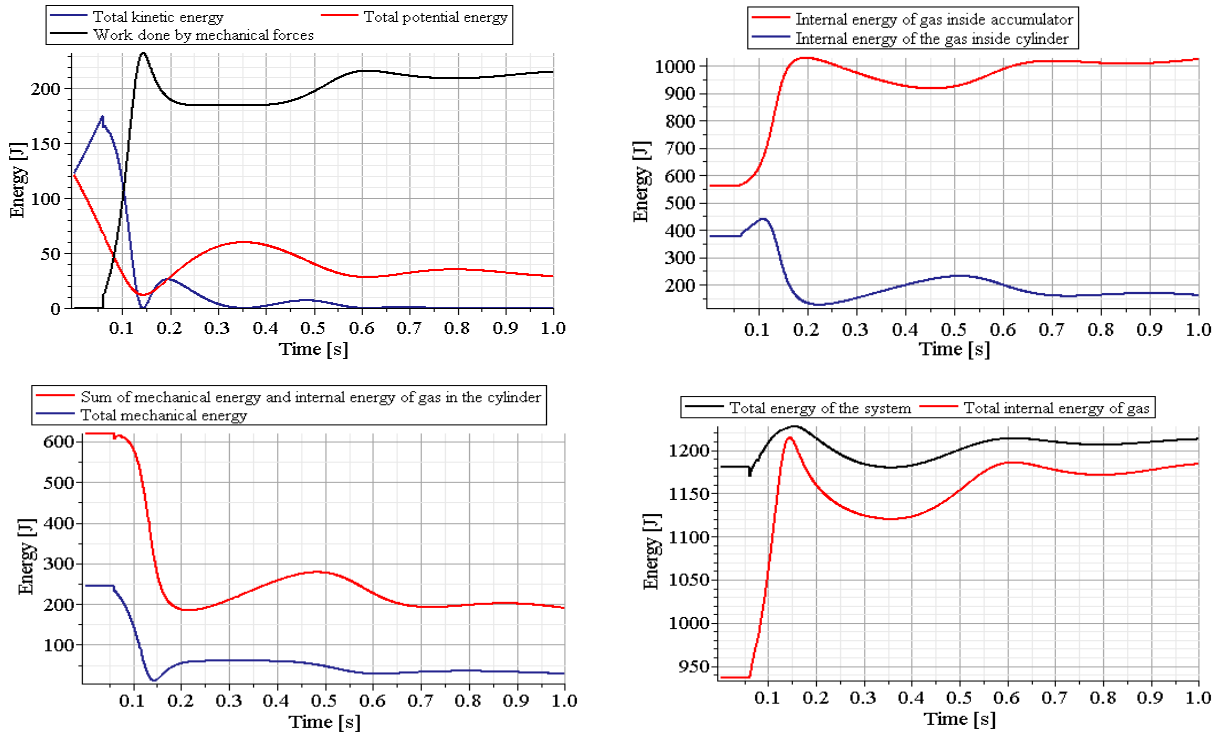

Fig. 3.1.8 Analysis of changes of system energy:
a) mechanical energy balance (Eq.3.1.15); b) change of internal energy (Eq.3.1.49a, b);
c) balance corresponding to lower chamber (Eq.3.1.49d,e); d) total energy of the system (Eq.3.1.49c,g)

Mathematical structure of the system of equations governing the absorber with accumulator can be explained by using the simplified 1DOF model which assumes isothermal conditions and simple model of the gas flow:

$$M\ddot{u}_2 + (p_2 - p_A)A = 0 \tag{3.1.50}$$

$$p_2 A(h_{02} - u_2) = m_2 R T_0, \quad p_3 V_3 = (m_t - m_2) R T_0$$

$$p_2 - p_3 = -C_V \dot{m}_2$$

$$\text{IC: } u_2(0) = 0, \dot{u}_2(0) = V_0, m_2(0) = m_{02}$$

By combing ideal gas laws for both chambers with equation of the flow, we obtain differential equation:

$$\frac{m_2 RT_0}{A(h_{02}-u_2)} - \frac{(m-m_2)RT_0}{V_3} = -C_V \dot{m}_2 \tag{3.1.51}$$

which can be solved analytically in order to find mass of the gas inside lower chamber of the cylinder and the corresponding gas pressure which can be expresses as:

$$p(t) = f_3\left(\int_0^t f_2\left(\int_0^t f_1(u_2)dt, C_V\right), \int_0^t f_1(u_2)dt,\ u_2\right) \tag{3.1.52}$$

According to Eq. 3.1.52 pneumatic force generated by the absorber depends not only on the actual piston displacement but also on the time history of piston displacement and on the time history of valve opening. Generated force is not a direct function of the actual piston velocity and actual valve opening, what is a typical feature of hydraulic shock absorbers.

Due to the fact that pressure differences which occur in equation of motion and in equation defining the gas flow are different, the integral forms of both equations can not combined and single equation of the second order describing the whole system (analogous to Eq. 3.1.39b) can not be derived. However, four governing equations (Eq. 3.1.50) can be combined into single differential equation of third order which describes motion of the impacting mass:

$$-C_V M\dddot{u}(h_0-u) - C_V\left(-\frac{M\ddot{u}}{A}+p_A\right)A\dot{u} + \left(-\frac{M\ddot{u}}{A}+p_A\right)RT_0 - \frac{mR^2T_0^{\,2}}{V_3} + \\ + \frac{(-M\ddot{u}+p_A A)A(h_0-u)RT_0}{V_3} = 0 \tag{3.1.53}$$

The above equation takes more complicated form than the corresponding equation for the system with exhaust to environment (Eq. 3.1.40). Except typical inertia term, the equation contains several terms with mixed displacement derivatives which are responsible for the energy dissipation (none of them is a classical velocity-dependent damping term). It can be proved that in case when the valve is closed or fully open $(C_V \to \infty, C_V = 0)$, only the inertia and stiffness terms remain present and Eq. 3.1.53 describes pneumatic spring.

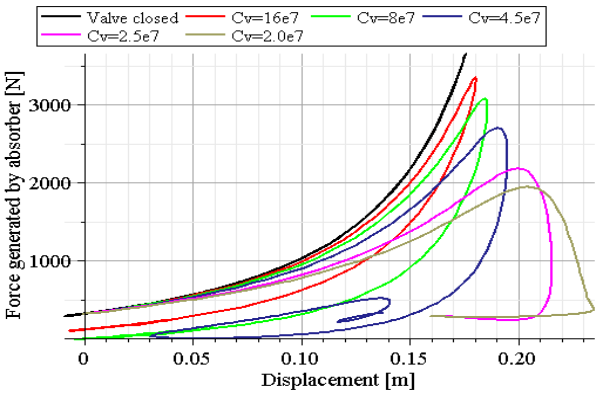

Fig.3.1.9 Influence of valve opening (represented by viscous resistance coefficient [Pa/(kg/s)]) on pneumatic force generated by the absorber and piston displacement

Similarly as previously, the developed numerical model will be used to investigate the influence of selected parameters on the dynamic response of the pneumatic cylinder. Initially,

the influence of valve opening on evolution of pneumatic force and on the amount of dissipated energy were considered, cf. Fig. 3.1.9.

The second intrinsic parameter which determines dynamic properties of the pneumatic system is initial pressure inside the cylinder and the accumulator. In the considered example pressure inside accumulator ranged between 10kPa and 400kPa, while pressure inside cylinder chamber was always equal to 200kPa. Response of the system with arbitrarily assumed valve opening is presented in Fig. 3.1.10. In the subsequent analyzed cases the energy dissipation was decreasing since the outflow of fluid to the accumulator was less effective and the inflow from the accumulator (which occurred at certain periods of the process) was increased.

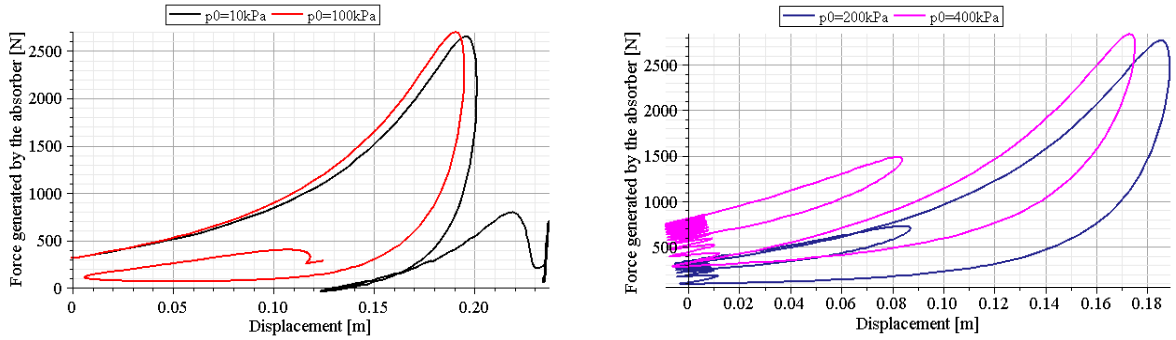

Fig.3.1.10 Influence of initial pressure in accumulator on force generated by the absorber

3.1.3 Absorber with valve between chambers

Last of the analyzed pneumatic cylinders (cf. Fig. 3.1.11a) contains two gas chambers located on both sides of the piston and a connection between them allowing for the fluid flow. Connection between the chambers can be located inside the piston or, alternatively, it may be designed as an external bypass. Due to applied method of modelling, which assumes uniform distribution of gas parameters, location of the connection between the chambers does not affect the form of the governing equations.

In both cases, considered pneumatic system is described by the system of equations governing the motion of the falling object and the piston:

$$M_1 \frac{d^2 u_1}{dt^2} - M_1 g + F_C = 0 \tag{3.1.54}$$

$$M_2 \frac{d^2 u_2}{dt^2} - M_2 g + F_P - F_C - F_D{}^{TOP} + F_D{}^{BOT} + F_{Fr} = 0 \tag{3.1.55}$$

Pneumatic force results from difference of pressure on both sides of the piston and external pressure and thus it is defined as:

$$F_P = p_2 A_2 - p_1 A_1 - p_A (A_2 - A_1) \tag{3.1.56}$$

Contact, delimiting and friction forces are defined as in the previous cases (vide Eqs. 3.1.3, 3.1.5, 3.1.6). Gas filling both chambers is described by ideal gas law:

$$p_1 V_1 = (m_t - m_2) R T_1 \quad \text{where} \quad V_1 = A_1 (h_{01} + u_2) \ , \ \ m_t = m_1 + m_2 \tag{3.1.57}$$

$$p_2 V_2 = m_2 R T_2 \quad \text{where} \quad V_2 = A_1 (h_{02} - u_2)$$

Flow of the gas will be described by general equation:

$$\dot{m}_2 = f(p_2, T_2, p_1, T_1, C(t)) \tag{3.1.58a}$$

However, often a simple model of the flow will be assumed:

$$p_2 - p_1 = -C_V(t)\dot{m}_2 - C_H(t)\dot{m}_2|\dot{m}_2| \tag{3.1.58b}$$

The balance of internal gas energy has the same form as usually:

$$dQ + dm_{in}\overline{H}_{in} - dm_{out}\overline{H}_{out} = d(m\overline{U}) + dW \tag{3.1.59a}$$

where specific gas enthalpy, specific gas energy and work done by gas are defined as:

$$\overline{H}_{in} = c_p T_{in}\,; \quad \overline{H}_{out} = c_p T\,; \quad \overline{U} = c_V T\ ; \quad dW = pdV \tag{3.1.59b}$$

For both lower and upper chamber of the cylinder the equation of energy balance has to contain enthalpy terms which indicate inflow/outflow of the fluid. In typical AIA application, piston moves downwards, pressure in the lower chamber is higher than pressure in the upper chamber and gas flows from the lower to upper chamber. The occurrence of the above conditions allows to specify a particular form of the enthalpy terms. The above situation, however, can be reversed during a backstroke. Let us note that summation of energy balances for both chambers leads to global energy balance in which the enthalpy terms are eliminated:

$$dQ_1 + dQ_2 = d(m_1\overline{U}_1) + d(m_2\overline{U}_2) + dW_1 + dW_2 \tag{3.1.59c}$$

In special cases, the above energy balance can be integrated analytically which will be effectively utilized in further analysis of governing equations.

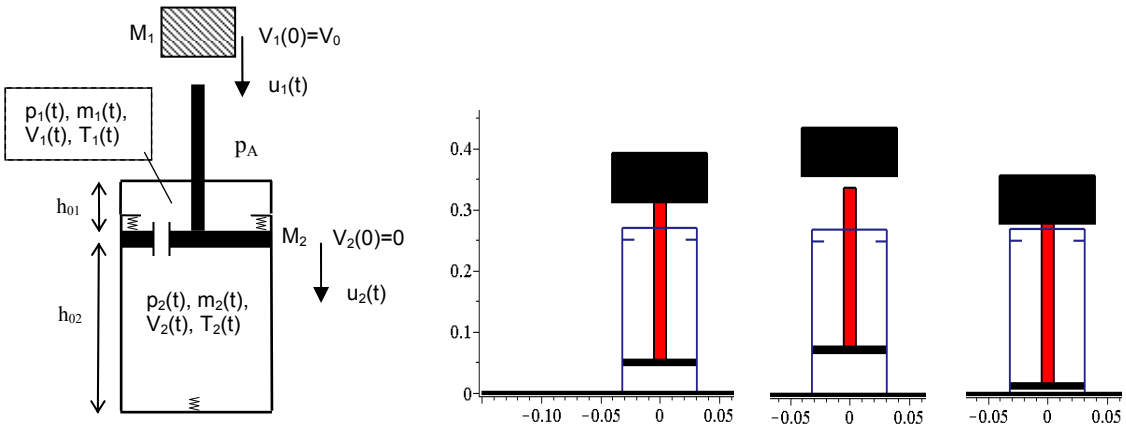

Fig.3.1.11a Pneumatic cylinder with valve between the chambers: a) scheme of the system, b) simulation performed in MAPLE software (t=0.15s, t=0.22s, t=0.69s, cf. Fig. 3.1.11b)

The above system of equations has to be complemented with initial conditions imposed on initial kinematics of the falling mass and the piston, as well as parameters of gas in both chambers. Resulting system of differential equations is of higher complexity than analogous system for a single-chamber absorber due to presence of two pressure chambers with changing volume and amount of gas. The system of governing equations can still be efficiently solved with fourth order Runge-Kutta method. In performed simulation, parameters of the system and simplifying assumptions ($F_{fr} = 0$, $C_V = const.$, $C_H = 0$, $\dot{Q} = 0$)

are the same as for previous absorbers, which enables direct comparison of the results.

Considered absorber has typical features of the pneumatic absorbers analyzed in previous sections including characteristic piston kinematics and change of the contact force. However, dissipative characteristics of the absorber is additionally influenced by pressure of gas in the chamber located above the piston. During the process the pressure of gas in both chambers is affected by movement of the piston and migration of gas between the chambers. In the initial stage of the process the effect of change of chambers' volumes prevails and thus pressure in the lower chamber increases and in the upper one decreases, which results in growth of the pneumatic force generated by the absorber. As the impact proceeds velocity of the piston is diminished and pressure difference raises, which causes that the influence of mass exchange becomes stronger and the influence of change of chambers' volumes becomes weaker. Finally, when the velocity of the piston is close to zero, pneumatic force achieves its maximum and further starts to decrease.

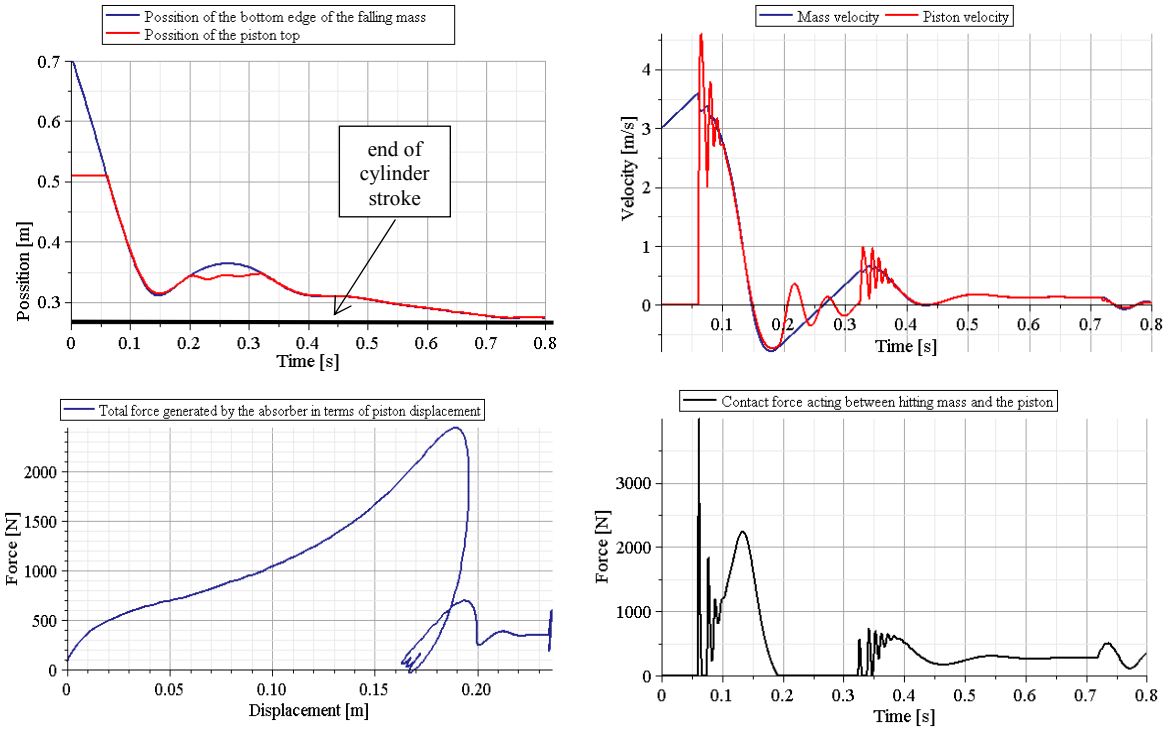

Fig.3.1.11b. Pneumatic cylinder with valve between the chambers: a), b) kinematics of the system, c) total force generated by the absorber , d) contact force between falling mass and the piston

The fact that gas removed from the lower chamber is transferred to the upper one causes that change of pneumatic force is larger than in case of release of gas to environment. As a consequence, the process of energy dissipation is more efficient and only a small rebound of the impacting object occurs. Typical response of the system with constant valve opening is presented in Fig. 3.1.11b and Fig. 3.1.11c.

During the entire process of energy dissipation the whole mass of the gas is transferred from the lower chamber to the upper one. Finally, pressure in both chambers is equilibrated, however its level is substantially increased as a result of change of mechanical energy of the impacting object into gas energy. Increase of gas internal energy is reflected in change of gas temperature, which is especially high in the upper chamber of the cylinder.

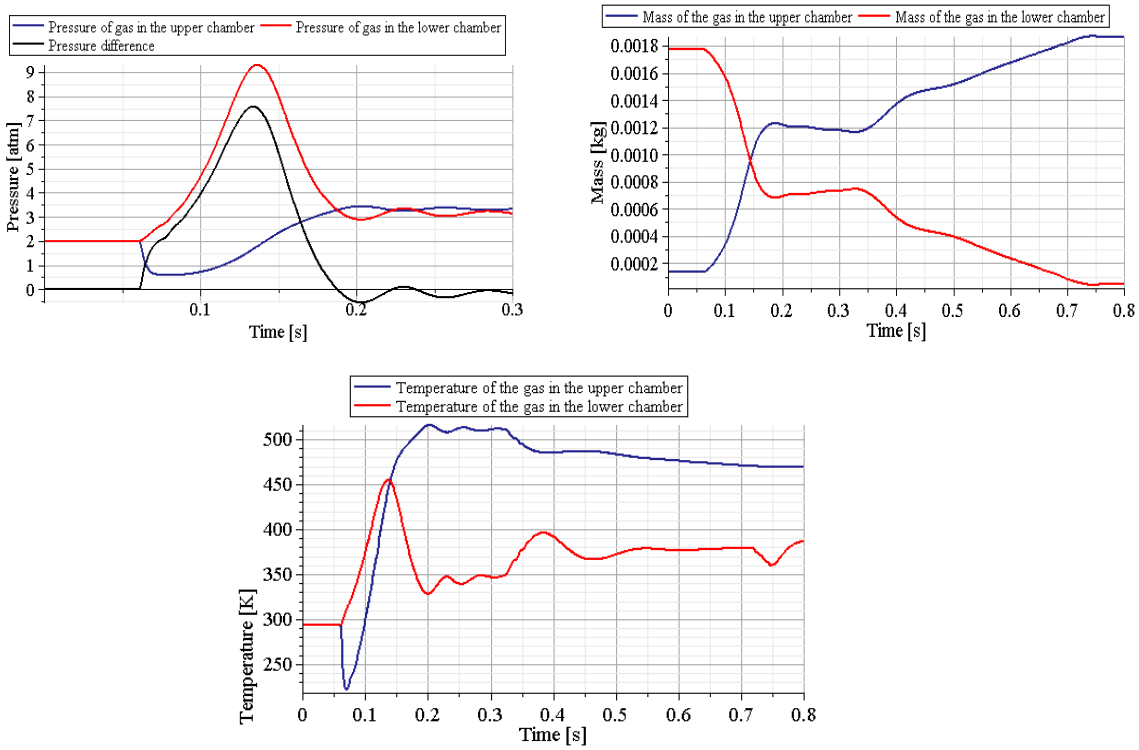

Fig.3.1.11 Pneumatic cylinder with valve between the chambers: a) pressures in both chambers and pressure difference, b) mass of gas in both chambers , c) temperature of gas in both chambers

The insight on **dissipative properties** of the considered system can be gained from the analysis of simple 1DOF model of the absorber which generates exclusively pneumatic force. For the typical stage of the absorber work when the piston moves down and gas flows from the lower chamber to the upper one the system is described by the equations:

$$M\ddot{u}+\left(\frac{m_2RT_2}{V_{02}-uA_2}A_2-\frac{m_1RT_1}{V_{01}+uA_1}A_1\right)=0 \tag{3.1.60}$$

$$\lambda A_{W1}(u)(T_{ext}-T_1)-\dot{m}_2c_pT_2=\dot{m}_1c_VT_1+m_1c_V\dot{T}_1-\frac{m_1RT_1}{V_{01}+uA_1}A_1\dot{u}$$

$$\lambda A_{W2}(u)(T_{ext}-T_2)+\dot{m}_2c_pT_2=\dot{m}_2c_VT_2+mc_V\dot{T}_2-\frac{m_2RT_2}{V_{02}-uA_2}A_2\dot{u}$$

$$\text{IC: } u(0)=u_0,\ \dot{u}(0)=V_0,\ T_1(0)=T_{01},\ T_2(0)=T_{02}$$

In above model the force resulting from ambient pressure acting on the piston is arbitrarily neglected. Moreover, the exchange of gas between both chambers $\dot{m}_1(t)=-\dot{m}_2(t)>0$ is arbitrarily assumed. A further argumentation follows the one for single chamber pneumatic cylinder (cf. Eqs. 3.1.14). In general case, the pneumatic force exerted on the piston reads:

$$F_p(u,t)=\frac{m_2(t)RT_2(t)}{V_{02}-uA_2}A_2-\frac{(m_t-m_2(t))RT_1(t)}{V_{01}+uA_1}A_1 \tag{3.1.60a}$$

Pneumatic force is composed of two terms and each of them indicates variable in-time nonlinear stiffness. Since temperature of the gas in each chamber is not independent, change of temperature has to be expressed in terms of other parameters. For considered stage of

absorber's work when gas flows from the lower to the upper chamber the above formula can be written in the form:

$$F_p(u,t) = \frac{m_2(t)RT_2(u,m_2,t)A_2}{V_{02} - uA_2} - \frac{(m_t - m_2(t))RT_1(u,m_2,T_2,t)A_1}{V_{01} + uA_1} \tag{3.1.60b}$$

Potential energy of the gas spring will be defined in an analogous manner as for the single chamber absorber:

$$E_p(\bar{t}) = -\int_{\bar{u}}^{u_{eq}} \widetilde{F}_p(u)du = -\int_{\bar{u}}^{u_{eq}} \left(\frac{\overline{m}_2 R\widetilde{T}_2(u,\overline{m}_2)}{V_{02} - uA_2} - \frac{(m_t - \overline{m}_2)R\widetilde{T}_1(u,\overline{m}_2)}{V_{01} + uA_1} \right) Adu \tag{3.1.60c}$$

where overbar indicates actual state of the system. Similarly as in case of single chamber system, the values of functions $\widetilde{T}_1(u)$ and $\widetilde{T}_2(u)$ are obtained from the energy balance (Eq. $3.1.60_{2,3}$) by setting $\dot{m}_1 = \dot{m}_2 = 0$ and $\lambda \to \infty$ or $\lambda = 0$ for isothermal and adiabatic system, respectively. Total mechanical energy of the system, i.e. sum of kinetic energy of mass and potential energy of pneumatic system, remains constant in case when the explicit dependence of mass and temperature on time vanishes. Such situation occurs when:

$$F_p(u) = \frac{m_{02}RT_2(u)}{V_{02} - uA_2}A_2 - \frac{(m_t - m_{02})RT_1(u)}{V_{01} + uA_1}A_1 \tag{3.1.60d}$$

i.e. for isothermal and adiabatic system with constant mass of the gas in both chambers. By contrast, in more general case, total energy is not conserved due to change of mass and temperature in time caused by exchange of enthalpy between the chambers and exchange of heat with the environment.

Let us further focus on adiabatic system with transfer of gas between the chambers. Dissipation of mechanical energy occurs when change of time dependent parameter (here: mass of the gas or temperature) causes decrease of absolute value of force F_p. Taking into account reduced equation of the energy balance ($\Delta H = \Delta U$) and dependence of the direction of the gas flow on actual pressure difference we conclude that dissipation of the energy occurs in two cases: i) $F_p^2 > F_p^1$ and $p_2 > p_1$ and ii) $F_p^2 < F_p^1$ and $p_2 < p_1$. In other cases mechanical energy of the system increases. Let us note that in case when $A_1 = A_2$ the condition $F_p^2 > F_p^1$ is equivalent to condition $p_2 > p_1$ which provides that dissipation of mechanical energy in considered system is permanent. Moreover, during transfer of gas between the chambers one term of pneumatic force decreases (as a result of mass and temperature decrease) and, simultaneously, the second term increases (as an effect of internal energy increase). Therefore, the effect of force reduction and energy dissipation caused by transfer of certain amount of gas is larger than for exhaust of the same amount of gas from lower chamber to environment.

Let us further determine change of gas temperature in both chambers during the adiabatic process. By using Eq. $3.1.60_3$ the temperature in the lower chamber $T_2(t)$ can be expressed analytically in terms of actual mass of the gas and actual chamber volume:

$$T_2(t) = T_0 \left(\frac{m_{02}}{h_{02}A_2} \frac{(h_{02} - u)A_2}{m_2(t)} \right)^{1-\kappa} \tag{3.1.61a}$$

Temperature inside the upper chamber, where inflow of the gas occurs, can be determined from the equation of energy balance for the upper chamber (Eq. 3.1.60$_2$)

$$T_1(t)=\frac{1}{m_1(t)}\left(\kappa\int_0^t\left[(h_{01}+u)A_1\right]^{\kappa-1}\dot{m}_1(\bar{t})T_2(\bar{t})d\bar{t}+\frac{T_{01}m_{01}}{\left(h_{01}A_1\right)^{1-\kappa}}\right)\left[(h_{01}+u)A_1\right]^{1-\kappa} \tag{3.1.61b}$$

The above integral formula indicates that temperature T_1 (and thus pneumatic force defined by Eq. 3.1.60a) depends on the whole time-history of the considered process. Therefore, an important difference between considered double chamber cylinder and previously analyzed systems with exhaust to environment and to accumulator occurs. In case of double chamber cylinder the non-locality of the pneumatic force in terms of mass of the gas and piston displacement appears in the basic stage of the system work, when lower chamber is compressed and upper chamber is decompressed by impacting object. Therefore, when mass of the gas is considered as the only force-controlling parameter, the characteristics of the pneumatic device can not be treated as elastic with variable in time nonlinear stiffness.

An alternative approach for determination of generated pneumatic force does not utilize equations of internal energy for both chambers but global balance of internal energy for the whole system (cf. Eq. 3.1.59c). Thus, the system of governing equations reads:

$$\begin{aligned} M\ddot{u}+p_2A_2-p_1A_1&=0 \\ \dot{U}_1+\dot{U}_2+\dot{W}_1+\dot{W}_2&=0 \end{aligned} \tag{3.1.62a}$$

Summation of the first equation integrated over displacement and the second equation integrated over time yields:

$$m_1c_VT_1-m_1c_VT_{01}+m_2c_VT_2-m_2c_VT_{02}+\tfrac{1}{2}M\dot{u}^2-\tfrac{1}{2}MV_0^2=0 \tag{3.1.62b}$$

and thus allows to calculate temperature inside upper chamber in terms of initial energy of the impacting object and its actual velocity:

$$T_1=T_{01}-\frac{m_2}{m_1}T_2+\frac{m_2}{m_1}T_{02}-\frac{M\dot{u}^2}{2c_Vm_1}+\frac{MV_0^2}{2c_Vm_1} \tag{3.1.62c}$$

Determined temperatures T_1 (Eq. 3.1.61a) and T_2 (Eq. 3.1.62c) allow to express pneumatic force generated by the absorber in terms of initial energy of the impacting object, its actual displacement and velocity:

$$F_p(m_2,u)=\frac{m_2(t)RT_2A_2}{V_{02}-uA_2}-\frac{RA_1}{V_{01}+uA_1}\left[m_1T_{01}-m_2(t)T_2+m_2(t)T_{02}-\frac{M\dot{u}^2}{2c_V}+\frac{MV_0^2}{2c_V}\right] \tag{3.1.62d}$$

The above formula indicates that pneumatic force generated by the absorber involves both nonlinear time-dependent stiffness terms and nonlinear damping terms which depend on mass of the impacting object. However, only the stiffness terms depend on actual mass of the gas in the chambers.

Finally, in case of isothermal process definition of the pneumatic force reads:

$$F_p(t)=\frac{m_2(t)RT_0}{V_{02}-uA_2}A_2-\frac{(m_t-m_2(t))RT_0}{V_{01}+uA_1}A_1 \tag{3.1.63}$$

and thus in isothermal case considered system involves only variable in time nonlinear stiffness.

In case of adiabatic or isothermal system with closed valve, the mass of the gas in both chambers is constant and the system acts as double-sided pneumatic spring. In case when valve opening does not cause any flow resistance, pressure in both chambers is equal, however, pneumatic force arises due to various effective areas on both sides of the piston. Two above extreme cases are defined by the formulae:

$$F_p^{\max}(u) = C_\kappa^2\left(\frac{m_{02}}{V_{02}-uA_2}\right)^\kappa A_2 - C_\kappa^1\left(\frac{m_t-m_{02}}{V_{01}-uA_1}\right)^\kappa A_1 \tag{3.1.63a}$$

$$F_p^{\min}(u) = C_\kappa\left(\frac{m_t}{V_{01}+V_{02}-u(A_2-A_1)}\right)^\kappa (A_2-A_1) \tag{3.1.63b}$$

where $C_\kappa^2 = RT_{02}\left(\frac{m_{02}}{V_{02}}\right)^{1-\kappa}$, $C_\kappa^1 = RT_{01}\left(\frac{m_{01}}{V_{01}}\right)^{1-\kappa}$, $C_\kappa = RT_0\left(\frac{m}{V_{01}+V_{02}}\right)^{1-\kappa}$ (3.1.63d)

Characteristics that can be obtained by applying various valve openings are located between two curves defined above.

Global balance of the system energy is obtained by integration of both equations of motion (Eq. 3.1.54 and Eq. 3.1.55) over displacement:

$$\int_{u_1^0}^{u_1} M_1 \frac{d^2\overline{u_1}}{dt^2}\, d\overline{u_1} - \int_{u_1^0}^{u_1} M_1 g\, d\overline{u_1} + \int_{u_1^0}^{u_1} F_c\, d\overline{u_1} = 0 \tag{3.1.64a}$$

$$\int_{u_2^0}^{u_2} M_2 \frac{d^2\overline{u_2}}{dt^2} d\overline{u_2} - \int_{u_2^0}^{u_2} M_2 g d\overline{u_2} + \int_{u_2^0}^{u_2} (p_2A_2 - p_1A_1 - p_A(A_2-A_1)) d\overline{u_2} - \tag{3.1.64b}$$

$$- \int_{u_2^0}^{u_2} F_C d\overline{u_2} - \int_{u_2^0}^{u_2} F_D^{TOP} d\overline{u_2} + \int_{u_2^0}^{u_2} F_D^{BOT} d\overline{u_2} + \int_{u_2^0}^{u_2} F_{fr} d\overline{u_2} = 0$$

By summing up the above equations we obtain:

$$\Delta E_k^1 + \Delta E_k^2 + \Delta E_p^1 + \Delta E_p^2 - W_{Fp} - W_C - W_D^{TOP} - W_D^{BOT} - W_{fr} = 0 \tag{3.1.65}$$

where ΔE_k and ΔE_p indicate changes of kinetic and potential energy of the falling mass and the piston while W_{Fp} indicates work done by pneumatic system:

$$W_{Fp} = -\int_{u_2^0}^{u_2} (p_2A_2 - p_1A_1 - p_A(A_2-A_1)) d\overline{u_2} \tag{3.1.66a}$$

which can be divided into a sum of three components:

$$W_{Fp} = W^2 + W^1 + W_p^A \tag{3.1.66b}$$

denoting work done by gas in the lower and upper chamber and work done by atmospheric pressure which are defined respectively as:

$$W^2 = -\int_{u_2^0}^{u_2} p_2\ A_2 d\overline{u_2} = \int_{V_2^0}^{V_2} p_2\ d\overline{V_2}\ , \qquad W^1 = \int_{u_2^0}^{u_2} p_1\ A_1 d\overline{u_2} = \int_{V_1^0}^{V_1} p_1\ d\overline{V_1} \tag{3.1.67a,b}$$

$$W^A = \int_{u_2^0}^{u_2} p_A\ (A_2 - A_1) d\overline{u_2} = p_A\ (A_2 - A_1)(u_2 - u_2^0) \tag{3.1.67c}$$

In case when simplified single degree of freedom model is utilized, global energy balance is reduced to the form:

$$\Delta E_k + \Delta E_p - W^2 - W^1 - W^A - W_{fr} = 0 \tag{3.1.68}$$

Internal energy balance for upper and lower chamber reads:

$$\Delta Q_2 + \Delta H_2 = \Delta U_2 + W^2 \tag{3.1.69a}$$

$$\Delta Q_1 + \Delta H_1 = \Delta U_1 + W^1 \quad \text{or} \quad \Delta Q_1 - \Delta H_2 = \Delta U_1 + W^1 \tag{3.1.69b}$$

The enthalpy term in both equations is exactly opposite since the enthalpy which is removed from one chamber is directly transferred to the other one. Summation of both above equations leads to thermodynamic balance of internal energy for the whole system:

$$\Delta Q_1 + \Delta Q_2 = \Delta U_1 + \Delta U_2 + W^1 + W^2 \tag{3.1.69a}$$

which can be also written in the form:

$$W_{Fp} = -\Delta U + \Delta Q + W_p^A \quad \text{or} \quad L_{Fp} = \Delta U + D_Q - W_p^A \tag{3.1.70}$$

By combining mechanical energy balance with global balance of internal energy we obtain equation defining change of total mechanical energy of the impacting object:

$$\Delta E_k + \Delta E_p - W_p^A = -(\Delta U + D_Q + D_{fr}) \tag{3.1.71a}$$

The above equation shows that mechanical energy of the falling object and work done by external pressure are changed into internal energy of the gas, energy transferred to the environment in the form of heat and work done by friction force. Total energy of the system (sum of mechanical energy and internal gas energy) is changed only by transfer of heat to the environment, work done by external pressure and work done by friction force, and it is completely not affected by transfer of gas between the chambers:

$$\Delta E = \Delta E_k + \Delta E_p + \Delta U = -D_Q - D_{fr} + W_p^A \tag{3.1.71b}$$

In a special case of adiabatic process with no friction force and negligible work done by external pressure the total energy of the system remains constant during the during the entire process of impact. Change of system energy is presented in Fig. 3.1.12a.

From thermodynamic point of view, three processes take place simultaneously during impact:

- kinetic energy of the impacting body is changed into gas internal energy,
- flow of the gas between the high-pressure and low-pressure chambers occurs (the process is not revealed by Eq. 3.1.71a),
- transport of energy in the form of heat between cylinder to environment takes place.

The first process results in change of kinetic and potential energy of the impacting object, however it does not cause energy dissipation. Moreover, due to the fact that time period of impact is short, the process of heat transfer to environment is insignificant and the process can be treated as adiabatic. Therefore, the dominating mechanism of impact energy dissipation is irreversible flow of the gas between high and low pressure chamber. Although it does not change total internal energy it changes the amount of internal gas energy which can be converted into mechanical work. As a result of coadjuvancy of the first and third process mechanical energy of the falling object is irreversibly changed into internal energy of the gas. Let us note that the influence of gas transfer between the chambers is not covered by global energy balances (3.1.71) which justifies the usage of the introduced notion of exergy.

After impact, the heat transfer through the cylinder walls occurs and surplus of temperature and the corresponding internal gas energy are reduced. After falling object is removed from the absorber, piston moves to its initial position due to a difference of areas subjected to action of pressure on both sides of the piston. Thus the system recovers its initial configuration both in terms of piston position and internal pressure.

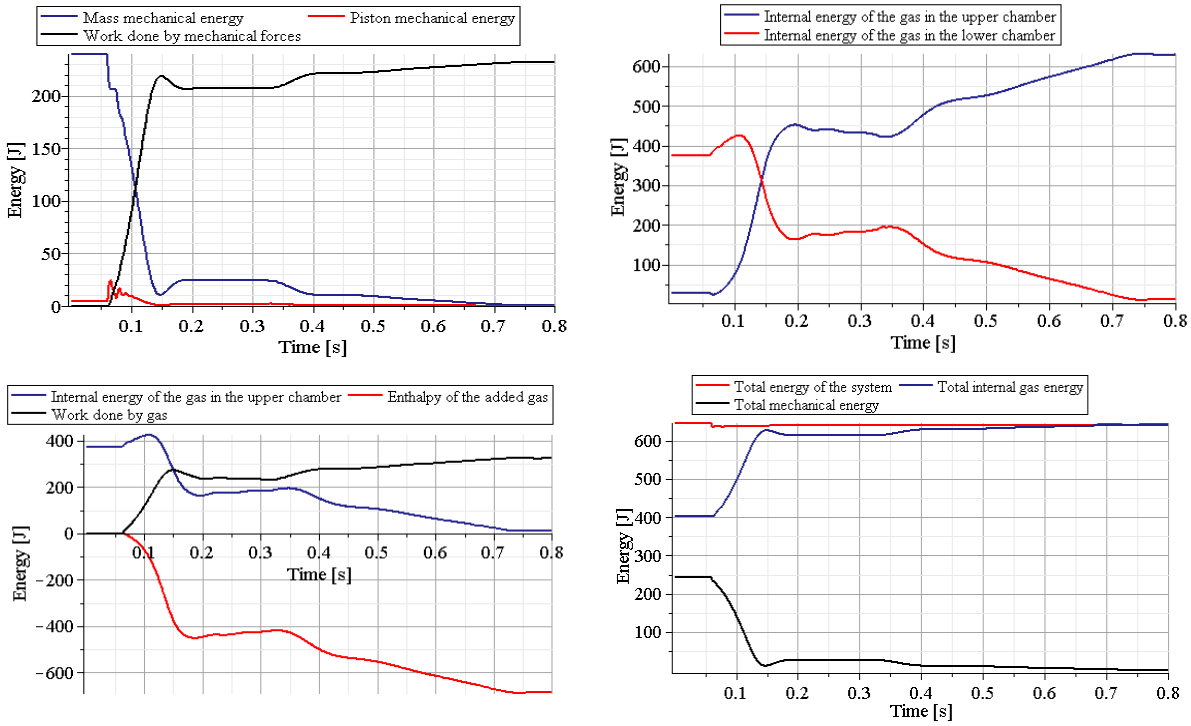

Fig.3.1.12a Analysis of change of system energy: a) mechanical energy balance (Eq. 3.1.68), b) change of internal energy of gas in both chambers (Eq. 3.1.69), c) balance of internal energy of gas in the lower chamber (Eq. 3.1.69a), d) global energy balance of the system (Eq.3.1.71a,b)

Further, the attention will be focused on mathematical description of the dissipation of the mechanical energy of the impacting object during the process. Similarly as in case of single chamber absorber we will utilize the notion of **exergy** X which indicates work that can be done by pneumatic system with fixed amount of gas in each chamber during transition from actual state $(\bar{t},\overline{V}_1,\overline{T}_1,\overline{T}_2,\overline{m}_1)$ to the 'referential state' in which mechanical energy of the impacting object is the largest $(t^{eq},V_1^{eq},T_1^{eq},T_2^{eq},m_1^{eq}=\overline{m}_1)$:

$$X(\bar{t}) = W_{Fp}\left(\bar{t} \to t^{eq}\right) = -L_{Fp}\left(\bar{t} \to t^{eq}\right) \tag{3.1.72a}$$

For double chamber cylinder the above formula is composed of three terms related to subsequent components of the pneumatic force:

$$X(\bar{t}) = \int_{\bar{t}}^{t_{eq}} p_2(\overline{m}_2, V_2, T_2)\frac{dV_2}{dt}dt + \int_{\bar{t}}^{t_{eq}} p_1(\overline{m}_1, V_1, T_1)\frac{dV_1}{dt}dt + p_A\,(A_2 - A_1)(u_2^{eq} - \bar{u}_2) \tag{3.1.72b}$$

where $\overline{m}_1$ and $\overline{m}_2$ denote fixed mass of gas inside each chamber. Similarly as previously, the introduced quantity indicates the amount of energy which will be transferred to impacting object when intentional dissipation (in this case exchange of gas between the chambers) will be stopped at time instant $\bar{t}$. By utilizing ideal gas law, introducing non-dimensional variable $\xi_1 = V_1 / V_1^{eq}$ and by performing integration by parts we obtain: (the overbars are omitted)

$$\begin{aligned} X = {} & m_2 R T_2 \ln\left(\frac{V_2^{eq}}{V_2}\right) - \int_t^{t_{eq}} m_2 R \dot{T}_2 \ln\left(\frac{V_2}{V_2^{eq}}\right)dt + \\ & + m_1 R T_1 \ln\left(\frac{V_1^{eq}}{V_1}\right) - \int_t^{t_{eq}} m_1 R \dot{T}_1 \ln\left(\frac{V_1}{V_1^{eq}}\right)dt + p_A\,(A_2 - A_1)(u_2^{eq} - u_2) \end{aligned} \tag{3.1.73a}$$

The above quantity depends on time-history of the process of transition from actual state to 'referential state'. In case of an adiabatic and isothermal processes the exergy can be expressed exclusively in terms of parameters of the system in actual and referential state. For the adiabatic process the formulae defining actual exergy reads:

$$\begin{aligned} X = {} & \frac{m_2 R T_2}{1-\kappa}\left(\left(\frac{V_2^{eq}}{V_2}\right)^{1-\kappa} - 1\right) + \frac{m_1 R T_1}{1-\kappa}\left(\left(\frac{V_1^{eq}}{V_1}\right)^{1-\kappa} - 1\right) + p_A\,(A_2 - A_1)(u_2^{eq} - u_2) = \\ & = m_2 c_V T_2 - m_2 c_V T_2^{eq} + m_1 c_V T_1 - m_1 c_V T_1^{eq} + p_A\,(A_2 - A_1)(u_2^{eq} - u_2) \end{aligned} \tag{3.1.73b}$$

The above definition is equivalent to the definition of the potential energy of the pneumatic system (Eq. 3.1.60c). Defined adiabatic exergy can be divided into specific exergy X^S (exergy of the gas contained in both cylinder chambers) and exergy of the environment X^{env}:

$$X = X^S + X^{env} = X^2 + X^1 + X^{env} \tag{3.1.74}$$

Exergy of the gas contained in both chambers has opposite sign, however, total exergy of the adiabatic system is always non-negative. Similarly as in case of single chamber absorber the specific exergy of the adiabatic system has especially simple interpretation since it equals change of the gas internal energy during the transition from the actual state to the referential state. Consequently, anergy of the gas equals its internal energy in the referential state. Accordingly, internal gas energy can be decomposed as follows:

$$U = X^S + A = \left(U - U^{eq}\right) + U^{eq} = \left(U_2 - U_2^{eq} + U_1 - U_1^{eq}\right) + \left(U_2^{eq} + U_1^{eq}\right) \tag{3.1.75a}$$

For isothermal process formula defining actual gas exergy takes the form:

$$X = m_2 R T_0 \ln\left(\frac{V_2^{eq}}{V_2}\right) + m_1 R T_0 \ln\left(\frac{V_1^{eq}}{V_1}\right) + p_A\,(A_2 - A_1)(u_2^{eq} - u_2) \tag{3.1.73c}$$

In this case, specific exergy is equal to heat which can be extracted from the environment in order to enable transition from actual to equilibrium state, and anergy of the gas equals the

difference of its initial energy and heat transferred from the environment:

$$U = X^S + A = \Delta Q^{t\to t^{eq}} + \left(U - \Delta Q^{t\to t^{eq}}\right) = \tag{3.1.75b}$$
$$= \Delta Q_2{}^{t\to t^{eq}} + \Delta Q_2{}^{t\to t^{eq}} + \left(U_2 - \Delta Q_2{}^{t\to t^{eq}} + U_1 - \Delta Q_1{}^{t\to t^{eq}}\right)$$

According to the Eq. 3.1.73a-c, we can calculate initial exergy of the system as a work that can be done during transition from the initial state to the corresponding referential state:

$$X^0 = m_2^0 R T_2^0 \ln\left(\frac{V_2^{0eq}}{V_2^0}\right) - \int_{t^0}^{t^{0eq}} m_2^0 R \dot{T}_2 \ln\left(\frac{V_2^0}{V_2^{0eq}}\right) dt + \tag{3.1.76a}$$
$$+ m_1^0 R T_1^0 \ln\left(\frac{V_1^{0eq}}{V_1^0}\right) - \int_{t^0}^{t^{0eq}} m_1^0 R \dot{T}_1 \ln\left(\frac{V_1^0}{V_1^{0eq}}\right) dt + p_A\,(A_2 - A_1)(u_2^{0eq} - u_2^0)$$

In case of adiabatic process the analogous formula takes the form:

$$X^0 = \frac{m_2^0 R T_2^0}{1-\kappa}\left(\left(\frac{V_2^{0eq}}{V_2^0}\right)^{1-\kappa} - 1\right) + \frac{m_1^0 R T_1^0}{1-\kappa}\left(\left(\frac{V_1^{0eq}}{V_1^0}\right)^{1-\kappa} - 1\right) + p_A\,(A_2 - A_1)(u_2^{0eq} - u_2^0) \tag{3.1.76b}$$
$$= m_2^0 c_V T_2^0 - m_2^0 c_V T_2^{0eq} + m_1^0 c_V T_1^0 - m_1^0 c_V T_1^{0eq} + p_A\,(A_2 - A_1)(u_2^{0eq} - u_2^0)$$

Finally in case of isothermal process we obtain:

$$X^0 = m_2^0 R T_0 \ln\left(\frac{V_2^{0eq}}{V_2^0}\right) + m_1^0 R T_0 \ln\left(\frac{V_1^{0eq}}{V_1^0}\right) + p_A\,(A_2 - A_1)(u_2^{0eq} - u_2^0) \tag{3.1.76c}$$

Initial exergy of the double-chamber pneumatic cylinder has similar interpretation as exergy of a single chamber cylinder. In particular, when the initial state is state of static equilibrium of the piston, the initial exergy X^0 indicates dissipation of mechanical energy of the impacting object between initial state and subsequent referential state in a process without transfer of gas between the chambers.

The above formula defining actual and initial exergy of the system allows to calculate change of exergy during the process $\Delta X = X - X_0$ or change of exergy between two arbitrary states of the system. The analysis of the system with constant volume of both chambers but with transfer of gas between the chambers indicates that two situations may occur:

- gas is transferred from the chamber located at this side of the piston where larger pneumatic force is generated: decrease of system exergy.
- gas is transferred from the chamber located at this side of the piston where smaller pneumatic force is generated: increase of the system exergy.

In general, decrease of gas exergy occurs when the gas transfer decreases absolute value of total force generated by the absorber and causes that the new state is closer to the state of equilibrium. During impact, the pneumatic force generated by gas enclosed in the lower chamber is higher than the force generated by force in the upper chamber, i.e. $p_2 A_2 > p_1 A_1 + p_A(A_2 - A_1)$. Moreover, pressure inside lower chamber is usually higher than pressure inside upper chamber. Therefore, gas is transferred from the lower to upper chamber causing decrease of the system exergy. Transfer of gas from lower to upper chamber can be treated as superposition of two processes: i) removing gas from the lower chamber and ii)

adding gas to upper chamber. Since each of these processes causes decrease of the system exergy the transfer of gas between the chambers is a more effective mechanism of energy dissipation than a release of gas to the environment.

An interesting feature of the considered system is the possibility of spontaneous increase of exergy. Such a process occurs when gas is transferred from the high pressure chamber which generates smaller component of the pneumatic force to the low pressure chamber which generates larger component of the pneumatic force. When the valve is opened briefly after impact the gas flows from the more inflated, but generating lower force upper chamber to the less inflated, but generating higher force lower chamber. Gas migration causes that position of equilibrium is moved upwards and exergy of the pneumatic system increases. As a result, speed of rebound can be larger than initial speed of impact which is in contradiction with the intuitive understanding of the behaviour of the absorber. The first law of thermodynamics is fulfilled since the increase of mechanical energy is compensated by decrease of gas internal energy. The second law of thermodynamics is also fulfilled since the considered irreversible process increases total entropy of the gas contained within the chambers, however it increases work that can be done by the system.

In the last step we will determine the work done by pneumatic system during transition $t_0 \to t$ during which mass of the gas changes $\left(m_1 \neq const, m_2 \neq const\right)$:

$$W_{Fp} = \int_{t_0}^{t} p_2(m_2, V_2, T_2)\dot{V}_2 dt + \int_{t_0}^{t} p_1(m_1, V_1, T_1)\dot{V}_1 dt + p_A\,(A_2 - A_1)(u_2 - u_2^0) \tag{3.1.77a}$$

which can be transformed into alternative form:

$$W_{Fp} = \int_{t_0}^{t} m_2 R T_2 \frac{\dot{V}_2}{V_2} dt + \int_{t_0}^{t} m_1 R T_1 \frac{\dot{V}_1}{V_1} dt + p_A\,(A_2 - A_1)(u_2 - u_2^0) \tag{3.1.77b}$$

By using similar methodology as in case of single-chamber cylinder we obtain general formula defining work done by gas:

$$\begin{aligned} W_{Fp} = {} & m_2 R T_2 \ln\left(\frac{V_2}{V_2^0}\right) - \int_{t_0}^{t} \left(\dot{m}_2 R T_2 + m_2 R \dot{T}_2\right) \ln\left(\frac{V_2}{V_2^0}\right) dt + mRT \ln\left(\frac{V_1}{V_1^0}\right) + \\ & - \int_{t_0}^{t} \left(\dot{m}_1 R T_1 + m_1 R \dot{T}_1\right) \ln\left(\frac{V_1}{V_1^0}\right) dt + p_A\,(A_2 - A_1)(u_2 - u_2^0) \end{aligned} \tag{3.1.77c}$$

In case of adiabatic process, an analytical formula defining work done by gas in terms of mass of the gas and chambers volume (analogous to 3.1.32b) can not be derived due to a relatively complex differential relation describing change of temperature inside the chamber with the inflow of the fluid. Therefore, a general formula (3.1.77c) has to be used and time integration has to be performed numerically. Finally, in case of isothermal process we obtain:

$$\begin{aligned} W_p = {} & m_2 R T_0 \ln\left(\frac{V_2}{V_2^0}\right) - \int_{t_0}^{t} \dot{m}_2 R T \ln\left(\frac{V_2}{V_2^0}\right) dt + m_1 R T_0 \ln\left(\frac{V_1}{V_1^0}\right) - \int_{t_0}^{t} \dot{m}_1 R T \ln\left(\frac{V_1}{V_1^0}\right) dt \\ & + p_A\,(A_2 - A_1)(u_2 - u_2^0) \end{aligned} \tag{3.1.78}$$

The above defined quantities allow to divide internal energy of the gas into exergy and anergy (Fig. 3.1.12b$_1$) and to calculate pneumatic dissipation of the mechanical energy of the

impacting object D_1, cf. Eq. 3.1.33 and pneumatic dissipation of total useful energy D_2, cf. Eq. 3.1.25c and Eq. 3.1.34. Overall change of total useful energy of the system is governed by the equation:

$$\Delta E^* = \Delta E_k + \Delta E_p + \Delta X = -D_2 - D_{fr} \tag{3.1.79}$$

In contrast to total energy of the system, total useful energy decreases during the whole impact process as a result of transfer of gas from the lower to the upper chamber (cf. Fig. 3.1.12a$_4$ vs. 3.1.12b$_2$). Moreover, change of useful energy of double-chamber absorber is qualitatively similar change of useful energy of single chamber absorber with exhaust to environment (Fig. 3.1.3b$_2$) which reflects that both systems are dissipative. In considered system without friction the useful energy denotes maximal energy of the impacting object which can be obtained if intentional dissipation by gas transfer will not be further performed.

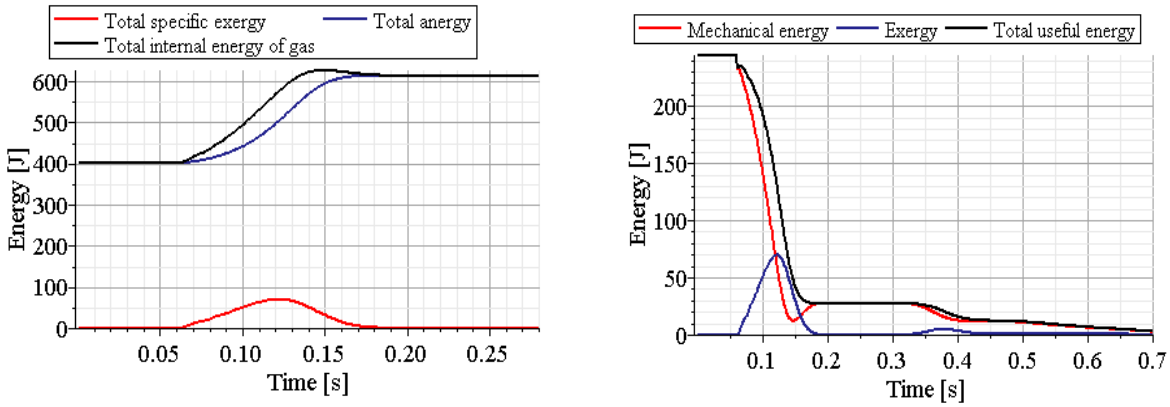

Fig. 3.1.12b Analysis based exergy and anergy: a) division of internal energy into specific exergy and anergy, b) change of mechanical energy, exergy and total useful energy of the system

The **mathematical structure** of the equations governing pneumatic system with valve between the chambers can be revealed by using simplified 1DOF model of frictionless system working under isothermal conditions and which assumes with simple model of the gas flow:

$$M\ddot{u} + (p_2 - p_1)A = 0 \tag{3.1.80}$$

$$p_2 A_1 (h_0 - u_2) = m_2 R T_0, \quad p_1 A_1 u_2 = (m_t - m_2) R T_0$$

$$p_2 - p_1 = -C_V \dot{m}_2$$

$$\text{IC: } u(0) = 0, \dot{u}(0) = V_0, p_1(0) = p_1^0, p_2(0) = p_2^0$$

Ideal gas law can be combined with equation of the gas flow, which leads to differential equation defining mass of the fluid inside the lower chamber. Analytic solution of this equation allows to obtain analytic formulae defining pressures p_1 and p_2 (and resulting pneumatic force) in terms of piston displacement and valve opening:

$$p_1(t) = \frac{\left(\left(\dfrac{mRT_0}{C_V} \displaystyle\int_0^t \frac{e^{\frac{RT_0}{C_V}\int_0^t \frac{V}{(V_{01}+u(t)A)(V_{02}-u(t)A)}dt}}{(V_{02}-u(t)A)}dt + m_{01} \right) e^{\frac{RT_0}{C_V}\int_0^t -\frac{V}{(V_{01}+u(t)A)(V_{02}-u(t)A)}dt} \right) RT_0}{V_{01}+u(t)A} \tag{3.1.81}$$

and

$$p_2(t)=\frac{\left(\left(\frac{mRT_0}{C_V}\int_0^t \frac{e^{\frac{RT_0}{C_V}\int_0^t \frac{V}{(V_{01}+u(t)A)(V_{02}-u(t)A)}dt}}{(V_{01}+u(t)A)}dt+m_{02}\right)e^{-\frac{RT_0}{C_V}\int_0^t \frac{V}{(V_{01}+u(t)A)(V_{02}-u(t)A)}dt}\right)RT_0}{V_{02}-u(t)A} \tag{3.1.82}$$

Therefore equation of motion can be written in a simplified manner:

$$M\ddot{u}+\frac{f\left(I_1\left(I_2(u),u,C_V\right),I_2(u),u,C_V\right)}{V_{02}-uA}-\frac{g\left(I_1\left(I_2(u),u,C_V\right),I_2(u),u,C_V\right)}{V_{01}+uA}=0 \tag{3.1.83}$$

where the symbol $I_{1/2}$ denotes integral. According to Eq. 3.1.82 and Eq. 3.1.83, pneumatic force generated by the absorber depends, in complicated integral manner, on piston displacement and valve opening, which indicates that it depends on time-history of the process. In comparison to analogous formula for single chamber cylinder (Eq. 3.1.38c), the dependence on valve opening is similar, however, dependence on piston displacement is of more complex form. The pneumatic force is evidently not a direct function of the actual piston velocity and actual valve opening, what is a typical feature of hydraulic shock absorbers. However, as a consequence of displacement history dependence, the response of the pneumatic system changes considerably for slow and fast impacts of the same kinetic energy.

An alternative method of derivation of a single equation governing the piston motion utilizes time integration of combined Eq. 3.1.80a and Eq. 3.1.80c which yields:

$$m_2=\frac{M}{C_V A}\left(\dot{u}-\dot{u}(0)\right)+m_{02} \tag{3.1.84}$$

By introducing ideal gas law into equation of mass motion and by utilizing the above formula we obtain:

$$M\ddot{u}+\frac{MRT_0}{C_V}\left(\frac{\dot{u}}{(h_{02}-u)A}+\frac{\dot{u}}{(h_{01}+u)A}\right)+\frac{m_{02}RT_0}{h_{02}-u}-\frac{m_t RT_0}{h_{01}+u}+ -\frac{MRT_0}{C_V}\left(\frac{V_0}{(h_{02}-u)A}+\frac{V_0}{(h_{01}+u)A}\right)=0 \tag{3.1.85}$$

In the above equation, three groups of terms can be distinguished, consecutively: i) damping terms which depend on piston displacement and mass of the impacting object, ii) nonlinear stiffness terms, iii) nonlinear stiffness terms which depend on initial momentum of the impacting object. Moreover, value of the flow resistance coefficient influences both damping and stiffness terms. The structure of the above formula and the analogous formula for single chamber cylinder with exhaust to environment is very similar. However, differentiation of Eq. 3.1.85 over time does not allow to eliminate dependence on initial velocity of the hitting object. Therefore, third order equation describing motion of the mass (analogous to Eq. 3.1.40) can not be derived.

For the sake of completeness let us also analyse the influence of valve opening and value of initial pressure inside cylinder on global dynamic properties of double-chamber pneumatic absorber. The influence of valve opening was intentionally analysed for relatively high values of resistance coefficient and for long time interval to observe behaviour of the under-damped system with response of vibration-type (Fig. 3.1.13a) and its transition to over-damped system with strongly dissipative characteristics (Fig. 3.1.13b).

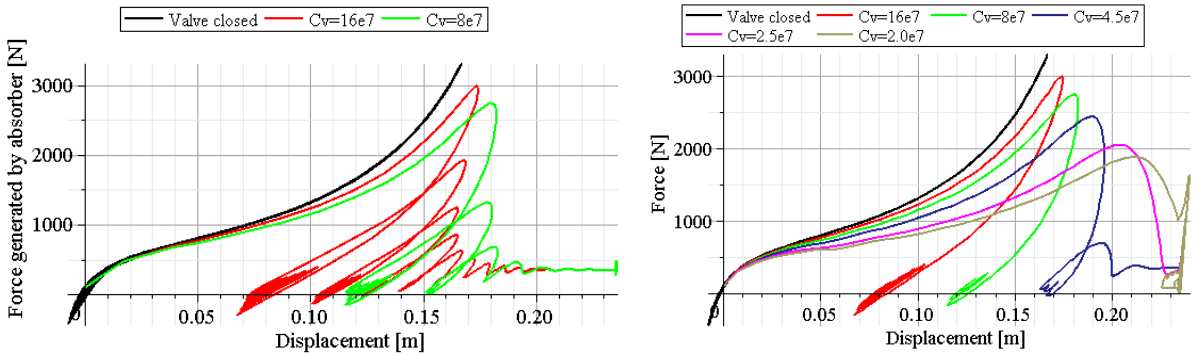

Fig.3.1.13 Influence of valve opening (represented by flow resistance coefficient [Pa/(kg/s)]) on force generated by the absorber: a) small valve opening: under-damped case, b) transition from elastic to dissipative characteristics

Value of initial pressure also significantly changes the dynamic characteristics of the absorber and its ability of energy dissipation. In the presented example various initial pressure is applied, however the valve opening is constant during the process and remains unaltered for subsequent impacts. Increase of initial pressure reduces utilized stroke of the absorber and changes maximal value of generated pneumatic force. The value of pressure, for which maximal value of pneumatic force is the smallest is, however, not known a priori.

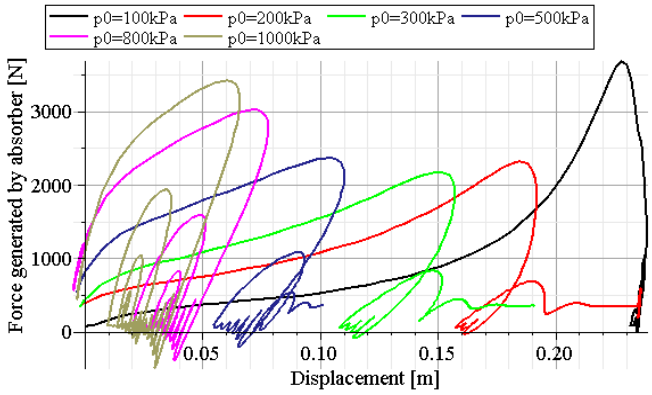

Fig.3.1.14 Influence of initial pressure on maximal pressure during impact and utilised stroke

Due to the fact that design of two-chamber pneumatic absorber resembles to some extend the classical hydraulic damper both devices will be compared against each other. Although the principle of energy dissipation is in both cases the same (kinetic energy is changed into heat which is further transferred to the environment), mathematical description and dynamic characteristics of both systems are completely different.

Hydraulic damper contains incompressible fluid which is forced to flow through the orifice and pneumatic cushion which compensates changes of internal absorber volume during

compression. The main consequence of incompressibility of the fluid is direct dependence of damping force on piston velocity. In the simplest case, this relation is linear or quadratic depending on type of applied fluid and considered numerical model. As a result, hydraulic damper can be described by single differential equation:

$$M\ddot{u} + p_0 A_p \left(\frac{V_0}{V_0 - uA_p} \right)^{\kappa} + sign(\dot{u}) \frac{1}{2} \frac{\rho A_h^{\ 3}}{C_d^{\ 2} A_0^{\ 2}} \dot{u}^2 = 0 \tag{3.1.86}$$

where the quantities p_0, V_0 and A_p denote initial pressure of gas, volume of the pneumatic cushion and pneumatic area, respectively, while ρ, A_h, C_d, A_0 indicate density of the hydraulic fluid, pneumatic area, discharge coefficient and cross-sectional area of discharge orifice. Equation (3.1.86) contains two separate terms describing elastic force and damping force causing energy dissipation. Consequently, control of the orifice width changes damping force and does not alter elastic force.

On the contrary, pneumatic absorber does not contain separate mediums which causes elastic force and damping. Moreover, general model of pneumatic absorber is more complicated than the model of hydraulic absorber since it is composed of several differential equations or, after transformation, a single equation with several complicated terms being combination of nonlinear stiffness and damping. Even in the simplest case of isothermal conditions, equation of mass motion contains integral terms where elastic and damping forces can not be separated from each other. Therefore, pneumatic absorber should not be considered from the perspective of similarity to hydraulic absorber since it may lead to confusion, especially, in case of more complicated, adaptive versions of both types of absorbers.

Comparison of three types of pneumatic absorbers

Three considered types of pneumatic absorbers (with outflow to environment, with outflow to accumulator and with valve between the chambers) have different dynamic characteristics and the choice of optimal type of absorber depends on its future application. Since all above systems are considered in the context of energy dissipation, the best evaluation method is based on comparison of change of pneumatic force in terms of piston displacement obtained for a constant, arbitrary assumed valve opening, Fig. 3.1.15. The area below plot of the force indicates work done on the pneumatic system. When the process is considered between points where force equals zero (the points of zero exergy), the area below the plot equals to dissipated mechanical energy.

It is clearly seen that dissipation obtained in the system equipped with an accumulator is the smallest, which is caused by increase of pressure inside accumulator. Moderate dissipation occurs in case of absorber with exhaust to environment where pneumatic force decreases at the final part of the stroke. Finally, the largest dissipation occurs when gas is transferred from the lower to the upper chamber of the cylinder since, as discussed, dissipation occurs due to removing fluid from compressed chamber and adding fluid to decompressed chamber. On the other hand, transfer of gas to the upper chamber increases its internal pressure and diminishes pressure difference between the chambers which causes that further flow of the gas is aggravated.

Another feature that can be compared is the correspondence of the fluid flow with desired dissipation of the energy. The process of energy dissipation is permanent only in case of single-chamber pneumatic cylinder with exhaust to environment. As long as pressure inside cylinder remains larger than external one, the outflow of the fluid occurs and exergy decreases. When pressure drops below external one, the inflow of the gas takes place, but exergy is still diminished, cf. Sec.3.1.1. Such a beneficial situation does not always occur in case of double-chamber cylinder with outflow to accumulator and with the absorber with valve between the chambers. The adverse process of increase of system energy takes place most easily in a system with the accumulator, when during backstroke gas enters main cylinder chamber where pressure is higher than the external one.

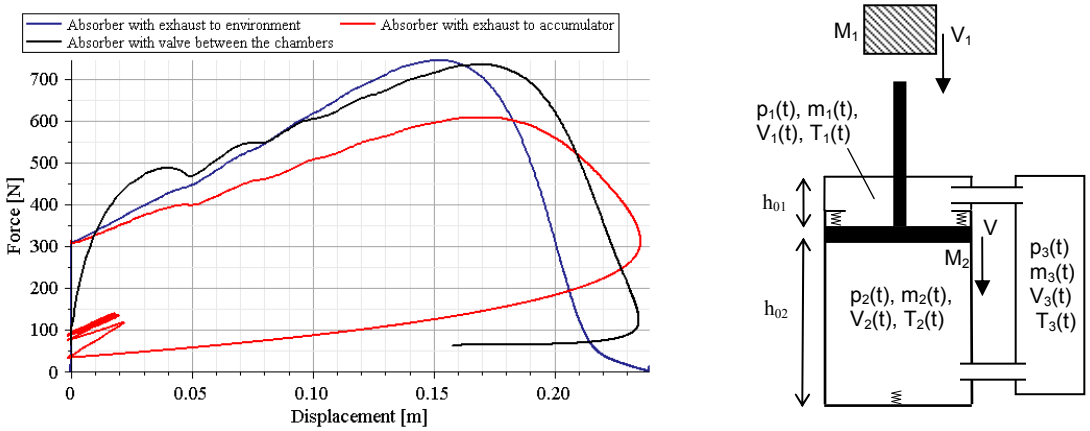

Fig. 3.1.15 a) Force-displacement characteristics obtained for three considered types of absorbers, b) Universal adaptive pneumatic absorber being generalisation of three analyzed adaptive absorbers

The next property concerns the possibility of absorbing the whole energy of impact. In single-chamber system the value of the force at the end of the process can be reduced to zero and the entire energy of the hitting object can be dissipated. On the contrary, in case of double-chamber cylinder located horizontally the force cannot be reduced to zero due to difference in effective area of the chambers on both sides of the piston and therefore the entire impact energy cannot be absorbed. Consequently, certain rebound of the impacting object will always occur. The largest rebound is expected in system with accumulator due an increase of exergy during backstroke.

The last feature, which distinguishes different types of pneumatic systems, is stability of position of static equilibrium and the corresponding ability of returning to initial state after impact. This feature of the pneumatic system can be treated as highly beneficial since it provides the possibility of multiple usage of the pneumatic device. The feature of stable static equilibrium is characteristic for closed pneumatic systems as the one with exhaust to accumulator (with initial accumulator pressure equal to initial cylinder pressure) and the one involving gas flow between two chambers of the cylinder. For non-ideal pneumatic absorber (involving friction force) the ability of returning to initial position also depends on value of static friction force.

Three described pneumatic absorbers can be integrated in a single pneumatic system containing two chambers on both sides of the piston, an accumulator and valves between each

chamber and accumulator, vide Fig. 3.1.15b. Such a generalized pneumatic system can be reduced to previously considered elementary pneumatic absorbers in the following way:

- by closing the upper valve and substantial increase of accumulator volume - to the system with exhaust to environment,
- by closing the upper valve only - to the system with accumulator,
- by opening both valves and reducing volume of the accumulator to minimum - to double-chamber pneumatic system with gas exchange between the chambers.

Comparison of 'falling object' and 'landing object' problems

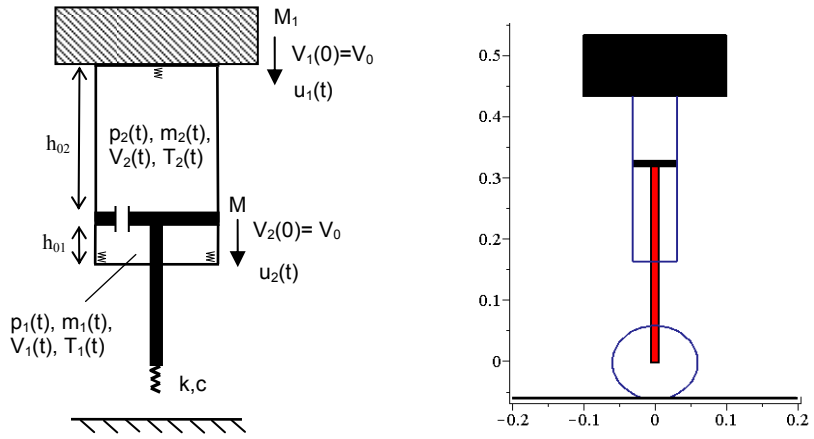

Fig 3.1.16 a) Definition of the 'landing object' problem, b) simulation performed in Maple software

Another, additional issue in modelling of pneumatic absorbers is a clear distinction between ‘falling object’ problem and ‘landing object’ problem. Since the case of rigid object falling into adaptive absorber located on the ground is often used as an experimental model for airplane landing gear, the relation of quantities obtained in both problems has to be clearly established. Comparison of results obtained in cases of 'falling object' and 'landing object' problems will be performed for double-chamber cylinder with internal flow between the chambers since this type of absorber is best suited to be applied as airplane landing gear. Equations describing landing of the object equipped with pneumatic absorber read:

$$M_1 \frac{d^2 u_1}{dt^2} - M_1 g + F_P + F_{fr} - F_D^{BOT} + F_D^{TOP} = 0 \tag{3.1.87a}$$

$$M_2 \frac{d^2 u_2}{dt^2} - M_2 g - F_p - F_{fr} + F_D^{BOT} - F_D^{TOP} + F_C = 0 \tag{3.1.87b}$$

where mass M_1 and displacement u_1 are related to the falling object, while mass M_2 and displacement u_2 are related to the piston and the wheel. Let us note that falling mass is not subjected to the action of contact force as it was in case of ‘falling object’ problem but instead, to forces generated by the absorber: pneumatic, friction and delimiting force. Each of these forces depends on mutual position and velocity of the falling mass and the piston. Moreover, the contact force which accounts for the force in the pneumatic tire is acting exclusively on the piston rod and depends on position of the wheel with respect to ground. Dependence of above forces on system kinematics is the following:

$$F_p = f(u_2 - u_1)\,, \quad F_{fr} = f(u_2 - u_1, \dot{u}_2 - \dot{u}_1)\,, \quad F_D = f(u_2 - u_1)\,, \qquad (3.1.88)$$
$$F_C = f(u_2, \dot{u}_2)$$

The system has to be supplemented with initial conditions imposed on initial position and velocity of the falling mass and the piston (usually of the same value) and parameters of the gas inside cylinder.

The comparison of the results obtained for two described models reveals very good correspondence of global response of the absorber, i.e., pressures of gas in both chambers (Fig. 3.1.17a) and total generated force. However, the comparison shows clear discrepancy between acceleration of the mass at the beginning of the process obtained from two above models (Fig. 3.1.17b). Moreover, the acceptable agreement of local response expressed in terms of contact force (Fig. 3.1.17c, error of ~14%) and acceleration of the piston (Fig. 3.1.17d) was obtained. The simple conclusion from the analysis is that the system with rigid object falling on the pneumatic cylinder can be used for modelling pneumatic landing gear; however, sum of forces generated by the absorber (not the contact force) should be considered as force acting on the falling object and should be used for calculation of the falling object deceleration. The above comment applies primarily to the first stage of impact when the contact force may suffer large variations (depending on mass of the piston and properties of the contact element, cf. Sec. 3.1.1).

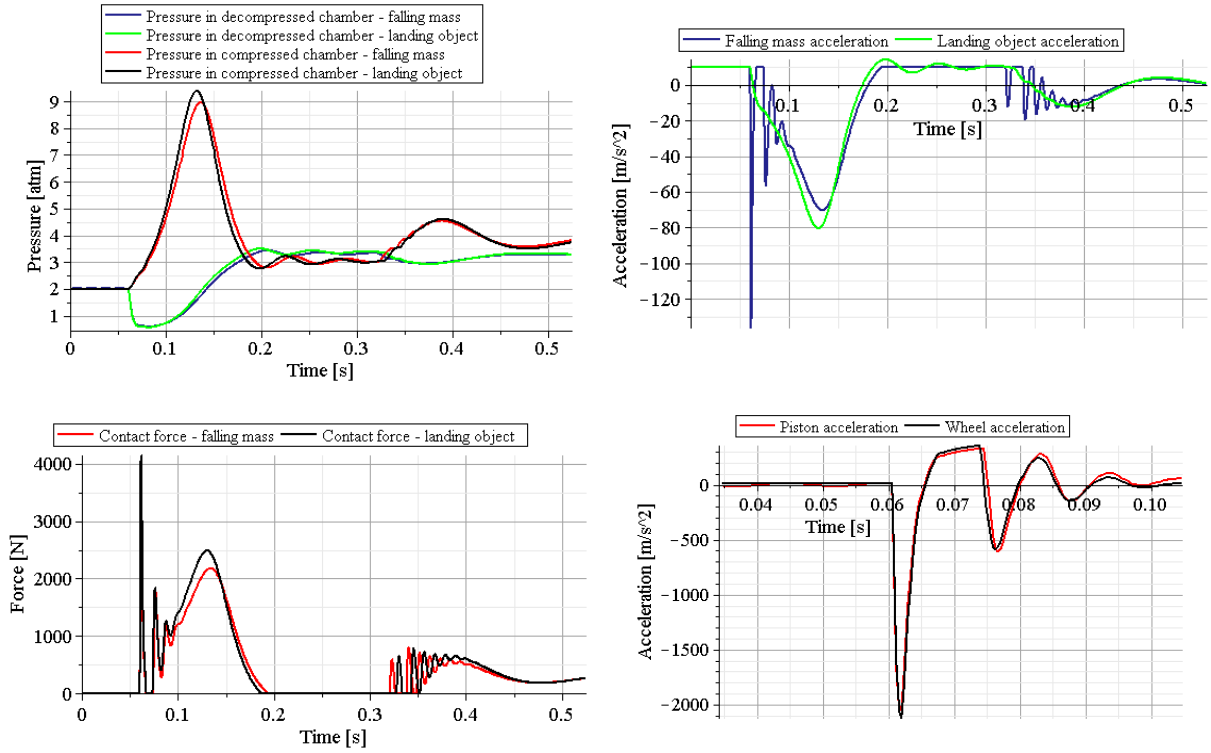

Fig 3.1.17 Comparison of the results obtained from the numerical analysis of falling object hitting stationary pneumatic cylinder and falling object with connected pneumatic cylinder

Simplified methods of modelling

Apart from the above precise methods of modelling, which take into account two mechanical degrees of freedom which appear in the model (falling mass and piston), several simplified

approaches can be proposed. Eventually, the following methods of modelling of pneumatic absorbers can be distinguished:

- 2DOF (already discussed in this chapter),
- 1.5 DOF (model which neglects inertia of the piston),
- Enhanced 1DOF (model which takes into account exclusively the inertia of the falling object, however allows for simplified modelling of the rebound),
- 1 DOF (the model which takes into account falling mass only).

Hereafter, let us focus on the absorber with valve located between the chambers impacted by the falling object. In case of 1.5 DOF model the equations of motion of falling object (Eq.3.1.54) remains unchanged, but equation of motion of the piston neglects the inertia term:

$$M_1 \frac{d^2 u_1}{dt^2} - M_1 g + F_C(u_1, \dot{u}_1, u_2, \dot{u}_2) = 0 \tag{3.1.89}$$

$$F_P(u_2) - F_C(u_1, \dot{u}_1, u_2, \dot{u}_2) - F_D{}^{TOP}(u_2) + F_D{}^{BOT}(u_2) + F_{Fr}(u_2) = 0 \tag{3.1.90}$$

The above system of equations has to be complemented with differential equation describing mass flow rate of the fluid, balances of internal energy in each chamber and definitions of all present forces (contact, pneumatic, delimiting and friction). The above model neglects inertia of the piston, however it takes into account compliance of the contact element. In case when simplified (velocity-independent) model of the contact and friction force is assumed, the second equation is no longer differential but becomes algebraic. However, due to complex form of Eq. (3.1.90), piston displacement can not be expressed analytically in terms of mass displacement. Therefore, the complete system of governing equations can not be simplified into system containing entirely differential equations and it should be qualified as system of differential-algebraic equations (DAEs).

Enhanced 1 DOF model utilises equation of motion of the falling mass in the form:

$$M_1 \frac{d^2 u_1}{dt^2} - M_1 g + F_P(u_2) - F_D{}^{TOP}(u_2) + F_D{}^{BOT}(u_2) + F_{fr}(u_2) = 0 \tag{3.1.91}$$

and equations governing thermodynamic part of the system. However, an additional procedure is used to simulate interaction of mass with weightless cylinder piston:

- Force generated by the absorber (being sum of pneumatic, delimiting and friction forces) is applied to the falling mass in case when it assumes positive values, i.e. when it acts in upward direction.
- When force generated by the absorber drops below zero (which indicates disconnection of piston and mass) it becomes inactive in a model. Moreover, the valve is arbitrarily closed to maintain system in unchanged state.
- When absorber force is positive, position of the piston is calculated basing on position of the mass; in other cases piston is set in equilibrium position.

Despite its simplicity, the method enables modelling of three cases of the falling mass rebound:

- the case of strong rebound when piston hits upper delimiter and mass disconnects from the piston,

- the case when piston rebounds but does not reach upper delimiter and mass disconnects in the middle of the cylinder stroke,
- the case of slight rebound without disconnection of piston and mass (the case when during entire rebound stage the absorber force preserves positive value).

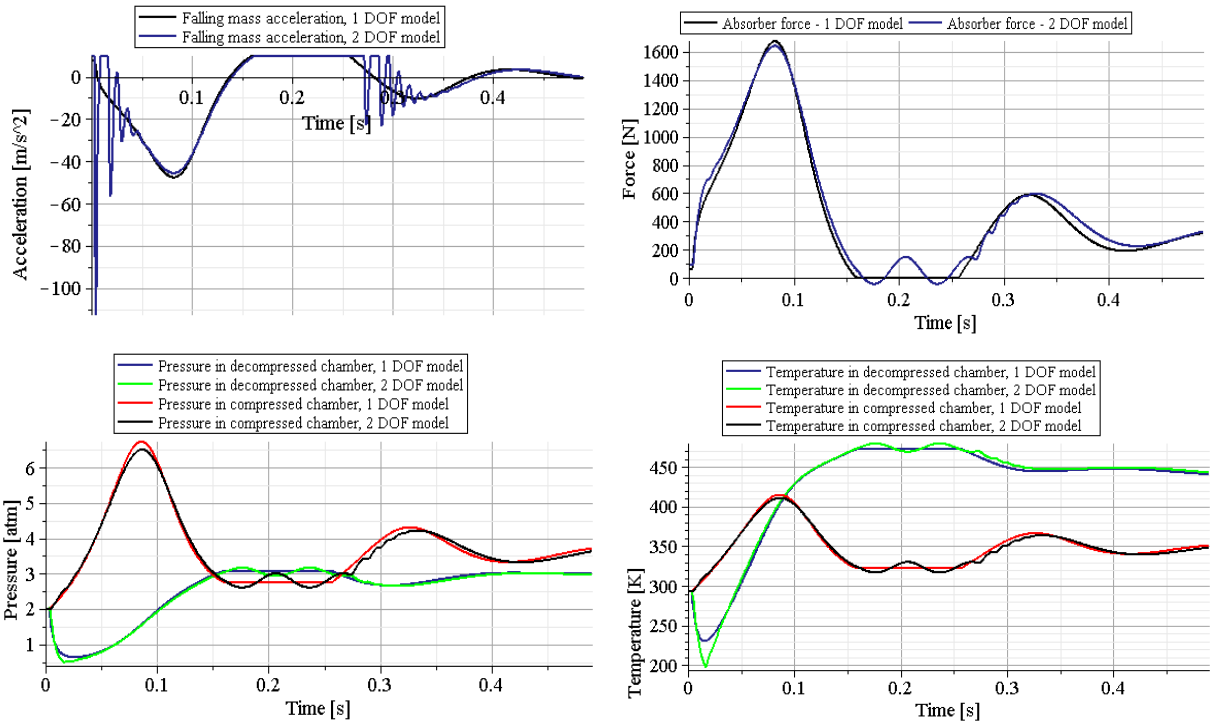

Fig.3.1.18 Comparison of results obtained by using enhanced 1 DOF model and 2 DOF model: a) falling mass acceleration, b) force generated by the absorber, c) pressures in both chambers, d) temperature in both chambers.

Enhanced 1DOF model allows to obtain results of a good correspondence with reference results from 2DOF model (Fig. 3.1.18b-d). However, it is not capable of modelling the phenomenon of initial rebounds of the piston from the falling mass and corresponding initial variation of the contact force and mass acceleration (Fig. 3.1.18a).

Finally, the simplest model of the absorber subjected to an impact loading is based exclusively on Eq. 3.1.91. In case of 'falling object problem' such a model refers to the situation when after collision the falling mass sticks to the piston and they move together during the rest of the process. On the contrary, in case of 'landing object problem', the model refers to the situation when after landing the wheel of the object can not disconnect from the ground. Distinction between the problems of 'falling object' and 'landing object' should be preserved by various assumption of the mass and initial velocities. Mass applied in one degree of freedom model of a 'falling object' problem should be equal to sum of masses of the hitting object and piston. Moreover, initial velocity should be calculated under assumption of inelastic collision of both objects. On the contrary, values of mass and initial velocity applied in one degree of freedom model of a 'landing object' problem should be equal to corresponding quantities in real situation and should not be altered.

Properties of 1DOF pneumatic systems with controllable gas exhaust subjected to an impact loading are precisely described in [256].

Numerical implementation issues

The implementation of the described above numerical models of three types of passive pneumatic absorbers was performed in three manners:

- 2DOF and 1DOF models were implemented from scratch in MAPLE software by introducing appropriate differential equations, next by solving them by fourth order Runge-Kutta method and, finally, by integrating them over time and displacement in order to obtain momentum and energy balances.
- 1 DOF models were implemented in commercial implicit finite element software ABAQUS Standard (finite element approach was not used). Since built-in functions of ABAQUS allow only for basic modelling of fluid-filled structures, additional features (energy balance, Saint-Venant model of the flow) were implemented by Fortran subroutines.
- 1 DOF models were implemented within explicit finite element software ABAQUS Explicit (FEM was again not utilized) which offers wide range of possibilities for modelling fluid filled structures with Uniform Pressure Method.

Results obtained from three above methods for three types of absorbers were precisely compared with each other and their good agreement was obtained. MAPLE models of pneumatic cylinders were developed for the purpose of further convenient introduction of the adaptation strategies. By contrast, ABAQUS models of pneumatic cylinders were treated as initial stage before modelling more complex adaptive pneumatic structures. ABAQUS Standard models were developed since they enable simple implementation of adaptation strategies by means of Fortran subroutines. ABAQUS Explicit models were implemented since explicit methods are well suited for simulation of fast dynamic events resulting in large deformations analysed in further chapters.

Summary of the Section 3.1

The section discussed the problem of simplified modelling and dynamical properties of three types of pneumatic absorbers. The proposed model based on ordinary differential equations reveals dynamic properties of the analyzed pneumatic systems including detailed insight on the process of energy dissipation. The difficulty of the model interpretation results from the following facts: i) description of the problem by several differential equations not a single one, ii) nonlinearity of the governing equations, iii) the lack of separate term corresponding to stiffness and damping in equation of motion. The model was investigated by using purely mechanical and thermodynamic approach and by combination of both. The importance of the notion of exergy of the pneumatic system as a good measure of energy dissipation was emphasized. Moreover, the features of the model were analyzed from both physical and mathematical point of view.

The above performed comprehensive and multithread analysis is required for understanding basic mechanical features of the pneumatic absorbers and can not be omitted before proceeding to more advanced problems of control and optimal design of the adaptive pneumatic absorbers. The features of the pneumatic absorbers are planned to be further investigated with the use of: i) Noether's theorems, ii) theory of the 'wandering sets', iii) Lagrangian and Hamiltonian formalism for description of the dissipative processes.

3.2. Pressure control strategies

All pneumatic absorbers considered in previous section were passive, i.e. valve opening was arbitrarily fixed and remained constant during the whole period of impact. Consequently, mass flow rate of the gas and resulting change of pressure inside cylinder chambers were dependent only on initial parameters of gas and impact characteristics. On the contrary, adaptive pneumatic cylinders are equipped with controllable valve whose opening can be changed during the impact process and which enables control of internal pressure inside cylinder chambers. Therefore, the next step in analysis of pneumatic absorbers is development of valve opening strategies (also called 'pressure control strategies') which allow to obtain adaptation of the absorber to actual impact loading.

From mathematical point of view, passive pneumatic cylinder is described by ordinary differential equations with constant coefficients. Control of pneumatic absorbers executed by change of characteristics of the valve during analysis is reflected in numerical model by time-dependence of the flow area $A(t)$ or resistance coefficient $C(t)$. Therefore, mathematical model of adaptive pneumatic cylinder is described by differential equations with variable coefficients. When closed control loop is applied, resistance coefficients depend on actual response of the system which introduces additional nonlinearity to governing equations.

Control objectives for adaptive pneumatic cylinders depend on their particular application within the wide range of possible applications of Adaptive Impact Absorption. In general, all control problems concerning adaptation of inflatable structures formulated in Chapter 2 can be adopted to pneumatic cylinders. Similarly, as in case of all adaptive inflatable structures, the main adaptation task is related to protection of the hitting object by dissipating the largest part of impact energy with minimal value of acceleration. As it was previously proposed, two separate control problems involving impacting object deceleration and its final kinetic energy can be formulated:

$$\text{Find } p_0, C(t) \quad \text{such that} \quad J_2 = \max_t \left|\ddot{u}(t)\right| \text{ is minimal} \tag{3.2.1}$$

$$\text{Find } p_0, C(t) \quad \text{such that} \quad J_3 = E_k(t_{end}) \text{ is minimal} \tag{3.2.2}$$

or the above objectives can be incorporated into a single control problem. Here, the attention will be given to the formulations related separately to minimisation of acceleration and minimisation of kinetic energy assuming that one of these quantities is of primary interest. Another group of problems is related to protection of the impacted cylinder by minimisation of pressure inside compressed chamber:

$$\text{Find } p_0, C(t) \quad \text{such that} \quad J_5 = \max_t p(t) \text{ is minimal} \tag{3.2.3}$$

An additional control problem relies on finding valve opening which maximizes load capacity of the structure (understood as maximal allowable impact energy) under condition that constraints imposed on maximal deceleration, maximal value of final kinetic energy and maximal value of pressure are not violated. Mathematical formulation of this problem reads:

$$\begin{aligned} &\text{Find } p_0, C(t) \quad \text{such that} \quad E_k(t_0) \quad \text{is maximal} \\ &\text{subject to: } \max_t \left|\ddot{u}(t)\right| < f_1, \quad E_k(t_{end}) < f_2, \quad \max_t p(t) < f_3 \end{aligned} \tag{3.2.4}$$

Additional constraints which have to be included in both types of the problems concern range of available initial pressure values, range of valve opening and speed of valve opening:

$$p_0 \in \langle p_{\min}, p_{\max} \rangle, \quad C(t) \in \langle C_{\min}, C_{\max} \rangle, \quad \frac{dC(t)}{dt} < \widetilde{C}_{\max} \tag{3.2.5}$$

In most of the considered problems only selected of these constraints will be applied.

3.2.1 Comments on impact identification techniques

As it was previously described a preliminary step of Adaptive Impact Absorption, which precedes the adaptation process, is identification of the impact loading. In general problem of impact identification, both location of the impact loading, its direction and time-variation have to be determined. Methods of impact identification can be divided into 'on-line' methods which identify impact at the very beginning of the process and 'off-line' methods which utilize measurements from the whole impact period and conduct precise post-factum identification. The most classical approach for identification of impact loading utilizes propagation of elastic waves inside considered structure [257]. An overview of methods based on inverse analysis utilized for indirect identification of the impact loading is presented in paper [258]. In turn, description of on-line methods of load identification techniques is presented in [259], where the authors introduce four time-domain methods and outline advantages and disadvantages of the particular approaches. The methods of dynamic load identification developed at IPPT PAN are related both to online methods (weigh-in-motion devices and impact identification devices [105 260]) and offline methods (identification of loading acting on truss and frame structures [261]).

In considered case of pneumatic absorbers, the procedures of impact identification can be developed both for 'impacting object problem' and 'landing object problem'. Here, the problem will be limited to the first case and, additionally, it will be assumed that impacting object is totally rigid. Since location and direction of the impact is known a priori, the identification problem is substantially simplified. The purpose of the identification is to determine mass and velocity of the impacting object exclusively by using sensors attached to the impacted absorber.

Two efficient methods for identification of two parameters of the rigid object hitting pneumatic absorber were proposed by Sekuła, et al. [262]. The first method is based on measurement of the contact force which acts between colliding bodies. The method utilises the so-called 'response map' which is prepared in advance and aggregates quantities that characterise measured contact force (such as its maximal amplitude or time when it is achieved) for various parameters of the impact loading. Identification is performed by comparing actually obtained response with the referential response from the prepared map. The second method utilises time integration of equation of falling mass motion and exploits the fact that at certain time instants, at the beginning of the process (t_1 and t_2), velocities of the colliding objects are exactly equal. Therefore, when integration is performed in the range (t_1, t_2) acceleration of the falling mass can be replaced by acceleration of the piston, which allows to calculate the unknown mass of the falling object M_1^{id} and its initial velocity V_1^{id} from the formula:

$$M_1^{id} = -\int_{t_1}^{t_2} F_C(t)dt \Big/ \left[\int_{t_1}^{t_2} (a_2(t) - g)dt\right], \qquad V_1^{id} = v_1(t_1) = v_2(t_1) \tag{3.2.6}$$

where F_C denotes contact force and a_2 denotes acceleration of the piston, which are both measured during impact.

The purpose of the further part of this section is general classification of mass and velocity identification methods and proposition of some additional techniques of impact identification. Since the contact force will be the main quantity utilized in proposed identification procedures, its sensitivity on impacting mass and velocity is crucial for the effectiveness of the identification process. Sensitivity analysis was conducted with the use of developed numerical model of the absorber (Fig. 3.2.1a). The influence of impacting object mass is nearly not reflected in the initial variation of the contact force and becomes distinct only in the second stage of impact. On the contrary, the influence of impact velocity is clearly observed during the whole impact process. Obtained results preliminary indicate that identification of the impacting mass will be more difficult and will require longer part of the impact period.

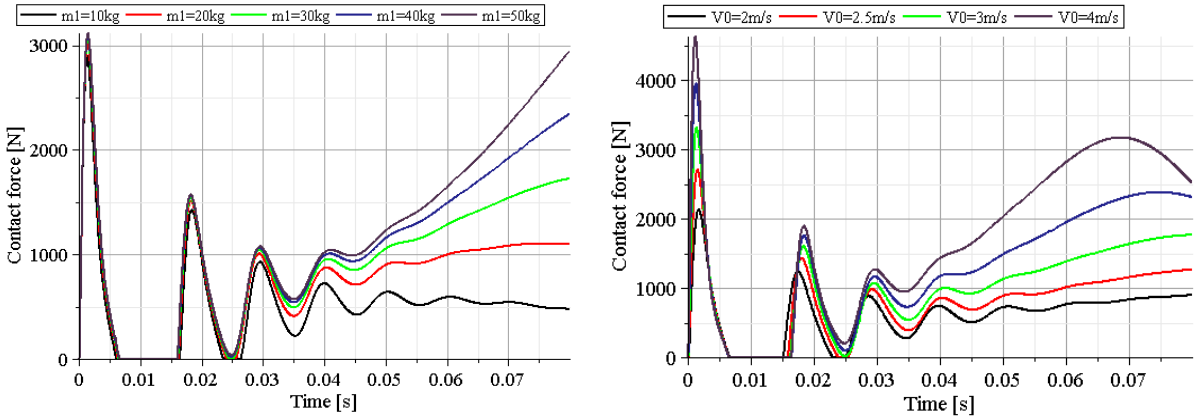

Fig.3.2.1a. Dependence of the contact force on mass and of the hitting object and its initial velocity

In general the methods that can be proposed for impact identification can be divided into three groups:

1. methods based on fitting actual and referential response of the system ('response-fitting approach' and 'response map approach'),
2. methods based directly on inverse analysis of the governing equations, which take into account constitutive relations defining contact material,
3. methods based on integral forms of governing equations and momentum conservation.

The first group of methods utilizes classical for defect identification problems 'response-fitting approach' based on minimisation of discrepancy between measured response of the system and the response obtained for assumed values of system's parameters. In case of impact identification where mass and velocity are being identified and the contact force $F_C^*(t)$ is utilized as system response, the corresponding minimisation problem takes the form:

$$\text{Find } \min_{M_1,V_0} f(M_1,V_0) = \int_0^{t_{end}} \left(F_C^*(t) - F_C(M_1,V_0,t)\right)^2 dt \tag{3.2.7}$$

In case when precise numerical model of the system is available the objective function can be calculated by solving system of differential equations and minimisation can be performed by means of gradient-based or heuristic optimisation method. Length of the time interval used for calculation of the objective function should be as short as possible to provide fast identification, but on the other hand it has to be long enough to capture dependence of the objective function on hitting object mass and its initial velocity. In practise, time t_{end} strongly depends on correspondence of the developed numerical model with experiment. In case of purely numerical identification (when 'measured' response is also obtained from the numerical model) utilization of the objective function being time integral of the first peak of the contact force allows to obtain satisfactory precision of the identification.

In practise, time of solution of the minimisation problem (which involves multiple solving of the differential equation) is much longer than time required for on-line impact identification and therefore the 'response map approach' has to be applied. In this method time-history of the contact force is computed in advance for discrete values of impact parameters (mass and velocity). Moreover, the identification can be performed with the use of values of contact force at selected time instants in order to speed up the computations. The corresponding optimisation problem reads:

$$\text{Find } \min_{M_1,V_0} f[M_1,V_0] = \sum_{i=1}^{n}\left(\frac{F_C^*(t_i) - F_C(M_1,V_0,t_i)}{F_C^*(t_i)}\right)^2 \tag{3.2.8}$$

and minimum is searched in a set of discrete values of mass and velocity. Effectiveness of the identification procedure depends on size of the prepared response map. Rare discretisation in terms of impact parameters and time, decreases identification precision or may lead to false results. On the other hand, dense discretisation elongates identification time and prevents conducting the identification process 'on-line'.

Shape of the objective function defined by Eq. 3.2.7 and Eq. 3.2.8 depends on length of time period used for the calculation of the objective function. In case when this period includes only initial stage of impact, the objective function depends mainly on impact velocity. As the length of the time period increases, the objective function becomes also dependent on mass of the hitting object which facilitates process of the identification, Fig. 3.2.1b.

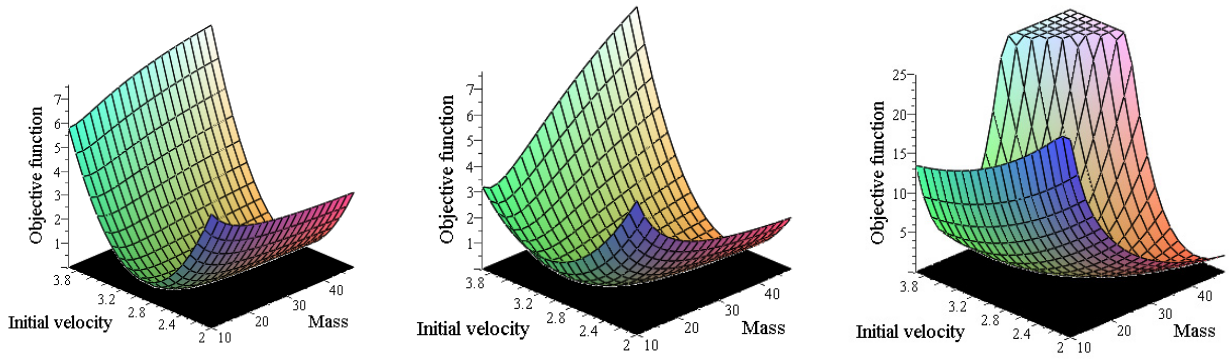

Fig.3.2.1b. Dependence of the objective function on time interval used for identification: a) t=10ms, b) t=40ms, c) t=80ms. Dependence on mass increases along with length of the time interval

An alternative method within 'response map approach' is based on selection of particular parameters which characterize measured response and which can be further used for

formulation of the objective function and unambiguous determination of impact loading (so-called 'feature extraction'). Since two quantities have to be identified, at least two features characterizing the response have to be defined. The approach allows for simplification of the definition of the objective function and therefore it enables its faster computation during the short time period dedicated to impact identification. Minimisation problem related to identification procedure takes the form:

$$\text{Find } \min_{M_1,V_0} f[M_1,V_0] = \left(\frac{p_1^* - p_1(M_1,V_0)}{p_1^*} \right)^2 + \left(\frac{p_2^* - p_2(M_1,V_0)}{p_2^*} \right)^2 \tag{3.2.9}$$

where parameters p_1^* and p_2^* are chosen from the following set: value of contact force at arbitrary time instants, value of force at first (or second) peak, duration of the first (or second) peak, time period between the peaks, integral of contact force calculated over certain time period. In case when numerical model was used, the identification procedure was successful regardless of the choice of pair of parameters. However, in case when 'response map' was prepared basing on experimental data, both parameters had to be clearly dependant on mass and velocity of impacting object to obtain proper shape of the objective function (similar to shape in Fig.3.2.2 b,c) and to make the process of identification possible. Qualitative and quantitative results of identification obtained by the use of 'response map approach' are presented in [262].

The second group of methods is based directly on inverse analysis of the governing equations and effectively takes into account constitutive relations defining properties of the contact material. Let us recall equations governing both objects motion together with the definition of the contact force acting between colliding objects (cf. Eq. 3.1.3-3.1.3) :

$$M_1 \frac{d^2 u_1}{dt^2} - M_1 g + F_C = 0 \tag{3.2.10a}$$

$$M_2 \frac{d^2 u_2}{dt^2} - M_2 g + F_P - F_C - F_D{}^{TOP} + F_{fr} = 0 \tag{3.2.10b}$$

$$F_C = k(u_1 - u_2 - d_0)^n \quad \text{or} \quad F_C = k(u_1 - u_2 - d_0)^n + c(u_1 - u_2 - d_0)(\dot{u}_1 - \dot{u}_2) \quad \text{for } u_1 - u_2 - d_0 > 0 \tag{3.2.10c}$$

Since during initial stage of impact the valve is closed and exchange of heat with environment is insignificant the equation of the energy balance simplifies to the analytical form (Eq.3.2.21) and generated pneumatic force is expressed in terms of piston displacement. The definition of the contact force can be arbitrary, however it is required that analytic definition of the contact force is known. Let us consider the system of governing equations at time period corresponding to the first peak of the contact force (before first rebound of the piston). In case when the contact force is measured and definitions of other forces (pneumatic, delimiting and friction) are known the following impact identification procedure can be proposed:

1. Differential equation 3.2.10b can be solved in order to find displacement of the piston u_2. Zero initial conditions for displacement and velocity of the piston at time instant when collision starts have to be assumed.

2. Differential equation 3.2.10c can be solved in order to find displacement of the impacting mass u_1 (equation defining the contact force has to be of the first order to avoid the defining initial velocity of the hitting object). As a result, displacement of the impacting object and its velocity, including value at the beginning of the collision, is determined.
3. Mass of the falling object can be identified by using direct or integral form of the equation 3.2.10a and previously determined kinematics of the impacting object.

In numerical example, two definitions of the contact force were considered: i) stiffness-based definition of the contact force and ii) definition including linear stiffness term and nonlinear stiffness-damping term (based on Eq. 3.2.10c with n=1). Initial velocity of the falling object was correctly identified in both cases and precise value of 2,8m/s was obtained at the beginning of the process. In numerical solution, mass of the falling object was found to oscillate severely at the initial and final part of the considered time interval, cf. Fig. 3.2.2 (in mass plots the peripheral parts of the identification period are appropriately shortened). However, in the middle of the identification period the value of identified mass stabilizes and its value closely corresponds to the value which was initially assumed.

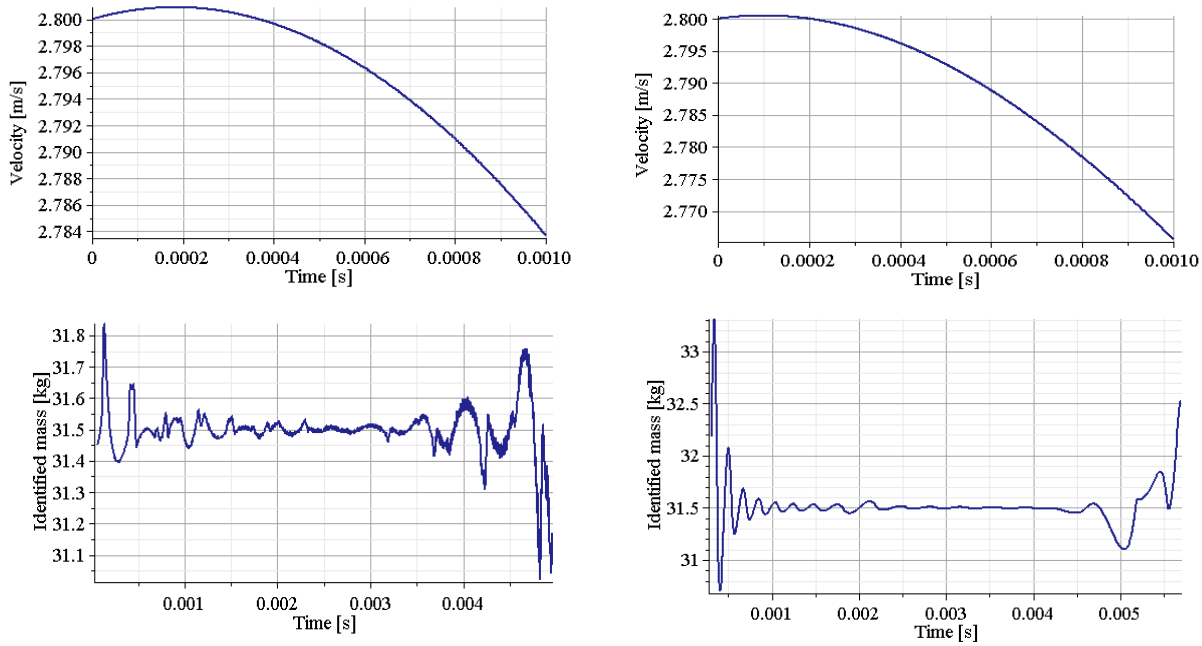

Fig. 3.2.2 Results of identification of impacting mass and velocity obtained by inverse analysis of governing equations: a) contact force with stiffness, b) contact force with stiffness and nonlinear damping. Assumed impact parameters M_1=31,5kg, V_0=2,8m/s.

The third group of the methods is based on determination of the mass of falling object and its initial velocity by using integral form of the governing equations. The main idea behind this method is that actual velocity and displacement of the impacting object can be expressed analytically in terms of impacting mass value, impact velocity and time integral from measured contact force. Further, impacting object velocity or displacement in certain time instants can be compared with (measured) corresponding quantity for the piston in order to assemble system of equations for determination of impact parameters. Such a formulation

of the method constitutes generalisation of the method described at the beginning of this section and defined by Eq. (3.2.6). Moreover, the method will be specified to the case of various definitions of the contact force.

The most important method of this type which concerns equalization of the mass velocity v_1 and piston velocity v_2 at certain time instants of the process t_1 and t_2. Integration of equation of impacting object motion over time allows to express both velocities as:

$$v_1(t_1) = v_1(t_0) + gt_1 - \frac{1}{M_1}\int_{t_0}^{t_1} F_C(t)dt\,, \quad v_1(t_1) = v_2(t_1) \tag{3.2.11a}$$

$$v_1(t_2) = v_1(t_0) + gt_2 - \frac{1}{M_1}\int_{t_0}^{t_2} F_C(t)dt\,, \quad v_1(t_2) = v_2(t_2) \tag{3.2.11b}$$

Subtraction of two above equations leads directly to formula:

$$M_1^{id} = \frac{-\int_{t_1}^{t_2} F_C(t)dt}{\left[v_2(t_2) - v_2(t_1)\right] - g(t_2 - t_1)}\,, \quad V_1^{id} = v_1(t_1) = v_2(t_1) \tag{3.2.11c}$$

which is fully equivalent to Eq. 3.2.6 and allows to determine mass of the hitting object from a single algebraic equation which involves integral of the measured contact force and measured piston kinematics. Initial velocity of the impacting object is determined directly from condition of being equal to piston velocity and it is determined at time instant t_1.

Determination of time instants, when velocity of the falling mass equals to the velocity of the piston (t_1 and t_2), depends on mechanical properties of the contact material and corresponding definition of the contact force. Time instants t_1 and t_2 can be easily determined in case of elastic contact force, i.e., when $F_C = kx^n$, $x = u_1 - u_2 - d_0$. Differentiation of the definition of contact force over time yields:

$$\frac{dF_C}{dt} = kn(u_1 - u_2 - d_0)^{n-1}(\dot{u}_1 - \dot{u}_2) \tag{3.2.12}$$

and thus indicates that time instants when both velocities are equal coincide with the extremum of the contact force (maximum or minimum if it exists). The advantage of this method is that, except the fact that contact force is elastic, neither the exact constitutive relation nor exact value of stiffness coefficient has to be known.

In a more general case of contact force being linear combination of stiffness and damping: $F_C = kx + c\dot{x}$, $x = u_1 - u_2 - d_0$ differentiation of the contact force over time gives:

$$\frac{dF_C}{dt} - k\left(\frac{du_1}{dt} - \frac{du_2}{dt}\right) - c\left(\frac{d^2u_1}{dt^2} - \frac{d^2u_2}{dt^2}\right) = 0 \tag{3.2.13a}$$

By reducing the second term and utilizing equation of motion of the falling mass, we obtain the equation (3.2.13b) which allows to determine time instants of velocities' equalisation in terms of mass of the hitting object. The whole system of equations for solving the identification problem reads:

$$\frac{dF_C(t)}{dt} - c\left(-\frac{F_C(t)}{M_1} + g - a_2(t)\right) = 0 \tag{3.2.13b}$$

$$M_1^{id} = -\int_{t_1}^{t_2} F_C(t)dt \left[\int_{t_1}^{t_2} \left(a_2(t) - g\right)dt\right]^{-1}, \qquad V_1^{id} = v_1(t_1) = v_2(t_1) \tag{3.2.13c}$$

Typical solution of the problem involves:

- assumption of mass M_1,
- calculation of time instants t_1 and t_2 from Eq. 3.2.13b,
- identification of mass and velocity according to Eq. 3.2.13c,
- repeating procedure with determined value of mass M_1^{id}.

Due to a large difference in masses of piston and falling object and their accelerations the influence of term dependant on mass M_1 is not significant. As a result convergence of the proposed procedure is very fast and impact parameters can be usually identified after several iterations. When the above model of the contact force involving viscous terms is applied, colliding objects velocities do not equalize at the time instant when the contact force reaches maximum but slightly later, cf. Eq. 3.2.13a and Fig. 3.2.3. The time shifts between peak of the contact force and time instant of equalization of the velocities were found to be different for both peaks of the contact force and strongly dependent on viscous coefficient used in Eq. 3.2.13a, however almost insensitive to parameters of the impact loading.

In case when contact force is defined as combination of stiffness term and stiffness-dependant damping term: $F_C = kx^n + cx\dot{x}$, $x = u_1 - u_2 - d_0$ its time derivative reads:

$$\frac{dF_C}{dt} - kn(u_1 - u_2 - d_0)^{n-1}\frac{d(u_1 - u_2)}{dt} - c\left[\frac{d(u_1 - u_2)}{dt}\right]^2 - c(u_1 - u_2 - d_0)\frac{d^2(u_1 - u_2)}{dt^2} = 0 \tag{3.2.14a}$$

By reducing the second and the third term and by using integral form of equation of the falling mass motion we obtain the following equation for determination of time instants t_1 and t_2 which involves mass of the impacting object M_1 and its initial velocity $v_1(t_0) = V_0$:

$$\frac{dF_C}{dt} - c\left[V_0(t - t_0) - \int_{t_0}^{t}\int_{t_0}^{t}\left(\frac{F_C(t)}{M_1} - g\right)dt - u_2 - d_0\right]\left(-\frac{F_C(t)}{M_1} + g - a_2(t)\right) = 0 \tag{3.2.14b}$$

Since the above procedure does not provide elimination of velocity of the impacting object (as it was in case of linear damping) it also does not provide numerical benefits and time instants of velocity equalisation can be as well determined directly by using definition of the contact force:

$$F_C = k\left[V_0(t - t_0) - \int_{t_0}^{t}\int_{t_0}^{t}\left(\frac{F_C(t)}{M_1} - g\right)dt - u_2 - d_0\right]^n \tag{3.2.14c}$$

where the term $cx\dot{x}$ was omitted as equal to zero. The whole system of equations for determination of impact parameters consists of Eq. (3.2.14b or 3.2.14c) and Eq. (3.4.13c). Unfortunately, it was found that the procedure which was proposed for system with linear

damping, in current case does not usually converge well. Therefore, the solution of the problem has to be searched by minimisation of the following objective function:

$$\text{Find } \min_{M_1,V_0} F(M_1,V_0) = \left(\frac{M_1 - M_1^{id})}{M_1}\right)^2 + \left(\frac{V_0 - V_1^{id}(t_0)}{V_0}\right)^2 \tag{3.2.15}$$

In the above formula identified velocity $V_1^{id}(t_0)$ is related to time instant of the beginning of impact and it can be obtained from typically identified velocity $V_1^{id} = v_1(t_1)$ by backward integration of the equation of mass motion. Solution of the above problem can be performed by means of gradient-based method. Complexity of the system of equations which has to be used for determination of the impact parameters and the necessity of solving optimization problem cause that method may be excessively time consuming to be applied for on-line impact identification.

Another method for determination of impact parameters takes advantage of conformity of displacements (vanishing of relative distance) of the falling object and the piston at the end of the first peak of the contact force (time t_{1u}) and at the beginning of the second peak (time t_{2u}), cf. Fig. 3.2.3. The above method can be applied in case when decrease of the contact force to zero implicates zero distance of both objects ($x = u_1 - u_2 - d_0 = 0$). Such condition is fulfilled for definitions of elastic contact force $F_C = kx^n$ and contact force with nonlinear damping $F_C = kx + cx\dot{x}$ (when for the whole rebound stage the condition $kx + cx\dot{x} > 0$ is satisfied), but not for the contact force defined as $F_C = kx + c\dot{x}$. The equations of conformity of both objects displacements at considered time instants read:

$$\begin{aligned} u_1(t_{1u}) &= V_0(t_{1u} - t_0) + \tfrac{1}{2} g(t_{1u} - t_0)^2 - \frac{1}{M_1}\int_{t_0}^{t_{1u}}\int_{t_0}^{t_{1u}} F_C(t)dt \;, \quad u_1(t_{1u}) - d_0 = u_2(t_{1u}) \\ u_2(t_{2u}) &= V_0(t_{2u} - t_0) + \tfrac{1}{2} g(t_{2u} - t_0)^2 - \frac{1}{M_1}\int_{t_0}^{t_{1u}}\int_{t_0}^{t_{1u}} F_C(t)dt \;, \quad u_1(t_{2u}) - d_0 = u_2(t_{2u}) \end{aligned} \tag{3.2.16}$$

and the equivalence of upper limits of both integrals is the result of contact force being zero between subsequent peaks of the contact force. Subtraction of the above two equations leads to a single equation:

$$V_0(t_{2u} - t_{1u}) + \tfrac{1}{2} g\left[(t_{2u} - t_0)^2 - (t_{1u} - t_0)^2\right] = u_2(t_{2u}) - u_2(t_{1u}) \tag{3.2.17}$$

which can be used for determination of the initial velocity of the impacting object $V_0 = v_1(t_0)$. Further, one of equations (3.2.16) can be used for determination of the impacting object mass. Let us note that, on the contrary to previous methods, the exact constitutive model of the contact material does not have to be known and the range of allowable constitutive relations has been extended. Furthermore, the method can be considered as slightly faster than the method based on equalisation of the velocities since it allows for determination of the impact parameters at the beginning of the second peak of the contact force.

The method can be generalized into the case of constitutive relations for which displacement of both objects are not equal at the end or beginning of contact force peaks, however in such a case, more complex identification procedure is required.

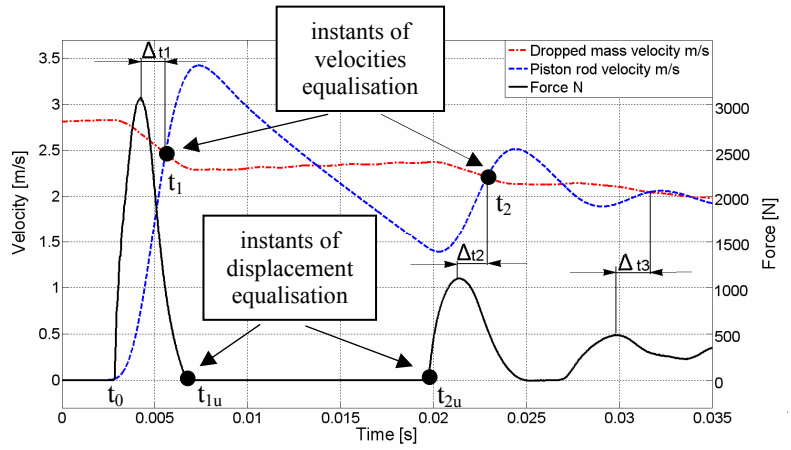

Fig. 3.2.3 Initial stage of the impact process utilized for identification of the impact parameters

Hybrid method of identification of impact parameters utilizes combination of equations from two above methods: one equation concerns equalisation of impacting objects velocities and the second one concerns equalisation of their displacements. In the simplest case of system with elastic contact element, velocities of both objects are equal at maximum of contact force (time instant t_1) and displacements are equal at the end of peak of the contact force (time instant t_{1u}), Fig. 3.2.3. The set of governing equations reads:

$$v_1(t_1) = V_0 + g(t_1 - t_0) - \frac{1}{M_1}\int_{t_0}^{t_1} F_C(t)\,, \quad v_1(t_1) = v_2(t_1) \tag{3.2.18}$$

$$u_1(t_{1u}) = V_0(t_{1u} - t_0) + \tfrac{1}{2} g(t_{1u} - t_0)^2 - \frac{1}{M_1}\int_{t_0}^{t_{1u}}\int_{t_0}^{t_{1u}} F_C(t)dt\,, \quad u_1(t_{1u}) - d_0 = u_2(t_{2u})$$

The hybrid method allows to shorten time of identification since both mass and velocity of the impacting object can be recognized after the first peak of the contact force. Let us note that in two artificial extreme cases of piston kinematics the above system of equations is indeterminate: i) when the piston is clamped and does not move during the process and ii) when the piston does not have any support, i.e. the force generated by absorber equals zero. In all cases lying between these two extremes, mass and velocity of the impacting object can be successfully recognized based on equations (3.2.18), however, the measurements and computations have to be performed with a large precision.

The following possibility of identification of the impact parameters utilizes the concept of coefficient of restitution which is defined as a ratio of final relative velocity of the impacting objects to their initial relative velocity. As a preliminary step of the method, coefficient of restitution has to be determined (either experimentally or numerically) in terms of mass of the hitting object and its initial velocity. The equations governing the method involve: i) the equalisation of displacements at the end of the first peak of contact force and ii) definition of the coefficient of restitution as ratio of final relative velocity of both objects (expressed in terms of unknown impacting mass M_1, unknown initial velocity V_0 and measured contact force $F_C(t)$) to their initial relative velocity V_0.

$$V_0(t_{1u}-t_0)+\tfrac{1}{2}g(t_{1u}-t_0)^2-\frac{1}{M_1}\int_{t_0}^{t_{1u}}\int_{t_0}^{t_{1u}}F_C(t)dt=u_2(t_{1u}) \tag{3.2.19}$$

$$R(M_1,V_0)=\frac{v_1(t_{1u})-v_2(t_{1u})}{V_0}=\frac{\left(V_0+g(t_{1u}-t_0)-\frac{1}{M_1}\int_{t_0}^{t_{1u}}F_C(t)\right)-v_2(t_{1u})}{V_0}$$

where R is the coefficient of restitution. Similarly to the previously described method which utilizes equality of displacements and velocities, the method based on restitution coefficient allows to identify impact parameters at the end of the first peak of the contact force. The important difference is, however, that in current method the constitutive relation defining the contact force does not have to be known.

The last of the proposed methods of identification of impact parameters utilizes definitions of the contact force formulated at two arbitrary time instants of the process. In these definitions the displacement and velocity of the impacting mass are expressed in terms of unknown mass of the impacting object and its initial velocity. Exemplary equations governing the method (for the definition of the contact force $F_C=kx+c\dot{x}$) read:

$$F(t_1)=k\left(V_0t_1-\frac{1}{M_1}\int_{t_0}^{t_1}\int_{t_0}^{t_1}F_C(t)dt-u_2(t_1)\right)+c\left(V_0-\frac{1}{M_1}\int_{t_0}^{t_1}F_C(t)dt-v_2(t_1)\right) \tag{3.2.20}$$

$$F(t_2)=k\left(V_0t_2-\frac{1}{M_1}\int_{t_0}^{t_2}\int_{t_0}^{t_2}F_C(t)dt-u_2(t_2)\right)+c\left(V_0-\frac{1}{M_1}\int_{t_0}^{t_2}F_C(t)dt-v_2(t_2)\right)$$

The above equations can be used for determination of mass and velocity of the impacting object in case when contact force and kinematics of the piston are measured during the impact process. On the contrary to the previous methods, this approach requires precise data concerning constitutive relation governing the contact material and knowledge of constitutive parameters *k* and *c*. Theoretically, the system can be assembled for time instant located at the beginning of the raising slope of the first peak of the contact force and the impact parameters can be identified almost infinitely fast. In practise, certain amount of time is required in order to obtain satisfactory precision of identification.

Most above methods, based on integral forms of the governing equations, were tested either numerically or experimentally [262]. Numerical models were used to investigate the influence of sampling frequency and signal noise on precision of the identification. Experimental testing of the identification methods was limited to ‘response map’ approach and to integral method which utilizes equalisation of impacting object velocities. In the latter case, the best precision of the identification was obtained when fixed time-shift between maximum of the contact force and time instant of velocities equalisation was assumed [262].

Optimal design of device for impact identification

Although in numerical examples impact parameters can be identified in most of the cases, the success of experimental procedure highly depends on parameters of the device used for identification (so called 'impactometer', cf. patent pending [263]) and the accuracy of the

performed measurements. Therefore, it is necessary to determine optimal parameters of the impactometer (pressure inside the cylinder, mass of the piston, stiffness and damping of the contact element) which are optimal from the point of view of precise impact identification, i.e. for which:

1. impact parameters can be recognized after the shortest part of the impact period,
2. inaccuracy of the measurements has minimal influence on the identification accuracy.

The optimality of the impactometer's parameters depends on the method used for identification. Let us further briefly analyze each of the previously described groups of impact identification methods in context of optimal design of impact identification device.

In case of the first group of methods based on 'response-fitting approach' or 'response map approach' (where measurement of the contact force is the only quantity used for impact identification) the most expedient feature is possibly distinct dependence of contact force on both mass and velocity of the impacting object during the first stage of impact. In such a case objective function (Eq. 3.2.7-3.2.9) is conducive for minimization and, as a result, the identification process is facilitated. The developed numerical model of the impact identification device indicates that although dependence on velocity of the impacting object is apparent in most of the cases, the dependence on mass of the hitting object can be considerably improved in two manners:

- by increasing pressure inside pneumatic cylinder,
- by increasing mass of the piston.

The only requirement for the second group of identification methods concerns constitutive relation of the contact material. The first issue is that constitutive relation has to be explicitly known and its parameters have to be easily determinable. The second issue is that characteristics of the contact material has to be independent of external conditions like temperature, time and wear in order to avoid the requirement of the secondary testing of the contact material.

Analysis of the third group of identification techniques (methods based on integral form of the governing equations) will be limited to the method based on equalization of velocities at certain time instant of the process. Optimal conditions for the identification procedure are obtained when contact material has purely elastic characteristics and, consequently, time instants t_1 and t_2 used for identification can be determined directly from time-history of the contact force. This allows to avoid complexity of the identification procedure which arises in case of other characteristics of the contact element.

More precise approach to optimal design of impactometer is based on analysis of main equation which is used for determination of the impacting mass (Eq. 3.2.11c). Since the quantities on the right hand side of the above formula are obtained from the measurements they usually contain errors due to limited accuracy of sensors. Therefore, the value of denominator (velocity difference between subsequent peaks) has to be possibly large in order to minimise the influence of velocity measurement inaccuracy on identified value of mass. Developed numerical model indicates that value of velocity difference depends on parameters of the impactometer. Numerical analysis of obtained velocity difference and corresponding identification accuracy had revealed the following features of the system:

- high initial pressure increases velocity difference and has beneficial influence on mass identification ,
- large mass of the piston causes similar effect as increase of pressure,
- large stiffness of the contact element aggravates mass identification.

Let us finally note that identification procedure is required as a preliminary step of adaptation when the control procedure assumes that valve should be opened starting from the beginning of the process. If, according to assumed control strategy, the valve has to remain closed during initial stage of impact, the separate procedure for impact identification does not have to be applied. Measurements performed during the initial, passive stage of impact can be used to execute determine optimal control strategy without explicit determination of hitting object mass and its initial velocity.

3.2.2 Strategies for deceleration minimisation

In this section various strategies for minimisation of deceleration of the impacting object are proposed and verified numerically. Two types of pneumatic absorbers are considered: the absorber with the exhaust of gas to the environment and absorber with the flow of gas between the chambers. Since single chamber absorber is the most basic adaptive pneumatic structure, adaptation strategies developed for this absorber can be treated as a reference and a starting point for elaboration of strategies for more complex types of pneumatic cylinders and other types of inflatable structures. Double-chamber absorber is studied in the context of future application as pneumatic landing gear for a small airplane. Although the attention will be focused on a problem of minimisation of hitting object deceleration, it will be shown that proposed strategies closely correspond to the problem of minimisation of final kinetic energy of the impacting object and thus, they lead to reduction of hitting object rebound.

Developed adaptation strategies can be divided not only in terms of assumed control objective but also in terms of type of applied algorithm. Both feed-forward control algorithms based on preliminarily recognized impact parameters and feedback control algorithms based on actual response of the system will be utilized. Adaptation strategies introduced in this section can be classified into the following five groups:

- **semi-active adaptation** where valve opening is adjusted to recognised impact scenario, however it remains constant during whole process;
- **active adaptation** with:
  - continuous control of valve opening where the valve opening is smoothly changed during the impact process;
  - on/off control of valve opening where during the impact process the valve is switched between two extreme positions;
  - proportional control where finite number of time intervals is defined and on each of them constant opening of the valve is adjusted;
  - discrete control where several various valve openings are predefined and their sequence and duration of the corresponding time intervals is searched.

The above control strategies differ in terms of number of allowed valve openings and number of time intervals (control steps) when the valve position remains constant. Division into the

above five groups is not very strict since classification of particular strategy changes continuously together with increase/decrease of the number of allowed valve openings or control intervals (cf. Fig. 3.2.22). The variety of investigated adaptation strategies results from the fact that diverse types of valves characterised by various operating principles can be used in a final application of the absorber.

In the first stage of analysis, no constraints on valve opening will be imposed which allows to determine properties of the valve required to execute optimal adaptation strategy. Further, certain constraints will be introduced in order to analyse change of the optimal adaptation algorithm and its influence on obtained deceleration of the hitting object. The control strategies will be developed for arbitrary assumed geometry of the absorber (length, diameter, division into chambers) and with the use of one degree of freedom model which properly simulates global response of the absorber being the quantity of interest in considered control problems.

Semi-active adaptation

Semi-active adaptation to a given impact loading (i.e. loading characterized by mass M and velocity V_0) will be defined as problem of finding two parameters: the initial pressure p_0 and the constant in time opening of the valve represented by the viscous resistance coefficient C_V, which minimise maximal value of hitting object deceleration:

$$\text{Find } p_0, C_V \quad \text{such that } J_2 = \max_t \left|\ddot{u}(t)\right| \text{ is minimal} \tag{3.2.21}$$

Let us initially consider one degree of freedom model of the horizontally located **single-chamber absorber** with exhaust to environment and adiabatic walls (cf. Fig. 3.1.2a). In case when only outflow of the gas occurs, equation of internal energy balance can be integrated analytically and thus mathematical model of the absorber takes the form:

$$M\ddot{u} + (p - p_A)A = 0, \qquad \dot{m}(t) = -\frac{(p - p_A)}{C_V}, \qquad \frac{p(h_0 - u)^\kappa}{m^\kappa} = \frac{p_0 h_0^{\ \kappa}}{m_0^{\ \kappa}} \tag{3.2.22a}$$

$$\text{IC: } u(0) = 0,\ \dot{u}(0) = V_0,\ m(0) = m_0$$

Alternative forms of the above system of equations can be obtained by eliminating pressure of the gas *p*:

$$M\ddot{u} + \left[C\left(\frac{m}{h_0 - u} \right)^\kappa - p_A \right] A = 0, \qquad \dot{m} = -\frac{1}{C_V}\left[C\left(\frac{m}{h_0 - u} \right)^\kappa - p_A \right] \tag{3.2.22b}$$

$$C = p_0 \left(\frac{h_0}{m_0} \right)^\kappa, \quad \text{IC: } u(0) = 0,\ \dot{u}(0) = V_0,\ m(0) = m_0$$

and by eliminating mass of the gas *m*:

$$M\ddot{u} + (p - p_A)A = 0, \qquad \left(\frac{1}{C} \right)^{\frac{1}{\kappa}} \left[\frac{1}{\kappa} p^{\frac{1}{\kappa} - 1} \dot{p}(h_0 - u) - p^{\frac{1}{\kappa}} \dot{u} \right] = -\frac{p - p_A}{C_V} \tag{3.2.22c}$$

$$C = p_0 \left(\frac{h_0}{m_0} \right)^\kappa, \quad \text{IC: } u(0) = 0,\ \dot{u}(0) = V_0,\ p(0) = p_0$$

Optimal initial pressure (i.e. initial pressure which corresponds to minimal force generated by the absorber and minimal deceleration of the impacting object) will be initially calculated for the case when the valve is closed and mass of the gas inside cylinder remains constant. In such a case integration of the equation of piston motion over displacement in the range $(0,u_{\max})$ yields:

$$\frac{MV_0^2}{2}=\frac{p_0h_0A}{\kappa-1}\left[\left(\frac{p_0}{p_{\max}}\right)^{1/\kappa-1}-1\right]-p_AAh_0\left[1-\left(\frac{p_0}{p_{\max}}\right)^{1/\kappa}\right] \tag{3.2.23a}$$

Analogous formula for isothermal process can be derived by using L'Hopital's rule:

$$\frac{MV_0^2}{2}=-p_0h_0A\ln\left(\frac{p_0}{p_{\max}}\right)-p_AAh_0\left(1-\frac{p_0}{p_{\max}}\right) \tag{3.2.23b}$$

The above formulae can be used to determine maximal pressure obtained during impact in terms of terms initial pressure. The analytical formula defining maximal pressure can be found for the following cases:

- isothermal process with $p_A=0$ (condition equivalent to presence of the upper chamber of the cylinder of zero volume):

$$p_{\max}(p_0)=p_0\exp\left(\frac{1}{2}\frac{MV_0^2}{p_0h_0A}\right) \tag{3.2.24a}$$

- isothermal process with $p_A\neq 0$:

$$p_{\max}(p_0)=-p_A\left[LW\left(-\frac{p_A}{p_0}\exp\left(\frac{MV_0{}^2}{2p_0h_0A}+\frac{p_A}{p_0}\right)\right)\right]^{-1} \tag{3.2.24b}$$

where the *LambertW* function which satisfies the equation: $LW(x)\exp(LW(x))=x$;

- and adiabatic process with $p_A=0$:

$$p_{\max}(p_0)=p_0\left[\exp\left(-\frac{1}{2}\left(\frac{\kappa}{\kappa-1}\right)\frac{MV_0^2\kappa-MV_0^2+2p_0h_0A}{p_0h_0A}\right)\right]^{-1} \tag{3.2.24c}$$

Further, optimal initial pressure can be calculated from the necessary condition for extremum of the function $p_{\max}(p_0)$ which leads to exactly the same result for three considered cases:

$$\frac{d(p_{\max})}{dp_0}=0\quad\rightarrow\quad p_0^{opt}=\frac{MV_0{}^2}{2h_0A}+p_A \tag{3.2.25}$$

Optimal value of initial pressure for adiabatic process with $p_A\neq 0$ was found numerically, however the result was exactly the same as above. Let us note that derived optimal pressure for the system with closed valve is exactly the same as constant pressure which should be used to stop the hitting object by using the whole stroke of the cylinder. Moreover, the above formulae allow to calculate maximal value of pressure which is reached during the process. Simple results are obtained in cases of:

- isothermal process with $p_A=0$:

$$p_{\max}(p_0^{opt}) = ep_0^{opt} = e\frac{MV_0^{\,2}}{2h_0A} \cong 2{,}72\frac{MV_0^{\,2}}{2h_0A} \tag{3.2.26a}$$

- adiabatic process with $p_A = 0$:

$$p_{\max}(p_0) = \exp\left(\frac{\ln(\kappa)\kappa}{\kappa-1}\right)p_0^{opt} = \exp\left(\frac{\ln(\kappa)\kappa}{\kappa-1}\right)\frac{MV_0^{\,2}}{2h_0A} \cong 3{,}24\frac{MV_0^{\,2}}{2h_0A} \tag{3.2.26b}$$

Optimal valve opening for arbitrary initial pressure can be calculated by using the condition that the piston is stopped at the vicinity of the cylinder bottom, and the whole mass of gas is removed from the cylinder. Integration of the equation of mass motion and the flow equation over time yields:

$$-MV_0 + \int_0^{t_{stop}} (p - p_A)A\,dt = 0\,, \qquad m_0 = \frac{1}{C_V^{\,opt}}\int_0^{t_{stop}} (p - p_A)\,dt \tag{3.2.27}$$

where V_0 is the initial velocity of the impacting object. The above formulae allow to determine limiting combination of pressure and valve opening for which piston does not hit cylinder bottom. For given value of p_0 we have:

$$C_V^{\,opt} = C_V^{\min}(p_0) = \frac{MV_0}{m_0A} = \frac{MV_0RT_0}{p_0h_0A^2} \tag{3.2.28}$$

The formula (3.2.28) defines minimal allowable (and thus optimal for deceleration minimisation) value of resistance coefficient for arbitrary value of initial pressure. The above result holds for both isothermal and adiabatic systems. If resistance coefficient is larger than defined by Eq. 3.2.28, the piston is stopped by using only a part of the cylinder stroke which results in larger piston deceleration. On the contrary, when flow resistance coefficient is lower than value determined from Eq. 3.2.28a the piston velocity is not reduced to zero by pneumatic force and piston hits bottom of the cylinder. The relation reversed to Eq. 3.2.28:

$$p_0^{\,\min}(C_V) = \frac{MV_0RT_0}{C_Vh_0A^2} \tag{3.2.29}$$

can be used for finding minimal allowable initial pressure for given valve opening. Optimal initial pressure for a given valve opening, represented by resistance coefficient, has to be searched numerically in the range $\left\langle p_0^{\min}, p_0^{\max}\right\rangle$. However, for flow resistance coefficients indicating relatively large openings of the valve, optimal initial pressure is located at the beginning of the range of allowable initial pressures, i.e. $p_0^{opt} = p_0^{\min}$, cf. Fig. 3.2.5a.

Let us further analyse basic features of the pneumatic system with optimal constant valve opening. By analogy to Eq. 3.1.39b, the system of governing equations can be written in the form of a single equation involving terms dependent on mass of the impacting object and its initial velocity:

$$M\ddot{u} + CA\left[\frac{M}{C_VA}\frac{\dot{u}}{h_0-u} + \left(m_0 - \frac{MV_0}{C_VA}\right)\frac{1}{h_0-u}\right]^{\kappa} - p_AA = 0\,, \qquad C = p_0\left(\frac{h_0}{m_0}\right)^{\kappa} \tag{3.2.30a}$$

By introducing optimal resistance coefficient C_V^{opt} defined by Eq. 3.2.28 we obtain:

$$M\ddot{u} + CA\left[\frac{m_0}{\dot{u}_0}\frac{\dot{u}}{h_0 - u}\right]^{\kappa} - p_A A = 0 \tag{3.2.30b}$$

As a result of the dependence of force generated by the absorber on term indicating ratio of actual and initial velocities $\dot{u}/\dot{u}_0$, the force generated for impacts of the same energy depends exclusively on piston displacement and does not depend on piston velocity, cf. Fig. 3.2.4. Therefore, single chamber pneumatic absorber with optimal constant valve opening is untypical dissipative system where for particular kinetic energy of impact the force-displacement characteristics is independent of mass and velocity of the impacting object.

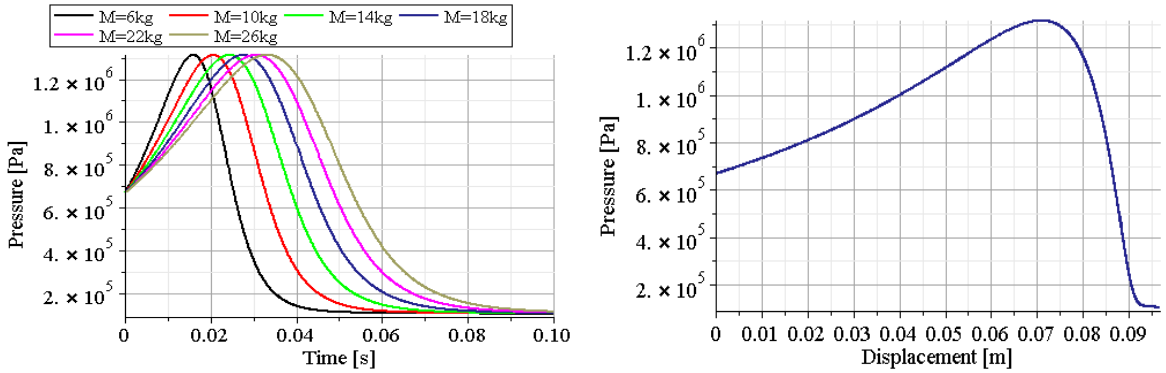

Fig. 3.2.4. Response of the single-chamber absorber with optimal valve opening defined by Eq. 3.2.28 to impact of the same energy but various masses and velocities of the impacting object

Due to the fact that according to Eq. 3.2.28 optimal resistance coefficient is a function of initial pressure, minimum of the objective function in the main problem of deceleration minimisation (Eq.3.2.21) can be searched in terms of pressure only. Let us analyse the simple case of isothermal system with $p_A = 0$. In such a case Eq. 3.2.30b simplifies to the form:

$$M\ddot{u} + \frac{m_0 R T_0}{\dot{u}_0}\frac{\dot{u}}{h_0 - u} = 0 \tag{3.2.30c}$$

and can be integrated analytically over time to obtain actual value of mass velocity:

$$V = \dot{u}_0 - \frac{1}{M}\frac{m_0 R T_0}{\dot{u}_0}\ln\left(\frac{h_0}{h_0 - u}\right) \tag{3.2.31}$$

By introducing the above formula back into Eq. 3.2.30c we obtain:

$$M\ddot{u} + \frac{m_0 R T_0}{\dot{u}_0}\frac{\left[\dot{u}_0 - \frac{1}{M}\frac{m_0 R T_0}{\dot{u}_0}\ln\left(\frac{h_0}{h_0 - u}\right)\right]}{h_0 - u} = 0 \tag{3.2.32}$$

The second term of the Eq. (3.2.32c) which indicates force generated by the absorber is expressed exclusively in terms of mass displacement, which is in a way delusive since the original equation (3.2.30) describes dissipative system. Optimal initial mass of the gas, optimal initial pressure as well as maximal force will be determined in the following way:

- displacement u_{ext} for which pneumatic force attains its maximum can be found from the condition: $dF_p(u)/du = 0$;
- maximal pneumatic force can be determined from Eq. 3.2.32: $F_p^{\max}(m_0) = F(u_{ext}, m_0)$;
- mass of the gas for which maximal value of pneumatic force is the smallest can be determined from the condition $dF_p^{\max}(m_0)/dm_0 = 0$;
- corresponding optimal value of initial pressure and maximal value of pressure can be determined by using definition of the pneumatic force.

All steps of the above procedure can be performed fully analytically, however particular formulae are fairly complicated. Finally, the following simple results for optimal semi-active system are obtained:

$$p_0^{opt} = \frac{MV_0^2}{2h_0A}, \qquad C_V{}^{opt} = \frac{2RT_0}{V_0A}, \tag{3.2.33}$$

$$p_{\max}(p_0^{opt}, C_V^{opt}) = \frac{e}{2}p_0^{opt} = \frac{e}{2}\frac{MV_0^2}{2h_0A} \cong 1{,}36\frac{MV_0^2}{2h_0A}$$

which indicates that optimal pressure is exactly the same as in case of closed valve and maximal pressure obtained during the process is decreased exactly twice (cf. Eq. 3.2.26a). Let us note that optimal resistance coefficient depends only on initial velocity of the impacting object which simplifies the adaptation procedure.

The corresponding results for adiabatic system with $p_A = 0$, as well as for isothermal and adiabatic system with, $p_A \neq 0$, were obtained numerically. For adiabatic system optimal value of initial pressure (and thus resistance coefficient) is the same as for isothermal system, however maximal value of pressure obtained during the process is slightly higher and equals:

$$p_{\max}(p_0^{opt}, C_V^{opt}) \cong 1{,}41p_0^{opt} = 1{,}41\frac{MV_0^2}{2h_0A} \tag{3.2.34}$$

Optimal parameters for the isothermal and adiabatic systems with $p_A \neq 0$ read:

$$p_0^{opt} = \frac{MV_0^2}{2h_0A} + p_A, \qquad C_V{}^{opt} = \frac{MV_0RT_0}{\left((MV_0^2)/(2h_0A) + p_A\right)h_0A^2} \tag{3.2.35}$$

and indicate that optimal initial pressure is again equal to corresponding pressure in case of closed valve. Here the initial pressure depends on impact energy, but optimal valve opening depends separately on mass of the hitting object and its velocity. Moreover, maximal value of pressure obtained during the process is not proportional to initial pressure (as it was in cases of $p_A = 0$), however it can be expressed as a function of initial pressure, external pressure and initial energy of the impacting object: $p_{\max} = f(p_0, p_A, MV_0^2)$.

The surface of maximal pressure in terms of initial pressure and flow resistance coefficient, together with line indicating minimal value of pressure for each valve opening is presented in Fig. 3.2.5a.

The similar analysis can be conducted for **double-chamber absorber** with valve between the chambers (similar to the absorber shown in Fig. 3.1.11a), which is located

horizontally, has adiabatic walls and negligible cross-sectional area of the piston rod. During the forward stroke the system is described by the following set of equations:

$$M\ddot{u}+(p_2-p_1)A=0\,,\qquad \dot{m}_2(t)=-(p_2-p_1)/C_V \tag{3.2.36}$$

$$\frac{p_2(h_{02}-u)^{\kappa}}{m_2^{\kappa}}=\frac{p_{02}h_{02}^{\kappa}}{m_{02}^{\kappa}}=C$$

$$m_1c_VT_1+m_2c_VT_2-m_1c_VT_{01}-m_{02}c_VT_{02}=\tfrac{1}{2}MV_0^2-\tfrac{1}{2}M\dot{u}^2$$

$$p_1(h_{01}+u)A=m_1RT_1\qquad p_2A(h_{02}-u)=m_2RT_2\qquad m_1+m_2=const.$$

$$\text{IC:}\;\; u(0)=0\,,\;\; \dot{u}(0)=V_0\,,\; m_2(0)=m_{02}$$

In the above system four algebraic equations couple six unknowns: p_1,p_2,T_1,T_2,u,m_2. Therefore, pressures p_1 and p_2 can be expressed exclusively in terms of piston displacement u and mass of the gas m_2 in order to be introduced into two initial differential equations ($3.2.36_{1,2}$). Although the mathematical model is more complicated than model describing absorber with exhaust to environment, the former procedure of derivation of optimal parameters can be followed.

Henceforth, the case when initial volume of the upper chamber is close to zero will be considered. When the valve remains closed only the compressed chamber contributes to the energy balance and optimal initial pressure for isothermal and adiabatic system is exactly the same as in case of single-chamber cylinder with $p_A=0$, cf. Eq. 3.2.25. Consequently, maximal value of pressure is defined by Eq. 3.2.26.

Optimal flow resistance coefficient can be obtained by integrating equation of motion and equation of the flow over time:

$$-MV_0+\int_0^{t_{stop}}(p_2-p_1)A\,dt=0\,,\qquad m_0=\frac{1}{C_V^{\;opt}}\int_0^{t_{stop}}(p_2-p_1)dt \tag{3.2.37}$$

Although the above equations are different than corresponding equations for single-chamber cylinder, exactly the same function defining minimal allowable (and thus optimal) resistance coefficient for given value of initial pressure was obtained (Eq. 3.2.28). Optimal value of initial pressure for assumed valve opening has to be searched numerically in the range $\left\langle p_0^{\min},p_0^{\max}\right\rangle$ where $p_0^{\min}$ is defined by Eq. 3.2.29. For the wide range of resistance coefficients optimal value of initial pressure is located between $p_0^{\min}$ and $p_0^{\max}$, and it has similar value independently on the value of flow resistance coefficient, see Fig. 3.2.5b. In turn, for relatively large opening of the valve the optimal initial pressure equals the lowest allowable pressure, i.e. $p_0^{opt}=p_0^{\min}$, cf. Fig. 3.2.5b.

Double-chamber absorber can be also described by a single equation involving mass of the impacting object (analogous to 3.2.30a). Thus, single equation governing system with optimal valve opening (analogous to 3.2.30b) can be also derived. For the isothermal case this equation reads:

$$M\ddot{u}+\frac{m_0RT_0}{\dot{u}_0}\left(\frac{\dot{u}}{h_{02}-u}-\frac{\dot{u}}{h_{01}+u}\right)=0 \tag{3.2.38}$$

and for adiabatic case it has a fairly complicated form due to influence of terms indicating

gas inflow to the upper chamber. The specific form of both equations causes that double-chamber absorber equipped with valve with optimal constant opening posses the feature of independence of force-displacement characteristics on impacting mass and velocity when impacts of the same energy are considered.

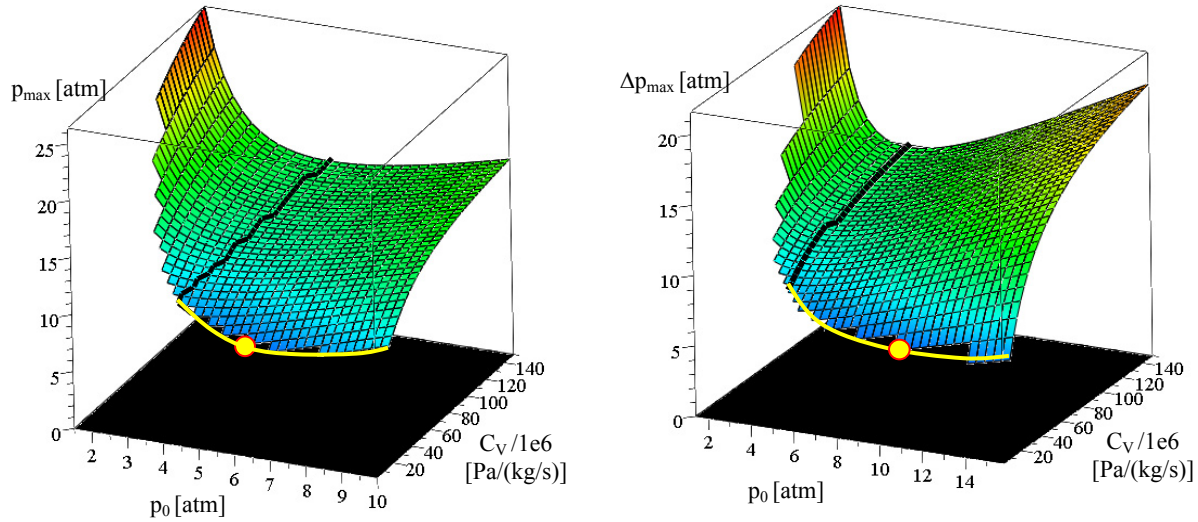

Fig. 3.2.5. Surfaces of maximal pressure / maximal pressure difference in terms of initial pressure and valve opening: a) system with exhaust to environment, b) system with valve between the chambers.

The procedure for deriving formula which defines pneumatic force explicitly in terms of piston displacement (Eq. 3.2.31-3.2.32) can be directly followed, however the resulting formula is too complex to find analytical function defining optimal initial pressure. Thus, global minimum of maximal pressure difference $\Delta p_{\max}$ (which is equivalent to global minimum of generated pneumatic force) was determined numerically. It was obtained for substantially higher value of initial pressure than in case of closed valve and it was dependent on impacting mass and impact velocity. The surface of maximal pressure difference in terms of initial pressure and flow resistance coefficient is presented in Fig. 3.2.5b.

The above derived formulae defining optimal initial pressure and optimal flow resistance coefficient for single- and double-chamber absorbers hold only for purely pneumatic system described by set of equations (3.2.22 and 3.2.36). In cases of pneumatic absorbers which involve friction or other forces, the solution of the optimisation problem (3.2.21) has to be searched numerically. However, due to the fact that considered systems are based mainly on pneumatic forces (not on friction or other forces) derived analytical formulae can be used as preliminary assessment of the optimal parameters.

Active adaptation with continuous valve control

Active adaptation of pneumatic absorber is formulated as the problem of determination of initial pressure in the absorber p_0 and continuous change of valve opening during the process $C_V(t)$ which minimizes extreme value of hitting object acceleration. Straightforward mathematical formulation of the problem reads:

$$\text{Find } p_0, C_V(t) \quad \text{such that } J_2 = \max_t \left|\ddot{u}(t)\right| \text{ is minimal} \tag{3.2.39}$$

Mathematical model of the adiabatic single-chamber absorber considered in the optimisation problem is more complicated than model considered in case of semi-active adaptation. Except the pneumatic forces generated by the absorber, also additional elastic and damping forces are taken into account in equation of impacting mass motion (Eq. $3.2.40_1$). Moreover, the flow resistance coefficient in the flow equation may change during the process. Modelling is limited to the case when outflow of the gas from the cylinder occurs and thus equation of energy balance can be transformed into analytical form. The complete set of governing equations reads:

$$M\ddot{u} + (p - p_A)A + ku + c\dot{u} = 0\,, \qquad \dot{m}(t) = -(p - p_A)/C_V(t) \tag{3.2.40}$$

$$\frac{\dot{p}}{p} = \kappa\frac{\dot{m}}{m} - \kappa\frac{\dot{V}}{V} \qquad \text{or} \qquad \frac{pV^{\kappa}}{m^{\kappa}} = \frac{p_0 V_0^{\kappa}}{m_0^{\kappa}} \qquad \text{for} \quad p > p_{ext}$$

IC: $u(0) = 0\,,\ \dot{u}(0) = V_0\,,\ p(0) = p_0\,,\ m(0) = m_0$

The procedure of active adaptation is composed of three following stages:

1. preliminary impact detection and identification of impacting mass and velocity;
2. determination of optimal change of pneumatic force in terms of time or piston displacement based on global energy balance or actual system kinematics;
3. control of the valve opening in order to provide predetermined optimal change of the pneumatic force generated by the absorber.

Ad. 1. The methods of impact identification were described in Sect. 3.2.1. Determined values of the impacting mass and impact velocity allow to compute energy which has to be dissipated and to determine desired change of the force generated by the absorber during the impact process. However, in case when adjustment of initial pressure is not possible, the control strategy typically involves the preliminary stage of pressure increase with the closed valve. In this situation real-time analysis of the system kinematics during initial stage of impact can be used for determination of further optimal control strategy and separate impact identification procedure is not required.

Ad. 2. Strategy of optimal adaptation which leads to minimal values of generated forces and minimal values of impacting object deceleration depends on the following features of the system:

- presence of additional forces generated by the absorber, i.e. elastic and friction forces dependent on piston displacement and velocity, respectively;
- constraints imposed on maximal valve opening and speed of valve opening.

Let us initially focus on the simplest case when only pneumatic force is generated by the absorber and no constraints on valve opening are imposed. Additionally, it will be assumed that initial pressure is preliminarily defined and it is lower than pressure equivalent to constant force required for stopping the impacting object by using the whole cylinder stroke: $p_0 < MV_0^2 / 2h_0A + p_A$.

Determination of optimal change of pneumatic force is based on a proposed adaptation strategy which consists of two main stages:

- keeping the valve closed in order to increase pneumatic force to desired level and to obtain required level of piston deceleration;
- control of valve opening aimed at maintaining constant level of internal pressure and constant level of force generated by the absorber.

Calculation of piston displacement when the second stage of adaptation begins is based on the condition that the mass is stopped by using the whole stroke of absorber h_0. Equations of motion describing optimally controlled single chamber absorber read:

$$M\frac{d^2u(t)}{dt^2}+\left(\frac{p_0{h_0}^{\kappa}}{(h_0-u(t))^{\kappa}}-p_A\right)A=0 \quad \text{for} \quad u(t)\in\left(0,u_x\right) \tag{3.2.41a}$$

$$M\frac{d^2u(t)}{dt^2}+\left(\frac{p_0{h_0}^{\kappa}}{(h_0-u_x)^{\kappa}}-p_A\right)A=0 \quad \text{for} \quad u(t)\in\left(u_x,h_0\right\rangle \tag{3.2.41b}$$

The variable u_x indicates piston displacement at time instant when the valve is opened and it can be calculated by comparing kinetic energy of the hitting object with work done by pneumatic force on piston displacement. Integration of Eqs 3.2.41a,b over displacement in the range from 0 to h_0 gives:

$$u_x=h_0-h_0\left[\frac{(\kappa-1)}{\kappa}\left(\frac{MV_0^2}{2p_0h_0A}+\frac{p_A}{p_0}\right)+\frac{1}{\kappa}\right]^{\frac{1}{1-\kappa}} \tag{3.2.42}$$

The result for isothermal process can be obtained by calculating limit of Eq. 3.2.42 when κ approaches 1. Pressure at time instant when the valve is being opened and which commence active stage of impact can be determined from the adiabatic ideal gas law:

$$p_x=p^{opt}=\frac{p_0{h_0}^{\kappa}}{(h_0-u_x)^{\kappa}}=p_0\left[\frac{(\kappa-1)}{\kappa}\left(\frac{MV_0^2}{2p_0h_0A}+\frac{p_A}{p_0}\right)+\frac{1}{\kappa}\right]^{\frac{-\kappa}{1-\kappa}} \tag{3.2.43}$$

Corresponding piston velocity can be calculated by using integral of Eq.3.2.41b over displacement in the range $(u_x,h_0\rangle$:

$$v_x=\left(\frac{2A(p_x-p_A)(h_0-u_x)}{M}\right)^{1/2} \tag{3.2.44}$$

Finally, acceleration of the hitting object can be calculated directly from the equation of motion which allows to determine the entire kinematics of the hitting object during the second stage of impact:

$$a_x=a^{II}=a^{opt}=-\frac{A(p^{opt}-p_A)}{M}, \qquad v^{II}=v_x+a^{opt}(t-t_x), \tag{3.2.45}$$

$$u^{II}=v_x(t-t_x)+\frac{a^{opt}(t-t_x)^2}{2}$$

In above formulae t_x indicates time of valve opening which can be determined from the numerical solution of Eq. 3.2.41a.

The formulae defining optimal pressure and acceleration hold until impacting mass approaches cylinder bottom and its velocity decreases to zero. At this time instant total

pneumatic force acting on the impacting object should be diminished in order to reduce impacting object deceleration and to obtain state of static equilibrium of the system. In the proposed adaptive system displacement of the piston u_x at which the valve is opened depends only on impact energy and, consequently, the whole force-displacement characteristics is identical for all impacts of the same kinetic energy. By contrast, change of pneumatic force in time depends on mass (or velocity) of the impacting object.

Although the above procedure for determination of the beginning of the second stage of adaptation is relatively simple, it has to be preceded by a complex procedure for identification of impact parameters. An alternative approach for determination of time instant of valve opening is based on tracking piston kinematics during the first (passive) stage of impact. The second stage begins at time instant t_x when piston deceleration reaches the value which maintained constant allows to stop impacting object by using the remaining part of the cylinder stroke:

$$t = t_x \quad \text{such that} \quad a(t_x) = -\frac{v(t_x)^2}{2(h_0 - u(t_x))} \tag{3.2.46}$$

Theoretically, determination of time t_x requires measurement of only one kinematical quantity since they are connected by differential and integral relations. Alternatively, measurement of internal pressure can be utilized since during passive stage of impact it is unambiguously correlated with piston displacement. The above procedure can not be applied when initial pressure inside cylinder should be separately adjusted at the beginning of the process, e.g. when it is too high for particular impact scenario and gas should be immediately released to provide minimal value of hitting object deceleration.

Ad. 3. In the second stage of adaptation valve opening is changed in real time in order to maintain constant level of force generated by the absorber. From the point of view of control theory this stage of adaptation is control with predefined output, known as problem of 'regulation'. In considered case of purely pneumatic absorber, optimal change of resistance coefficient, which allows to maintain constant pneumatic force starting from arbitrary assumed state defined by parameters u^*, p^*, m_0 can be determined analytically. For this purpose, the condition of pressure being constant is introduced into analytical form of the equation energy balance (Eq. 3.2.40$_4$) to obtain:

$$m = \left(\frac{p}{p^*}\right)^{1/\kappa}\left(\frac{h_0 - u(t)}{h_0 - u^*}\right)m_0 = \left(\frac{h_0 - u(t)}{h_0 - u^*}\right)m_0 \tag{3.2.47}$$

Further, required mass flow rate of gas and required resistance coefficient of the valve are determined by time differentiation of Eq. 3.2.47 and by utilizing the definition of the mass flow rate through the valve:

$$q = \dot{m} = -\frac{v(t)\,p_0 h_0 A}{(h_0 - u^*)RT_0}, \qquad C_V = \frac{(p^* - p_A)(h_0 - u^*)RT_0}{v(t)\,p_0 h_0 A} \tag{3.2.48}$$

In a control procedure, arbitrary parameters defining state of the system at time instant of valve opening u^*, p^* have to be replaced by previously determined optimal parameters u_x, p_x (cf. Eq. 3.2.42, Eq. 3.2.43). Eventually, the control procedure is defined as follows:

$$C_V \to \infty \quad \text{for} \quad t < t_x$$
$$C_V(v) = \frac{(p_x - p_A)(h_0 - u_x)RT_0}{v p_0 h_0 A} \quad \text{for} \quad t \geq t_x \tag{3.2.49a}$$

The control variable C_V is expressed here in terms of parameters of the system at time t_x (pressure p_x and displacement u_x) and in terms of actual piston velocity v. By substituting actual velocity of the piston by the previously determined function describing optimal change of its velocity (Eq. 3.2.45$_2$) we obtain an alternative form of the control procedure:

$$C_V \to \infty \quad \text{for} \quad t < t_x$$
$$C_V(t) = \frac{(p^{opt} - p_A)(h_0 - u_x)RT_0}{v^{II}(t) p_0 h_0 A} \quad \text{for} \quad t \geq t_x \tag{3.2.49b}$$

In contrast to the previous case, now the control variable is not defined in terms of actual velocity of the piston but explicitly in terms of time. Moreover, the formula (3.2.49) clearly reveals the dependence of optimal resistance coefficient on impact energy (cf. Eq. 3.2.43) and mass of the impacting object (cf. Eq. 3.2.44, Eq. 3.2.45). Proposed adaptation algorithms can be viewed in two manners:

- as feedback control system with on-line identification of time instant of valve opening t_x and with feedback to piston velocity (Eq. 3.2.49a),
- as feed-forward control system where optimal change of flow resistance coefficient is predefined at the beginning of the impact process on the basis of recognized impact mass and impact velocity (Eq. 3.2.49b).

Both adaptation algorithms applied to the model of ideal pneumatic system lead to the same results in case when there are no constraints on valve opening imposed. However, both procedures behave differently in case when constraints imposed on maximal valve opening become active at certain time period of the impact. The control algorithm based on Eq. 3.2.49a allows for continuation of the procedure of maintaining constant predefined pressure when the constraint becomes inactive. On the contrary, the control procedure defined by Eq. 3.2.49b is deregulated by active constraint (due to unexpected increase of pressure and change of predicted system kinematics) and does not act properly when constraint becomes inactive. Consequently, both methods are characterised by various robustness when uncertainties or interferences of the system occurs.

Numerical verification of the proposed adaptation strategy was performed for three impacts of the same energy, but characterized by various masses and velocities of the impacting object cf. Fig. 3.2.6a. The simulations reveal that after passive stage of impact where pressure is not released the valve has to be open to a certain extend (determined by impact and absorbers parameters, cf. Eq.3.2.49a,b) and then it has to be gradually closed until the end of the process. According to derived formulae and conducted simulations the inverse of the optimal flow resistance coefficient changes proportionally to piston velocity - it decreases linearly in terms of time, but nonlinearly in terms of piston displacement (cf. Eq. 3.2.48). The reverse dependence is observed for the mass of the gas inside cylinder. Optimal adaptation requires, the same for each scenario, linear reduction of mass of gas in terms of piston displacement (cf. Eq. 3.2.47), which differs in terms of time.

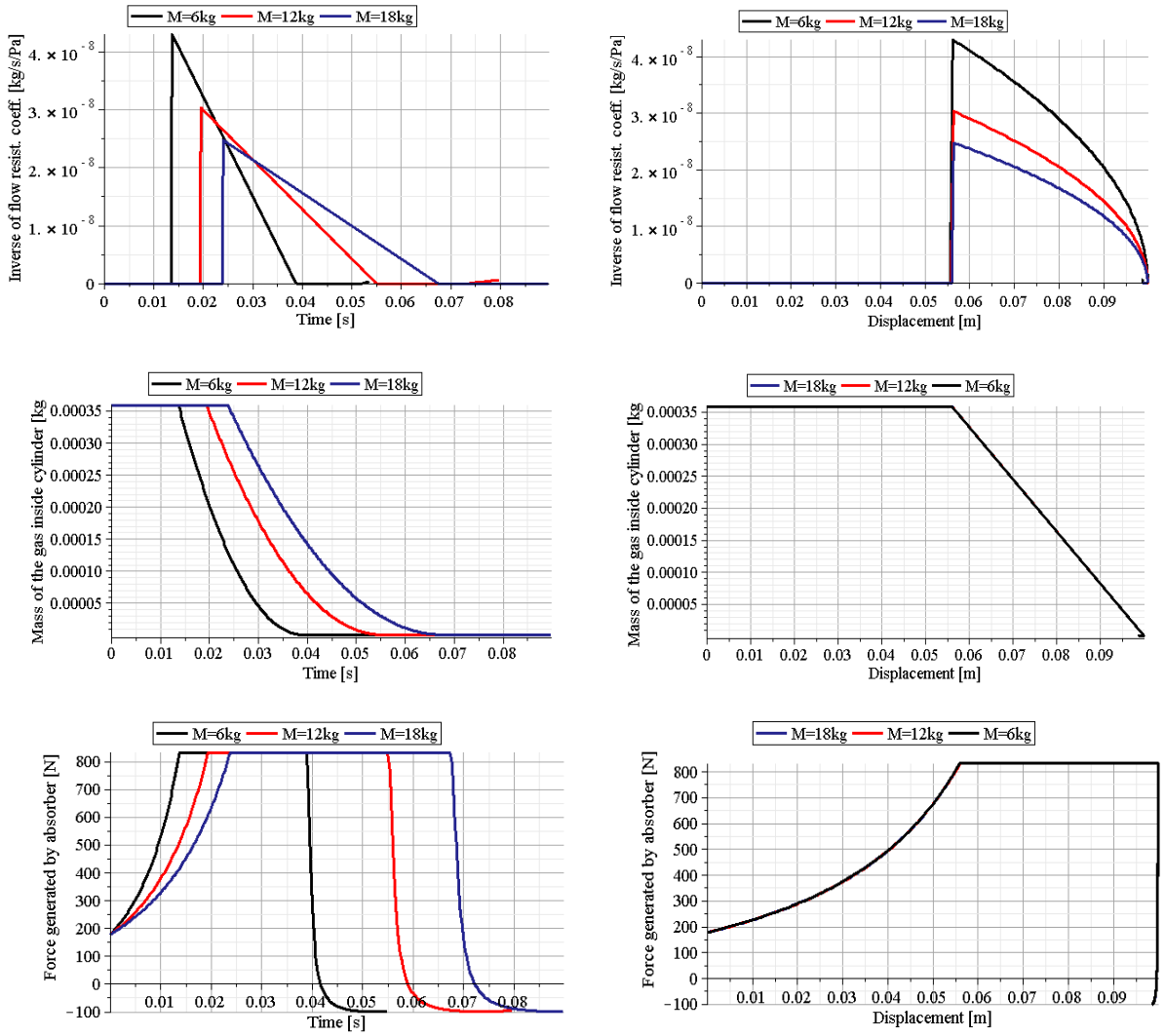

Fig.3.2.6. Active adaptation of pneumatic absorber to impact of the same energy but various masses and velocities: a) optimal valve opening, b) mass flow rate of gas, c) force generated by the absorber

In case when initial pressure of gas inside cylinder can be also adjusted, active adaptation strategy enables to maintain constant level of force generated by the absorber during the whole impact process. Optimal initial pressure equals to constant pressure which allows to stop the hitting object by using the whole stroke of the absorber. In turn, the optimal flow resistance coefficient is determined on the basis of Eq. 3.2.48b. Both control parameters are exactly the same for the processes which take place under isothermal or adiabatic conditions and they are defined as follows:

$$p_0 = p^{opt} = \frac{MV_0^2}{2Ah_0} + p_A \quad , \quad C_V(t) = \frac{(p_0 - p_A)RT_0}{v^{II}(t)p_0 A} \tag{3.2.50}$$

The smallest resistance coefficient, which corresponds to the largest valve opening is required at the very beginning of impact. Minimal flow resistance coefficient expressed in terms of impact and absorber parameters equals:

$$C_V(t) = \frac{MV_0RT_0}{2\left((MV_0^2)/2h_0A + p_A\right)h_0A^2} \tag{3.2.51}$$

and it is exactly two times smaller than previously derived flow resistance coefficient required for semi-active adaptation procedure (cf. Eq. $3.2.35_2$).

In case when initial pressure is higher than optimal pressure defined by Eq. ($3.2.50_1$), it instantly results in excessive forces generated by the absorber and excessive initial value of hitting object acceleration. Consequently, the adaptation strategy, that can be proposed, should minimize the period during which acceleration level remains excessive. Such a strategy assumes full opening of the valve from the beginning of the process until time instant when condition (3.2.46) is reached and further change of valve opening according to Eq. $3.2.49b_2$ until the end of the process.

Let us further considered the influence of **additional forces** in the equation of motion of the hitting mass: elastic force (caused for instance by spring located inside a cylinder) and damping force dependent on piston velocity (caused for instance by friction of the piston and cylinder walls). The equation of mass motion supplemented by two above terms reads:

$$M\ddot{u} + (p - p_A)A + ku + c\dot{u} = 0 \tag{3.2.52}$$

Moreover, it will be assumed that the second term of Eq. 3.2.52 prevails over the third and fourth term which indicates that response of the absorber is based mainly on pneumatic force. In considered system the optimal change of force generated by the absorber is defined by the equations:

$$M\frac{d^2u(t)}{dt^2} + \left(\frac{p_0 {h_0}^{\kappa}}{(h_0 - u(t))^{\kappa}} - p_A\right)A + ku + c\dot{u} = 0 \quad \text{for} \quad u(t) \in (0, u_x) \tag{3.2.53a}$$

$$M\frac{d^2u(t)}{dt^2} + \left(\frac{p_0 {h_0}^{\kappa}}{(h_0 - u_x)^{\kappa}} - p_A\right)A + ku_x + c\dot{u}_x = 0 \quad \text{for} \quad u(t) \in (u_x, h_0\rangle \tag{3.2.53b}$$

In the second (active) stage of impact, all components of force generated by the absorber (pneumatic, elastic and damping force) change in time and only their sum indicating total force generated by the absorber remains constant. In Eq. 3.2.53b all forces are artificially assumed to be constant and equal to value at time instant of valve opening t_x, which allows to determine optimal kinematics of the impacting mass.

Determination of the beginning of the second stage of impact, which is defined by the quantity u_x or alternatively t_x can be determined:

- by analytical integration of Eqs. 3.2.53a,b over displacement (which is possible if only elastic force is present) in order to find displacement u_x;
- numerically by solving differential equation (3.2.53a) and by checking kinematical condition defining optimal acceleration (Eq. 3.2.46).

The complete state of the pneumatic system, defined by quantities p_x, v_x, a_x can be determined in similar manner as it was performed for purely pneumatic system (cf. Eqs. 3.2.43-3.2.45). Knowledge of the above parameters allows to find optimal kinematics of the system during the second stage of impact and corresponding change of elastic and damping force. The condition of equivalence of total absorber force at time instant of valve opening and during the entire second stage of impact:

$$\left(p_x - p_A\right)A + ku_x + c\dot{u}_x = \left(p^{opt}(t) - p_A\right)A + ku(t) + c\dot{u}(t) \tag{3.2.54a}$$

allows to determine optimal change of pressure inside cylinder:

$$p^{opt}(t) = p_x - A^{-1}k\left(u(t) - u_x\right) + A^{-1}c\left(\dot{u}_x - \dot{u}(t)\right) \tag{3.2.54b}$$

The above equation clearly reveals that in system involving additional elastic force the pneumatic force has to decline during active stage of impact in order to compensate increase of elastic force caused by spring compression. On the contrary, additional damping force causes that pneumatic force has to gradually rise during the process in order to compensate the decrease of damping force related to reduction of piston velocity (Fig.3.2.7, Fig. 3.2.8).

Optimal change of mass of the gas inside cylinder can be determined from the adiabatic ideal gas law and by taking into account optimal change of pressure inside cylinder defined by Eq. 3.2.54b:

$$m = \left(\frac{p^{opt}}{p_x}\right)^{1/\kappa}\left(\frac{h_0 - u}{h_0 - u_x}\right)m_0 = \left(\frac{p_x - A^{-1}k\left(u - u_x\right) + A^{-1}c\left(\dot{u}_x - \dot{u}\right)}{p_x}\right)^{1/\kappa}\left(\frac{h_0 - u}{h_0 - u_x}\right)m_0 \tag{3.2.55}$$

Required mass flow rate is obtained by simple differentiation over time:

$$q = \frac{m_0}{h_0 - u_x}\left(\frac{1}{p_x}\right)^{1/\kappa}\left[\begin{array}{l} -\dfrac{A^{-1}}{\kappa}\left[p_x - A^{-1}k\left(u - u_x\right) + A^{-1}c\left(\dot{u}_x - \dot{u}\right)\right]^{\frac{1}{\kappa}-1}\left(k\dot{u} + c\ddot{u}\right)\left(h_0 - u\right) \\ -\left[p_x - A^{-1}k\left(u - u_x\right) + A^{-1}c\left(\dot{u}_x - \dot{u}\right)\right]^{\frac{1}{\kappa}}\dot{u} \end{array}\right] \tag{3.2.56}$$

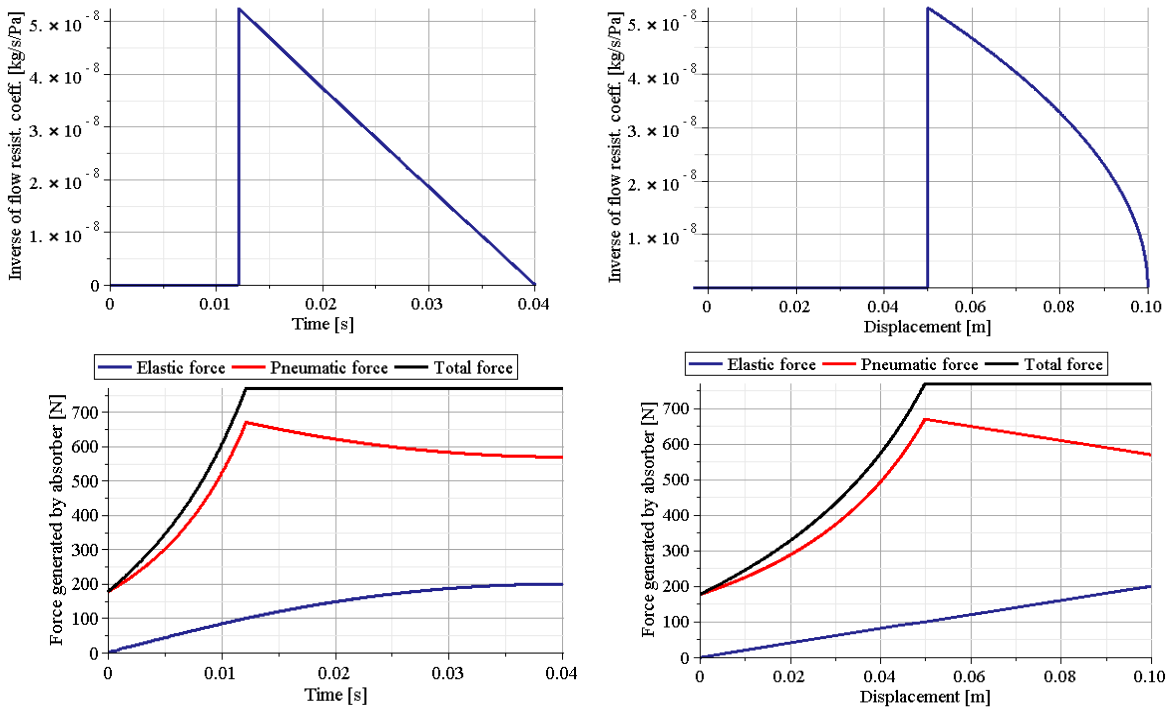

Fig.3.2.7. Active adaptation of pneumatic absorber including additional elastic force:
a) optimal valve opening, b) obtained pneumatic, elastic and total force

Flow resistance coefficient which enables maintaining constant value of force generated by the absorber starting from displacement u_x can be determined from the equation defining

mass flow rate of the fluid and it equals:

$$C_V(u,\dot{u},\ddot{u}) = \frac{(p_x - p_A)RT_0(h_0 - u_x)}{p_0 h_0 A}\left(\frac{1}{p_x}\right)^{-1/\kappa} \times \left[\quad\right]^{-1} \tag{3.2.57}$$

It can be seen that even for such a simple problem with definition of the equation of motion with two additional terms (Eq. 3.2.52), the control law becomes fairly complicated. The final form of the control algorithm can be written in two equivalent forms analogous to Eq. 3.2.49a and Eq. 3.2.49b with C_V defined by Eq. 3.2.57. In case when formula (3.2.57) is directly applied, the adaptation algorithm can be treated as feedback control with feedback to piston displacement, velocity and acceleration. On the contrary, when optimal kinematics is introduced into the Eq. 3.2.57, the resistance coefficient is expressed explicitly in terms of impact parameters and time, and the system can be treated as feed-forward. The results of application of the second type of control procedure in case of additional elastic force and friction force are depicted in Fig. 3.2.7 and 3.2.8, respectively.

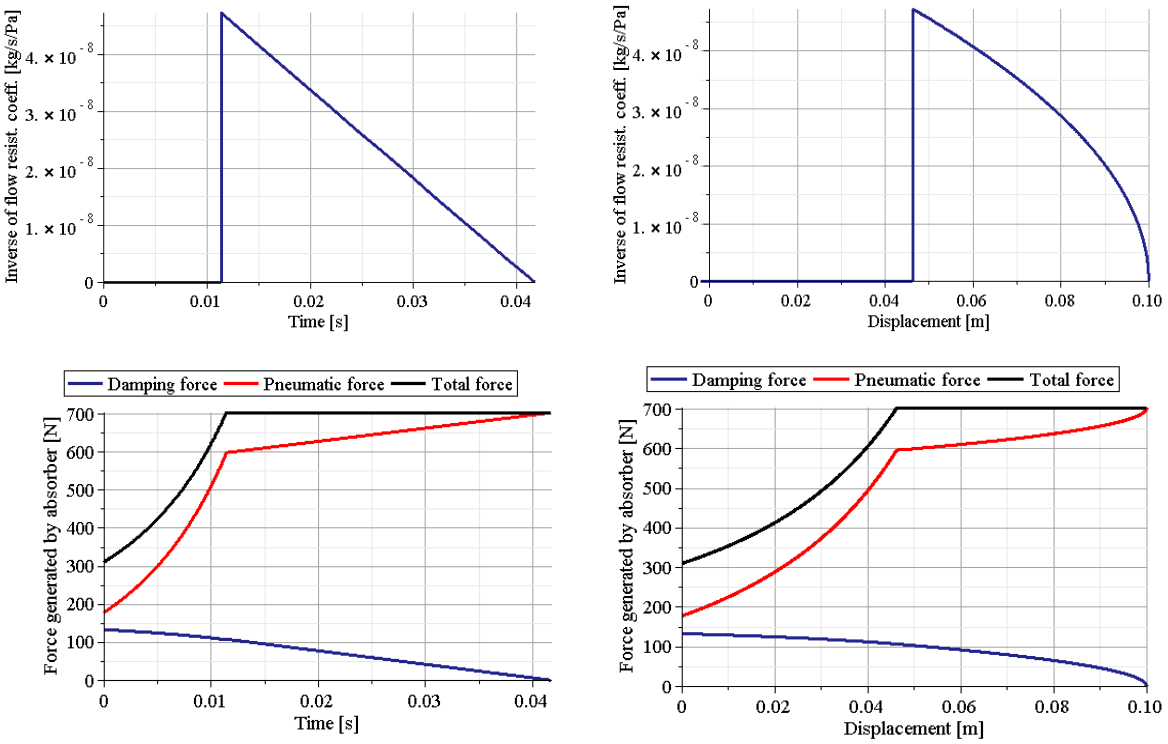

Fig.3.2.8. Active adaptation of pneumatic absorber including additional friction:
a) optimal valve opening , b) obtained pneumatic force, friction force and total force

Adaptation procedure becomes more complex when **constraints on extreme valve opening** or maximal speed of valve opening are imposed. In further analysis, purely pneumatic absorber will be considered and constraint on maximal valve opening $A_V^{\max}$ (represented by minimal value of resistance coefficient $C_V^{\min}$) will be imposed. The constraint on minimal valve opening will not be established. Moreover, natural constraint that valve opening can not be smaller than zero does not have to be separately introduced into mathematical model since it is automatically incorporated into proposed procedure of

determination of optimal change of pneumatic force. Eventually, the flow resistance coefficient C_V is confined to the range:

$$C_V^{\min} < C_V < \infty \tag{3.2.58}$$

In case when the constraint on maximal valve opening becomes active, the control strategy based on Eq. 3.2.49a or Eq. 3.2.49b appears not to be optimal since it results in undesired increase of pneumatic force at the beginning of the active stage of impact. Therefore, separate adaptation strategy for the case of active constraint has to be proposed. Similarly as previously, such a strategy is composed of the initial passive stage where valve remains closed and the second stage where valve opening is controlled. However, two intrinsic differences are the following:

- valve opening during the second stage of impact should provide arbitrary constant level of pressure (not fixed level of pressure),
- time of valve opening should be determined as a result of optimization procedure.

The first issue is related to definition of the flow resistance coefficient in active stage of impact. The definition (3.2.49a) allows for maintaining constant pressure starting from the initial state defined by parameters u_x, p_x, m_0. By contrast, the current procedure should allow for maintaining constant pressure whenever it is possible starting from an arbitrary state of the system defined by parameters: u^*, p^*, m^*. In such a case optimal mass of the gas in the cylinder can be calculated as:

$$m = \left(\frac{p}{p^*}\right)^{1/\kappa}\left(\frac{h_0 - u(t)}{h_0 - u^*}\right)m^* = \left(\frac{h_0 - u(t)}{h_0 - u^*}\right)\frac{p^*V^*}{RT^*} = \frac{\left(h_0 - u(t)\right)\left(p^*\right)^{\frac{1}{\kappa}}A}{RT_0\left(p_0\right)^{\frac{1}{\kappa}-1}} \tag{3.2.59}$$

where the Eq. 2.3.20c had been used. Further, required mass flow rate of the fluid and required resistance coefficient can be determined by time differentiation of Eq. 3.2.59 and by application of mass flow rate definition:

$$q = \dot{m} = \frac{v(t)\left(p^*\right)^{\frac{1}{\kappa}}A}{RT_0\left(p_0\right)^{\frac{1}{\kappa}-1}}, \quad C_V = \frac{\left(p^* - p_A\right)RT_0\left(p_0\right)^{\frac{1}{\kappa}-1}}{v(t)\left(p^*\right)^{\frac{1}{\kappa}}A} \tag{3.2.60}$$

Since value of pressure at which adaptation procedure begins is arbitrary, the value p^* can be replaced with the actual value of pressure inside cylinder $p(t)$. Moreover, flow resistance coefficient C_V has to be confined by its minimum value $C_V^{\min}$. Eventually, the control procedure which enables maintaining constant level of actual pressure starting from arbitrary time instant t_x takes the form:

$$C_V(t) \to \infty \quad \text{if} \quad t < t_x \tag{3.2.61}$$

$$C_V{}^{OPT} = \frac{(p(t) - p_A)RT_0 p_0{}^{1/\kappa - 1}}{Av(t)\,p(t)^{1/\kappa}}$$

$$C_V(v,p) = C_V{}^{OPT} \quad \text{if} \quad t \geq t_x \quad \text{and} \quad C_V{}^{OPT} > C_V^{\min}$$

$$C_V(v,p) = C_V{}^{\min} \quad \text{if} \quad t \geq t_x \quad \text{and} \quad C_V{}^{OPT} < C_V^{\min}$$

The above adaptation algorithm can be treated as feedback system with feedback to actual value of pressure inside cylinder and actual value of piston velocity. Let us note that in case of active constraint on valve opening the formula analogous to Eq. 3.2.49b where control parameters were defined directly in terms of time can not be explicitly determined. Furthermore, when actual pressure $p(t)$ in equation $(3.2.61_2)$ is replaced by constant value p_x (indicating pressure at time t_x), the algorithm allows for maintaining constant level of predefined pressure.

The second issue in development of optimal adaptation strategy is determination of time instant defining the end of passive stage of impact. In considered case with active constraint on valve opening, time instant when the second stage should begin can not be, however, calculated on the basis of the identified impact energy (cf. Eq. 3.2.41) or determined from kinematic relations of the system (cf. Eq. 3.2.46). Instead, time of valve opening has to be optimised in order to minimize the maximal value of pressure and hitting object acceleration. The corresponding optimization problem reads:

$$\text{Find } t_x \text{ such that } J_2 = \max_t \left|\ddot{u}(t)\right| \text{ is minimal} \tag{3.2.62}$$

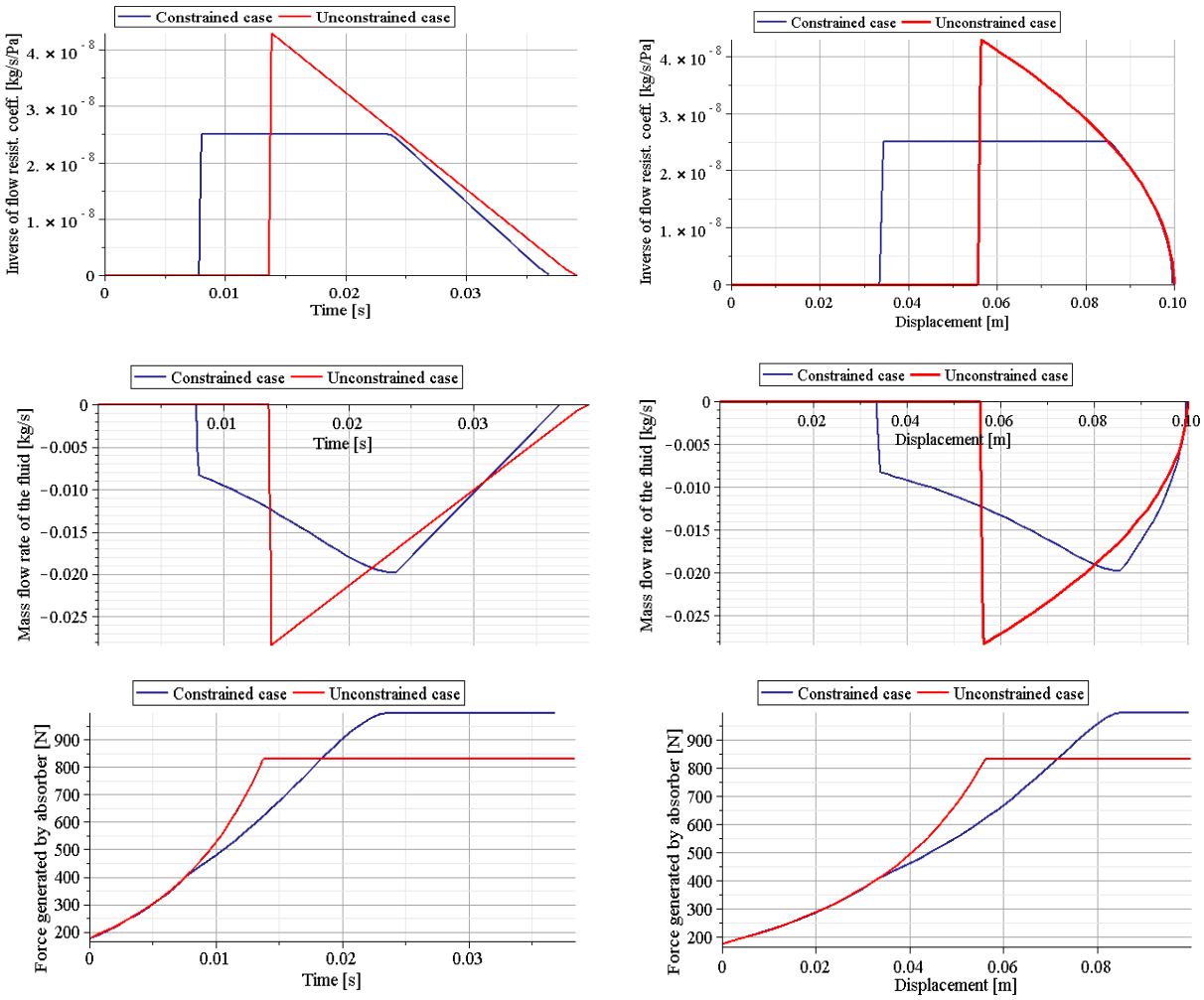

Fig. 3.2.9. Active adaptation of pneumatic absorber with/without constraints imposed on maximal valve opening: a) optimal valve opening, b) mass flow rate of the gas, c) pneumatic force in terms of time and piston displacement

Due to the fact that in unconstrained problem the value of optimal resistance coefficient C_V^{OPT} is gradually decreasing during the second stage of the process, in current constrained case the constraint on valve opening becomes active at the beginning of this stage. Consequently, optimisation procedure results in earlier opening of the valve than in unconstrained case. The valve remains fully open until it enables maintaining constant level of internal pressure. Further pneumatic force is maintained constant until the end of the cylinder stroke by gradual decrease of valve opening.

The numerical example (Fig. 3.2.9) shows the influence of active constraint on optimal change of flow resistance coefficient, mass flow rate of gas during the process and pneumatic force generated by the absorber. Application of the above described control strategy results in different optimal opening of the valve and higher level of generated force.

The problem of active adaptation was also solved for **double-chamber cylinder** with controlled flow between the chambers and adiabatic walls. The system will be considered during forward stroke of the piston, when pressure in compressed chamber is higher than in decompressed chamber and thus direction of the flow is fixed. In such a situation, considered adaptive pneumatic cylinder is described the following set of equations:

$$M\ddot{u} + p_2 A_2 - p_1 A_1 = 0\,; \qquad \dot{m}_2 = -\left(p_2 - p_1\right)/\, C_V(t) \tag{3.2.63a,b}$$

$$\frac{\dot{p}_2}{p_2} = \kappa\frac{\dot{m}_2}{m_2} - \kappa\frac{\dot{V}_2}{V_2} \quad \text{or} \quad \frac{pV^\kappa}{m^\kappa} = \frac{p_0 V_0^{\,\kappa}}{m_0^{\,\kappa}} \quad \text{for} \quad p_2 > p_1 \tag{3.2.63c}$$

$$\frac{\dot{p}_1}{p_1} = \kappa\frac{\dot{m}_1}{p_1 V_1}\frac{p_2 V_2}{m_2} - \kappa\frac{\dot{V}_1}{V_1} \quad \text{for} \quad p_2 > p_1 \tag{3.2.63d}$$

$$m = m_{10} + m_{20}\,, \quad V_1 = A_1(h_{10} + u)\,, \quad V_2 = A_2(h_{20} - u) \tag{3.2.63e}$$

IC: $u(0) = 0\,,\ \dot{u}(0) = V_0\,,\ p_1(0) = p_{10}\,,\ p_2(0) = p_{20}\,,\ m_1(0) = m_{10}\,,\ m_2(0) = m_{20}\,,$

The above system of equations is more complex than the system which governs single-chamber absorber due to presence of an additional differential equation describing energy balance inside decompressed chamber where inflow of the gas occurs. As in case of a single-chamber cylinder the control problem relies on finding optimal initial pressure and change of valve opening which provides minimal value of force generated by the absorber and minimal value of hitting object acceleration. Consequently, typical procedure of solution of the control problem is composed of preliminary step of impact identification, determination of optimal change of force generated by the absorber and determination of optimal change of flow resistance coefficient.

Kinematics of the optimally controlled system without constraints imposed on valve opening is described by the following equations of motion:

$$M\frac{d^2u(t)}{dt^2} + \frac{p_{20}h_{20}^{\,\kappa}}{(h_{20} - u(t))^\kappa}A_2 - \frac{p_{10}h_{10}^{\,\kappa}}{(h_{10} + u(t))^\kappa}A_1 = 0 \quad \text{for} \quad u(t) \in \left(0, u_x\right) \tag{3.2.64}$$

$$M\frac{d^2u(t)}{dt^2} + \frac{p_{20}h_{20}^{\,\kappa}}{(h_{20} - u_x)^\kappa}A_2 - \frac{p_{10}h_{10}^{\,\kappa}}{(h_{10} + u_x)^\kappa}A_1 = 0 \quad \text{for} \quad u(t) \in \left(u_x, h_0\right\rangle$$

Where the variable u_x indicates piston displacement at time instant when the valve is opened and it can be determined from the energy balance of the system (integration of Eqs. 3.2.64 over displacement). Parameters defining state of the system at time instant of valve opening assume especially simple form in case of zero initial volume of the upper chamber $h_{10} = 0$ and equal area of the piston in both chambers $A_1 = A_2$. In such a case piston displacement at time instant of valve opening equals:

$$u_x = h_{20} - h_{20}\left[\frac{(\kappa-1)}{\kappa}\left(\frac{MV_0^{\,2}}{2p_{20}h_{20}A}\right)+\frac{1}{\kappa}\right]^{\frac{1}{1-\kappa}} \tag{3.2.65}$$

and allows to determine pressure inside compressed chamber and force generated by the absorber at time instant of valve opening:

$$p_x = \frac{p_{20}h_{20}^{\ \kappa}}{(h_{20}-u_x)^{\kappa}} = p_0\left[\frac{(\kappa-1)}{\kappa}\left(\frac{MV_0^2}{2p_{20}h_{20}A}\right)+\frac{1}{\kappa}\right]^{\frac{-\kappa}{1-\kappa}}, \quad F_x = A_2 p_x \tag{3.2.66}$$

Corresponding velocity of the piston can be found from the energy balance:

$$v_x = \left(\frac{2A_2 p_x (h_{20}-u_x)}{M}\right)^{1/2} \tag{3.2.67}$$

and allows to find optimal kinematics of the system during the second stage of impact:

$$a_x = a^{II} = a^{opt} = -\frac{Ap_x}{M}, \quad v^{II} = v_x + a^{opt}(t-t_x), \quad u^{II} = v_x(t-t_x) + \frac{a^{opt}(t-t_x)^2}{2} \tag{3.2.68}$$

Both in case when impact is not recognized as well as in case when model of pneumatic cylinder involves elastic or friction forces, parameters of valve opening have to be determined on-line from the Eq. 3.2.46.

The next step in development of control procedure is determination of optimal change of flow resistance coefficient, which has to be preceded by determination of pressures and mass of the gas in both chambers of the cylinder since none of these quantities are explicitly known. Optimal change of pressures and change of mass of the gas can be found from the following system of equations resulting directly from the main system of governing equations (3.2.63):

$$p_2 = A_2^{-1}(F_x + p_1 A_1), \qquad m_2 = \left(\frac{p_2}{p_x}\right)^{1/\kappa}\left(\frac{V_2}{V_{2x}}\right)m_{20} \tag{3.2.69}$$

$$\frac{\dot{p}_1}{p_1} = -\kappa\frac{\dot{m}_2}{p_1 V_1}\frac{p_2 V_2}{m_2} - \kappa\frac{\dot{V}_1}{V_1}, \qquad \text{IC: } p_1(t_x) = p_{1x}$$

where the optimal kinematics of the system:

$$V_1 = A_1(h_{10} + u^{II}), \qquad V_2 = A_2(h_{20} - u^{II}) \tag{3.2.70}$$

has to be preliminarily introduced. In next step optimal change of the flow resistance coefficient can be determined in accordance to assumed adaptation strategy and by using

definition of the flow resistance coefficient:

$$C_V(t) \to \infty \quad \text{for} \quad t < t_x \tag{3.2.71}$$

$$C_V^{opt}(t) = -\frac{p_2 - p_1}{\dot{m}_2} \quad \text{for} \quad t \geq t_x$$

In the above equation, change of the resistance coefficient is not defined in terms of actual parameters of the process, but explicitly in terms of time. Therefore, the above control procedure defines feed-forward control system which determines optimal change of flow resistance coefficient on the basis on recognized impact energy and velocity.

Alternatively, change of the flow resistance coefficient can be determined analytically in terms of actual parameters of the pneumatic system. For this case differential equation of energy balance for the upper chamber has to be replaced with analytical energy balance for the whole structure (cf. Eq. 3.1.62b). System of algebraic equations for determination of change of systems parameter during the process reads:

$$p_2 = A_2^{-1}\left(F_x + p_1 A_1\right), \qquad m_2 = \left(\frac{p_2}{p_x}\right)^{1/\kappa}\left(\frac{V_2}{V_{2x}}\right)m_{20} \tag{3.2.72}$$

$$\tfrac{1}{2}MV_0^2 - \tfrac{1}{2}M\dot{u}^2 = \frac{p_1V_1}{\kappa - 1} + \frac{p_2V_2}{\kappa - 1} - \left(m_{10}c_VT_{10} + m_{20}c_VT_{20}\right)$$

The above system of equations allows to express change of system parameters p_1, p_2, m_2 in terms of system kinematics defined by functions $u, \dot{u}$. Finally, feedback control algorithm involves change of the flow resistance coefficient during the second stage of impact defined in terms of piston displacement, velocity and acceleration:

$$C_V \to \infty \quad \text{for} \quad u < u_x \tag{3.2.73}$$

$$C_V(u, \dot{u}, \ddot{u}) = C_V^{\,opt} = -\frac{p_2 - p_1}{\dot{m}_2} \quad \text{for} \quad u \geq u_x$$

The above control law is more complicated than control law derived for single chamber absorber (cf. Eq. 3.2.49a) which depends exclusively on piston velocity. Moreover definition of the optimal resistance coefficient involves mass of the impacting object and its initial velocity (cf. Eq. 3.2.72) which implies the requirement of preliminary impact identification.

In case of isothermal process the system of equations for determination of optimal pressures and mass of the gas in both chambers involves three simple equations:

$$p_2 = A_2^{-1}\left(F_x + p_1 A_1\right), \qquad p_1V_1 = m_1RT_0, \qquad p_2V_2 = m_2RT_0 \tag{3.2.74}$$

which allow to determine change of flow resistance coefficient in terms piston displacement and velocity:

$$C_V^{\,opt}(u, \dot{u}) = \frac{\left[F_x(A_1u + A_1h_{10} - A_2u + A_2h_{20}) + RT_0m(A_1 - A_2)\right]RT_0}{\dot{u}A_1A_2\left[F_x(2u + h_{10} - h_{20}) + RT_0m\right]} \tag{3.2.75}$$

In special case when area of the piston in both chambers is equal $A_1 = A_2$ the above formula simplifies to:

$$C_V^{\ opt} = -\frac{VRT_0}{\dot{V}_2\left[\left(\frac{p_0}{\nabla p_x}+1\right)V - 2V_2\right]} \tag{3.2.76}$$

The corresponding control law can be expressed in the form analogous to (3.2.73) or alternatively (3.2.71). Consequently, the adaptation algorithm can be treated as feedback control system where valve opening is based on actual piston displacement and piston velocity and (in case when optimal kinematics of the system is explicitly introduced) as feed-forward control system where optimal valve opening is preliminarily determined as a function of time on the basis of initially recognized impact energy and velocity.

The remaining part of the control problem is to find optimal initial pressure in both chambers for which maximal force generated by the absorber is the smallest. In case when different values of pressure can be applied in both chambers the solution is trivial and results from equivalence of initial pressure difference and optimal constant force:

$$p_{10} = 0, \quad p_{20} = \frac{MV_0^{\ 2}}{2h_{20}A_2} \tag{3.2.77}$$

In case when initial pressure in the whole system has to be uniform, it should provide possibly high initial force but on the other hand it should provide the possibility of maintaining constant optimal force at the end of the process (when the whole stroke is utilized and internal pressure is increased to p_{end}). Theoretical result can be obtained from the equations:

$$p_{end} = p_1 = p_2 = \frac{MV_0^{\ 2}}{2h_{20}(A_2 - A_1)}; \qquad \tfrac{1}{2}MV_0^{\ 2} = \frac{p_{end}V_{end}}{\kappa - 1} - \frac{p_0V_0}{\kappa - 1} \tag{3.2.78}$$

and it requires infinitely large opening of the valve at the end of the process.

Corresponding numerical example concerns the case of adiabatic process. Both difference between effective area of the chambers on both sides of the piston and initial volume of decompressed chamber are taken into account. Performed numerical simulations indicate that maintaining constant level of pneumatic force requires change of valve opening which achieves its maximum in the middle of the active stage of the process, Fig. 3.2.10a. Change of resistance coefficient is now nonlinear both in terms of time and in terms of piston displacement.

During the active stage of impact pressure in both chambers increases, however pressure difference gradually diminishes. As a result of the applied control strategy the force is maintained on a possibly low constant level and the whole stroke of the absorber is utilized, which results in optimal mitigation of impacting object deceleration.

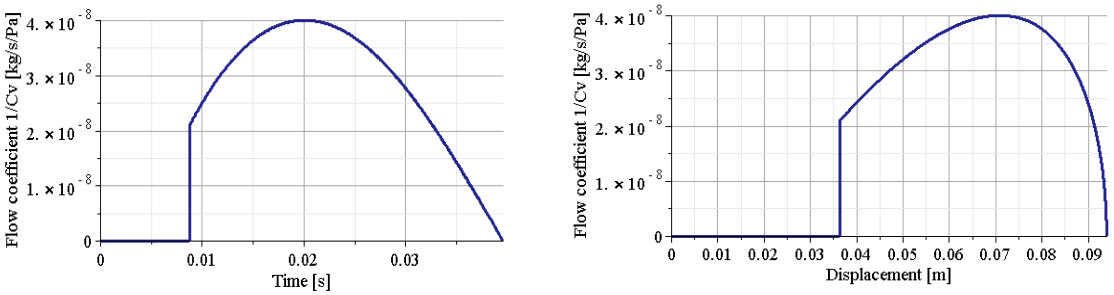

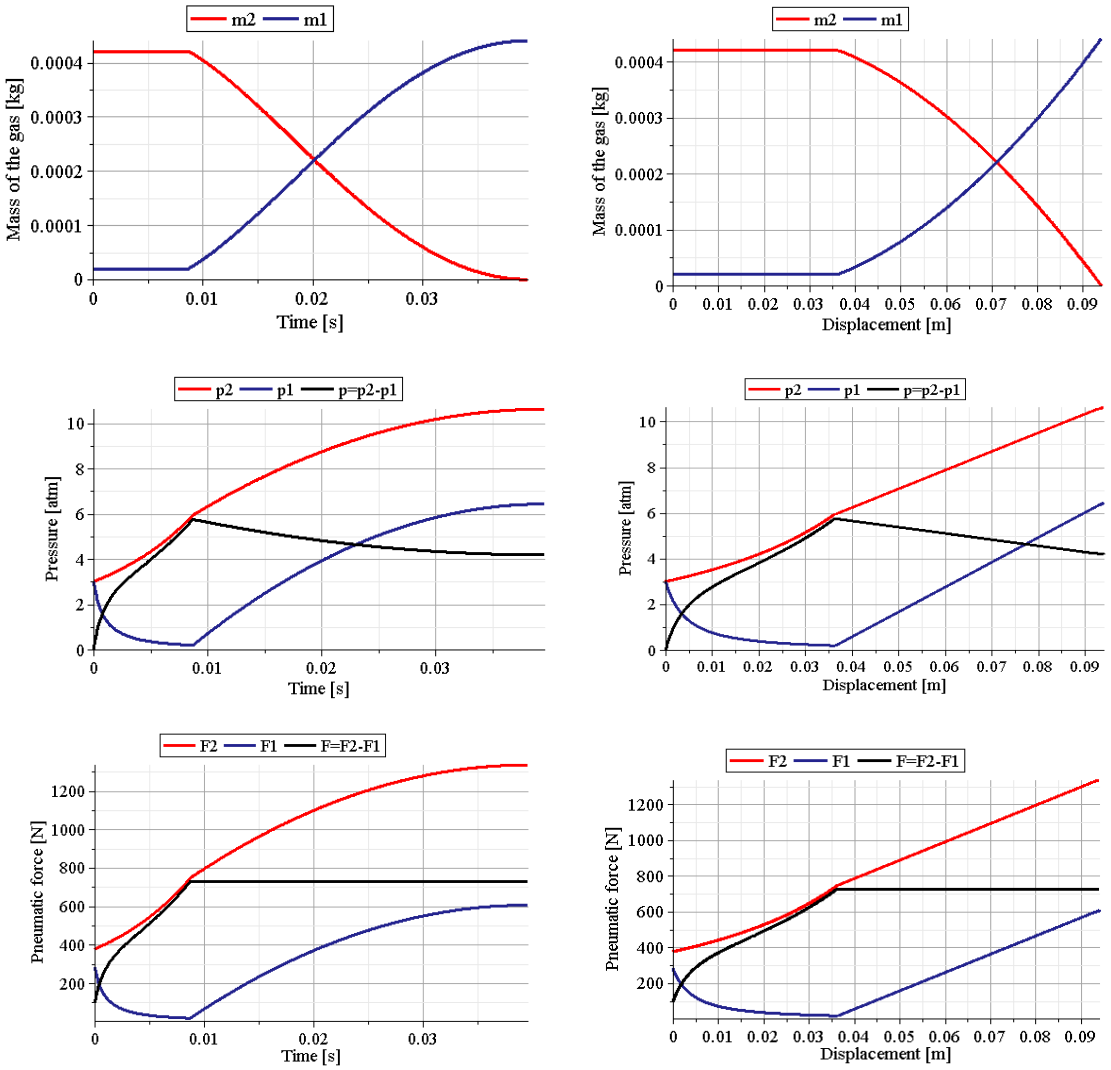

Fig.3.2.10. Active adaptation of purely pneumatic absorber: a) change of flow resistance coefficient, b) change of mass of the gas in both chambers, c) pressure of gas in both chambers, d) pneumatic force generated in both chambers and total force generated by the absorber

In case when additional forces are present in the equation of piston motion the strategy of optimal adaptation can be developed in similar manner. Parameters of the system at time instant of initial valve opening can be computed by analytical or numerical integration of equation of motion for the case of additional elastic and friction force, respectively. In such a case optimal pneumatic force does not remain constant and its desired change can be determined from kinematics of the system. Optimal change of flow resistance coefficient can be computed from Eq. 3.2.69-73 for adiabatic system and from Eq. 3.2.74-76 for the isothermal system and in each case the time variation of optimal pneumatic force has to be taken into account.

In case of **constraints imposed on maximal valve opening** more complex procedures of adaptation have to be developed. Two algorithms of adaptation will be proposed depending on the type of system under consideration:

- generalization of the control law and optimization of selected parameters can be used for the isothermal system;

- the method based on solution of separate systems of differential equations for subsequent stages of the process and optimization of selected parameters can be applied for adiabatic system.

The algorithm of adaptation is simpler in the first case (i.e. for isothermal process) since for such systems analytical form of the control law exists (Eq. 3.2.75). Initially, the control law has to be generalized in order to maintain actual value of the pneumatic force, not the value which is initially predefined. By taking advantage of the discretion of choice of the value of pneumatic force which has to be maintained constant, the fixed value F_x will be replaced by actual value of pneumatic force expressed in terms of pressure: $p_2 A_2 - p_1 A_1$. Generalized form of the control law for isothermal system reads:

$$C_V^{\,opt}(u,\dot{u},p_2,p_1)=\frac{\left[\left(p_2A_2-p_1A_1\right)\left(A_1u+A_1h_{10}-A_2u+A_2h_{20}+RT_0m(A_1-A_2)\right]RT_0\right.}{\dot{u}A_1A_2\left[\left(p_2A_2-p_1A_1\right)\left(2u+h_{10}-h_{20}+RT_0m\right)\right]} \tag{3.2.79}$$

In a special case when area of the piston in both chambers is equal we obtain:

$$C_V^{\,opt}=-\frac{VRT_0}{\dot{V}_2\left[\left(\frac{p_0}{\left(p_2-p_1\right)}+1\right)V-2V_2\right]} \tag{3.2.80}$$

Similarly, as in case of single chamber system, the control law is defined as follows:

$$C_V \to \infty \quad \text{for} \quad t < t_x \tag{3.2.81}$$

$$C_V(u,\dot{u},p_2,p_1)=C_V^{\,opt} \quad \text{if} \quad t \geq t_x \quad \text{and} \quad C_V^{\,opt} > C_V^{\min}$$

$$C_V(u,\dot{u},p_2,p_1)=C_V^{\,\min} \quad \text{if} \quad t \geq t_x \quad \text{and} \quad C_V^{\,opt} < C_V^{\min}$$

In case of active constraint, the time instant of valve opening is not known a priori and it has to be determined by solving the following simple optimization problem:

$$\text{Find } t_x \text{ such that } J_2=\max_t\left|\ddot{u}(t)\right| \text{ is minimal} \tag{3.2.82}$$

As a result of applied control strategy the process can be divided into four stages, Fig. 3.2.11:

1. increase of pneumatic force while the valve is closed,
2. sudden opening of the valve to a certain extend and gradual increase of valve opening in order to maintain constant level of generated pneumatic force,
3. maintaining full opening of the valve which results in increase of the pneumatic force due to active constraint on valve opening,
4. gradual reduction of valve opening in order to maintain constant pneumatic force.

The following two methods of tuning up the above adaptation strategy can be proposed:

- softening of the absorber during the initial, previously passive, stage of the process by partial constant opening of the valve,
- modification of the second, active stage of impact by applying full opening of the valve before time instant when pneumatic force starts to increase above the initially assumed level.

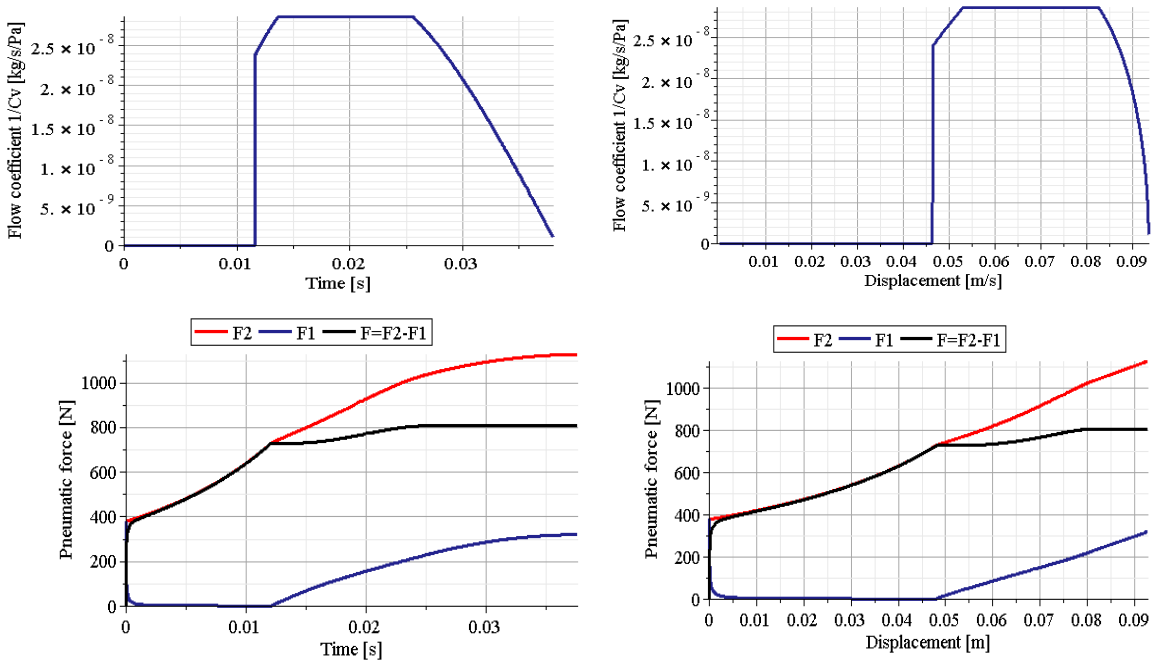

Fig.3.2.11. Basic strategy of active adaptation of pneumatic absorber involving limitation on maximal valve opening: a) valve opening , b) resulting pneumatic force

In the first case the corresponding optimization problem relies on finding initial constant valve opening $C_V{}^1$ and time instant when the valve starts to maintain constant force t_x^1:

$$\text{Find } C_V{}^1, t_x^1 \text{ such that } J_2 = \max_t |\ddot{u}(t)| \text{ is minimal} \tag{3.2.83}$$

Performed numerical simulations indicate that for assumed impact scenario such a formulation of the problem does not lead to reduction of force generated by the absorber and to decline of maximal level of hitting object deceleration.

In the second case, the optimization problem involves searching for time instant t_x^1 when the valve is initially opened to maintain constant pneumatic force and time instant t_x^2 when the valve becomes fully open:

$$\text{Find } t_x^1, t_x^2 \text{ such that } J_2 = \max_t |\ddot{u}(t)| \text{ is minimal} \tag{3.2.84}$$

The numerical analysis indicates that optimal solution is obtained when $t_x^1 = t_x^2$, i.e. full valve opening is applied instantly at the beginning of the second stage of impact. As a result pneumatic force acting on the hitting object is only insignificantly decreased (<1%) in comparison to generic active adaptation strategy. Comparison of constrained and unconstrained adaptation strategy (Fig. 3.2.12) reveals the increase of generated pneumatic force and reduction of the utilized stroke of the cylinder being a result of active constraint.

In case of adiabatic system in which impact parameters are not identified, the basic difficulty is that the flow resistance coefficient can not be found analytically in terms of actual state of the system. Therefore, numerical procedure of adaptation is not based on solving single system of differential equations with appropriately changing value of the flow resistance coefficient, but rather on solving different systems of differential equations for subsequent stages of the process. In case of basic adaptation procedure the following stages of the process can be distinguished:

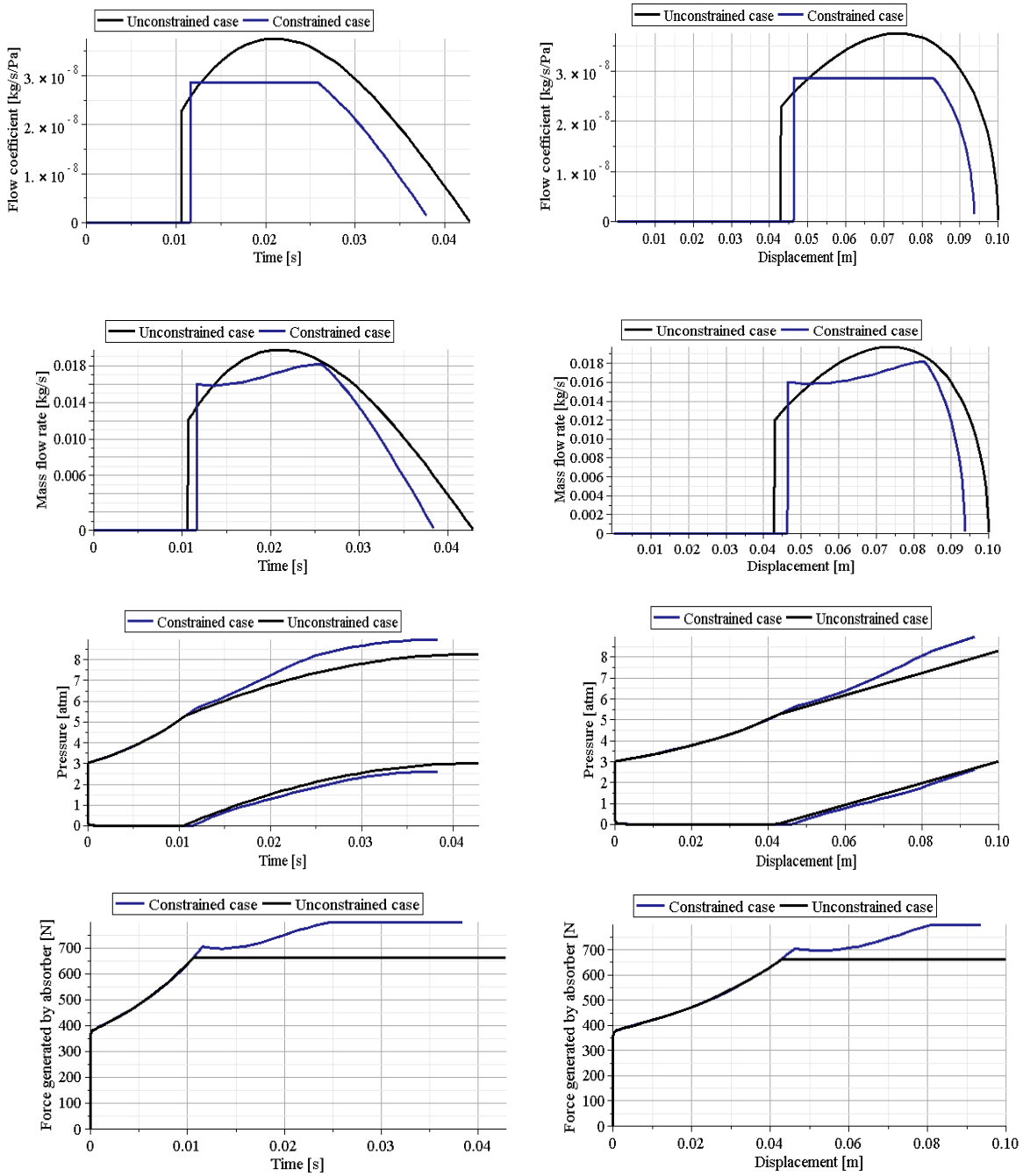

Fig.3.2.12. Comparison of unconstrained and constrained active adaptation strategy: a) valve opening, b) mass flow rate, c) resulting pressures in both chambers, d) resulting pneumatic force

1. solution of generic system of equations (3.2.63) with the closed valve;
2. solution of system of equation (3.2.69) for determination of resistance coefficient $C_V^{opt} > C_V^{\min}$ (from Eq.3.2.71$_2$) which allows to maintain constant level of pneumatic force, continuation of solution until $C_V^{opt} = C_V^{\min}$;
3. solution of generic system of equations (3.2.63) with minimal resistance coefficient $C_V^{\min}$ indicating full opening of the valve; parallel computation of optimal resistance coefficient $C_V^{opt} < C_V^{\min}$ which allows to maintain constant pneumatic force; continuation of solution until $C_V^{opt} = C_V^{\min}$;

4. solution of system of equations (3.2.69) for determination of resistance coefficient $C_V^{opt} > C_V^{\min}$ (Eq.3.2.71$_2$) which maintains constant pneumatic force until the end of the process, i.e. until impacting object velocity is reduced to zero.

Further stage of development of active adaptation strategy assumes optimization of time instant of initial valve opening according to (Eq. 3.2.82). In the next step the adaptation strategy can be tuned according to (Eq. 3.2.83 or Eq. 3.2.84) similarly as it was performed in case of isothermal system.

Active adaptation with on/off valve control

'On/off' control of valve opening is similar to 'continuous control' of valve opening in a sense that it allows to maintain (almost) constant level of force generated by the absorber during the second stage of impact. The substantial difference is that constant level of force is not obtained by continuous change of valve opening, but by fast commutative switching of the valve between 'open' and 'closed' positions. The control law defines opening of the valve in terms of actual force generated by the absorber $F(t)$, optimal value of that force F^{opt} and assumed range of tolerance ΔF^{tol}:

$$F(t) > F^{opt} + \Delta F^{tol} \;\rightarrow \text{ valve open} \tag{3.2.85}$$

$$F(t) < F^{opt} - \Delta F^{tol} \;\rightarrow \text{ valve closed}$$

$$\left\{F^{opt} - \Delta F^{tol} < F(t) < F^{opt} + \Delta F^{tol}\right\} \text{ and } \; dF/dt < 0 \;\rightarrow \text{ valve open}$$

$$\left\{F^{opt} - \Delta F^{tol} < F(t) < F^{opt} + \Delta F^{tol}\right\} \text{ and } \; dF/dt > 0 \;\rightarrow \text{ valve closed}$$

The above control law provides that the valve is opened above the upper tolerance level in order to decrease actual value of generated force by letting the gas out of the compressed chamber and it is closed below the lower tolerance level in order to increase generated force due to movement of the piston. Between the tolerance levels the valve opening depends on the value of the first derivative of force over time. In an alternative, practically equivalent approach the valve maintains its previous position between the tolerance levels.

In the first approximation it can be assumed that average value of pneumatic force during active stage of the process lies exactly in the middle of the tolerance range and therefore optimal level of force F^{opt} may be assumed as equal to optimal level of force in strategy with continuous valve control. Due to the fact that maximal force obtained during the process equals to $F(t) \cong F^{opt} + \Delta F^{tol}$, the range of tolerance should be maximally reduced in order to minimize force generated by the absorber. On the other hand, smaller range of tolerance results in the requirement of faster opening and closing of the valve.

Although the method is relatively simple, it involves several substantial advantages intrinsic both to numerical and practical implementation:

- the control law which allows to maintain constant force assumes the same form regardless of the type of the system (1DOF or 2DOF), thermodynamic conditions (isothermal and adiabatic system), the presence of additional forces, etc.
- the control law involves feedback exclusively to actual value of force generated by the absorber (which can be expressed in terms of gas pressure) and it does not involve

feedback to piston displacement and piston velocity as it was in case of algorithm of continuous control,

- implementation of the method does not require development of the numerical model of the fluid flow through controllable valve,
- in practical realisation the method allows to avoid difficulties related to mechanical properties of the controllable valve (such as hysteresis of a piezoelectric stack) and its interaction with the fluid flow.

On the other hand successful implementation of 'on/off strategy' requires application of the valve with much shorter response time than 'continuous strategy'. Application of the valve with insufficiently short response time results in increase of force generated by the absorber or causes that realisation of the on/off strategy becomes impossible.

Numerical example concerning single chamber pneumatic absorber presents application of the on/off strategy for various ranges of tolerance levels (cf. Fig. 3.2.13). In both cases the length of time intervals when the valve is closed remains similar during the process since it depends on velocity of the piston and volume of the chamber, which both are simultaneously decreasing. On the contrary, the length of time intervals when the valve is open depends only on decreasing volume of the chamber and mass flow rate through the valve and it theoretically tends to zero at the end of the process. In practical applications this singularity of the control algorithm does not occur since the whole stroke of the cylinder is never utilized. Minimal length of time period of valve opening which can be determined from presented analysis determines minimal range of tolerance level which can be assumed and thus the minimal value of force which can be obtained by using particular type of the valve.

Two drawbacks of the above method based on maintaining pneumatic force between the tolerance levels are the following:

- the method does not directly take into account the limitation of the valve speed,
- the method results in excessive fluctuations of the pneumatic force at the initial part of the active stage of impact.

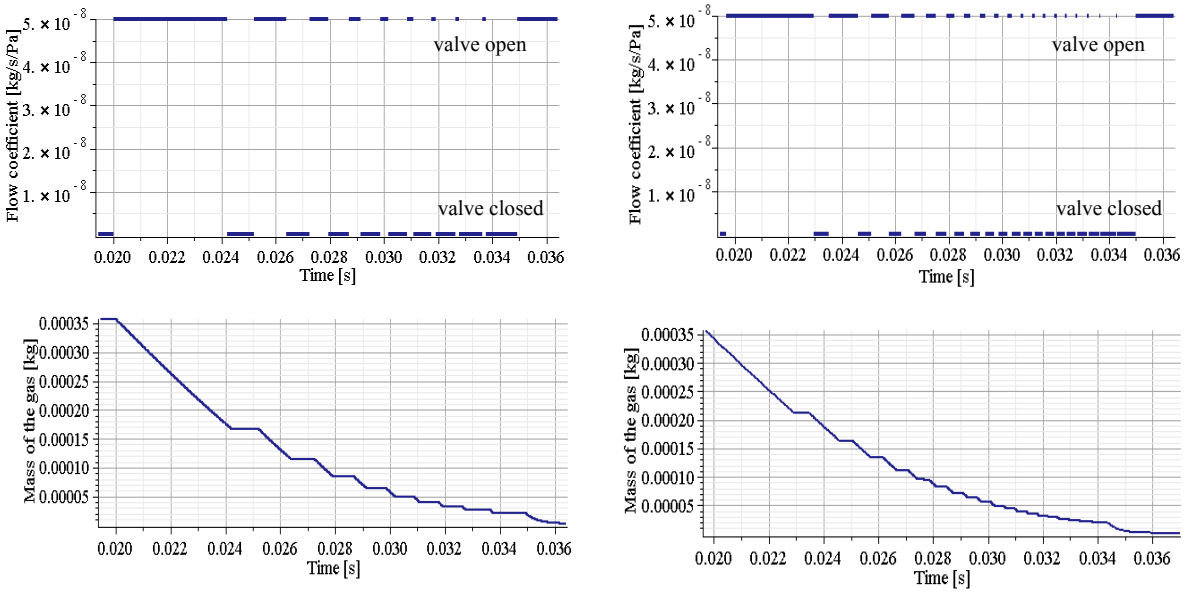

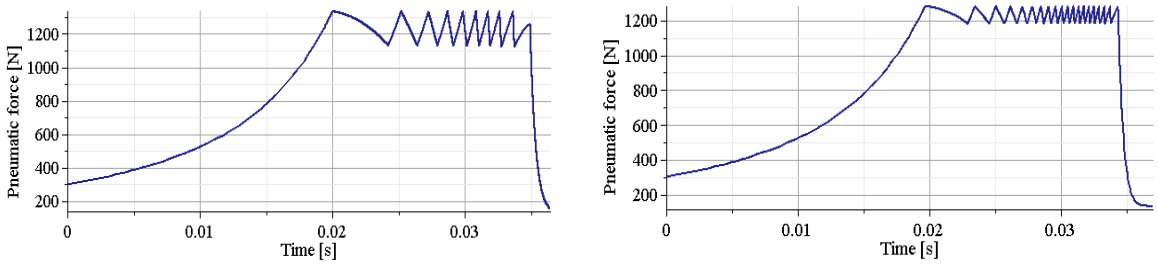

Fig. 3.2.13. Comparison of 'on/off' adaptation strategy of a single- chamber pneumatic absorber for two tolerance levels: a) valve opening, b) mass of gas inside cylinder, c) force generated by absorber

In the following considerations, the limitation on speed of valve opening will be taken into account in a simplified way by imposing condition that valve position can be changed in discrete equally distributed time instants of the process. In this strategy pressure is maintained at the vicinity of the assumed level at the beginning of the active stage of impact. Due to limitations imposed on speed of valve opening, the procedure results in excessive decrease of force generated by the absorber during the final part of the process. Therefore, assumed level of constant force F^{opt} has to be slightly increased in order to ascertain the possibility of dissipation of the whole kinetic energy of the impacting object. Corresponding control law takes the form:

$$\text{For } t_n = n\Delta t: \quad \text{if } F(t) > F^{opt} \text{ then 'open the valve'} \qquad (3.2.86)$$

$$\text{if } F(t) < F^{opt} \text{ then 'close the valve'}$$

The results of application of the above adaptation strategy to single-chamber cylinder are presented in Fig. 3.2.14. In this example valve is changed in 150 time instants during active stage of impact which leads to substantial variations of force at the end of the process.

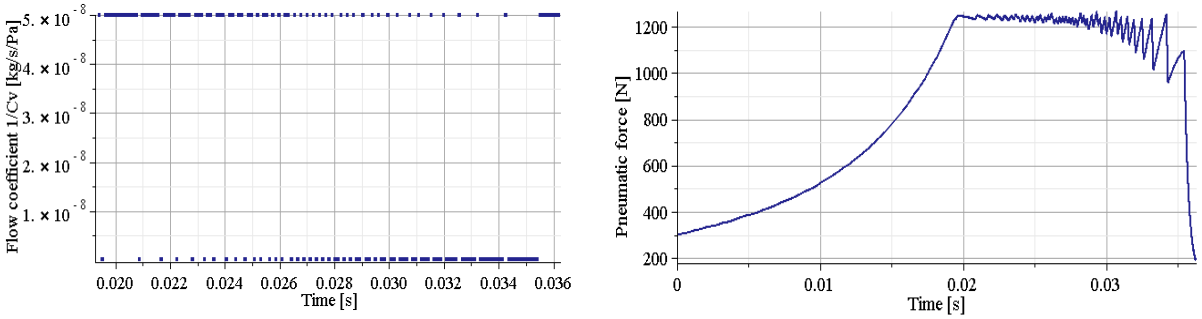

Fig.3.2.14. Alternative on/off adaptation of a single-chamber pneumatic absorber with exhaust to environment: a) valve opening, b) pneumatic force generated by absorber

Both previously described 'on-off' adaptation strategies were applied for double-chamber cylinder with valve located between the chambers. Let us note that in case of both adaptation strategies fluctuations of total force are caused by fluctuations of force generated in compressed chamber. Moreover, in the second adaptation strategy, limitation imposed on speed of valve opening results in double-sided fluctuations of pneumatic force generated by the absorber at the end of the process, Fig. 3.2.15.

Both presented in this section adaptation strategies can be easily considered in conjunction with constraints imposed on maximal valve opening.

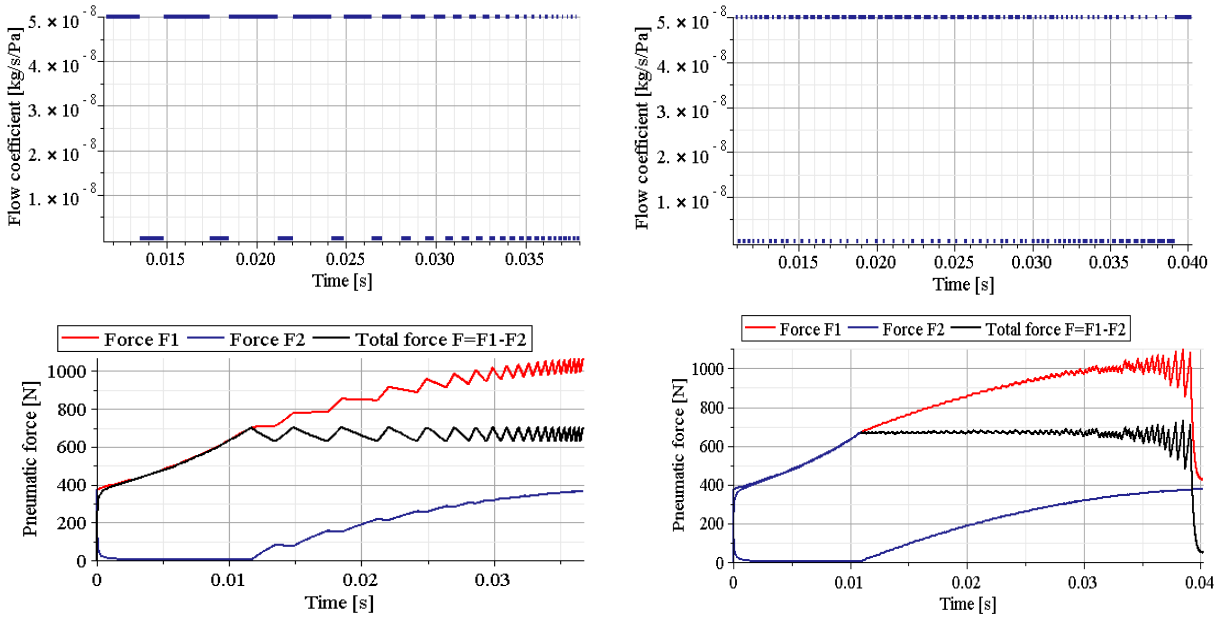

Fig.3.2.15. Two methods of 'on/off' adaptation of a double chamber pneumatic absorber with valve between the chambers: a) valve opening, b) generated pneumatic force

Active adaptation with proportional valve control

In 'proportional control', valve opening is adjusted proportionally on finite number of time intervals which may be of equal or various durations. 'Proportional control' methods are developed for the case of valve whose opening can be changed limited number of times during the process. Proposed control algorithms are based on the following techniques:

1. calculation of resistance coefficient according to precise analytical formula,
2. approximation of analytical value of resistance coefficient,
3. numerical computation of resistance coefficient,
4. analytical calculation of optimal flow resistance coefficient and determination of optimal length of time interval of single valve opening,
5. numerical computation of optimal flow resistance coefficient and optimal length of time interval of single valve opening.

Ad. 1. Precise analytical formula defining flow resistance coefficient on each time interval is based on general formula applied in case of continuous control (cf. e.g. Eq. 3.2.60 and 3.2.80 for single- and double- chamber absorbers, respectively). The method assumes that active stage of impact is divided into several time intervals of equal duration and flow resistance coefficient is computed at the beginning of each of them. Consequently, the method provides that exactly constant value of pneumatic force is maintained only at the beginning of considered time interval.

In case of single-chamber pneumatic cylinder, where optimal valve opening gradually decreases during active stage of impact, application of constant resistance coefficient calculated at the beginning of each time interval results in slight decrease of pneumatic force during the subsequent control steps. Therefore, the formula defining flow resistance coefficient has to be complemented with the correction coefficient k of value greater than the one, which depends on number of considered time intervals. Definition of optimal value of

each flow resistance coefficient for isothermal conditions takes the form (cf. Eq. 3.2.60):

$$C_V^{(i)} = k\frac{(p_{(i)} - p_A)RT_0}{Av_{(i)}p_{(i)}} \tag{3.2.87}$$

where index $'i'$ indicates time instant at the beginning of the considered time interval.

The corresponding formula for double- chamber pneumatic absorber with equal area of the piston in both chambers reads (cf. Eq. 3.2.80):

$$C_V^{(i)} = -k\frac{VRT_0}{\dot{V}_{2(i)}\left[\left(\frac{p_0}{\Delta p_{(i)}}+1\right)V - 2V_{2(i)}\right]} \tag{3.2.88}$$

Considering that optimal flow resistance coefficient achieves its minimal value in the middle of the active stage of impact, application of flow resistance coefficient calculated at the beginning of each interval causes increase of pneumatic force during subsequent steps at the first part of the active stage of impact and decrease of pneumatic force during subsequent steps at second part of active stage of impact. Consequently, the best results can be obtained by changing correction coefficient in the middle of active stage of impact. The results of adaptation performed for single- and double- chamber cylinder, nine time intervals and constant value of correction coefficient are presented in Fig. 3.2.16 (only the second stage of impact, where force is intended to be maintained constant is presented).

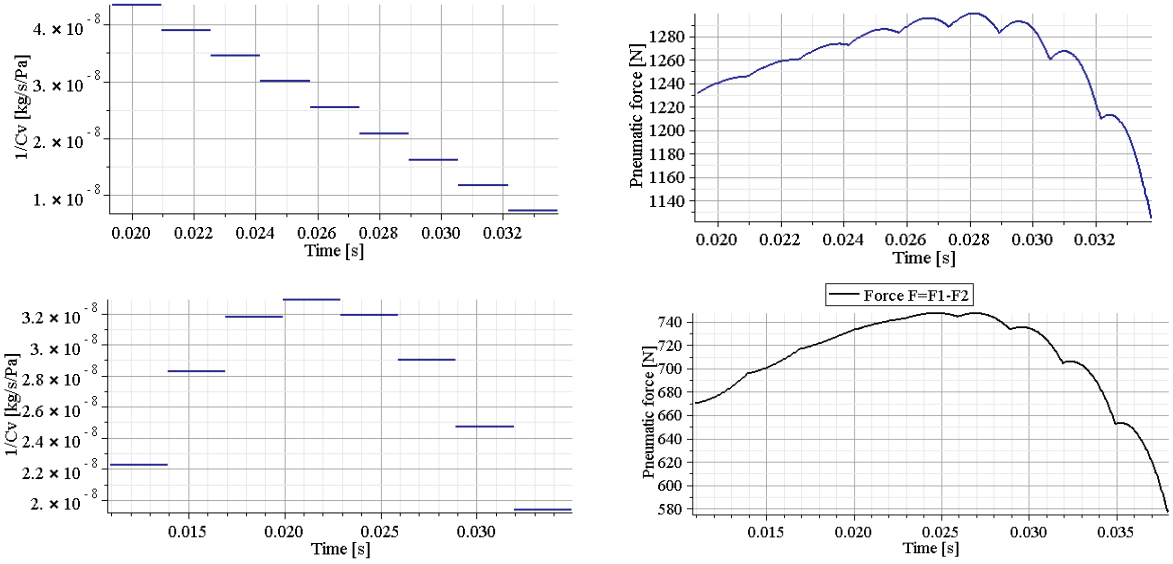

Fig.3.2.16. Proportional control with the use of precise analytical value of flow resistance coefficient (active stage of impact only): a) single-chamber cylinder k=1,12; b) double- chamber cylinder k=1,05

Ad. 2. Approximated method of determination of analytical value of resistance coefficient is based on the following assumptions: i) at the end of considered time interval pneumatic force (in case of single- chamber absorber also internal pressure) achieves optimal value and ii) during considered time interval piston velocity decreases linearly in time and corresponding piston deceleration remains constant. Under such assumptions mass of the gas at the beginning and at the end of considered time can be expressed as:

$$m_{(i)} = \frac{p_{(i)}(h_0 - u_{(i)})}{RT_0}, \quad m_{(i+1)} = \frac{p_{opt}(h_0 - u_{(i)} - v_{(i)}\Delta t - \frac{1}{2}a_{(i)}(\Delta t)^2)}{RT_0} \tag{3.2.89}$$

The above quantities allows to determine approximate formula defining mass flow rate of the fluid during considered time interval and approximate formula defining optimal flow resistance coefficient which reads:

$$C_V^{(i)} = \frac{(p_{(i)} - p_A)RT_0\Delta t}{p_{(i)}(h_0 - u_{(i)})A - p_{opt}(h_0 - u_{(i)} - v_{(i)}\Delta t - \frac{1}{2}a_{(i)}(\Delta t)^2)A} \tag{3.2.90}$$

Implementation of the above control strategy to single-chamber absorber (Fig. 3.2.17a) results in smaller oscillations of force generated by absorber than in case of strategy based on precise value of flow resistance coefficient (Fig. 3.2.16a).

Ad. 3. Alternatively, the resistance coefficient of the valve can be determined numerically for each time interval. Three strategies that can be distinguished within this method are the following:

- computation of valve opening which gives desired minimal (final) value of force generated by the absorber at each time interval (lower tolerance method),
- computation of valve opening which gives desired maximal value of force generated by the absorber (upper tolerance method),
- computation of valve opening for which maximal and minimal value of pneumatic force are equally distant from the desired value.

The method results in similar level of oscillations of pneumatic force as previous method based on approximate value of flow resistance coefficient (Fig. 3.2.17b). The strong advantage of the method is that it provides control on direction of force oscillations and maximal value of oscillations in one direction.

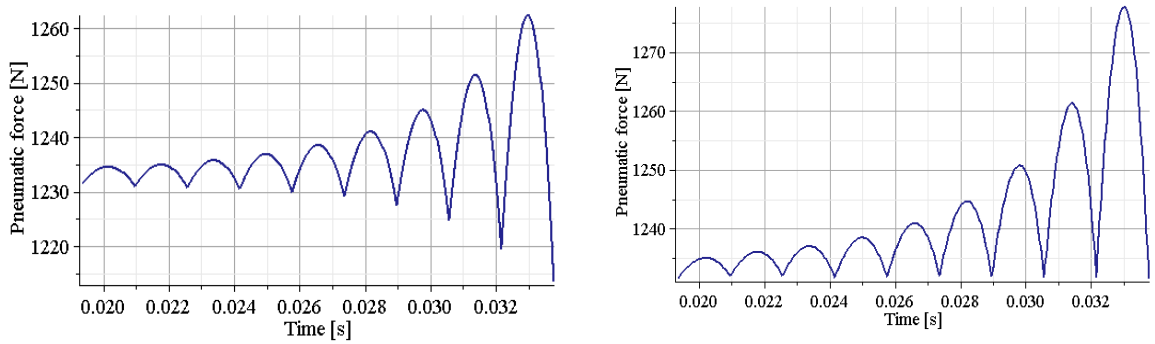

Fig.3.2.17. Proportional control with the use of: a) approximate value of flow resistance coefficient, b) numerically determined value of flow resistance coefficient (lower tolerance method)

Ad. 4. Two previous methods result in large fluctuations of pneumatic force generated by the absorber at the end of the process. This disadvantage can be overcome by a proper choice of length of time interval at which valve opening is adjusted. The approach is based on the following steps:

- value of resistance coefficient at the beginning of each step is assumed to be equal to precise analytical value with appropriate correction coefficient, cf. Eq. 3.2.87,

- each control interval is accomplished when pneumatic force drops below the level of assumed lower tolerance.

The method results in decrease of length of the time interval of single valve opening as the process proceeds. High oscillations of pneumatic force are mitigated but at the cost of larger number of applied time intervals, cf. Fig. 3.2.18. The oscillations of pneumatic force can be further arbitrarily decreased by reducing correction coefficient and consequently by reducing the lengths of all time intervals of constant valve opening. Let us note that the method allows for setting only the lower tolerance of the pneumatic force, not the upper one.

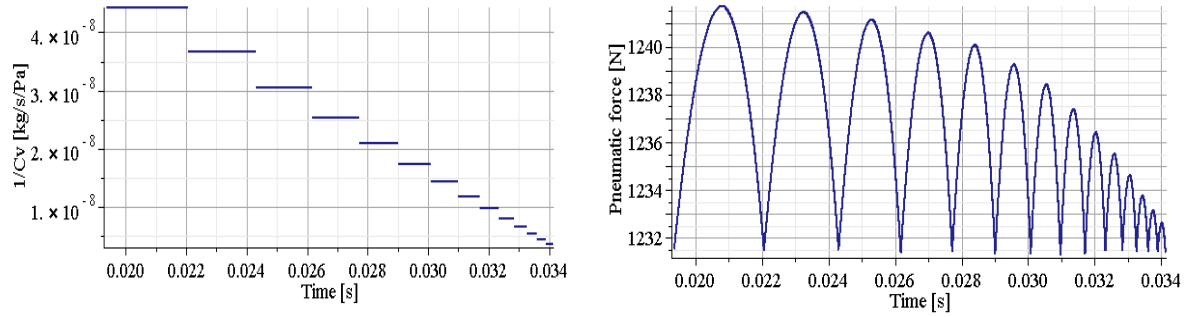

Fig.3.2.18. Proportional control with analytical determination of resistance coefficient and adjustment of the length of time interval: a) assumed resistance coefficient, b) resulting pneumatic force

Ad. 5. The last of the proposed methods of proportional control combines the method of numerical determination of flow resistance coefficient and adjustment of length of time interval of constant valve opening. The method allows for setting both upper and lower tolerance and therefore, can be classified as double-sided tolerance method. The control strategy is based on the following steps:

- numerical computation of the flow resistance coefficient for which upper tolerance of the pneumatic force is reached,
- termination of the control interval at time instant when pneumatic force reaches lower tolerance level.

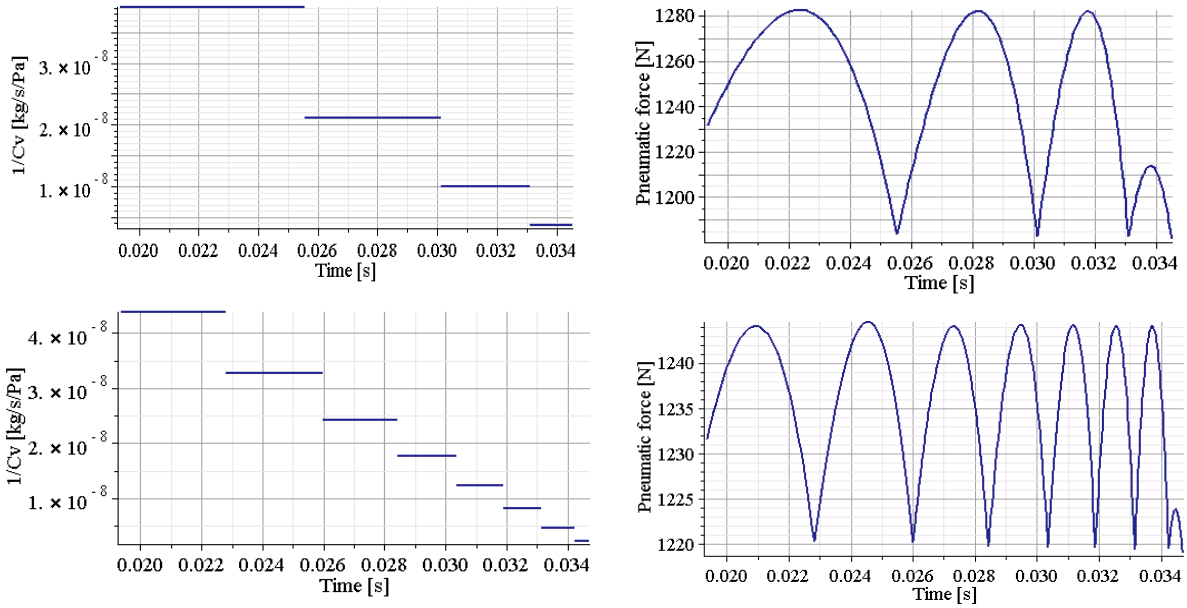

Fig.3.2.19. Proportional control with numerical computation of resistance coefficient and adjustment of the length of time interval : a) assumed flow resistance coefficient, b) resulting pneumatic force

Active adaptation with discrete valve control

The strategy of discrete control of valve opening assumes finite number of positions of the valve head (and corresponding flow resistance coefficients) allowed during the process. In the simplest case, the sequence and duration of particular valve openings are the unknowns in the corresponding optimisation problem. In a more complicated case, size of the valve openings are also subjected to optimisation. The following types of control problems will be considered:

1. only one positions of valve opening is allowed, i.e. the valve may be opened only once during the process and its position has to remain fixed,
2. two positions of the valve opening defined on two time intervals can be applied,
3. finally three positions of valve opening defined on three time intervals are used.

In case when the flow coefficient is also adjusted, the problem of discrete adaptation can be classified as located between semi-active adaptation and active adaptation with proportional control in terms of number of time intervals defined.

Ad. 1. If only one position of valve opening is allowed (the valve is closed and partially/fully open) adaptation strategy is based on the resemblance to semi-active adaptation strategy and contains initial step aimed at increase of pneumatic force followed by step with constant valve opening. When valve opening is arbitrarily assumed (C_V^*), simple corresponding optimization problem relies on finding time instant of valve opening:

$$\text{Find } t_x^1 \text{ such that } \quad J_2 = \max_t \left|\ddot{u}(t)\right| \text{ is minimal} \tag{3.2.91}$$

The above problem will be analyzed for single-chamber absorber working under isothermal conditions and with initial pressure lower than the optimal one (cf. Eq. $3.2.35_1$). The strategy of finding optimal time of valve opening (or equivalently pressure at which the valve is opened) depends on relation of imposed value of flow resistance coefficient C_V^* to optimal value of resistance coefficient C_V^{OPT} (cf. Eq. 3.2.28), which indicates valve opening for which the whole stroke of the cylinder is utilized. Let us note that the value of optimal flow resistance coefficient can be calculated not only for the initial parameters of the system but also for the actual ones:

$$C_V^{OPT}(t) = \frac{MV(t)RT_0}{p(t)\left[h_0 - u(t)\right]A^2} = \frac{MV(t)RT_0}{p_0 h_0 A^2} \tag{3.2.92}$$

and it is decreasing during the first stage of the process when the valve remains closed. Two cases can be distinguished basing on relation of the imposed value of resistance coefficient to the optimal one:

- $C_V^* \geq C_V^{OPT}(0)$ which indicates that piston will not reach the bottom of the cylinder independently of assumed time of valve opening,
- $C_V^* < C_V^{OPT}(0)$, which indicates that opening of the valve at the beginning of the process will result in collision of the piston with the bottom cylinder wall.

In the first case there are no indications for additional confinement of the time domain in which optimal time of valve opening t_x^1 is searched. However, in the second cases the valve should remain closed until actual optimal value of resistance coefficient $C_V^{OPT}(t)$ drops to the

value of imposed resistance coefficient C_V^*, which allows to avoid collision of the piston against cylinder bottom. The optimal time of valve opening should fulfil the following conditions:

$$\text{if } C_V^* \geq C_V^{OPT}(0) \text{ then } t_x^1 > 0 \tag{3.2.93}$$

$$\text{if } C_V^* < C_V^{OPT}(0) \text{ then } t_x^1 > \tilde{t} \text{ such that } C_V^* = C_V^{OPT}(\tilde{t})$$

In none of the above cases optimal time of valve opening equals the time at the beginning of the allowable range defined by Eq. 3.2.93 (for which the largest part of the cylinder stroke is used) as it could be expected. Optimal pressure of valve opening can not be found analytically, but it can be easily determined numerically by using one-dimensional optimization algorithm.

In case when value of the flow resistance coefficient is not arbitrarily imposed and its adjustment is the goal of adaptation, the corresponding optimization problem reads:

$$\text{Find } t_x^1, C_V^{\,1} \text{ such that } J_2 = \max_t \left|\ddot{u}(t)\right| \text{ is minimal} \tag{3.2.94}$$

Although the problem (3.2.94) is, in general, more complicated than the problem (3.2.91) it has fully analytical solution for the case of single-chamber cylinder working under isothermal conditions. At first, optimal flow resistance coefficient has to provide utilization of the whole cylinder stroke and it is defined by Eq. 3.2.92. Moreover, it was found that value of pressure at which the valve is opened is exactly the same as in case of continuous control strategy and it can be determined from the simple two-stage energy balance (3.2.41) or from the kinematic condition (3.2.46). For the considered isothermal system, pressure and piston displacements at which the valve has to be opened are equal:

$$p_x = p_0 \exp\left(\frac{MV_0^{\,2} - 2A(p_0 - p_A)h_0}{2Ap_0h_0}\right); \qquad u_x = h_0\left(1 - \frac{p_0}{p_x}\right) \tag{3.2.95}$$

The velocity of the piston at time instant of valve opening which can be determined from the energy balance of the first stage of impact allows to find analytical formula for optimal flow resistance coefficient according to Eq. 3.2.46 and Eq. 3.2.92:

$$C_V^{\,OPT} = \frac{M^{1/2}\left[2A(p_x - p_A)(h_0 - u_x)\right]^{1/2} RT_0}{p_0 h_0 A^2} \tag{3.2.96}$$

Ad. 2. More advanced case of discrete control assumes two time intervals in active stage of impact and two values of the flow resistance coefficients $\left(C_V^{1*}, C_V^{2*}\right)$. The sequence of valve opening should mimic the optimal opening of the valve in continuous adaptation strategy and therefore larger valve opening should be applied first. The corresponding optimisation problem relies on finding two time instants when position of the valve changes:

$$\text{Find } t_x^1, t_x^2 \text{ such that } J_2 = \max_t \left|\ddot{u}(t)\right| \text{ is minimal} \tag{3.2.97}$$

The possibility of using two openings of the valve during active stage of impact allows to make an attempt to maintain approximately constant level of pneumatic force (with two concave intervals). Therefore, the indications for optimal choice of time instants at which valve position changes are the following:

- pressure p_x^1 (related to time t_x^1) should be relatively close to optimal pressure level for active adaptation defined by Eq.(3.2.95$_1$)
- time t_x^2 should fulfil condition $C_V^{2^*} > C_V{}^{OPT}(t_x^2)$ to avoid collision of the piston against bottom of the cylinder.

Finally, both time instants can be found numerically by means of one of the classical optimisation algorithms with initial conditions and bounds on optimisation variables defined above. Typically, the optimisation results in similar level of pneumatic force at both time intervals. The exact equalisation of both peaks of force is not always possible depending on assumed values of flow coefficients, Fig. 3.2.20b.

In case when flow resistance coefficients are also subjected to optimisation the optimisation problem takes the form:

$$\text{Find } t_x^1, C_V{}^1, t_x^2, C_V{}^2 \text{ such that } J_2 = \max_t \left|\ddot{u}(t)\right| \text{ is minimal} \tag{3.2.98}$$

and four parameters of the system have to be optimized. Similarly, as in previously considered case, pressure $p_x{}^1$ should be relatively close to optimal pressure level defined by Eq. 3.2.95$_1$. Moreover, the optimization problem can be significantly simplified due to following facts:

- flow resistance coefficient $C_V{}^1$ should generate slight initial increase of the pneumatic force (beginning of the first concave interval of the pneumatic force) which is obtained for resistance coefficient insignificantly larger than the one for the active system,
- similarly as in problem defined by Eq.3.2.94, the time of valve opening t_x^2 can be determined from the kinematic condition (Eq. 3.2.46),
- the second flow resistance coefficient $C_V{}^2$ should provide utilization of the whole cylinder stroke and therefore, it should be determined from Eq. 3.2.92.

Finally, the optimization has to be performed over only two well-defined and strictly bounded variables t_x^1 and $C_V{}^1$. In the conducted numerical example, results obtained by classical optimisation methods were compared against the results obtained from systematic search of the feasible domain in order to exclude the possibility of finding local minimum. The results of adaptation with predefined and optimized values of resistance coefficients are presented in Fig. 3.2.20.

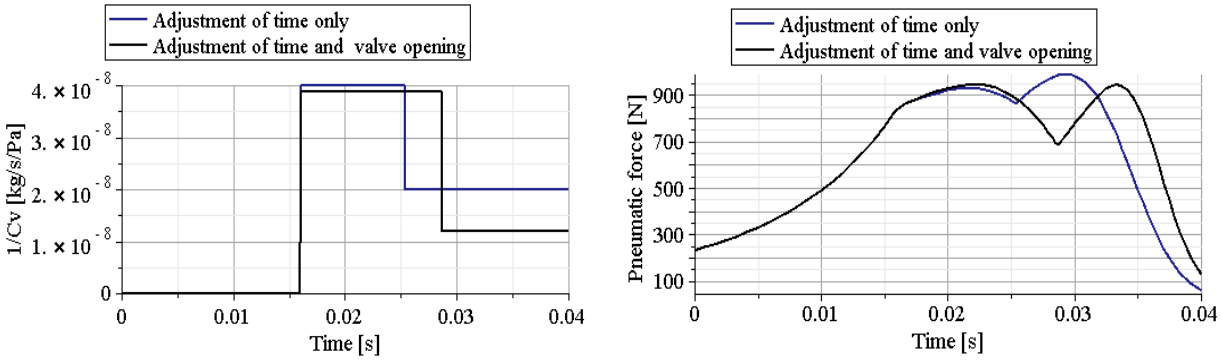

Fig.3.2.20. Two-stage discrete control of single-chamber pneumatic cylinder: a) applied change of valve opening , b) obtained change of pneumatic force

Ad. 3. Finally, when three values of valve opening are considered, the optimization problem can be defined either in the classical form where piston acceleration is minimized:

$$\text{Find } t_x^1, t_x^2, t_x^3 \text{ such that } J_2 = \max_t |\ddot{u}(t)| \text{ is minimal} \tag{3.2.99a}$$

or as minimization of time integral of difference of currently obtained mass acceleration $a(t)$ and optimal acceleration $a^{opt}(t)$ calculated over assumed time interval:

$$\text{Find } t_x^1, t_x^2, t_x^3 \text{ such that } J_2 = \int_0^{t^{end}} \left[a(t) - a^{opt}(t)\right]^2 dt \text{ is minimal} \tag{3.2.99b}$$

In the simplified approach, the time of the first valve opening should be assumed as equal to corresponding time in continuously controlled system which reduces the optimization problem into two variables. Both approaches lead to similar results which are compared in Fig. 3.2.21.

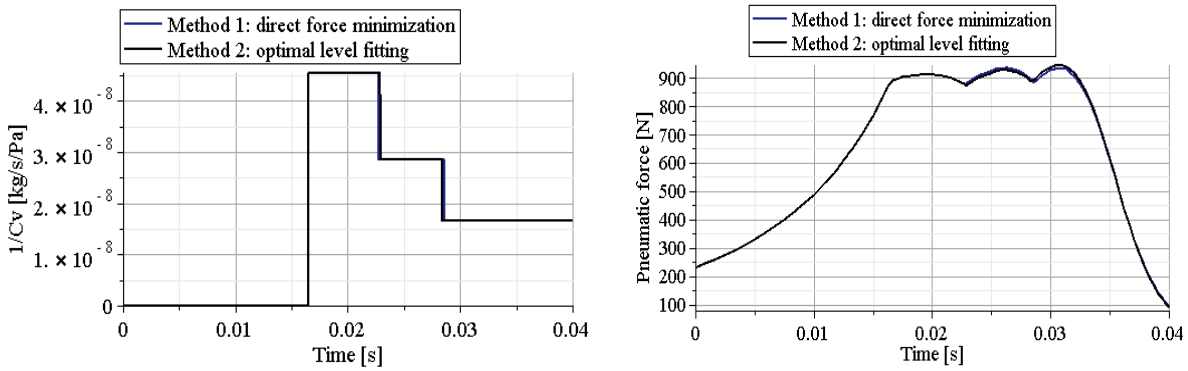

Fig.3.2.21. Three-stage discrete control of single chamber pneumatic cylinder: a) change of valve opening , b) obtained change of pneumatic force

In case when values of flow resistance coefficients constitute additional optimization variables, the classical method of solution of the optimization problem:

$$\text{Find } t_x^1, C_V^{\,1}, t_x^2, C_V^{\,2}, t_x^3, C_V^{\,3} \text{ such that } J_2 = \max_t |\ddot{u}(t)| \text{ is minimal} \tag{3.2.100}$$

can be replaced with step-by-step procedure based on, introduced in previous section, algorithm of 'proportional control' involving adjustment of resistance coefficient and adjustment of length of time interval of constant valve opening. The proposed procedure involves the following steps:

- assumption of upper and lower level of tolerance of the pneumatic force,
- numerical determination of flow resistance coefficient for which upper tolerance of the pneumatic force is reached,
- termination of the control interval at time instant when pneumatic force reaches lower tolerance level,
- adjustment of the tolerance level in order to obtain exactly three time periods of a constant valve opening (cf. also Fig.3.2.19).

Classification of all presented in this section methods of adaptation aimed at minimisation of force generated by the absorber (and impacting object deceleration) is shown in Fig. 3.2.22.

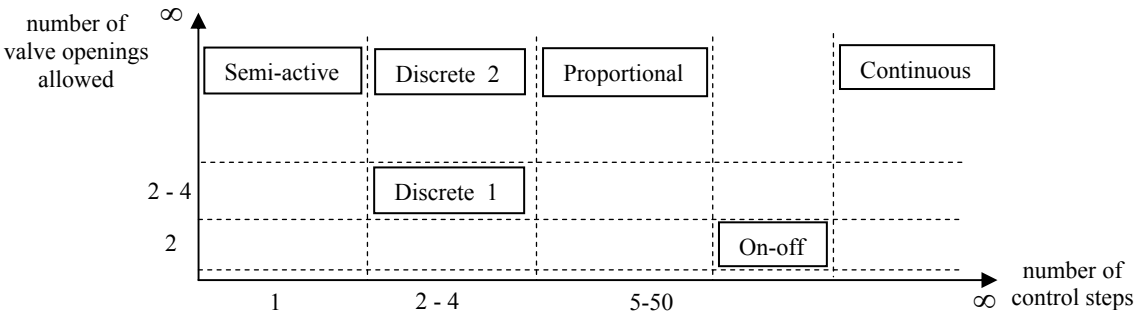

Fig. 3.2.22. Classification of methods of adaptation aimed at minimisation of decelerations.

3.2.3. Maximisation of energy dissipation

Another objective of adaptation strategy is to provide maximal dissipation of mechanical energy of the hitting object during impact. This objective is equivalent to minimisation of mechanical energy of the hitting object at the end of the process and to minimization of hitting object rebound.

Dissipation of mechanical energy was defined in Section 3.1.1 as a difference between work done on pneumatic system during the process L_{Fp} and actual exergy of the system X, cf. Eq. 3.1.34. Let us calculate dissipation of the mechanical energy which occurs between initial state and the subsequent 'referential state' where mechanical energy of the impacting object achieves maximal value and $X = 0$:

$$D_1(t_{end}) = L_{Fp}(t_{end}) - X(t_{end}) = L_{Fp}(t_{end}) = \int_{u_0}^{u_{\max}} F_{p_1}(t)du - \int_{u_{eq}}^{u_{\max}} F_{p_2}(t)du \tag{3.2.101}$$

In above formula the first integral indicates work done on absorber during forward-stroke $\langle u_0, u_{\max} \rangle$ when the force $F_1(t)$ is generated and the second integral indicates work done during backstroke $\langle u_{\max}, u_{eq} \rangle$ when the force $F_2(t)$ is generated. In a standard process both integrals are positive. Time t_{end} corresponding to the 'referential state' of the system has to be defined separately for horizontal and vertical position of the absorber.

In case of system located horizontally the only component of the mechanical energy is kinetic energy. During rebound stage of impact mechanical energy of the hitting object is increasing as long as the object is subjected to action of the contact force. Maximal value of kinetic energy is achieved when hitting object is separated from the piston and contact force between hitting object and the piston vanishes, $F_C = 0$. Separation of piston and hitting object may occur in two situations:

- when the piston reaches end of the cylinder and it is stopped by the mechanical delimiter,
- in the middle of the rebound stage when return movement of the piston is stopped by negative pneumatic force.

The condition corresponding to the first case expressed in terms of piston velocity and force generated by the absorber reads:

$$t_{end} = t \in \langle t^1_{stop}, \infty) \text{ such that } \dot{u}_2(t) \le 0 \text{ and } F_P - F_D^{TOP} + F_{Fr} = 0 \tag{3.2.102a}$$

where t^1_{stop} indicates time instant when impacting object is stopped for the first time. However, in case of stiff and short delimiting spring it can be simplified to the form:

$$t_{end} = t \in \left\langle t^1_{stop}, \infty \right) \text{ such that } u_2(t) = h_0 \tag{3.2.102b}$$

Similarly, the condition related to the second case can be defined as:

$$t_{end} = t \in \left\langle t^1_{stop}, \infty \right) \text{ such that } \dot{u}_2(t) \le 0 \text{ and } F_P + F_{Fr} = 0 \tag{3.2.102c}$$

The above conditions define state of the system at which exergy of the system equals zero, i.e. pneumatic absorber is in equilibrium with the environment and cannot perform any work on impacting object. At time instant t_{end} rebound velocity of the hitting object achieves maximal value and further remains constant. Therefore, energy dissipation D_1 can be clearly interpreted as difference between the initial and final kinetic energy of the hitting object.

In case of <u>vertical absorber</u> located in a gravitational field, an additional component of mechanical energy is the potential energy. During rebound stage of impact the kinetic energy of the hitting object achieves its maximum when external forces acting on the hitting object (in this case contact force and gravity force) are in equilibrium. In turn, mechanical energy of the hitting object achieves its maximum in two situations:

- when hitting object is separated from the piston (at the external end of cylinder or in the middle of its stroke) and contact force is reduced to zero,
- when hitting object is moving together with the piston and they reach their highest position in the middle of the cylinder stroke without separating from each other.

In the first case the corresponding conditions are formulated in similar manner as previously, however they are complemented with gravitational force acting on the piston:

$$t_{end} = t \in \left\langle t^1_{stop}, \infty \right) \text{ such that } \dot{u}(t) \le 0 \text{ and } -M_2 g - F_P - F_D{}^{TOP} + F_{Fr} = 0 \tag{3.2.103a}$$

and

$$t_{end} = t \in \left\langle t^1_{stop}, \infty \right) \text{ such that } \dot{u}(t) \le 0 \text{ and } -M_2 g - F_P + F_{Fr} = 0 \tag{3.2.103b}$$

In turn, in the second case definition of the corresponding time t_{end} reads:

$$t_{end} = t \in \left\langle t^1_{stop}, \infty \right) \text{ such that } \dot{u}_1(t) = 0 \tag{3.2.103c}$$

The above condition refers to the situation, when during rebound stage of impact the force generated by the absorber is not reduced to zero due to influence of the gravity force acting on the impacting object. When piston reaches highest position the force generated by the absorber fulfils the condition: $0 < F(t) < M_1 g$. Both definitions of time t_{end} provide that for vertical absorber energy dissipation D_1 has clear interpretation as a difference between initial mechanical energy of the hitting object and maximal potential energy during the first rebound.

Finally, the problem of <u>maximal energy dissipation</u> can be formulated as follows:

$$\text{Find } C_V(t), t \in \left\langle 0, t_{end} \right\rangle \text{ such that } D_1 \text{ is maximal} \tag{3.2.104}$$

The problem of maximisation of energy dissipation (3.2.104) can be decomposed into two separate problems related to:

- maximisation of the first integral (change of mechanical energy during forward stroke of the piston)

  Find $C_V(t), t \in \langle 0, t_{end} \rangle$ such that $\int_{u_0}^{u_{\max}} F_1(t)du$ is maximal (3.2.105)

- minimisation of the second integral (recapture of the energy during backstroke)

  Find $C_V(t), t \in \langle 0, t_{end} \rangle$ such that $\int_{u_{end}}^{u_{\max}} F_2(t)du$ is minimal (3.2.106)

In case of horizontal absorber, value of the first integral equals the initial mechanical energy of the impacting object independently of valve opening, resulting pressure inside cylinder chambers and piston displacement. The impacting object is always stopped, either by pneumatic force or delimiting spring. On the contrary, in case of vertical absorber value of the first integral equals:

$$\int_{u_0}^{u_{\max}} F_1(u)du = \tfrac{1}{2} M V_0^2 + Mg\left(u_{\max} - u_0\right) \tag{3.2.107}$$

and it is the largest when hitting object is stopped in the vicinity of the cylinder bottom due to larger change of the potential energy. Therefore maximization of the first integral relies on utilizing the whole available stroke of the cylinder.

The first stage of minimisation of the second integral (related to rebound stage of impact) is the minimisation of the exergy at time instant when hitting object is stopped:

$$X(t_{\max}) = \int_{u_{eq}^*}^{u_{\max}} F_{p_2}(\overline{m}, u, T)du \tag{3.2.108}$$

where $F_{p_2}(\overline{m}, u, T)$ indicates force generated by the absorber during rebound stage of impact in a special case when intended dissipation gas transfer is not conducted ($\overline{m}$ denotes constant mass of gas inside absorber chambers). Exergy of the system depends on volume and pressure of the gas at the end of the forward stroke and it is reduced to zero when the system is in static equilibrium with the environment. Therefore, the objective which has to be fulfilled during forward stroke of the piston is to provide that pneumatic system is possibly close to static equilibrium at time instant when the piston is stopped. When the above objective is successfully fulfilled the whole impact energy is dissipated during the forward stroke of the piston and rebound stage of impact vanishes.

In contrast, in case when obtaining state of static equilibrium at time instant when the piston is stopped is not possible (e.g. due to constraints imposed on valve opening) pressure has to be released further during the rebound stage with maximal allowable opening of the valve. The above procedure is the most effective when volume of gas which has to be released is small, i.e. when piston is stopped at the vicinity of the cylinder bottom. In such a case, small mass flow rate allows for substantial reduction of pressure and for fast approaching the equilibrium state. Finally, the following three indications may be given:

1. valve opening during forward stroke should minimise exergy of the absorber at time instant when the hitting object is stopped,
2. among states of the same exergy the states with high pressure and small volume of the positive chamber are preferable since the corresponding gas exergy can be reduced faster,
3. during backstroke the valve should remain open as long as it reduces value of pneumatic force generated by the absorber.

Most of the adaptation strategies aimed at minimisation of the hitting object deceleration described in previous section (except the ones in which constraints on maximal valve opening are imposed) provide that the hitting object is stopped just before reaching cylinder bottom and thus, the state of zero exergy is obtained. Therefore, they provide dissipation of whole kinetic energy during forward movement of the piston. In this context, minimisation of impacting object deceleration can be considered as equivalent to maximisation of energy dissipation and minimisation of impacting object rebound.

3.2.4. Minimization of internal pressure

Previously considered adaptation procedures were aimed at protection of the impacting object by mitigating it acceleration or rebound. On the contrary, the objective of the current control strategy is to protect impacted object by minimisation of internal pressure inside positive chamber of the absorber. Minimisation of pressure reduces internal forces generated inside absorber walls and therefore, protects absorber against global failure and possible bursting.

Previously developed strategies, which were aimed at minimisation of impacting object acceleration, are equivalent to strategies aimed at minimisation of internal pressure when two conditions are fulfilled:

- considered pneumatic absorber contains single-pressure chamber,
- pneumatic force is the only component of force generated by the absorber.

In all other cases independent control strategies has to be elaborated due to influence of force resulting from pressure inside the upper chamber of the absorber and the influence of additional forces generated by the absorber, as for instance friction force. Similarly as in case of acceleration minimisation, adaptation strategies can be divided into semi-active and active with continuous, on/off, proportional and discrete control of valve opening (cf. Sec. 3.2.2). However, only semi-active strategy and active strategy with continuous valve control will be briefly analysed.

In most of the problems of acceleration minimisation mathematical formulation of the optimisation problem did not require explicit condition enforcing dissipation of the impact energy during forward movement of the piston. The cases when piston collides against the cylinder bottom were automatically eliminated as non-optimal due to large value of deceleration caused during direct collision by delimiting spring. By contrast, neglecting condition of energy dissipation in the problem of pressure minimisation would lead to solutions completely disregarding energy dissipation. Therefore, two following approaches can be applied:

- explicit formulation of the condition of dissipation of whole impact energy during forward stroke,
- artificial closing of the valve when piston approaches the vicinity of the cylinder bottom which causes sudden pressure increase and qualifies strategy as non-optimal.

General problem of semi-active adaptation relies on finding initial pressure and constant in time valve opening for which maximal pressure value inside positive chamber is minimal:

$$\text{Find} \quad p_0, C_V \ \text{such that} \ \ J_4 = \max_t p(t) \ \ \text{is minimal} \tag{3.2.109}$$

Initially, the problem was considered for single-chamber absorber with significant influence of velocity-dependant friction force, described by the equations:

$$M\ddot{u} + (p - p_A)A + c\dot{u} = 0\,, \qquad \dot{m}(t) = -(p - p_A)/\,C_V \tag{3.2.110}$$

$$\frac{p(h_0 - u)^{\kappa}}{m^{\kappa}} = \frac{p_0 h_0{}^{\kappa}}{m_0{}^{\kappa}} = C$$

$$\text{IC:} \ \ u(0) = 0\,,\ \dot{u}(0) = V_0\,,\ m(0) = m_0$$

Similarly, as in case of semi-active acceleration minimisation, optimal opening of the valve has to be determined separately for each value of initial pressure and, as it appeared, it provides utilisation of the whole stroke of the absorber. Due to presence of the friction force the optimal value of the flow resistance coefficient can not be found analytically, but it has to be determined by numerical solution of the equation defining maximal piston displacement:

$$u(p_0, C_V) = u_{\max} = h_0 \tag{3.2.111}$$

where $u(t)$ is defined by solution of the system of differential equations (3.2.110). In the second step, optimal initial pressure can be determined by using gradient-based optimisation procedure. Finally, solution of the problem of pressure minimisation results in different value of initial pressure and different value of resistance coefficient than problem of semi-active acceleration minimisation, see Fig. 3.2.23.

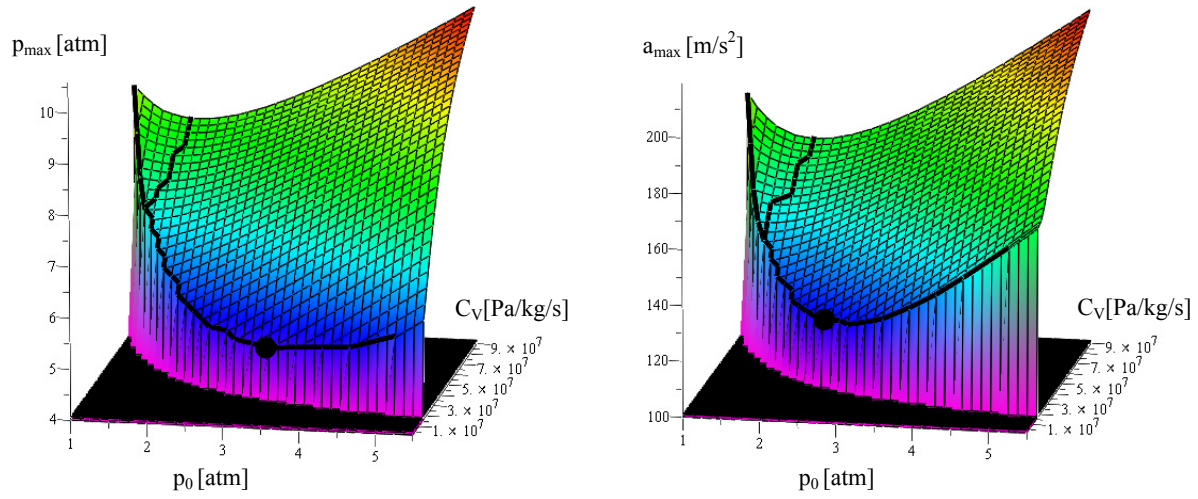

Fig.3.2.23. Comparison of semi-active adaptation of single chamber absorber with influence of friction force aimed at minimization of internal pressure and hitting object acceleration (minimum obtained for 3.37atm and 2.6atm)

Similar situation occurs in case of semi-active adaptation of double chamber cylinder with valve located between the chambers, described by system of Eq. 3.2.36. In case when initial volume of the upper chamber tends to zero and friction force does not occur, optimal value of the flow resistance coefficient can be calculated analytically (cf. Eq.3.2.33$_2$). Optimal value of pressure has to be found numerically and it is usually lower than optimal pressure being solution of the problem of acceleration minimization.

The strategy of active adaptation assumes the initial stage of pressure increase and the second stage when pressure in positive chamber remains constant. Development of the strategy is similar as in case of acceleration minimisation and it is composed of two steps: i) calculation of minimal level of pressure in compressed chamber which maintained constant allows to stop the piston just before cylinder bottom, ii) finding valve opening which allows to realize the strategy of maintaining constant pressure.

In case of single-chamber pneumatic absorber with significant contribution of the friction force, the equations governing two stages of the impact process read:

$$M\ddot{u}+\left(\frac{p_0 h_0{}^{\kappa}}{(h_0-u)^{\kappa}}-p_A\right)A+c\dot{u}=0 \quad \text{for} \quad u(t)\in(0,u_x) \tag{3.2.112}$$

$$M\ddot{u}+\left(\frac{p_0 h_0{}^{\kappa}}{(h_0-u_x)^{\kappa}}-p_A\right)A+c\dot{u}=0 \quad \text{for} \quad u(t)\in(u_x,h_0\rangle$$

where the quantity u_x indicates piston displacement at time instant dividing two stages of the process. The equation governing the second stage has an analytical solution:

$$u_{II}=u_x+\frac{1}{c^2}\left[-Me^{-\frac{ct}{M}}\left(v_x c-A(p_x-p_A)\right)-Ac(p_x-p_A)t+Mv_x c+MA(p_x-p_A)\right] \tag{3.2.113}$$

$$v_{II}=\frac{du_{II}}{dt}=\frac{1}{c}\left[e^{-\frac{ct}{M}}\left(v_x c+A(p_x-p_A)\right)-A(p_x-p_A)\right]$$

which obviously depends on state of the system at the end of the first stage of the process, i.e. at time instant when the valve is opened: pressure of gas p_x and piston velocity v_x. The above equations can be used to determine time instant when velocity of the hitting object drops to zero t_{end} and to calculate final displacement of the hitting object u_{end}:

$$t_{end}=-\frac{M}{c}\ln\left(\frac{A(p_x-p_A)}{V_0 c+A(p_x-p_A)}\right) \tag{3.2.114}$$

$$u_{end}=u_x+\frac{M}{c^2}\left[-A(p_x-p_A)\left[1+\ln\left(\frac{A(p_x-p_A)}{v_x c+A(p_x-p_A)}\right)\right]+v_x c+A(p_x-p_A)\right]$$

Due to the fact that minimal level of pressure is obtained in case when the whole stroke of the cylinder is utilized, optimal parameters can be identified on the basis of the simple condition $u_{end}=h_0$, which has to be systematically checked during solution of the differential equations governing the first stage of the process. In case of zero friction force (when minimisation of pressure is equivalent to minimisation of acceleration) this condition simplifies to Eq. 3.2.42.

Maintaining constant level of pressure requires changing of the flow resistance coefficient according to the following control law:

$$C_V(t) \to \infty \quad \text{for} \quad t < t_x \tag{3.2.115}$$

$$C_V(v) = \frac{(p_x - p_A)(h_0 - u_x)RT_0}{v^{II}(t)\, p_0 h_0 A} \quad \text{for} \quad t \geq t_x$$

which was derived in Sec.3.2.2. The strategy results in maintaining constant level of pressure and simultaneous decrease of hitting object acceleration due to gradual decrease of the friction force.

Let us further consider double-chamber absorber with exhaust of gas from the lower chamber to environment and with no friction force. Optimally controlled absorber is described by the following equations corresponding to two subsequent stages of the process:

$$M\frac{d^2u(t)}{dt^2} + \frac{p_{20}h_{20}{}^{\kappa}}{(h_{20} - u(t))^{\kappa}}A_2 - \frac{p_{10}h_{10}{}^{\kappa}}{(h_{10} + u(t))^{\kappa}}A_1 = 0 \quad \text{for} \quad u(t) \in (0, u_x) \tag{3.2.116}$$

$$M\frac{d^2u(t)}{dt^2} + \frac{p_{20}h_{20}{}^{\kappa}}{(h_{20} - u_x)^{\kappa}}A_2 - \frac{p_{10}h_{10}{}^{\kappa}}{(h_{10} + u(t))^{\kappa}}A_1 = 0 \quad \text{for} \quad u(t) \in (u_x, h_0\rangle$$

The second term in the second equation remains constant as a result of controllable gas exhaust. The above equations can be integrated analytically in order to obtain parameters of the system at optimal time instant of valve opening. Due to the fact that constant pressure is maintained constant and pressure is released to environment optimal change of the resistance coefficient is described by exactly the same equation as in case of single chamber system (Eq. 3.2.115). Since the influence of pressure inside the upper (decompressed) chamber on total force generated by the absorber is relatively small, the minimization of pressure is, in this case, almost equivalent to minimisation of total force generated by the absorber, Fig. 3.2.24 (upper plots).

In case of different design of the absorber where the valve is located between the chambers the equations governing optimally adapted system contain an additional differential equation which governs balance of internal energy of gas enclosed in upper chamber of the absorber (change of internal pressure inside upper chamber due to simultaneous increase of chamber volume and inflow of the gas from the lower chamber). The system of equations governing change of pressure within both chambers reads:

$$V_1 = A_1(h_{10} + u^{II}), \qquad V_2 = A_2(h_{20} - u^{II}) \tag{3.2.116}$$

$$m_2 = \left(\frac{p_2}{p_{2x}}\right)^{1/\kappa}\left(\frac{V_2}{V_{2x}}\right)m_{20} = \frac{V_2}{V_{2x}}m_{20}$$

$$\frac{\dot{p}_1}{p_1} = -\kappa\frac{\dot{m}_2}{p_1V_1}\frac{p_{2x}V_2}{m_2} - \kappa\frac{\dot{V}_1}{V_1}$$

$$\text{IC:}\ \ u(t_x) = u_x,\ \dot{u}(t_x) = V_x,\ p_1(t_x) = p_{1x},\ p_2(t_x) = p_{2x}$$

and the quantities with the (second) index 'x' corresponds to time instant of valve opening.

The third equation can be transformed into the form:

$$\frac{\dot{p}_1}{p_1} = \frac{\kappa p_{2x}\dot{V}_1}{V_1 p_1} - \kappa\frac{\dot{V}_1}{V_1} \quad \text{or} \quad \frac{1}{p_1}\frac{dp_1}{dV_1} = \frac{\kappa p_{2x}}{V_1 p_1} - \frac{\kappa}{V_1} \tag{3.2.117}$$

which can be solved analytically to obtain:

$$p_1 = p_{2x} + CV_1^{-k}, \qquad C = \frac{p_{1x} - p_{2x}}{V_{1x}^{-k}} \tag{3.2.118}$$

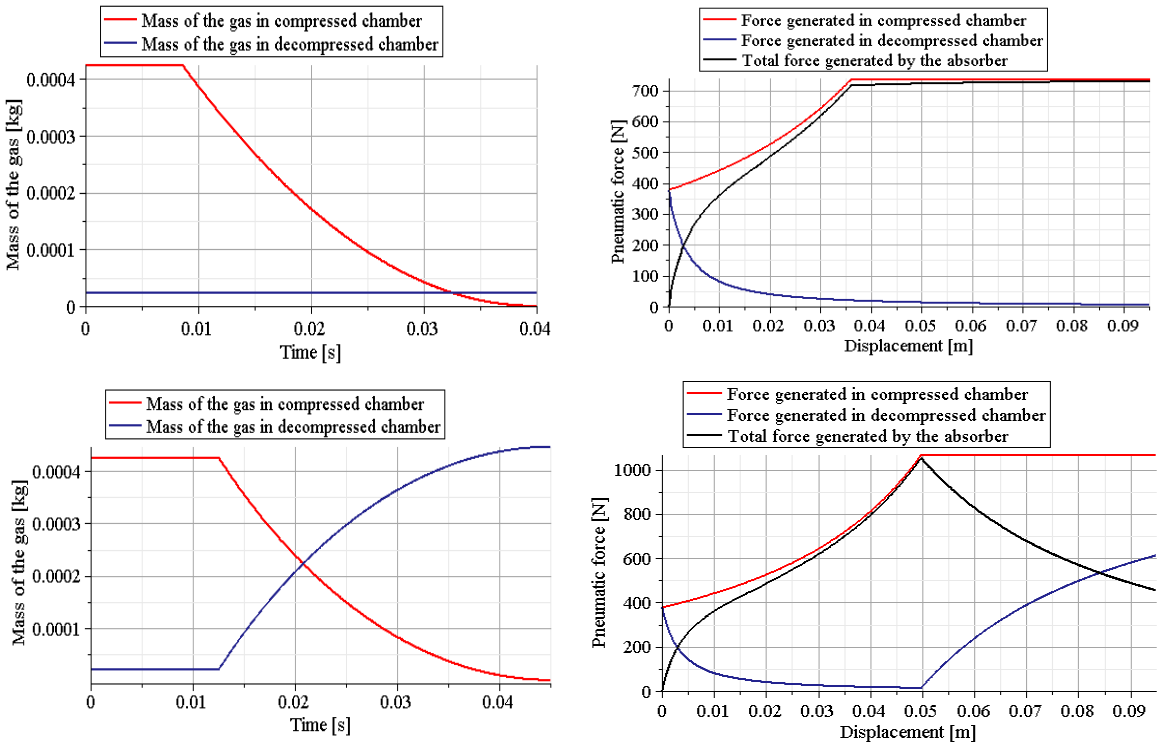

Fig.3.2.24. Minimization of pressure in double chamber cylinder with exhaust to environment (upper plots) and with valve between the chambers (lower plots): a) mass of the gas in both chambers, b) resulting change of force

Therefore, in contrast to analogous system which is aimed at maintaining constant pneumatic force, pressures in both chambers and pneumatic force generated by the absorber can be expressed in terms of piston displacement. As a result, the system of equations governing kinematics of the system in two stages of the process can be written in the form:

$$M\frac{d^2u(t)}{dt^2} + \frac{p_{20}h_{20}^{\ \kappa}}{(h_{20}-u(t))^{\kappa}}A_2 - \frac{p_{10}h_{10}^{\ \kappa}}{(h_{10}+u(t))^{\kappa}}A_1 = 0 \quad \text{for} \quad u(t)\in(0,u_x) \tag{3.2.119}$$

$$M\frac{d^2u(t)}{dt^2} + \frac{p_{20}h_{20}^{\ \kappa}}{(h_{20}-u_x)^{\kappa}}A_2 - \left[p_{2x} + (p_{1x}-p_{2x})\left(\frac{A_1(h_{10}+u(t))}{V_{1x}}\right)^{-k}\right]A_1 = 0$$

$$\text{for} \quad u(t)\in(u_x, h_{20}\rangle$$

which can be integrated over displacement in the range $(0, h_{20}\rangle$ and compared with identified impact energy in order to find the displacement u_x indicating time instant of valve opening.

The control law for the second stage of the process is given in the form of analytical formula defining resistance coefficient in terms of piston velocity and upper chamber pressure and allows to maintain constant pressure in compressed chamber of the absorber:

$$C_V(t) \to \infty \quad \text{for} \quad t < t_x \tag{3.2.120}$$

$$C_V(v, p_1) = \frac{(p_x - p_1)(h_{20} - u_x)RT_0}{v p_{20} h_{20} A} \quad \text{for} \quad t \geq t_x$$

Due to substantial gas inflow to the upper chamber its influence of total force generated by the absorber is relevant. Therefore, the solution of the problem of pressure minimisation is completely different than problem of acceleration minimisation, cf. Fig. 3.2.24. Comparison of results obtained from analyzed systems indicates that double-chamber cylinder with exhaust to environment is more efficient in terms of reduction of positive chamber pressure and protection of the impacted object.

3.2.5. Load capacity maximization

The last considered adaptation procedure is not related directly to a particular impact scenario defined by hitting object mass and impact velocity but to general properties of the absorber. The objective of current adaptation strategy is to find value of initial pressure and change of valve opening which maximizes load capacity of the pneumatic absorber. Load capacity will be further defined as maximal energy of the impacting object which does not violate constraints imposed on quantities minimised in previous adaptation strategies, i.e. maximal deceleration, maximal energy after rebound and maximal value of internal pressure. General formulation of the problem reads:

$$\text{Find} \quad p_0, C_V \ \text{such that} \ J_4 = E_k^0 \ \text{is maximal} \tag{3.2.121}$$

$$\text{subject to:} \ \max_t \left|\ddot{u}(t)\right| < f_1, \quad E_k(t_{end}) < f_2, \quad \max_t p(t) < f_3$$

The problem of maximisation of the load capacity is relatively simple when only one main constraint (typically regarding maximal acceleration or pressure) is taken into account and **no constraints on valve opening are imposed**. Let us initially consider purely pneumatic (friction-less) single-chamber pneumatic absorbers with exhaust to environment. The highest load capacity of the absorber can be obtained when active adaptation strategy with continuous control of valve opening is applied. In case of limitation imposed on maximal deceleration of the hitting object $a_{\max} = \max_t \left|\ddot{u}(t)\right|$, maximal pressure inside cylinder and piston displacement at time instant when the valve becomes open can be expressed as:

$$p_{\max} = \frac{Ma_{\max}}{A} + p_A \ ; \ u_x = h_0 \left[1 - \left(\frac{p_0}{p_{\max}}\right)^{\frac{1}{\kappa}}\right] = h_0 \left[1 - \left(\frac{Ap_0}{Ma_{\max} + Ap_A}\right)^{\frac{1}{\kappa}}\right] \tag{3.2.122}$$

Let us note that maximal force generated by the absorber depends on mass of the impacting object. In case when mass of the hitting object is known (and maximal impact velocity is searched), maximal allowable impact energy can be calculated directly by integration of the

equations of impacting object motion corresponding to two stages of the process (in the form Eq.3.2.41a,b) over displacement. The resulting formula defining maximal impact energy is equivalent to reverse form of Eq. 3.2.43:

$$E_k^{\max} = p_0 h_0 A \left[\frac{\kappa}{\kappa - 1} \left(\left(\frac{p_{\max}}{p_0} \right)^{\frac{\kappa-1}{\kappa}} - \frac{1}{\kappa} \right) - \frac{p_A}{p_0} \right] \tag{3.2.123}$$

and indicates that maximal allowable impact energy increases together with mass of the hitting object and initial pressure inside the absorber. In turn, when initial velocity of the hitting object is known (and maximal mass is searched) determination of maximal impact energy relies on solving the equation:

$$\tfrac{1}{2} M V_0^{\,2} = E_k^{\max}(M) \tag{3.2.124}$$

where the right hand side is defined by Eq. 3.2.123. The corresponding valve opening which provides constant level of pressure (and also constant force and hitting object acceleration) is defined by Eq. 3.2.49a,b. When the constraints are imposed on internal pressure inside absorber chamber the formulae (3.2.123, 3.2.124) hold, however maximal pressure is not defined by (Eq. 3.2.122) but assumed a priori. Maximal allowable kinetic energy of the impacting object is then independent on its mass and velocity.

In case of purely pneumatic double- chamber absorber with zero initial volume of the upper chamber and constraint imposed on maximal acceleration of the impacting object, the methodology of determining maximal kinetic energy is similar as in case of single chamber absorber. Maximal pressure in the compressed chamber can be determined from the Eq. 3.2.122 with ambient pressure $p_A = 0$, the maximal energy that can be applied to the absorber is defined by Eq. 3.2.123 or Eq. 3.2.124 (also with $p_A = 0$). Finally, change of flow resistance coefficient which allows to maintain constant pneumatic force generated by the absorber is defined for adiabatic system by Eq. 3.2.71 and Eq. 3.2.73, and for isothermal system by Eq. 3.2.75.

When constraints on maximal pressure in compressed chamber are imposed the process of maximisation of the load capacity relies on application of active adaptation strategy defined by Eq. 3.2.120 composed of stage of pressure increase and stage when pressure remains constant. Determination of maximal kinetic energy is based on integration of Eq. 3.2.119 over displacement, where the quantity p_{2x} indicates maximal allowable pressure in the lower chamber and the quantity u_x indicates displacement when maximal pressure is achieved.

Problems of maximisation of the load capacity become more complicated in case when the main constraint (i.e. maximal acceleration or maximal internal pressure) are considered in conjunction with **constraints imposed on maximal valve opening**. Due to the fact that active constraint causes that neither minimal force generated by the absorber nor minimal pressure generated in the compressed chamber is unambiguously defined by energy of the hitting object, mass of the hitting object has to be assumed and velocity maximised or vice versa. Hereafter, let us assume the first possibility and maximize initial velocity of the impacting object. Proposed solution of the problem posed is composed of two steps:

- development of procedure for finding change of valve opening which minimizes hitting object acceleration or internal pressure for given impact velocity (typical procedures were proposed in Sec. 3.2.2 and 3.2.4); as a result implicit function defining maximal acceleration or pressure in terms of impact velocity $a_{\min} = f_1(V_0)$ or $p_{\max} = f_2(V_0)$ is obtained (both functions are expected to be monotonous);
- finding velocity of the hitting object for which minimal acceleration/pressure achieves predefined limit value, i.e. solving equation $f_1(V_0) = a^{\max}$ or $f_2(V_0) = p^{\max}$ which due to implicit form of the function f_1 or f_2 has to be performed by using optimization techniques.

The above procedure is a straightforward generalisation of the procedure applied for case when constraints on valve opening were not imposed. Despite simple methodology, the corresponding numerical computations become complex since for each impact velocity minimal acceleration has to be searched iteratively (the procedure for finding optimal time instant of valve opening is iterative), and further iterative procedure is required for solving equation aimed at finding maximal velocity.

In case when **two types of constraints** are imposed (on maximal acceleration and maximal pressure), the problem of maximisation of the load capacity is the related to a straightforward problem of minimisation of weighted sum of maximal acceleration and maximal pressure which reads:

$$\text{Find} \quad p_0, C_V \text{ such that } J_4 = a \max_t a(t) + b \max_t p(t) \text{ is minimal} \qquad (3.2.125)$$

which was not solved in Sec. 3.2. and remains open. Nevertheless, some indications and approximate solution regarding maximization of the initial kinetic energy subject to simultaneous acceleration and pressure constraint will be given.

The situation is the simplest in case of single-chamber absorber where adaptation strategy aimed at maintaining constant level of pressure is fully equivalent to maintaining constant level of hitting object acceleration. The comparison of force which is generated by the absorber when pressure of the gas achieves maximal allowable value: $F_p = A(p_{\max} - p_A)$ and force generated by the absorber which causes maximal allowable acceleration $F_a = Ma_{\max}$ allows to determine which condition is critical for determination of the load capacity of the absorber. Optimal adaptation strategy assumes maintaining constant level of the lower of two above forces. Further, maximal kinetic energy of the impacting object can be computed by two-stage integration of force generated by the absorber.

In case of double-chamber absorber with zero initial volume of the upper chamber, the preliminary step also relies on comparison of maximal force resulting from maximal pressure condition $F_p = Ap_{\max}$ and maximal force resulting from acceleration condition $F_a = Ma_{\max}$. In case when $F_p < F_a$ the proposed adaptation strategy is based on:

- keeping the valve closed until force generated by the absorber achieves value $F_{p,}$
- maintaining constant level of pressure in compressed chamber until the end of cylinder stroke (the procedure results in decrease of hitting object acceleration and therefore, the possibility of exceeding limit acceleration value does not occur).

On the contrary, in case when $F_a < F_p$ the following strategy should be applied:

- keeping the valve closed until force generated by the absorber reaches the value F_p
- maintaining constant level of hitting object acceleration until the end of cylinder stroke (the procedure results in increase of pressure inside lower chamber of the cylinder and therefore the risk of exceeding maximal pressure value occurs),
- optional: maintaining constant level of pressure in the compressed chamber once it reaches maximal allowable value, which results in (unfavourable) decrease of hitting object acceleration.

The whole procedure is more complex when mass of the hitting object is not known since maximal allowable pneumatic force F_a can not be directly determined. Although the proposed algorithm utilizes only two simple adaptation strategies aimed at maintaining constant acceleration and constant pressure, it results in finding maximal load capacity of the absorber.

Numerical implementation of proposed control strategies

Implementation of presented adaptation strategies based on methods of optimisation and control was performed in the following manners:

- in case of models implemented directly in MAPLE as ordinary differential equations:

  1. application of build-in commands allowing for 'on-line' changing of the coefficients of the differential equations according to actually obtained solution including inequality-based conditional statements (method for control purposes),

  2. automatic multiple stop and restart of the numerical analysis at particular time instants in order to analyze previously obtained results and change equations' coefficients in the continued analysis accordingly (method for control purposes),

  3. establishing connection to MATLAB (by defining function which generates MAPLE input file, runs the analysis and reads selected results) and utilising MATLAB procedures included in 'Optimisation Toolbox' and 'Direct Search and Genetic Algorithm Toolbox' for solving optimisation problems;

- in case of models implemented in commercial FEM code ABAQUS Standard the feedback control was obtained by utilizing Fortran subroutines interacting with the numerical analysis: URDFIL subroutine for reading results at each time step of the analysis, DISP subroutine for direct changing of internal pressure and finally UFIELD subroutine for changing parameters of the flow;
- for models implemented in explicit FEM code ABAQUS Explicit the feedback control was obtained by establishing connection to MATLAB software (by defining function which generates ABAQUS input file, runs finite element analysis and finally reads selected results) and by utilizing MATLAB optimisation procedures.

Implementation of various methods of solving optimisation and control problems for adaptive pneumatic absorbers (being the simplest of considered pneumatic structures) gives precise insight to drawbacks and advantages of each method. It also establishes good starting point for simulation and implementation of adaptation strategies for more complex inflatable structures as thin walled inflatable steel structures and adaptive 'flow control - based' airbags

considered in further chapters of this thesis. On the other hand, described methods of numerical implementation of models of inflatable structures are also suitable for simulation of other types of adaptive structures especially the ones dedicated for Adaptive Impact Absorption.

The choice of the most efficient methodology of numerical implementation depends on type of optimisation/control problem considered and type of the structure being optimised/controlled. The methodology of using separate software for performing numerical analysis (MAPLE or ABAQUS in this case) and using MATLAB (and its optimisation toolboxes) for implementation of optimisation and control procedures was found to be convenient and effective. The effort required for coupling two separate numerical codes pays off due to high specialisation of software applied for both purposes. Therefore, mainly this methodology will be applied for solving optimisation and control problems related to other types of inflatable structure.

Summary of the Section 3.2

The section presents various strategies aimed at adaptation of two types of pneumatic cylinders to actual impact loading. The section starts with presentation of load identification techniques aimed at determination of parameters of rigid impacting object. Further described adaptation strategies are oriented towards minimisation of impacting object deceleration and rebound, minimisation of internal pressure and, finally, at maximisation of the load capacity. Moreover, the strategies are divided according to type of applied control.

The attention is focused on minimisation of impacting object deceleration. Proposed semi-active adaptation reveals the characteristic features of the system with constant valve opening. Active adaptation strategies with continuous control of valve opening effectively utilize numerical model of the analyzed system which, despite its nonlinearity, in many cases allows to find analytical function defining the control law. Application of such approach is possible due to lack of external excitation and description of the considered problem by homogenous differential equations. Continuous control strategies are also developed for the case of insufficient valve opening and additional forces generated by the absorber. The following methods of adaptation utilize discrete valve openings or predefined time intervals. The relation between minimisation of deceleration and minimisation of rebound is also discussed. Proposed methodologies and conducted simulations show that control of generated pneumatic force and minimisation of the impacting object deceleration can be performed in a variety of methods by utilizing valves of different operating principles.

The following part briefly describes semi-active and active strategies aimed at minimisation of internal pressure and maximisation of the system load capacity. The continuous strategies of maintaining constant pressure are compared against strategies for maintaining constant deceleration. The proposed methods for maximising the load capacity effectively utilize previously elaborated strategies for pressure and deceleration minimisation.

The section presents miscellaneous methodologies for controlling dynamic characteristics of the adaptive pneumatic cylinder and reveals the ability of effective mitigating dynamic response of the hitting object and impacted structure. The wide range of analyzed control objectives, methodologies and numerical examples provides comprehensiveness and thoroughness of the considerations.

3.3. Optimal design of adaptive pneumatic absorbers

In many practical cases the engineering problem is not only to develop control strategy for mitigation of hitting object or impacted structure response but also to design the adaptive impact absorbing device, i.e. to find optimal dimensions of the cylinder, optimal pressure range and required parameters of the controllable valve. Let us stress the fact that in case of adaptive structure the typical design methodology in which parameters of the structure are selected to minimize certain objective function (typically total cost or weight) with respect to constraints defined by structure response (typically maximal stress or deflection) can not be directly followed. The response of the adaptive structure depends not only on structure parameters and external loading but also on the adaptation strategy which is intended to be applied, cf. Fig. 3.3.1. In turn, the adaptation strategy itself also depends on parameters of the system, not only in terms of coefficients values but also in terms of the general algorithm of adaptation, cf. adaptation strategy for minimization of hitting object acceleration with and without constraints imposed on valve opening.

Therefore, the problem of optimal choice of parameters is inherently connected with considered adaptation strategy. In the most general approach, the problems of finding optimal topology, choice of optimal parameters and development of adaptation strategy should be considered simultaneously.

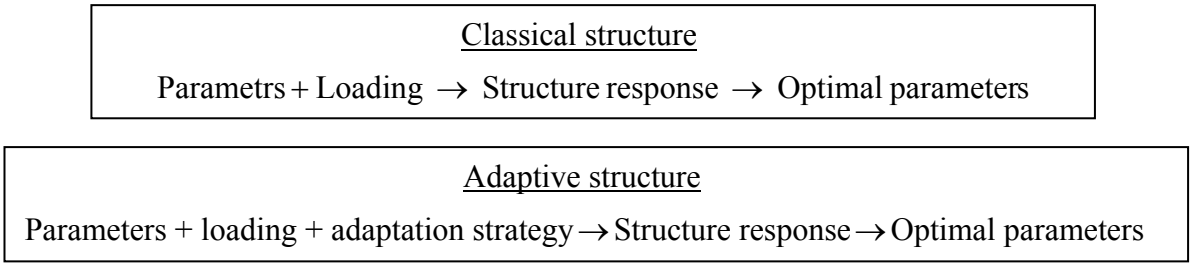

Fig.3.3.1. Difference in design methodology of classical and adaptive structure

The problem of optimal design will be discussed for double-chamber cylinder which will be analysed in the context of application as landing gear for a small aerial vehicle. The aim of the current task is to find optimal dimensions of the pneumatic absorber and the required parameters of the valve, i.e.:

- the length of both chambers of the absorber h_{01}, h_{02}
- cross-section area of both chambers A_1, A_2
- maximal pressure difference for which the valve remain airtight $\Delta p_{\max}$
- required mass flow rate through the valve $q_{\max}$ (for certain parameters of the gas in both chambers of the absorber).

The initial data for calculation of these parameters will be mass of the landing object M, maximal landing velocity V_0, maximal allowable level of deceleration of the landing object a_{max} and maximal pressure of gas inside compressed chamber of the cylinder p_{max}.

The procedure for determination of optimal parameters will be based on model of the absorber reduced to a single mechanical degree of freedom. We will effectively utilize the following governing equations which are valid during forward movement of the piston when $p_2 > p_1$: (cf. Fig. 3.1.11a)

$$M\ddot{u} - Mg + A_2 p_2(t) - A_1 p_1(t) = 0 \tag{3.3.1a}$$

$$\frac{p_2 V_2^{\kappa}}{m_2^{\kappa}} = \frac{p_{02} V_{02}^{\kappa}}{m_{02}^{\kappa}} \tag{3.3.1b}$$

$$\frac{\dot{p}_1}{p_1} = \kappa \frac{\dot{m}_1}{p_1 V_1} \frac{p_2 V_2}{m_2} - \kappa \frac{\dot{V}_1}{V_1} \quad \text{or alternatively} \tag{3.3.1c}$$

$$\tfrac{1}{2} M V_0^2 - \tfrac{1}{2} M \dot{u}^2 + Mgu = \frac{p_1 V_1}{\kappa - 1} + \frac{p_2 V_2}{\kappa - 1} - \left(m_{01} c_V T_{01} + m_{02} c_V T_{02} \right) \tag{3.3.1d}$$

where the equation (3.3.1c) describes energy balance for the upper chamber where inflow of the gas occurs and alternative equation (3.3.1d) describes balance of the energy of the whole system. Ideal gas law has been already incorporated into the above equations. Moreover, the following relations between mass of gas and volumes of the chambers hold:

$$V_1 = A_1 \left(h_{10} + u \right), \qquad V_2 = A_2 \left(h_{20} - u \right), \qquad m_1 + m_2 = m_{01} + m_{02} = const. \tag{3.3.1e}$$

The most important task of the landing gear is dissipation of the kinetic energy of the landing with minimal value of the landing object deceleration. Therefore, **optimal design of the absorber** will be based on adaptation strategy aimed at deceleration minimisation (cf. Sec. 3.2.2) which provides that both above objectives are fulfilled.

The first step in calculation of optimal parameters of pneumatic cylinder is, therefore, assumption of optimal kinematics of the absorber with initial stage of force increase and further stage when generated pneumatic force remains constant. Equations of motion of for the two subsequent stages of impact reads:

$$M \frac{d^2 u}{dt^2} - Mg + \frac{p_0 {h_{02}}^{\kappa}}{(h_{02} - u)^{\kappa}} A_2 - \frac{p_0 {h_{01}}^{\kappa}}{(h_{01} + u)^{\kappa}} A_1 = 0 \quad \text{for} \quad u \in \left(0, u_x\right) \tag{3.3.2a}$$

$$M \frac{d^2 u}{dt^2} - Mg + \frac{p_0 {h_{02}}^{\kappa}}{(h_{02} - u_x)^{\kappa}} A_2 - \frac{p_0 {h_{01}}^{\kappa}}{(h_{01} + u_x)^{\kappa}} A_1 = 0 \quad \text{for} \quad u \in \left(u_x, u_{\max}\right\rangle \tag{3.3.2b}$$

where u_x indicates value of piston displacement when the valve becomes open and u_{max} indicates maximal allowable displacement of the piston (which is arbitrarily assumed and usually indicates position in the vicinity of the end of absorber stroke). By integrating above equations over displacement in the range from 0 to u_{max} one obtains:

$$\begin{aligned} \frac{M {V_0}^2}{2} + Mgu_{\max} = {} & \frac{p_0 A_2 {h_{02}}^{\kappa} (h_{02} - u_x)^{-\kappa+1}}{\kappa - 1} - \frac{p_0 A_2 h_{02}}{\kappa - 1} + \frac{p_0 A_1 {h_{01}}^{\kappa} (h_{01} + u_x)^{-\kappa+1}}{\kappa - 1} \\ & - \frac{p_0 A_1 h_{01}}{\kappa - 1} + \left(\frac{p_0 {h_{02}}^{\kappa} A_2}{(h_{02} - u_x)^{\kappa}} - \frac{p_0 {h_{01}}^{\kappa} A_1}{(h_{01} + u_x)^{\kappa}} \right) \left(u_{\max} - u_x \right) \end{aligned} \tag{3.3.3}$$

The above equation allows to find displacement u_x, corresponding maximal force acting on the falling object during impact F_x and corresponding maximal acceleration $a_{max} = a_x$:

$$F_x = \frac{p_0 {h_{02}}^{\kappa} A_2}{(h_{02} - u_x)^{\kappa}} - \frac{p_0 {h_{01}}^{\kappa} A_1}{(h_{01} + u_x)^{\kappa}}, \qquad a_{\max}(p_0, h_{01}, h_{02}, A_1, A_2) = \frac{F_x}{M} - g \tag{3.3.4}$$

Maximal value of pressure inside positive chamber $p_2^{\max}$ is obtained at the end of the process when the piston is nearly stopped and it approaches its lowest position in the vicinity of the cylinder bottom but the force level is still maintained constant, cf. Fig. 3.2.10. At this time instant the whole mechanical energy of the impacting object is changed into internal gas energy. Corresponding parameters of the pneumatic system can be determined from the following system of algebraic equations:

$$p_2^{\max} A_2 - p_1^{\max} A_1 = F_x \tag{3.3.5}$$

$$\tfrac{1}{2} M V_0^2 + M g u_{\max} = \frac{p_1^{\max} V_1^{end}}{\kappa - 1} + \frac{p_2^{\max} V_2^{end}}{\kappa - 1} - \left(m_{02} c_V T_{02} + m_{02} c_V T_{02} \right)$$

where the quantities V_1^{end} and V_2^{end} are known since they are determined by displacement u_{max}. Moreover $p_1^{\max}$ denotes pressure corresponding to $p_2^{\max}$, i.e. obtained at the end of the process, however it does not indicate maximal pressure obtained in decompressed chamber. In a special case when maximal piston displacement equals the cylinder stroke, pressure of gas inside both chambers at time instant when the piston is stopped equals:

$$p_1^{\max} = \frac{m_{10} c_V T_{10} + m_{20} c_V T_{20} + \tfrac{1}{2} M V_0^{\,2} + M g h_{02}}{(\kappa - 1)^{-1} (h_{01} + h_{02}) A_1} \tag{3.3.6}$$

$$p_2^{\max}(p_0, h_{01}, h_{02}, A_1, A_2) = \frac{F_x + p_1^{\max} A_1}{A_2}$$

Above analytical formulae (3.3.4$_2$) and (3.3.6$_2$) explicitly define maximal acceleration of the hitting object and maximal pressure in terms of initial parameters of the impacting object, initial pressure and searched geometrical parameters of the absorber. By assuming dimensions of decompressed chamber, cross-sectional area of the piston rod (which often results from technological limitations) and initial pressure, one can calculate minimal length h_{02} and minimal cross section A_2 of the cylinder, which are required to fulfil the conditions imposed on maximal deceleration and maximal pressure.

State of the system after equilibration of pressures in both chambers after impact can be determined from the algebraic equation analogous to (3.3.5$_b$) but with $p_1^{\max} = p_2^{\max} = p^{end}$:

$$\tfrac{1}{2} M V_0^2 + M g u_{\max} = \frac{p^{end} (V_1^{end} + V_2^{end})}{\kappa - 1} - (m_{01} c_V T_{01} + m_{02} c_V T_{02}) \tag{3.3.7}$$

Pressure p^{end} determines characteristics of the absorber after impact when valve remains open and both chambers can be treated as a single gas volume:

$$F_p(u) = \frac{p^{end} (V^{end})^{\kappa}}{\left(V^{end} - (A_2 - A_1)(u - u_{\max}) \right)^{\kappa}} (A_2 - A_1) \tag{3.3.8a}$$

where $V^{end} = V_1^{end} + V_2^{end}$. Position of static equilibrium of the system can be determined by comparing above force with weight of the impacting mass. Since the characteristics of the absorber is relatively flat, the equilibrium may be obtained at the end of the cylinder with the use of delimiting springs. Moreover, position of equilibrium changes as gradual cooling of gas due to transfer of heat to the environment occurs. Since stiffness of the absorber after impact

depends on areas of both chambers, it can be utilized as an additional condition for finding optimal geometry of the absorber or optimal initial pressure.

The first step of finding optimal **parameters of the valve** is determination of the maximal pressure difference for which the valve has to remains airtight, i.e. for which leakages of the fluid do not occur or are insignificantly small. As it is presented in Fig. 3.2.10 (Section. 3.2.2) the largest pressure difference occurs at the end of the first stage of the impact just before opening of the valve and equals:

$$\Delta p_{\max} = \frac{p_0 {h_{02}}^{\kappa}}{(h_{02} - u_x)^{\kappa}} - \frac{p_0 {h_{01}}^{\kappa}}{(h_{01} + u_x)^{\kappa}} \tag{3.3.9}$$

In further stage of active adaptation strategy maintaining constant force generated by the absorber requires gradual closing of the valve through where flow of the fluid occurs. During the second stage of impact pressure difference is slightly smaller than Δp_{max} which allows to preliminarily presume that realisation of the process of closing the valve will be possible. However, actual pressure difference can be used only for rough estimation of forces acting on the valve head during closing of the valve. Precise determination of these forces requires using methods of computational fluid dynamics and it will be an objective of analysis of piezoelectric valve in Chapter 7.

Calculation of maximal mass flow rate through the valve requires preliminary determination of change of gas parameters during the second stage of impact. Since total force generated by the absorber remains constant and kinematics of the system is defined by Eq. $3.3.2_b$, change of pressure and mass of the gas in both chambers can be determined from the following set of algebraic equations:

$$p_2 = A_2^{-1}\left(F_x + p_1 A_1\right), \qquad \frac{p_2 V_2^{\kappa}}{m_2^{\kappa}} = \frac{p_{02} V_{02}^{\kappa}}{m_{02}^{\kappa}} \tag{3.3.10}$$

$$\tfrac{1}{2} M V_0^2 - \tfrac{1}{2} M \dot{u}^2 + Mgu = \frac{p_1 V_1}{\kappa - 1} + \frac{p_2 V_2}{\kappa - 1} - \left(m_{10} c_V T_{10} + m_{20} c_V T_{20}\right)$$

Determined change of mass of the gas allows to calculate required mass flow rate of gas $q = -\dot{m}_2$ corresponding to actual parameters of gas in both chambers.

Developed conditions defining maximal pressure difference for which the valve remains airtight and maximal mass flow rate through the valve can be treated either as requirements for the valve (when it is intended to be designed) or as additional conditions for selecting geometrical parameters of the system (when particular type of the valve is intended to be applied).

Application to design of adaptive pneumatic landing gear

The above methodology was utilized to design adaptive pneumatic landing for Unmanned Aerial Vehicle (UAV), i.e. to find optimal geometry of the absorber and required properties of the valve. The initial data for the design of landing gear included:

- mass of the UAV: $M = 8{,}5kg$, maximal touchdown velocity: $V_0 = 3{,}3m/s$
- maximal admissible vertical deceleration during landing: $a_{\max} = 70m/s^2$

- maximal pressure in compressed chamber of the absorber: $p_2^{\max} = 16atm$
- initial pressure in absorber chambers: $p_0 = 6atm$
- maximal stroke of the absorber $u_{\max} = h_{02} - 0.01m$

Basic parameters of the adaptive absorber were determined by using balance of energy of the landing object and comparing obtained deceleration and pressure with assumed limiting values. The following parameters were obtained:

- length of the absorber: $h_0 = 0{,}11m$
- length of decompressed chamber: $h_{01} = 0{,}005m$, compressed chamber: $h_{02} = 0{,}095m$
- cylinder diameter: $d = 32mm$, piston rod diameter: $d_T = 12mm$

Further, thermodynamic part of the model was utilized to determine required parameters of the controllable valve:

- maximal pressure difference for which the valve remains airtight: $\Delta p = 8{,}45atm$
- range of pressure difference during second stage of landing: $\Delta p = 7{,}25atm - 8{,}45atm$
- range of pressure values in compressed chamber: $p_2 = 8{,}97atm - 16{,}3atm$
- maximal required mass flow rate : $q_{\max} = 14{,}8g/s$ (corresponding pressure difference: $\Delta p = 7{,}79atm$, corresponding upstream pressure $p_2 = 13{,}0atm$).
- maximal value of resistance coefficient $C_V = 52{,}5\dfrac{MPa}{kg/s}$, $1/C_V = 0{,}019\dfrac{kg/s}{MPa}$

After the process of landing, internal pressure inside cylinder reaches the value $p_{end} = 9{,}86atm$, and static equilibrium of the system can be obtained with fully expanded absorber. On the contrary, when temperature of the gas decreases to the level of external temperature static equilibrium of the system can be obtained with fully compressed absorber. Both above facts indicate that application of additional delimiting springs at the ends of the cylinder is required.

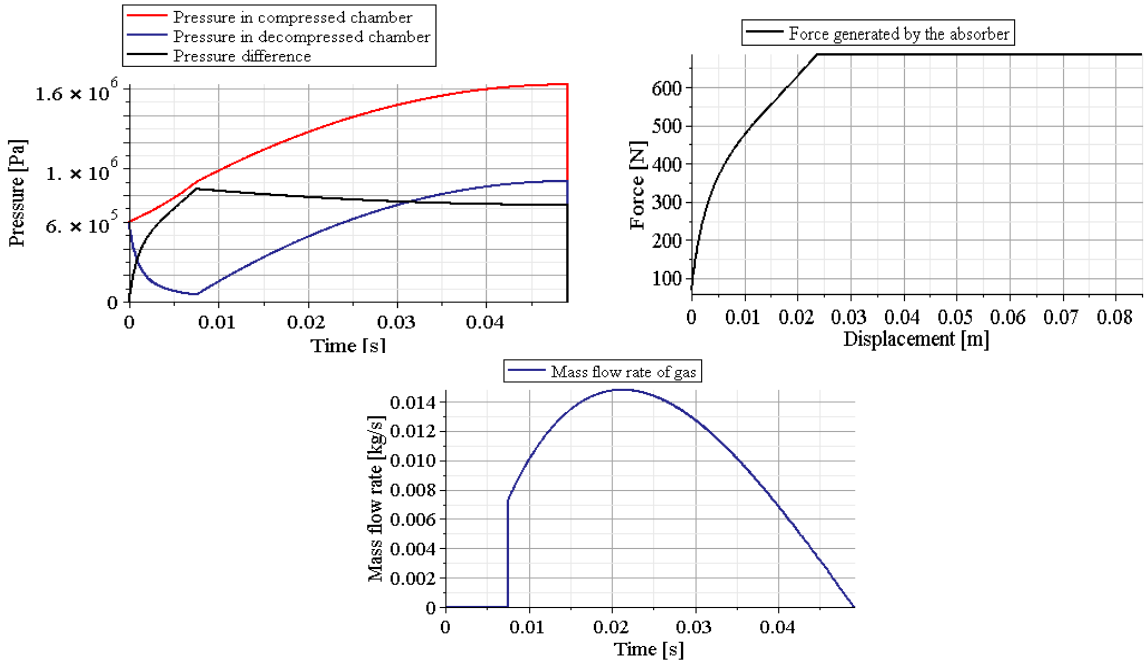

Fig.3.3.1. Characteristics of the double-chamber absorber with optimal parameters determined from simplified 1DOF model

Simulation of the landing gear with optimal absorber

In the following step, full 2 DOF model of the system was utilized to simulate performance of the adaptive pneumatic absorber characterized by optimal parameters during the process of landing. The simulation was preceded by the following steps:

- development of the model of the wheel of the aerial vehicle, which was assumed in the form: $F_k = k(p)x^2 + c(p)x\dot{x}$; where p is wheel pressure and it was adjusted to obtain desired deflection of the wheel during the process,
- development of the model of the friction force: $F_t = F_0 \tanh(a\dot{x})$,
- the model of the gas flow through the valve was assumed either in a simple form: $q = (p_2 - p_1)/C_V$ or it was described by Saint-Venant model of the flow (Eq. 3.2.28).

The following step was assumption of the set of differential equations describing dynamics of the landing gear. Set of governing equations takes the form, Fig. 3.3.2:

$$M_1 \frac{d^2u_1}{dt^2} - M_1 g + F_P - F_{Fr} - F_D^{BOT} + F_D^{TOP} = 0 \tag{3.3.11}$$

$$M_2 \frac{d^2u_2}{dt^2} - M_2 g - F_p + F_{Fr} + F_D^{BOT} - F_D^{TOP} + F_C = 0$$

where mass M_1 and displacement u_1 are related to the landing aerial vehicle , whereas mass M_2 and displacement u_2 are related to the wheel (together with piston and piston rod). Pneumatic force F_P, friction force F_{Fr} and both forces which delimit movement of piston at the ends of the cylinder F_D depend on mutual position or velocity of the falling mass and the piston. By contrast, contact force F_C depends exclusively on position and velocity of the wheel:

$$F_p = f(u_2 - u_1), \quad F_{Fr} = f(\dot{u}_2 - \dot{u}_1), \quad F_D = f(u_2 - u_1), \quad F_C = f(u_2, \dot{u}_2) \tag{3.3.12}$$

All thermodynamic relations were defined in an analogous manner as in previous models described in this chapter.

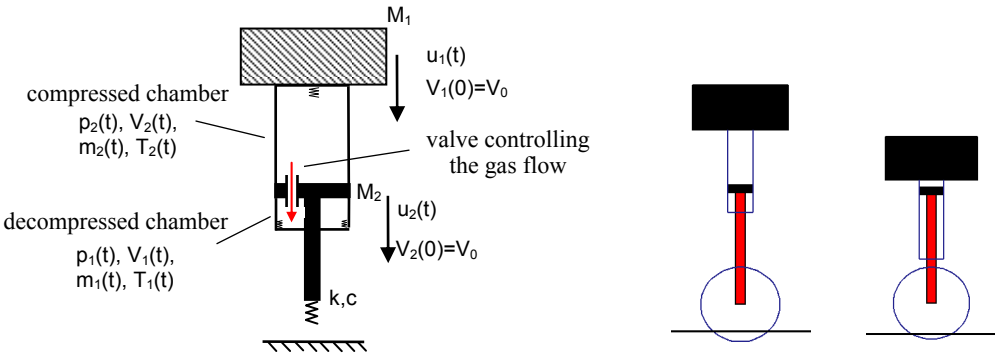

Fig.3.3.2. Numerical model of the adaptive pneumatic landing gear: a) theoretical model, b) visualization of the process of landing

In the following step, two adaptation strategies were implemented:

- adjustment of time instant and magnitude of constant valve opening ('discrete' control)
- maintaining constant, possibly low value of deceleration during the process of landing ('on/off' control).

In the first strategy the valve remains closed during the initial stage of landing in order to enable a fast increase of the force generated by the absorber. The time of valve opening and flow resistance coefficient (representing valve opening) are adjusted by means of optimization procedure which minimizes force generated by the absorber taking into account the constraint imposed on maximal absorber stroke, Fig. 3.3.3a.

In the second strategy the valve also remains closed during the initial stage of the process. Optimal level of constant force generated by the absorber F_{OPT} is determined by using energy conservation law, which indicates the equality of potential and kinetic energy of the landing object and energy dissipated by the absorber and the wheel.

$$\Delta E_{K1} + \Delta E_{P1} + \Delta E_{K2} + \Delta E_{P2} = -(D_{ABSORBER} + D_{WHEEL}) \tag{3.3.13}$$

Alternatively, the time of valve opening can be determined from the kinematical condition:

$$a_1 = V_1^2 / 2(u_{\max} - (u_1 - u_2)) \tag{3.3.14}$$

where the value $u_{\max} = 0{,}085m$ is arbitrarily assumed and denotes maximal stroke of the absorber. In further part of the landing process the valve is simultaneously opened and closed in order to maintain constant value of generated force (Fig. 3.3.3b). The signal that controls the valve opening I_n depends on actual value of force generated by the absorber:

$$I_n = 1 \quad \text{if} \quad F > F_{OPT} + \Delta F_{TOL} \quad \text{(valve open)} \tag{3.3.15}$$

$$I_n = 0 \quad \text{if} \quad F < F_{OPT} - \Delta F_{TOL} \quad \text{(valve closed)}$$

$$I_n = I_{n-1} \quad \text{if} \quad F_{OPT} - \Delta F_{TOL} < F < F_{OPT} + \Delta F_{TOL}$$

where: ΔF_{TOL} is assumed tolerance of the force level. The coefficient characterizing the valve was slightly larger than the one determined from 1 DOF model, in order to execute on-off control strategy: $1/C_V = 0{,}025(kg/s)/MPa$. The applied strategy enables to stop the landing object by using minimal level of the force generated by the absorber and with minimal corresponding deceleration. During the final stage of the process, when velocity of the landing object is relatively small, the force generated by the absorber is gradually reduced in order to smoothly diminish the force below the wheel and its deflection and to obtain state of static equilibrium of the system. The results of the numerical simulation conducted for the most harsh landing condition, (M=8,5kg, V_0=3,3m/s) are presented in Fig. 3.3.4 and Fig. 3.3.5.

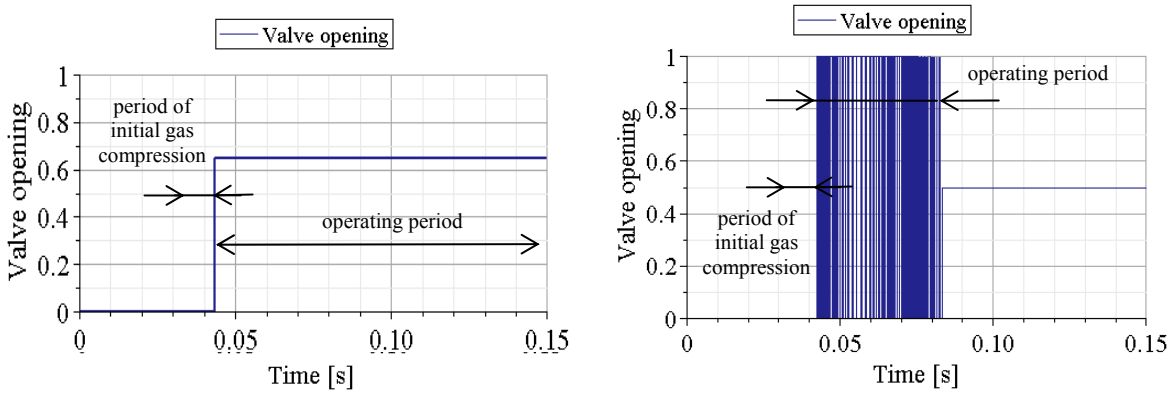

Fig. 3.3.3 Applied adaptation strategy: a) discrete control, b) on-off control

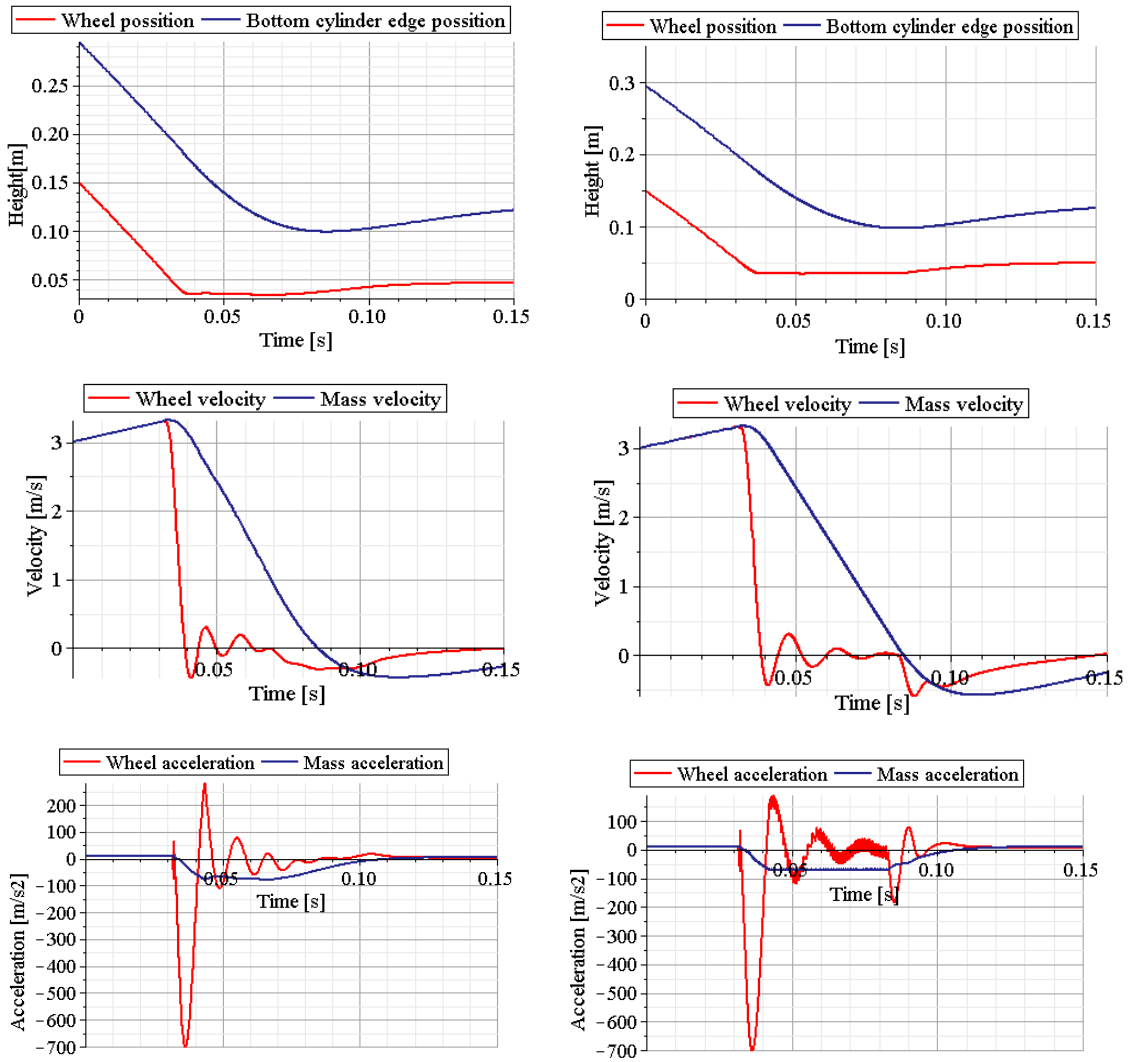

Fig. 3.3.4 Kinematics of the landing gear: a) discrete control, b) on-off control

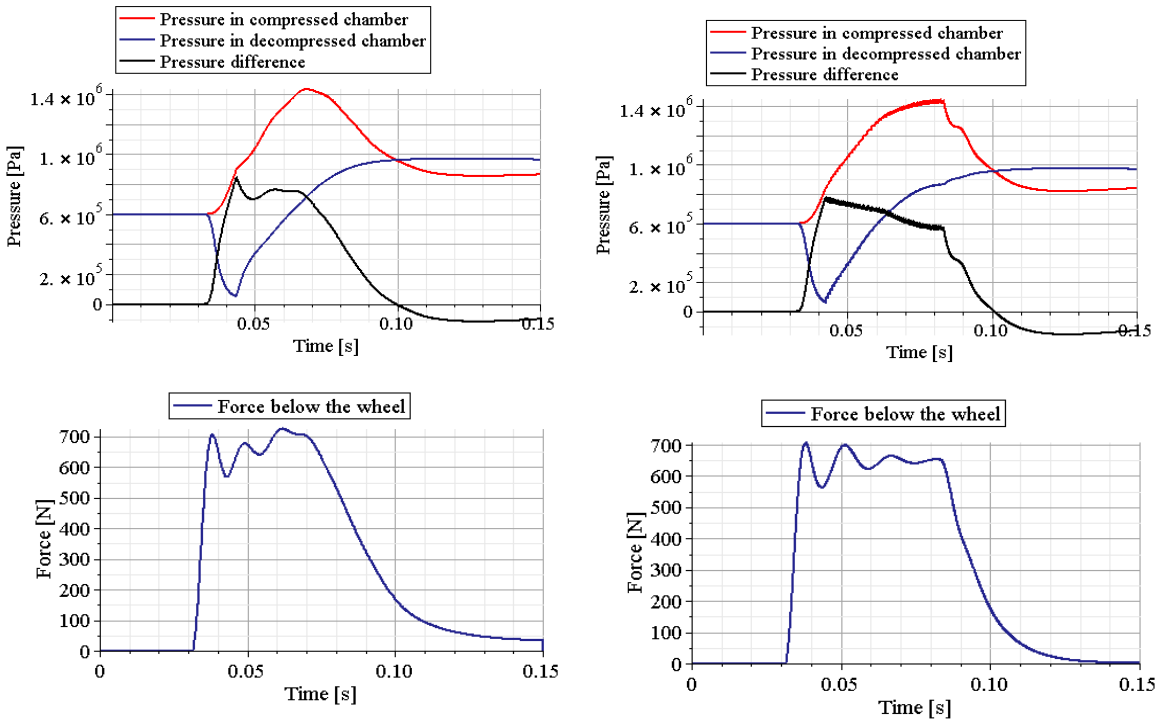

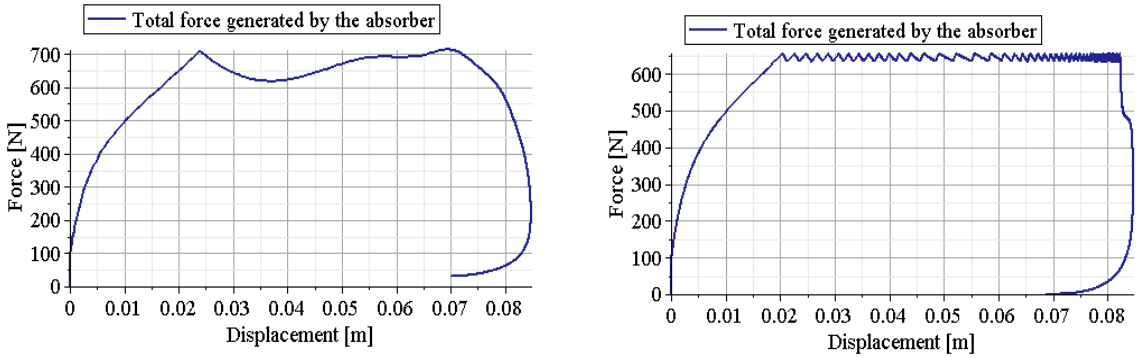

Fig. 3.3.5 Results of the applied adaptation strategies: change of pressures in both chambers and pressure difference, change of force below the wheel and change of force generated by the absorber: a) discrete control, b) on-off control

Results obtained from 2DOF model with implemented 'on/off' control strategy, in general, confirm the results predicted by simplified single degree of freedom model, cf. Fig. 3.3.1. The results from the simplified model were slightly overestimated (cf. plots of pressures and absorber force) since simplified model does not take into account the compliance of the wheel and corresponding dissipation of the impact energy. Nevertheless, the proposed methodology allowed to design adaptive pneumatic landing gear which fulfills preliminarily assumed requirements related to maximal deceleration and pressure and to determine properties of the valve which allows to execute assumed control strategy.

	Discrete control	On-off control
Maximal generated force	712N	654N
Maximal deceleration	79,19m/s^2	71,94 m/s^2
Absorber efficiency	83,9%	**90,4%**
Landing gear efficiency	72,6%	**76,7%**

Table1. Comparison of quantitative results obtained for adaptive pneumatic landing gear with single-stage and real-time control strategy

Conducted simulations confirmed the feasibility of proposed concept of dissipating kinetic energy of the landing object by means of double-chamber pneumatic absorber. Results of simulations indicated that both proposed control strategies allow to avoid rebound of the landing object and to obtain favorable, almost constant level of force generated by the absorber. Real-time control of valve opening enables to obtain unprecedented very high efficiency of the absorber which exceeds 90%.

Summary of the Section 3.3

The current section addresses the problem of optimal design of the adaptive pneumatic absorbers. The undertaken problem substantially differs from the optimal design of the passive structure since it has to take into account adaptive response of the designed system. The section proposes the methodology of optimal choice of dimensions, initial pressure and parameters of the valve of double chamber absorber intended to be applied as a adaptive landing gear of small aerial vehicle. High effectiveness of the pneumatic landing gear controlled by two strategies is proved by numerical simulations.

3.4. Experimental verification

The concept of adaptive pneumatic absorber was verified experimentally by using typical industrial pneumatic cylinder, constructed piezoelectric valve and laboratory free-fall drop testing stand. The following tasks were performed during the laboratory tests:

1. The correctness of developed numerical model of pneumatic absorber was confirmed,
2. The influence of initial pressure and valve opening on dynamic characteristics of the absorber and the amount of energy dissipated was investigated,
3. On/off adaptation strategy was implemented and superiority of the adaptive absorber over the passive one was proved.

Description of the experimental stand

Adaptive pneumatic absorber was built on a basis of typical industrial double chamber pneumatic cylinder with the diameter of 63mm and stroke of 250mm. Two design options of the absorber were considered: the system where the valve controls the exhaust of gas from lower (compressed) chamber to environment and the system where the valve controls flow of the gas between lower and upper chamber of the cylinder. In both cases the controllable valve was mounted in the port in the lower cylinder chamber, cf. Fig. 3.4.1a. Additionally, in the second case outlet of the valve was connected to the port in the upper cylinder chamber such that pneumatic system was isolated from the environment. Moreover, compressor was used to modify the initial pressure inside the pneumatic cylinder by the use of dedicated pressure regulator. In conducted experiments free falling mass was impacting the piston of the cylinder via a rubber bumper and response of the pneumatic system was observed.

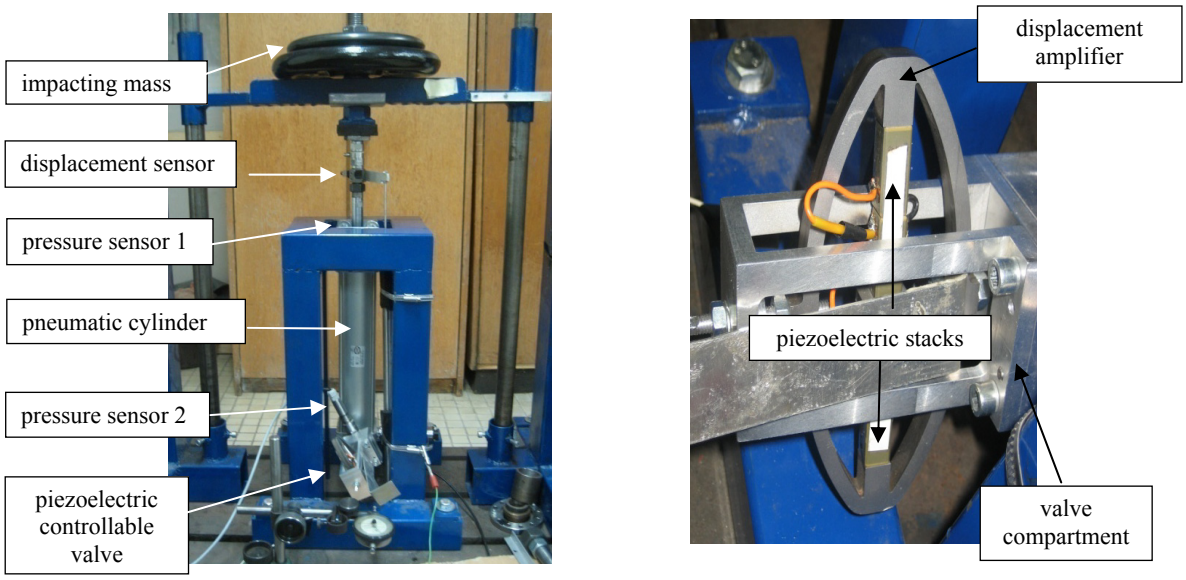

Fig.3.4.1. a) Adaptive pneumatic absorber, b) Controllable valve based on piezoelectric stack

The valve controlling flow of the fluid (cf. Fig. 3.4.1b) consisted of piezoelectric stack, valve head sealed by rubber gasket, displacement amplifier and metal compartment. Piezoelectric stack produced by Cedrat company was located perpendicularly to the direction of the valve head movement due to application of ellipsoidal structure which served for

increasing range of the valve head displacement. In a basic configuration the valve head remained closed preventing flow of the gas. Applied electric signal had caused elongation of the piezoelectric stack, deformation of the displacement amplifier in vertical and horizontal direction, corresponding movement of the valve head, and finally it had invoked flow of the gas. The valve provided stroke of the valve head of 0.14mm and delay in response of the valve in respect to applied control signal was less than 2ms.

The measurement were performed by using two dynamic pressure sensors (Peltron and Honeywell), two accelerometers dedicated to impact measurements (Brüel & Kjær 4397), LVDT displacement sensor, dynamic force sensor and optical switch. Pressure sensor were connected to the ports in both chambers of the cylinder. Measured change of pressure in each chamber during impact was used to calculate actual pressure difference and actual level of pneumatic force generated by the absorber. Signal from the optical switch allowed to determine vertical velocity of the falling mass at time instant just before impact and therefore to determine the exact value of kinetic energy of the impacting object.

The accelerometers were attached to the falling mass and to the piston of the cylinder. The signal from accelerometers was integrated to obtain change of velocities and displacements of the falling mass and the piston during the process. Computed displacements were compared with the displacement obtained from the movie recorded by the high-speed camera and with the displacements obtained by LVDT sensor. During the whole experiment contact force between falling mass and the piston was measured by dynamic force sensor.

Experimental testing of semi-active system

In the fist stage of the experiment the simplest pneumatic system consisting of two chambers and valve between the lower chamber and environment was investigated. Initial pressure inside cylinder was equal to 1atm and response of the system was tested for various constant in time valve openings. Expected reduction of maximal pressure value, increase of the cylinder stroke and corresponding decrease of hitting object rebound was observed, which indicates that absorber characteristics changes from nearly elastic to dissipative, cf. Fig. 3.4.2. In the following tests (Fig. 3.4.3) the maximal stroke of the absorber was artificially diminished by changing initial position of the piston in the cylinder. In this case, the piston reached bottom of the cylinder which caused activation of the automatic brake (the second peak of the pressure plot) and rebound of the impacting object was not totally mitigated.

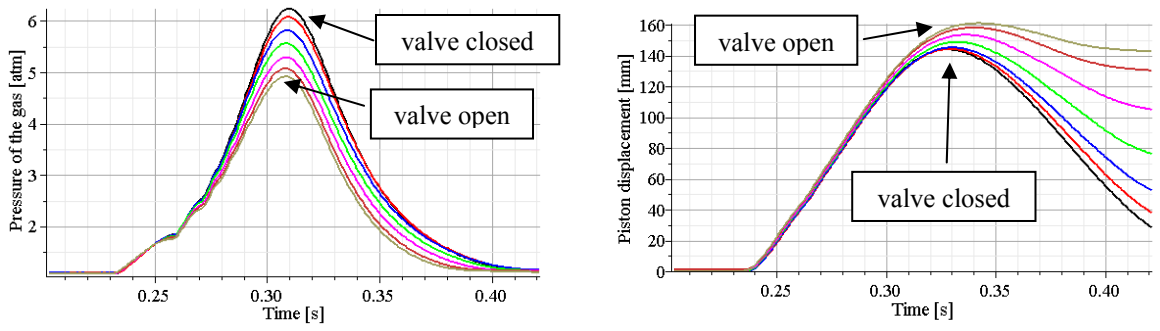

Fig.3.4.2. Response of two-chamber pneumatic system with exhaust to environment for various valve openings: a) pressure in terms of time, b) hitting object displacement in terms of time

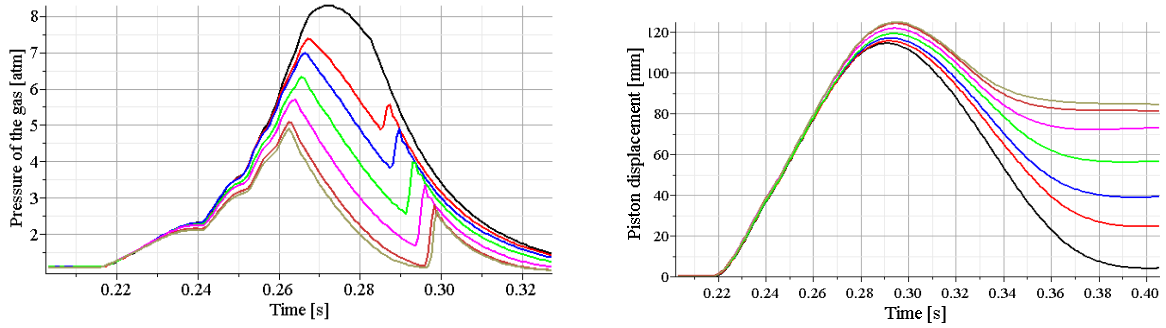

Fig.3.4.3. Response of two-chamber pneumatic system with exhaust to environment for various valve openings: a) pressure in terms of time, b) hitting object displacement in terms of time

In the next part of the experiment the connection between two chambers of the cylinder, allowing for controlled gas migration from the lower to upper chamber, was established. The influence of initial pressure and opening of the valve on generated force and dissipative properties of the system was investigated. The experiment was performed for two values of initial pressure p_0=1atm and p_0=3atm and seven positions of the valve head (which remained constant during each impact), cf. Fig. 3.4.4. Initially, the valve separating the chambers had remained closed. When pressure of 1atm was used, maximal displacement was relatively large and force-displacement characteristics reflected adiabatic compression of the lower chamber. By contrast, in case when initial pressure was equal to 3atm the system operated in the initial range of force-displacement characteristics which is close to linear, and final displacement of the piston was substantially reduced.

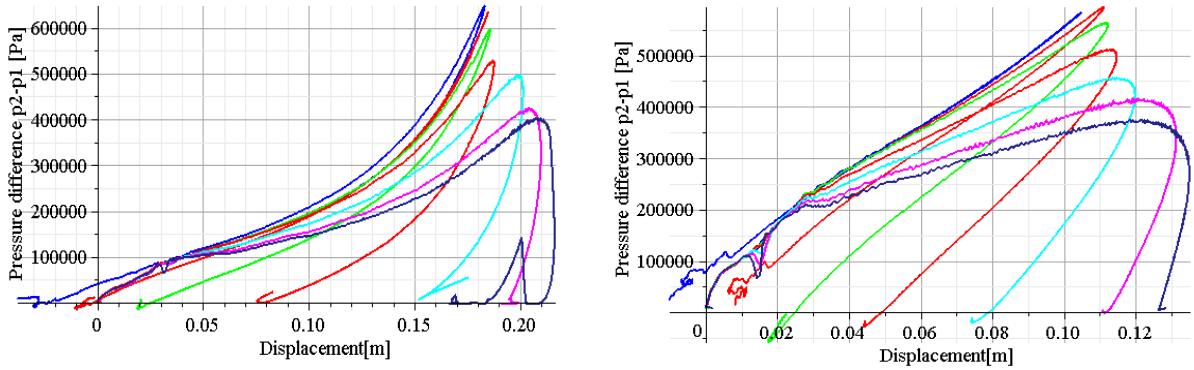

Fig. 3.4.4 Difference of pressure between the chambers for various valve openings:
a) initial pressure 1atm, b) initial pressure 3 atm

When opening of the valve was increased, the system became more dissipative, maximal value of pressure gradually decreased and stroke of the piston was increasing. In case of initial pressure of 1atm maximal valve opening allowed for using the whole stroke of the cylinder and dissipation of the whole kinetic energy of impact. In case of initial pressure of 3atm maximal allowable valve opening was not large enough to provide optimal reduction of pressure during the process. As a result, maximal value of pressure difference (and level of force generated by the absorber) obtained in both cases was similar, cf. Fig. 3.4.5. However, in case when larger opening of the valve would be possible, pressure could be reduced more efficiently and system with higher initial pressure would be more advantageous.

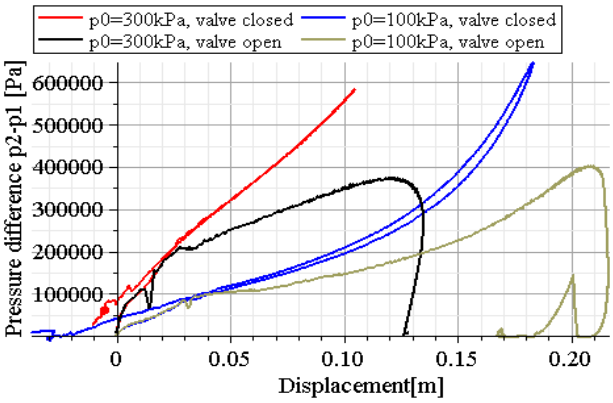

Fig. 3.4.5 Pneumatic force in terms of piston displacement for initial pressure 1atm and 3 atm obtained in case of closed and fully open valve

On the other hand, higher initial pressure allows for obtaining higher level of the pneumatic force at the beginning of the piston stroke and therefore to absorb impact of a larger energy with the same constraint on maximal allowable pneumatic force. The problem of optimal adjustment of initial pressure and valve opening for minimisation of generated force and the problem of optimal adjustment of these parameters for maximisation of the absorber load capacity were addressed in Sec. 3.2.2 and Sec. 3.2.5, respectively.

Results of the experiment were compared with the results obtained from the numerical models developed in previous sections in order to verify the simplifying assumptions applied in numerical modelling. Both global response of the system (falling object kinematics, pressures in both chambers and force generated by absorber) and local response of the system (piston kinematics and contact force) were compared and in most of the cases satisfactory correspondence of results was obtained. Possible discrepancies between both models arise due to the following reasons:

- main simplifying assumption related to homogeneity of gas parameters (especially gas temperature) in each chamber may not be exactly fulfilled during the whole process;
- the simplified formula describing flow of the fluid may not be accurate, especially at the beginning of the process when high variation of the gas flow occurs;
- precise determination of the contact force requires considering complex hyper-elastic properties of the rubber element located between falling mass and piston.

The comparison presented below concerns impact of the mass of 27,2kg with initial velocity 2,7m/s against double-chamber cylinder with initial pressure equal to 2,9atm and partially open valve.

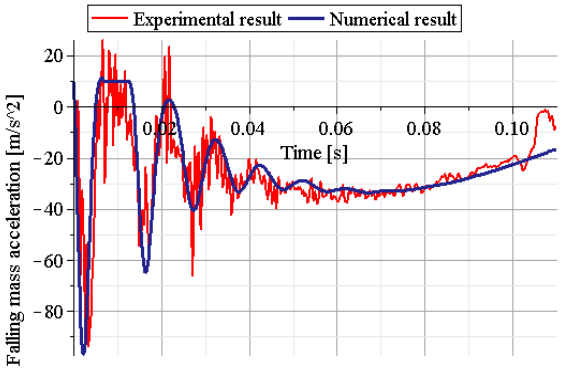

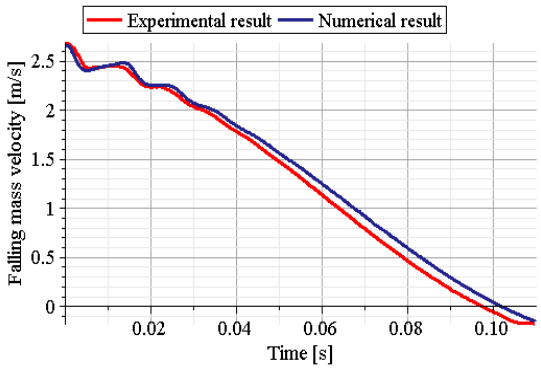

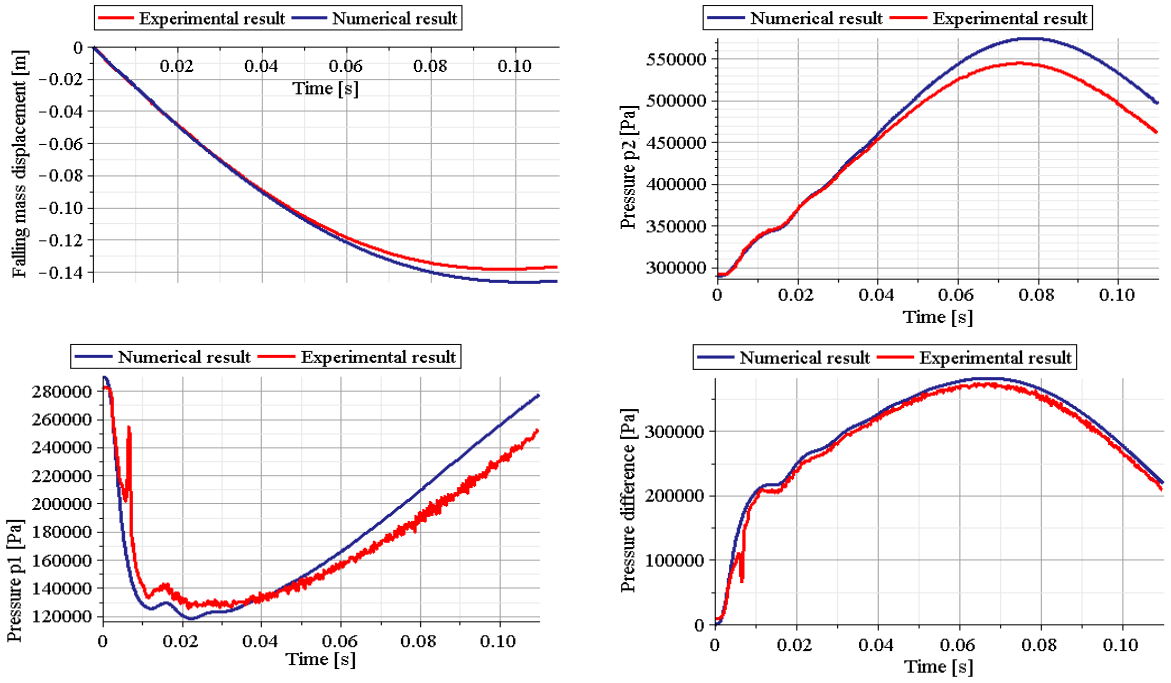

Fig. 3.4.6 Comparison of falling mass kinematics, pressure in both chambers and pressure difference obtained from the numerical analysis and from the experiment

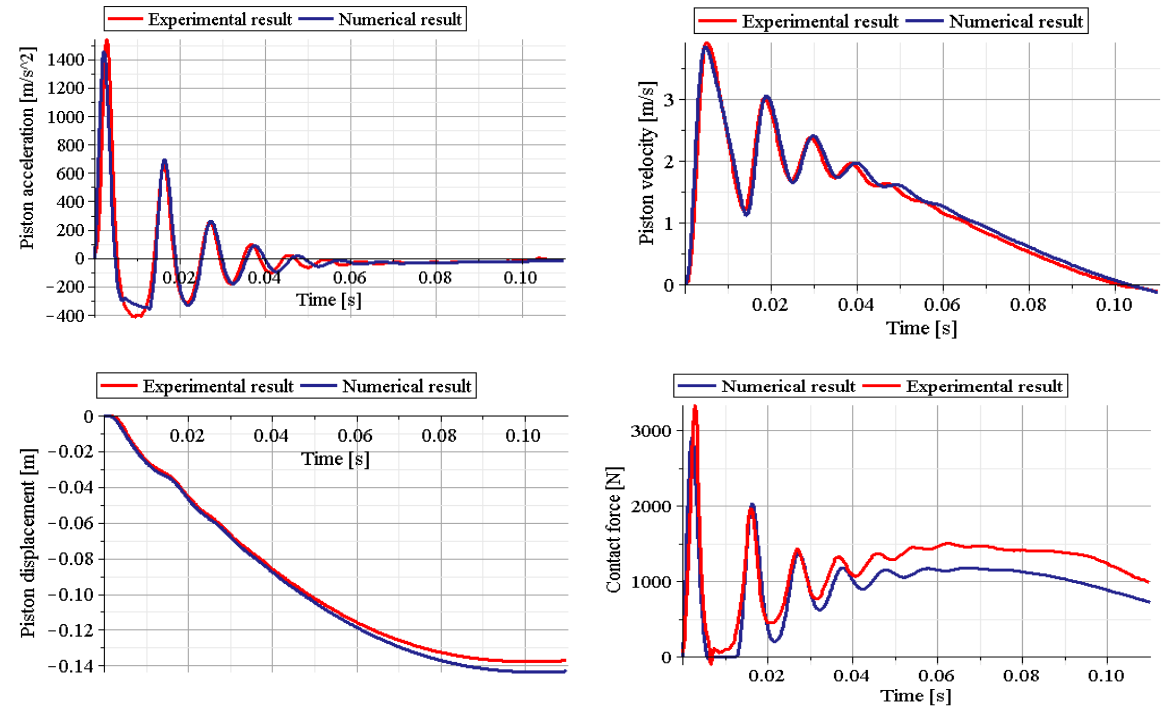

Fig.3.4.7. Comparison of piston kinematics and contact force obtained from the numerical analysis and from the experiment

Experimental implementation of the adaptive system

The final stage of the research was experimental testing of active adaptation strategy aimed at minimisation of pressure difference between the chambers. Such a goal of adaptation was not considered previously among proposed adaptation strategies; however, it is closely related to

minimization of force generated by the absorber (with the only difference that disparity in effective area of the piston in each chamber is disregarded). The adaptation strategy is, in a classical way, composed of initial step when pressure difference increases and the second step where pressure difference is maintained on a constant level. The second stage of the process is realized by simultaneous opening and closing of the valve (on/off strategy):

$$p_2(t) - p_1(t) < \Delta p^{opt} - \Delta_{tol} : \text{ valve closed} \qquad (3.4.1)$$

$$p_2(t) - p_1(t) > \Delta p^{opt} + \Delta_{tol} : \text{ valve open}$$

$$p_2(t) - p_1(t) - \Delta_{tol} < \Delta p^{opt} < p_2(t) - p_1(t) + \Delta_{tol} : \text{no change of valve opening}$$

which was chosen for experimental implementation due to its simplicity and robustness. The implementation of the active adaptation strategy was conducted by means of Labview system and Field Programmable Gate Array (FPGA) device[1]. The strategy described by Eq. 3.4.1 which utilizes pressure values to determine actual required valve possition was implemented by means of Labview system and further sent to the FPGA device. During the impact process FPGA device collected actual signals from pressure sensors in real-time and had sent the electric signal to the piezoelectric stack. As a consequence, the control strategy was executed in real time during the impact process.

For assumed impact scenario minimal pressure difference which could be maintained constant was equal 3,7atm due to limitations of maximal opening of the applied piezoelectric valve. Therefore, only part of the cylinder stroke was utilized and pressure difference was not optimally reduced, cf. Fig. 3.4.7. In semi-active adaptation strategy with constant valve opening used for the sake of comparison the maximal piston displacement was exactly the same as in case of active system. Let us note that in both cases the whole impact energy is not dissipated and both strategies result in partial rebound of the hitting object. Nevertheless, comparison of pneumatic force generated by the absorber in case of semi-active and active adaptation strategy (cf. Fig. 3.4.7) proves that active adaptation leads to a significant reduction of the pneumatic force generated by the absorber during impact and confirms the finality of applying real-time control.

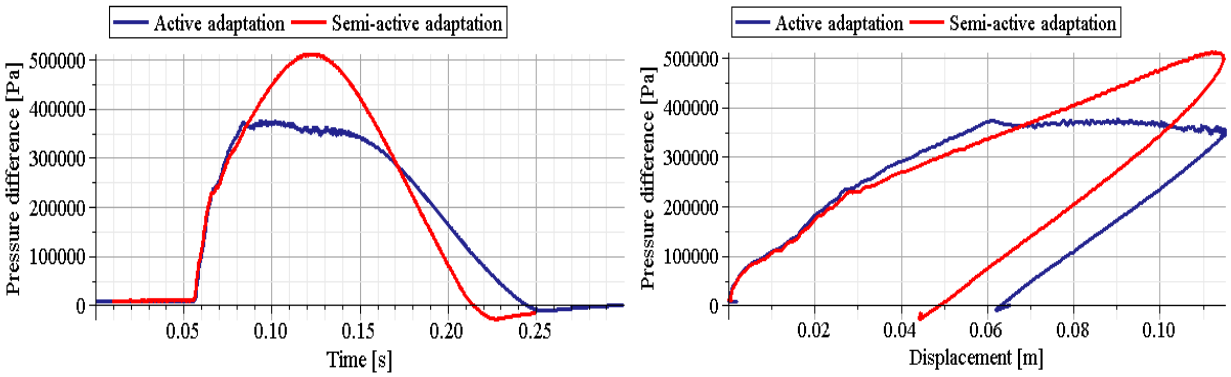

Fig.3.4.8. Comparison of experimental semi-active and active adaptation: a) pressure difference in terms of time, b) pressure difference in terms of displacement

[1] The control system was implemented by dr G.Mikułowski from IPPT PAN.

Summary of the Section 3.4

The section presents experimental verification of the concept of applying adaptive pneumatic cylinders with controllable valves for efficient dissipation of the impact energy. Both the system with controlled release of pressure to environment and the system with controlled flow between the chambers were analyzed. The results of the experiments conducted with the use of devices with constant valve opening were verified against previously developed numerical models. Finally, the controllable valve based on piezoelectric stack was used to execute the strategy of maintaining constant pressure difference during the impact process. The section proves that practical realisation of the real-time control of pneumatic force during the impact process is feasible and ultimately confirms the correctness of the concept of adaptive pneumatic cylinders.

CHAPTER 4 - CFD MODELS OF ADAPTIVE PNEUMATIC CYLINDERS

The current chapter constitutes direct continuation of the previous one since it also concerns modelling and control of the adaptive pneumatic cylinders. The intrinsic difference is that here we will consider these impact scenarios where Uniform Pressure Method can not be applied for description of gas enclosed within cylinder chambers. Instead, the proposed, more complex method of numerical analysis will be based on coupling of the Navier-Stokes equations describing the gas and the equation describing dynamics of the piston. Since the core of the method is numerical solution of the Navier-Stokes equations, which will be done conducted with the use of methods of Computational Fluid Dynamics, the developed models of pneumatic cylinders will be referred to as 'CFD models'.

The main feature of the CFD model is that it accounts for the wave propagation effects which occur inside pneumatic cylinders during impact. Such effects are evoked by two factors: i) movement of the piston after impact which causes local increase of pressure as an effect of gas compression, ii) opening of the valve which causes local decrease of pressure as an effect of gas outflow. Wave effects are important for global response of the system when time of impulse propagation along the cylinder (and consequently time of relaxation) is relatively long in comparison to the whole period of impact. Accordingly, the CFD model should be applied in case of impacts with relatively high initial velocity. By contrast, in case of impacts with small initial velocity, when the relaxation time is short in comparison to impact period, the application of CFD-based model instead of the UPM model is related to a much higher and unjustified numerical cost. On the other hand, the advantage of the introduced method is that it does not require preliminary determination of the analytical model of the gas flow through the valve which is a compulsory step of the UPM modelling.

Nowadays, the methods of computational fluid dynamics are widely applied in the process of design and optimisation of the shock absorbers. However, in most cases application of the CFD methods is aimed at examination of the particular components of the absorbers, not the whole devices. For example, in papers [264 265], numerical models are used to analyse flow of oil through various components and valves of hydraulic shock absorbers. The authors of [266] merge numerical simulations allowing to predict flow characteristics of the valves with simple dynamic model of the absorber in order to determine its global performance and damping characteristics. Moreover, in [267] combination of the computational fluid dynamics and analytical modelling of deformation of solid parts of the valve is utilized to simulate response of disc-spring valve system in hydraulic absorber. In more advanced papers [268] and [269], optimisation of a disc-spring valve system is performed with the use of coupled FSI model. Moreover, the simulation of flow developed inside active hydraulic absorber equipped with piezoelectric valve was conducted with the use of the ALE method in [240].

The chapter starts with the development of 2D model of a single-chamber adaptive pneumatic cylinder which utilizes the ALE approach for modelling of deforming fluid domain and exploits various techniques for modelling of the controllable valve. The model is compared with the UPM model and the influence of valve opening on dynamic response of the system is investigated. Moreover, two valve control strategies aimed at maintaining constant deceleration of the piston are developed. The following parts of the chapter pertain to

modelling and comparison of two types of double-chamber absorber, as well as, to brief discussion of the possibilities of application of other modelling methods such as CEL (fixed grid), purely Lagrangian and hybrid approach. In the last part of the chapter, modelling and control of 1D pneumatic system is considered.

4.1. Modelling and control of single-chamber systems

The CFD-based models of adaptive pneumatic cylinders can be obtained directly by reduction of the full models of Adaptive Inflatable Structures based on fluid-structure interaction approach. However, in case of pneumatic cylinders, deformation is limited to unidirectional compression caused by movement of the piston, which substantially simplifies description of the mechanical part of the coupled problem.

In order to develop the model of the system, solid part of the model Ω_S will be divided into two separate parts: cylinder walls and cylinder piston, $\Omega_S = \Omega_W \cup \Omega_P$. An arbitrary friction force will be applied between these two parts in order to account for the resistance which occurs during piston sliding. Due to the fact that deformation of cylinder walls and cylinder piston is small, its influence on the global response of the system can be neglected. Therefore, numerical analysis of the problem can be divided into two separate stages:

- determination of the global response of the system including movement of the piston and change of parameters of gas inside cylinder,
- calculation of internal forces generated inside cylinder walls.

In the first stage of solution cylinder walls are assumed to be fixed in space and equations describing their mechanical equilibrium are dissembled from numerical model of the system. Moreover, equations describing mechanical equilibrium of the piston are replaced by equation of the piston motion. It is assumed that during the process the transfer of heat through the walls of the piston and cylinder occurs so the equation of energy balance for the solid part of the system is taken into account. Moreover, the Navier-Stokes equations for the fluid part are considered in a full form. Consequently, during the first stage of numerical solution the system remains fully coupled from thermal point of view, however mechanical coupling is degenerated. After computation of cylinder pressure and piston displacement, as a second step of solution, strain and stress fields inside the cylinder walls and inside the piston can be determined. The second stage is not of interest and will be skipped in further considerations.

Pneumatic cylinders can be successfully modelled by using both Arbitrary Lagrangian Eulerian method and fixed grid method, however, for the sake of conciseness only ALE formulation will be precisely described below.

Modelling of single-chamber systems

Let us initially consider the model of pneumatic cylinder consisting of one pressure chamber Ω_F , solid walls Ω_W , piston Ω_P and an orifice of a constant diameter, cf. Fig. 4.1a. The equations governing solid part of the system during the first stage of the numerical analysis, i.e. equation of piston motion and energy conservation law formulated in the ALE frame of reference take the form, cf. Sec. 2.2.2:

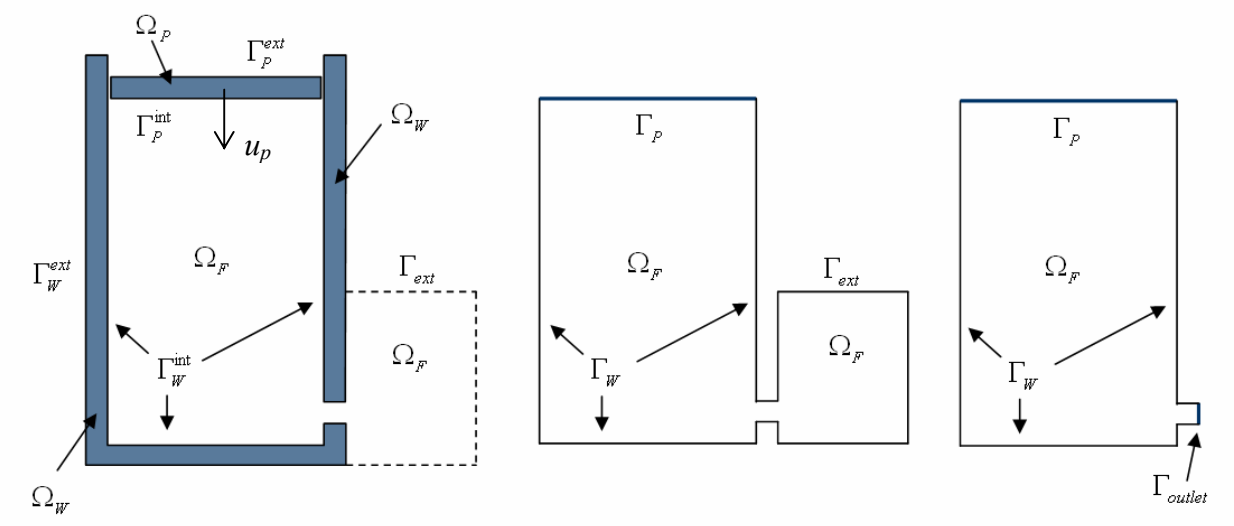

Fig. 4.1 CFD model of single-chamber pneumatic cylinder: a) with full modelling of heat transfer through cylinder walls, b) with isothermal or adiabatic walls, c) with isothermal and adiabatic walls and outlet boundary condition

$$M\frac{d^2u_P}{dt^2}+\int_A\left(\left(\boldsymbol{\sigma}_{\mathbf{f}}(\Gamma_P^{\text{int}})\mathbf{n}\right)\cdot\mathbf{n}-p_0\right)dA+F_{fr}=0 \qquad \text{at } \Gamma_P \tag{4.1.1}$$

$$\rho_{\mathbf{S}}\frac{\overline{D}}{\overline{D}t}(Je)=-\overline{\text{Div}}(J\mathbf{q}_{\mathbf{S}}\mathbf{F}^{-\mathbf{T}}) \qquad \text{in } \Omega_W\cup\Omega_P \tag{4.1.2}$$

In the above formulae M indicates mass of the impacting object and F_{fr} is friction force between the piston and cylinder walls which is, in general, an arbitrary function of piston velocity, its position in cylinder and internal pressure. In the considered model the energy conservation law (Eq. 4.1.2) concerns only internal energy e and neglects terms corresponding to internal stresses and internal energy production (cf. Eq. 2.2.60). The equation is written in general ALE form, however Jacobian J equals unity and thus Eq. 4.1.2 reduces to a simple heat transfer equation. Thermal boundary conditions have to be formulated at external boundaries of both cylinder walls and the piston:

$$T_S=\widetilde{T}_S \quad \text{or} \quad -\mathbf{q}_S\cdot\mathbf{n}=h(T_{ext}-T_S) \quad \text{on} \quad \Gamma_W^{ext}\cup\Gamma_P^{ext} \tag{4.1.3}$$

Balance equations for the fluid formulated in ALE frame of reference are the same as in general model of the inflatable structure:

$$\frac{\overline{D}(J_\chi\rho_{\mathbf{f}})}{\overline{D}t}+\overline{\text{Div}}\left[\rho_{\mathbf{f}}J_\chi\left(\mathbf{v}_{\mathbf{f}}-\frac{\partial\hat{\mathbf{u}}_{\mathbf{f}}}{\partial t}\right)\mathbf{F}_\chi^{-\mathbf{T}}\right]=0 \tag{4.1.4}$$

$$\frac{\overline{D}(\rho_{\mathbf{f}}J_\chi\mathbf{v}_{\mathbf{f}})}{\overline{D}t}+\overline{\text{Div}}\left[\rho_{\mathbf{f}}J_\chi\mathbf{v}_{\mathbf{f}}\otimes\left(\mathbf{v}_{\mathbf{f}}-\frac{\partial\hat{\mathbf{u}}_{\mathbf{f}}}{\partial t}\right)\mathbf{F}_\chi^{-\mathbf{T}}\right]=\overline{\text{Div}}\left[J_\chi\boldsymbol{\sigma}_{\mathbf{f}}{}^{\mathbf{T}}\mathbf{F}_\chi^{-\mathbf{T}}\right]+\rho_{\mathbf{f}}J_\chi\mathbf{f} \tag{4.1.5}$$

$$\frac{\overline{D}(\rho_{\mathbf{f}}J_\chi E_f)}{\overline{D}t}+\overline{\text{Div}}\left[\rho_{\mathbf{f}}J_\chi E_f\left(\mathbf{v}_{\mathbf{f}}-\frac{\partial\hat{\mathbf{u}}_{\mathbf{f}}}{\partial t}\right)\mathbf{F}_\chi^{-\mathbf{T}}\right]= \tag{4.1.6}$$

$$=-\overline{\text{Div}}\left[J_\chi\mathbf{q}_{\mathbf{f}}\mathbf{F}_\chi^{-\mathbf{T}}\right]+\overline{\text{Div}}\left[J_\chi(\boldsymbol{\sigma}_{\mathbf{f}}\mathbf{v}_{\mathbf{f}})\mathbf{F}_\chi^{-\mathbf{T}}\right]+\rho_{\mathbf{f}}J_\chi\mathbf{f}\cdot\mathbf{v}_{\mathbf{f}}$$

The gradient $\mathbf{F}_{\chi}^{-\mathrm{T}}$ and Jacobian J_{χ} for the fluid domain are not equal to corresponding quantities for the solid, however they typically assume simplified form due to unidirectional compression of the fluid domain. For the sake of precise modelling of the outflow of the gas through the orifice, a part of external region located in the vicinity of the orifice has to be modelled. Mechanical and thermal conditions at the boundary with the external region Γ_{ext} ('opening' boundary conditions) read:

$$\mathbf{v}_{\mathbf{f}} = \widetilde{\mathbf{v}}_{\mathbf{f}} \quad \text{or} \quad \boldsymbol{\sigma}_{\mathbf{f}}\mathbf{n} = -p^{ext}\mathbf{n} \quad \text{or} \quad \dot{m} = \widetilde{q}_V \quad \text{on} \ \Gamma_{ext} \tag{4.1.7}$$

$$T_{\mathbf{f}} = \widetilde{T}_{\mathbf{f}} \quad \text{on} \ \Gamma_{ext}$$

Boundary conditions concerning fluid velocity and thermal coupling conditions have to be formulated at internal boundaries of the cylinder walls:

$$\mathbf{v}_{\mathbf{f}} = 0 \quad \text{on} \ \Gamma_W^{\text{int}} \tag{4.1.8}$$

$$T_{\mathbf{S}} = T_{\mathbf{f}} \quad \text{and} \quad \mathbf{q}_{\mathbf{S}} \cdot \mathbf{n} = \mathbf{q}_{\mathbf{f}} \cdot \mathbf{n} \quad \text{on} \ \Gamma_W^{\text{int}}$$

where the first equality can be treated as boundary condition and it provides that fluid velocity is not altered by mesh motion. The second equality denotes thermal coupling condition. Similar conditions are formulated at the internal boundary of the piston, however various conditions are imposed on fluid velocity perpendicular $\mathbf{v}_{\mathbf{f}\perp}$ and parallel to the piston $\mathbf{v}_{\mathbf{f}\parallel}$:

$$\mathbf{v}_{\mathbf{f}\perp} = v_P, \quad \mathbf{v}_{\mathbf{f}\parallel} = 0 \quad \text{on} \ \Gamma_P^{\text{int}} \tag{4.1.9}$$

$$T_{\mathbf{S}} = T_{\mathbf{f}} \quad \text{and} \quad \mathbf{q}_{\mathbf{S}} \cdot \mathbf{n} = \mathbf{q}_{\mathbf{f}} \cdot \mathbf{n} \quad \text{on} \ \Gamma_P^{\text{int}}$$

Arbitrary equation governing mesh deformation inside fluid domain has general form:

$$\frac{\partial \hat{\mathbf{u}}_{\mathbf{f}}}{\partial t} = \mathbf{D}(\hat{\mathbf{u}}_{\mathbf{f}}) \quad \text{in} \ \Omega_f \tag{4.1.10}$$

but now $\mathbf{D}$ is differential operator which contains spatial derivatives in the direction of piston movement only. Boundary / coupling conditions for the field $\hat{\mathbf{u}}_{\mathbf{f}}$ defining deformation of the referential coordinate system read:

$$\hat{\mathbf{u}}_{\mathbf{f}\perp} = u_P, \quad \hat{\mathbf{u}}_{\mathbf{f}\parallel} = 0 \quad \text{on} \ \Gamma_P^{\text{int}} \tag{4.1.11}$$

$$\hat{\mathbf{u}}_{\mathbf{f}} = 0 \quad \text{on} \ \Gamma_{W\_bottom}^{\text{int}} \quad \text{and} \quad \hat{\mathbf{u}}_{\mathbf{f}\perp} = 0 \quad \text{on} \ \Gamma_{W\_latteral}^{\text{int}}$$

and cause that fluid mesh is compressed by movement of the piston and slides over horizontal walls of the cylinder. Finally, initial conditions for the fluid, cylinder walls, piston and displacement of the referential coordinate system are the following:

$$\rho_{\mathbf{f}}(0) = \widetilde{\rho}_{\mathbf{f}}, \quad \mathbf{v}_{\mathbf{f}}(0) = 0, \quad T_{\mathbf{f}}(0) = \widetilde{T}_{\mathbf{f}} \tag{4.1.12}$$

$$T_{\mathbf{S}}(0) = \widetilde{T}_{\mathbf{S}}, \quad T_P(0) = \widetilde{T}_P, \quad u_P(0) = 0, \quad v_P(0) = \widetilde{v}_P$$

$$\hat{\mathbf{u}}_{\mathbf{f}}(0) = \widetilde{\mathbf{u}}_{\mathbf{f}}$$

The above equations can be used for simulation of the response of passive pneumatic cylinder with constant valve opening subjected to an impact load.

The presented above numerical model of pneumatic cylinder can be simplified by neglecting modelling of heat transfer through cylinder walls (cf. Fig. 4.1b). Instead, walls of the cylinder can be assumed to be either isothermal or adiabatic. In such a case, the only equation governing solid part of the system is equation of piston motion:

$$M\frac{d^2u_P}{dt^2}+\int_A\left(\left(\boldsymbol{\sigma}_{\mathbf{f}}(\Gamma_P^{\text{int}})\mathbf{n}\right)\cdot\mathbf{n}-p_0\right)dA+F_f=0 \qquad \text{in } \Omega_P \tag{4.1.13}$$

Consequently, thermal boundary condition for the cylinder walls has to be omitted. Equations governing the fluid part of the problem (4.1.4-4.1.6), mechanical and thermal boundary conditions for external fluid region (4.1.7) and mechanical boundary / coupling conditions for internal fluid region (4.1.8a, 4.1.9a) are not altered. By contrast, thermal coupling conditions for the fluid (4.1.8b, 4.1.9b) are replaced by a simple boundary conditions indicating isothermal or adiabatic walls:

$$T_{\mathbf{f}}=T_{ext} \quad \text{on} \quad \Gamma_W\cup\Gamma_P \quad \text{for isothermal wall} \tag{4.1.14}$$

$$\mathbf{q}_{\mathbf{f}}\cdot\mathbf{n}=0 \quad \text{on} \quad \Gamma_W\cup\Gamma_P \quad \text{for adiabatic wall}$$

The initial conditions for cylinder walls, piston and fluid are the following:

$$\rho_{\mathbf{f}}(0)=\widetilde{\rho}_{\mathbf{f}}, \quad \mathbf{v}_{\mathbf{f}}(0)=0, \quad T_{\mathbf{f}}(0)=\widetilde{T}_{\mathbf{f}} \tag{4.1.15}$$

$$u_P(0)=0, \quad v_P(0)=\widetilde{v}_P$$

The model can be further simplified by avoiding modelling of external region of the cylinder and by superseding it with outlet boundary condition, cf. Fig. 4.1.c. Boundary conditions at outlet are related to mechanical part of the problem ('outlet boundary conditions') read:

$$\mathbf{v}_{\mathbf{f}}=\widetilde{\mathbf{v}}_{\mathbf{f}} \quad \text{or} \quad \boldsymbol{\sigma}_{\mathbf{f}}\mathbf{n}=-p^{ext}\mathbf{n} \quad \text{or} \quad \dot{m}=\widetilde{q}_V \quad \text{on} \quad \Gamma_V \tag{4.1.16}$$

The model of pneumatic cylinder with adiabatic/isothermal walls and model of pneumatic cylinder with simplified modelling of the outflow were implemented by using commercial CFD software ANSYS CFX. The results of numerical analyses will be presented in further part of this section and the comparison of the response of passive and adaptive cylinder subjected to impacts with high initial velocities will be performed.

Numerical examples presented in this section concern single-chamber pneumatic cylinder of dimensions: 30cm width, 60cm length, cf. Fig. 4.2a. For the sake of simplicity and computational efficiency the model is two dimensional. It contains only one layer of elements in the plane of the picture and utilizes symmetry boundary conditions applied on both front and back surfaces. Middle part of the bottom edge of the cylinder (of length 4cm) constitutes the valve which will be further used for controlled gas exhaust. When the valve remains closed, 'wall' boundary condition is prescribed at the location of outlet. By contrast, when the valve becomes open, the 'outlet' boundary condition is applied and external pressure, outflow velocity or mass flow rate of gas can be imposed.

In the preliminary analysis, pneumatic cylinder with the closed valve is subjected to kinematic excitation, i.e. prescribed piston displacement $d = 0{,}3m$ with constant velocity $V = 40\frac{m}{s}$. In order to simplify the system of governing equations isothermal conditions of the analysis ($T = 20C$) are assumed. The kinematic excitation is applied during transient CFD analysis as moving boundary problem. The referential coordinate system (and the computational mesh) is arbitrarily moving together with the piston at the upper boundary of the fluid domain, it is sliding along the horizontal cylinder walls and it is fixed at the bottom of the cylinder. Moreover, mesh stiffness inside fluid domain is controlled during the analysis and increased near boundaries or in the regions where it becomes strongly distorted.

Mechanical boundary conditions for the fluid are in agreement with the movement of the fluid domain boundaries. Fluid velocity equals piston velocity at the upper edge, it equals zero at the bottom edge and, moreover, no slip boundary conditions are assumed on cylinder walls. All the above conditions provide that the fluid is properly affected by piston motion and it is not dragged by motion of the mesh at the cylinder side-walls.

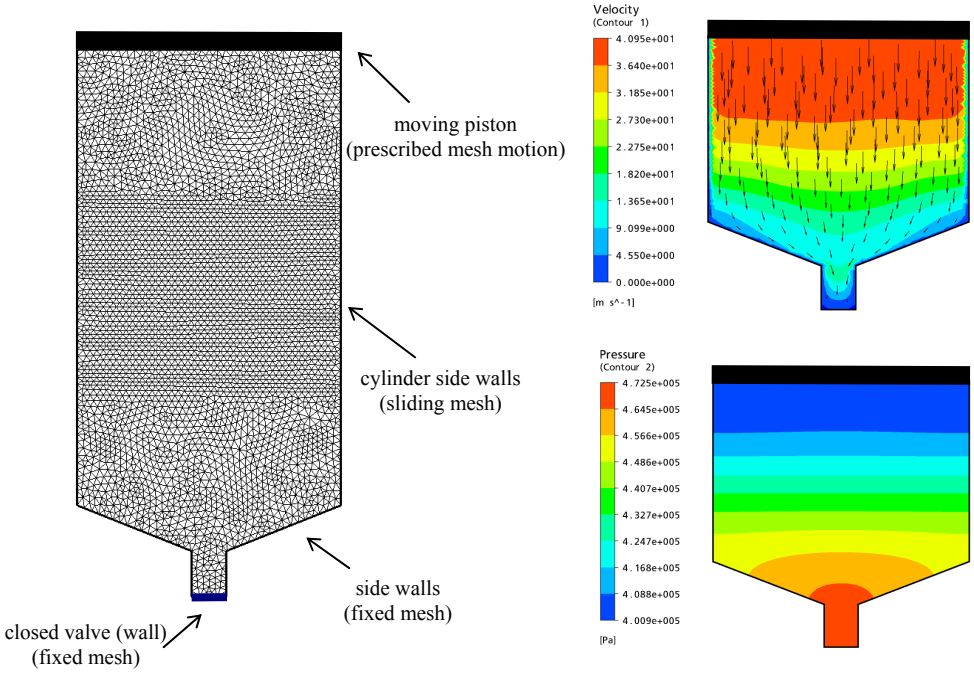

Fig. 4.2. Pneumatic cylinder with closed valve subjected to kinematical excitation:
a) numerical model of the system, b) fluid velocity distribution for d=0,3m and v=40m/s,
c) pressure distribution for d=0,3m and v=40m/s,

Results of the numerical analysis performed by means of Finite Volume Method are presented in Fig. 4.2.b. As a result of applied kinematic excitation and boundary conditions, fluid velocity ranges from 0m/s at the bottom and the side cylinder walls to 40m/s at the piston, cf. Fig. 4.2b. Applied excitation velocity of 40m/s is large enough to cause non-uniform distribution of pressure inside fluid domain. During the process of gas compression, the zones of higher pressure are moving from the top to the bottom of the cylinder and back and simultaneously the distribution of pressure inside cylinder becomes equalized. At the end of the process, when the piston reaches its final location, the relative difference of pressure equals 17,8%, see Fig. 4.2c.

In the following numerical analyses various velocities of kinematical excitation were applied in order to estimate the range of velocities for which the CFD modelling of the process is required. As it was expected, for relatively low excitation velocities (1-5m/s) the change of average pressure exerted on a piston resembles a force-displacement characteristics which is obtained with the use of uniform pressure method, cf. Fig. 4.3. Above this range of impact velocities, the influence of non-uniform pressure distribution is significant and it has to be taken into account during determination of average pressure (and force) acting on the piston. As the velocity of excitation increases, the initial range of constant pressure elongates and the value of initial constant pressure raises. Eventually, for the highest considered speed of excitation of 80m/s, the average pressure exerted on piston remains constant during the substantial part of the piston stroke and it increases only at the end of the process.

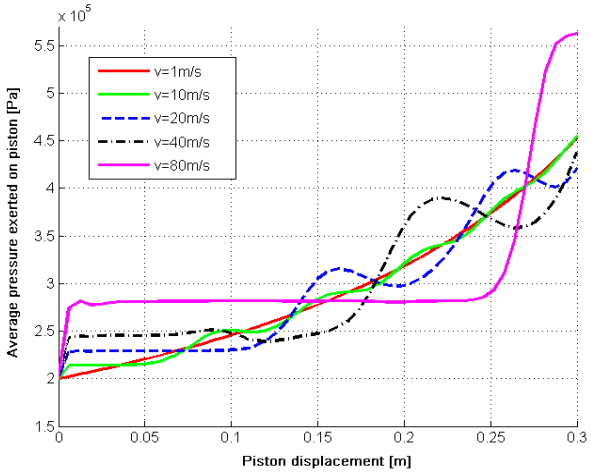

Fig. 4.3. Pneumatic cylinder with closed valve subjected to kinematic excitation: average pressure exerted on piston for various excitation velocities

The analysis was repeated after supplementing the model with the third Navier-Stokes equation governing balance of gas energy and assuming adiabatic walls of the cylinder. The results obtained from numerical simulation (pressure distribution inside cylinder and average pressure exerted on piston) were qualitatively similar to the results obtained from the isothermal model. However, final distribution of gas temperature was considerably non-uniform and moreover, the range of obtained temperatures was substantially lower than the one obtained from the analytic UPM-based model. The explanation stems from the fact that in case of uniform gas compression and closed valve almost no convection occurs. Thus, heat transfer is caused almost only by conduction which is slow with respect to total duration of the process.

In the next step, pneumatic cylinder was subjected to dynamic excitation, which in a simplified way models impact loading by assuming arbitrary mass of the hitting object and its initial velocity. In general, the dynamics of the piston is governed by equation of motion which involves forces generated by pneumatic absorber:

$$M\frac{d^2u}{dt^2} - Mg + \int_A \left(\left(\boldsymbol{\sigma}_{\mathbf{f}}(\Gamma_P)\mathbf{n}\right)\cdot\mathbf{n} - p_0\right)dA + F_{fr}(u,\dot{u},t) = 0 \tag{4.1.17}$$

$$\text{IC: } v(0) = v_0, \quad u(0) = 0$$

The subsequent terms of the above equation indicate inertia of the impacting mass, gravity force, force exerted on the piston by compressed gas and external pressure and friction force acting between piston and cylinder sidewalls. Discretisation of the above equation in time domain allows to derive a formula defining displacement of the mass in subsequent time instants of the process in terms of actual displacement, actual velocity and total force exerted on the piston:

$$u_{n+1} = u_n + v_n \Delta t - \frac{\int_A \left(\left(\boldsymbol{\sigma}_{\mathbf{f}} (\Gamma_P) \mathbf{n} \right) \cdot \mathbf{n} - p_0 \right) dA}{M} \Delta t^2 \tag{4.1.18}$$

In the above formula gravity and friction force were neglected as not being the main subject of the analysis. Actual displacement of the impacting mass can be determined at each step of the transient CFD analysis and introduced to the model as arbitrary movement of the fluid boundary. The above proposed simple procedure enables to perform simplified impact simulation within standard fluid dynamics software and it can be applied both for systems with closed valve, systems with constant valve opening and adaptive systems with controllable gas exhaust. The procedure was implemented in ANSYS CFX by using the CFX Expression Language (CEL).

In the initial numerical example the system with closed valve was considered. Single-chamber pneumatic cylinder was subjected to several impact scenarios of the same energy of 125J but various excitation velocities ranging from 1m/s to 80m/s. Since from the point of view of fluid the dynamic excitation can be treated as a special case of kinematic excitation, the fluctuations of average pressure acting on the piston during impact are similar as previously described.

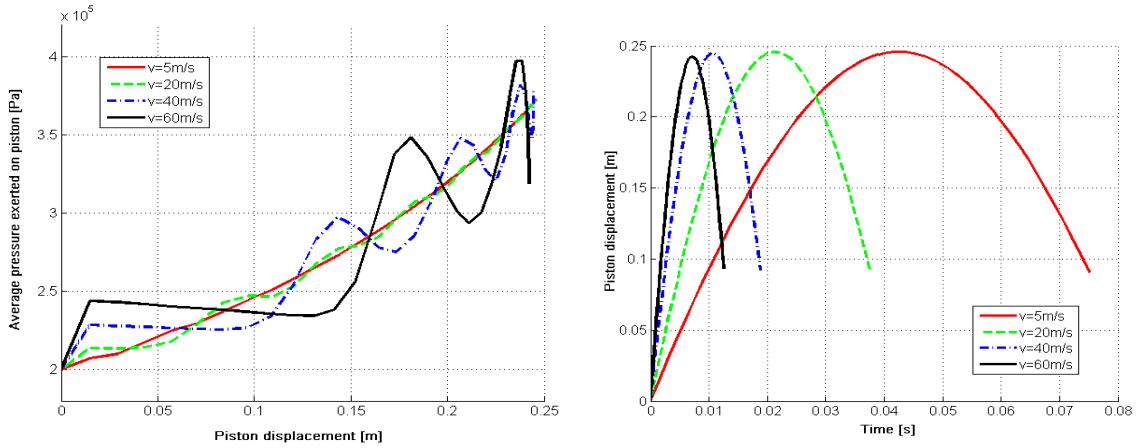

Fig. 4.4. Response of pneumatic cylinder with a closed valve to impacts of the same energy but various velocities: a) average pressure exerted on piston, b) time-history of piston displacement

For the impact velocities higher than ~20m/s average pressure exerted on piston clearly reveals the wave nature of the phenomenon. High excitation velocities result in oscillations of force exerted on piston during the process. In case of highest considered impact velocity the initial stage of the process when force acting piston remains almost constant is clearly visible, cf. Fig. 4.4a. Since the impact applied to the piston is in all cases characterised by the same energy it causes identical maximal displacement of the piston, Fig. 4.4b. The force exerted on piston expressed in terms of displacement is very similar for the forward-

stroke and backstroke which indicates that the influence of gas viscosity is relatively small and global characteristics of the system is close to elastic.

Adaptivity and control of single-chamber system

In general, all theoretical models of Adaptive Inflatable Structure with controllable valve introduced in Sec. 2.2.3 (model based on boundary condition control, orifice width control and valve head control) can be applied for modelling adaptive pneumatic cylinders. Two of these models, i.e.:

- the model based on change of value of b.c. imposed at outlet and
- the model based on combination of change of the orifice width and outlet size.

were selected to be applied for simulation of the controllable valve in adaptive single-chamber cylinder. In both above cases the lack of continuum modelling of the solid walls simplifies the numerical implementation since it eliminates the inexactness of modelling solid body in the vicinity of the outlet, caused either by introduction of artificial boundary condition or introduction of additional, non-physical stresses, cf. Sec. 2.2.3.

The model based on arbitrary change of value of imposed boundary condition at outlet is the most convenient for numerical implementation since it does not require any changes in topology of the model of the pneumatic cylinder. In general, three types of boundary conditions can be imposed at outlet: external pressure, outflow velocity or mass flow rate of gas. Change of external pressure is an artificial condition which can not be executed in practice and thus the method was not implemented. By contrast, change of the outflow velocity and change of mass flow rate at outflow can be obtained as a result of the valve operation and thus such a modelling method can be treated as acceptable simplification of the real situation. Regarding the model based on change of the orifice width, its implementation is also facilitated since required change of topology concerns only the fluid domain.

Since the considered CFD model of the pneumatic cylinder is based on discretisation of the domain and numerical solution of the Navier-Stokes equations, it remains relatively complicated. Therefore, the analysis of adaptive system will not be as comprehensive as for the UPM-based model. Instead, it will be limited to investigation of the influence of controlled gas exhaust on pressure distribution and a single control objective of maintaining preliminarily assumed constant level of piston deceleration.

Preliminary **numerical example** presents the influence of outlet boundary condition on response of pneumatic cylinder subjected to dynamic excitation (E=125J, V_0=50m/s). Central part of the cylinder bottom, which constitutes the valve, was replaced by subsonic outlet where arbitrary mass flow rate of gas or, alternatively, outlet velocity was imposed. Initially, constant value of applied boundary condition during single numerical analysis was assumed. In subsequent numerical analyses the value of imposed outlet boundary condition was increased and its qualitative influence on pressure distribution and fluid velocity at time instant of stopping the piston was observed, Fig. 4.5. As expected, outflow of the fluid caused reduction of a mean value of pressure inside the cylinder and larger difference of pressure between top and bottom wall. Moreover, imposing constant mass flow rate of gas and constant outflow velocity at outlet resulted in different distribution of fluid pressure and velocity inside the cylinder, Fig. 4.5.

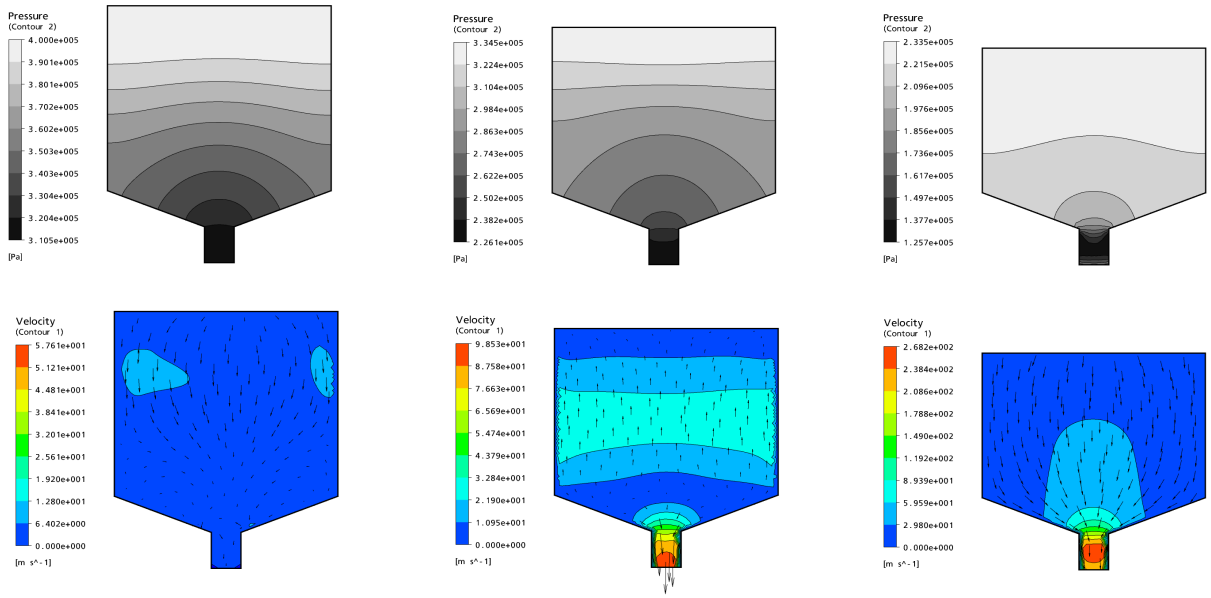

Fig. 4.5. Qualitative influence of outlet boundary condition on pressure and fluid: a) closed valve, b) influence of mass flow rate 0,1kg/s, c) influence of outflow velocity 240m/s

The quantitative influence of outlet boundary condition on global response of the system is reflected by change of average pressure exerted on piston and change of piston displacement during the process, Fig. 4.6. When outflow of gas is performed the oscillations of the average value of pressure still arise, however they are mitigated together with the decrease of mass of gas inside cylinder. As a result of interaction of two contradictive processes (compression of gas chamber causing pressure increase and gas release causing pressure reduction) maximal value of average pressure does not occur at maximal piston displacement but in the middle of the piston stroke.

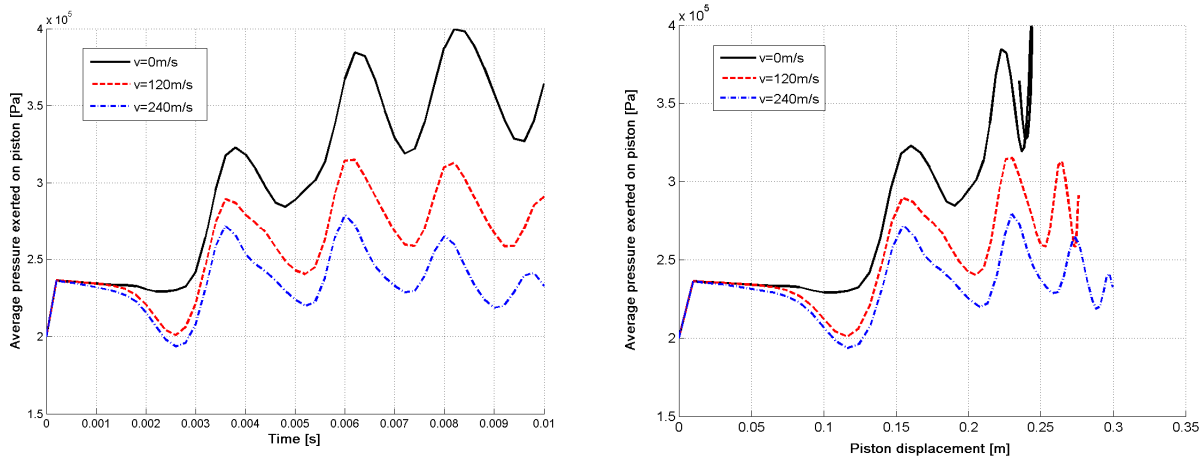

Fig. 4.6. Quantitative influence of mass flow rate of gas imposed at outlet on average pressure exerted on the piston: a) average pressure in terms of time, b) average pressure in terms of displacement

As a result of pressure release, maximal displacement of the piston increases and its deceleration simultaneously decreases. Unfortunately, large displacement of the piston causes large deformation of the finite volume mesh which results in difficulties with convergence of the numerical solution and possible termination of the analysis. The problem was solved by: i)

precise control of the mesh stiffness during numerical analysis, ii) multiple remeshing of the fluid region during numerical analysis when mesh becomes distorted and mapping of the solution into new mesh; nevertheless the satisfactory results were not always obtained.

More sophisticated numerical example concerns adaptive pneumatic cylinder in which feedback control system is implemented in order to change outflow of the fluid depending on actual response of the system. The cylinder is subjected to dynamic excitation caused by arbitrary mass applied with initial velocity. During dynamic analysis, boundary condition applied at outlet is changed depending on the actual value of piston deceleration. The difficulty in modelling feedback systems is the requirement of coupling of the particular input of the system (in this case value of the outlet boundary condition) and actual results of the numerical analysis. Models of the adaptive pneumatic cylinder with feedback control were implemented in two ways:

- by utilising CFX Expression Language (CEL) in a similar manner as it was done for updating position of the piston during dynamic analysis,
- by linking CFX with MATLAB and by performing multiple automatic restarts of the CFD analysis.

Due to the fact that the latter option provides more flexibility in further development of the control strategies, it was applied for developed numerical models. MATLAB was used to initialise data for the CFD analysis, to generate input file, run CFD simulation and, finally, to read selected results. Further, the input parameters were changed accordingly and numerical analysis was restarted by using previously obtained results as the initial conditions for continued analysis. Eventually, proposed methodology of simulation of adaptive pneumatic cylinder subjected to impact load differs from the typical CFD analysis in two manners: i) CEL is used to update position of the piston and ii) MATLAB is used to change value of outlet b.c. during analysis according to assumed adaptation strategy.

The following task in simulation of adaptive pneumatic cylinders is development of the control strategy, i.e. finding change of the outflow velocity at outlet during the impact process which minimises certain objective function. In considered example, the purpose of the control strategy is to obtain desired change of piston acceleration which involves two stages:

i) initial increase of deceleration to a predefined level while closed valve,
ii) maintaining piston deceleration at constant predefined level.

Thus, mathematically the control problem relies on finding control function (fluid velocity at outlet $\mathbf{v}_f$) which minimises difference between optimal and obtained piston acceleration:

$$\text{Find } \mathbf{v}_f(\Gamma_V, t) \text{ such that } \int_{t_x}^{t_{end}} [a_{opt}(t) - a(t)]^2 dt \text{ is minimal} \tag{4.1.19}$$

where t_x indicates time instant when desired decceleration is achieved. In order to simplify the problem the outflow velocity was assumed to be perpendicular to the outlet boundary and to be uniformly distributed along the outlet. The above assumptions reduce vector function of space and time $\mathbf{v}_\mathrm{f}(\Gamma_V, t)$ to a scalar function of time $v_f(t)$.

Since the problem is of transient type the control is performed at the several subsequent time intervals (control steps) during which outflow velocity v_f remains constant.

The main prerequisite for development of the control algorithm is a substantial delay which occurs between change of outflow velocity and change of force exerted on piston. In proposed control algorithm the length of the control step Δt_C is approximately equal to maximal time interval when the influence of outflow velocity on force exerted on piston is still not observed. Although this time interval depends on actual cylinder stoke and internal pressure (and thus it changes during impact), for the sake of simplicity constant averaged length of all control steps $\Delta t_C = 1ms$ was assumed. Apart from the control steps of duration Δt_C, the algorithm utilizes the concept of 'predictive analyses' of duration $2\Delta t_C$, which precede each control step and which are aimed either at predicting future value of generated force or determination of the proper value of applied outflow velocity, Fig. 4.7a,b.

The process of impact starts with passive stage (Stage I) when the valve remains closed (v_f=0) in order to achieve fast increase of pneumatic force and piston deceleration to desired level. During this stage 'predictive analyses' are performed in order to detect time instant, when pneumatic force achieves required value, with an appropriate advance. The second stage of impact commences at discrete time instant being starting point for predictive analysis in which optimal value pneumatic force is exceeded (F_{pist}>F_{opt}).

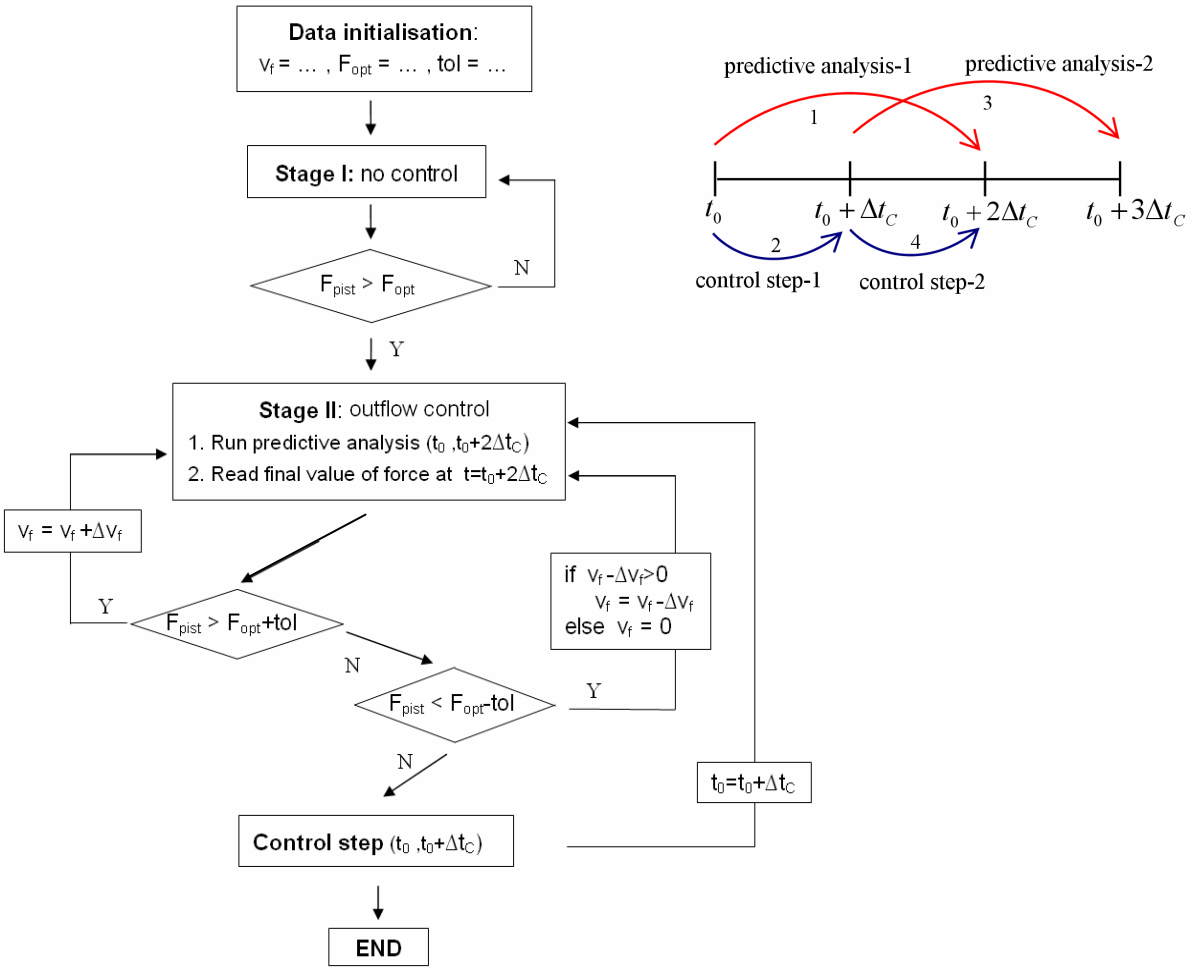

Fig. 4.7. a) Scheme of numerical procedure for controlling force generated by absorber (and piston acceleration), b) the concept of predictive analysis utilized in a control algorithm

In the active stage of impact (Stage II) the first predictive analysis utilizes predefined nonzero trial value of the outflow velocity v_f in order to determine change of pneumatic force

at time interval $\langle t_0, t_0 + 2\Delta t_C \rangle$. The simple algorithm for finding the optimal outflow velocity is based on comparison of force F_{pist} obtained at time instant $t_0 + 2\Delta t_C$ with arbitrary assumed optimal value F_{opt}. If obtained force is located outside assumed tolerance range, the correction of the outflow velocity is introduced and the 'predictive analysis' is repeated at the same time interval. By contrast, if pneumatic force fits the tolerance range, the value of outflow velocity is used to perform the control step at time interval $t_0 + \Delta t_C$. The considered first control step provides proper value of piston acceleration a time instant $t_0 + 2\Delta t_C$.

The next predictive analysis, performed at time interval $\langle t_0 + \Delta t_C, t_0 + 3\Delta t_C \rangle$, serves for determination of the outflow velocity during the second control step $\langle t_0 + \Delta t_C, t_0 + 2\Delta t_C \rangle$ and value of pneumatic force at time instant $t_0 + 3\Delta t_C$. Thanks to proper choice of Δt_C, the second control step does not alter value of force at time $t = t_0 + 2\Delta t_C$. The whole procedure is repeated for the subsequent control steps, cf. Fig. 4.7.

The results of application of the proposed control algorithm in case of the impact of energy E=125J and velocity V_0=50m/s are presented in Fig. 4.8a,b. Active stage of impact starts at time instant t_0=5ms. Imposing nonzero outflow velocity at initial control step (5-6ms) does not change pneumatic force within this time interval, however it allows to decrease value of force in the following one (6-7ms). Sudden increase of the outflow velocity for three further control intervals (6-9ms) and its gradual decrease (9-12ms) allow for maintaining constant value of total pneumatic force during substantial part of the process. The control procedure is able to keep constant value of force level as long as gas is compressed. When rebound of the piston starts (t=12ms) the value of pneumatic force decreases despite the fact that the valve is closed. Maintaining constant level of force would require gas inflow which, however, in considered case of impact absorption is purposeless.

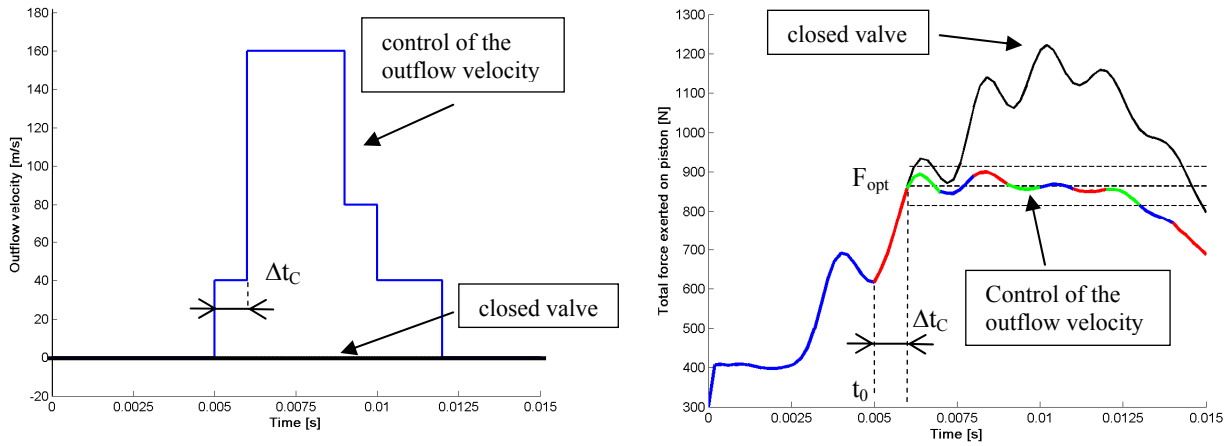

Fig. 4.8. Control of piston acceleration by changing outflow boundary condition:
a) applied change of outflow velocity b) resulting acceleration of the piston

Another possible approach to development of a control algorithm for fast impact scenarios is based on preliminary assumption of the algorithm developed for the UPM approach and further introduction of additional modifications in order to eliminate the influence of wave effects. This methodology is expected to be better suited for the impacts for which the UPM modelling gives similar results as full CFD modelling (range of impact velocities 20-40m/s).

Different method of modelling of controlled outflow from adaptive pneumatic cylinder is based on changing width of the orifice, where outflow of the fluid occurs and simultaneous changing size of the outlet where the outflow boundary condition is imposed, Fig. 4.9. Thus the method can classified as junction of 'boundary condition control' and 'orifice width control', Sec 2.2.3. The method is more complex than the change of outlet boundary condition value since changing the orifice width within the ALE approach requires introducing additional moving boundaries in the fluid domain, Fig.4.9. Therefore, in considered model the movement of the finite volume mesh is prescribed not only at the location of the piston (as it was in previous case) but also at walls adjacent to the outlet. Moreover, in case of adaptive systems, movement of the orifice walls will depend on actual results of the numerical analysis.

The orifice can be modelled and discretized by two methods:

- Single fluid domain embracing cylinder region and orifice region can be defined. During the movement of the orifice walls in inner direction, the outlet is narrowed and interior parts of the bottom cylinder wall simultaneously extend. During the process topology of the mesh is preserved, cf. Fig. 4.9a
- Separate fluid domain for the cylinder and the orifice regions can be defined and an interface between these two regions can be established. During movement of the orifice walls the outlet shrinks and part of the interface is simultaneously changed into the wall of the fluid domain (change of the b.c. type occurs). The mesh slides on the interface between cylinder and orifice region, cf. Fig. 4.9b.

The disadvantage of the first method is that the cylinder mesh may become strongly distorted in the vicinity of the orifice, single element of the cylinder region is significantly expanded and several elements are narrowed. The distortion of the orifice mesh also occurs, however it can be provided that the mesh is deformed in almost uniform manner. On the other hand, in the second method the cylinder mesh is not altered, however the discrepancies and numerical errors during sliding of the mesh at the interface between two regions are probable to occur.

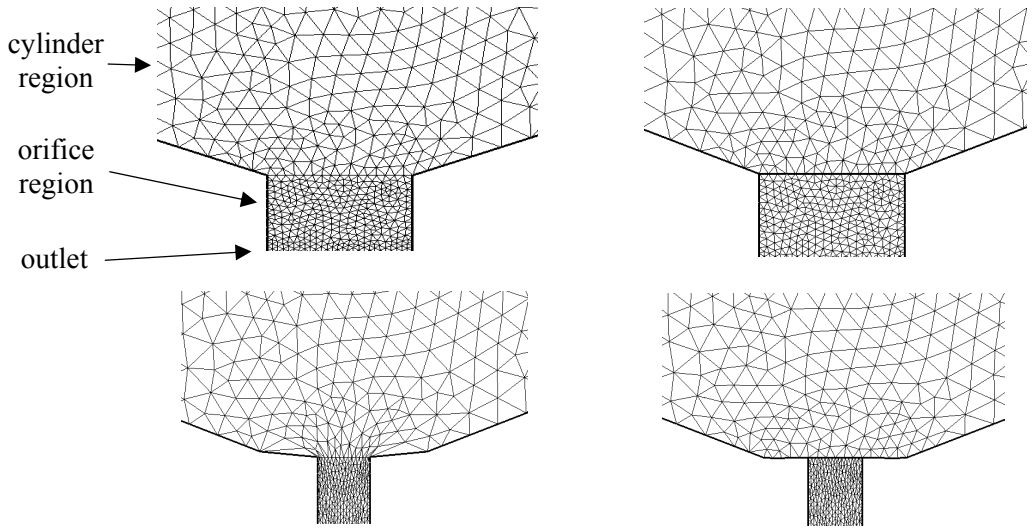

Fig. 4.9. Comparison of two methods of changing orifice width: a) initial computational mesh, b) distorted computational mesh after changing the orifice width

An alternative for application of the outlet boundary condition of variable size is modelling of the external fluid region in the vicinity of the outlet and imposing 'opening' boundary condition at the boundaries of this region, cf. Fig. 4.10b. Modelling of the orifice region can be performed by two above introduced methods, i.e. using single fluid domain and using separate regions with interfaces (cf. Fig. 4.9). When the second option of modelling is used, an additional interface between the orifice region and the external region has to be defined. When external region is modelled, the outflow of the fluid is controlled directly by change of the width of the orifice region located between internal and external fluid domains and the method can be classified as 'orifice width control'. Modelling of the controllable outflow from cylinder with the use of external region instead of outlet boundary condition reduces the difficulties related to convergence of the numerical solution due to smooth change of the pressure and velocity fields in considered domain.

Since the methods based on changing the size of outlet and the method based on changing the width of the orifice simulate the same physical phenomenon, they were compared against each other to confirm the equivalence of both methods of modelling. In the numerical example the cylinder was subjected to dynamic excitation and an arbitrary change of outlet size/orifice width was assumed. Due to the fact that satisfactory correspondence of the numerical results in terms of pressure and velocity distribution was obtained, the model with the outlet boundary condition was selected to be applied in further simulations as being more computationally effective due to a reduced number of degrees of freedom.

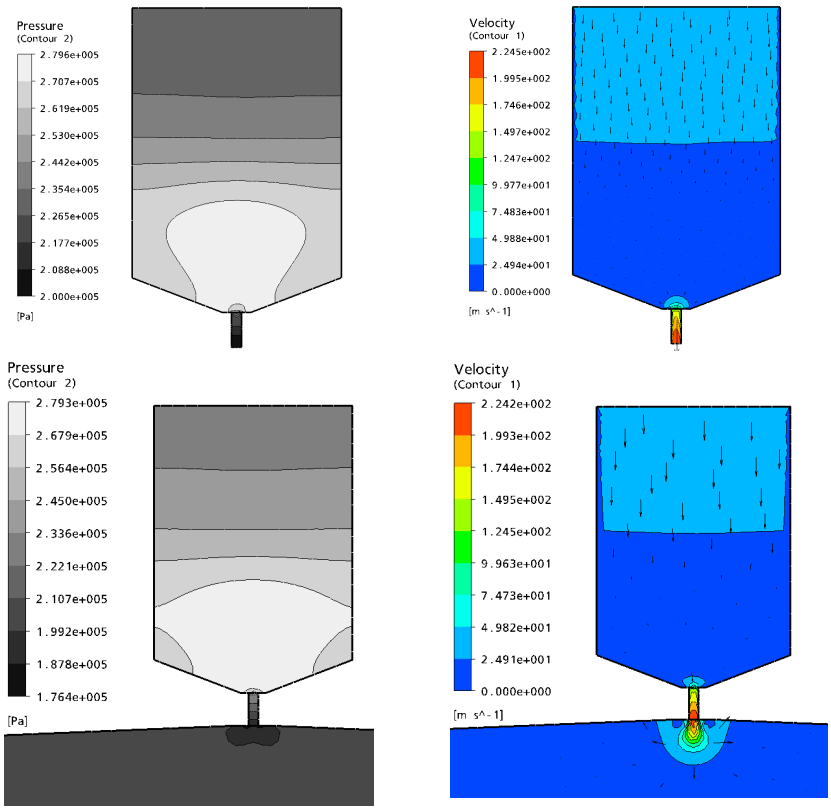

Fig. 4.10. Comparison of numerical results obtained by using simplified model with outlet boundary condition and full model with orifice between cylinder and environment

As a next step, a procedure of controlling orifice/outlet width aimed at obtaining arbitrarily assumed change of piston deceleration was developed. Mathematically, the problem was formulated similarly as in case of outflow velocity control (cf. Eq. 4.19). The present control problem is to find change of size of the outlet during the process which minimizes time integral of difference between assumed and obtained piston deceleration:

$$\text{Find } \left|\Gamma_V(t)\right| \text{ such that } \int_{t_x}^{t_{end}} [a_{opt}(t) - a(t)]^2 dt \text{ is minimal} \tag{4.1.20}$$

where the norm $\left|\ \right|$ indicates the length of the of the part of the boundary where outlet b.c. is defined. Since sudden change of the outlet size may cause numerical errors or convergence difficulties, continuous modification of the outlet size is the preferable method of control. It will be obtained by replacing control variable $\left|\Gamma_V(t)\right|$ indicating actual width of the orifice, and by control variable v_{or} indicating velocity of the orifice wall perpendicular to the outlet.

The first stage of the process (Stage I) is aimed at initial increase of the acceleration level with the closed valve. During this stage maximal size of the outlet is assumed, however outflow of the gas does not occur since boundary condition denoting the 'wall' is applied at the location of outlet. At the end of passive stage, when desired value of piston deceleration is detected by predictive analysis, 'wall' boundary condition is removed and external pressure is imposed at outlet and the valve becomes fully open.

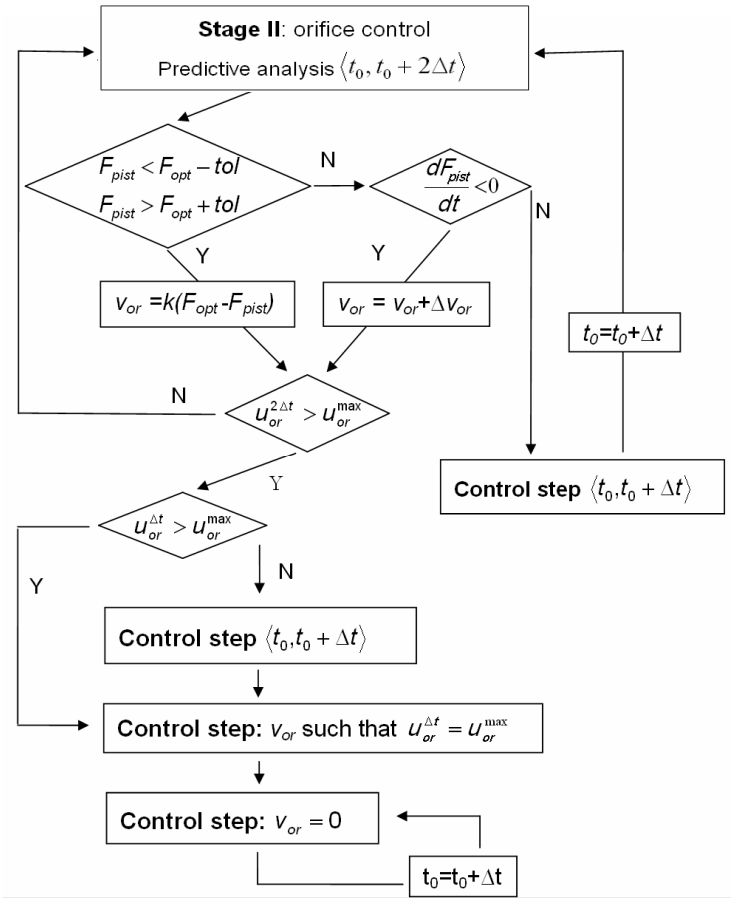

Fig. 4.11. Scheme of a procedure for controlling piston deceleration by changing outlet size

During the second stage of the process (Stage II) velocity of the orifice wall is controlled in order to fulfil assumed control objective and to maintain constant level of generated pneumatic force and piston deceleration (Fig. 4.11). Similarly as in case of outflow velocity control, the active stage of impact contains subsequent steps of predictive analysis followed by control steps of a half shorter duration, cf. Fig. 4.7b.

Preliminarily assumed size of the outlet is relatively large, it causes fast stabilisation of total force exerted on piston and its further decrease. Therefore, the control procedure is aimed at reduction of the orifice width which is counteraction to excessive drop of pressure and decrease of force acting on the piston. In a control procedure the feedback is established between velocity of the orifice walls and pneumatic force exerted on piston.

If pneumatic force obtained at the end of the predictive analysis is outside the range of force tolerance, speed of orifice walls (directed inside) is changed proportionally to the difference between optimal and actual force value. Thus, the algorithm provides that speed of outlet size reduction increases when obtained force is too low and vice versa. If total force is located within tolerance level but its value decreases, the valve speed is increased by an arbitrary value. The last part of the procedure (lower part of the scheme in Fig. 4.11) is related to final part of the process. When updated valve velocity causes that displacement of the orifice walls at the end of predictive step $u_{or}^{2\Delta t}$ is larger than maximal allowable value $u_{or}^{\max}$, one or two control steps leading to minimal size of the outlet are performed and zero velocity is assumed in a further part of the process.

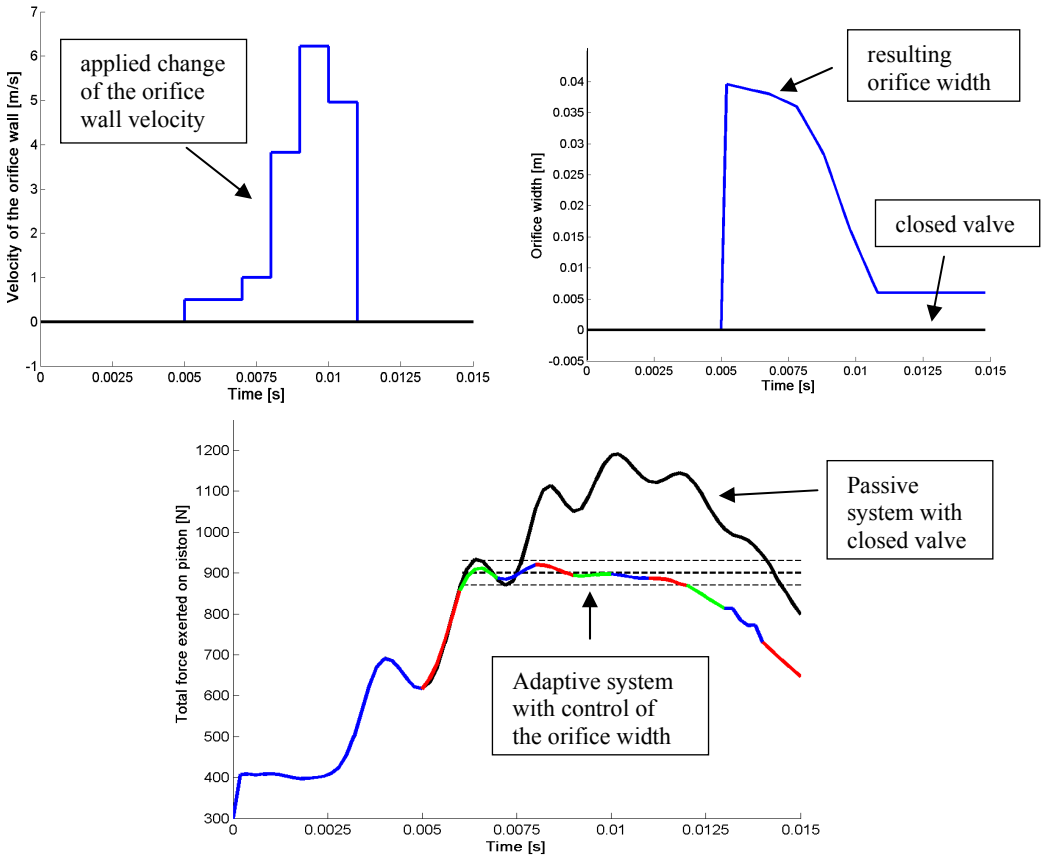

Fig. 4.12. Control of piston deceleration by changing size of the outlet: a) applied velocity of the orifice wall, b) change of the orifice width, c) resulting force exerted on piston

Similarly as in case of system controlled by outflow velocity, the control system applied herein allows to reduce total value of force exerted on piston and to maintain it on a constant level during the second part of impact, before the rebound occurs, cf. Fig. 4.12c. The velocity of the orifice wall determined from the control algorithm permanently remains positive (Fig. 4.12a) which indicates that orifice width is gradually decreasing during active stage the process (Fig. 4.12b) and the valve is being gradually closed. Such a control scheme corresponds to the results obtained in previous example where optimal outflow velocity was initially maintained on a high level and was gradually reduced during the second part of the active stage of impact, cf. Fig. 4.8a.

Modelling of modified versions of pneumatic cylinders

The above modelling and control considerations concern the simplest possible adaptive pneumatic cylinder with exhaust to the external environment. However, two basic modifications of the system topology can be made. First of all, the system can be equipped with additional closed chamber located above the piston. Since controlled gas inflow or outflow to this chamber does not occur, its simulation is straightforward. The chamber can be modelled by introducing an additional fluid region, with one moving boundary, governed by the classical Navier-Stokes equations with appropriate boundary conditions. The additional closed upper chamber was omitted in the CFD model of pneumatic cylinder since its influence on general scheme of the proposed control algorithms is subsidiary.

At second, the gas from the chamber below the piston, instead of being released to environment, can be released to a closed fixed volume chamber which serves for accumulation of the compressed gas for future usage. The CFD modelling of system with exhaust to accumulator differs from full modelling of the system with exhaust to environment only by definition of boundary conditions for the external fluid region. Namely, the conditions defining external pressure have to be replaced by conditions defining wall of the chamber. Moreover, the outflow to additional chamber can not be modelled by means of outlet boundary condition with imposed external pressure since distribution of pressure inside accumulator during the process is not a priori known.

The detailed comparison of dynamic response of passive and adaptive pneumatic cylinders of various designs was presented in Chapter 3 dedicated to the UPM-based approach.

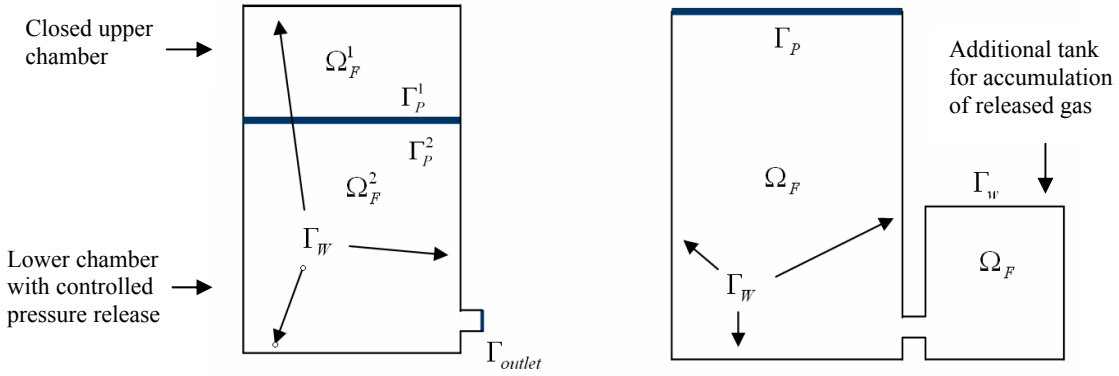

Fig. 4.13. Models of modified versions of adaptive pneumatic cylinder: a) with an additional upper chamber above the piston, b) with an outflow to a fixed volume chamber (accumulator)

4.2. Modelling of double-chamber systems

The systems which contain two pressure chambers and a controllable valve allowing for controlled gas flow between the chambers will be analysed separately since they involve particular differences in modelling methodology.

Let us initially consider the complete model of double-chamber pneumatic cylinder with the orifice of a constant width located inside the piston, Fig. 4.14a. Due to the fact that in ALE approach the topology of the considered system has to be preserved, it will be assumed that the orifice allowing for the flow of the fluid between the chambers always exists, however it can be reduced to a small size such that the flow of the fluid is almost totally blocked. Basic assumptions for modelling of the system will be similar as in case of single-chamber cylinder. In the first step of the analysis, external walls of the cylinder will be assumed to be fixed in space and piston will be treated as a rigid body with one degree of freedom. Dynamics of the piston is governed by equation of motion similar to Eq. 4.1.1 but without the term indicating influence of external pressure:

$$M\frac{d^2u_P}{dt^2}+\int_A\left(\boldsymbol{\sigma}_{\mathbf{f}}(\Gamma_P)\mathbf{n}\right)\cdot\mathbf{n}dA+F_f=0 \qquad \text{at } \Gamma_P \tag{4.2.1}$$

Moreover, transfer of heat through cylinder walls and through the piston is described by equation identical to Eq. 4.1.2. Corresponding thermal boundary conditions for the solid region are formulated only at the external wall of the cylinder and read:

$$T_S=\widetilde{T}_S \quad \text{or} \quad -\mathbf{q}_S\cdot\mathbf{n}=h(T_f-T_S) \quad \text{on} \quad \Gamma_W^{ext} \tag{4.2.2}$$

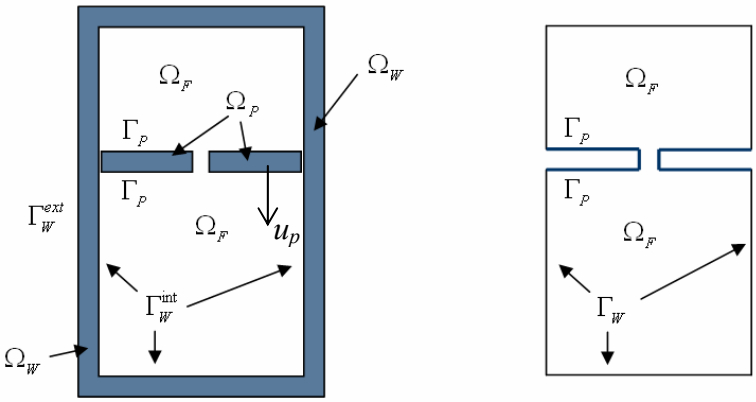

Fig. 4.14. CFD model of double-chamber chamber pneumatic cylinder: a) including modelling of heat transfer through cylinder walls, b) with isothermal or adiabatic walls

The methodology of modelling both chambers of the cylinder as a single fluid domain provides that fluid contained inside cylinder can be described by single set of the Navier-Stokes equations (4.1.4-4.1.6). Despite the fact that topology of double-chamber system differs substantially from the topology of single-chamber system, coupling conditions between fluid and solid formulated at cylinder walls (4.1.8) and at piston (4.1.9) remain valid. The only substantial difference in comparison to a single-chamber cylinder arises in the

definition of coordinate system deformation. Differential equation governing mesh deformation remains the same as previously:

$$\frac{\partial \hat{\mathbf{u}}_{\mathbf{f}}}{\partial t} = \mathbf{D}(\hat{\mathbf{u}}_{\mathbf{f}}) \quad \text{in } \Omega_f \tag{4.2.3}$$

However, boundary conditions are defined at the top and bottom of the piston, at top and bottom cylinder walls and at lateral cylinder walls:

$$\hat{\mathbf{u}}_{\mathbf{f}\perp} = u_P, \quad \hat{\mathbf{u}}_{\mathbf{f}\parallel} = 0 \quad \text{on } \Gamma_P \tag{4.2.4}$$

$$\hat{\mathbf{u}}_{\mathbf{f}} = 0 \quad \text{on } \Gamma^{\text{int}}_{W\_bottom} \cup \Gamma^{\text{int}}_{W\_top} \quad \text{and} \quad \hat{\mathbf{u}}_{\mathbf{f}\perp} = 0 \quad \text{on } \Gamma^{\text{int}}_{W\_latteral}$$

The above equations remain valid when width of the orifice changes during numerical analysis. Finally, initial conditions formulated for solid and fluid bodies have the same form as in case of single-chamber system (cf. Eq. 4.1.12).

In the simplified model of the cylinder, heat transfer through cylinder walls and piston is not modelled, but instead all external walls of the fluid region are assumed to be isothermal or adiabatic. In such a case modelling of the solid part of the cylinder is reduced to equation of piston motion. All thermal equations formulated for the solid body and corresponding coupling conditions have to be omitted or replaced by adiabatic or isothermal boundary conditions:

$$T_{\mathbf{f}} = T_{ext} \quad \text{on} \quad \Gamma_W \cup \Gamma_P \quad \text{for isothermal wall} \tag{4.2.5}$$

$$\mathbf{q}_{\mathbf{f}} \cdot \mathbf{n} = 0 \quad \text{on} \quad \Gamma_W \cup \Gamma_P \quad \text{for adiabatic wall}$$

An alternative model can be obtained by considering two chambers of the cylinder as separate fluid domains and by defining artificial interface which constitutes outlet for one chamber and inlet for the other and which provides exchange of the fluid. The conditions at outlet Γ_V^1 and inlet Γ_V^2 are coupled by values of imposed boundary and coupling condition:

$$\text{BC:} \quad \mathbf{v}_f^1 = \widetilde{\mathbf{v}}_f \quad \text{on} \quad \Gamma_V^1 \tag{4.2.6a}$$

$$\text{CC:} \quad \dot{m}_1 = -\dot{m}_2 \quad \text{on} \quad \Gamma_V^{1/2}, \quad T_f^1 = T_f^2 \quad \text{on} \quad \Gamma_V^{1/2} \tag{4.2.6b}$$

The condition (4.2.6a) is intended to be applied at the outlet from one of the chambers. Resulting mass flow rate and temperature at outlet are applied as inlet conditions for the second chamber. Although the above method of modelling seems artificial, its essence is the possibility of controlling fluid exchange by changing boundary condition (its type, value or size) instead of changing width of the orifice.

In further **numerical examples,** two types of double-chamber pneumatic cylinder utilizing various connections of the chambers will be considered:

- the absorber with the orifice located inside the piston, Fig. 4.15,
- the absorber with the external bypass located outside the cylinder and equipped with flow control device, Fig. 4.16.

In the first case, the possibility of controlling the flow of the fluid is provided by change of the orifice width during the process. In the second case, control of the fluid flow is obtained

by change of the position of an additional empty region which models the valve head. Two proposed methods of flow control directly refer to general methods introduced in Sec.2.2.2.

In numerical models of both systems, the piston is represented by an empty region inside a fluid domain. The model which contains the orifice located inside the piston (Fig. 4.15a) has relatively simple topology, however it involves a problem of modelling of the moving orifice, which from the point of view of computational fluid dynamics requires special handling. In considered case, the orifice moves horizontally and its width is simultaneously changed during numerical analysis. Vertical displacement of the lateral walls of the orifice is determined by actual displacement of the piston which is governed by equation of motion:

$$M\frac{d^2u_P}{dt^2} - Mg + \int p_2^{pist}(x,t)dA_2 - \int p_1^{pist}(x,t)dA_1 + F_f(u,\dot{u},t) = 0 \tag{4.1.7}$$

$$\text{IC: } v(0) = v_0, \quad u(0) = 0$$

In the above equation the third and fourth integral terms denote fluid forces exerted on both sides of the piston. On the contrary, the width of the orifice is arbitrarily changed during the analysis according to assumed control strategy and it usually depends on actual or predicted piston acceleration. Discretisation of the single fluid domain can be performed in two manners (Fig. 4.15):

- single fluid domain can be defined for the whole region occupied by fluid,
- separate fluid domains for upper chamber, the orifice region and the lower chamber can be defined and interfaces between these regions can be introduced.

In the first method, vertical displacement of the orifice and control of its width are obtained by imposing vertical and horizontal displacement of orifice walls and adjacent skew walls (Fig. 4.15b). The second method is more complex due to an introduction of domain interfaces, however it provides a better control over mesh stiffness and mesh deformation during the impact process.

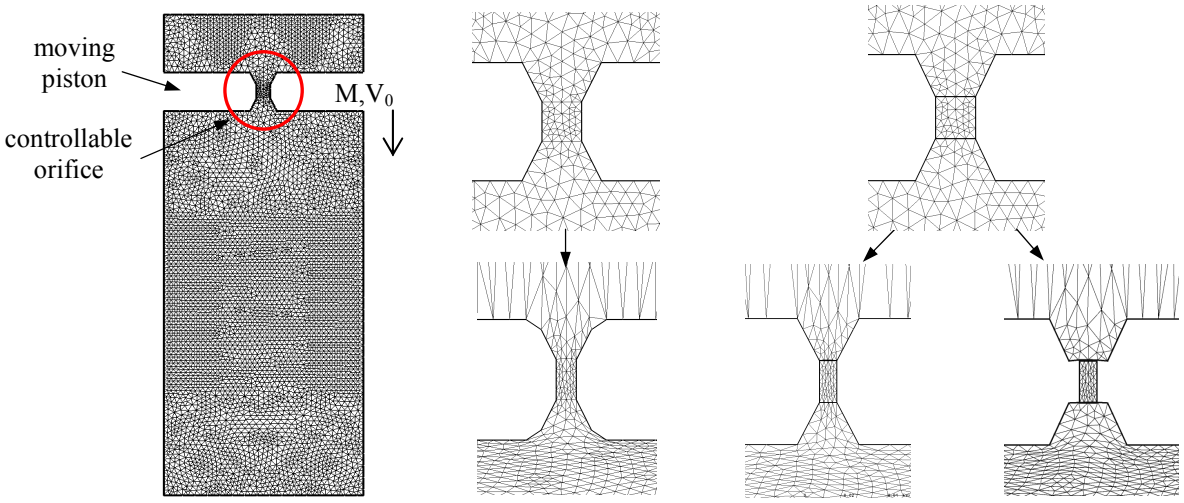

Fig. 4.15. Numerical model of double-chamber cylinder with controllable orifice: a) considered fluid domain, b) and c) methods of discretization of the orifice region

The method enables separate definition of the vertical and horizontal displacement of the mesh at the walls of the orifice, adjacent skew walls and at the interface which allows to change width of the orifice in two manners (Fig. 4.15c). In the first option, mesh in the region adjacent to the orifice deforms and topology of the mesh is preserved. By contrast, the second one utilizes sliding of the orifice mesh along domains interfaces.

The described above model of adaptive pneumatic cylinder was implemented into ANSYS CFX. Equation of piston dynamics was discretized (in similar manner as in Eq. 4.1.18) and movement of the piston was introduced to the model as displacement of interior boundaries of the fluid domain. Width of the orifice was presumed to be either constant or changed according to assumed feed-forward or feedback control strategy. Exemplary response of double-chamber cylinder caused by dynamical excitation is presented in Fig. 4.16. (width of the orifice is linearly decreasing during the process).

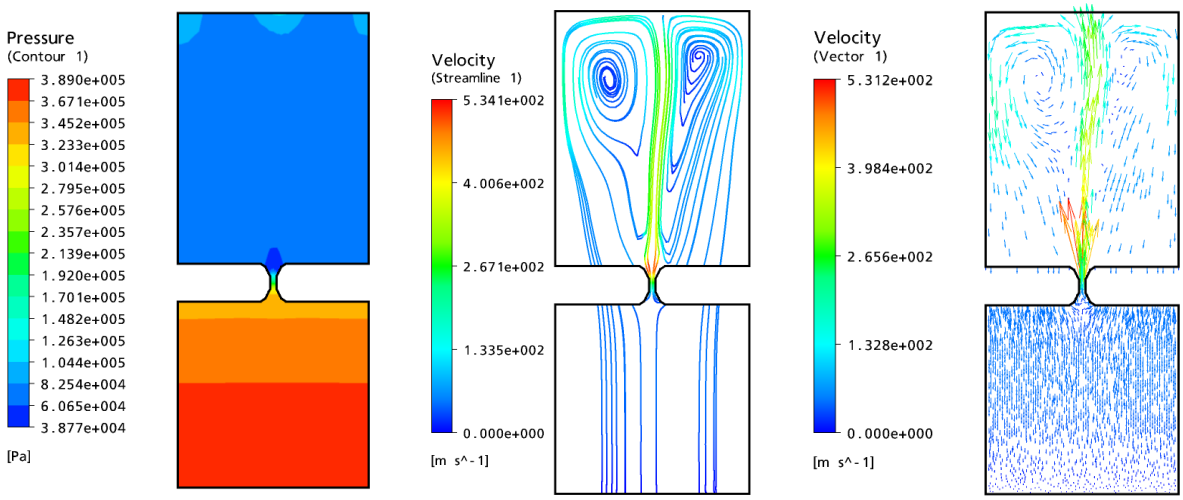

Fig. 4.16. Dynamic response of double-chamber pneumatic cylinder with internal orifice: a) pressure distribution, b) streamlines, c) velocity vectors

An alternative topology of double-chamber adaptive pneumatic cylinder contains external bypass allowing migration of gas between the chambers (Fig. 4.1.16). The bypass is equipped with the simple valve which allows to control the gas flow between the chambers. Although the model seems to be more complex, it provides that movement of the piston and movement of the valve head are separated from each other, which facilitates dicretization of the fluid domain and execution of valve head displacement. In the considered model only the valve head is modelled and direct change of its position is regarded as externally applied control. The mechanism of the valve head movement is not considered, however limitations of valve head displacement resulting from the operating principle of the valve can be introduced into the model. The developed computational model of the absorber, together with typical response to dynamic excitation, is depicted in Fig. 4.17.

Qualitatively, the response of double-chamber cylinder with connection between the chambers resembles the response of single-chamber cylinder with exhaust to environment. When double-chamber system is subjected to kinematic or dynamic excitation and the valve remains closed, change of total force exerted on piston is caused by changes of pressure in both chambers. Force acting on the piston is affected by increase of average pressure in the

lower chamber, by decrease of average pressure in the upper chamber and, moreover, by effects arising from propagation of pressure waves in both chambers. The wave effects depend on the stage of the process, actual pressure value and dimensions of both chamber. Therefore, the oscillations of total force acting on the piston may be magnified or reduced in comparison to oscillations occurring in a single-chamber system.

When the orifice width (or valve opening) allows for substantial flow of the fluid, average pressure inside the chambers is being equilibrated and thus total force exerted on piston decreases. Moreover, oscillations of the pneumatic force are diminished (in a sense damped), similarly as it occurred in case of single-chamber cylinder, see Fig. 4.6. Together with increase of valve opening, the characteristic of the device becomes more dissipative, its maximal displacement rises and backward movement of the piston is reduced.

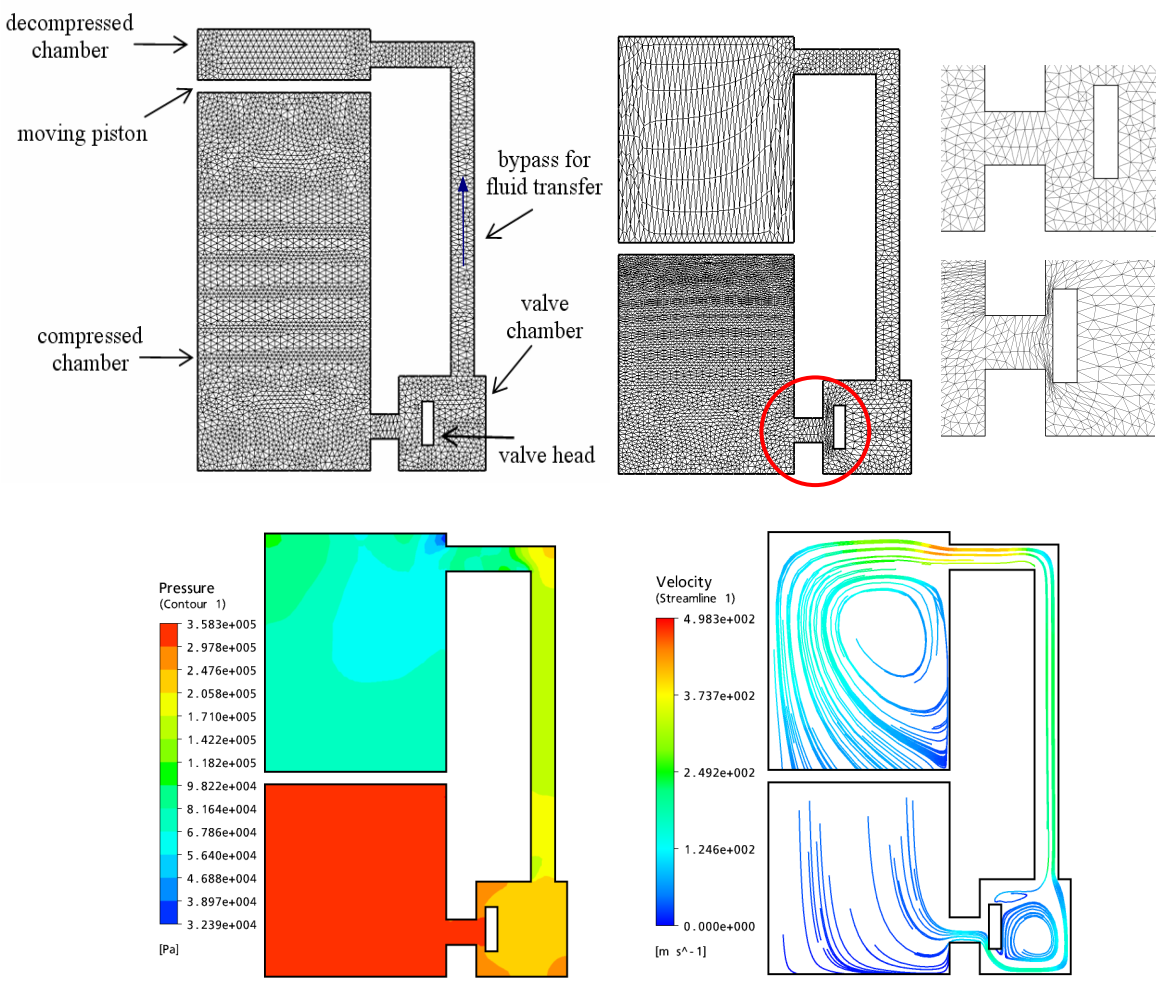

Fig. 4.17. Dynamic response of double-chamber pneumatic cylinder with an external bypass: a) initial computational mesh, b) deformed mesh, c) details of mesh deformation in the valve region, d) pressure distribution, e) streamlines

Typical control strategy for double-chamber pneumatic cylinder is aimed at obtaining arbitrarily assumed change of force generated by the absorber and it can be based on a control scheme developed for a single-chamber adaptive pneumatic cylinder (Fig. 4.11). However, important differences appear in previously considered delay between applied control and its

influence on force exerted on piston. In case of adaptive system with orifice located inside the piston the delay of applied control can be neglected since the influence of change of the orifice width on force exerted on piston is almost instant. On the contrary, in case of adaptive system with bypass the effect of valve head movement is observed on upper and lower surface of the piston with different delay. The above fact complicates development of control strategy and does not allow for direct application of the concept of predictive analysis of a proper duration. Development and implementation of the control strategies for double-chamber cylinders based on continuous change of the orifice width and change of the valve head position are planned as a further step of research.

Comments on application of 'fixed grid' and 'Lagrangian' approach

Another possibility for modelling of double-chamber adaptive pneumatic cylinders is 'fixed grid' method (cf. Sec. 2.2.2 for general description). In case of 'fixed grid' method the whole region of space that can be possibly occupied by fluid (i.e. region between upper and lower cylinder wall) is discretized by the stationary Eulerian mesh. In the most general case, the piston and the valve head are modelled as solid bodies defined on Lagrangian mesh which is superimposed on stationary Eulerian mesh (Coupled Eulerian Lagrangian method). Discretization of piston and the valve head allows for modelling their deformation and heat transfer occurring during the process. Alternatively, the piston and the valve head can be modelled as rigid bodies and the piston dynamics can be governed exclusively by equation of motion. In the latter case, the method is often referred to as 'Immersed Solid' method which arises from CEL method by replacing deformable solid body by rigid object.

Modelling of pneumatic cylinders with 'fixed grid method' posses all features of 'fixed grid' modelling of general fluid-structure interaction problems described in Sect. 2.2.2. The main advantage of the method is that the initial topology of the system does not have to be preserved. In case of double-chamber pneumatic cylinder with controllable connection between the chambers, the above feature allows for multiple separation and connection of the fluid regions during numerical analysis (multiple full closing and opening of the valve). On the other hand, the main disadvantage of the method is the possibility of leakages of the fluid through the piston when computational mesh is not fine enough. Moreover, since the method is often implemented in solvers based on explicit scheme of integration (as ABAQUS/Explicit), it is prone to stability problems due to a high speed of fluid deformation.

An elementary example of application of fixed grid method was implemented in ABAQUS/Explicit and it concerns double-chamber cylinder with closed valve subjected to dynamic excitation (Fig. 4.18). The obtained non-uniform distribution of pressure inside lower chamber was found to be in qualitative agreement with the results from ALE approach. However, observed behaviour of gas inside upper chamber was clearly incorrect. When gas pressure dropped below atmospheric pressure as a result of chamber elongation, the gas had stopped expanding and was gathered in the upper side of the chamber, which is a transparent artefact. Accordingly, the fixed grid method will be further applied only in cases of pressure being positive and results will be treated with limited reliance.

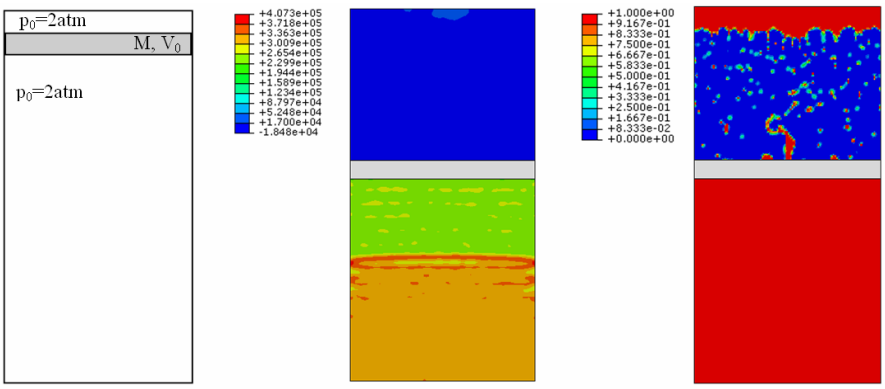

Fig. 4.18. Modelling of single-chamber passive pneumatic cylinder by fixed grid approach: a) numerical model, b) pressure distribution (overpressure [Pa]), c) distribution of the fluid inside considered domain (1- region filled with fluid, 0 – region filled with void)

Purely Lagrangian approach (Lagrangian modelling of fluid and solid domains) can be successfully applied only when motion of the fluid particles is relatively small and it can be followed by Lagrangian mesh. In case of pneumatic cylinders such a situation occurs when considered fluid chamber is completely closed and no outflow of the fluid occurs, as in example of single-chamber cylinder in Fig. 4.19. During piston displacement the mesh becomes distorted (compressed) in regions where pressure is increased. At the bottom of the cylinder, where pressure is equal to the initial one, the elements are of their original size, cf. Fig. 4.19b. In case of adaptive pneumatic cylinder with open valve, fluid particles may move outside the cylinder and tracking them with Lagrangian mesh becomes impossible. Therefore, the Lagrangian method appears to be an alternative for ALE and CEL (Eulerian) approaches only for the purpose of modelling closed pneumatic cylinders.

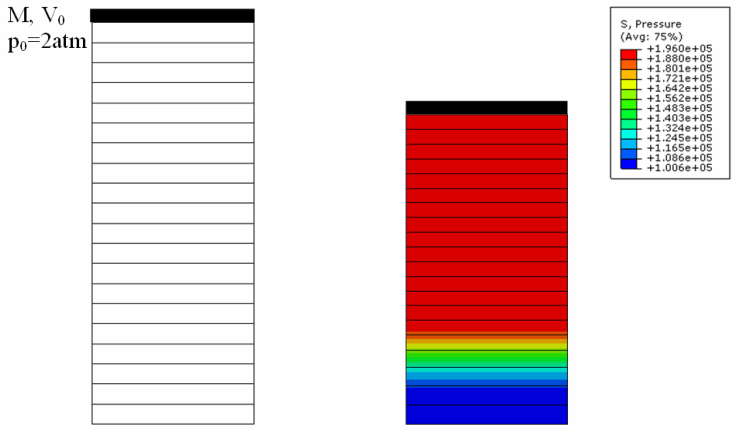

Fig. 4.19. Modelling of single-chamber passive pneumatic cylinder with Lagrangian approach a) numerical model, b) pressure distribution at intermediate time instant of the process

4.3. Hybrid approach to modelling adaptive pneumatic cylinders

Hybrid methods of modelling adaptive pneumatic cylinders can be derived directly from theoretical model of Adaptive Inflatable Structure developed in Sect. 2.4. The hybrid approach can be applied both in case of full model which takes into account heat transfer

through cylinder walls and the simplified model with adiabatic or isothermal walls. In both cases, an important simplification, in comparison to general hybrid model, is that mechanical coupling conditions between fluid and cylinder walls do not have to be considered.

In this section, the considerations will be limited to development of a hybrid model of double-chamber pneumatic cylinder, Fig. 4.20. The substantial part of the cylinder will be modelled by Uniform Pressure Method, while the valve region will be modelled more precisely by using the Navier-Stokes equations. Since the piston is adjacent exclusively to UPM region, its equation of motion has a simple form:

$$M\frac{d^2u_P}{dt^2} + (p_2 - p_1)A + F_{fr} = 0 \tag{4.3.1}$$

where u_P denotes displacement of the piston, p denotes pressure inside cylinder determined from Uniform Pressure Method and F_{fr} is the friction force. The heat transfer through immobile cylinder walls and through the piston is described by the equation:

$$\rho_{\mathbf{S}}\frac{de_S}{dt} = -\nabla\cdot\mathbf{q_S} \qquad \text{in } \Omega_S \cup \Omega_P \tag{4.3.2}$$

Boundary conditions are formulated for the solid domain at its external boundary:

$$T_S = T_{ext} \quad \text{or} \quad -\mathbf{q_S}\mathbf{n} = h(T_{ext} - T_S) \quad \text{on} \quad \Gamma_S \tag{4.3.3}$$

Fluid inside each UPM region is described in classical manner by ideal gas law and in case of adiabatic system by energy conservation law in the form:

$$\dot{Q}_1 + \sum \dot{m}_{in}\overline{H}_{in} - \sum \dot{m}_{out}\overline{H}_{out} = \dot{U} + \dot{W} \qquad \text{in } \Omega_F^{UPM} \tag{4.3.4}$$

where $\dot{Q}_1$ denotes transfer of heat through walls of the cylinder, $\sum \dot{m}_{in}\overline{H}_{in}$ denotes enthalpy flux caused by gas inflow to each chamber and $\sum \dot{m}_{out}\overline{H}_{out}$ denotes enthalpy flux caused by gas outflow from each chamber. Moreover, U and W indicate internal energy and work done by gas, respectively. The Navier-Stokes equations describing the fluid in the valve region have standard form (Eq. 4.1.4-4.1.6), however they have to be complemented with non-standard coupling conditions at the boundary with the UPM region.

In general, three types of boundary/coupling conditions have to be formulated: conditions between fluid regions modelled by the UPM method and cylinder walls and piston, conditions between fluid region modelled by the Navier-Stokes equations and cylinder walls and, finally, coupling conditions between fluid regions modelled by two approaches. Conditions between UPM fluid region and solid wall at Γ_{FS}^{UPM} take the form:

$$V_f^{UPM} = \int d\Omega_f^{UPM} \tag{4.3.5}$$

$$T_S = T_f^{UPM} \quad \text{on} \quad \Gamma_{FS}^{UPM} \quad \text{and} \quad \int(\mathbf{q_S}\cdot\mathbf{n})d\Gamma_{FS}^{UPM} = \dot{Q}_1$$

where the first condition indicates equality of actual volume of the fluid employed in equation of gas state and actual volume of the UPM fluid domain which changes due to movement of the piston. Mechanical coupling conditions are not formulated here explicitly since they are included in the equation of piston motion (Eq. 4.4.1). Thermal coupling conditions are related

to conformance of temperatures of fluid and solid wall and total transfer of heat to the fluid. Coupling conditions at the boundary of region modelled by the Navier-Stokes equations and solid wall Γ_{FS}^{FSI} take the form:

$$\mathbf{v_f} = 0 \quad \text{on} \quad \Gamma_{FS}^{FSI} \tag{4.3.6}$$

$$T_\mathbf{S} = T_\mathbf{f} \quad \text{and} \quad \mathbf{q_S} \cdot \mathbf{n} = \mathbf{q_f} \cdot \mathbf{n} \quad \text{on} \quad \Gamma_{FS}^{FSI}$$

Moreover, both fluid regions are coupled by mechanical and thermal coupling conditions formulated at their common boundary $\Gamma_F^{NS/UPM}$:

$$\boldsymbol{\sigma}_\mathbf{f}\mathbf{n} = -p_f^{UPM}\mathbf{n} \quad \text{on} \quad \Gamma_F^{NS/UPM}, \qquad \int (\mathbf{v_f} \cdot \mathbf{n}) \rho_f d\Gamma_F^{NS/UPM} = \dot{m}_f^{UPM} \tag{4.3.7}$$

$$T_f = T_f^{UPM} \quad \text{on} \quad \Gamma_F^{NS/UPM}, \quad \int \left((\mathbf{v_f} \cdot \mathbf{n}) \rho_f \right) c_p T_f d\Gamma_F^{NS/UPM} = \sum \dot{m}_{in/out} \overline{H}_{in/out} \quad \text{on} \quad \Gamma_F^{NS/UPM}$$

The last condition (enthalpy flux equality) results from equality of mass flow rates and temperatures. Finally, the initial conditions are formulated for fluid region modelled by the UPM approach:

$$\rho_\mathbf{f}(0) = \widetilde{\rho}_\mathbf{f}, \quad T_\mathbf{f}(0) = \widetilde{T}_\mathbf{f} \tag{4.3.8}$$

and for the fluid modelled by the Navier-Stokes equations:

$$\rho_\mathbf{f}(x,y,0) = \widetilde{\rho}_\mathbf{f}, \quad T_\mathbf{f}(x,y,0) = \widetilde{T}_\mathbf{f}, \quad \mathbf{v_f}(x,y,0) = \widetilde{\mathbf{v}}_\mathbf{f} \tag{4.3.9}$$

Initial conditions related to solid part concern initial velocity of the piston and temperature:

$$v_P(0) = \widetilde{v}_P, \quad T_S(0) = \widetilde{T}_S \tag{4.3.10}$$

An alternative, simplified hybrid model of the pneumatic cylinder assumes adiabatic or isothermal walls of the cylinder. In such a case thermal coupling conditions between fluid and cylinder walls are replaced by thermal boundary conditions and coupling between two fluid regions remains unchanged. The hybrid model of double-chamber adaptive pneumatic cylinder with orifice located inside the piston is more complicated in terms of division into UPM- and NS-modelled regions since mutual location of both regions changes during the process due to a movement of the piston. Moreover, equation of piston dynamics contains terms corresponding to both UPM- and NS- modelled regions.

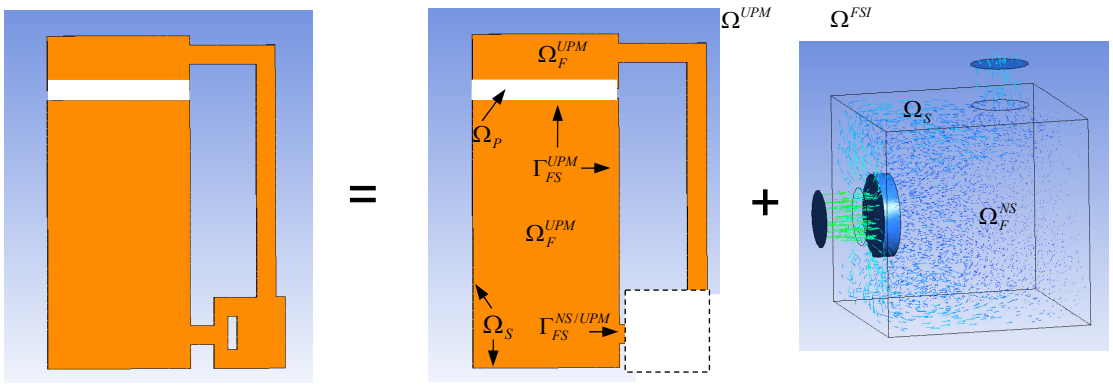

Fig. 4.20. Hybrid approach for modelling of double chamber pneumatic cylinder: decomposition of the considered domain into parts modelled by UPM approach FSI approach.

4.4. One-dimensional CFD models of pneumatic cylinders

The model of adaptive pneumatic cylinder can be further simplified by performing reduction to one spatial dimension. One-dimensional model can still be regarded as 'CFD model' since the Navier-Stokes equations are used and, consequently, wave propagation effects are taken into account. Adaptive pneumatic cylinder will be considered under isothermal conditions, which allows to neglect the third N-S equation governing the energy balance. In momentum equation viscosity of the gas will be taken into account, to avoid change of the parabolic equation into a hyperbolic one. Solid part of the model will be confined to equation of motion of the piston. The main advantage of proposed 1D model is that, at first, it is clear from mathematical point of view and, secondly, it is numerically effective.

In the current approach the Navier-Stokes equations being core of the method will be considered as the main set of governing equations. In considered case general ALE form of these equations (4.1.4-4.1.5) can be reduced into two partial differential equations defined in terms of fluid velocity u and density ρ, which in the Eulerian frame of reference read:

$$\frac{\partial \rho}{\partial t} + \frac{\partial (\rho u)}{\partial x} = 0 \tag{4.4.1a}$$

$$\rho \frac{\partial u}{\partial t} + \frac{\partial}{\partial x}\left(\rho RT - \mu \frac{\partial u}{\partial x} \right) = -\rho u \frac{\partial u}{\partial x} \tag{4.4.1b}$$

Dirichlet boundary conditions can be imposed on fluid density and fluid velocity at the boundaries of considered one-dimensional domain:

$$\rho(0,t) = \overline{\rho}(t) \quad \text{or} \quad u(0,t) = \overline{u}(t) \tag{4.4.2a}$$

and they define static pressure or inflow/outflow velocity, respectively. Alternatively, the Neumann boundary conditions can be imposed on the flux term of both equations:

$$\rho(0,t)u(0,t) = \overline{q}(t) \quad \text{or} \quad \rho(0,t)RT - \mu \frac{\partial u}{\partial x}(0,t) = \overline{\sigma}(t) \tag{4.4.2b}$$

and they denote mass flow rate of the fluid and external force, respectively. Alternative form of the equation (4.4.1b) reads:

$$\frac{\partial (\rho u)}{\partial t} + \frac{\partial (\rho u^2)}{\partial x} + \frac{\partial}{\partial x}\left(\rho RT - \mu \frac{\partial u}{\partial x} \right) = 0 \ , \ \text{where:} \quad \frac{\partial (\rho u^2)}{\partial x} = \frac{\partial (\rho u)}{\partial x} u + \rho u \frac{\partial u}{\partial x} \tag{4.4.3}$$

The Dirichlet and Neumann boundary conditions for the above equation take the form:

$$\rho(0,t)u(0,t) = \overline{q}(t) \quad \text{and} \quad \rho(0,t)RT - \mu \frac{\partial u}{\partial x}(0,t) = \overline{\sigma}(t) \tag{4.4.4}$$

The Dirichlet boundary condition for Eq. 4.4.3 is exactly the same as the Neumann boundary condition for the Eq. 4.4.1b. The second term of Eq. 4.4.3 is not considered as a part of the flux term since it can be divided into convective part of time derivative and nonlinear term. Therefore, Eq. 4.4.4 does not generate a new boundary condition.

The above preliminary considerations allow to formulate two distinct models of passive pneumatic cylinder, where:

- piston is modelled as point mass which dynamics is governed by ordinary differential equation and PDEs are used only for modelling gas inside cylinder (Fig. 4.21a),
- piston is modelled as a solid body and PDEs are used for modelling both the piston and the gas inside cylinder (cf. Fig. 4.21b).

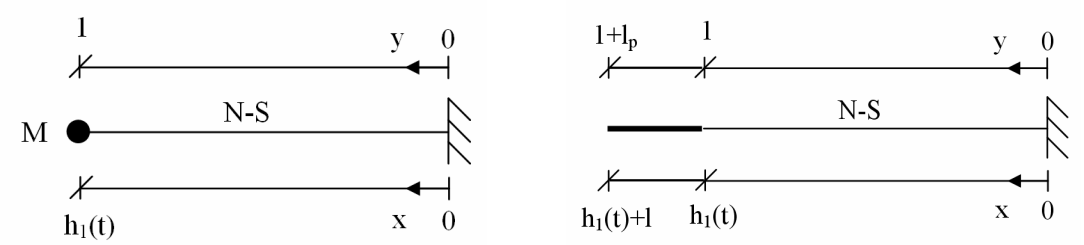

Fig. 4.21. One-dimensional model of passive pneumatic cylinder: a) point mass and continuous fluid domain, b) two continuous domains modelling piston and fluid

In the first method, the model of pneumatic cylinder is composed of single domain where the Navier-Stokes equations are defined, one stationary boundary indicating the wall and one mobile boundary where cylinder piston is located. In case of **kinematical excitation** when velocity of the left boundary $f(t)$ is imposed, piston inertia does not have to be taken into account. Thus, mathematical model is composed of the Navier-Stokes equations defined on a deforming domain and the Dirichlet boundary conditions at both ends:

$$\frac{\partial \rho}{\partial t}+\frac{\partial(\rho u)}{\partial x}=0 \qquad x\in\left(0,h_1(t)\right) \tag{4.4.5a}$$

$$\rho\frac{\partial u}{\partial t}+\frac{\partial \rho}{\partial x}RT-\mu\frac{\partial^2 u}{\partial x^2}=-\rho u\frac{\partial u}{\partial x} \qquad x\in\left(0,h_1(t)\right)$$

$$\text{BC: } u(h_1(t),t)=f(t) \text{ and } \dot{h}_1(t)=f(t); \qquad u(0,t)=0 \tag{4.4.5b}$$

$$\text{IC: } u(x,t)=u_0(x), \qquad \rho(x,0)=\rho_0(x), \qquad h_1(0)=h_{01}$$

The strong disadvantage of such a formulation is that it contains boundary condition which is imposed on a moving boundary. Solution of the problem requires change of variables (u,ρ) into $(\tilde{u},\tilde{\rho})$ which allows to transform the problem into deforming domain:

$$u(x,t)=\tilde{u}(y,t), \qquad \rho(x,t)=\tilde{\rho}(y,t), \tag{4.4.6}$$

$$y=\psi(x,t)=x/h_1(t) \quad \Rightarrow \quad x=yh_1(t)$$

The above procedure is equivalent to transformation of the governing equations from the Eulerian coordinate system to the referential coordinate system. Consequently, time and space derivatives of both variables are connected by relations:

$$\frac{\partial u}{\partial t}=\frac{\partial \tilde{u}}{\partial t}+\frac{\partial \tilde{u}}{\partial y}\frac{\partial \psi}{\partial t}, \qquad \frac{\partial u}{\partial x}=\frac{\partial \tilde{u}}{\partial y}\frac{\partial \psi}{\partial x}, \qquad \frac{\partial^2 u}{\partial x^2}=\frac{\partial^2 \tilde{u}}{\partial^2 y}\left(\frac{\partial \psi}{\partial x}\right)^2+\frac{\partial \tilde{u}}{\partial y}\frac{\partial^2 \psi}{\partial x \partial y}\frac{\partial \psi}{\partial x} \tag{4.4.7a}$$

where:

$$\frac{\partial \psi}{\partial t}=\psi_t=-\frac{x\dot{h}_1(t)}{h_1(t)^2}=-\frac{y\dot{h}_1(t)}{h_1(t)}, \qquad \frac{\partial \psi}{\partial x}=\psi_x=\frac{1}{h_1(t)} \tag{4.4.7b}$$

Let us note here that transformation of the coordinate system could be easily performed since in case of kinematical excitation both displacements of the boundaries are known a priori (displacement of the right boundary equals zero and displacement of left boundary equals time integral of velocity imposed at the boundary *f(t)*). After transformation to new variables, equations governing the problem read:

$$\frac{\partial\widetilde{\rho}}{\partial t}+\frac{\partial\widetilde{\rho}}{\partial y}\psi_t+\widetilde{\rho}\frac{\partial\widetilde{u}}{\partial y}\psi_x+\widetilde{u}\frac{\partial\widetilde{\rho}}{\partial y}\psi_x=0 \qquad y\in(0,1) \tag{4.4.8a}$$

$$\widetilde{\rho}\frac{\partial\widetilde{u}}{\partial t}+\widetilde{\rho}\frac{\partial\widetilde{u}}{\partial y}\psi_t+\frac{\partial\widetilde{\rho}}{\partial y}\psi_x RT-\mu\frac{\partial^2\widetilde{u}}{\partial y^2}(\psi_x)^2=-\widetilde{\rho}\widetilde{u}\frac{\partial\widetilde{u}}{\partial y}\psi_x \qquad y\in(0,1)$$

$$\text{BC:}\ \ \widetilde{u}(1,t)=f(t), \qquad \widetilde{u}(0,t)=0 \tag{4.4.8b}$$

$$\text{IC:}\ \ \widetilde{u}(y,0)=\widetilde{u}_0(y), \qquad \widetilde{\rho}(y,0)=\widetilde{\rho}_0(y)$$

which is a typical formulation of initial-boundary value problem.

In case when **dynamics of the mass** is incorporated into the problem, the boundary/coupling conditions at left boundary of the domain concern both compatibility of velocities and equation of equilibrium of the mass:

$$\text{BC:}\ u(h_1(t),t)=\dot{h}_1(t), \quad \rho(h_1(t),t)RT-\mu u_x(h_1(t),t)=M\ddot{h}_1(t), \quad u(0,t)=0 \tag{4.4.9}$$

Both above conditions can be written in the form of a single condition such that system of boundary and coupling conditions for the problem (4.4.5a) reads:

$$\text{BC:}\ \rho(h_1(t),t)RT-\mu u_x(h_1(t),t)=M\dot{u}(h_1(t),t); \qquad u(0,t)=0 \tag{4.4.10}$$

$$\text{IC:}\ \ u(x,t)=u_0(x), \quad \rho(x,0)=\rho_0(x), \quad h_1(0)=h_{01}, \quad \dot{h}_1(0)=v_0$$

The condition imposed at left boundary can be treated as the Neumann boundary condition which, however, is not a typical one since its value is not predefined but depends on time derivative of the solution at the boundary $\dot{u}(h_1(t),t)$. Boundary conditions (4.4.9) require transformation into deforming domain which is governed by Eqs (4.4.6, 4.4.7) and which leads to the following form of the boundary conditions in a new coordinate system:

$$\text{BC:}\ \ \widetilde{u}(1,t)=\dot{h}_1(t), \qquad \frac{\partial\widetilde{\rho}}{\partial y}(1,t)\psi_x RT-\mu\frac{\partial\widetilde{u}}{\partial y}(1,t)\psi_x=m\ddot{h}_1(t), \qquad \widetilde{u}(0,t)=0 \tag{4.4.11}$$

The intrinsic difference, in comparison to previously considered system with kinematic excitation, results from the fact that function $h_1(t)$ involved in differential equations (4.4.8a) and in boundary conditions (4.4.11) is not known a priori but depends on actual solution at the boundary. Numerical solution of such formulated problem can not be obtained in a straightforward way by using typical commercial solvers for partial differential equations. However, it can be solved by combining standard PDE solver with simple optimisation procedure aimed at finding actual displacement of the mass. The proposed procedure is based on the following algorithm executed at several equally distributed time-steps of the analysis:

- value of piston displacement h_1 is assumed,
- time derivative $\dot{h}_1(t)$ is calculated and applied as Dirichlet condition at left boundary,

- N-S equations (in a form transformed into new coordinate system) are solved by PDE solver,
- value of the flux at left boundary is calculated and condition of equilibrium of the left boundary (Eq. 4.4.11b) is checked; discrepancy of forces is considered as minimized objective function,
- value of displacement $h_1(t)$ is changed and the procedure is repeated until objective function is minimized and equilibrium of the left boundary is satisfied.

Alternatively, converse procedure can be applied, i.e. after assuming $h_1(t)$:

- second time derivative $\ddot{h}_1(t)$ is calculated and applied as Neumann condition at the left boundary,
- N-S equations are solved by PDE solver,
- calculated fluid velocity at left boundary is used to check the condition of kinematic compatibility at left boundary (4.4.11a); discrepancy of velocities is considered as minimized objective function,
- value of displacement $h_1(t)$ is changed and procedure is repeated until objective function is minimized and kinematic compatibility at the left boundary is satisfied.

The above procedure resembles, to some extend, two main classical methods used for analysis of the truss structures: the 'direct stiffness method' where values of generalised displacement are assumed and matched to fulfil equilibrium equations, and 'direct displacement method' where values of element forces are assumed and matched to fulfil conditions of geometrical compatibility. The difference between approach applied here and in truss theory is that unknown value is determined by optimisation procedure instead by solving system of algebraic equations. Although more efficient methods of numerical solution can be developed, the proposed procedure is easy for numerical implementation when standard PDE solver is available. The method can be applied not only to passive pneumatic cylinders, where zero fluid velocity at right boundary is imposed, but also for adaptive pneumatic cylinders, where outflow b.c. at right boundary is prescribed.

In the second proposed method of 1D modelling of pneumatic cylinder, both the piston and the fluid are modelled in continuous way and they are in governed by partial equilibrium equations. However, the piston is made of relatively stiff material with linear characteristics in considered range of small deformation. This fact has two consequences: i) deformation of the piston domain may be assumed as negligible; ii) piston can be described by wave equation. The Navier-Stokes equations describing fluid inside the cylinder are defined on the deforming domain with left mobile boundary. The system of governing differential equations reads:

$$\frac{\partial \rho_F}{\partial t} + \frac{\partial (\rho_F u_F)}{\partial x} = 0 \qquad x \in \left(0, h_1(t)\right) \tag{4.4.12}$$

$$\rho_F \frac{\partial u_F}{\partial t} + \frac{\partial \rho_F}{\partial x} RT - \mu \frac{\partial^2 u_F}{\partial x^2} = -\rho_F u_F \frac{\partial u_F}{\partial x} \qquad x \in \left(0, h_1(t)\right)$$

$$\rho A \frac{\partial^2 u_S}{\partial t^2} - EA \frac{\partial^2 u_S}{\partial x^2} = 0 \qquad x \in \left(h_1(t), h_1(t) + l\right)$$

Coupling conditions between these two regions are established by providing geometrical compatibility and equilibrium of internal forces at common interface:

$$\text{CC: } u_F(h_1(t),t) = \dot{u}_S(h_1(t),t) \tag{4.4.13}$$

$$\rho_F(h_1(t),t)RT - \mu\frac{\partial u_F}{\partial x}(h_1(t),t) = -EA\frac{\partial u_S}{\partial x}(h_1(t),t)$$

Boundary and initial conditions include zero Dirichlet condition imposed on the right edge, Neumann condition imposed on the left edge (modelling external force applied to the piston) and zero initial conditions for the whole system:

$$\text{BC: } EA\frac{\partial u_S}{\partial x}(h_1(t)+l) = F_{imp}(t), \quad u_F(0) = 0 \tag{4.4.14}$$

$$\text{IC: } u_F(x,0) = 0,\ \rho_F(x,0) = 0,\ u_S(x,0) = 0,\ \dot{u}_S(x,0) = 0$$

The initial step of solution is the transformation of the differential equations and boundary conditions into mobile coordinate system which follows motion of the piston. Due to the fact that wave equation is defined on a domain which is moving in space but is not deforming, it does not have to be transformed. Model based on two PDEs is expected to be equivalent to the model based on a single PDE in terms of distribution of pressure inside pneumatic cylinder, however, it also allows to determine distribution of stresses inside the piston.

Control of pneumatic cylinder, both in case of kinematical and dynamical excitation, is aimed at obtaining desired level of force at the left boundary where the piston is located. Since the model is one-dimensional, the number of control possibilities is restricted. Namely, the methods based on change of the size of the outlet width of the orifice and position of the valve head are not applicable. Nonetheless, control of the system can be performed in two manners:

- by changing value of the outflow boundary condition at the right boundary,
- by applying displacement of the right (previously fixed) boundary.

Here, the second option will be precisely analysed since the first one was already considered for two-dimensional CFD model. Model of adaptive pneumatic cylinder with two moving boundaries (Fig. 4.22) is governed by the following set of equations:

$$\frac{\partial\rho}{\partial t} + \frac{\partial(\rho u)}{\partial x} = 0 \qquad x \in \left(h_1(t), h_2(t)\right) \tag{4.4.15a}$$

$$\rho\frac{\partial u}{\partial t} + \frac{\partial\rho}{\partial x}RT - \mu\frac{\partial^2 u}{\partial x^2} = -\rho u\frac{\partial u}{\partial x} \qquad x \in \left(h_1(t), h_2(t)\right)$$

$$\text{BC: } u(h_1(t),t) = \dot{h}_1(t), \quad \rho(h_1(t),t)RT - u_x(h_1(t),t) = M\ddot{h}_1(t); \quad u(h_2(t),t) = \dot{h}_2(t) \tag{4.4.15b}$$

$$\text{or} \quad \rho(h_1(t),t)RT - \mu u_x(h_1(t),t) = m\dot{u}(h_1(t),t); \quad u(h_2(t),t) = \dot{h}_2(t)$$

$$\text{IC: } u(x,t) = u_0(x), \quad \rho(x,0) = \rho_0(x), \quad h_1(0) = h_{01}, \quad h_2(0) = h_{02}, \quad \dot{h}_1(0) = v_0$$

In the above model the direction of the x axis is reversed. Position of the mass and position of the piston are defined by coordinates $h_1(t)$ and $h_2(t)$, respectively.

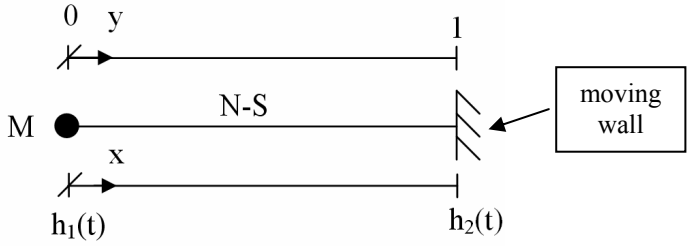

Fig. 4.22. One-dimensional model of adaptive pneumatic cylinder in which control is executed by introducing mobile left boundary.

In direct simulation of adaptive pneumatic cylinder, where $h_1(t)$ is unknown function while $h_2(t)$ is arbitrarily assumed, the method of solution developed for a passive system can be directly applied. By contrast, the control problem is to find function $h_2(t)$ for which global (integral) discrepancy between obtained value of mass acceleration $\ddot{h}_1(t)$ and assumed optimal value $\ddot{h}_{1opt}(t)$ is the smallest:

Find $h_2(t)$ that minimises $J = \int_0^t (\ddot{h}_1(t) - \ddot{h}_{1opt})^2 dt$ or (4.4.16)

$$J = \int_0^t \left[M^{-1} \left[\rho(h_1(t),t)RT - \mu u_x(h_1(t),t) \right] - \ddot{h}_{1opt}(t) \right]^2 dt$$

where $u(x,t)$ and $h_1(t)$ are solution of the problem (4.1.15)

Twin definition of the minimized functional indicates that it can be expressed both in terms of acceleration of the mass and in terms of solution of partial differential equation at the left boundary. The function $h_2(t)$ does not appear explicitly in the minimised functional but in the set of differential equations governing the problem.

The first step of solving the control problem is transformation of the equations and boundary conditions into a new coordinate system defined as:

$$u(x,t) = \tilde{u}(y,t), \quad \rho(x,t) = \tilde{\rho}(y,t) \tag{4.4.17}$$

$$y = \psi(x,t) = \frac{x - h_1(t)}{h_2(t) - h_1(t)} \quad \Rightarrow \quad x = h_1(t) + y(h_2(t) - h_1(t))$$

Time and space derivatives of fluid velocity and density are transformed according to (4.4.7a), however, time and space derivatives of the transfer function ψ assume different values than defined by Eq. 4.4.7b. Finally, system of governing equations takes the form (4.4.8a) while boundary and initial conditions for the system read:

$$\text{BC: } \tilde{u}(0,t) = \dot{h}_1(t), \quad \frac{\partial \tilde{\rho}}{\partial y}(0,t)\psi_x RT - \mu \frac{\partial \tilde{u}}{\partial y}(0,t)\psi_x = M\ddot{h}_1(t); \quad \tilde{u}(1,t) = \dot{h}_2(t) \tag{4.4.18}$$

$$\text{IC: } \tilde{u}(y,t) = u_0(y), \quad \tilde{\rho}(y,0) = \rho_0(y), \quad \dot{h}_1(0) = v_0$$

Typical solution of the control problem requires assuming the control function $h_2(t)$, solving direct problem (Eq. 4.4.8a) to find functions $u(x,t), \rho(x,t), h_1(t)$ which satisfy kinematic compatibility and equilibrium conditions at the left boundary and further updating of the function $h_2(t)$ in order to minimise integral difference between obtained and assumed mass

acceleration. Due to the fact that finding solution of the direct problem (4.4.15) requires iterative procedure (iterations over time instants and over actual values of h_1), the above method would be ineffective and time consuming. On the other hand, the nonlinearity of the governing equations and the lack of analytical or semi-analytical solutions prevent application of classical methods of solving optimal control problems.

In a simplified approach, global control problem (4.1.16) can be divided into a set of simpler problems related to particular steps of solution (time instants of the process). In this method displacement of the right boundary at particular step of solution is adjusted to minimise acceleration difference at the following step, i.e. with certain time delay. The applied time shift is caused by wave propagation effects involved in the problem. The 'discrete formulation' of the control problem reads:

$$\text{Find } h_2(t_n) \text{ that minimises } \quad J = \ddot{h}_1(t_{n+1}) - \ddot{h}_{1opt}(t_{n+1}) \quad \text{or} \tag{4.4.19}$$

$$J = M^{-1}\left[\rho(h_1(t_{n+1}), t_{n+1})RT - u_x(h_1(t_{n+1}), t_{n+1})\right] - \ddot{h}_{1opt}(t_{n+1})$$

Although this formulation is simpler than global formulation (4.1.16), it remains numerically expensive, especially when direct solution for given displacement of the right boundary has to be found by proposed iterative procedure.

Here, we will consider the 'strong form of the control problem' where optimal value of the controlled quantity (optimal displacement of the piston $h_{1opt}(t)$) is explicitly introduced into governing equations of the problem. In this formulation governing equations (4.4.8a) are used, but boundary conditions assume untypical form:

$$\text{BC:} \quad u(0,t) = \dot{h}_{1opt}(t), \quad \frac{\partial \widetilde{\rho}}{\partial y}(0,t)\psi_x RT - \mu \frac{\partial \widetilde{u}}{\partial y}(0,t)\psi_x = M\ddot{h}_{1opt}(t), \tag{4.4.20}$$

$$u(1,t) = \dot{h}_2(t)$$

In this case, partial differential equation is accompanied by both Dirichlet and Neumann boundary conditions at the left boundary and the value of right boundary condition is one of the unknowns in the problem. The following algorithm of the solution can be proposed:

- for each time instant value of wall displacement h_2 is assumed and $\dot{h}_2$ is imposed as Dirichlet b.c. at right boundary,
- $\dot{h}_{1opt}(t)$ is calculated and imposed as Dirichlet b.c. at left boundary,
- system of governing equations (4.4.8a) is solved by PDE solver,
- value of flux at left boundary is calculated and condition of equilibrium of the left boundary (4.4.20b) is checked,
- value of wall displacement h_2 is changed and the procedure is repeated until equation of piston equilibrium at the left boundary is satisfied.

Alternatively, the opposite procedure can be applied, i.e. after assuming h_2 and imposing Dirichlet b.c. at the right boundary:

- $\ddot{h}_{1opt}(t)$ is calculated and Neumann b.c. at left boundary is imposed,
- system of governing equations (4.4.8a) is solved by PDE solver,

- obtained fluid velocity at the left boundary is utilized to check the condition of kinematic compatibility a the left boundary,
- value of displacement h_1 is changed and procedure is repeated until condition of kinematic compatibility is satisfied.

The algorithm for solving such formulated optimisation problem is similar to the algorithm for solving the straightforward problem (4.4.8), except that h_2 is the main unknown in the optimisation problem, and, therefore, it has to be assumed at the beginning of each step of the procedure and applied as the Dirichlet boundary condition.

Since the formulation of the problem is not typical, the existence of the solution of the problem is not certain. In general, it is not known whether for assumed piston displacement, there exists a function describing displacement of the right boundary for which both Dirichlet and Neumann conditions at the left boundary are satisfied. Solution of the 'strong form' of the control problem is probable to exist in case when piston assumed piston displacement $h_1(t)$ arises as a slight modification of the solution of the direct problem (Eq. 4.4.8).

Both simplified formulations of the global control problem (Eq. 4.4.19 and 4.4.20) are equivalent to the general formulation of the control problem (Eq. 4.4.16) under the same conditions, i.e. when no constraints on displacement of the right boundary are imposed and the assumed trajectory of the piston can be exactly followed (i.e. global error in general formulation of the control problem can be minimised to zero). Considering 'strong form of control problem' can be treated as preliminary step before solving general control problem (4.4.16). If the solution of 'strong control problem' can not be found than general procedure of solving control problem has to be applied.

For the sake of simplicity the method was not implemented for the Navier-Stokes equations but for the **Burgers equation** which is the equivalent to the second N-S equation (Eq. 4.4.3) under assumption that fluid density remains constant. The Burgers equation was used due to the fact that its numerical solution does not cause numerical difficulties and it can be obtained by most of PDE solvers. However, it has to be clearly stated that the Burgers equation can not be used for modelling of pneumatic cylinders with large piston displacement.

We will consider the system depicted in Fig. 4.22 with one moving boundary and with point mass located at the other, described by the Burgers equation in the form:

$$\frac{du}{dt} - \frac{d^2u}{dx^2} = -\frac{d(u^2)}{dx}, \qquad x \in \langle h_1(t), h_2(t) \rangle \tag{4.4.21a}$$

The boundary conditions for the problem are formulated in similar manner as for the Navier-Stokes equations, i.e. at the left boundary with point mass both kinematic conformity and equilibrium conditions are assumed (both Dirichlet and Neumann conditions), while at the right boundary only kinematic compatibility is assumed (only Dirichlet condition):

$$\text{BC:} \quad u(h_1(t),t) = \dot{h}_1(t), \quad u_x(h_1(t),t) = m\ddot{h}_1(t); \qquad u(h_2(t),t) = \dot{h}_2(t) \tag{4.4.21b}$$

$$\text{or} \quad u_x(h_1(t),t) = m\dot{u}(h_1(t),t); \qquad u(h_2(t),t) = \dot{h}_2(t)$$

Moreover, arbitrarily assumed initial conditions for the problem read:

$$\text{IC:}\quad u(x,t)=\sin\left(\pi\frac{x-h_{01}}{h_{02}-h_{01}}\right),\qquad h_1(0)=h_{01},\quad h_2(0)=h_{02},\qquad \dot{h}_1(0)=v_0 \tag{4.4.21c}$$

After the following transformation to new coordinate system:

$$u(x,t)=\tilde{u}(y,t),\qquad y=\psi(x,t)=\frac{x-h_1(t)}{h_2(t)-h_1(t)} \tag{4.4.22}$$

The governing equation reads:

$$\frac{\partial\tilde{u}}{\partial t}+\frac{\partial\tilde{u}}{\partial y}\psi_t-\frac{\partial^2\tilde{u}}{\partial y^2}(\psi_x)^2=-\tilde{u}\frac{\partial\tilde{u}}{\partial y}\psi_x\ ,\qquad y\in(0,1) \tag{4.4.23a}$$

While boundary conditions for the system are formulated as follows:

$$\text{BC:}\quad \tilde{u}(0,t)=\dot{h}_1(t),\qquad -\frac{\partial\tilde{u}}{\partial y}(0,t)\psi_x=m\ddot{h}_1(t),\qquad \tilde{u}(1,t)=\dot{h}_2(t) \tag{4.4.23b}$$

and

$$\text{IC:}\quad \tilde{u}(y,t)=\sin(\pi y),\qquad \dot{h}_1(0)=v_0 \tag{4.4.23c}$$

After above transformation of the Burgers equation and corresponding boundary conditions into moving coordinate system two problems were solved numerically (cf. Fig. 4.23.):

- 'direct problem' in which displacement of the right boundary $h_2(t)$ was arbitrarily assumed and piston displacement $h_1(t)$ was calculated,
- 'control problem' where previously computed displacement of the piston $h_1(t)$ was assumed and displacement of the right boundary $h_2(t)$ was recalculated.

In both cases, previously developed numerical procedures were applied and numerical solution was obtained by combining MATLAB built-in PDE solver with MATLAB optimisation procedure for finding value of function $h_1(t)$ or $h_2(t)$ (in direct and control problem, respectively) with the use of condition of equilibrium at the left boundary. Exemplary results of application of the proposed algorithm are presented in Fig. 4.23.

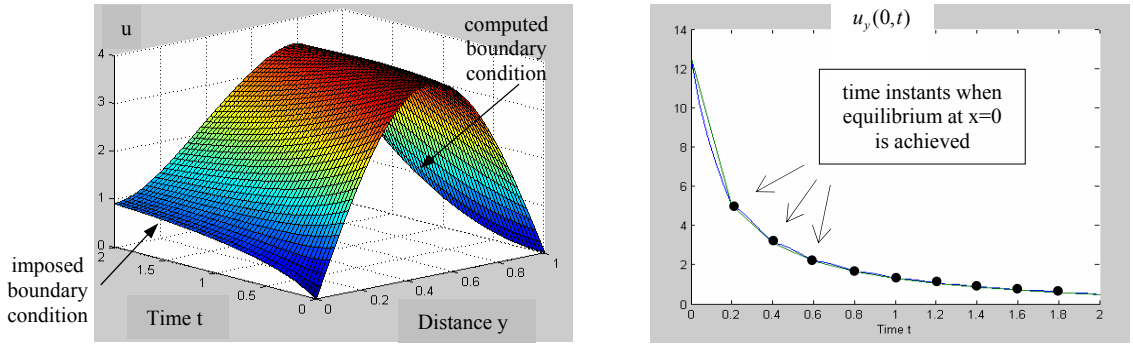

Fig. 4.23. Solution of the control problem with point mass at the left boundary and moving right boundary (Fig. 4.22), b) equilibrium at the boundary with point mass, curves: $u_y, -M\ddot{h}_1/\psi_x$

Summary of Chapter 4

The chapter presents the methods of modelling, simulation and control of adaptive pneumatic cylinders subjected to impacts of high initial velocity. Analyzed systems are modelled with the use of Navier-Stokes equations coupled with equation of dynamics of the piston and they additionally incorporate various models of controllable valves.

The most precise analysis is conducted for single chambers cylinders for which the models with full heat transfer through the walls and with simplified thermodynamic modelling of the walls are described. The models implemented in commercial CFD software allow to investigate qualitative change of dynamic response of a closed system caused by high velocity of impact and to estimate conditions when CFD modelling is required. Further, two simplified models of gas outflow from the cylinder are introduced and their influence on dynamic response is investigated. Finally, two algorithms of valve control aimed at maintaining constant level of generated pneumatic force are proposed. The control algorithms are based on the concept of 'predictive analysis' and they are successfully implemented with the use of CFD code coupled with external software.

The following part of the chapter discusses modelling of simulation of double chamber cylinder. The controlled gas flow between the chambers requires different modelling methods than outflow to environment. Two proposed options utilize orifice of controllable width located inside the piston and external bypass with controllable valve head. Modelling of double chamber cylinder is also performed with the use of hybrid method based on combination of UPM approach and Navier-Stokes equations. The chapter finishes with description of modelling of 1D adaptive pneumatic system where the control is introduced by movement of one of the boundaries. The example transparently reveals the underlying mathematical description of the gas medium occupying deforming space region.

The chapter expands the range of applicability of adaptive pneumatic cylinders into impacts with high initial velocity. Presented considerations and simulations preliminarily prove that in case of fast impacts adaptation to actual loading can be conducted and may lead to desired change of the dynamic response of the system. However, due to different nature of the occurring phenomena, more sophisticated numerical tools for modelling, as well as, different control algorithms have to be applied.

CHAPTER 5 - CRASHWORTHINESS OF ADAPTIVE INFLATABLE STRUCTURES

Thin-walled structures are commonly used in transport and mechanical industry because of their large stiffness, durability and small weight. Additionally, thin-walled structures made of steel effectively absorb the energy of axial loading due to the process of plastic folding. The above features cause that thin-walled steel elements are often applied in the crashing zones of trains, cars and other energy absorbing structures.

Mechanics of thin-walled structures subjected to large deformations can be analysed by both analytical and numerical methods. Analytical methods of crashworthiness were originated in the paper by Alexander [15] in the context of longitudinal crushing of a steel tube. Analytical methods assume certain folding pattern which depends on structure geometry and characteristics of material in order to calculate the amount of energy dissipated during the process of crushing. By contrast, numerical methods for solving crashworthiness problems are based on space and time discretisation and they usually utilise the nonlinear Finite Element Method with explicit scheme of integration of equations of motion.

Impact energy absorption of thin-walled absorbers of various cross sections and shapes and their applications were studied in books by Johnes and Wierzbicki [17 18 19] and, more recently, for instance by Kim and Wierzbicki [270 271] or Han and Yamazaki [272]. The research done on various types of thin-walled absorbers is reviewed in paper [273], while more general overview related to energy absorbing capabilities of various materials and structures is presented in book [274]. A full review of conventional thin-walled impact energy absorbers will not be performed here, since it can be found exemplary in [95] and [101]. Instead, the attention will be focused on methods of increase and control of their crashworthiness capabilities.

Improvement of crashworthiness of structures subjected to axial loading by filling them with granular material (like sand or grain) and by taking advantage of friction forces generated between granules during impact was proposed by Lee [95]. In turn, Zhang [101] examined the usage of the buckling initiators activated just before expected impact in order to reduce initial peak of crushing force. Moreover, thin-walled absorbers composed of two sections joined by pyrotechnic connectors, which can be detached during impact to reduce absorber stiffness, were proposed and tested experimentally by Ostrowski [91]. Another important concept is filling axially loaded circular tubes with compressed gas in order to take an advantage of the effect of gas compression during an impact and to affect the shape of deformation of thin-walled absorber, cf. Zhang et al. [101]. The above concept was also studied by Greń [275] who had developed precise analytical model of the process of crushing assisted by gas pressure. The application of the above concept to control stiffness of the vehicle longitudinal frontal members was studied by Pipkorn [276].

In contrast to previously mentioned solutions, the concept presented in current chapter is focused on thin-walled structures subjected to lateral impact. In case of lateral loading, thin-walled structure easily undergoes buckling and local plastic yielding, and as a result only small part of the impact energy is dissipated. However, as it will be shown in the following

sections, filling thin-walled structure with gas and controlling its release during the impact process significantly increases thin-walled structure durability. The chapter starts with a simple experiment where aluminium beverage can is subjected to the action of transverse force and the influence of internal pressure on buckling phenomenon is observed. Further, numerical analyses of impact subjected inflatable thin-walled structures are conducted and general conclusions concerning the effects of structure inflation are drawn. In the following part, simplified two-dimensional model of adaptive multi-chamber inflatable barrier is developed and strategies of pressure adjustment for maximisation of structure load capacity are proposed. Finally, the model of inflatable barrier is used to demonstrate the possibilities of adaptation aimed at minimisation of hitting object acceleration, minimisation of internal pressure and obtaining desired deformation.

Several concepts presented within this Chapter are included in the patent claim [277]. Some parts of the chapter were published as conference papers [278] and [279], related to buckling of the aluminium can and optimisation of the inflatable barrier, respectively.

5.1. Properties of air inflated thin-walled structures

5.1.1. Basic experiment: buckling of the inflated can

Basic experiment confirming the beneficial influence of filling thin-walled structure with compressed air was conducted on aluminium beverage can[2]. In the initial experiment an empty can was not sealed so internal pressure was equal to ambient pressure. Right end of the can was clamped around the circumference of the cylinder. Left end was reinforced by special ring and subjected to action of vertical force **F** acting upwards. As a result of applied boundary conditions and external force, the can was acting as a cantilever. Applied loading caused bending of the can, tension of its lower wall and compression of the upper.

During the experiment value of vertical force was gradually increased. Sudden collapse of the structure was observed when vertical force achieved 155N and it was caused by buckling of the cylinder sidewalls. The buckling region covered large part of the can located between its middle part and the support (cf. Fig. 5.1.1a). Moreover, buckling shape was symmetrical on both sides of the cylinder. The collapse of the structure occurred at relatively small displacement of the left edge of the can which indicates small work done by external force before buckling.

In the second stage of the experiment the cylinder was sealed and inflated with compressed gas under pressures: 0,2MPa, 0,4MPa, 0,6MPa and 0,8MPa. During the experiment the internal pressure was not externally changed or controlled. Additional loading of the can caused by applied internal pressure acts against buckling due to following reasons:

- it reduces compressive stresses arising at prone to buckling upper wall of the cylinder,
- it aggravates inward deformation of cylinder walls which occurs during buckling of the empty can.

The value of critical force causing buckling of the structure was gradually increasing (up to 610N for internal pressure of 0,6MPa). Along with an increase of critical force, the area of

[2] The experiment was performed by Mr. Rafał Chmielewski at IPPT PAN.

buckling was decreasing and moving into the direction of the support, cf. Fig. 5.5.1b. Buckling phenomena occurred at apparently larger displacement of the left (free) end of the can which indicates significant increase of work done by external force and corresponding increase of energy absorbed by inflated can in comparison to generic case of an empty can.

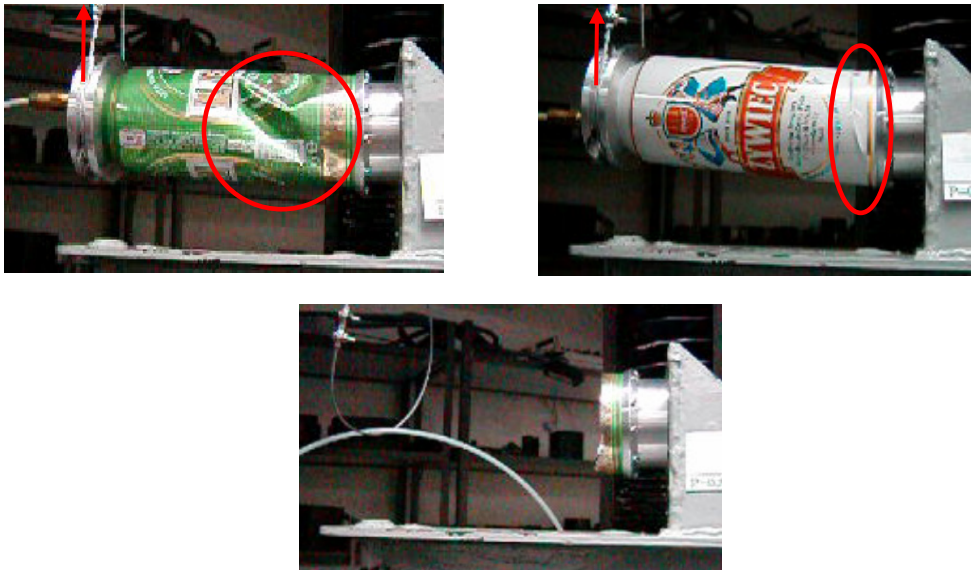

Fig.5.1.1: Deformation of the beverage can with internal pressure: a) 0 MPa, b) 0,6 MPa, c) 0,8MPa

In the last considered case of pressure of 0,8MPa, the maximal value of applied force was equal to approx. 700N, however a total destruction of the can occurred briefly after buckling because of the sudden burst in the vicinity of the support. The burst was caused either by exceeding maximal allowable tensile stress in the lower part of the can or by crack which appeared at the certain point of the bucking area and propagated around the can in the vicinity of the support.

The experiment clearly reveals two important features of the inflatable thin-walled structures. Primarily, the durability of thin-walled structures to lateral loading and the amount of dissipated energy can be substantially increased by the use of compressed gas. On the other hand, application of high internal pressure is related to a danger of sudden destruction or blast of the structure, which implicates the requirement of precise pressure control. Both above facts justify application of Adaptive Inflatable Structures equipped with controllable valves serving for real-time control of internal pressure.

Corresponding numerical analyses

The problem of inflated can was simulated numerically by using the Finite Element Method for modelling of thin-walled structure and by applying uniformly distributed loading perpendicular to the surface of the can to account for the influence of pressure of compressed gas. Performed simulations were treated as a preliminary step before modelling of more complex inflatable thin-walled structures. The following numerical analyses were performed:

1. Static analysis of bending of empty and inflated can
2. Linear buckling analysis of empty and inflated can during bending
3. Nonlinear analysis of bending and buckling of the can

4. Linear buckling analysis of the can during axial compression
5. Modal analysis of empty and inflated can

Thin-walled cylindrical shell structure considered in numerical simulations had the dimensions of the aluminium can: length l=170mm, radius of the base r=33mm and thickness of the wall t=0,1mm. Thickness of both bases of the cylinder was equal to 0,5mm to model large stiffness of the reinforcing ring from the experiment. Because of the lack of precise material data it was assumed that material is fully isotropic. Young modulus of the aluminium and Poisson ratio were assumed to be equal to E=56GPa and $\nu = 0{,}33$ which provides agreement of the numerical analysis with buckling experiment. Numerical simulations were performed with two finite element codes where four and eight-node shell elements were used.

Static analysis of bending of the inflated can was aimed at investigating the influence of internal pressure on distribution of internal stresses in cylinder walls. Internal pressure was modelled as distributed loading applied perpendicularly in the outer direction at all internal walls of the cylinder. Applied vertical load was distributed along the circumference of the left base of the cylinder. At this stage of analysis, characteristics of the material was assumed as linear elastic, however, equilibrium equations were established in actual configuration.

The problem of bending of the inflated can consists of the first step of inflation (increase of pressure loading) and the second step of bending (increase of external force). In finite element notation the problem solved reads:

$$\begin{aligned} &\text{Step 1: } \mathbf{K}(\mathbf{Q}_\mathbf{p},\mathbf{q})\mathbf{q} = \mathbf{Q}_\mathbf{p}(p,\mathbf{q}) \\ &\text{Step 2: } \mathbf{K}(\mathbf{Q}_\mathbf{p}^{\max},\mathbf{Q}_\mathbf{F},\mathbf{q})\mathbf{q} = \mathbf{Q}_\mathbf{p}(p^{\max},\mathbf{q}) + \mathbf{Q}_\mathbf{F}(F,\mathbf{q}) \end{aligned} \tag{5.1.1}$$

where $\mathbf{K}$ is the stiffness matrix whose arguments indicate the dependence on actually applied loading $\mathbf{Q}$ and actual deformation of the structure $\mathbf{q}$. The quantity $\mathbf{Q}_\mathbf{p}(p,\mathbf{q})$ is the load vector caused by internal pressure p (in particular: $\mathbf{Q}_\mathbf{p}^{\max} = \mathbf{Q}_\mathbf{p}(p^{\max},\mathbf{q})$) and $\mathbf{Q}_F(F,\mathbf{q})$ is the load vector caused by external force $\mathbf{F}$ of a magnitude F. Both load vectors depend on actual deformation of the structure since pressure loading is perpendicular to the walls of the can and external force is assumed to follow structure deformation. The case when both forces are applied simultaneously:

$$\mathbf{K}(\mathbf{Q}_\mathbf{p},\mathbf{Q}_\mathbf{F},\mathbf{q})\mathbf{q} = \mathbf{Q}_\mathbf{p}(p,\mathbf{q}) + \mathbf{Q}_\mathbf{F}(F,\mathbf{q}) \tag{5.1.2}$$

is not equivalent to problem (5.1.1) which is reflected in different arguments of the stiffness matrix and consequently different path of structure equilibrium. Significant simplification of the problem (5.1.1) is obtained by setting equilibrium equations in initial (undeformed) configuration. In such a case the problem solved reads:

$$\mathbf{K}\mathbf{q} = \mathbf{Q}_\mathbf{p}(p) + \mathbf{Q}_\mathbf{F}(F) \tag{5.1.3}$$

and can be decomposed into two simpler problems:

$$\begin{aligned} &\mathbf{K}\mathbf{q}_\mathbf{p} = \mathbf{Q}_\mathbf{p}(p) \quad \text{and} \quad \mathbf{K}\mathbf{q}_\mathbf{F} = \mathbf{Q}_\mathbf{F}(F) \\ &\mathbf{q} = \mathbf{q}_\mathbf{p} + \mathbf{q}_\mathbf{F} \end{aligned} \tag{5.1.4}$$

where $\mathbf{q}_\mathbf{p}, \mathbf{q}_\mathbf{F}$ indicate displacements caused by internal pressure and vertical force. Total displacement $\mathbf{q}$ can be calculated as a sum of the two above displacements according to

superposition principle. The formula (5.1.4) reveals, in a simplified manner, the expected influence of internal pressure on distribution of internal forces in considered structure and its deformation.

The exemplary results of numerical simulation based on Eq. 5.1.1 are related to the case of bending force equal to 165N (value of buckling force obtained from numerical linear buckling analysis) and two values of internal overpressure: 0MPa and 0,4MPa. In case of zero internal overpressure, the distribution of longitudinal stress is very regular with tension region at the lower side and compression regions at the upper side of the cylinder (Fig. 5.1.2a). Although deformation of the cylinder is relatively small, the influence of geometry change on distribution of internal forces is reflected in slightly unsymmetrical distribution of longitudinal stress on the bottom and on the top of the cylinder.

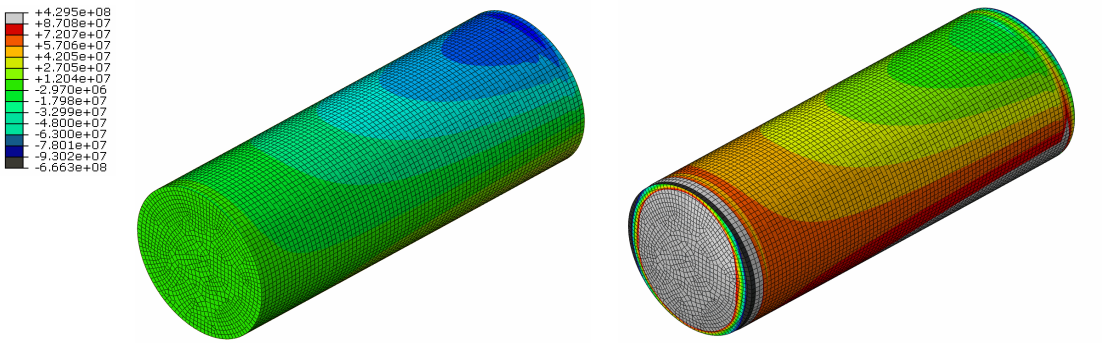

Fig.5.1.2: Distribution of the longitudinal stress [Pa] at outer side of the shell caused by bending of the can by force 165N: a) empty can, b) internal overpressure of 0.4MPa

When only internal pressure is applied, it causes nearly uniform longitudinal and circumferential tensile stresses in the sidewalls of the cylinder (except the peripheral regions of clamping and free end). Consequently, interaction of internal pressure and bending force leads to a reduction of longitudinal compressive stresses in the upper part of the cylinder with simultaneous increase of longitudinal tensile stresses in the lower part (cf. Fig. 5.1.2b).

Although finite element analysis reveals vague effect of bending of cylinder walls (slight variation of stress across shell thickness), the distribution of stresses can be estimated by means of membrane shell theory [280] which assumes that equilibrium of shell is provided without the presence of the bending forces. Analytical formulae defining stress in the longitudinal direction at critical points on top and bottom of the cylinder in the vicinity of support read:

1. First load case: force acting at the end of the cantilever F=165 N, no internal overpressure:

$$\sigma_{top} = -\frac{Mr}{J} = -\frac{Flr}{\frac{\pi}{4}(r^4 - (r-t)^4)} = -82{,}36MPa\,, \qquad \sigma_{bottom} = 82{,}36MPa \tag{5.1.5}$$

2. Second load case: force F=165N, internal overpressure p=0,4 MPa

$$\sigma_{top} = -\frac{Mr}{J} + \frac{pr}{2t} = -16{,}4MPa\,, \qquad \sigma_{bottom} = \frac{Mr}{J} + \frac{pr}{2t} = 148{,}5MPa \tag{5.1.6}$$

Both of the above results are in agreement with results of FEM simulations. The obtained results indicate that buckling of the empty can occurs at relatively low value of stress (below

plastic limit of the aluminium) and the process can be treated as elastic buckling. On the other hand, when the cylinder is subjected to action of internal pressure of 0,8 MPa and bended by the force of 700N (extreme conditions in the experiment) the maximal longitudinal stress calculated according to Eq. 5.1.6 equals 481MPa and exceeds yield strength of aluminium. Therefore, the phenomenon obtained in the experiment, in case of high internal pressure, should be rather treated as elasto-plastic buckling.

In the next step, the **linear buckling analysis** of the empty and inflated can during bending by the vertical force was conducted. The analysis of the inflated can was performed in two subsequent steps:

- initial pre-stress where distributed loading modelling gas pressure is applied,
- eigenvalue buckling analysis where critical value of the bending load is searched.

$$\begin{aligned} &\text{Step 1: } \mathbf{K}\mathbf{q}_\mathbf{p} = \mathbf{Q}_\mathbf{p} \quad \text{or} \quad \mathbf{K}(\mathbf{Q}_\mathbf{p}, \mathbf{q}_\mathbf{p})\mathbf{q}_\mathbf{p} = \mathbf{Q}_\mathbf{p} \\ &\text{Step 2: } \left[\mathbf{K}(\mathbf{Q}_\mathbf{p}^{\max}, \mathbf{q}_\mathbf{p}) - \lambda \mathbf{K}_{\mathbf{Q}_\mathbf{F}}\right]\mathbf{v} = \mathbf{0} \end{aligned} \tag{5.1.7}$$

The first step is a static analysis in which cylinder is subjected to action of internal pressure. The analysis can be executed either as geometrically linear or nonlinear one. The first step is aimed at obtaining pre-stressed (and in case of nonlinear analysis deformed) configuration of the structure $\mathbf{q}_\mathbf{p}$ and corresponding stiffness matrix $\mathbf{K}(\mathbf{Q}_\mathbf{p}^{\max}, \mathbf{q}_\mathbf{p})$ which are used as a base state for the buckling analysis. In the second step of the analysis, global stiffness matrix is composed of base stiffness matrix $\mathbf{K}$ and load stiffness matrix $\mathbf{K}_{\mathbf{Q}_\mathbf{F}}$ corresponding to external vertical load of a value equal to unity. The step is aimed at finding value of external bending load for which Eq. (5.1.7b) has nontrivial solutions, i.e. for which global stiffness matrix of the system becomes singular. Eigenvalues λ are determined as solution of the equation:

$$\det\left[\mathbf{K}(\mathbf{Q}_\mathbf{p}^{\max}, \mathbf{q}_\mathbf{p}) - \lambda \mathbf{K}_{\mathbf{Q}_\mathbf{F}}\right] = \mathbf{0} \tag{5.1.8}$$

which further allows to find value of critical bending loading $\lambda\mathbf{Q}_\mathbf{F}$, total value of critical loading $\mathbf{Q}_\mathbf{p} + \lambda\mathbf{Q}_\mathbf{F}$ and eigenvectors $\mathbf{v}$.

Values of the critical bending force for an empty cylinder computed with the use of two solvers are equal to 165N and 171N, which is only slightly higher than the value of critical force obtained from the experiment. The first buckling shape includes longitudinal deformations arising on both sides of the cylinder, cf. Fig.5.1.3a. The fact that the subsequent values of the critical forces are close to each other indicates that the loss of stability of real structure may involve combination of several initial buckling shapes from the numerical analysis. The buckling shape obtained from the numerical simulations is slightly different than the deformation shape obtained during the experiment, however in both cases the deformation occurs along the longitudinal direction of the cylinder.

In the next step, simulation of buckling was performed for several values of internal pressure inside the cylinder. The increase of pressure in subsequent numerical analyses caused change of buckling shape (cf. Fig. 5.1.3a, b) and corresponding increase of critical vertical force (cf. Fig. 5.1.4). For the pressure range of 0-0,5atm the first buckling shape covers most part of the cylinder sidewalls. However, in case when initial pressure is higher, the shape of

buckling significantly changes. The area of buckling is decreased and it is located only in the vicinity of the support. In case of inflated structure a buckling phenomenon is associated with a smaller overall deformation of the structure and thus buckling itself can be considered as less dangerous for the structure operation.

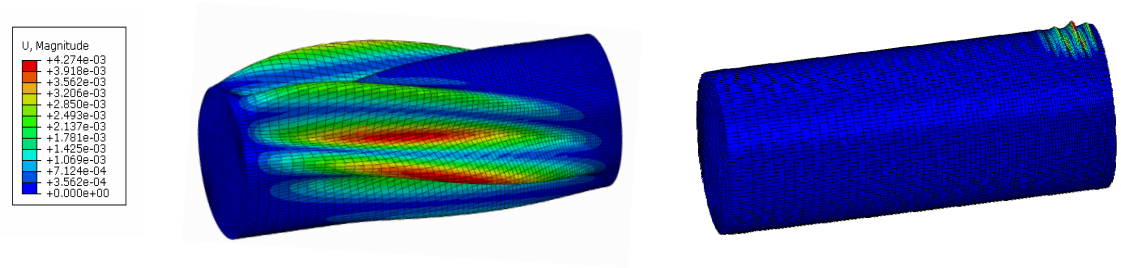

Fig. 5.1.3: Change of buckling shape as a result of increase of internal pressure in the cylinder: a) p=0MPa, b) p=0.35MPa

Increase of internal pressure is also associated with the increase of critical bending force, cf. Fig. 5.1.4. Computed value of critical force was found to increase fast for low values of internal pressure but further its growth is reduced and remains almost linear. Additionally, linear static analysis was conducted for each value of internal pressure and the value of vertical force which causes exceeding of ultimate tensile strength (500MPa) at the bottom of cylinder wall was computed.

Results of the analysis performed for pressures 0 - 1,3 MPa reveal that two ranges of pressure can be distinguished (Fig. 5.1.4). When initial pressure is in the range (0-0,975MPa) buckling of the can occurs at lower value of vertical force than bursting of the bottom wall. The point of intersection of both computed curves indicates theoretical optimal pressure of 0,975 MPa at which buckling of the top wall and bursting of the bottom wall of the cylinder occur theoretically simultaneously. The vertical force that can be applied to the structure equals 678 N and it is 4,1 times larger than the initial force causing collapse (165N). Finally, when internal pressure is higher than optimal value of 0,975MPa buckling of the cylinder does not occur and its destruction is caused by bursting of the bottom wall.

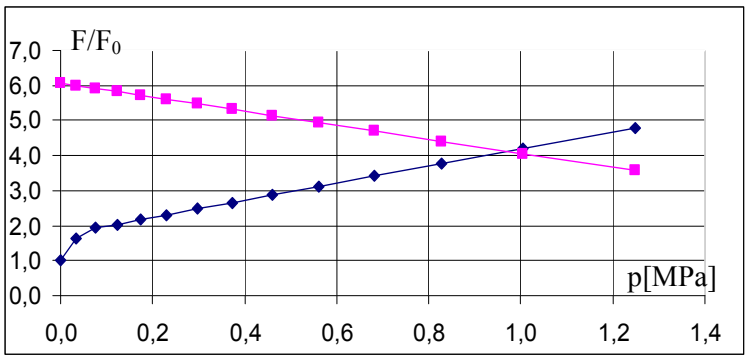

Fig. 5.1.4: Force causing buckling of the can (increasing function) and force causing bursting of the can (decreasing function) in terms of gas pressure (both divided by initial buckling force of 165N).

Nonlinear analysis of bending and buckling of the can was performed in order to verify results from linear buckling analysis and to analyse the post-buckling behaviour of the can with large deformation and nonlinear characteristics of the material. In case of nonlinear

analysis, no special procedure of capturing buckling phenomenon is required. Nevertheless, buckling force at which sudden increase of can deformation occurs can be clearly observed.

Nonlinear analysis of buckling and bending of the can was performed by using dynamic explicit solver in order to avoid the difficulties related to convergence of the analysis conducted with implicit method. The period of the analysis was selected as sufficiently long in order to neglect inertia of the structure, but simultaneously not excessively long in order to provide reasonable computation time (t=0,05s). In the initial analysis, the characteristics of material was assumed as linear elastic in order to obtain correspondence with preceding linear buckling analysis. Similarly as in case of static analysis, numerical procedure is composed of initial step when the can is pre-stressed by internal pressure and the main step when it is bended by vertical force:

$$\begin{aligned} &\text{Step 1: } \mathbf{M}\ddot{\mathbf{q}} + \mathbf{C}\dot{\mathbf{q}} + \mathbf{K}(\mathbf{Q}_\mathbf{p}, \mathbf{q})\mathbf{q} = \mathbf{Q}_\mathbf{p}(p(t), \mathbf{q}), \quad t \in \langle 0, t_1 \rangle \\ &\text{Step 2: } \mathbf{M}\ddot{\mathbf{q}} + \mathbf{C}\dot{\mathbf{q}} + \mathbf{K}(\mathbf{Q}_\mathbf{p}^{\max}, \mathbf{Q}_\mathbf{F}, \mathbf{q})\mathbf{q} = \mathbf{Q}_\mathbf{p}(p(t_1), \mathbf{q}) + \mathbf{Q}_\mathbf{F}(F(t), \mathbf{q}), \quad t \in \langle t_1, t_2 \rangle \end{aligned} \tag{5.1.9}$$

However, because of relatively long analysis time and resulting small influence of inertial and damping forces the governing equations are practically identical to Eq. (5.1.1).

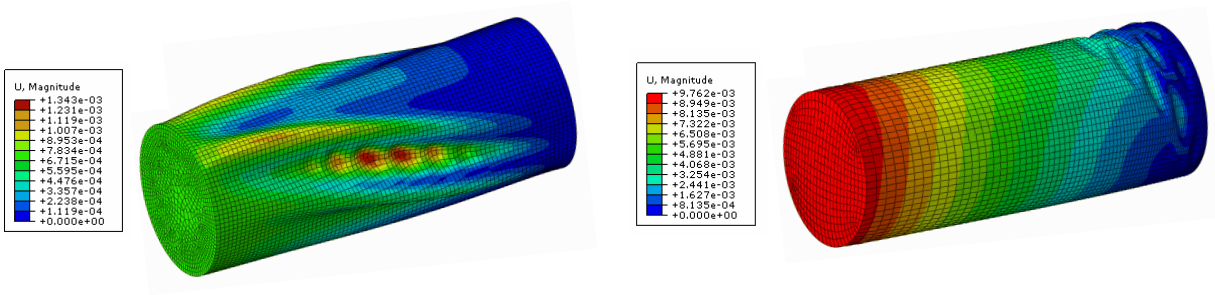

Fig.5.1.5: Buckling shapes obtained from nonlinear explicit dynamic analysis:
a) p=0MPa, b) p=0.3MPa

The results obtained by means of presented methodology confirm, in general, the previous results from the linear buckling analysis. In case when the can is not inflated or when the value of pressure is low, buckling occurs at a large area of cylinder sidewalls, symmetrically on both sides, cf. 5.1.5a. Computed value of the first buckling force for an empty cylinder is only 11,9% higher than the value obtained from the linear buckling analysis conducted with the same solver, cf. Table 5.1. Buckling of the can starts when vertical displacement of loaded edge of the cylinder equals approx. 2mm. The fact that pre-buckling displacement is relatively small, however not negligible, indicates that linear buckling analysis constitutes acceptable approximation of buckling phenomenon, but on the other hand it explains certain difference in values of buckling forces computed by two proposed methods.

For pressures of 0,08-0,09atm and higher the shape of buckling changes and concentrates at the vicinity of the support, cf. Fig. 5.1.5b. Buckling force of the inflated cylinder obtained from the explicit dynamic analysis remains higher than the value from linear buckling analysis if the same model and solver are used, cf. Table 5.1. As the structure becomes inflated, the displacement at which buckling occurs gradually increases and it reaches 9,5mm for internal pressure of 0,9MPa. The increase of pre-buckling displacement

justifies the increase of difference between values of critical force obtained by linear and nonlinear (explicit) bucking analysis. For the largest considered values of pressure, the linear buckling analysis can be used only for rough approximation of the real buckling force.

	0MPa	**0,1MPa**	**0,3MPa**	**0,5MPa**	**0,7MPa**	**0,9MPa**
ANSYS	165,5 N	331,4 N	405,1 N	492,4 N	576,5 N	640,9 N
ABAQUS STD	171,2 N	270,4 N	340,3 N	410,5 N	480,8 N	551,2 N
ABAQUS XPL	~191 N	~280 N	~404 N	~506 N	~645 N	~779 N

Table.5.1: Comparison of buckling force obtained from linear buckling analysis (ANSYS and ABAQUS STD) and nonlinear buckling analysis (ABAQUS XPL)

The last step of numerical investigation was an attempt of simulation of bursting of the can during bending with high internal pressure (0,8MPa). Due to the lack of exact data of the aluminium utilized for production of the can, material data was fitted to qualitative results of the conducted experiment. Elastic stage of deformation is assumed to occur in the range 0-200MPa (E=56GPa), while plastic stage of deformation in the range 200-400MPa (with maximal strain equal 0,4). Rupture of the material is assumed to occur at 300MPa.

The form of cylinder destruction obtained by the numerical simulation clearly resembles the results of the conducted experiment. The can bursts at the vicinity of the support and, moreover, ruptured part is torn in the longitudinal direction. The maximal value of force obtained from the simulation is c.a. 30% higher than the force obtained from buckling analysis.

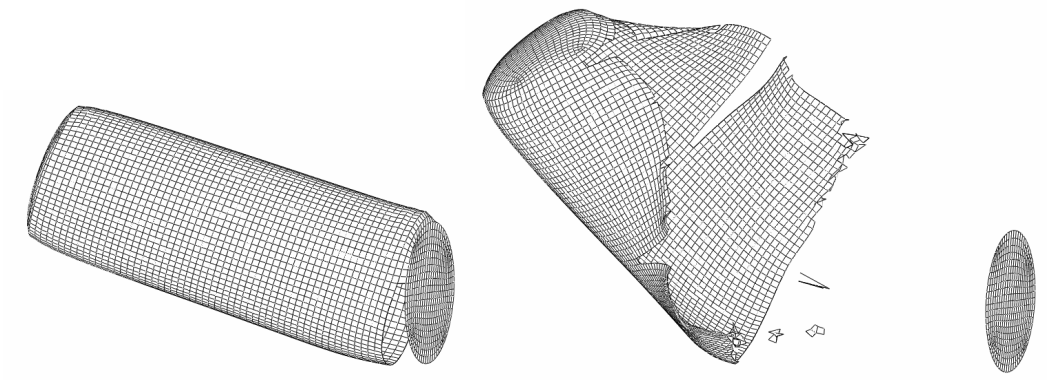

Fig.5.1.6: Two stages of simulation of bursting of the can: a) initiation of bursting F=711N, b) total destruction of the can

Apart from the numerical simulations related to the experiment presented above, two additional simulations were performed:

- linear analysis of buckling of empty and inflated can during axial compression,
- modal analysis of empty and inflated can.

Linear analysis of buckling caused by axial load relies on solving two-step problem (5.1.7) in which $\mathbf{Q}_F$ indicates axial loading applied at free end of the cylinder and uniformly distributed along its circumference. The problem differs from the previously considered buckling under action of the bending force only by the direction of the applied loading $\mathbf{Q}_F$

and physical sense of the load stiffness matrix $\mathbf{K}_{Q_F}$.

The problem of buckling of cylindrical shells is widely considered in classical literature concerning shell structures, cf. Flügge [281]. The phenomenon of buckling of free-supported cylindrical shell under axial loading and pressure can be described fully analytically by assuming sinusoidal buckling shapes and by introducing them into differential equations of shell buckling. Finally, the formula for determination of the non-dimensional parameter defining axial loading q_2 in terms of number of half-waves along cylinder length (n) and number of half-waves along cylinder circumference ($2m$) reads [281]:

$$q_2(n,m) = \frac{\left\{(1-\nu^2)\lambda^4 + k\left[\left(\lambda^2+\nu^2\right)^4 - 2(\nu\lambda^6 + 3\lambda^4 m^2 + (4-\nu)\lambda^2 m^4 + m^6) + 2(2-\nu)\lambda^2 m^2 + m^4\right]\right\}}{\lambda^2\left(\lambda^2+m^2\right)^2 + \lambda^2 m^2} \qquad (5.1.10)$$

In above formula the parameter λ depends on value of n and cylinder geometry: $\lambda = n\pi r / l$, while k depends solely on thickness of cylinder wall and its radius: $k = t^2/(12r^2)$. Minimal value of non-dimensional loading parameter q_2 can be determined by minimization of Eq. 5.1.10 over parameters n and m:

$$\text{Find } \{n,m\} \text{ such that } q_2(n,m) \text{ is minimal; } m,n \text{ are integers} \qquad (5.1.11)$$

Minimum is usually obtained for n=1 and therefore minimization over m is sufficient for finding critical value of loading parameter q_2. Further, the value of critical axial force which causes buckling of the cylinder can be calculated as:

$$F = 2\pi r D q_2(n,m) \qquad (5.1.12)$$

where $D = Et/(1-\nu^2)$. The value of critical force determined from Eq. 5.1.12, as well as values of critical forces corresponding to subsequent buckling shapes, are in very good agreement with results obtained from the linear buckling analysis performed by means of finite element method.

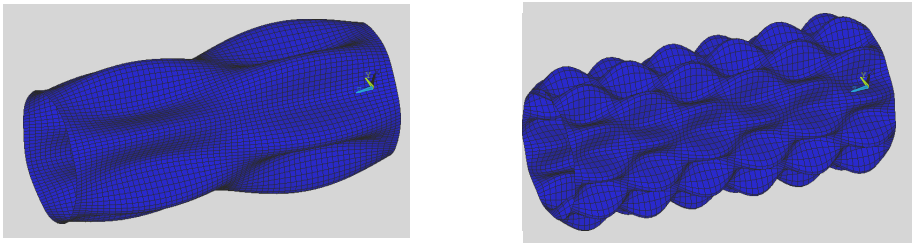

Fig. 5.1.7: Typical buckling shapes of the cylindrical shell under axial loading (no internal pressure): a) the second mode, b) the fourth mode

Similar calculations can be performed for distributed loading applied perpendicularly at the sidewalls of the cylinder which is equivalent to the gas pressure. Moreover, the problem of simultaneous action of axial loading and pressure can also be approached fully analytically. According to conclusions drawn by Flügge, internal pressure does not substantially change the value of critical compressive axial force, however, axial tension increases the resistance to buckling caused by an external pressure. The above conclusions were fully confirmed by performed finite element - based simulations.

The following simulations correspond to the situation when one end of the cylinder is clamped and axial loading is applied at the other end where no kinematic constraints are imposed. The lack of symmetry of the loading and boundary conditions causes that the analysis of buckling can not be easily performed analytically. The conducted numerical analyses reveal that buckling of the cylinder has rather local character and it is concentrated in the vicinity of the free end of the cylinder, cf. Fig. 5.1.8a.

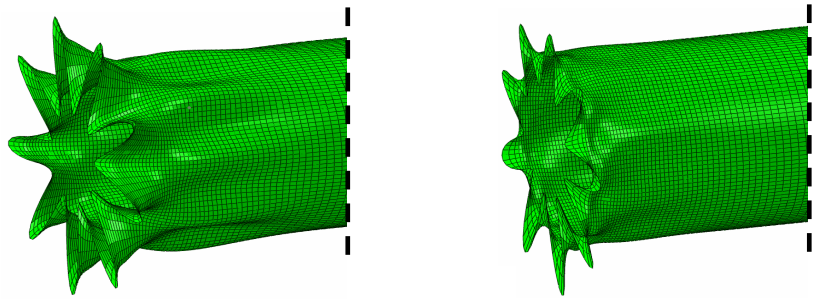

Fig.5.1.8: Comparison of buckling shape obtained for various internal pressures: a) p=0MPa, b) p=0,07MPa

The applied internal pressure causes, in general, stiffening of the cylindrical shell and it is reflected both in buckling shapes and in the value of the critical force. Even for low values of pressure, the buckling area steadily moves in the direction of free end and gradually occupies smaller part of the cylinder, cf. Fig. 5.1.8b. At certain value of pressure (in considered case 0.08MPa) buckling shape changes and does not contain characteristic weaving of the free end of the cylinder. The value of critical force increases in the range of pressure 0-0.08MPa and then remains at almost constant value, see Table 2.

Pressure [MPa]	0	0,01	0,02	0,03	0,04	0,05	0,06	0,07	0,08	0,09	0,1
Force [N]	4071	4501	4729	4890	5002	5091	5159	5210	5236	5235	5231

Table.2. Change of critical force of axially compressed cylinder in terms internal pressure

Modal analysis of the inflated can was performed in order to investigate change of basic dynamic characteristics caused by internal pressure. Similarly as in case of buckling analysis, modal analysis of the inflatable structure is preceded by the initial step where distributed loading modelling gas pressure is applied. This stage of analysis is aimed at obtaining pre-stressed and deformed configuration of the structure which serves as a starting point for the second stage where classical modal analysis is performed. The mathematical formulation of the problem reads:

$$\begin{aligned} &\text{Step 1: } \mathbf{K}(\mathbf{Q}_\mathrm{p},\mathbf{q}_\mathrm{p})\mathbf{q}_\mathrm{p} = \mathbf{Q}_\mathrm{p} \\ &\text{Step 2: } \left[\mathbf{K}(\mathbf{Q}_\mathrm{p},\mathbf{q}_\mathrm{p}) - \omega^2\mathbf{M}\right]\boldsymbol{\varphi} = \mathbf{0} \end{aligned} \tag{5.1.13}$$

where ω is natural frequency of the system and $\boldsymbol{\varphi}$ indicates subsequent modes of vibration. Initial pre-stress of the structure by internal pressure generates internal forces and corresponding deformation of the structure which influence stiffness matrix used in modal analysis. Consequently, initial prestress affects eigen-frequencies and modal shapes of the inflated structure determined from Eq. 5.1.13b.

Since the most significant effect of internal pressure is a uniform tension of the inflated structure, the frequencies of structure vibration increase. The effect is significant even when the gas inside the cylinder is under low pressure (see Table 3) and it corresponds to subsequent vibration modes of the structure. Change of the vibration frequency is often accompanied with change of the modal shape, which in case of inflated structure is characterized by smaller number of 'waves' in the circumferential direction, cf. Fig. 5.1.9. Let us note that two characteristic features of the structure considered within this section, i.e. buckling force and frequency of vibration are not independent from each other since they are connected by the dynamic criterion of the stability loss. More detailed studies on vibrations of cylindrical shells filled with fluid or exposed to fluid flow are presented in papers [282 283].

	p=0	**p=0,2**	**p=0,4**	**p=0,6**
Mode I	830,25	2556,0	2959,3	3189,9
Mode II	880,67	2709,3	3297,6	3900,8
Mode III	1005,6	3083,8	4243,7	5133,1
Mode IV	1079,8	3809,7	4670,9	5148,8

Table.3: Change of frequency of vibration [Hz] caused by internal pressure [MPa] (modes related to deformation of the cylinders sidewalls)

The final conclusion from the experiment and simulations conducted in this section is that application of internal pressure can substantially alter state of stress of the structure, the value of the buckling force and frequencies of structure vibrations. Therefore, stability of the state of equilibrium, as well as basic dynamic properties and energy dissipation capabilities of thin-walled structures can be effectively controlled by means of internal pressure.

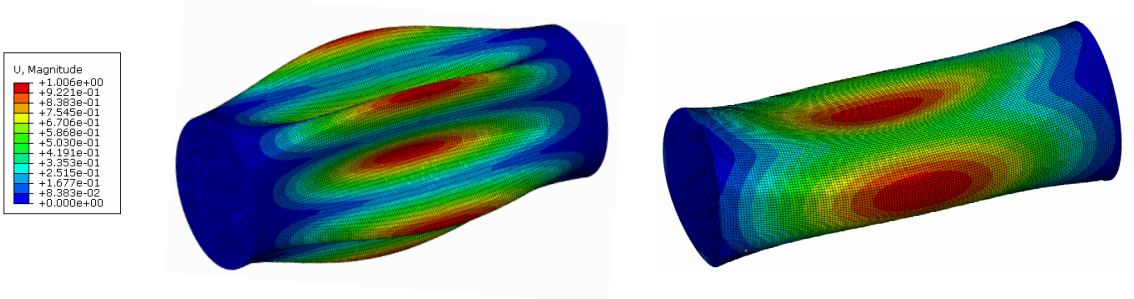

Fig. 5.1.9: Change of first vibration mode of the cylinder caused by internal pressure: a) p=0MPa, b) p=0,6MPa

5.1.2. Analysis of basic inflatable structures

The following section is dedicated to basic numerical analysis of several types of thin-walled structures and an attempt of their improvement by using compressed gas. The following engineering structures will be examined:

- inflatable compartments inside hull of the ship,
- inflatable door of the passenger car,
- inflatable road barrier.

For each type of structure the influence of internal pressure on structure durability and energy absorption capabilities will be analysed. Range of required pressure value will be estimated and benefits of dividing the structure into several pressurised chambers with various pressures will be examined. Presented examples will be further used to develop simplified two-dimensional model of thin-walled inflatable barrier for which precise algorithms of pressure adjustment will be elaborated.

Inflatable hull compartments

The first of the proposed concepts is inflation of the compartments located inside hull of the ship in order to increase hull durability and to prevent its penetration in case of open-sea ship collisions.

One of the most dangerous collision scenarios is an impact of ship with a bulbous bow against double hull carrier, cf. Fig. 5.1.10a. The thorough numerical simulations of such collision was performed by Wiśniewski and Kołakowski [284]. In this study, the hull of the struck ship was composed of inner and outer hull, stiffeners and hull plating, while the bulbous bow of the striking ship was assumed to be a rigid body. The struck ship was still, and the striking ship was moving in horizontal direction such that collision occurred at right angle. The results of numerical simulations conducted in [284] indicate that typical damage of the struck ship caused by impact of moderate velocities involves total penetration of the carrier hull.

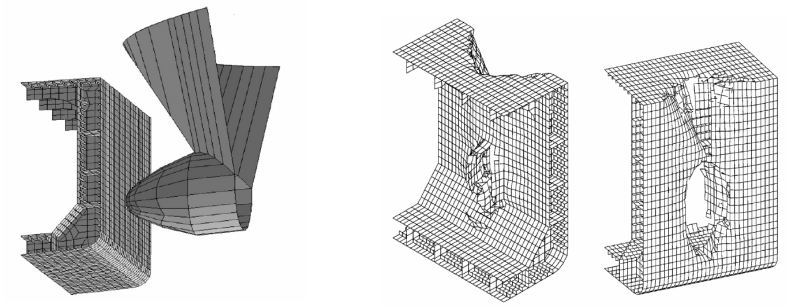

Fig. 5.1.10: Collision of double- hull carrier and ship with a bulbous bow: a) numerical model of the problem, b) typical damage of the struck ship [284]

The finality and effectiveness of the inflation of hull compartments was examined by using simplified numerical example in which rectangular prism of dimensions 6m x 4m x 1,5m and thickness of 0,015m which models single compartment of the ship hull is impacted by rigid sphere of diameter 1,6m which models a bulbous bow, cf. Fig. 5.1.11. The proposed simplified simulation is based on the mentioned previously simulation of ship collision in terms of basic dimensions and material properties. The characteristics of the compartment material were assumed as elasto-plastic with hardening. Tensile failure of the steel occurs when ultimate plastic strain ($\varepsilon = 0{,}17$ at $\sigma = 400\text{MPa}$) is exceeded in all Gauss points of the element.

In the initial simulation, empty compartment was subjected to impact characterized by fixed velocity equal to 10m/s but various masses of the striking object. Two types of displacement boundary conditions were considered:

- suppression of displacements of the lower edge of the compartment only,
- suppression of displacements of both upper and lower edge.

Since deformation of the compartment differs significantly in both cases, the process of impact and the influence of inflation will be analysed separately for each type of structure.

In the first case, when the edge of the upper surface remains unconstrained, both upper and lower surface of the chamber are simultaneously involved in the process of impact absorption. After the impact, the upper surface deflects until contact with the lower surface occurs. In the following stage, both surfaces remain in contact and deflect together. The lower surface usually ruptures first which is the result of kinematic boundary conditions applied along all its edges. Finally, the upper surface of the chamber also bursts and total penetration by the hitting object occurs. In the considered example, all stages of the process take place for the impacting mass of 800 tons and above, Fig. 5.1.11.

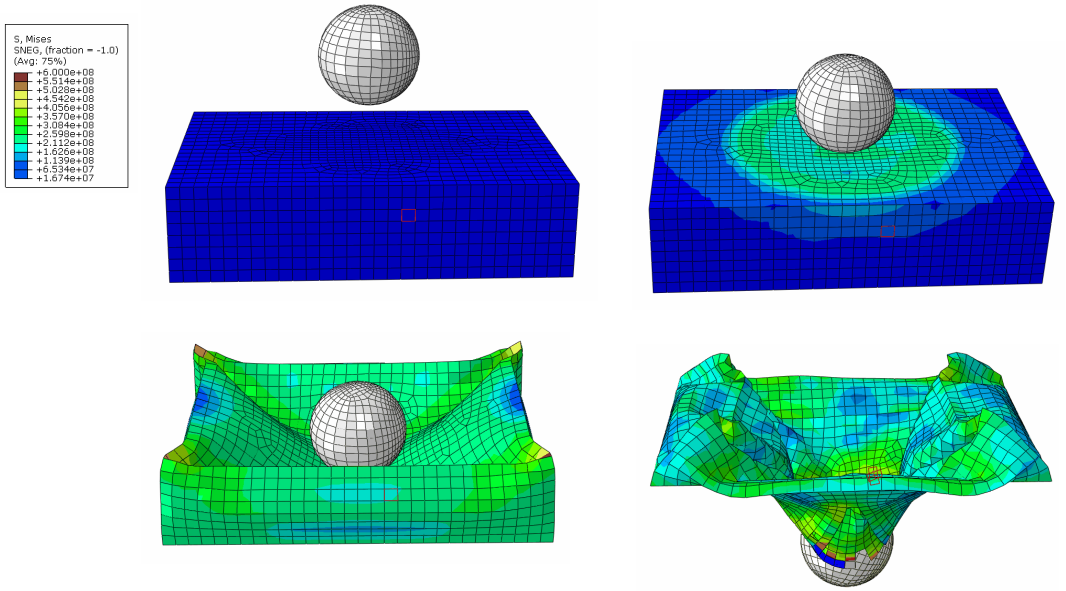

Fig.5.1.11: Simulation of impact against empty compartment (M=800tons, V=10m/s): a) initial stage of impact, b) impact process with final full penetration of the compartment

Beneficial influence of chamber inflation is the most transparent during the first stage of impact when internal pressure increases resistance of the upper surface against impact loading. In the second stage of impact when both surfaces come into contact, the advantageous effect of inflation relies on increase of global stiffness of the compartment. At time instant when lower surface is ruptured, the influence of internal pressure is totally suppressed due to immediate pressure release.

In the presented numerical example (Fig. 5.1.12), the impact loading is exactly the same as previously and internal pressure is maintained at the lowest constant level for which a qualitative difference in response is observed (p=4atm). Applied internal pressure allows to avoid rupture of the upper surface and therefore it prevents the penetration of the compartment by impacting object. Substantially higher value of constant internal pressure (p>8atm) allows to obtain a different mode of deformation in which destruction of lower

surface is prevented, however the upper surface bursts. Although none of the above strategies allows to maintain total structural integrity of the compartment, the presented example clearly indicates that internal pressure allows to avoid full penetration by impacting object and to control type of compartment failure.

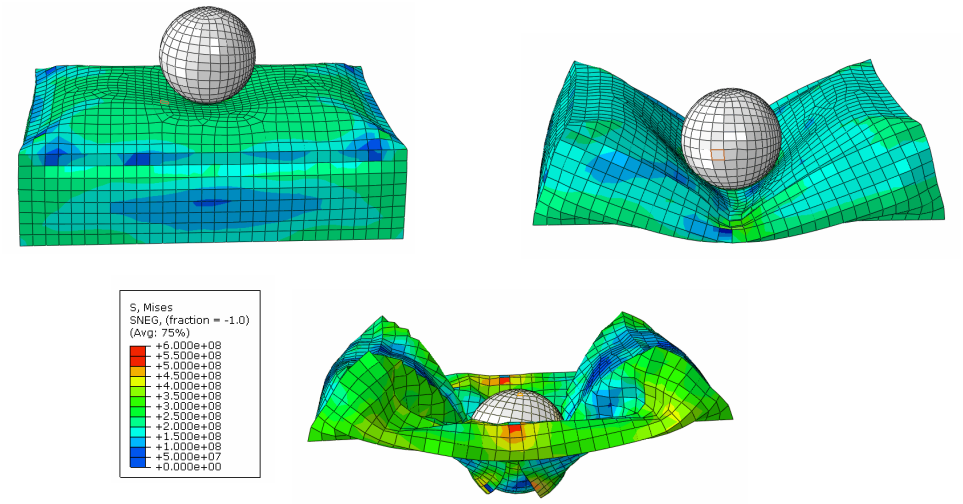

Fig.5.1.12: Simulation of impact against inflated compartment (M=800tons, V=10m/s, p=4atm): a) initial stage of impact, b) intermediate stage of impact, c) final stage of impact with rupture of the lower surface only

In case of the second type of boundary conditions, when displacement of the upper edge of the compartment is constrained, both surfaces of the cuboid respond almost independently. Kinematic constraints imposed on upper surface do not allow for its large deflection and contact with the lower surface. Therefore, the impacting object is initially being stopped by the upper surface and when it ruptures - by the lower surface, cf. Fig. 5.1.13a. Mass of the object which causes penetration of the upper layer is substantially lower than in previous case and equals 150tons.

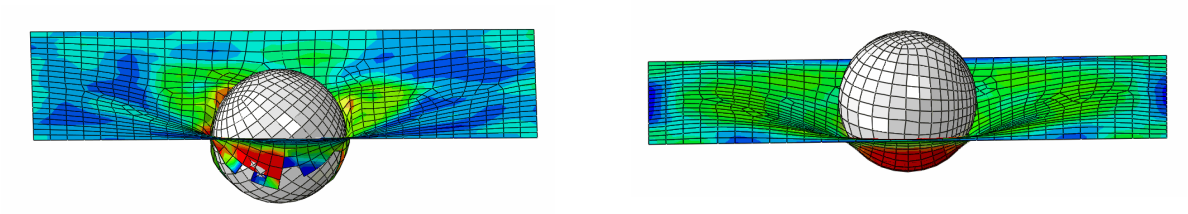

Fig.5.1.13: Simulation of the impact process (M=150tons, V=10m/s): a) final deformation of an empty compartment, b) final deformation of the inflated compartment

Despite different operating principles the internal pressure can still be used to improve durability of the structure against impact loading. In this case, pressure will be applied to avoid rupture of the upper layer of the compartment. In the numerical example internal pressure is maintained at a lowest constant level (p=6atm) for which failure of the upper surface of the cuboid does not occur. The strategy results in rebound of the impacting body and allows to preserve the integrity of the compartment, Fig. 5.1.13b. In the considered case, internal pressure can be used only for increasing the durability of the upper surface and it has no beneficial influence on the response of the lower surface.

Inflatable door of the car

The second proposed concept is inflation of the door of the passenger car in order to increase its durability in case of lateral impact against narrow objects. Lateral collision with objects such as pole, lantern or tree is a typical accident scenario and in case of higher velocities it may causes severe destruction of the whole body of the car, cf. Fig. 5.1.14a. Lateral impact is also included as a mandatory crash-test for each produced car according to the European New Car Assessment Programme (Euro-NCAP). In this test, the car is propelled sideways at 29kph into a rigid pole of a diameter 25,4mm, Fig. 5.1.14b.

Fig.5.1.14: Lateral impact thin-walled door of the passenger car: a) deformation of the car after lateral impact with high velocity, b) scenario of NCAP 'Pole side impact' test

The concept of inflatable door is based on division of its internal space into sealed chambers (Fig. 5.1.15), appropriate inflation of each chamber depending on actual impact scenario and release of gas during impact. The division into pressure chambers can be performed by stiff partitions made of the same material as the door itself or, alternatively, by elastic membrane partitions. In case when the partitions are stiff they substantially increase durability of the door against side impact. Therefore, the direct comparison of empty and inflated structure can be done only for structures of the same topology.

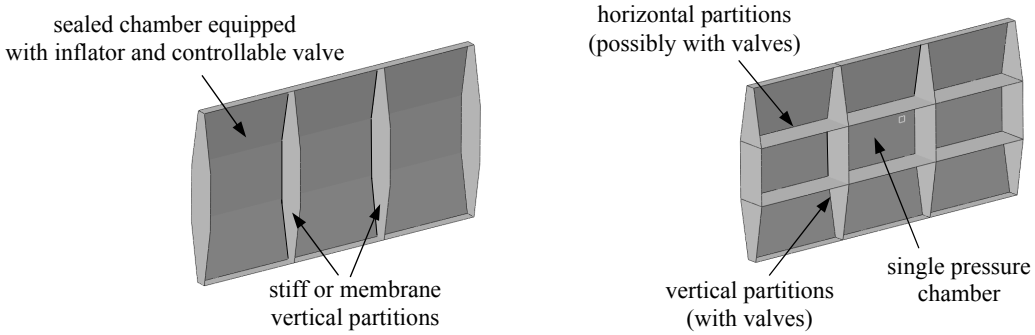

Fig.5.1.15: The concept of multi-chamber inflatable door of the passenger car with:
a) vertical division into three vertical chambers, b) both-directional division into nine chambers

Numerical simulations within this section are based on NCAP pole side impact test. In the numerical simulation immobile door of the car (dimensions: 1m x 0,6m x 0,1m, thickness 0,001m) supported in out-of-plane direction on lateral edges are subjected to impact of a rigid pole of fixed mass and velocity (M=1000kg, V=4m/s and V=8m/s). The main requirement for the door of the car is to minimise deformation caused by the hitting object in order to protect passenger's area. Therefore, maximal deflection of the door is the main quantity observed in each simulation. Since deformation of the structure strongly

depends on kinematic constraints imposed on in-plane displacement of the left and right edge of the door, two types of kinematic boundary conditions (free and blocked) will be considered separately.

The first example concerns three-chamber structure with fixed displacement of lateral edges and impact with velocity of 8m/s, Fig.5.1.16. The impact results in substantial deformation of the structure with maximal displacement of the central part of 0,22m. Simple strategy of internal pressure control assumes inflation of central chamber with twice higher pressure than the lateral chambers and maintaining constant pressure during the impact process.

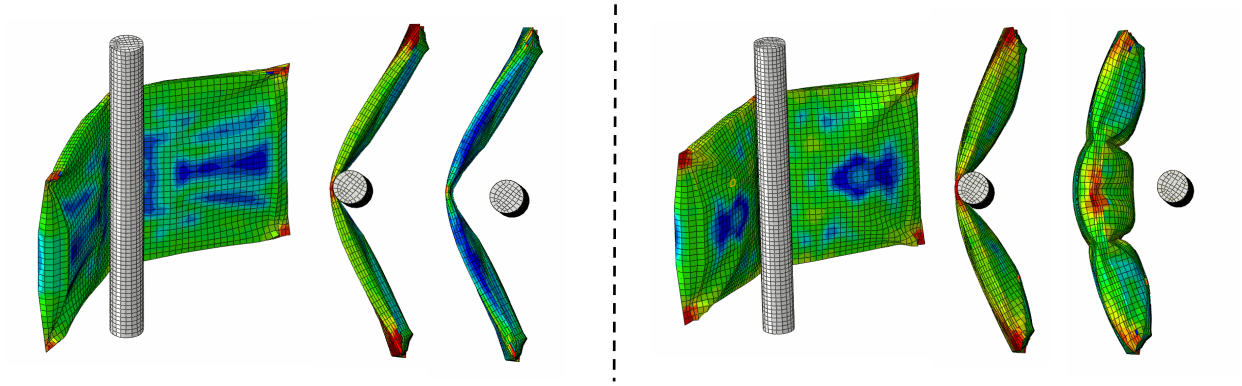

Fig.5.1.16: Response of three-chamber structure to lateral impact (M=1000kg, V=8m/s, suppressed in-plane displacement): a) no inflation, b) constant pressure: 2.5atm, 5atm, 2.5atm.

The application of the above strategy (with pressures 2,5atm, 5atm, and 2,5atm) results in a substantial change of deformation shape and decrease of maximal displacement to 0,17m. Moreover, increase of stresses was observed only in certain small regions of the structure, particularly at corners and edges. The effect of inflation is clearly visible after rebound of the impacting object, Fig. 5.1.16. After the impact, generic empty structure remains fully deflected by impacting object while inflated structure partially retains its initial configuration simultaneously remaining bulged by internal pressure.

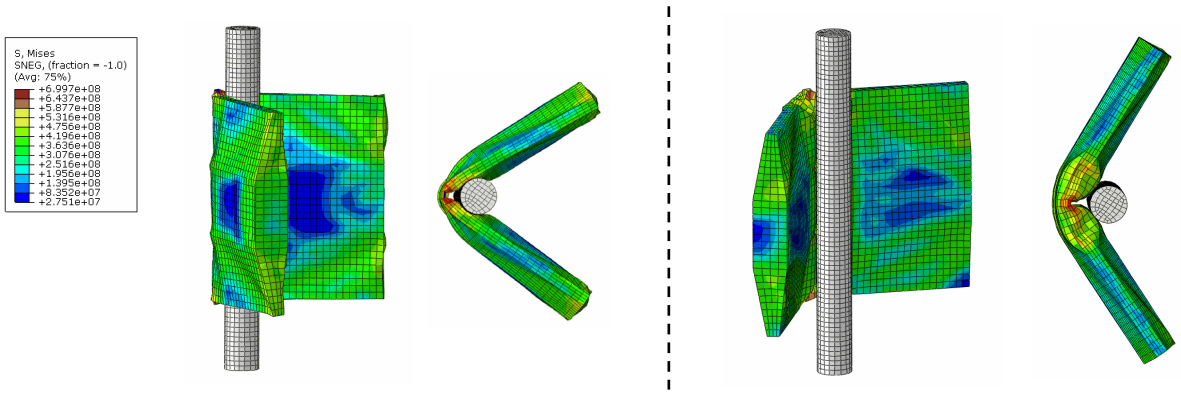

Fig.5.1.17: Response of nine-chamber structure on lateral impact (M=1000kg, V=4m/s, free in-plane displacement): a) no inflation, b) constant pressure of 5atm

The influence of inflation is even more apparent in case of structure with free in-plane displacement of the lateral edges (free-supported structure). In numerical simulation

the structure divided into nine chambers was subjected to impact with initial velocity equal to 4m/s. Despite larger initial stiffness of the structure and smaller impact energy, the deformation of the structure is significant (max. displacement: 0,38m) and it is stopped only due to squeeze of the pole, Fig. 5.1.17a. Inflation of the structure with uniform pressure of 5atm allows to change the shape of structure deformation (Fig. 5.1.17b) and to decrease maximal displacement by approx. 40% (to 0,23m).

Both presented examples indicate that application of internal pressure allows to increase global stiffness of thin-walled structure and to control (and substantially diminish) depth of penetration caused by impacting object.

Inflatable road barrier

The last considered concept of inflatable thin-walled structure is a multi-chamber inflatable traffic barrier, cf. Fig. 5.1.18a. Traffic barriers are mounted at the edges of the road in order to prevent errant vehicles against falling out of the road and being subjected to obstacles or hazards located nearby. They can be divided into three groups depending on their stiffness:

- flexible barriers (as metal beam fence, cable barriers, corrugated rail systems),
- semi-rigid barriers (as standard guardrail barrier described below),
- rigid barriers (as block of reinforced concrete).

Standard guardrail barriers are constructed of sigma posts, distance spacer and a guardrail, Fig. 5.1.18a. They dissipate energy of impact by deformation of the elements of barrier, friction between barrier and the car and deformation of the car's body. Semi-rigid barriers usually allow for deformation up to ~1m in case of the harshest impact. In Poland the requirements for design of the traffic barriers are regulated by the code PN-EN 1317. Accordingly, the barriers are designed to sustain impact of heavy vehicle with large initial velocity but simultaneously to provide acceptably low level of deceleration of light vehicles. Since above requirements are contradictory, a typical passive barrier cannot fulfil both of them in an optimal way.

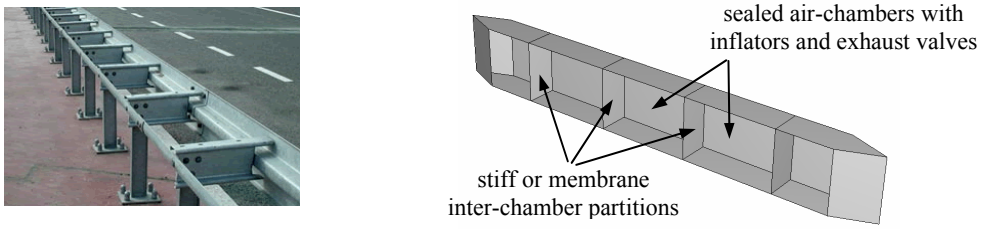

Fig.5.1.18: Comparison of two various designs of a traffic barrier: a) standard guardrail design, b) the concept of adaptive inflatable road barrier

Some innovative concepts of barriers include the possibility of adaptation to actual impact conditions. As an example, one of the concepts is based on a cable net equipped with hydraulic absorbers on both sides which allow to control the force used for stopping the car. Since such a barrier is designed for impact at right-angle and it requires substantial operational space, its application as a typical roadside barrier is strongly limited. Another concept utilizes the special panel which extends from the surface of the road and stops the vehicle [285]. The system is activated by sensor embedded in surface of the road which

recognizes type and velocity of the approaching vehicle. Moreover, the concept of flexible barrier equipped with internal airbags was proposed in [286], however the structure was not considered as adaptive and the possibilities of adjustment to actual impact scenarios were not discussed.

The potential of application of compressed gas inside thin-walled road barrier was examined with the use of conceptual design presented in Fig. 5.1.18b. In numerical simulations, the barrier of dimensions 3m x 0,2m x 0,4m and material thickness of 3mm was subjected to perpendicular and skew (45 degrees) impact of the rigid body of dimensions of the car, mass 1000kg and velocity of 16m/s. The presented results concern three-chamber inflatable barrier with thin steel partitions of thickness 1mm.

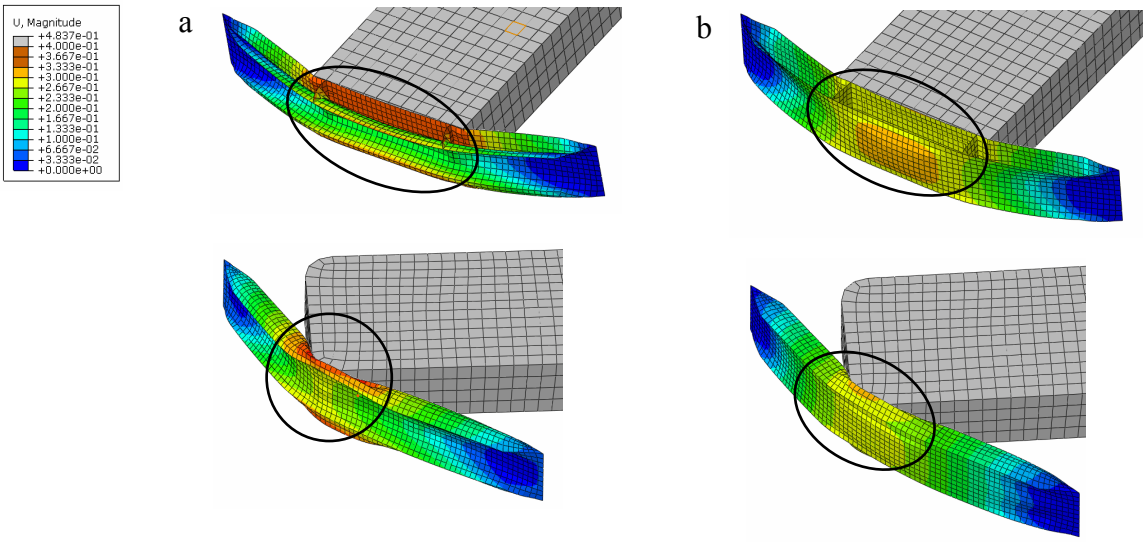

Fig.5.1.19: The influence of internal pressure on response of the barrier subjected to perpendicular and skew impact: a) empty barrier, b) barrier inflated with pressures: 3atm, 5atm, 3atm.

In case when the barrier is not inflated the perpendicular impact, Fig. 5.1.19 (top), causes folding of the of the upper wall, crushing of the internal partitions and substantial reduction of the barrier width during the process. Inflation of the barrier increases local stiffness of each pressure chamber, changes local stress distribution and prevents crushing of the internal partitions. As a result, the barrier preserves its original width, its global stiffness increases and way of stopping the impacting object is reduced (0,34m to 0,28m). In case of skew impact the influence of internal pressure causes distribution of the deformed zone along the length of the barrier instead of concentration in one distinct location, cf. Fig. 5.1.19 (bottom).

The above examples show that inflation of the particular chambers allows to control shape of local deformation of thin-walled structure and to influence zones where stress concentration arises or distribute them into larger area.

5.2. Adaptive inflatable multi-chamber barrier

Strategies of optimal adjustment of pressure during impact will be developed for a simple two-dimensional frame, Fig. 5.2.1. The structure under consideration may contain arbitrary number of pressure chambers separated by stiff or elastic partitions. Each

chamber is assumed to be equipped with inflators and controllable valves which allow for real-time control of internal pressure. The loading is applied at the upper beam of the structure which models lateral (non-axial) impact. The model accounts for both material and geometrical nonlinearities: elasto-plastic material with hardening is assumed and equilibrium equations are set in an actual configuration.

Although the proposed model of the inflatable structure is relatively simple (and therefore computationally effective), it possesses the main features of three-dimensional thin-walled inflatable steel structures analysed in previous section of this chapter. Therefore, obtained results and conclusions could serve as a basis for design of three-dimensional thin-walled inflatable structures of more complex design.

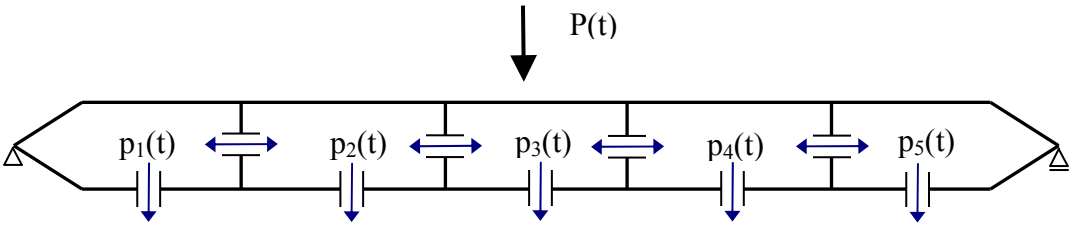

Fig. 5.2.1: Two-dimensional frame structure with several separate pressure chambers considered in the optimization problem

The problem of pressure adjustment will be aimed at finding optimal initial distribution of pressure inside the chambers and its optimal change during the impact process. Here, the above task will be formulated rather as optimization than a control problem. The optimisation will be performed primarily with respect to functions describing changes of pressure in particular chambers. Corresponding objective functions will be based on the criteria of maximization of the load capacity of the barrier (Sec.5.2.1) and its optimal adaptation to a given impact loading (minimization of hitting object deceleration, minimization of internal pressure and obtaining assumed deformation of the structure, Sec. 5.2.2). The constraints will be formulated by using kinematic conditions imposed on maximal displacement and final deformation of the frame. Considered objective functions and constraints usually depend on applied pressure changes in a complicated way since they are obtained from nonlinear dynamic analysis.

Influence of internal pressure (linear static case)

The preliminary step before solving aforementioned optimisation problems will be linear static analysis aimed at evaluation of the influence of internal pressure on distribution of internal forces in selected elements of the frame.

The frame is modelled by Bernoulli beam elements. Since the structure is statically indeterminate, internal forces can not be found by using equilibrium equations only. Instead, they can be determined in a classical way by the 'force method' or, alternatively, the finite element method which allows to obtain the exact solution when physical shape functions are used. In the latter approach, solution of the global equilibrium equation $\mathbf{Kq} = \mathbf{Q}$ allows to find deformation of each element of the frame (longitudinal displacement $u(x)$ and deflection $w(x)$) and to calculate internal forces (normal forces, transverse forces and bending moments) according to formulae $N = EAu'$, $T = EJw'''$, $M = EJw''$, respectively. In the

following examples only the value of bending moment will be considered since it causes the largest values of generated stresses.

In the first example, the frame contains one chamber and it is loaded in the middle of the upper span by a point load **P**. When structure is not inflated solution of the problem $\mathbf{Kq} = \mathbf{P}$ yields linear distribution of bending moments on the upper span with the largest bending moment at its middle point (M_1=18,54 kNm), Fig.5.2.2a. In case when the frame is additionally subjected to internal pressure *p,* the equilibrium is described by the equation:

$$\mathbf{Kq} = \mathbf{P} + p\mathbf{Q}_\mathbf{p} \tag{5.2.1a}$$

where $\mathbf{Q}_\mathbf{p}$ indicates load vector which models distributed loading of a uniform value. The problem of finding optimal value of pressure *p* reads:

$$\text{Find } p \text{ such that } \max M_n(x) \text{ is minimal} \tag{5.2.1b}$$

where $M_n(x)$ denotes maximal bending moment which results from solution of the problem (5.2.1a). Since applied internal pressure causes reduction of bending moment at the upper beam but simultaneously increases bending moment at the lower beam, the optimal strategy is based on equalizing both bending moments. The strategy results in decrease of maximal bending moment to 11,72kNm which is equivalent to increase of load capacity by 58,4%.

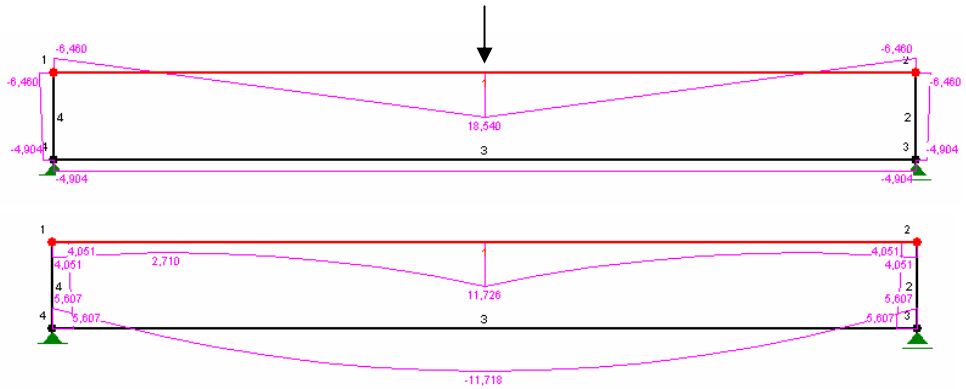

Fig.5.2.2: Reduction of bending moment obtained by uniform pressure. Load capacity: a) 1 b) 1,58.

Further improvement can be achieved by applying internal pressure only in selected parts of the structure. To avoid an adverse effect of increase of bending moment at the lower beam, the structure was divided horizontally into two separate pressure chambers by internal partition with two joints in its middle part, Fig. 5.2.3. Only the upper chamber was inflated. The structure equipped with internal chamber of horizontal length *d* inflated with pressure *k* is described by the equation:

$$\mathbf{K}(d)\mathbf{q} = \mathbf{P} + p\mathbf{Q}_\mathbf{p}(d) \tag{5.2.2a}$$

The corresponding optimisation problem is to find optimal length of the chamber and optimal value of pressure multiplier:

$$\text{Find } d,p \text{ such that } \max M_n(x) \text{ is minimal} \tag{5.2.2b}$$

For each length of the upper chamber optimal value of internal pressure *p* allows to equalise bending moments at the upper beam in its middle and in locations where internal chamber is attached. Optimal value of the parameter *d* was found by testing several types of structures

with various lengths of the upper chamber. Finally, the largest reduction of the bending moment (to 4,79kNm) and corresponding largest increase of load capacity (286%) was obtained in case when the length of the upper chamber equals the total length of the frame.

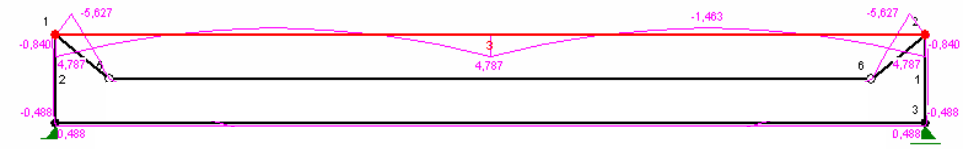

Fig.5.2.3: Reduction of bending moment obtained by horizontal division and uniform pressure in the internal upper chamber. Load capacity: 2,58.

5.2.1 Maximisation of the load capacity

This section investigates the possibilities of increasing load capacity of dynamically loaded structure by a precise adjustment of initial inflation and release of pressure during the impact process. Load capacity of the considered structure will be defined as maximal impact energy which can be applied to the structure. Consequently, an objective of the corresponding optimization problem will be maximisation of impact energy.

Mathematical formulation

The finite element model of the frame subjected to dynamic loading is in general described by nonlinear equation of motion:

$$\mathbf{M}(m)\ddot{\mathbf{q}} + \mathbf{C}\dot{\mathbf{q}} + \mathbf{K}(\mathbf{q})\mathbf{q} = \mathbf{F}(\mathbf{p},\mathbf{q}) + \mathbf{F_I}(t) \qquad (5.2.3)$$

$$\mathbf{q}(0) = \mathbf{q}_0 \,,\, \dot{\mathbf{q}}(0) = \dot{\mathbf{q}}_\mathbf{0}$$

where vector $\mathbf{p}(t) = \{p_1(t), p_2(t), ..., p_n(t)\}$ denotes changes of pressures in each chamber of the frame. The impact applied to the upper beam can be modelled by one of the following:

- a priori assumed right hand side force vector $\mathbf{F_I}$(t),
- mass of the hitting object m added in selected nodes of the frame and corresponding initial velocity V_0 (being part of the vector $\dot{\mathbf{q}}_\mathbf{0}$),
- contact conditions defined between inflatable structure and rigid object of mass m approaching the structure with velocity V_0 .

In any option of impact modelling, the vector $\mathbf{F}$ ($\mathbf{p}$,$\mathbf{q}$) is present in governing equation since it provides coupling between the frame structure and gas enclosed inside. In case of passive inflatable structure pressure $\mathbf{p}(t)$ is unambiguously defined in terms of initial pressure and actual chamber deformation.

On the contrary, in case of adaptive inflatable structure pressures inside cavities can be used to control dynamic response since they influence right hand side load vector $\mathbf{F}$ and displacements $\mathbf{q}$, likewise. Due to the fact that control will be applied by direct change of pressures (not the flow coefficients) the approach will be called 'direct pressure control'. Arbitrary change of internal pressure, which affects right hand side vector $\mathbf{F}$ can be treated, from the point of view of control theory, as control by external forces (active control). However, only the value of pressure can be controlled. Direction of the distributed loading resulting from internal pressure is predefined by actual configuration of the structure.

Moreover, it will be assumed that after the inflation stage the presure of gas is either constant or gradually decreases as the impact proceeds. Due to the fact that during the process volumes of the chambers typically decline, maintaining constant value of pressure (or its decrease) requires release of gas from the chambers. Since the gas is only released, no additional energy is added to the system, the structure remains adaptive and fulfils the paradigm of Adaptive Impact Absorption.

In the following part of this section impact of the rigid body will be considered. For given location and direction of impact, the solution of the problem (5.2.3) can be written as vector function $\mathbf{q}(m,V_0,\mathbf{p},t)$ where argument m denotes mass of the hitting object and V_0 denotes value of its initial velocity. The function $\mathbf{q}(m,V_0,\mathbf{p},t)$ is not defined explicitly in terms of its arguments but it has to be obtained from nonlinear dynamic analysis typically conducted by Finite Element Method. Let us note that values of components of vector $\mathbf{q}$ at arbitrary time instant t_x do not depend exclusively on values of pressures at time t_x but also on values of pressure during the whole period (0-t_x).

Henceforth, it will be assumed that the impact velocity V_0 is fixed so the solution of the problem (5.2.3) can be written as $\mathbf{q}(m,\mathbf{p},t)$ and deformation of the frame, its internal forces and load capacity are defined exclusively by mass of the hitting object. In further analysis two special quantities will be used:

- function $\mathbf{q}_m(m,\mathbf{p},t)$ being component of $\mathbf{q}(m,\mathbf{p},t)$ which denotes displacement of the node of the upper beam located in the center of the impact zone (displacement of 'central impacted node'),
- vector $\mathbf{q}(m,\mathbf{p},t_{stop})$ which indicates deformation of the structure at time instant when impacting mass is stopped, i.e. at instant when velocity of the hitting object approaches zero for the first time.

Arbitrarily assumed set of all admissible values of mass will be denoted by Ω_m and arbitrarily assumed set of all admissible functions describing change of pressure will be denoted by $\Omega_{\mathbf{p}}$. Both sets are assumed to be positive. Additionally, functions being components of vector $\mathbf{p}$ cannot exceed a fixed upper limit.

Definition of the load capacity of the structure requires introducing conditions which describe limits of its admissible state. These conditions can be defined in various ways including typical conditions imposed on maximal level of stress and maximal elongation of members. However, here the kinematic approach will be used and conditions describing admissible state of the structure will based exclusively on its deformation. Hereafter, deformation of the structure will be considered as admissible if two conditions are satisfied:

1. contact of the lower and upper beam of the frame during the impact process does not occur,
2. maximal displacement of the lower span during the impact process does not exceed a limit value.

Let us introduce two scalar functions describing deformation of the structure. The first function $D(m,\mathbf{p},t)$ describes distance between central impacted node and the lower span of the frame, which can be expressed in terms of displacement of the impacted node $\mathbf{q}_m$ and displacements of the nodes located at the lower span $\mathbf{q}_{\mathbf{low}}$:

$$D(m,\mathbf{p},t) = \mathrm{dist}\left(\mathbf{q}_m(m,\mathbf{p},t), \mathbf{q}_{\mathbf{low}}(m,\mathbf{p},t)\right) \tag{5.2.4a}$$

The second function $q_{max}(m,\mathbf{p},t)$ describes maximal deflection of the structure (i.e. the largest among vertical displacements of the nodes located at the lower beam $\mathbf{q}_{\mathbf{low}}^{\mathbf{vert}}$), which is expected to occur at time instant when impacting mass is stopped:

$$q_{\max}(m,\mathbf{p},t_{stop}) = \max\ \mathbf{q}_{\mathbf{low}}^{\mathbf{vert}}\ (m,\mathbf{p},t_{stop}) \tag{5.2.4b}$$

Set of admissible deformations of the frame S_q can now be defined as:

$$S_q = \{\mathbf{q}(m,\mathbf{p},t) \text{ satisfying conditions}: \tag{5.2.5}$$

$$1)\ D(m,\mathbf{p},t) > 0 \quad \text{for } t \in \left(0, t_{stop}\right\rangle$$

$$2)\ q_{\max}(m,\mathbf{p},t_{stop}) \le q_{adm}\}$$

The problem of maximisation of allowable impact energy can be formulated as follows: find maximal mass which can be applied to the structure with optimally controlled internal pressure and which does not violate kinematic conditions imposed on structure deformation. Corresponding mathematical formulation of the problem reads:

$$\begin{gathered}\text{Find: } \{m,\mathbf{p}\} \text{ such that } \Psi(m,\mathbf{p}) = m \text{ is maximal} \\ \text{subject to: } \mathbf{q}(m,\mathbf{p},t) \in S_q\end{gathered} \tag{5.2.6}$$

where S_q is defined by (5.2.5). Therefore, the problem of maximisation of allowable impact energy relies not only on finding maximal mass but also on finding optimal change of pressure inside chambers of the frame. Although the objective function $\Psi(m,\mathbf{p})$ is extremely simple (being equal to one of the arguments), the constraint depends in complicated way on both optimisation variables. Therefore, the main difficulty in solving the above optimisation problem is to account for complicated constraint imposed on a set of optimisation variables $\Omega_m \times \Omega_{\mathbf{p}}$.

Further, we will simplify the problem (5.2.6) and we will rearrange it to the form convenient for numerical computations. Let us introduce the set $S_m(\mathbf{p})$ being the subset of Ω_m containing all values of impacting mass which cause admissible deformation of the structure for arbitrarily assumed change of internal pressure inside the chambers (Fig. 5.2.4):

$$S_m(\mathbf{p}) \subseteq \Omega_m \tag{5.2.7}$$

$$S_m(\mathbf{p}) = \{m \text{ such that } \mathbf{q}(m,\mathbf{p},t) \in S_q\}$$

The functional $\Phi_m(\mathbf{p})$ will indicate load capacity of the structure, i.e. maximal impacting mass which can be applied to the structure for given changes of internal pressure:

$$\Phi_m(\mathbf{p}) = \max\{m \in S_m(\mathbf{p})\} = \max\{m \text{ such that } \mathbf{q}(m,\mathbf{p},t) \in S_q\} \tag{5.2.8}$$

By using the function $\Phi_m(\mathbf{p})$, the problem (5.2.6) can be decomposed into the form:

$$\text{Find } \max_{\mathbf{p}}\{\Phi_m(\mathbf{p})\},\ \mathbf{p}\in\Omega_{\mathbf{p}}$$
$$\text{where } \Phi_m(\mathbf{p}) = \max_m\{m \text{ such that } \mathbf{q}(m,\mathbf{p},t)\in S_q\} \tag{5.2.9}$$
$$\text{and } S_q \text{ is defined by (5.2.5)}$$

Let us note that formulation (5.2.9) involves two separate stages of optimisation. At the first stage maximal mass which causes admissible deformation of the structure for given changes of pressures inside the chambers is searched (calculation of the objective function $\Phi_m(\mathbf{p})$). The goal of the second stage is to find changes of pressures inside chambers for which value of mass that can be applied to the structure is the largest (maximisation of the objective function $\Phi_m(\mathbf{p})$).

In order to simplify the **first stage** of the procedure, it will be assumed that maximal value of impacting mass is obtained at the boundary of allowable set of optimisation variables. We will define limiting deformations of the structure corresponding to both introduced kinematic conditions. The set of limiting deformations corresponding to a lack of collision of the spans Γ^1_{Sq} involves reduction of distance between mass and lower span to an infinitesimal value δ at time instant of stopping the mass t_{stop}. Mathematically, the above conditions can be written in the form:

$$\Gamma^1_{Sq} = \{\mathbf{q}(m,\mathbf{p},t_{stop}) \text{ satisfying conditions}:$$
$$1)\ D(m,\mathbf{p},t_{stop}) = \delta\ ;\quad 2)\ \left.\frac{dD(m,\mathbf{p},t)}{dt}\right|_{t=t_{stop}} = 0\ ;\quad 3)\ \left.\frac{d^2D(m,\mathbf{p},t)}{dt^2}\right|_{t=t_{stop}} > 0\ \} \tag{5.2.10}$$

Due to fact that maximal displacement of the lower span also occurs at time t_{stop} , the set of limiting deformations corresponding to maximal displacement of the lower span is defined as:

$$\Gamma^2_{Sq} = \{\mathbf{q}(m,\mathbf{p},t_{stop}) \text{ satisfying condition}: \tag{5.2.11}$$
$$q_{\max}(m,\mathbf{p},t_{stop}) = q_{adm}\ \}$$

The above approach allows to detect limiting deformation of the structure by examining only infinitesimal time interval in the vicinity of time instant t_{stop}, not the whole period of the impact. Further, we can define functional $\Gamma^1_{Sm}(\mathbf{p}) = m^1(\mathbf{p})$ which returns mass which causes limiting deformation Γ^1_{Sq} (i.e. infinitesimal distance between beams at time t_{stop}):

$$\Gamma^1_{Sm}(\mathbf{p}) \subseteq \Omega_m \tag{5.2.12}$$
$$\Gamma^1_{Sm}(\mathbf{p}) = \{m \text{ such that } \mathbf{q}(m,\mathbf{p},t_{stop})\in\Gamma^1_{Sq}\ \}$$

and functional $\Gamma^2_{Sm}(\mathbf{p}) = m^2(\mathbf{p})$ which returns mass which causes limiting deformation Γ^2_{Sq} (i.e. maximal displacement of the lower span at time t_{stop}):

$$\Gamma^2_{Sm}(\mathbf{p}) \subseteq \Omega_m \tag{5.2.13}$$
$$\Gamma^2_{Sm}(\mathbf{p}) = \{m \text{ such that } \mathbf{q}(m,\mathbf{p},t_{stop})\in\Gamma^2_{Sq}\ \}$$

Maximal mass which can be applied to the structure $\Phi_m(\mathbf{p})$ can be determined by choosing smaller of the values $\Gamma^1_{Sm}(\mathbf{p})$ and $\Gamma^2_{Sm}(\mathbf{p})$:

$$\Phi_m(\mathbf{p}) = \begin{cases} \Gamma^1_{Sm}(\mathbf{p}) & \text{when} \quad \Gamma^1_{Sm}(\mathbf{p}) \le \Gamma^2_{Sm}(\mathbf{p}) \quad \text{(a)} \\ \Gamma^2_{Sm}(\mathbf{p}) & \text{when} \quad \Gamma^1_{Sm}(\mathbf{p}) > \Gamma^2_{Sm}(\mathbf{p}) \quad \text{(b)} \end{cases} \tag{5.2.14}$$

Taking into account the condition (5.2.14) we can divide the set of pressures $\Omega_{\mathbf{p}}$ into two subsets $\Omega^1_{\mathbf{p}}$ and $\Omega^2_{\mathbf{p}}$ where (5.2.14a) and (5.2.14b) are fulfilled, respectively.

The **second step** of solving the optimization problem (5.2.9) is finding maximum of the functional $\Phi_m(\mathbf{p})$ where vector $\mathbf{p}$ contains n functions describing change of pressure inside the chambers of the frame in terms of time. The difficulty in solving this optimisation problem results from the fact that considered functional is not defined analytically in terms of function describing pressure changes. Moreover, the objective function can not be obtained directly from nonlinear dynamic analysis but has to be searched iteratively according to (5.2.12) and (5.2.13). Additionally, the functional $\Phi_m(\mathbf{p})$ is not smooth because it is composed of functionals $\Gamma^1_{Sm}(\mathbf{p})$ and $\Gamma^2_{Sm}(\mathbf{p})$.

According to the above difficulties, variational problem has to be transformed into classical optimisation problem by substitution of continuous functions describing changes of pressures in time by discrete optimisation variables, i.e.:

- values of pressure in each chamber at selected time instants or
- coefficients of functions describing change of pressure.

The above procedure substantially simplifies considered optimisation problem and allows to apply the classical methods of optimisation. However, finding solution remains complicated due to the fact that calculation of the objective function is time consuming and a number of iterations that can be performed in the optimisation problem is strongly limited. Moreover, gradient-based methods are prone to find local minima due to possible inaccuracies which may occur both in solution of strongly nonlinear mechanical problem and in the procedures for finding maximal mass (5.2.12, 5.2.13). Further simplifications of the considered optimisation problem can be obtained by:

1. analysis of the sensitivity of functionals $\Gamma^1_{Sm}(\mathbf{p})$ and $\Gamma^2_{Sm}(\mathbf{p})$ with respect to parameters of functions **p,** which allows to choose parameters which substantially influence the value of the objective function,
2. approximation of functionals $\Gamma^1_{Sm}(\mathbf{p})$ and $\Gamma^2_{Sm}(\mathbf{p})$ in terms of parameters of functions **p**.

Analysis of sensitivity of functionals $\Gamma^1_{Sm}(\mathbf{p})$ and $\Gamma^2_{Sm}(\mathbf{p})$ allows to determine 'dominant parameters' and to perform initial optimisation with respect to these parameters only. In the following (optional) step of optimisation, the remaining variables should be considered. An alternative approach assumes the first step of optimisation with respect to initial pressures in the cavities and further step of optimisation with respect to parameters describing release of pressure during the impact process. In turn, approximation of functionals $\Gamma^1_{Sm}(\mathbf{p})$ and $\Gamma^2_{Sm}(\mathbf{p})$ allows to determine which geometrical constraint (Γ^1_{Sq} or Γ^2_{Sq}) is critical for structure load capacity and to substantially facilitate computation of the objective function.

In case of two-dimensional frame structure loaded in the middle of the upper span both conditions imposed on frame deformation are, in most cases, adversative. Inflation of the structure allows to prevent collision of the spans and increases mass $\Gamma^1_{Sm}(\mathbf{p})$. On the other hand, high value of internal pressure, for which collision of the spans does not occur, increases deflection of the lower span and thus decreases mass $\Gamma^2_{Sm}(\mathbf{p})$, cf. Fig. 5.2.4. Therefore, maximum load capacity is expected to be achieved when both limit conditions imposed on final structure deformation are fulfilled. Consequently, maximum of the functional $\Phi_m(\mathbf{p})$ is expected to be found for pressure vector $\mathbf{p}$ which belongs to the subset $\Omega^{12}_{\mathbf{p}}$ being solution of the equation:

$$\mathbf{p} \in \Omega^{12}_{\mathbf{p}} : \ \Gamma^1_{Sm}(\mathbf{p}) - \Gamma^2_{Sm}(\mathbf{p}) = 0 \tag{5.2.15}$$

Solving above equation is not efficient since it requires determination of both limiting surfaces $\Gamma^1_{Sm}(\mathbf{p})$ and $\Gamma^2_{Sm}(\mathbf{p})$. Therefore, two alternative methods can be proposed. The first method of finding subset $\Omega^{12}_{\mathbf{p}}$ is based on calculation of deflection of the lower span evoked by mass $\Gamma^1_{Sm}(\mathbf{p})$ causing collisions of the spans:

$$q^1_{\max}(\mathbf{p}) = q_{\max}(\Gamma^1_{Sm}(\mathbf{p}), \mathbf{p}, t_{stop}) \tag{5.2.16}$$

and comparing it with the limit value:

$$\mathbf{p} \in \Omega^{12}_{\mathbf{p}} : \ q^1_{\max}(\mathbf{p}) - q_{adm} = 0 \tag{5.2.17}$$

Equation (5.2.17) is more convenient for numerical implementation than equation (5.2.15) since having calculated mass $\Gamma^1_{Sm}(\mathbf{p})$ displacement $q^1_{\max}(\mathbf{p})$ can be obtained directly from solution of (Eq. 5.2.3) while calculating $\Gamma^2_{Sm}(\mathbf{p})$ requires solving the inverse problem (Eq. 5.2.13). The second method of finding subset $\Omega^{12}_{\mathbf{p}}$ is converse. It is based on calculation of the distance between the spans evoked by mass $\Gamma^2_{Sm}(\mathbf{p})$ causing maximal displacement of the lower span:

$$D_2(\mathbf{p}) = D_2(\Gamma^2_{Sm}(\mathbf{p}), \mathbf{p}, t_{stop}) \tag{5.2.18}$$

and by checking whether conditions defining the first limiting state (5.2.10) are fulfilled:

$$\mathbf{p} \in \Omega^{12}_{p} : D_2(\mathbf{p}) = \delta, \ \left.\frac{dD_2(m,\mathbf{p},t)}{dt}\right|_{t=t_{stop}} = 0, \ \left.\frac{d^2D_2(m,\mathbf{p},t)}{dt^2}\right|_{t=t_{stop}} > 0 \tag{5.2.19}$$

Finally, the optimization problem assumes the form:

$$\text{Find: } \max\{\Phi_m(\mathbf{p})\} = \max\{\Gamma^1_{Sm}(\mathbf{p})\} = \max\{\Gamma^2_{Sm}(\mathbf{p})\}, \ \mathbf{p} \in \Omega^{12}_{\mathbf{p}} \tag{5.2.20}$$

where $\Omega^{12}_{\mathbf{p}}$ is defined by (5.2.15 or 5.2.17 or 5.2.19)

The values of mass corresponding to each element of set $\Omega^{12}_{\mathbf{p}}$ are causing deformation with contact of the spans and limit displacement of the lower beam at the time instant of stopping the impacting object. Therefore, the initial set of pressure functions $\Omega_{\mathbf{p}}$ is confined to the set $\Omega^{12}_{\mathbf{p}}$ containing pre-selected functions for which allowable mass of the impacting object is expected to be the largest.

Nevertheless, the above proposed choice of optimal set $\Omega^{12}_{\mathbf{p}}$ should be rather treated as a conjecture which has to be verified for a particular structure subjected to optimisation.

In a simple case of inflatable structure with single-pressure chamber the introduced quantities: $\Gamma^1_{Sm}(\mathbf{p})$, $\Gamma^2_{Sm}(\mathbf{p})$ and $\Omega^{12}_{\mathbf{p}}$ have a very simple geometrical interpretation. The quantities $\Gamma^1_{Sm}(\mathbf{p})$ and $\Gamma^2_{Sm}(\mathbf{p})$ indicate curves located on a plane defined by allowable pressure and mass $\Omega_m \times \Omega_{\mathbf{p}}$. At each point of these curves the corresponding limiting deformation of the frame is obtained. The set $\Omega^{12}_{\mathbf{p}}$, being intersection of two curves, constitutes solution of the optimisation problem.

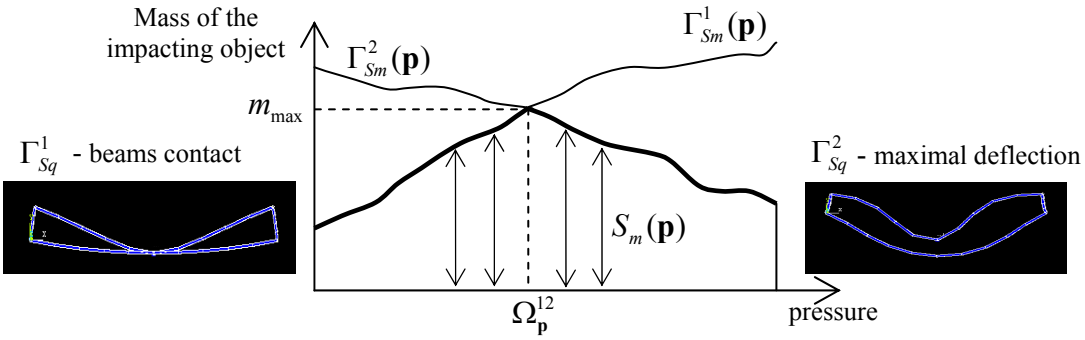

Fig.5.2.4: Geometrical interpretation of the considered optimisation problem with two constraints

In case of two-dimensional optimisation (for example searching for constant values of pressures in three-chamber frame in case of central impact) the $\Gamma^1_{Sm}(\mathbf{p})$ and $\Gamma^2_{Sm}(\mathbf{p})$ are surfaces located in space defined by mass and two components of pressure vector $\Omega_m \times \Omega_{\mathbf{p}}$. The set $\Omega^{12}_{\mathbf{p}}$ is a space curve located at intersection of the above surfaces. The solution of the optimisation problem is maximal mass located at the curve $\Omega^{12}_{\mathbf{p}}$.

Numerical examples

In order to demonstrate the effect of internal pressure on load capacity of the structure two numerical models of the inflatable frame structure were developed:

- The first model utilizes distributed loading to account for the influence of internal pressure. Consequently, the model is well suited for adaptation strategies based on 'direct pressure control'. The model is implemented within commercial FEM code ANSYS which uses implicit scheme of integration of equations of motion.
- The second model utilizes description of internal gas by the equations of Uniform Pressure Method (cf. Sect. 2.3, also part concerning multi-chamber systems). Consequently, the adaptation strategies may directly use functions describing change of pressure or flow resistance coefficient of the valves. The model is implemented within FEM code ABAQUS Explicit which uses explicit scheme of integration.

Solution of the above formulated control problems requires combining Finite Element Method and optimisation techniques. The proposed methodology of solution utilises linkage between MATLAB utilized finite element codes ANSYS and ABAQUS. In both cases the whole optimisation procedure is governed by MATLAB software. In case when ANSYS is used, scheme of the whole procedure is the following:

1. Initial value of impacting mass and initial parameters describing change of pressures are set in MATLAB.

2. ANSYS solver is launched to conduct nonlinear dynamic analysis (by the Newmark integration scheme and the Newton-Raphson algorithm).
3. ANSYS built-in optimisation procedures are used to solve inverse problems (5.2.12) and/or (5.2.13) required to calculate the load capacity of the structure $\Phi_m(\mathbf{p})$.
4. Either, MATLAB optimisation tools are used to find maximal impacting mass directly by solving the optimisation problem (5.2.9) with definition of the load capacity (5.2.14), or
5. preselected set $\Omega_{\mathbf{p}}^{12}$ is found by solving Eq. 5.2.17 or Eq. 5.2.19 and maximal impacting mass is found by solving optimisation problem (5.2.20).

The following numerical examples concern one- and three- dimensional frame structures with fixed and sliding supports impacted in various positions at the upper span.

Example 1: single-chamber frame, central impact (ANSYS)

The derived mathematical formulation and proposed solution methodology were utilized in elementary example of finding maximal load capacity of the frame with a single pressure chamber, cf. Fig. 5.2.5. All beams of the frame have a squared cross-section of dimensions of 0,02m x 0,02m. Material of the frame is bilinear elasto-plastic with Young modulus of E=210GPa, yield stress level of 500MPa and strength coefficient equal to $K=E/10$. Impact loading applied in central part of the upper beam is implemented in numerical model by additional mass located in central part of the frame and its initial velocity (V_0=2m/s). Moreover, maximal admissible deflection of the structure equals u_{max} = 0,18m.

When the frame is not inflated, its load capacity is exhausted due to collision of the spans which occurs at small maximal deflection of the frame. Load capacity of the structure $\Phi_m(\mathbf{p}) = \Gamma_{Sm}^1(\mathbf{p}) = m_{\max}$ determined by solving the inverse problem (5.2.12) equals 540kg. In the following simulations, distributed loading modelling internal pressure was applied gradually from the beginning of impact such that maximal value of pressure was obtained after 0,01s. For arbitrary value of internal pressure, load capacity of the structure is determined by comparison of masses which cause two types of limiting deformation, according to Eq.5.2.14. In general, applied inflation of the frame changes its dynamic response in three ways:

- load capacity of the structure substantially increases,
- way of stopping the impacting object extends,
- period of impact elongates

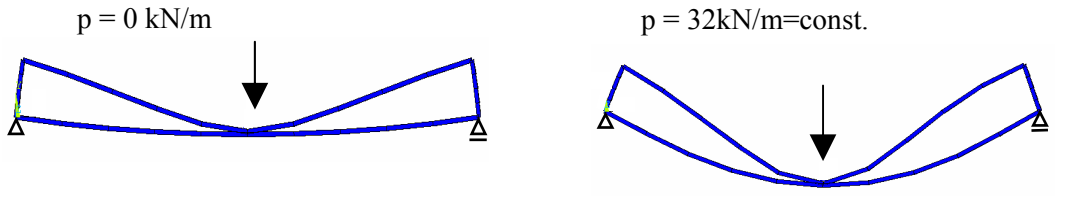

m_{max} = 540kg, u_{max} = 0,035m, t_{stop} = 0,12s

m_{max} = 2710kg, u_{max} = 0,18m, t_{stop}= 0,31s

Fig.5.2.5: Limit deformation of a single-chamber frame: a) empty, b) optimally inflated

Computation of optimal pressure was preceded by determination of preselected set of pressures $\Omega_{\mathbf{p}}^{12}$ for which both limiting conditions imposed on structure deformation are fulfilled. In considered one-dimensional case, preselected set contains only one element which denotes optimal value of pressure (p=32kN/m=const.). In case of optimal inflation, maximal impacting mass equals 2710kg which indicates 502% increase in load capacity in comparison to the generic structure.

Example 2a: three-chamber frame, central impact (ANSYS)

The second example concerns three-chamber frame with stiff partitions and supports fixed in vertical and horizontal direction, cf. Fig. 5.2.7. Material properties, velocity of impact and maximal deflection of frame remain the same as in Example 1. Impact loading is applied in the middle of the upper span. Applied boundary conditions cause that the structure has larger stiffness and high pressure values are required to alter its properties. Maximal value of pressure will be arbitrarily confined to p_{max}=1600kN/m.

The first part of the example concerns the case, when, after initial inflation stage, pressures in all chambers remain constant. Consequently, vector $\mathbf{p}$ has two constant components p_1 and p_2 which denote pressures in lateral and middle cells, respectively. In the first step of the solution procedure, the surface $\Gamma_{Sm}^{1}(\mathbf{p})$ which indicates minimal mass that causes contact of the beams is determined. Since the surface is regular and depends almost linearly on both pressure values it can be easily approximated in the whole pressure domain.

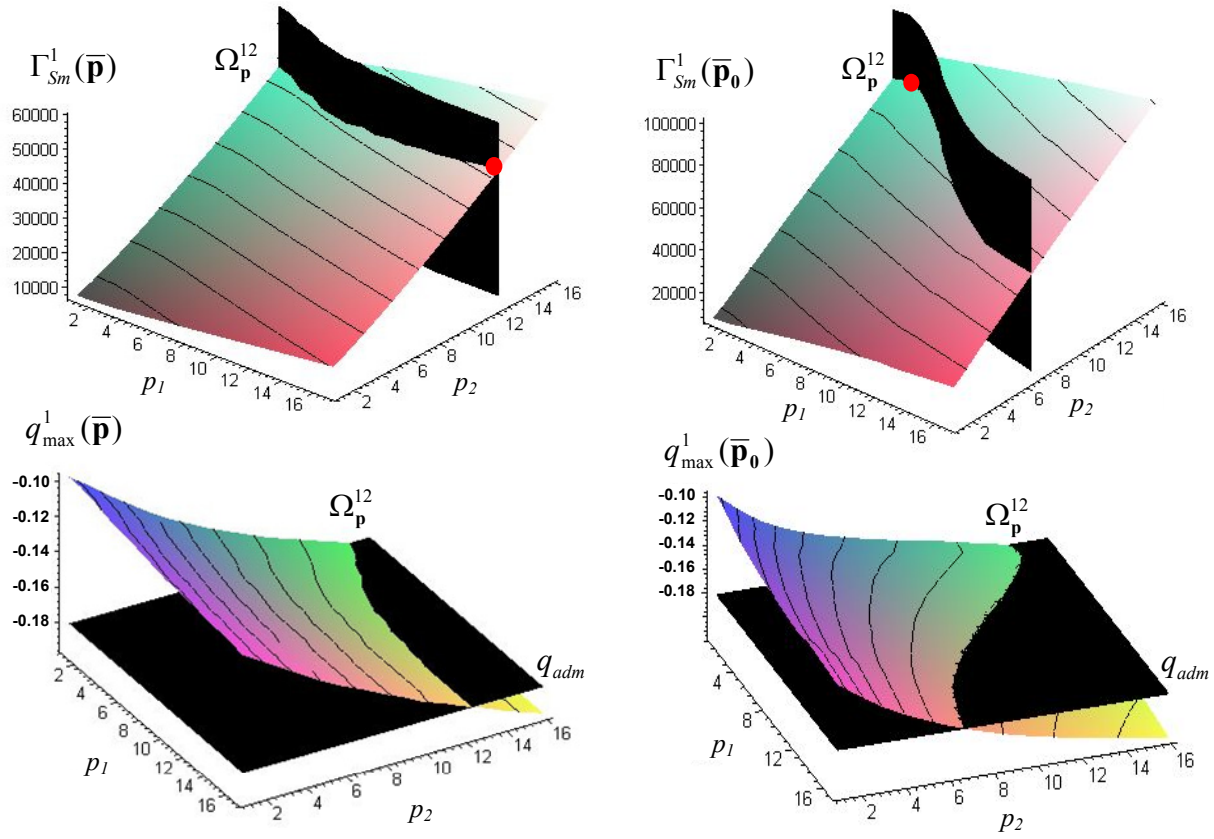

Fig.5.2.6: Surfaces $m^1(\overline{\mathbf{p}})$ and $q_{\max}^{1}(\overline{\mathbf{p}})$ in terms of non-dimensional pressure $\overline{\mathbf{p}}$:
a) constant pressure, $\overline{\mathbf{p}} = \mathbf{p}/(100\text{kN/m})$; b) linear decrease of pressure, $\overline{\mathbf{p}}_0 = \mathbf{p}_0/(300\text{kN/m})$.

In a second step of solution, displacement of the lower span evoked by mass causing collision of the spans $q^1_{\max}(\mathbf{p})$ is calculated according to Eq. 5.2.16. Intersection of this surface with the horizontal plane which denotes maximal allowable deflection (u_{max} = 0,18m) generates curve $\Omega^{12}_{\mathbf{p}}$ being solution of Eq. 5.2.15 and Eq. 5.2.17. In the last step, the curve $\Omega^{12}_{\mathbf{p}}$ is projected into surface $\Gamma^1_{Sm}(\mathbf{p})$ in order to find maximal allowable mass of the impacting object.

The whole procedure is illustrated in Fig. 5.2.6a, the obtained results are presented in Table 4 (2nd row) and the final frame deformation is depicted in Fig. 5.2.7a. Maximal load capacity is obtained for maximal value of pressure in the lateral chambers and moderate value of pressure in central chamber (1600kN/m and 1147kN/m, respectively) and it is 6,1 times higher than load capacity of the generic empty frame.

$\mathbf{p}_1(0)$ [kN/m]	$\mathbf{p}_2(0)$ [kN/m]	$\mathbf{p}_1(t_{stop})$ [kN/m]	$\mathbf{p}_2(t_{stop})$ [kN/m]	$q_1^{\max}$ [m]	t_{stop} [s]	**m** [kg]
0	0	0	0	0,04	0,152	**7596**
1600(max)	1147	1600	1147	0,18	0,213	**46374**
400	3925	0	0	0,18	0,265	**68489**

Table 4: Comparison of structure load capacity for various change of internal pressure

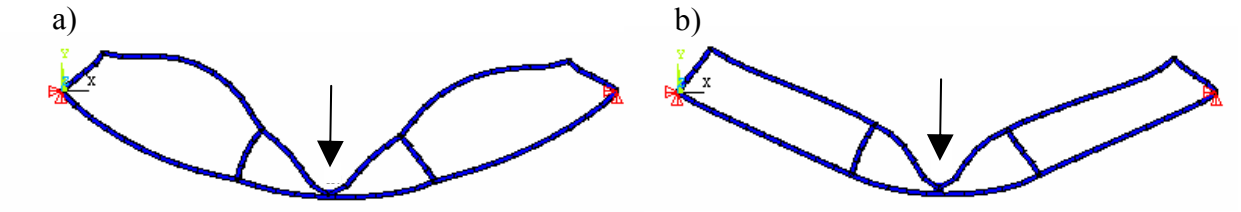

Fig 5.2.7: Deformation of the optimally inflated frame impacted by maximal mass:
a) constant pressure; b) linear release of pressure

The second part of the example concerns the case of linear decrease of pressure in all chambers of the frame. In such a case, vector describing changes of pressure can be replaced by vector of initial pressures $\mathbf{p_0}$ and parameter t_{end} which indicates time instant when pressure is reduced to zero. Moreover, solution of the fundamental problem (5.2.3) can be written in the form:

$$\mathbf{q} = \mathbf{q}(m, \mathbf{p}_0, t_{end}, t) \tag{5.2.21}$$

Time instant t_{end} is not directly subjected to optimisation but it is assumed to be equal to the time when impacting object is stopped t_{stop}. Time t_{stop} is not known a priori and, in general, it depends on both the pressure inside the cavities and the impacting mass. The procedure of finding time t_{end} can be incorporated into procedure of finding function $\Gamma^1_{Sm}(\mathbf{p}_0)$ which, in such case, is formulated as follows:

$$\text{Find } \{m, t_{end}\} \text{ such that } \mathbf{q}(m, \mathbf{p}_0, t_{end}, t_{stop}) \in \Gamma^1_{Sq} \text{ and } t_{stop} = t_{end} \tag{5.2.22}$$

The above formulation allows to avoid computation of time t_{end} separately for each assumed value of impacting mass. In the alternative approach, time t_{end} can be approximated beforehand in terms of vector of initial pressures and impacting mass.

In the first step of solution procedure, the surface $\Gamma^1_{Sm} = m^1$ can be determined in terms of vector of initial pressures $\mathbf{p_0} = \{p_1, p_2\}$. The assumed maximal values of initial pressure are exactly three times higher than maximal values of constant pressure ($p_0^{\max}$ = 4800 kN/m) since pressure release increases safety of inflatable structure. As a result, larger values of mass causing collision of the spans $m^1(\mathbf{p}_0)$ are obtained. In the second step of the procedure, displacement of the lower span corresponding to mass $m^1(\mathbf{p}_0)$ is computed. Obtained surface $q^1_{\max}(\mathbf{p_0})$ is now more sensitive to value of pressure in lateral chambers, which results in different shape of the curve $\Omega^{12}_{\mathbf{p}}$ where both limiting conditions are fulfilled, cf. Fig. 5.2.6b. Finally, maximal value of impacting mass is obtained for a low value of pressures in the lateral chambers and high value of pressure in the central one (400kN/m and 3925kN/m, respectively) and it is 9,01 times larger than in case of generic (not inflated) frame structure. The solution procedure is presented in Fig. 5.2.6b, detailed comparison of results is collected in Table 4 (3rd row) and the corresponding deformation of the structure is presented in Fig. 5.2.7b.

Example 2b: three-chamber frame, lateral impact (ANSYS)

The increase of structure load capacity was also examined for the case of non-central impact, i.e. impact applied to one of the lateral chambers of the frame. In such a case load capacity of non-inflated structure is over 40% smaller as compared to central impact and it is exhausted due to contact of upper and lower beam of the impacted left chamber, see Fig. 5.2.8a. Analysis of sensitivity of structure deformation on internal pressure in each chamber leads to the following conclusions:

1. exclusive inflation of the central chamber with no pressure release is not beneficial since it causes excessive outer deformation of the central chamber of the frame and decreases distance between upper and lower beams of the lateral chambers,
2. inflation of the right chamber influences only local deformation of the frame and has almost no influence on global load capacity.

According to the above features of the pneumatic system, the inflation of the impacted and central chamber was precisely examined. Although both conditions defining limiting deformation of the frame remain valid, the displacement of the lower span is relatively small and corresponding constraints in the optimisation problem are not active. Therefore, maximal mass of the impacting object can be found by maximisation of the function $m^1(\mathbf{p})$. In the considered case, function $m^1(\mathbf{p})$ is monotonic and maximal mass of the impacting object is obtained for the highest allowable pressure which counteracts collision of the spans in the most effective way.

In case of system with pressure release, the significant increase in load capacity was obtained for maximal initial inflation of the left chamber and linear decrease of pressure until the end of the process, cf. Table 5. Deflection of the inflated structure remained small and load capacity achieved the limit value due to collision of upper and lower beam. Additional inflation of the middle chamber of the frame (with the same initial pressure and its simultaneous decrease) leads to only a small improvement of the load capacity of the frame (approx. 5%).

$\mathbf{p}_1(0)$ [kN/m]	$\mathbf{p}_1(t_{stop})$ [kN/m]	$q_{\max}$ [m]	t_{stop} [s]	**m** [kg]
0	0	0,056	0,112	**4350**
2500(max)	2500(max)	0,121	0,192	**52000**
5000(max)	0	0,143	0,248	**76000**

Table.5: Comparison of structure load capacity for different values of pressure (lateral impact)

In the two above investigated cases the optimal solution is not achieved on the line of intersection of surfaces $m^1(\mathbf{p})$ and $m^2(\mathbf{p})$ since this line is located outside the area of admissible pressures (the set Ω_p^{12} is not a subset of Ω_p).

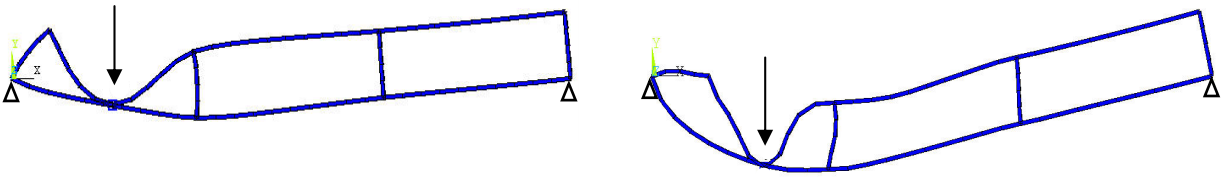

Fig 5.2.8: Deformation of three-chamber frame in case of lateral impact:
a) empty chambers; b) linear decrease of pressure in left chamber

The following numerical examples were also conducted with the use of explicit finite element code ABAQUS XPL. In the following numerical simulations the impact is modelled by introducing separate rigid object and by defining contact conditions between this object and the frame. As a result of applied explicit scheme of integration a single simulation of the impact process is always accomplished even in case of small hardening and resulting large deformation of the frame.

In case when ABAQUS is used the optimisation problem was formulated in general form (5.2.9) in which mass of the impacting object is maximised and inequality constraints are imposed on structure deformation. The whole optimisation procedure was based on the following algorithms:

- ABAQUS solver is launched to conduct nonlinear dynamic analysis by means of explicit integration scheme,
- MATLAB gradient-based optimisation procedure is used to compute the value of the objective function $\Phi_m(\mathbf{p})$,
- MATLAB 'pattern search-based' or 'genetic algorithm-based' optimisation procedure is used to maximise the objective function over parameters describing change of pressure within the chambers.

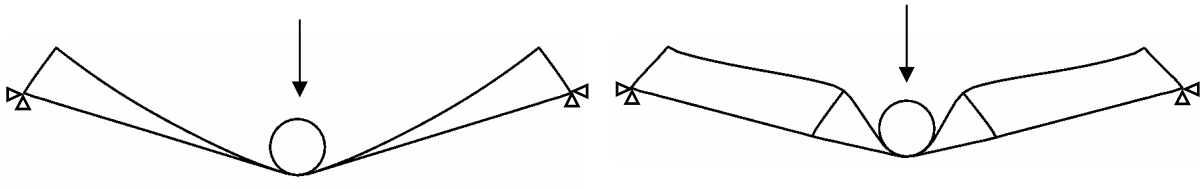

Fig. 5.2.9: Simulation of impact of a rigid object against one- and three-chamber frame performed by means of explicit Finite Element Method

Example 3: single-chamber frame, central impact (ABAQUS)

The initial example concerns single-chamber frame impacted in the middle of the upper span. Although the global dimensions of the considered structure are the same as in Example 1 (cf. Fig. 5.2.5), the cross section of the beams is reduced to 0,004m x 0,01m (thickness x out of plane dimension). Material of the frame is bilinear elasto-plastic with Young modulus of E=210GPa, yield stress level of $\sigma_{pl} = 400$MPa and ultimate plastic strain of $\varepsilon = 0{,}18$ at $\sigma = 700$MPa. The velocity of impact is now increased to $V_0 = 10$m/s and maximal deflection of the structure is confined to u_{max} = 0,1m.

Since dimensions, material properties and applied loading are substantially altered, the results of previous and current simulations can not be directly compared. Moreover, the problem will be solved without preliminary assumption that load capacity of the impacted structure is maximal when both limit conditions imposed on deformation are fulfilled.

Basic indications for optimal change of pressure are obtained from the analysis of the three basic scenarios of pressure adjustment:

- constant mass of gas inside the chamber (no pressure release) (a)
- constant pressure during the whole impact period (b)
- linear decrease of pressure until time instant of stopping the hitting object (c)

For each of the above pressure adjustment strategies, the curves defining limiting deformation ($\Gamma^1_{Sm}(p)$ and $\Gamma^2_{Sm}(p)$ corresponding to contact of the beams and maximal deflection) were determined and used for finding maximal allowable mass of the impacting object. Performed analysis allows to estimate required value of pressure (~1,1MPa), time instant of stopping the mass (35-55ms) and maximal mass which can applied to the structure (~17kg).

The largest load capacity of the structure was obtained for the slow decrease of pressure to nonzero value (case ‘c’) which preliminarily indicates that this scheme of pressure adjustment should be analysed further and it should be tuned by the optimisation procedure. Decrease of pressure inside the frame was defined in several various ways in order to cover the possibly wide range of functions which may describe optimal change of pressure. The following parameters, directly correlated with change of pressure, were utilised:

1. inflation pressure p_2, pressure at time instant of stopping the mass p_3,
2. inflation pressure p_2, time when pressure is decreased to arbitrarily value $p_2/3$,
3. pressure in subsequent time instants of the analysis: p_2, p_3, p_4, p_5, p_6.

The subsequent methods of pressure adjustment do not directly utilize functions describing change of pressure, but instead they use coefficients describing change of valve opening. In these methods the following parameters were used:

4. inflation pressure p_2, coefficient describing valve opening c_2,
5. inflation pressure p_2, valve opening at the beginning of impact c_2, valve opening at time instant of stopping the impacting object c_3,
6. inflation pressure p_2, valve opening at the beginning of impact c_2, time instant when valve becomes closed t_3,
7. inflation pressure p_2, valve opening in subsequent time instants of the analysis: c_2, c_3, c_4, c_5, c_6.

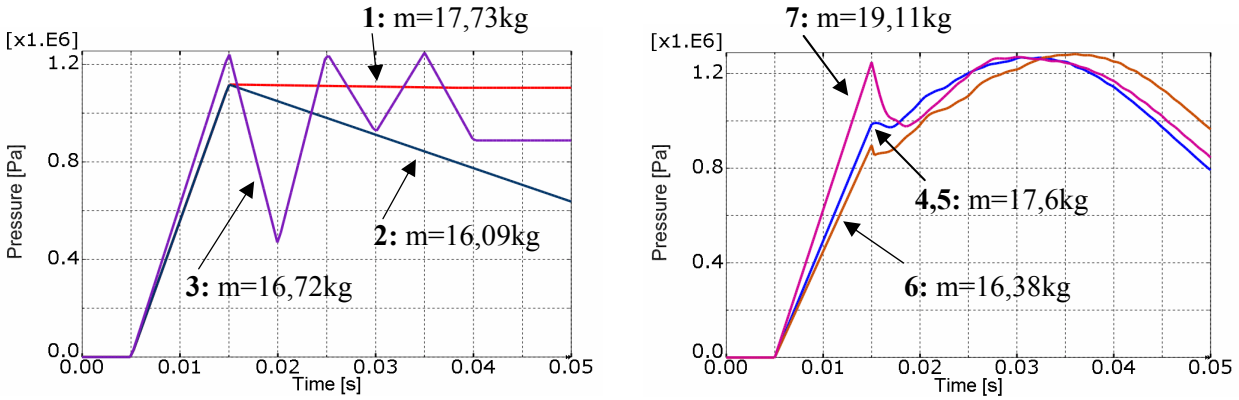

Fig. 5.2.10: Tuning of pressure release strategy by means of optimisation procedure: a) 'direct pressure control', b) indirect control utilizing coefficient of valve opening

In case of 'direct pressure control', the obtained functions describing pressure change are not 2nd order continuous and, moreover, they are substantially different from each other (Fig. 5.2.10a). Smoother changes of pressure are obtained in second group of methods when resistance coefficient is utilised (Fig. 5.2.10b). Finally, the largest load capacity (m=19,11kg) is obtained by the most complex of the proposed methods where initial pressure and flow coefficients defined in several time instants of the process are subjected to optimisation.

The obtained results reveal difficulties in minimisation of functional which depends on a continuous function defining change of pressure. On the other hand, they prove the effectiveness of the proposed methodology of diverse discretisation of aforementioned continuous function.

Example 4: three-chamber frame, central impact (ABAQUS)

In the last example three-chamber frame is subjected to a central impact of the rigid object. The goal is to find optimal distribution of pressures and load-bearing capacity of the structure.

The procedure of pressure adjustment was based on assumption of three basic scenarios of pressure change: a) constant mass of gas inside the chamber, b) constant value of pressure, c) linear decrease of pressure during the impact process. For each of the above strategies, both surfaces defining limiting deformation Γ^1_{Sm} and Γ^2_{Sm} were determined in terms of vector of initial pressure $p = \{p_1, p_2\}$, Fig. 5.2.11a-c. For low values of initial pressure mass corresponding to both critical conditions increases in terms of p_1 and p_2. The surface representing collision of the beams Γ^1_{Sm} is located below the surface representing maximal displacement Γ^2_{Sm}, which indicates collision of the beam is critical for the load capacity.

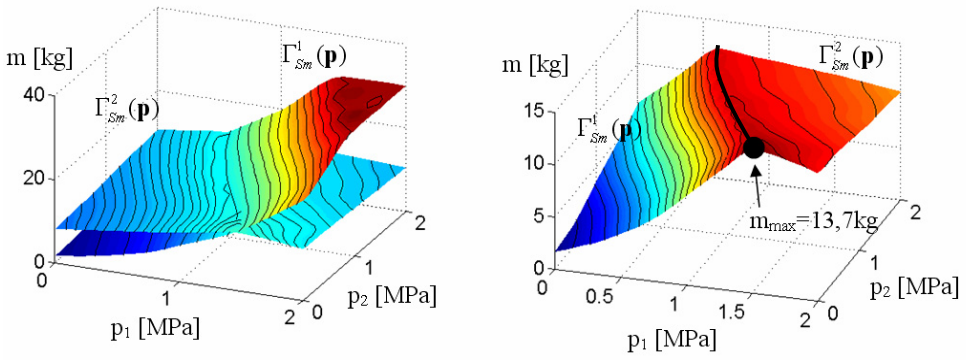

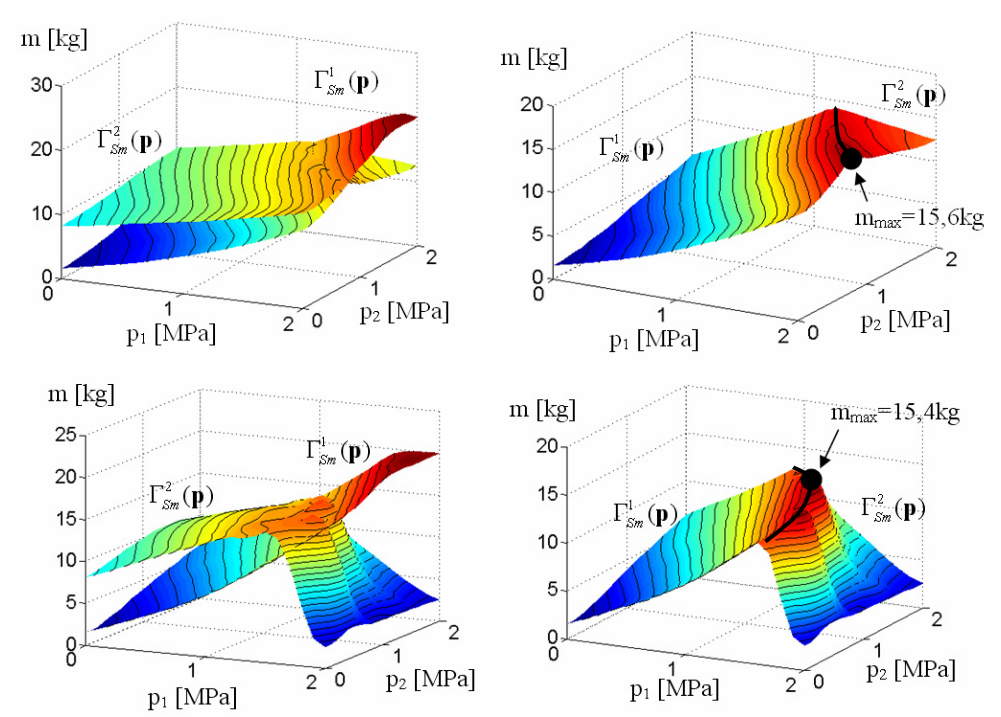

Fig. 5.2.11: Surfaces of both constraints (limiting deformation) for the case of: a) constant mass of the gas, b) constant pressure, c) linear decrease of pressure

After intersection of both surfaces, the surface indicating maximal allowable displacement Γ^2_{Sm} starts to decrease and it is located below the surface indicating collision of the beams Γ^1_{Sm}. The shape of function Γ^2_{Sm} indicates that internal pressure increases the value of mass causing maximal admissible deflection in these impact scenarios where collision of the spans occurs, but decreases the value of mass in impact scenarios where collision of spans does not occur. Eventually, the load capacity $\Phi_m(\mathbf{p})$ is defined by the surface Γ^1_{Sm} for low values of pressure and by the surface Γ^2_{Sm} for high values of pressure.

In each considered case maximal allowable mass of the impacting object is located at the intersection of surfaces representing limiting deformation (curve $\Omega^{12}_{\mathbf{p}}$). Shape of this curve in space defined by parameters p_1, p_2,m (and corresponding maximal value of mass) depends on assumed scenario of pressure change. The largest load capacity of the structure is obtained by maximal assumed inflation of the lateral chambers, moderate inflation of central chamber and by maintaining constant level of pressure during the process (m_{max}=15,6kg). The above result can be improved by applying optimisation procedure, similarly as in Example 3. Due to the fact that linear decrease of pressure leads to similar results, the increase in load capacity obtained by means of optimisation procedure is not expected to be significant.

5.2.2. Methods of adaptation to impact

In this section the impact scenario will be arbitrarily predefined (by mass, velocity and location) and pressure adjustment will be aimed to fulfil one of the following objectives:

- control of hitting object deceleration,
- minimisation of pressure inside chambers of the frame,
- obtaining assumed deformation of the structure.

Control of impacting object deceleration

The first objective of pressure adjustment is a mitigation of impact by minimization of forces and decelerations acting on the hitting object. Similarly as in case of pneumatic cylinder, change of internal pressure influences actual global stiffness of the inflatable structure and, therefore, allows to control forces counteracting the impact loading and to alter level of deceleration of the impacting body.

Time-history of the deceleration of the hitting object strongly depends on whether the collision of both spans of the frame occurs. In case when impact energy is relatively low and maximal displacement of the upper span is smaller than initial width of the frame, the hitting object acceleration depends mainly on stiffness of the upper beam and plot of acceleration is relatively smooth, Fig. 5.2.12a. On the contrary, in case when impact energy is high and causes collision of the spans, two stages of the process can be distinguished, Fig. 5.2.12b:

i) the first stage when deceleration of the hitting object is low since it results from stiffness of the upper span only (t=0-0.05s) and

ii) the second stage when both spans contribute to deceleration of the hitting object and, therefore, deceleration is additionally increased.

Both of the stages are separated from each other by the peak of acceleration which indicates beginning of beams contact.

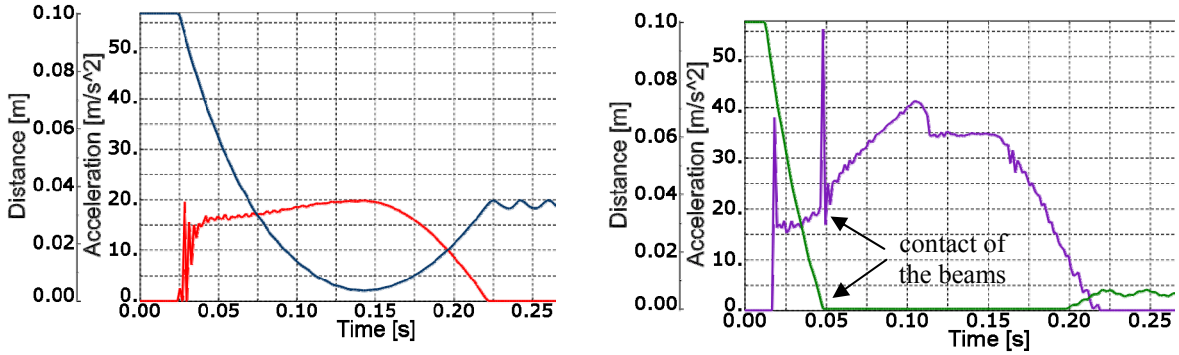

Fig 5.2.12: Two typical time-histories of hitting object acceleration (absolute value): a) low energy impact (M=500kg, V=2m/s), b) high energy impact with collision of the spans (M=500kg, V=4m/s)

In the first aforementioned case, the value of the hitting object acceleration can be controlled by means of internal pressure, however, it can not be decreased since internal pressure causes growth of the global stiffness of the structure. Therefore, the advantage of structure inflation is confined to the possibility of maintaining exactly constant value of hitting object deceleration and precise control of reduction of penetration by the hitting object.

On the contrary, in case of high energy impact, although internal pressure increases stiffness of the upper beam, it allows to avoid collision of upper and lower span of the frame. Therefore, precisely adjusted internal pressure enables decrease of hitting object deceleration by extending the first stage of impact and by alleviation (or complete elimination) of the second stage of impact.

The corresponding optimisation problem relies on finding change of pressure inside the chambers of the frame which minimises maximal value of hitting object acceleration $\ddot{u}_M(t)$. The direct formulation of this optimisation problem reads:

$$\begin{aligned} &\text{Find } \mathbf{p}(t) \text{ such that } \Phi(\mathbf{p}(t)) \text{ is minimal} \\ &\text{where } \Phi(\mathbf{p}(t)) = \max_t \left|\ddot{u}_M(t)\right| \end{aligned} \tag{5.2.23}$$

In an alternative approach, the objective function can be defined as time integral of discrepancy between assumed and obtained acceleration of the impacting object:

$$\Phi(\mathbf{p}(t)) = \int_0^{t_{stop}} \left[\ddot{u}_M(t) - \ddot{u}_M^{opt}(t)\right]^2 dt \tag{5.2.24}$$

The acceleration $\ddot{u}_M^{opt}$ is assumed to be constant and defined a priori. In the considered problem, it typically indicates constant minimal deceleration which allows to avoid collision of upper and lower beam of the frame. In order to obtain full compatibility with the formulation (5.2.23), the value of constant acceleration $\ddot{u}_M^{opt}$ should be separately subjected to optimisation.

Similarly as in case of maximisation of the load capacity, the above optimisation problem has variational form since minimised objective function $\Phi(\mathbf{p}(t))$ depends on continuous function $\mathbf{p}(t)$ describing changes of pressures in time. Finding the exact solution of the variational problem is difficult since for each assumed change of pressure the value of the functional Φ has to be determined numerically by means of nonlinear finite element analysis.

The above optimisation problem can be substantially simplified by discretisation of optimised function $\mathbf{p}$ and objective function Φ in time domain and by performing optimisation separately for each time instant. The procedure is feasible since the value of pressure in considered time step instantly affects value of hitting object decceleration. As a result, initial optimisation problem is decomposed into a series of simpler ones, where objective function and design variables are defined in selected time instants t_k:

$$\begin{aligned} &\text{Find } \mathbf{p}(t_k) \text{ such that } \Phi(\mathbf{p}(t_k)) \text{ is minimal} \\ &\Phi(\mathbf{p}(t_k)) = \left[\ddot{u}_M(t_k) - \ddot{u}_M^{opt}\right]^2 \end{aligned} \tag{5.2.25}$$

Discretisation of the optimisation problem can coincide with time discretisation of the basic dynamic problem, however, it can also be substantially coarser in order to speed-up solution. The local problem (5.2.25) is not as general as global problem (5.2.24) and may not lead to optimal minimisation of decelerations. However, in many cases when $\ddot{u}_M^{opt}$ is correctly chosen, objective functions (5.2.25) related to subsequent time instants can be minimized to zero which indicates that global solution was found.

Alternatively, the optimisation problem can be defined in terms of hitting object displacement instead of deceleration. The optimal displacement of the hitting object $u_m^{opt}(t)$ can be determined on the basis of its initial velocity and optimal acceleration $\ddot{u}_M^{opt}$. The continuous objective function of the corresponding optimisation problem reads:

$$\Phi(\mathbf{p}(t)) = \int_0^{t_{stop}} \left[u_m(t) - u_m^{opt}(t)\right]^2 dt \tag{5.2.26}$$

Similarly, as previously, the problem can be decomposed into a series of simpler problems formulated for selected time instants t_k. The intrinsic difference is that the influence of the applied internal pressure on displacement of the impacting object is not immediate. Therefore, the delay between applied pressure and response of the structure (of the length of one optimisation step) has to be accounted for in the definition of the objective function:

$$\Phi(\mathbf{p}(t_k)) = \left[u_m(t_{k+1}) - u_m^{opt}(t_{k+1})\right]^2 \qquad (5.2.27)$$

The derived optimization problem can be solved for the structure equipped with several pressure chambers, however, control of the pressure inside single, appropriately selected chamber usually allows for satisfactory reduction of the deceleration level. Basic analysis of sensitivity of the hitting object deceleration with respect to values of pressure inside the chamber indicates that inflation of the impacted chamber is typically the most effective. For the sake of simplicity, the structure considered in further examples will contain one pressure chamber only.

Example 1: low energy impact (ANSYS)

The first numerical example concerns low energy impact (M=500kg, V=2m/s) applied to the frame with single pressure chamber and one sliding support. Since the impact of empty structure does not cause collisions of the beams, corresponding change of acceleration is relatively smooth, cf. Fig. 5.2.12a. Therefore, the purpose of pressure adjustment is to maintain exactly constant level of hitting object deceleration ($a = 20m/s^2$) which allows to stop the object by using the stroke equal to initial width of the frame (0,1m) after the time of 0,1s.

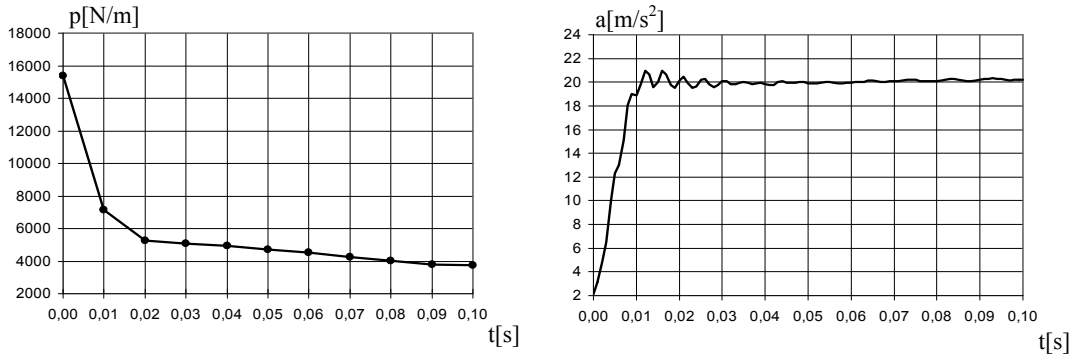

Fig. 5.2.13: Adjustment of pressure in case of low energy impact (10 steps of optimisation): a) optimal change of pressure in time; b) resulting deceleration of the impacting object

The problem was solved by using simplified model of impact where mass of the hitting object is added into mass matrix of the frame structure. Computation of the optimal pressure was performed according to formulation 5.2.27. In each step of the optimisation procedure the pressure was adjusted to conform the displacement of the impacting object to the assumed second order curve $u(t) = V_0 t - \frac{1}{2}at^2$. High value of the internal pressure is required at the beginning of the impact, but further optimal value of pressure is gradually declining, Fig.5.2.13a. Objective function is diminished almost to zero so the assumed and obtained displacements of the impacting object nearly overlap and the level of the acceleration remains approximately constant during the impact process, see Fig. 5.2.13b.

Example 2: high energy impact (ABAQUS)

The second example concerns high energy impact (M=500kg, V=4m/s). Such an impact applied to the empty frame causes collisions of upper and lower beam (clearly reflected in the plot of hitting object deceleration, cf. Fig. 5.2.12b and 5.2.14b) and results in high value of deceleration during the second stage of the process. Therefore, internal pressure will be used to decrease maximal deceleration level and to maintain its constant, possibly low value during the whole period of impact.

In this case, simulation of collision was performed with the model comprising separate rigid object. Adjustment of internal pressure was conducted according to general formulation of the optimisation problem (Eq. 5.2.23). However, continuous function describing change of pressure $p(t)$ was replaced by two parameters:

- time period of structure inflation (which starts at the instant of impact): t_{inf}
- value of pressure which is maintained constant during the impact process: p_{inf}

Although the above formulation is strongly simplified in comparison to the original one, optimal values of both introduced parameters provide almost constant value of hitting object deceleration during the main stage of impact (before rebound). They provide a relevant compromise between an increase of stiffness of the upper beam caused by internal pressure during the first stage of impact and an increase of global stiffness due to collision of the beams during the second stage. Despite the fact that the way distance of stopping the impacting body is reduced from 0,213m to 0,168m, the level of impacting object deceleration decreases from 55,02m/s^2 (or 41,5m/s^2 excluding peak) to 34,9m/s^2.

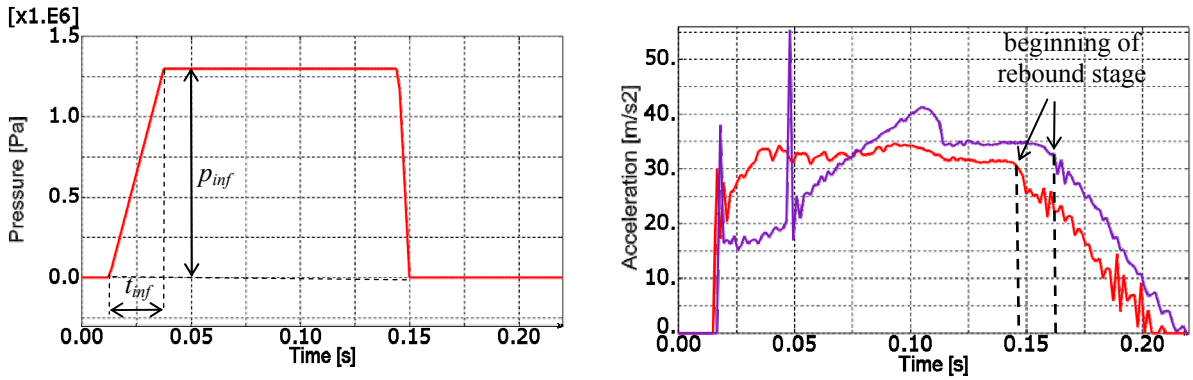

Fig. 5.2.14: Adjustment of pressure in case of high energy impact: a) optimal change of pressure in time, b) comparison of hitting object acceleration for passive and controlled structure

Minimisation of internal pressure

The second considered objective of pressure adjustment is sustaining given impact (of energy not exceeding the limit value found in Sec. 5.2.1) by using the smallest possible inflation of the structure. The problem of minimal inflation of the structure corresponds to minimisation of the energy which has to be initially introduced to the system. According to the classical AIA terminology, the problem can be treated as minimisation of introduced 'distortions', i.e. the quantities being a measure of required changes of the system during adaptation.

Let us initially define domain of the considered optimization problem. By analogy to Eq. 5.2.7 we can introduce mapping $S_{\mathbf{p}}(m)$ which defines the subset of $\Omega_{\mathbf{p}}$ containing all vectors of pressures $\mathbf{p}=\{p_1,p_2,...,p_k\}$ for which impact of the object of given mass causes admissible deformation of the structure S_q:

$$\begin{gathered} S_{\mathbf{p}}(m)\subseteq\Omega_{\mathbf{p}} \\ S_{\mathbf{p}}(m)=\left\{\mathbf{p}\ \text{such that}\ \mathbf{q}(m,\mathbf{p},t)\in S_q\right\} \end{gathered} \tag{5.2.28}$$

The set S_q is defined by Eq. 5.2.5 and involves two conditions imposed on structure deformation. In case of the simplest considered structure, i.e. single chamber frame in which pressure is maintained constant, $S_{\mathbf{p}}(m)$ has simple graphical interpretation and it denotes admissible range of pressure, see Fig. 5.2.15.

For small impacting mass, deformation of the structure is admissible regardless of applied internal pressure and set of admissible pressures $S_{\mathbf{p}}(m)$ covers the whole set $\Omega_{\mathbf{p}}$. In case of larger impacting mass, constraints imposed on structure deformation become active and the set $S_{\mathbf{p}}(m)$ becomes additionally constrained by $\Gamma^1_{Sm}(\mathbf{p})$ and $\Gamma^2_{Sm}(\mathbf{p})$ (curves in Fig. 5.2.15). When impacting mass is larger than $\Gamma^1_{Sm}(\mathbf{0})$, the set of admissible pressures $S_{\mathbf{p}}(m)$ does not contain initial point $\mathbf{p}=\mathbf{0}$ which means that the inflation of the structure is required to sustain given impact loading. Finally, for maximal value of the impacting mass m_{max} only one combination of pressures provides admissible deformation. For mass higher than m_{max} admissible vector of pressures does not exist.

Further, general problem of minimisation of 'effort' undertaken to sustain given impact loading will be defined. Objective function of the optimisation problem can be formulated in the several alternative ways, for instance as:

- sum of initial pressures in all chambers or sum of squares of initial pressures in all chambers (a),
- approximate value of internal energy or enthalpy of gas required for initial inflation of the structure (b),
- work done by internal pressure on structure deformation during inflation (c) .

The corresponding optimisation problems read:

$$\text{Find: } \min\left\{\Phi(\mathbf{p}(t))\right\}, \mathbf{p}\in S_{\mathbf{p}}(m) \tag{5.2.29}$$

$$\text{where: } \Phi(\mathbf{p}(t))=\sum p_i^0 \quad \text{or} \quad \Phi(\mathbf{p}(t))=\sum (p_i^0)^2, \tag{a}$$

$$\Phi(\mathbf{p}(t))=\tfrac{1}{\kappa-1}\sum (p_i^0)V_i^0=\sum (m_i^0)c_V T_i^0 \quad \text{or} \quad \Phi(\mathbf{p}(t))=\tfrac{\kappa}{\kappa-1}\sum (p_i^0)V_i^0=\sum (m_i^0)c_p T_i^0, \tag{b}$$

$$\Phi(\mathbf{p}(t))=\sum \int_{V_i^0}^{V_i^{end}} p_i(t)dV_i=\sum \int_{t_0}^{t_{end}} p_i(t)\dot{V}_i dt \tag{c}$$

and i indicates summation over chambers of the inflatable structure. Although in the first and the second case, the objective function is defined analytically in terms of pressure, the definition of the domain $S_{\mathbf{p}}(m)$ is complicated and its determination requires nonlinear dynamic finite element analysis of the structure. In this context, the problem is similar to the problem of finding maximal load capacity of the structure (cf. Sec. 5.2.1): it involves

simple objective function and fairly complicated constraints. Typical methods for this type of optimisation problems are based on searching of the boundary of feasible domain where maximum of the objective function is expected to be obtained. Methods of this type are based on moving along the boundary of the feasible domain and tracking active constraints [287].

By analogy to methodology applied in Sec 5.2.1 (Eq. 5.2.12), we can introduce mapping $\Gamma^1_{Sp}(m)$ which defines subset of $S_{\mathbf{p}}(m)$ containing vectors of pressures corresponding to deformations Γ^1_{Sq}:

$$\begin{aligned} \Gamma^1_{Sp}(m) &\subseteq S_{\mathbf{p}}(m) \\ \Gamma^1_{Sp}(m) &= \left\{\mathbf{p} \text{ such that } \mathbf{q}(m,\mathbf{p},t) \in \Gamma^1_{Sq}\right\} \end{aligned} \tag{5.2.30}$$

and mapping $\Gamma^2_{Sm}(m)$ which defines subset of $S_p(m)$ containing vectors of pressures corresponding to deformations Γ^2_{Sq}:

$$\begin{aligned} \Gamma^2_{Sp}(m) &\subseteq S_p(m) \\ \Gamma^2_{Sp}(m) &= \left\{\mathbf{p} \text{ such that } \mathbf{q}(m,\mathbf{p},t) \in \Gamma^2_{Sq}\right\} \end{aligned} \tag{5.2.31}$$

Alternatively, $\Gamma^1_{Sp}(m)$ and $\Gamma^2_{Sp}(m)$ can be determined as a set of solutions of the following equations:

$$\Gamma^1_{Sp}(m):\ \Gamma^1_{Sm}(\mathbf{p}) = m\,, \quad \Gamma^2_{Sp}(m):\ \Gamma^2_{Sm}(\mathbf{p}) = m \tag{5.2.32a}$$

The shape of plots in Fig. 5.2.15 indicates that boundary of set $S_{\mathbf{p}}(m)$ consists of curves $\Gamma^1_{Sp}(m)$, $\Gamma^2_{Sp}(m)$ where limit deformation is attained, and lines $\Gamma_p^{\min}$, $\Gamma_p^{\max}$ which arbitrarily restricts set $\Omega_{\mathbf{p}}$. Nontrivial solution of the optimisation problem (5.2.29) is expected to be achieved within set $\Gamma^1_{Sp}(m)$ since it is the closest to the point $\mathbf{p}=\mathbf{0}$. Therefore, simplified version of the optimisation problem reads:

$$\text{Find: } \min\left\{\Phi(\mathbf{p}) \text{ such that } \mathbf{p} \in \Gamma^1_{Sp}(m) \text{ and } \Gamma^1_{Sm}(\mathbf{p}) < \Gamma^2_{Sm}(\mathbf{p})\right\} \tag{5.2.33}$$

which differs from the original formulation (5.2.29) only by definition of the admissible pressure set. Considering only boundary of the allowable pressure set reduces dimension of the optimisation problem and, therefore, simplifies its solution.

The following simplification can be obtained by preliminary approximation of the function $\Gamma^1_{Sm}(\mathbf{p})$. In further part of the section three chamber frame subjected to central impact will be considered and constant or linearly decreasing pressure inside the chambers will be assumed. In such a case, the limiting surfaces of mass $\Gamma^1_{Sm}(\mathbf{p})$ is very regular (cf. Fig. 5.2.6) and it can be approximated by a linear function:

$$\Gamma^1_{Sm}(\mathbf{p}) = a_0 + \sum_{i=1}^{k} a_i p_i \tag{5.2.34}$$

where a_0 is the mass which can be applied to the empty (not inflated) structure, a_i indicates influence of the pressure p_i on the value of the maximal mass $\Gamma^1_{Sm}(\mathbf{p})$.

Intersection of the approximated surface with the surface of constant mass m^* allows to find boundary $\Gamma^1_{Sp}(m)$:

$$\Gamma^1_{Sp}(m^*): a_0 + \sum_{i=1}^{k} a_i p_i = m^* \tag{5.2.35}$$

In a further step the optimal combination of pressure has to be searched along the line (5.2.35). In case when mass m^* is larger than minimal mass located at the curve $\Omega^{12}_{\mathbf{p}}$ where both limit conditions are fulfilled, line $\Gamma^1_{Sp}(m^*)$ and curve $\Omega^{12}_{\mathbf{p}}$ intersect and not the entire line $\Gamma^1_{Sp}(m^*)$ constitutes boundary of admissible pressure set, cf. Fig. 5.2.15b. When two intersections occur, the optimization has to be performed in the domain which is not continuous. Therefore, in both above cases, the procedure of checking whether the second condition imposed on structure deformation is not violated has to be incorporated into the solution of the optimisation problem.

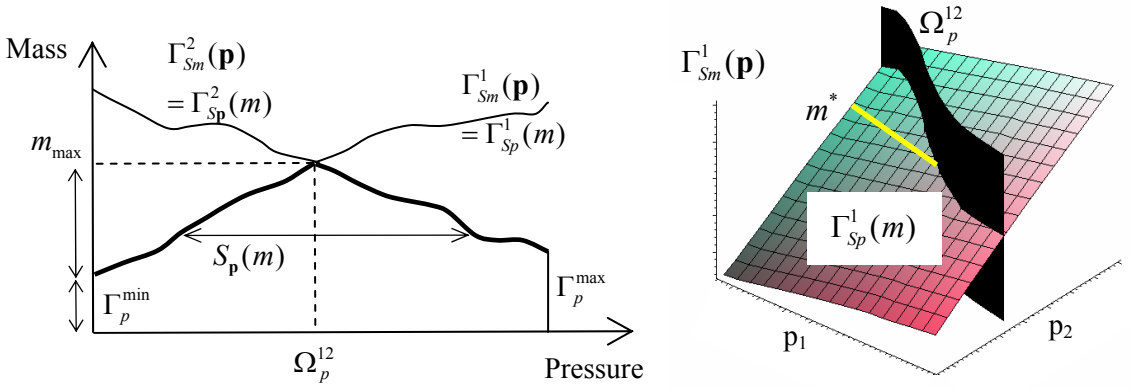

Fig. 5.2.15: Graphical interpretation of the proposed approach: a) characteristic values in 1D optimisation, b) typical shape of admissible pressure domain in case of 2D optimisation

Example 1: (ANSYS)

The numerical example concerns three chamber frame (Fig. 5.2.7) subjected to central impact of object with mass of 40ton and velocity of 2m/s. General features of the considered structure were investigated in Example 2a (Sec. 5.2.1) where both limiting surfaces and maximal load capacity of the structure were determined.

The coefficients of the plane which approximates surface $\Gamma^1_{Sm}(\mathbf{p})$ were found by means of least squares method and they are equal to: $a_0 = 7596$ kg , $a_1 = 4{,}736 \frac{kg \cdot m}{kN}$, $a_2 = 27{,}009 \frac{kg \cdot m}{kN}$. The line of intersection of this surface with a plane corresponding to the constant mass can determined from the equation:

$$a_0 + a_1 p_1 + a_2 p_2 = m^* \Rightarrow p_2(p_1) = -\tfrac{a_1}{a_2} p_1 + \tfrac{m^* - a_0}{a_2} \tag{5.2.36}$$

The solution of the above equation defines straight line on the plane (p_1,p_2), where the minimum of the objective function will be searched. According to the fact that considered mass is smaller than minimal value of mass at the curve $\Omega^{12}_{\mathbf{p}}$, optimisation can be performed in the whole range of pressure $\mathbf{p} \in \Omega_{\mathbf{p}}$. By substituting Eq. 5.2.36 into a definition of the objective function Eq. 5.2.29b we obtain optimisation problem expressed in terms of a single variable (p_1) and objective function defined as:

$$\Phi(p_1) = 2p_1V_1 + p_2V_2 = (2V_1 - \tfrac{a_1}{a_2}V_2)p_1 + \tfrac{m^* - a_0}{a_2}V_2 \tag{5.2.37}$$

In the considered case where $V_1 = V_2$ and $a_1 << 2a_2$ the objective function is increasing in terms of p_1. Therefore, minimum is obtained for $p_1 = 0$ and $p_2 = 1199{,}7\,\frac{kN}{m}$ which indicates that the inflation of the central chamber is the most effective way of sustaining impact of a given mass.

In a more general case of structure with unequal volumes of central and lateral chambers, the inflation of the central chamber is the most beneficial when coefficient before variable p_1 in Eq. 5.2.37 is positive, i.e. as long as the inequality:

$$\frac{a_1}{V_1} < \frac{2a_2}{V_2} \tag{5.2.38}$$

holds. In an opposite situation, objective function is obtained for maximal value of p_1 and value of p_2 determined from (5.2.36) which indicates that diversified inflation of all chambers is optimal.

The optimisation problem was also solved for the case when objective function is defined in a quadratic form:

$$\Phi(\mathbf{p}) = 2(p_1)^2 + (p_2)^2 = \left[2 + (\tfrac{a_1}{a_2})^2\right](p_1)^2 - \left[2\,\tfrac{a_1}{a_2}\,\tfrac{m^* - a_0}{a_2}\right]p_1 + (\tfrac{m^* - a_0}{a_2})^2 \tag{5.2.39}$$

Function $\Phi(\mathbf{p})$ achieves its minimum for the argument p_1 equal to:

$$p_1 = -\frac{b}{2a} = \frac{\frac{a_1}{a_2}\frac{m^* - a_0}{a_2}}{2 + (\frac{a_1}{a_2})^2} \tag{5.2.40}$$

For the considered three-chamber frame, the optimal values of pressures in lateral and central chambers are: $p_1 = 103{,}1\,\frac{kN}{m}$, $p_2 = 1181{,}7\,\frac{kN}{m}$. Therefore, it can be concluded that formulation of the objective function as a sum of pressure squares results in distribution of initial pressure to lateral cells in optimal design.

Control of structure deformation

The last objective of pressure adjustment is to control the process of structure deformation in order to obtain predefined final configuration, regardless of applied loading. Although the problem of controlling final deformation of the structure may seem artificial, it is known and developed in smart structures literature, cf. exemplary [288].

In case of considered inflatable thin-walled frame, the assumed objective is to obtain maximal compression of the selected chambers, i.e. to minimize distance between upper and lower beam of selected chambers in final deformation. Such formulation allows to control locations of arising of main plastic hinges which are the major mechanism of energy dissipation. Moreover, maximal compression of the chamber entails substantial amount of impact energy used for gas compression and the possibility of dissipation of this energy in a controlled way.

The distance between upper and lower beam of each chamber will be described mathematically by function D_i which depends on deformation of the upper and lower beam

of the considered chamber ($\mathbf{q}_{upper}$ and $\mathbf{q}_{lower}$, respectively). The mathematical formulation of the above defined optimisation problem reads:

$$\begin{aligned} &\text{Find} \ \ \min \left\{ \Phi(\mathbf{p}(t)) \middle| \mathbf{p}(t) \in \Omega_p \right\} \\ &\text{where}: \ \Phi(\mathbf{p}(t)) = \sum_{i=1}^{n} D_i(\mathbf{q}_{upper}(t_x), \mathbf{q}_{lower}(t_x)) \end{aligned} \tag{5.2.41}$$

The objective function is here defined as a sum of distances between upper and lower beam in selected chambers of the frame and it may concern only one (usually impacted) or several chambers. The considered time instant t_x may indicate the end of impact when the impacting mass is stopped or time instant when total distance is minimal. In both cases time instant t_x is not preliminarily known since it depends on applied loading and time-history of pressure changes during the process. Moreover, it is not known a priori which points of the spans will be closest to each other in final configuration and thus kinematics of the whole upper and lower span has to be observed during the analysis.

The formulated objective function is based on deformation of the structure similarly as in problem of minimisation of hitting object deceleration (Eq.5.2.27) where optimal displacement of the impacted node was predefined. However, the two substantial differences which distinguish the current problem are the following:

1. the objective function is not defined in every time instant of the process but only at certain time instant t_x ,
2. the objective function does not concern single node of the structure but it rather corresponds to global deformation of the structure.

The above features indicate that the whole problem can not be decomposed into a series of simpler problems formulated for particular time instants and, therefore, can not be solved by methods used in case of acceleration minimisation (cf. Example 1). In order to transform continuous variational problem (5.2.41) into classical optimisation problem, continuous functions **p**(t) will be substituted by coefficients of functions describing change of pressure in every chamber. Desired deformation of the structure will be obtained either by means of heuristic methods which utilise knowledge about impact location and energy for prediction of deformation and optimal inflation or, alternatively, by means of gradient-based optimisation procedures.

In the above optimisation problem, admissible shape of deformation is not restricted by previously defined conditions of collision of the mass and lower beam Γ_{Sq}^1 and maximal displacement of the lower span Γ_{Sq}^2. Deformation of the structure does not have to be contained in the set S_q defined by Eq. 5.2.5.

Example 1: three chamber frame, central impact

Initially, the optimisation problem was solved for three-chamber inflatable frame subjected to central impact. The structure is equipped with one sliding support which causes that deformation invoked by impact loading is relatively large and strongly depends on change of pressure in particular chambers of the frame.

Maximal compression of all chambers, which is not a typical deformation in case of central impact, can be obtained, however, negative values of pressure have to be applied in both lateral chambers, cf. Fig. 5.2.16.

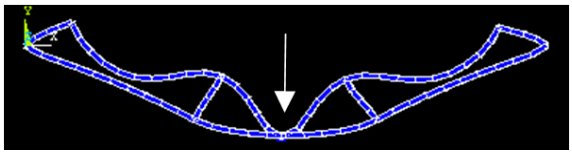

Fig. 5.2.16: Desired deformation of the structure obtained by means of negative pressures

In case when constant positive values of pressure in all chambers are assumed, the optimisation problem contains only three variables. Performed analysis of the optimisation problems aimed at compression of single chambers allow to draw the following conclusions:

- solution of the optimisation problem was often ambiguous and depended on choice of the starting point which means that particular deformation of the structure can be obtained by various combination of pressures,
- appropriate adjustment of constant positive pressure allows to obtain full compression of arbitrarily selected chamber,
- deformation of the frame is the most sensitive on value of pressure in central chamber.

As an example, the dependence of impact scenario (deformation type, maximal displacement of mass and time of stopping the mass) on pressure inside central chamber is presented in Table 6. (impacting mass: M=8600kg, pressures in lateral chambers: $p_1=p_3=0$kN/m).

p_2 [kN/m]	q_{max} [m]	t_{stop} [s]	Type of deformation, compressed chamber:
330	0,45	0,724	central
345	0,33	0,536	left
400	0,24	0,285	first left , afterwards right

Table.6: Influence of inflation on structure deformation

More precise control of final deformation shape can be obtained by introducing controlled release of pressure. The subsequent example, concerning distribution of the central impact into two chambers of the frame, reveals the influence of speed of pressure release on final deformation of the structure. Two schemes of pressure adjustment were considered:

- deformation of lateral chambers obtained by application of relatively high initial pressure (p=450kN) in central chamber, small pressures in the lateral ones and by performing slow release of pressure from the central chamber (t=0-0,6s), Fig. 5.2.17a
- deformation of central and right chamber obtained by exactly the same initial inflation but fast release of pressure from central chamber (t=0-0,3s), Fig. 5.2.17b.

The obtained change of deformation (5.2.17a to 5.2.17b) is associated with substantially larger displacement of the impacting mass and longer time of the process. Application of the above strategies allows for diverse distribution of the central impact and for controlling the locations of arising of the main plastic hinges.

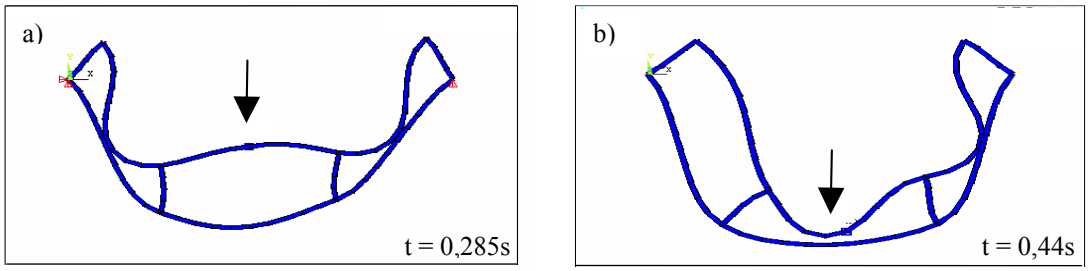

Fig. 5.2.17: Control of structure deformation: a) slow release of pressure in central chamber, b) fast release of pressure in central chamber.

Example 2: three chamber frame, lateral impact

In a further step, the problem of optimal distribution of pressure for various locations of the impact loading was examined. The example shows that optimal strategy of inflation depends not only on mass and velocity of the impacting object but also on impact location.

In the two considered examples of lateral loading (applied over left chamber or over right pillar, cf. Fig. 5.2.18a,b), the objective of pressure adjustment was to distribute impact into adjacent chambers of the frame. Applied heuristic strategy of adaptation assumes that external packages, which are most exposed to destruction, are inflated to a high pressure at the beginning of impact. In a further stage, pressure inside peripheral chambers can be decreased, however, gas has to be transferred to the central chambers to avoid their abrupt deformation, Fig. 5.2.18.

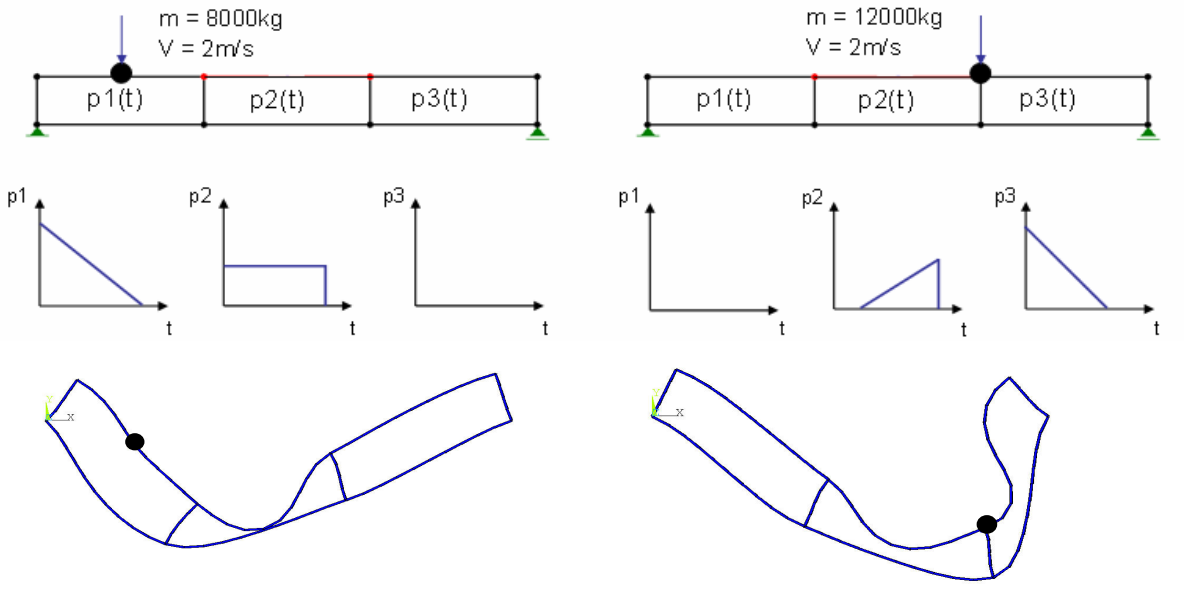

Fig. 5.2.18: Strategy of the pressure distribution during lateral impact: a) over left chamber, b) over right pillar

In case of an impact applied over left chamber, the applied strategy of pressure control leads to a full compression of the central chamber instead of peripheral one. In turn, when impact is applied over right pillar, appropriate tuning of the proposed strategy allows to obtain compression of both central and right chamber. Moreover, the strategy of pressure adjustment is not exactly the same in case of impact applied symmetrically at right and left side of the frame (over the pillar or in the middle of the chamber) due to influence of the sliding support.

Example 3: five chamber frame, lateral and central impact

The promising results were also obtained by controlling internal pressure in five-chamber thin-walled frame. Division of the structure into five sections allows to adjust pressure in different parts of the structure and provides precise control over structure deformation.

Typical response to the impact loading applied over peripheral left chamber involves large deformation of the impacted chamber and insignificant deformation of the other chambers. Under certain inflation of the left part of the frame (two lateral and central chambers) the structure becomes sensitive to the value of pressure and deformation shape changes. Precise adjustment of initial value and intensity of pressure release allows to obtain deformation of the second or alternatively third (central) chamber of the frame, cf. Fig. 5.2.19. The qualitative modification of the structure deformation is associated with a change of maximal deflection of the frame and with a change of total time of deformation.

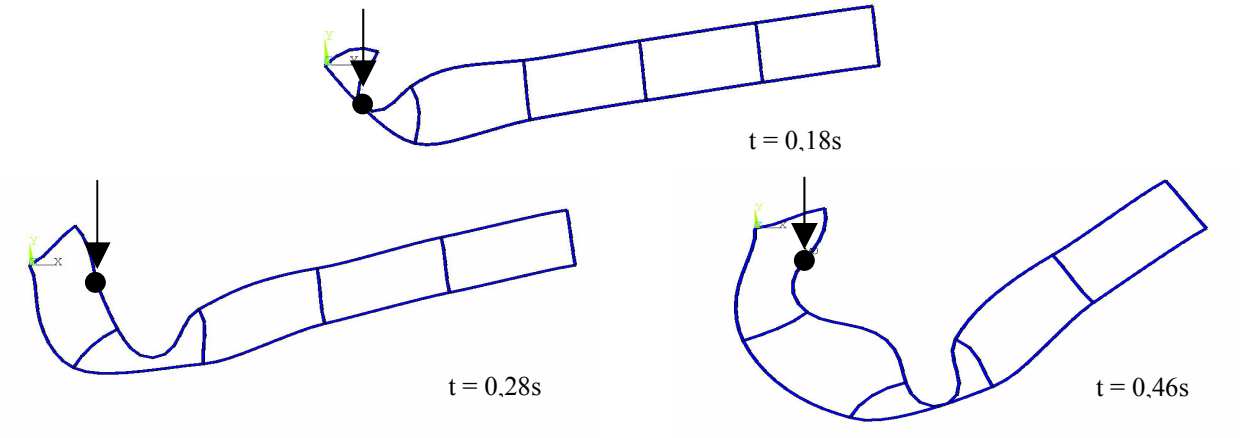

Fig. 5.2.19: Various deformations of the frame obtained in case of lateral impact:
a) no inflation, b) and c) inflation causing change of deformation shape

In case of strong central impact, the largest deformation occurs in central chamber and it is related to a large maximal deflection of the frame, cf. Fig. 5.2.20a. Application of high pressure exclusively in the central chamber of the frame allows to avoid its large compression and to distribute deformation into two sides of the frame, cf. Fig. 5.2.20b. The main benefit of this strategy is generation of two plastic hinges instead of one and corresponding increase of the efficiency of energy dissipation by structural part of the system.

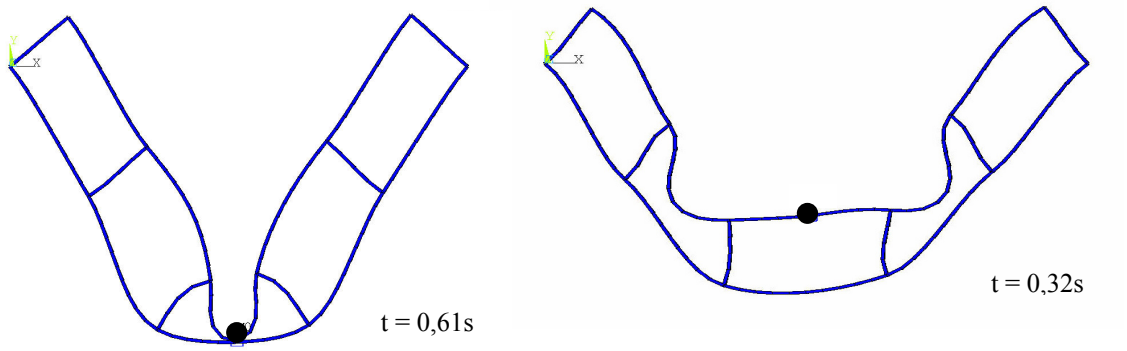

Fig. 5.2.20: Various deformations of the frame obtained in case of lateral impact:
a) no inflation, b) inflation of central chamber causing change of deformation shape

Summary of Chapter 5

The chapter analyzes basic mechanical properties of thin-walled crashworthy structures filled with compressed gas and investigates the possibilities of controlling their dynamic response to lateral impact by managing change of pressure during the impact process.

The first sections presents experiment proving beneficial influence of inflation on buckling of the aluminium can, followed by series of numerical analyses. Conducted simulations show the effect of pressure on stress distribution in the walls of the bended can and, moreover, reveal the qualitative and quantitative influence of inflation on value of the buckling force, buckling shape, possibility of can bursting and its frequencies of vibrations. Further numerical examples concern various inflated structures subjected to impact loading: hull compartments, door of the car and road barrier. For each structure different beneficial aspect of internal pressure is revealed. Adjustment of pressure allows to control type of failure and prevent penetration by impacting object, to increase global stiffness and decrease maximal deflection and, in the last case, to influence local zones of large deformation and stress concentration.

In the following section the attention is focused on pressure adjustment strategies for impact subjected 2D frame structure with several pressure chambers. The main problem addressed is maximisation of the load capacity of the structure by means of internal pressure changed on-line during the impact process. The mathematical formulation of the corresponding optimisation problem is precisely described and possibilities of problem simplifications are discussed. Proposed methods of solution are tested by using frame structures of different material characteristics, number of chambers and boundary conditions. The examples show that in certain cases the profit in load capacity may be significant. The following optimisation problems are oriented towards control of impacting object deceleration and minimisation of pressure values required to sustain given impact loading. In turn, the last group of examples shows the possibility of controlling final shape of structure deformation and location of plastic hinges by means of internal pressure.

Presented examples indicate that wide range of mechanical features of thin-walled structures, as well as, their dynamic response to lateral impact loading can be enhanced by the use of internal pressure. Solutions of the formulated optimisation problems prove that compressed gas allows to obtain intended change of response and large beneficial effects, however initial adjustment and release of pressure in particular chambers has to be precisely controlled.

CHAPTER 6 - ADAPTIVE 'FLOW CONTROL - BASED' AIRBAGS

The chapter is dedicated to development of the concept of adaptive 'flow-control based airbags' [289], i.e. airbags which are equipped with controllable valves providing optimal release of pressure during impact. The term 'airbag' is here expanded over the classical meaning since it embraces miscellaneous strongly deformable structures made of compliant material (not necessarily fabric) filled with gas. The chapter is composed of two independent parts, where two types of the systems based on adaptive airbags are proposed and analysed.

The first section concerns inflatable torus-shaped fender which mitigates the process of docking of small ships to offshore structures such as offshore wind turbines towers. Numerical models of various complexity, which enable simulation of ship impact against a tower protected by inflatable fender, are developed. In all models, impact of the ship is considered as unidirectional. The conducted simulations involve interaction between ship movement, fender deformation, change of internal pressure and tower vibrations during impact. Pressure control strategies are aimed at protection of both the ship and the tower and they take into account contribution of the above mentioned factors.

The second section introduces the concept of an adaptive external airbags for helicopter's emergency landing. In this case, release of gas occurs due to both fabric leakage and flow through controllable valve. Therefore, only part of the gas outflow can be controlled. Contrary to inflatable torus example, dynamics of the falling object is not considered uni-directionally but it involves all displacements and rotations related to rigid body motions. Consequently, pressure release strategies are aimed not only at controlling vertical motion of the falling object but also its rotation and angular acceleration.

6.1. Inflatable fenders for protecting offshore wind turbines

Wind turbines are one of the main sources of renewable energy. Current wind energy capacity installed in the EU countries equals 84GW (as of end 2010) and provides energy production of 142TWh (4,2% of European demand) [290]. Moreover, the contribution of wind energy to a total energy production is still increasing and it is expected that installed capacity will exceed 200GW before 2020. The largest wind generators currently operating provide up to 5MW of power and the increase of their effectiveness is still required. This can be achieved by locating wind turbines in regions where the wind conditions are more beneficial, for instance in offshore regions, where the wind flows with higher and more constant velocity. Additional advantages of locating wind turbines offshore include the availability of large open spaces and the lack of noise and aesthetics-related inconveniences for inhabitants. Wind turbines are usually situated in shallow continental shelves in the vicinity of large ports (for example on the North Sea). Such locations evoke a comparatively low overall cost for wind turbine installation and energy transportation.

In offshore regions wind turbines are exposed to harsher environmental conditions. The main threats for offshore wind generators are very strong winds and ice loading in winter [291]. Typical method of reducing ice forces acting on a structure is using ice braking cones which serve as passive or semi-active tuned mass dampers as proposed by Kärnä et al [292] and Mróz et al [93 293]. Moreover, the concept of reducing the effects of strong wind gusts

by using adaptive blade-hub connection controlled by magneto-rheological clutch was proposed and tested experimentally [94]. Another threat is the possibility of large tanker vessel collision and the risk of resulting environmental pollution. The indications for the design of offshore wind turbines which reduces the probability of the tanker vessel damage were given by Lehmann et al [294, 295]. Additional dangers for offshore structures are collisions involving small service ships which have to dock to wind turbine towers for the purpose of maintenance and monitoring. Such collisions occur especially often during rough sea conditions and can lead to a serious damage to both the wind generator tower and the ship. Therefore, an efficient system providing safety for docking operations is required. In this section the concept of adaptive torus-shaped pneumatic fender attached to the wind turbine tower is proposed and its feasibility is verified.

The section is based on author's papers [296 297]. It is organised in the following way: initially, the concept of adaptive pneumatic fender is introduced and its operation principles are described. Next, a full model of the wind turbine is presented and reduced to the water level. Then, three models of a ship impact against the tower protected by inflatable structure are considered (Sec. 6.1.1). The most precise, 3D model is used to simulate operation of the passive fender and to verify the correctness of the simpler models. By contrast, the most rudimentary, 1D model allows to estimate the response of the structure without conducting the finite element analysis. Two- dimensional, adequately precise and computationally effective model is used to develop miscellaneous pressure control strategies oriented toward mitigation of ship and tower response (Sec. 6.1.2). The main goal of the performed analyses is to compare the results obtained by applying various pressure adjustment strategies and to prove the effectiveness of AIA approach in comparison to a baseline passive case.

6.1.1. Concept of inflatable torus and modelling methods

The Adaptive Inflatable Structure used for protecting offshore wind turbine against collisions of small ships is torus-shaped and surrounds the tower as shown in Fig. 6.1.1. It is located at the water level and it may be partially submerged. The dimensions of the inflatable fender are limited to c.a. 2m in height and 1m in width due to requirements of fast inflation and pressure release during impact. Moreover, maximal operating pressure is arbitrarily confined to 20atm.

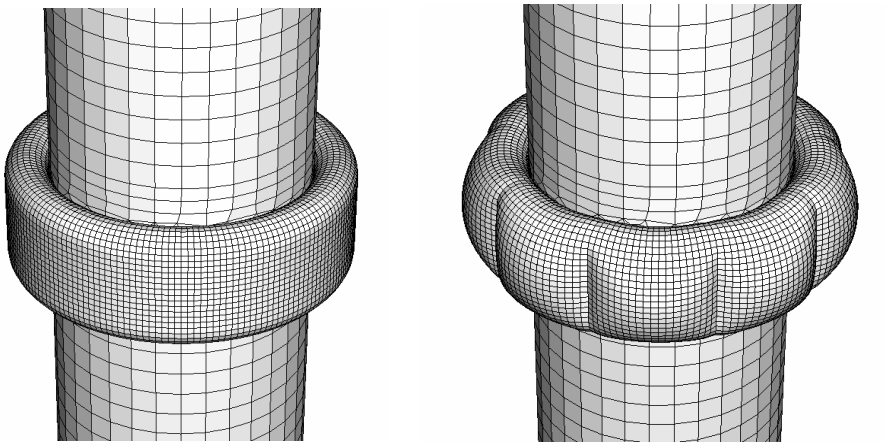

Fig.6.1.1. Adaptive Inflatable Structure surrounding the wind turbine tower: a) no inflation, b) uniform inflation of all chambers.

The walls of the pneumatic structure can be made of rubber reinforced by steel fibres or any other material which provides high durability and allows for large deformations during the impact of a ship. In order to obtain the possibility of better adaptation to various impact scenarios, the inflatable structure is divided into several separate air chambers located around the tower (Fig. 6.1.1 and Fig. 6.1.2). The exact design of the AIS and the required internal pressures are determined by the range of possible impact energies and they will be precisely defined while considering the conditions for optimal impact absorption.

Proposed pneumatic fender is intended to be permanently inflated to a relatively low pressure which provides mitigation of ship impacts of small kinetic energy. Additional inflation is planned before any stronger collision. It is executed for each chamber separately by a compressor located inside the tower or, alternatively, by a fast-reacting pyrotechnic system. The pressure of gas increases a total stiffness of the fender, which thus counteracts movement of the ship more effectively. As a result, appropriately inflated structure allows to prevent direct collision between the ship and the tower and to avoid corresponding excessive forces and accelerations. The usage of compressed air causes that the proposed protective structure can be easily adapted to various impact energies and scenarios. Value of initial internal pressure can be adjusted and varied between the chambers according to ship velocity, its mass and the area of contact with pneumatic structure.

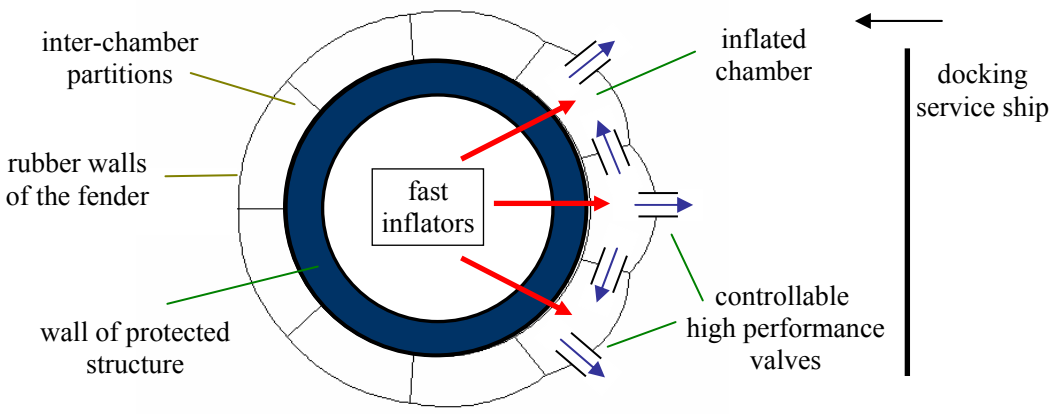

Fig. 6.1.2. Horizontal projection of the inflatable structure protecting the tower.

During collision or docking of the ship controlled release of pressure is executed by opening controllable high performance valves. Such valves are mounted inside external walls of inflatable fender, as well as in internal inter-chamber partitions such that they enable the gas flow between the chambers and outside the structure. Release of pressure allows to control global stiffness of the pneumatic structure (resulting from stiffness of rubber and internal pressure) during the subsequent stages of impact. Consequently, total force acting on docking ship and its deceleration can be controlled and impact energy can be dissipated.

The adaptation procedure can be successfully applied providing that ship impact is sufficiently well recognized. The initial velocity of approaching ship and impact direction can be determined by means of ultrasonic velocity sensors. Moreover, fender can be equipped with accelerometers, piezoelectric pressure sensors and displacement / deformation sensors located inside the torus chambers, which allow to track the dynamic response of the system.

The impacting object mass and its initial kinetic energy can be recognised during the initial stage of impact by using measurements from the above sensors and by applying procedures described in detail in Sect. 3.2.1.

The purpose of applying pneumatic structure is to mitigate the response of both the ship and the wind turbine tower. In particular, the inflatable structure allows to minimise ship deceleration, to avoid ship rebound, to decrease stresses arising at the location of the collision and, finally, to mitigate tower vibrations.

Model of the wind turbine tower

Let us analyse the finite-element model of a typical wind turbine, as shown in Fig. 6.1.3, which was introduced in [293]. Considered tower is 88m high and its foundation is located 6m below the water level. The tower consists of beam elements with circular sections and an external radius varying from 1,16 to 2,11m. The wind turbine has three 40-meter long blades which are modelled by shell elements. Four flanges located along the tower and three components of the turbine are modelled by point masses. Moreover, the tower is equipped with the cone structure located at the water level which serves as a protection against ice loading. In present case, the ice-braking cone will be replaced by inflatable fender designed to mitigate docking operations.

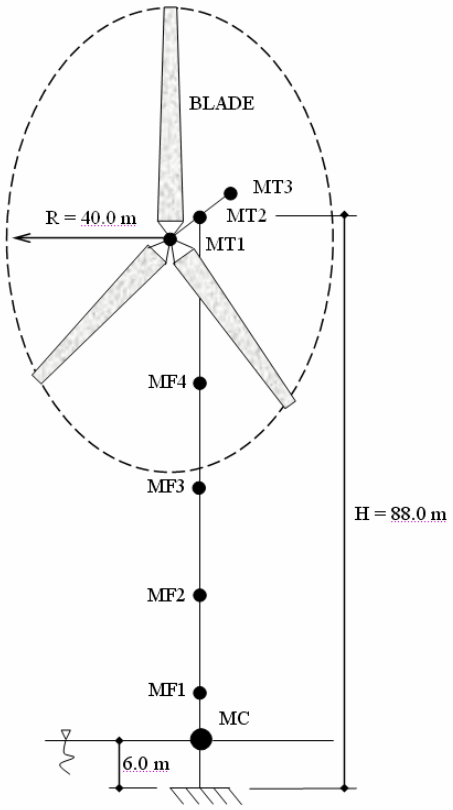

Blades (shell elements):
first own frequency $\omega_1 = 1.30$ Hz
weight of blade $G_B = 7006$ kg

Tower (beam elements):
47 elements with circular section
radius R = 1,16 ÷ 2,11 m
thickness t = 0,014 ÷ 0,040 m
weight of the tower $G_T = 186\,782$ kg

Point masses (MASS elements):
MT1 = 13 000 kg
MT2 = 31 800 kg } turbine
MT3 = 35 000 kg
MF1 = 4 200 kg
MF2 = 3 200 kg } flanges
MF3 = 1 900 kg
MF4 = 2 300 kg
MC = 49 620 kg - ice loading protecting cone

Total weight of the structure:
G = 3 x 7006 kg + 186 782 kg + 141 020 kg =
= 348 820 kg

Fig.6.1.3. Numerical model of the wind turbine tower by A. Mróz [293].

Part of the tower located nearby the water level is of greatest interest because of the collision considered. Reduction to one-dimensional model, at the water level, can be performed with the use of modal analysis of the structure [22]. For every particular vibration mode, mass, stiffness and damping of the reduced model are given by the formulae:

$$M = \frac{1}{\phi_{nC}} \int_0^H m(z)\phi_n^2(z)dz = \frac{M_n}{\phi_{nC}^2} \tag{6.1.1}$$

$$K = \omega_n^2 M = (2\pi f_n)^2 M \tag{6.1.2}$$

$$C = 2\xi\omega_n M \tag{6.1.3}$$

where: $\phi_n(z)$ is the mode shape, ϕ_{nC} is the normalised value of the mode on the water level, M_n is the generalised mass calculated for this mode and ω_n is the circular frequency. The values of ϕ_{nC}, M_n, f_n can be obtained directly from modal analysis of the structure presented in Fig. 6.1.3. The damping coefficient ξ is assumed to be equal to 0,5%. The resulting mass, stiffness and damping parameters of the reduced 1D model corresponding to two initial global modes of vibration are presented in Table 1 and they will be exploited in further sections.

	f_n[1/s]	ϕ_{nC}	M_n[kg]	M[kg]	K[N/m]	C[Ns/m]
Mode 1	0,33147	1,584 e-3	116 748	0,4653e11	0,2018e12	0,9690e9
Mode 2	0,38503	1,021 e-3	34 646	0,3318e11	0,1942e12	0,8029e9

Table 1. Parameters of the 1D model at the water level.

Three-dimensional model of collision between a ship and a tower

For the purpose of precise modelling of the influence of pneumatic fender and its properties on the process of ship impact against the wind turbine tower, a three-dimensional finite element model was developed, Fig. 6.1.1 and 6.1.4. The model contains only the lower part of the wind turbine tower and the upper part is modelled by additional masses attached at the upper edge. The tower consists of shell elements with thickness increased at the water level, while the torus-shaped fender can be modelled with either shell of membrane elements. The gas inflating the chambers is simulated by using Uniform Pressure Method according to formulae introduced in Sect. 2.3 (cf. part concerning multi-chamber systems). In considered case, the major part of pneumatic torus is located above the water and only a small part is submerged so pressure exerted by water is not taken into account. Typical deformation of the torus caused by initial inflation is presented in Fig. 6.1.4a.

Impact of the ship is defined as a contact problem. The ship is modelled as a rigid surface with a prescribed mass and area which is approaching the tower with initial velocity, Fig. 6.1.4b. The contact conditions are defined between the ship and the rubber wall of inflatable structure and between the rubber wall and the wall of the tower. When ship collision occurs the walls of the fender deform, chamber volume decreases (Fig. 6.1.4b) and pressure rises. During this stage, the release of the gas to environment and migration of gas between the chambers can be controlled by changing the resistance coefficients of the valves. Finally, the ship is stopped and possibly bounces from the inflatable structure. In case when the impact energy is too high or the control is adjusted improperly, the pneumatic structure is not able to stop the ship and collision against the tower wall occurs.

The numerical tool used for 3D simulations was the FEM code ABAQUS/Explicit which is well suited for this type of problems due to applied explicit scheme of integration and the function of ‘surface-based cavities’ which allows for modelling fluid-filled chambers.

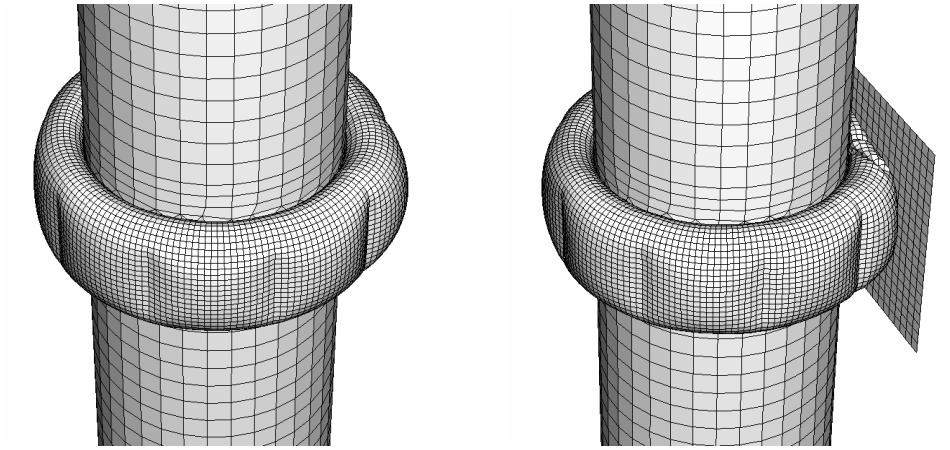

Fig.6.1.4. Three-dimensional model of collision: initial inflation and deformation during ship impact.

Two-dimensional model of collision

Two-dimensional model corresponding to water level was implemented to reduce the time of analysis and to examine various options for inflatable structure design. The model consists primarily of elastic Timoshenko beam elements used for modelling of tower and fender walls. Since the mass obtained from reduction of the full model (Table 1) is located in the middle of the structure, the additional elements connecting the mass with the walls of the tower are required, Fig. 6.1.5. The stiffness of the tower is modelled by an additional element connected to its middle point. The numerical software used for the analysis of 2D model was ABAQUS/ Standard. Although it's disadvantage is application of implicit integration methods, it enables the usage of Fortran subroutines for convenient implementation of additional models of gas flow and closed-loop control of gas release. An alternative methodology for conducting 2D simulations was application of ABAQUS/Explicit and coupling it to external software (MATLAB) in order to controlled gas outflow during the analysis.

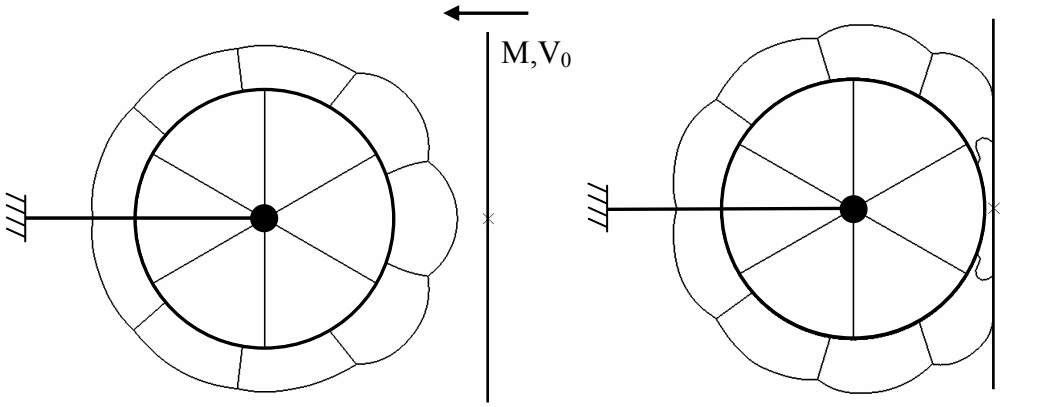

Fig.6.1.5. Two-dimensional model of collision: initial state and resulting deformation.

A parametric analysis performed with the use of two-dimensional model was utilised to investigate basic features of the inflatable structure. Various dimensions, number of chambers, material properties and thickness of the fender wall were considered. Indications for proper choice of these parameters and optimal design of the torus-shaped fender are as follows:

- value of pressure required to stop the ship can be decreased by using wide chambers (i.e. torus structure with large external radius),
- consequently, wide chambers are more beneficial for reduction of ship deceleration,
- chambers which are too long (along tower circumference) can not absorb strong impacts with initial atmospheric pressure and additional inflation is required,
- the use of longer chambers helps to decrease the local stresses in the tower wall,
- in long and narrow chambers large deformations and stresses appear after the initial inflation in the outer wall of the fender,
- the use of larger number of chambers allows us to adjust pressure more precisely to the actual impact scenario.

Taking into account all of the above mentioned conditions, as well as, the maximal admissible pressure, allowable stress of rubber and the maximal initial increase of chamber volume, the inflatable fender was designed as composed of nine chambers of a width 0,7m with walls of thickness 1cm made of reinforced rubber of alternate Young's modulus equal 150MPa.

Simplified one-dimensional spring-piston model of collision

Finally, the problem of ship collision with a tower protected by a pneumatic structure was reduced to a simple two degree of freedom system with a single air chamber modelled by an air spring (Fig. 6.1.6). The model allows for a basic estimation of required pressure values and for assessment of the inflatable fender efficiency.

The total force resulting from the action of compressed air equals $A(p(t)-p_A)$ and it acts when the ship is in contact with the inflatable structure. Since the pneumatic force always pushes the tower and the ship away from each other, the term $A(p(t)-p_A)$ is neglected when it becomes negative. Moreover, pneumatic force vanishes after ship rebound when the inflatable fender regains its original size h_0, i.e. when $u_2(t)=u_1(t)$. In case of impact with ship rebound, the response of the system can be divided into two stages: i) the first, when both objects are in contact and ii) the second stage when tower undergoes free vibrations.

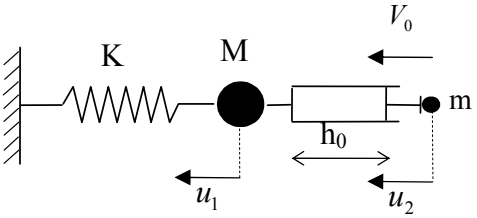

Fig.6.1.6. Two degree of freedom model of collision between the ship and the tower.

The equations governing the problem read:

$$M\frac{d^2u_1(t)}{dt^2}+Ku_1(t)-\begin{Bmatrix}(p(t)-p_A)A & \text{for} \quad p(t)\geq p_A \quad \text{and} \quad u_2(t)>u_1(t)\\ 0 & \text{otherwise}\end{Bmatrix}=0 \tag{6.1.4a}$$

$$m\frac{d^2u_2}{dt^2}+\begin{Bmatrix}(p(t)-p_A)A & \text{for} \quad p(t)\geq p_A \quad \text{and} \quad u_2(t)>u_1(t)\\ 0 & \text{otherwise}\end{Bmatrix}=0 \tag{6.1.4b}$$

$$IC: \quad u_1(0)=0,\ \dot{u}_1(0)=0,\ u_2(0)=0,\ \dot{u}_2(0)=V_0 \tag{6.1.4c}$$

When gas is released, the pressure in compressed chamber of the fender is defined by the equation:

$$p(t) = \frac{p_0 V_0^{\kappa}}{m_0^{\kappa}} \frac{m(t)^{\kappa}}{V(t)^{\kappa}}, \qquad V(t) = A(h_0 + u_1(t) - u_2(t)) \tag{6.1.5}$$

where $m(t)$ denotes actual mass of the gas inside the chamber and $V(t)$ denotes its volume. Summation of the equation (6.1.4a) integrated over u_1 and (6.1.4b) integrated over u_2 leads to the balance of the energy for the whole system in the form:

$$\tfrac{1}{2} M V_1(t)^2 + \tfrac{1}{2} K u_1(t)^2 - \int_0^{u_1 - u_2} \left(p(t) - p_A\right) A d(u_1 - u_2) + \tfrac{1}{2} m[V_2(t)^2 - V_0^2] = 0 \tag{6.1.6}$$

By using definitions of kinetic energy E_k, potential energy E_p, work done by gas W_p and work done by external pressure W_{pA} the above equality can be written as:

$$E_p^{tower} + E_k^{tower} - W_p - W_{pA} + \Delta E_k^{ship} = 0 \tag{6.1.7a}$$

Further, by using balance of internal gas energy we obtain the formula:

$$-\Delta E_k^{ship} + W^{atm} = E_k^{tower} + E_p^{tower} + \Delta U - \Delta Q - \Delta H \tag{6.1.7b}$$

which clearly indicates that change of the ship kinetic energy (ΔE_k^{ship}) and work done by atmospheric pressure (W^{atm}) are converted into kinetic and potential energy of the tower (E_k^{tower}, E_p^{tower}), internal gas energy, heat transferred to environment and enthalpy of the gas removed from the system. Since tower displacement is very small in comparison to the ship displacement, the term $u_1(t)$ can be neglected in the definition of the air-spring volume (Eq. 6.1.5$_b$). In such a case, the equations describing the system (Eq. 6.1.4) are separated. The second, nonlinear equation can be solved to determine ship displacement, while the solution of the first equation can be obtained by treating its last term as time-dependent excitation.

In the case of adiabatic system in which mass of the gas inside chamber remains constant, the energy balance at time instant when the ship stops is described by the equation:

$$\tfrac{1}{2} m V_0^2 + p_A A u_2^{\max} = \frac{p_0 h_0 A}{\kappa - 1} \left[\left(\frac{h_0}{h^{\min}} \right)^{\kappa - 1} - 1 \right] \tag{6.1.8}$$

where $u_2^{\max}$ denotes maximal ship displacement and $h^{\min}$ denotes minimal cylinder length.

For the considered spring-piston model, the problems of pressure minimization and ship deceleration minimisation are equivalent. Minimal ship deceleration which prevents collision with tower is constant and can be determined from the kinematics of the system. The corresponding optimal pressure inside cylinder can be calculated from the energy balance:

$$\ddot{u}_2^{opt} = -V_0^2 / 2h_0, \quad p^{opt} = \frac{m V_0^2}{2 h_0 A} + p_A, \tag{6.1.9}$$

The above relations hold until ship displacement of ship equals h_0 and its velocity is reduced to zero. At this moment infinitesimally small amount of gas remains in the cylinder and thus internal pressure instantly becomes equilibrated with atmospheric pressure (either due to release of infinitesimal mass of gas or infinitesimal backward movement of the piston).

Consequently, total force acting on ship and its acceleration are reduced to zero and rebound of ship is totally mitigated. The applied pressure control strategy causes that ship impact can be treated as inelastic collision, whereas it resembles elastic collision in case when pressure release is not performed. Due to the fact that impulse transmitted to the tower in inelastic collision is two times smaller, velocity of the tower after impact is reduced twice.

Change of cylinder volume and change of mass of the gas corresponding to optimal pressure and kinematics can be determined from the geometrical relations and the ideal gas law (Eq. 6.1.5). If mass flow rate of gas is assumed to be proportional to pressure difference, the formula defining time evolution of optimal resistance coefficient in terms of impacting mass and impact velocity reads (cf. Eq. 3.2.49$_b$ for $u_x = 0$):

$$C_V(t) = \frac{(p^{opt} - p_A)RT_0}{p^{opt} A \dot{u}_2^{opt}(t)} \tag{6.1.10}$$

The above solution is valid for both isothermal and adiabatic processes and it holds when no constraints on resistance coefficient are imposed.

Comparison of collision models

The results obtained with the use of three of the above models (full 3D, 2D at the water level and 1D spring-piston model) were compared with each other in order to verify correctness and reveal limitations of simplified modelling. Comparison of the basic dynamic response of the system equipped with passive fender (pressure and volume of the chamber, ship deceleration and stress in the tower wall) was performed for two impact scenarios of 60 ton ship (V=3m/s and V=6m/s), see Table 2.

	Velocity [m/s]	p_0 [atm]	V_0 [m^3]	p^{max} [atm]	V^{min} [m^3]	Accel. [-m/s^2]	Stress [MPa]
1D	3	2	2,91	4,11	1,41	17,8	-
2D	3	2	2,95	3,74	1,54	19,5	84,2
3D	3	2	2,60	3,52	1,47	21,8	33,8
1D	6	4	3,26	10,68	1,22	58,6	-
2D	6	4	3,57	8,92	1,55	58,4	243
3D	6	4	2,97	9,72	1,22	68,9	108

Table 2. Comparison of results obtained by using different models of collision.

Primarily, it was observed that the global stiffness of the chambers in 2D model is too small since the connection of each chamber with the tower wall at the top and the bottom of the inflatable torus is not taken into account. Thus, radial deformation of 2D structure caused by strong initial inflation is larger than deformation of 3D structure. Moreover, 2D modelling does not capture vertical deformation of the chambers so ship-torus contact area and chamber volume computed for the same ship position (i.e. distance from the tower) are slightly different for both models. As a result, maximal internal pressure and ship deceleration obtained from two- and three- dimensional model are not precisely equal.

The conducted simulations indicate that maximal pressure obtained by using 2D model is underestimated for high-energy impacts and overestimated for low-energy impacts. Ship accelerations computed by 2D model are always lower than accelerations computed by full 3D model. The maximal von Mises stress in the tower wall obtained by using both models can not be directly compared because of different geometry of the wall, however stress obtained from two-dimensional model is usually around 2,5 times larger. The general conclusion from the performed comparison is that 2D modelling captures the dynamic response of the system the most precisely when chambers of the inflatable fender become long and narrow (in circumferential and radial dimensions, respectively).

Simplified 1D modelling completely neglects initial expansion of the air chambers and their transverse deformation (expansion coefficients have to be assumed on the basis of 2D or 3D model). The introduced spring-piston modelling can be used for rough estimation of basic dynamic response of the system.

6.1.2. Control strategies for mitigation of ship and tower response

General guidelines for pressure adjustment

The main task of the inflatable torus is to prevent direct impact of the ship against the tower wall. When the inflatable structure is not sealed and inflated, it can stop the object of comparatively low kinetic energy of 0,2 MJ. In case of stronger impacts, a contribution of gas pressure is required to avoid ship contact with the tower. Due to the fact that the front chamber (the one which is the most exposed to impact, cf. Fig. 6.1.5) is crucial for operation of the pneumatic fender, it will be inflated with the highest pressure. Adjacent chambers act as auxiliary and their pressure will be set to 30-50% of pressure in the front chamber.

Let us initially consider the system where only initial pressure is adjusted and all valves remain closed. Value of initial pressure which provides that the ship is stopped in the very vicinity of the tower wall will be referred to as minimal initial pressure $p_0^{\min}$. The value of pressure $p_0^{\min}$ was calculated for various impact energies (0,756-2,56MJ) by using 2D finite element model, see Table 3. The assumption of isothermal process was applied. The first example shows the impact of energy 0,756 MJ (29,5% of maximal energy considered) can be absorbed by using initial atmospheric pressure in the front chamber.

Mass [ton]	Velocity [m/s]	Energy [kJ]	Impulse [t*m/s]	$p_0^{\min}$ [atm]	$p_0^{\max}$ [atm]	Stress [MPa]	Displ. [m]
42,00	6	756	252	1	7,09	193	0,00299
67,00	6	1206	402	1,45	11,67	340	0,00481
52,00	8	1664	416	1,95	15,04	470	0,00499
66,00	8	2112	528	2,50	18,11	611	0,00635
80,00	8	2560	640	2,95	20,51	692	0,00770

Table 3. Response of the structure calculated for various impact energies.

Maximal pressure p^{max} corresponds to minimal volume of the chamber obtained when the ship nearly touches the tower wall. Maximal front chamber pressure, highest stress arising in the tower wall and maximal displacement of the tower top computed for various impact energies are presented in Table 3.

Moreover, maximal initial pressure p_0^{max} was introduced due to excessive stresses arising in walls of inflatable structure and its excessive deformation after too strong initial inflation. It was assumed that maximal initial deflection of inflatable structure can not exceed 0,6m and maximal stress after inflation should be smaller than 30 MPa. Corresponding maximal initial pressure p_0^{max} equals 4atm and it is independent on impact energy.

In further simulations, the tower protected by the pneumatic structure was subjected to impact of the same energy (0,64 MJ) but of various velocities, cf. Table 4. Initial pressure inside the front chamber was equal 1,8 atm in all cases. The values of the maximal pressure, displacement of the tower top and maximal stresses in the tower wall were observed.

Mass [ton]	Velocity [m/s]	Energy [MJ]	Impulse [t·m/s]	p_0 [atm]	p^{max} [atm]	Accel. [-m/s^2]	Stress [MPa]	Displ. [m]
20,00	8	0,64	160	1,8	4,879	124,6	140,1	0,00191
35,56	6	0,64	213,36	1,8	4,916	69,33	133,8	0,00255
80,00	4	0,64	320	1,8	4,926	31,3	135,9	0,00379

Table 4. Response of the structure to slow and fast impact of the same energy.

Moreover, all computations were repeated under assumption of adiabatic conditions. Two groups of performed simulations allow to draw the following conclusions concerning initial pressure adjustment and system response for various impact scenarios:

- initial pressure, for which the whole front AIS chamber is compressed, depends approximately linearly on impact energy (and it is lower for adiabatic process),
- for given initial inflation, maximal pressure depends nonlinearly on impact energy (and it is higher for adiabatic process),
- for the same impact energy maximal ship acceleration increases proportionally to the square of ship velocity and decreases inversely proportionally to ship mass,
- maximal stress in the tower wall depends on the highest pressure in front AIS chamber,
- displacement of the tower top is proportional to the impulse of the ship and it is relatively very small.

The above conclusions are in agreement with equations describing simplified air-spring model. Contrary to the above examples, in further sections a controlled release of pressure will be executed. The following inflatable systems will be considered:

1. reference passive system: initial pressure adjusted to the harshest ship impact (i.e. $p_0 = p_0^{max} = 4\text{atm}$), no pressure release;
2. system with semi-active adaptation strategy: only initial pressure or both initial pressure and constant in time valve opening adjusted to particular impact;
3. system with active adaptation strategy: valve opening controlled in-real time during the impact process.

Mitigation of ship response: minimisation of ship deceleration

Further, we will consider exemplary impact of 60 ton ship approaching the tower with the velocity 6 m/s, two semi-active and two active strategies of adaptation. All simulations will be conducted with the use of the previously introduced two-dimensional model (Fig. 6.1.5). Inflation of the chambers will be executed during initial 200 ms of the analysis and collision of the ship with pneumatic fender will occur directly afterwards. Distribution of pressures inside fender chambers will be fixed (100% in front cavity, 50% in adjacent cavities, and 10% in the other ones) and it will not be subjected to optimisation.

The first objective of control is minimisation of ship deceleration during impact. In considered system, the equivalence of deceleration- and pressure- minimisation problems is disrupted due to influence of forces resulting from deformation of fender walls and change of contact area between ship and inflatable structure during collision. In the simplest semi-active system only initial pressure is adjusted and mass of the gas inside fenders chambers remains constant. Optimal initial pressure p_0^{opt} is searched in the range of allowable initial pressures $\left(p_0^{\min}, p_0^{\max}\right)$ by means of gradient-based method. Minimal ship acceleration of 58,84 m/s^2 (Fig. 6.1.7) is obtained for the highest allowable initial pressure ($p_0^{\max} = 4\text{atm}$), which is the consequence of significant expansion of the front chamber after inflation. Thus, semi-active system without pressure release is equivalent to the passive one. Minimal ship acceleration corresponds to the case when only a part of the inflatable structure stroke is used, which indicates the possibility of further system improvement.

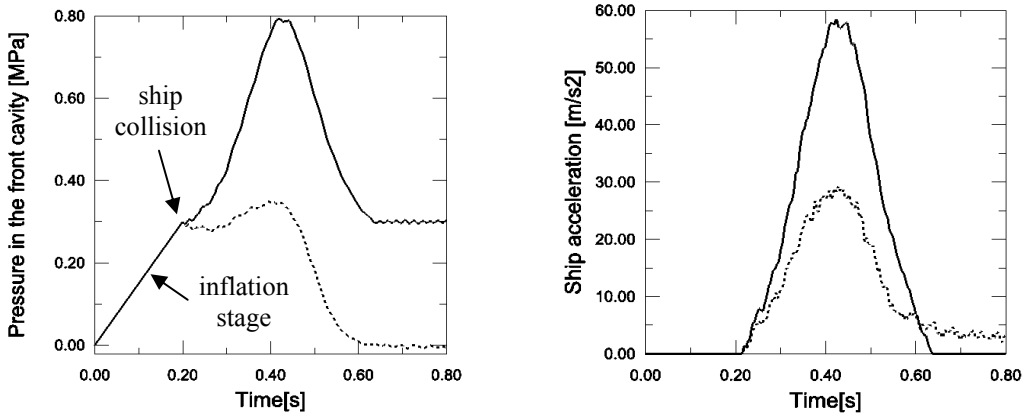

Fig.6.1.7. Semi-active acceleration mitigation without (continuous line) and with pressure release (dashed line): a) overpressure in the front chamber, b) corresponding ship acceleration.

More advanced type of semi-active system includes the exhaust valves which are opened at time instant when the ship approaches the inflatable structure. The opening of the valves is adjusted to particular impact scenario, but it remains constant during the whole event. In considered case the gas is released from three front chambers, which are essential for impact absorption, directly to environment. Performed release of gas causes decrease of pressure inside fender chambers, reduction of global force acting on the ship and increase of fender compression. Minimal ship acceleration of 29,14m/s^2 (Fig.6.1.7) is obtained for the case when maximal ship displacement achieves its limit, i.e. when the ship is stopped exactly before the tower wall. Accomplishment of the above strategy requires the valve of minimal resistance coefficient $C_V = 275 \frac{kPa}{kg/s}$ and maximal mass flow rate of gas $q = 1{,}27 \frac{kg}{s}$.

Further decrease of ship deceleration can be obtained by active control of valves opening during impact. In this strategy the valves remain closed until ship acceleration achieves the level, which maintained constant allows to stop the ship by using the remaining stroke of the fender. Therefore, determination of the time instant of valve opening is based on actual ship velocity, deceleration and distance to the tower (cf. Eq. 3.2.46).

The proposed methodology of maintaining constant ship deceleration utilises 'proportional control' of valve opening during the second stage of impact. In the applied strategy the value of resistance coefficient and the length of time interval of constant valve opening are adjusted in several consecutive steps in order to achieve approximately constant deceleration level, Fig. 6.1.8 (cf. proportional control of pneumatic cylinders in Sec. 3.2.2, strategy no.5). Alternatively, another strategies of proportional control or on/off control can be applied, however they require valve of considerably higher operating speed.

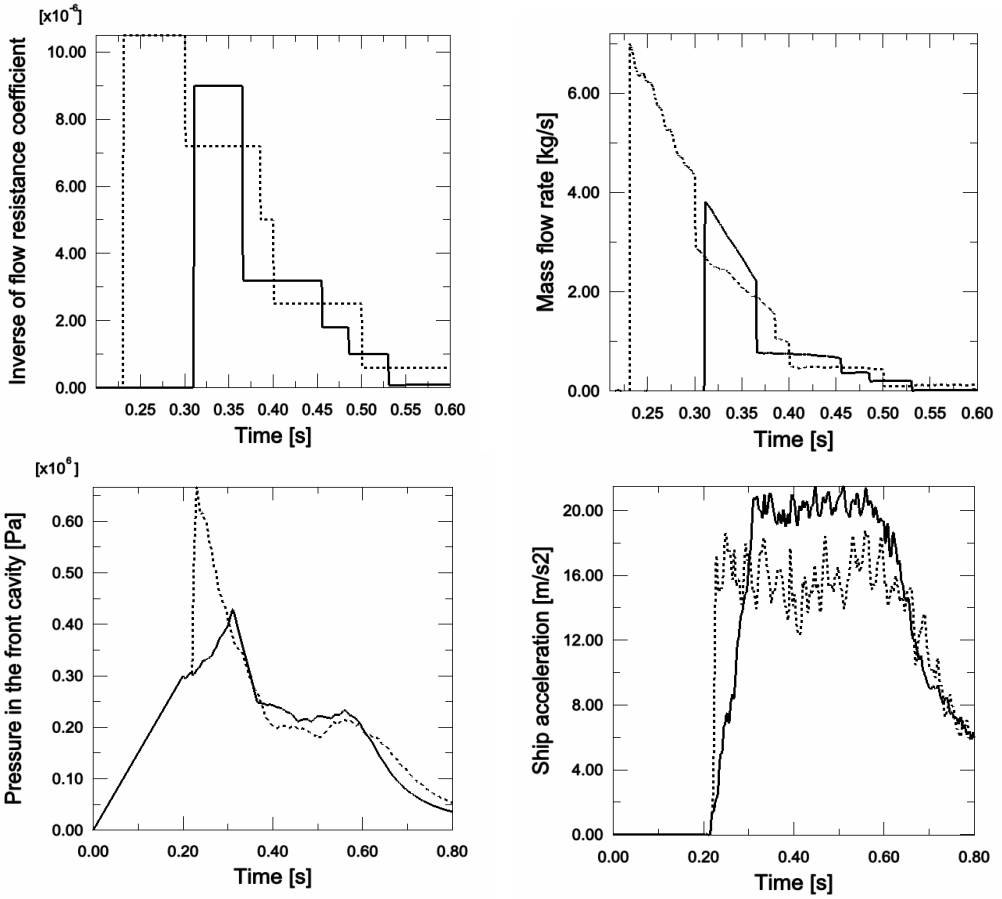

Fig.6.1.8. Two strategies of active acceleration mitigation: i) pressure only released during impact (continuous line), ii) additional inflation at the beginning of impact (dashed line).

The adaptation procedure is initiated at 110 milliseconds after the contact between ship and inflatable structure occurs (t=0,310s), when ship acceleration equals 21,2m/s^2, Fig. 6.1.8 (continuous line). During controlled stage of impact, the inverse of resistance coefficient which represents valve opening and corresponding mass flow rate of gas gradually decrease, Fig. 6.1.8a,b. Optimal value of pressure declines for several dozen milliseconds due to initial fast increase of ship/fender contact area and then it remains at similar level, Fig. 6.1.8c. As a result, ship deceleration is maintained nearly exactly constant (Fig. 6.1.8d) and its small oscillations are caused by vibrations of inflatable structure walls and discrete nature of applied

control procedure. Maximal acceleration obtained by this method is eventually reduced to 21,56 m/s^2, however high mass flow rate of gas (3,9kg/s) is required at the initial stage of impact.

Finally, an attempt to keep constant ship decceleration during the whole period of impact was made. Disadvantageous slow increase of acceleration in passive stage of impact (200-310 ms) can be avoided by additional inflation of the main chamber at time instant when the ship approaches inflatable structure. Due to the fact that in current strategy the whole stroke of the fender is optimally utilised, required level of ship deceleration is now lower than previously and theoretically equals $a^* = 16{,}4\text{m/s}^2$. To obtain desired deceleration level, the internal pressure inside front chamber is increased to 7,6atm at the initial stage of impact, immediately after ship contact, Fig. 6.1.8c. In a further stage of impact, large valve opening and corresponding mass flow rate of gas ($q = 7$ kg/s) are required to maintain constant level of deceleration, Fig. 6.1.8a,b. Since fast initial inflation causes strong vibration of the whole pneumatic fender, precise control of deceleration was aggravated. Eventually, ship deceleration was reduced to 18,76m/s^2 which constitutes 32% of acceleration in passive case.

Three methods of ship deceleration minimisation which involve change of amount of gas inside pneumatic fender during the impact process (strategy with constant valves opening, strategy with initial gradual increase of deceleration level and strategy involving additional initial inflation) are compared in Fig. 6.1.9.

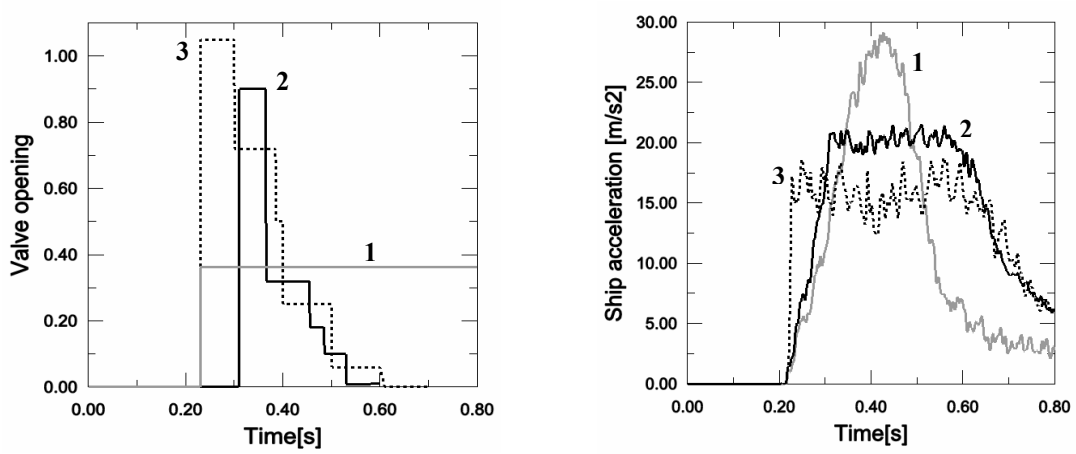

Fig.6.1.9. Comparison of three control strategies involving pressure release:
a) applied valve opening, b) resulting ship acceleration.

An alternative version of the active adaptation strategy, which allows to maintain constant deceleration level, utilises internal pressure as the main control parameter. Theoretically, optimal value of pressure can be determined from the simplified equation of ship motion which takes into account the forces arising during fender compression:

$$Ma^*(t) + \sum_{n=1..3} A_n(u, p_n)\, p_n(t) + P^{AIS}(u, p) = 0 \qquad (6.1.11)$$

where $a^*(t)$ is the optimal value of acceleration and $A_n(u, p_n)$ is the contact area between ship and each pneumatic chamber, which depends on actual ship position and internal pressure. The component $P^{AIS}(u, p)$ indicates force acting on the ship caused directly by deformed walls of the fender. The disadvantage of the method is that it requires preliminary determination of force P^{AIS} in terms of actual pressure and ship location.

Such a difficulty can be overcome by comparing actual and optimal state of the system for each time step of the finite element analysis. The procedure is started after initial stage of pressure increase, at time instant when values of pressure and acceleration reach optimal level. Thus, in the following step of analysis, the actual and optimal states of the system are close to each other and it can be assumed that the force P^{AIS} and the contact area A are equal for both of them. By subtracting equation of motion describing actual and optimal state of the system we obtain simple expression defining pressure modification which has to be applied at every time step in order to maintain constant ship deceleration:

$$\Delta p(t) = \frac{M(a^* - a(t))}{\sum_{n=1..3} A_n(u, p_n)} \tag{6.1.12}$$

The corresponding required mass flow rate of gas and continuous change of resistance coefficients can be computed by using previously determined optimal change of pressure and change of chamber volumes obtained from the finite element analysis.

Mitigation of ship response: minimisation of ship rebound

Considered torus-shaped pneumatic fender serves as a docking facility and ship rebound is not a desired phenomenon. Thus, the next control objective is to reduce ship rebound, i.e. to minimise ship velocity, after collision, possibly to zero. Equation of energy balance for ship collision with inflatable torus is analogous to Eq. 6.1.7b, but it is complemented with term indicating strain energy of deformed fender walls (ΔE^{AIS}). For the case of adiabatic systems equation of energy conservation reads:

$$-\Delta E_k^{ship} + \Delta W^{ext} = \Delta U + \Delta E^{AIS} + \Delta E^{tower} - \Delta H \tag{6.1.13}$$

In systems without pressure release, main part of ship kinetic energy (ΔE_k^{ship}) is converted into internal gas energy (ΔU) and a small part is converted into strain energy of the fender walls (ΔE^{AIS}). Kinetic and potential energy of the tower (ΔE^{tower}) can be neglected due to small displacement and velocity of the tower. During the rebound stage of impact gas expands, its internal energy decreases and it is transferred back to the ship.

In contrast to the above situation, in semi-active or active system with pressure release internal gas energy is not accumulated but it is dissipated by letting the air out of the chambers (ΔH). In such systems rebound of the ship is correlated with exergy of the gas (its ability to perform mechanical work) at time instant when the ship is stopped. Since exergy depends on gas pressure and volume at time instant of stopping the ship, it can be effectively reduced by applying controlled gas release.

Initially, semi-active strategies for reduction of ship rebound will be considered. Since adjustment of initial pressure itself does not cause energy dissipation, the value $p_0 = p_0^{\max} = 4atm$ will be arbitrarily assumed. When the system with a closed valve is applied, final kinetic energy of the ship is only 2% lower than the initial one, Fig. 6.1.10 (continuous line). Nonetheless, ship rebound can be effectively reduced by using semi-active system comprising valves with constant openings (Fig. 6.1.10, dashed line). Minimal final ship velocity V=1,25m/s is obtained when valves' openings provide that the whole stroke of pneumatic fender is utilized. Consequently, optimal resistance coefficient has exactly the

same value as in case of semi-active deceleration mitigation. In considered example, gas pressure at time instant of stopping the ship is not totally reduced (to an ambient pressure), however, final chamber volume is minimal and work that can be done by gas is relatively small. Therefore, semi-active system is very efficient and allows to dissipate almost 96% of initial kinetic energy of the ship.

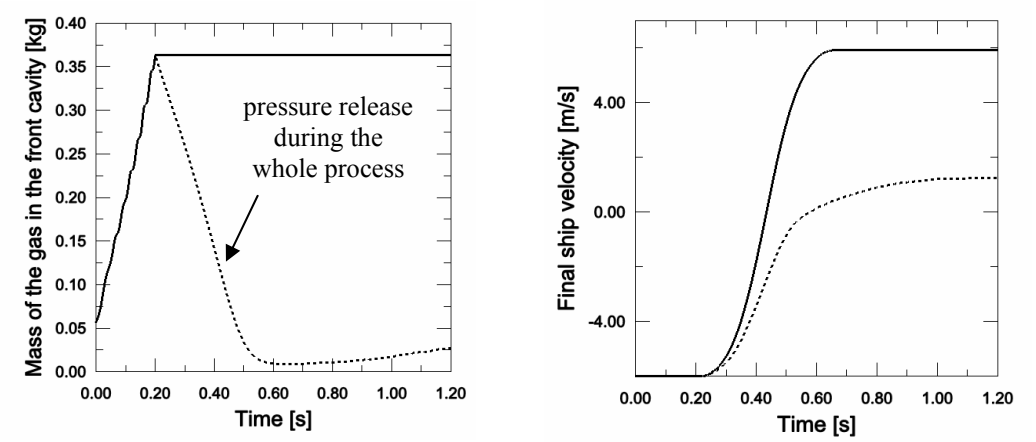

Fig.6.1.10. Semi-active adaptation without (continuous line) and with (dashed line) pressure release: a) mass of the gas in the front cavity, b) corresponding velocity of the ship.

In the first proposed active strategy the valves' openings remain constant while ship crashes the fender, as in semi-active approach. When ship velocity approaches zero (at time 0,54s) the valves are fully opened to release surplus of pressure, cf. Fig 6.1.11a (continuous line). This way gas pressure is reduced to atmospheric pressure, gas has no capability of expansion and cannot perform mechanical work. Then, the valves are closed and backward deformation of the fender chambers is prevented due to arising under-pressure. The result of this strategy is the reduction of rebound velocity to 1,05 m/s, Fig 6.1.11b (continuous line). The non-zero final ship velocity is the consequence of ship interaction with strongly deformed walls of pneumatic fender which push the ship away from the tower.

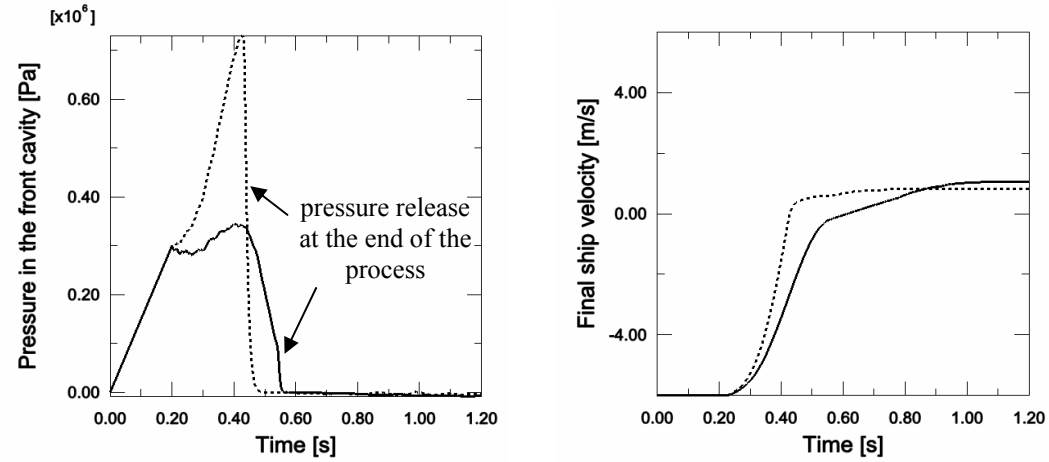

Fig.6.1.11. Two active adaptation strategies for reduction of ship rebound: a) pressure of the gas in the cavity, b) corresponding final velocity of the ship

An adverse influence of pneumatic fender walls can be further decreased by minimising their deformation and thereby the amount of accumulated strain energy. In the

second proposed control strategy the valves remain closed during the whole compression stage of impact to achieve the largest possible stiffness of pneumatic torus. The ship is stopped after crushing only a part of inflatable structure at time 0,42s. Then, immediate gas release is executed until pressure is reduced to the ambient one, Fig. 6.1.11a (dashed line), and the valves are closed again. As a result, the rebound velocity is reduced to 0,82 m/s which indicates that more than 98% of the initial ship energy is dissipated.

Another methodology of rebound mitigation is based on changing stiffness of partitions between front torus chambers during impact. This strategy allows to reduce strain energy accumulated in deformed front outer walls of the fender and to transfer it into kinetic energy to other parts of the pneumatic structure. Application of this method requires different construction of the torus partitions (e.g. as adaptive pneumatic cylinders) and introduction of additional controller into the system.

Mitigation of tower response: minimisation of stresses in tower wall

Another, equally important purpose of applying adaptive pneumatic fender is optimal mitigation of tower response during ship impact. In particular, pneumatic structure reduces local stresses in the front tower wall by preventing direct contact of the ship and the tower, which is achieved by applying initial pressure higher than $p_0^{\min}$ for each particular impact (cf. Table 3). During fender compression front tower wall is subjected to bending caused by pressure loading and its internal forces depend approximately on actual value of pressure. Therefore, the minimization of stresses in tower wall is approximately equivalent to the minimisation of front chamber pressure.

The reference case for performed comparison will be passive system with closed valve and initial pressure $p_0^{\max} = 4\text{atm}$. In such a system maximal internal pressure reaches 9,4atm and stresses in tower wall exceed 240MPa, Fig. 6.1.12a (continuous line). Optimal adjustment of initial pressure (to $p_0 = 2{,}7\text{atm}$) causes only a slight decrease of maximal pressure and, consequently, insignificant reduction of stresses (Fig. 6.1.12a, dashed line). In turn, semi-active system with pressure release is the most efficient when fender is inflated with maximal initial pressure $p_0^{\max}$ and constant valve opening provides that the whole fender stroke is utilised. In such a system maximal pressure is decreased to 4,49atm which causes that stresses in tower wall are diminished to 104.5MPa (Fig. 6.1.12b, continuous line).

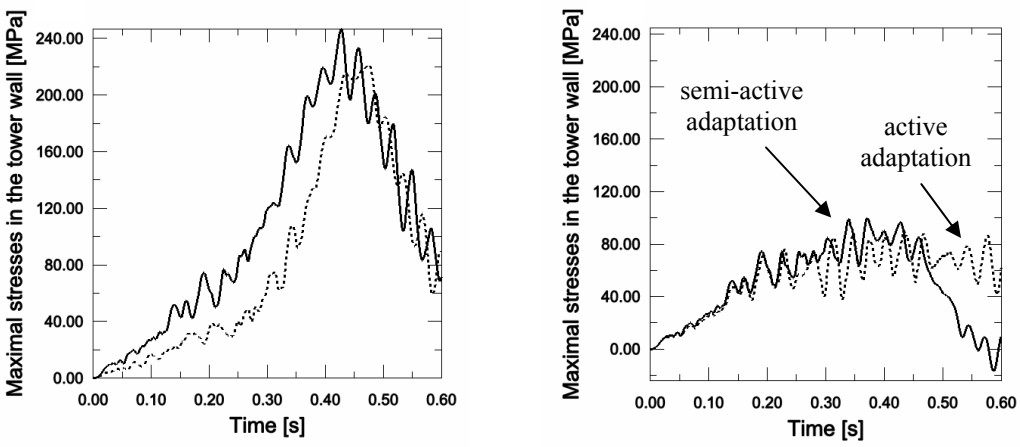

Fig.6.1.12. Minimisation of stress in tower wall: a) passive system and semi-active system without pressure release, b) semi-active and active system with pressure release

The proposed active strategy of stress minimisation relies on maintaining constant, possibly low value of pressure during the impact process. For impact energies lower than 1,25 MJ constant pressure which allows to stop the ship in the vicinity of the tower wall does not exceed maximal initial pressure $p_0^{\max}$. Thus initial pressure can be optimally adjusted and further maintained constant during the entire impact period. By contrast, for impact energy higher than 1,25MJ optimal strategy assumes inflation to maximal allowable pressure $p_0^{\max}$, the initial stage of pressure increase and the second stage when pressure remains constant.

For considered impact of 60 tons ship with the velocity 6 m/s (impact energy 1,08MJ) optimal value of initial pressure was determined directly from FEM simulations of ship impact and it equals $p_0 = p^{opt} = 3{,}68\text{atm}$. Obtained results allow to determine corresponding mass of the gas and required valve opening. Mass of the gas in front cavity increases during the inflation stage and it is reduced to keep constant level of pressure when fender is compressed by the ship, Fig.6.1.13a. During the rebound stage of impact, mass of the gas is again increased in order to maintain pressure constant (this stage is redundant and could be as well excluded from the analysis). Change of system parameters during the process of gas release is defined by the following simple equations:

$$\frac{p_0 V_0^{\kappa}}{m_0^{\kappa}} = \frac{p^{opt} V^{\kappa}}{m^{\kappa}} \Rightarrow m(t) = \frac{m_0}{V_0} V(t) = \frac{p^{opt}}{RT_0} V(t) \tag{6.1.14}$$

$$q(t) = \frac{dm(t)}{dt} = \frac{p^{opt}}{RT_0}\frac{dV(t)}{dt} \quad ; \qquad \frac{1}{C_V(t)} = \frac{p^{opt}}{RT_0(p^{opt} - p_A)}\frac{dV(t)}{dt}$$

The derived formula defining change of resistance coefficient is equivalent to the formula (3.2.115) defining continuous valve control in pneumatic cylinder. Change of resistance coefficient obtained from numerical analysis is irregular due to oscillations of chamber volume during the impact process, Fig. 6.1.13b. Since pressure difference remains constant, the inverse of resistance coefficient $1/C_V$ is proportional to mass flow rate of gas $q(t)$.

The proposed strategy provides significant reduction of pressure in comparison to the semi-active case (3,68atm vs. 4,49atm). However, high frequency vibrations of the tower wall arise and aggravate significant minimisation of stresses. Finally, the stresses are reduced to 91,9MPa (Fig. 6.1.12b) and the active system is 12% more effective than the semi-active one.

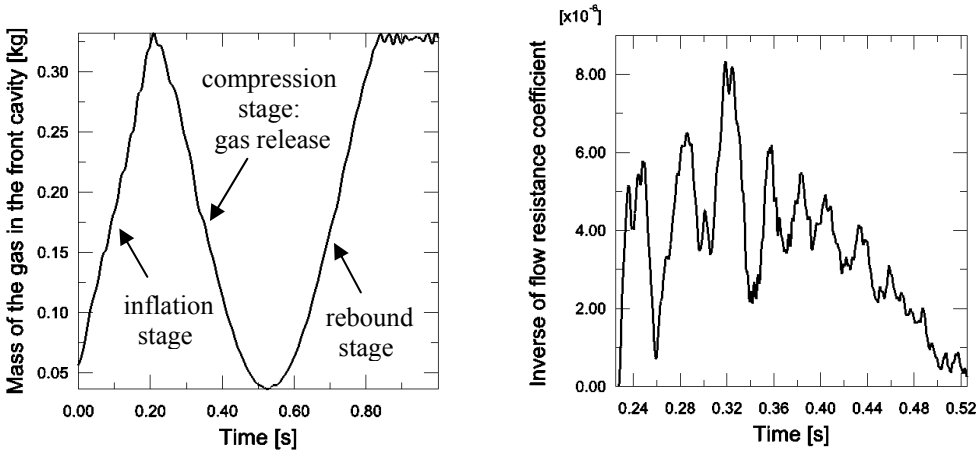

Fig.6.1.13. Active strategy of stress minimisation: a) mass of the gas in the cavity, b) inverse of resistance coefficient during compression stage of impact.

Mitigation of tower response: minimisation of tower vibrations

The last goal of pressure adjustment is to minimise the amplitude of tower vibrations after impact. This objective can be alternatively understood as a minimisation of the energy transmitted to the tower during ship collision. Due to the fact that impact time is relatively short in comparison to period of tower vibration, maximal tower displacement depends on ship impulse [22]. Impulse transmitted to the tower is proportional to mass of the ship and difference of its initial and final velocity. Hence, minimisation of tower vibrations is approximately equivalent to minimisation of ship rebound and vibration amplitude can be reduced maximally by 50%.

When semi-active system with closed valves is used, maximal tower displacement is almost independent of initial pressure and equals 4,58-4,60mm, which is in agreement with the result obtained by using simple model of elastic collision. Application of semi-active system with pressure release being the result of constant valve opening (Fig. 6.1.14a) causes that amplitude of tower vibration is reduced as presented in Table 6.1.14b. The best result (2,67mm) is obtained for the lowest resistance coefficient (i.e. the largest valve opening) for which the ship does not directly collide with the tower wall.

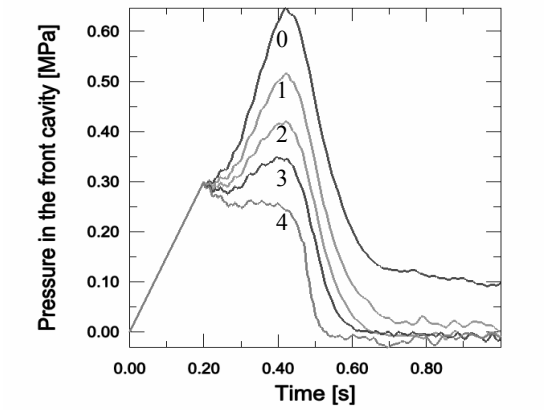

No.	C_V [Pa/(kg/s)]	Max. pressure [atm]	Displacement [m]
0	1 000 000	7,46	0,00405
1	500 000	6,15	0,00348
2	350 000	5,19	0,00299
3	275 000	4,49	0,00267
4	200 000	4,00	0,00336

Fig.6.1.14. Semi-active mitigation of tower vibrations: a) change of pressure in front chamber b) corresponding response of the tower

In the following step, active strategies which were previously developed for minimisation of ship rebound were investigated. The most effective procedure assumes constant valve opening and additional release of pressure at time instant when ship velocity is decreased to zero. By using such a strategy maximal tower displacement is reduced to 2,51mm. Keeping the valve closed and executing pressure release only when the ship is stopped (which is the most effective for rebound mitigation) results in slightly larger tower displacement, probably due to shorter impact time.

Let us note that the equivalence of the problems of ship rebound minimisation and tower vibrations mitigation holds only when structure own frequency is adequately low. For structures with short period of vibrations another control strategy has to be applied.

Summary of Section 6.1

The proposed Adaptive Inflatable Structure surrounding the tower at the water level can effectively protect the offshore wind turbine and the ship in case of collision. Adjustment of

initial pressure and controlling its release adapts the inflatable structure to various impact conditions and significantly increases system effectiveness. A controlled release of pressure helps to dissipate a major part of the impact energy and thus to decrease ship rebound and tower vibrations. Precise control of the valve flow enables minimisation of ship acceleration and reduction of stress in the tower wall.

Semi-active adaptation is the most efficient when maximal admissible initial pressure is applied and constant valve opening allows to utilise the whole stroke of pneumatic structure. Conducted simulations clearly indicate the advantage of semi-active structure over the passive one since it reduces ship acceleration and stresses in tower wall by over 50% and ship rebound velocity by nearly 80%. In turn, active adaptation (with real-time control valve opening) was found to be more effective for mitigation of ship response (profit up to 36% in comparison to semi-active case) than for alleviation of tower vibration and stresses (profit up to 12%). However, the execution of active adaptation strategies requires more sophisticated electronic control system and more power supply.

In the following stages of research the possibilities of constructing high speed and stroke controllable valves which allow to execute required high mass flow rates should be examined. Furthermore, the mathematical description of the gas flow should be adjusted to experimental data. During the design process of particular inflatable fender full 3D model should be used for numerical computations according to described limitations of simplified modelling. In particular, more accurate modelling of the material chosen for inflatable torus (for instance reinforced rubber) should be included into numerical model. Finally, an experimental verification of the whole system is required to test out its functioning and effectiveness.

6.2. Adaptive airbags for emergency landing

Classical airbag systems are commonly used in automotive industry to provide safety of the occupants during collisions since the 1980s. Despite many years of development and improvement, car airbags remain passive systems where only initial inflation is adjusted to actual impact scenario. After airbag deployment gas is released by fabric leakage only and precise control of internal pressure is not performed. This indicates that airbag response is still not optimal and it can be significantly improved by introducing controllable gas exhaust. On the other hand, the possibilities of application of airbags systems outside automotive industry are still not fully exploited. Both above facts constitute motivation for the research undertaken herein.

The section concerns application of adaptive external airbags for mitigation of crash or emergency landing of the flying objects, like rotorcrafts, UAVs or spacecrafts. Crash of the flying objects is inevitably related to risk of passengers' lives and serious damage of the structure. The extensive full scale crash tests of rotorcrafts and aircrafts, involving tests with external airbags, were performed at NASA Langley Research Centre [298]. In particular, external airbag system protecting 'crew escape module' of strategic bomber F-111 (Fig. 6.2.1a) was tested at various impact attitudes and ground types in order to refine initial airbag design. Despite the improvements made, the design was evaluated as non-satisfactory as the crew injury rate was higher than in case of alternative rescue systems [151]. Moreover, external airbag system developed by Rafael company was tested with the use of helicopter BELL 216 [148 149], Fig. 6.2.1b. Although neither precise parameters of applied airbags nor the results of the tests were published, the experiment was claimed to be successful due to decrease of accelerations acting on dummies and significant reduction of helicopter damages during landing. The other known application of the external airbags is system installed in helicopter Anakonda (version of PZL-W3 Sokół) which serves for landing on water.

Fig.6.2.1. System of external airbags: a) F-111 crew escape module equipped with an external airbag [298], b) emergency airbags attached to helicopter undercarriage [148]

Concerning space exploration, external airbags were successfully applied in Mars Pathfinder mission to attenuate landing of the spacecraft on Mars, cf. Fig. 1.4. Although the airbags surrounding the spacecraft were designed as non-vented and several rebounds occurred during the landing, the system effectively protected the space probe against possible damages. External airbags (together with retrorockets and parachutes) are also planned to be applied in new spacecraft NASA Orion as a system protecting the capsule during return landing on Earth. [151]. Moreover, the design and optimisation of the airbags intended to be installed in Beagle II Mars Lander (spacecraft by European Space Agency) is discussed in

paper [299]. Although the most commonly used airbags in astronautics are non-vented, the authors of [300] conclude that passively vented airbags or airbags with controlled outflow may have significant advantages. Let us stress the fact that all known external airbag systems being currently in use are passive and they do not provide the possibility of controlled release of pressure during landing.

Due to the fact that airbags systems are commonly used in automotive industry the process of airbag inflation and deployment as well as the process of occupant/airbag collision are the subject of intensive experimental and numerical analysis for over 30 years. Early numerical models of the airbag systems were based mainly on Uniform Pressure Method with additional modelling of the inflating jet and leakage through airbag fabric [215 216 301]. Starting from the middle 90's, the methods based on full modelling of the Fluid-Structure Interaction problem with the use of Navier-Stokes equations were extensively developed [302 303 304] and approaches which utilise fixed background Eulerian grid had gained the largest popularity. The UPM method can be used with satisfactory precision when impact of the occupant occurs after full deployment of the airbag where internal pressure is approximately uniform. By contrast, FSI methods have to be applied in the so-called "out-of-position" (OOP) situations where occupant impact occurs before airbag is fully deployed, occupant is directly subjected to jet of the gas from the inflator and internal pressure inside the airbag is evidently non-uniform. The comparison of both simulation methods with the use of various numerical approaches and solvers is presented in papers [305 306 307].

The alternative, recently developed method of airbag modelling is the so-called Corpuscular Particle Method, in which gas in modelled as a set of rigid particles in random motion and, moreover, kinetic molecular theory is utilised [308]. Recent papers in the field are dedicated to both development of new methods of airbag modelling and to optimisation of airbag behaviour (for instance by using two stage inflators) [309].

Concept of the adaptive airbags system

In this section, an innovative system for emergency landing composed of external 'flow control - based' airbags is proposed. The possibility of controlled release of gas from the airbags has crucial importance for system effectiveness since it provides wide range of system adaptation and, as a result, optimal response during various landing scenarios. The proposed system (Fig. 6.2.2, Fig. 6.2.3) consists of sensor system for identification of landing conditions, hardware controller, initially folded external airbags attached to the bottom side of the landing object, fast pyrotechnic inflators, and finally controllable valves mounted either on body of the landing object or in membrane of the airbag.

The initial stage of the process of emergency landing is identification of touchdown conditions. Since the impact problem is three dimensional, in general three inclination angles, three components of linear velocity and three components of the angular velocity have to be identified. This step is planned to be conducted with the use of system of ultrasonic velocity sensors placed in several locations of landing object undercarriage. Moreover, in general case, mass of the object and its rotational inertia have to be recognised during initial stage of impact. Complex system for identification of these parameters being the generalisation of system proposed for 1D case (cf. Section 3.2.1) is currently under development.

Shortly before touch down airbags are deployed and inflated by fast pyrotechnic inflators based on deflagration of the flammable material. The value of initial pressure inside each of the airbags is precisely adjusted to previously identified touchdown conditions. During the process of landing actual state of the system is monitored by dedicated system of sensors. Actual position and acceleration of the helicopter is determined by rotation/displacement sensors and accelerometers, respectively. Moreover, actual value of pressure inside each airbag is measured by piezoelectric pressure sensors and, at the same time, strains in airbags fabric are registered by airbag tension sensors (strain gauges, etc.)

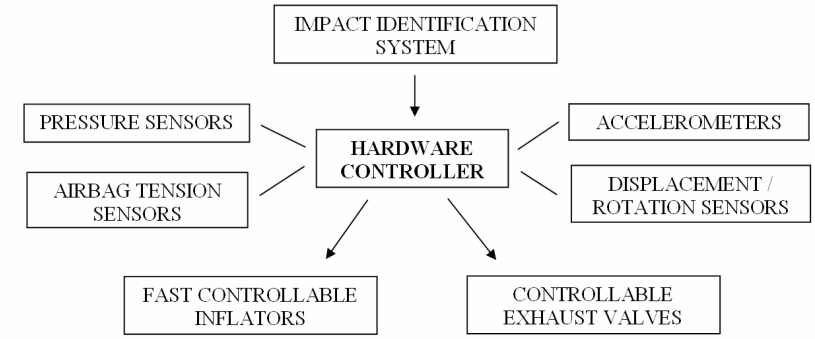

Fig. 6.2.2: Concept of the emergency landing system: interaction of system of sensors, hardware controller, inflators and adaptive valves.

During the whole process of landing, pressure inside airbags is controlled according to predefined control strategy and actual measurements from the sensors. Gas is released from airbags by fabric leakage and by additional controllable high performance valves (e.g. membranes valves described in Chapter 7). General objective of the emergency system is to mitigate global dynamic response by reduction of generated forces and decelerations, stabilisation of the landing object or, in case of extremely severe landing, preserving its structural integrity. For particular landing objects and certain touchdown conditions, the emergency landing system can be linked with (also controllable) landing gear to provide their complementary interaction and optimal global response.

In conducted numerical simulations of emergency landing it will be assumed that airbag deployment and inflation is completed before collision with the ground. Therefore, the process of airbag inflation or impact against airbag which is currently being deployed does not have to be considered. Accordingly, the Uniform Pressure Method was conceded as sufficiently precise tool for the preliminary simulation of system effectiveness. In further examples airbags attached to the landing object will be modelled by two methods:

- reduced Uniform Pressured Method where airbag compression is modelled analytically, similarly as compression of single-chamber pneumatic cylinder, and discrepancies in operation principles are taken into account by considering additional terms/coefficients in governing ordinary differential equations;
- full Uniform Pressure Method where deformation of the airbag is precisely modelled by partial differential equations solved by finite element method.

In further part of this section both models will be applied to two- and three-dimensional simulations of landing. Pressure control strategies will be initially developed for a single airbag, then for 2D reduced and full UPM models and, finally, for 3D models, Fig. 6.2.3.

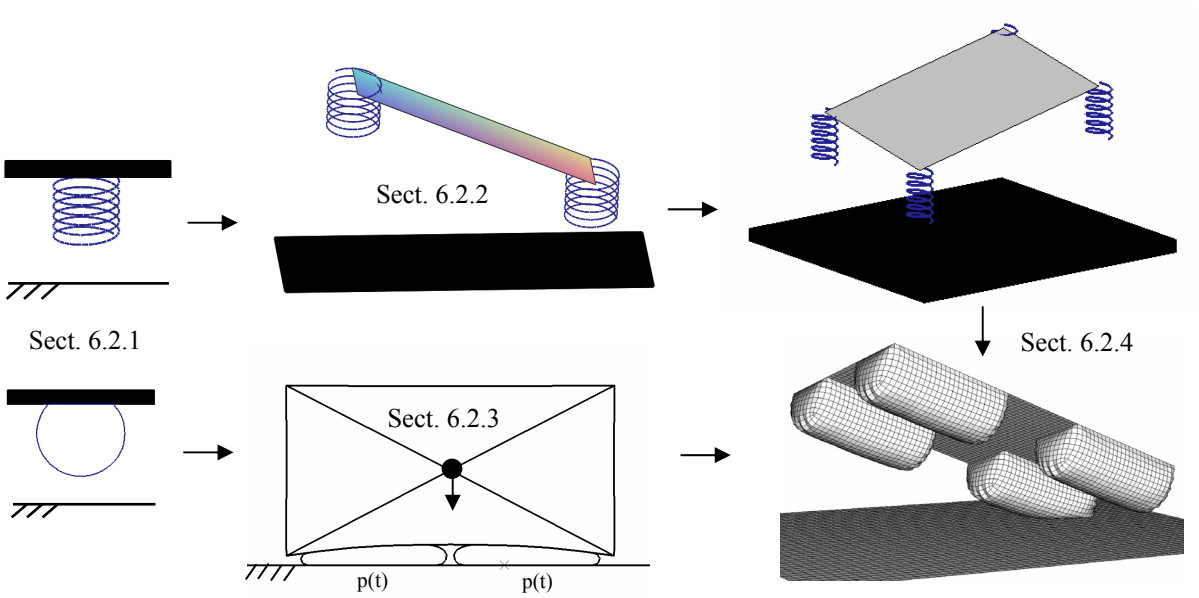

Fig.6.2.3. Tabulation of considered models and outline of the section:
upper row: models based on reduced UPM, lower row: models based on full UPM.

6.2.1. Basic models of an adaptive airbags

Model based on reduced Uniform Pressure Method

The basic indication for developing 'reduced UPM' model of an adaptive airbag is the intuitive analogy of the response of compressed airbag and response of the compressed single-chamber pneumatic cylinder. The main advantage of the method is elimination of complex simulation of the airbag deformation during impact which involves modelling airbag fabric and changeable contact conditions and which typically requires application of FEM. Instead, 'reduced UPM' approach utilises analytical description of airbag deformation as a function of airbag compression and, in case of highly extensible fabric, function of internal pressure.

Before deriving governing equations of the method let us analyse the subsequent stages of compression of the membrane airbag attached to the lower surface of the falling object located in parallel to the ground, Fig. 6.2.4 (external pressure and gravity are omitted):

1. stage before contact with the ground: forces acting on the falling object, i.e., force resulting from internal airbag pressure F_p and vertical force resulting from membrane tension F_m are equal, Fig. 6.2.4a;
2. compression of the lower part of the airbag (lasts until upper and lower area of the airbag A_m and A_C are equal): force F_m resulting from membrane tension is decreased due to reduction of lateral airbag surface A_A which is exposed exclusively to action of internal pressure, Fig. 6.2.4b;
3. uniform compression of an airbag from upper and lower side: upper surface of airbag comes into contact with bottom surface of the falling object which causes generation of the contact force $F_C = (A_C - A_m)p$, Fig. 6.2.4c.

For each of the above stages of the process, the equations of equilibrium of weightless airbag and the falling object clearly indicate that force acting on the falling object equals the product of contact area and internal pressure: $F = A_C p$.

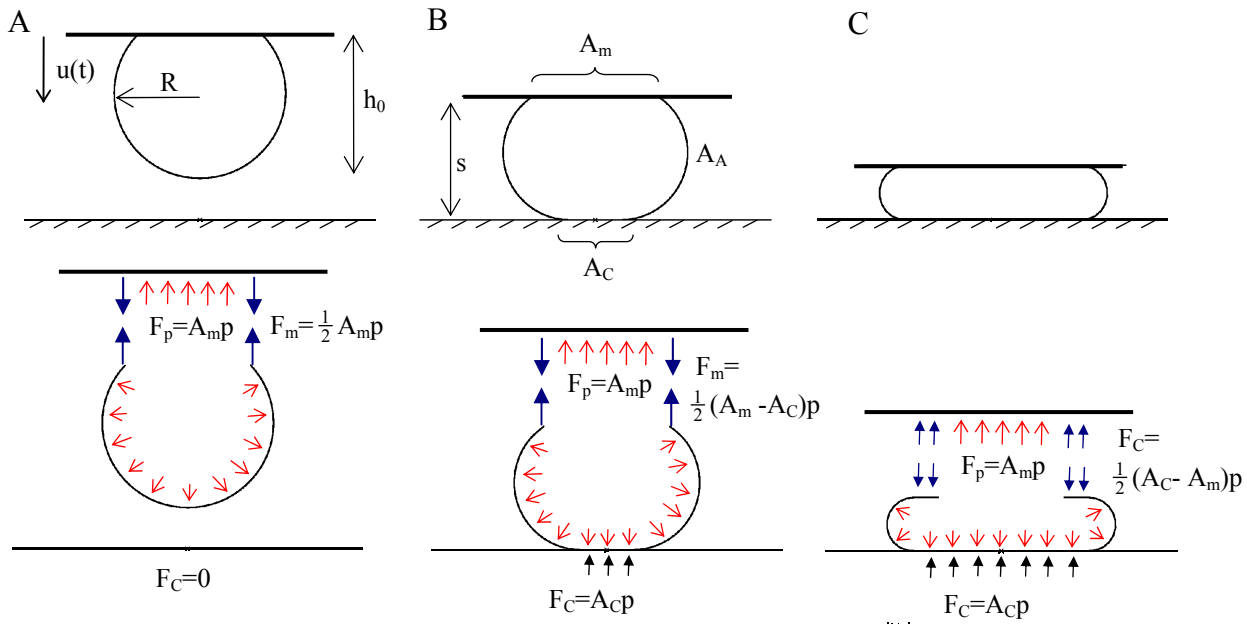

Fig.6.2.4. Three stages of membrane airbag deformation: a) free falling, b) compression of the lower side, c) uniform compression of both sides of an airbag; the sentence of pictures is obtained as a result of full UPM analysis performed in ABAQUS software

According to the above analysis, the main facts that have to be taken into account in development of reduced UPM model of the airbag are the following:

- the area of contact between the airbag and the ground, where contact force is generated, changes during the analysis (typically rises);
- volume of the airbag does not change linearly with airbag compression;
- release of pressure from the airbag is caused partially by fabric leakage and area through which leakage occurs changes during the process;
- in case when airbag fabric has substantial stiffness on compression, shearing and bending, it results in generation of additional forces during airbag compression (the airbag cannot be treated as membrane).

All mentioned phenomena can be treated as first-order effects which cause that the response of compressed airbag is substantially different than the response of compressed single-chamber pneumatic absorber.

Let us denote initial shape of the surface of inflated, but free of external excitations, airbag by $\Gamma_0(p)$, its initial area by $A_0(p)$ and volume by $V_0(p)$. Let us further consider uniform compression of an airbag as presented in Fig. 6.2.4. The first step of the model development is to determine deformation of the airbag surface as a function of actual airbag stroke and pressure, $\Gamma = \Gamma(s, p)$. The problem can be substantially simplified by assuming inextensibility of airbag fabric, which results in independence of airbag shape on internal pressure (in certain range of pressure higher than p_{atm}): $\Gamma(s, p) = \Gamma(s)$ and constant area of the airbag surface $A(p) = A_0$. Under above assumption, the shape of airbag Γ can be determined analytically by analysing the sequence of stages depicted in Fig. 6.2.4 and by utilising corresponding basic geometrical relations. In the next step, volume of an airbag $V_0(p)$, area of contact with the ground $A_C(p)$ and free surface through which fabric leakage occurs $A_A(p)$ can be found by calculating appropriate integrals of the airbag surface.

Alternatively, searched volume and area can be obtained directly from 'full UPM' model where finite element method is used for determine airbag deformation. Exemplary approximate formulae for 2D model of the cylindrical airbag read:

$$A_C(s) = aR(h_0 - s), \quad s \in \langle 0, h_0 \rangle \tag{6.2.2a}$$

$$V(s) = R^2\left[b - c(h_0 - s) - d(h_0 - s)^2 - e(h_0 - s)^3\right] \tag{6.2.2b}$$

$$A_A(s) = A_0 - A_C(s) \quad \text{if } s > 2R - 2(2R - h_0) \tag{6.2.2c}$$

$$A_A(s) = A_0 + A_m - 2A_C(s) \quad \text{if } s < 2R - 2(2R - h_0)$$

The above equations indicate that contact area $A_C(s)$ is increasing linearly with airbag compression, but airbag volume $V(s)$ is decreasing faster during the second part of the process (stage C in Fig. 6.2.4). The definition of the contact area $A_A(s)$ depends on whether contact of the airbag envelope with falling object occurs (stage B vs. stage C).

In developed 'reduced UPM' model, the influence of the gas leakage through airbag fabric is taken into account by considering an additional term in the equation governing change of mass of gas inside airbag. Mass flow rate of material leakage $\dot{m}_A$ depends on pressure difference and density of the gas. Finally, additional forces $F_A(s,p)$ arising as a result of deformation of airbag fabric of considerable stiffness are reflected in the numerical model by additional force terms in the equation of falling object motion. The value of these forces has to be preliminarily determined in terms of airbag stroke and pressure. The additional 'structural' forces causes that deformation of the airbag does not exactly follow the sequence presented in Fig. 6.2.4. In particular, the force F_m can assume negative values.

Numerical model of basic dynamical system involving object falling in parallel to the ground (Fig. 6.2.5) is typically reduced to a single mechanical degree of freedom since mass of the material airbag is small in comparison to mass of the falling object. Reduction to a single degree of freedom causes certain difficulties when full rebound of the hitting object occurs. Possible solution is the use of the equivalent of 'enhanced UPM' approach (cf. Sect. 3.1.3) where pneumatic force acting on the falling object is deactivated when it becomes negative and appropriate control of airbag shape during rebound is performed. Finally, the equations governing 1DOF model of the object equipped with airbag modelled by 'reduced UPM' take the form:

$$M\frac{d^2u}{dt^2} - Mg + F_p(s,p) + F_A(s,p) = 0 \tag{6.2.3}$$

$$F_p(s,p) = (p - p_A)A_C(s) \quad \text{if} \quad s < h_0 \ \text{ and } \ p - p_A > 0$$

$$pV = mRT$$

$$\dot{Q} + \sum \dot{m}_{in}\overline{H}_{in} - \sum \dot{m}_{out}\overline{H}_{out} = \dot{U} + \dot{W}$$

$$\dot{m} = \dot{m}_V + \dot{m}_A \quad \text{where:} \quad \dot{m}_V = -\frac{p - p_A}{C_V(t)}, \ \dot{m}_A = -C_A A_A(s)\frac{\sqrt{2(p - p_A)p}}{\sqrt{RT}}$$

$$\text{IC:} \ \ u(0) = 0, \ \dot{u}(0) = v_0, \ p(0) = p_0, \ m(0) = m_0,$$

, see also general equations of UPM approach in Sect. 2.3. The stroke of the airbag is, in the most general case, a function of object displacement and internal pressure $s = s(u, p)$.

The verification of the reduced UPM approach against full UPM model was conducted for parallel compression of cylindrical airbag whose deformation is described by Eqs. 6.2.2a-c and which is presented in Fig. 6.2.5a. The comparison was performed in terms of kinematic and thermodynamic quantities, and in both cases satisfactory correspondence of results was obtained, cf. Fig. 6.2.5b.

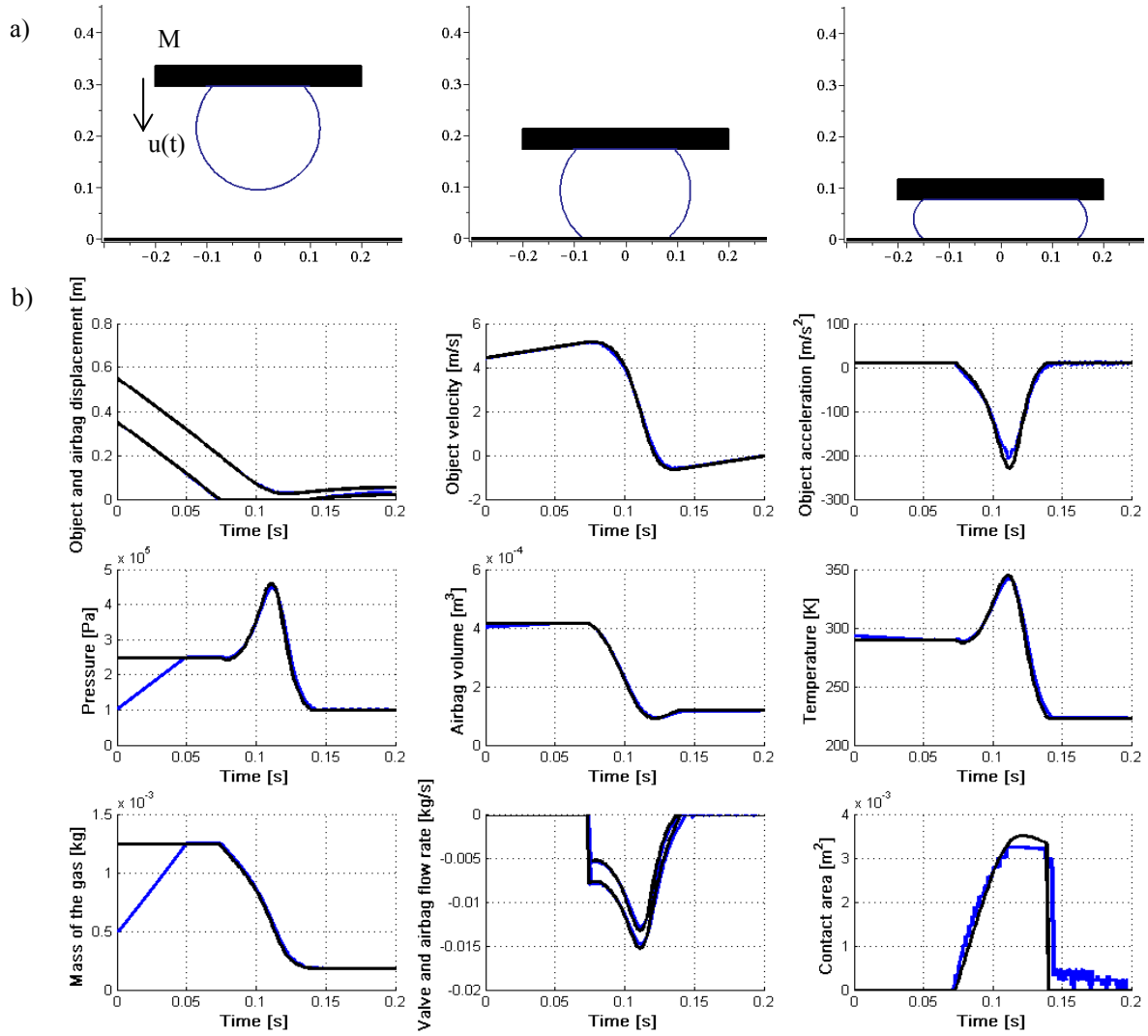

Fig.6.2.5. a) Deformation of cylindrical airbag during compression (reduced UPM model implemented in MAPLE), b) Comparison of results obtained by 'reduced UPM method' and 'full UPM method'

The developed model of airbag is based exclusively on physical principles and geometrical considerations and moreover it does not require linearization or omission of the selected terms. Therefore, the above model is expected to be more precise than classical models based on defining alternate stiffness and damping terms which are intended to model airbag response in an approximate way, cf. e.g. [95].

One of the goals of development of the numerical model was to investigate the influence of two characteristic features of an airbag (i.e. variable contact area and fabric leakage) on dynamic response of the system during compression. In Fig. 6.2.6 black line

represents response of the falling object with attached single- chamber pneumatic cylinder with constant area of contact with the ground and constant valve opening (the reference case).

The gradual increase of contact area with the ground during impact (blue line) is reflected by progressive increase of hitting object deceleration, progressive increase of pressure and higher value of maximal pressure. Moreover, higher pressure difference results in larger mass flow rate of gas through the valve and larger release of gas from the airbag during the process. The impact period is shorter than in case of constant contact area and ends up with object rebound. Consequently, pneumatic cylinder and airbag are characterized by different force-displacement characteristics which define their dissipative properties.

In turn, additional release of gas from the cylinder, which models fabric leakage (red line), increases dissipative capabilities of the pneumatic system. Maximal level of pressure and acceleration is substantially reduced. Mass flow rate through the valve is decreased, however, because of fabric leakage the total mass of gas removed from the pneumatic structure is larger. In considered case almost the whole kinetic energy of the hitting object is dissipated and its rebound does not occur. In case of airbag with a fabric leakage both described effects mutually complement each other.

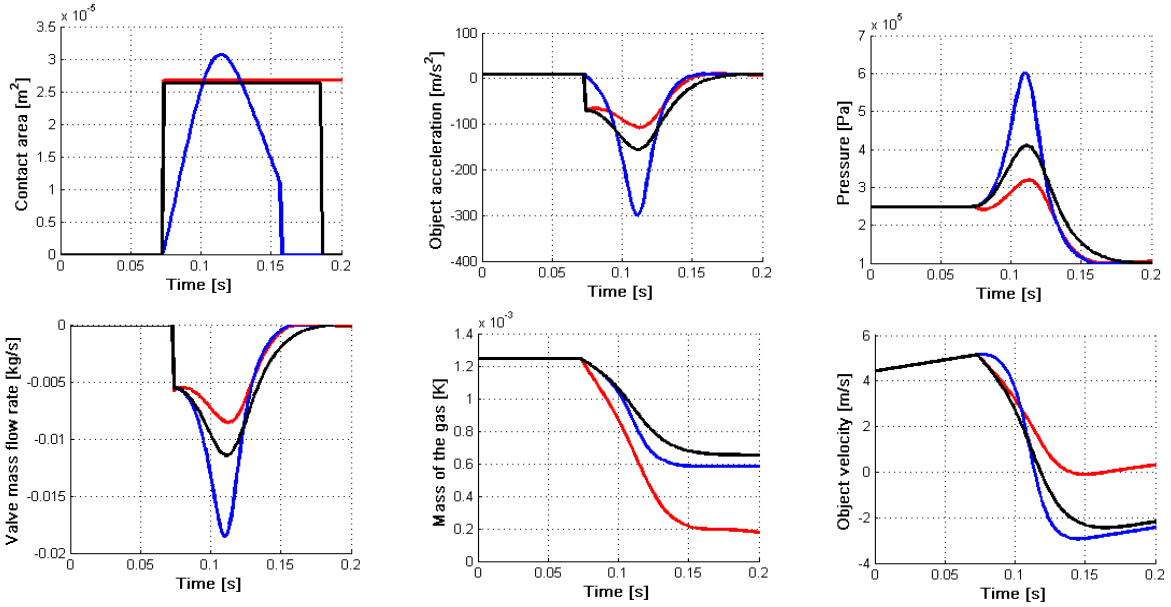

Fig.6.2.6. Influence of variable contact area and fabric leakage on response of the pneumatic structure: a) reference single-chamber absorber (black), b) influence of variable contact area (blue), c) influence of fabric leakage (red).

Adaptation strategies

Similarly as in case of all adaptive inflatable structures, the most important objective of airbag adaptation is minimisation of deceleration of the protected object. It can be performed by using modified versions of miscellaneous strategies proposed in Sect. 3.2.2 for adaptive pneumatic cylinders subjected to impact of external object. However, here the scope will be confined to ‘active adaptation’ with ‘continues control of valve opening’ , which is the most advanced from the point of view of control theory and leads to most accurate results (exactly constant level of deceleration). The other important objective of adaptation, which can be approached by active adaptation, is minimisation of internal pressure inside airbag. Two

above objectives of adaptation will be considered in parallel. In case of adaptive 'flow control - based' airbags, similarly as in case of adaptive pneumatic cylinders, the adaptation procedure consists of three steps: 1) preliminary impact identification, 2) determination of optimal time instant of valve opening and 3) optimal tuning of the valve opening.

Ad. 1. The identification of landing conditions is intended to be executed by standard methods described previously. Since identification of mass of the landing object is difficult to accomplish exclusively on the basis of airbags response during initial stage of the process, the separate device ('Impactometer') attached to the landing object and operating according to principles described in Sec. 3.2.1 should be applied.

Ad. 2. In case of active strategy of deceleration minimisation the process of optimal stopping of the landing object is composed of the first stage when force acting on the object (and consequently its deceleration) is increasing while the valve is closed and the second stage when the force is maintained on a constant level. Due to the fact that during the first stage leakage of gas through the fabric occurs, it cannot be described by a single differential equation. Consequently, equations defining two stages of the process can not be integrated analytically in order to find parameters of the system, which define time instant of valve opening. Therefore, the most general method for determination of these parameters is based on comparison of actual level of acceleration, actual velocity of the object and remaining stroke of the airbag, cf. Eq. 3.2.46. In a special case when the airbag is airtight and no fabric leakage occurs, two subsequent stages of the process are described by the equations:

$$M\frac{d^2u}{dt^2} - Mg + \left(\frac{p_0V_0^{\kappa}}{V(u)^{\kappa}} - p_A\right)A_C(u) = 0 \quad \text{for} \quad u(t) \in (0, u_x) \tag{6.2.4a}$$

$$M\frac{d^2u}{dt^2} - Mg + \left(\frac{p_0V_0^{\kappa}}{V(u_x)^{\kappa}} - p_A\right)A_C(u_x) = 0 \quad \text{for} \quad u(t) \in (u_x, h_0\rangle \tag{6.2.4b}$$

where $u(t)$ denotes displacement of the falling object measured from the time instant when contact of the airbag with the ground occurs. Integration of two above equations in the range $(0, h_0\rangle$ yields:

$$\tfrac{1}{2}Mv(0)^2 + Mgh_0 = \int_0^{u_x}\left(\frac{p_0V_0^{\kappa}}{V(u)^{\kappa}} - p_A\right)A_C(u)du + \left(\frac{p_0V_0^{\kappa}}{V(u_x)^{\kappa}} - p_A\right)A_C(u_x)(h_0 - u_x) \tag{6.2.4c}$$

Although the integral on the right hand side of Eq. 6.2.4c can be calculated analytically only in certain cases, the above equation allows to determine displacement u_x (and corresponding parameters of the system) when controllable valve has to be opened.

Similarly, in case of active strategy of pressure minimisation the process is composed of the initial stage when internal pressure is increasing while closed valve and the second stage when it is maintained on a constant level. The condition which defines beginning of the second stage reads:

$$t = t_x \quad \text{such that} \quad \frac{Mv(t_x)^2}{2} + Mg(h_0 - u(t_x)) = \int_{u(t_x)}^{h_0} p(t_x)A_C(u)du \tag{6.2.5a}$$

In a special case when the airbag is sealed and no fabric leakage occurs two stages of the process can be described by the equations:

$$M\frac{d^2u}{dt^2} - Mg + \left(\frac{p_0 V_0^{\kappa}}{V(u)^{\kappa}} - p_A\right) A_C(u) = 0 \quad \text{for} \quad u(t) \in (0, u_x) \tag{6.2.5b}$$

$$M\frac{d^2u}{dt^2} - Mg + \left(\frac{p_0 V_0^{\kappa}}{V(u_x)^{\kappa}} - p_A\right) A_C(u) = 0 \quad \text{for} \quad u(t) \in (u_x, h_0\rangle \tag{6.2.5c}$$

Let us note that Eq. (6.2.5b,c) are analogous to Eq. (6.2.4a,b) and the only difference is the area of the airbag in the second equations. Integration of two above equations in the range $(0, h_0\rangle$ leads to the formula:

$$\tfrac{1}{2}Mv(0)^2 + Mgh_0 = \int_0^{u_x}\left(\frac{p_0 V_0^{\kappa}}{V(u)^{\kappa}} - p_A\right) A_C(u)du + \int_{u_x}^{h_0}\left(\frac{p_0 V_0^{\kappa}}{V(u_x)^{\kappa}} - p_A\right) A_C(u)du \tag{6.2.5d}$$

which allows to determine displacement u_x, corresponding pressure p_x contact area A_x and mass of the gas m_x.

Ad. 3. In case of deceleration minimisation during the second stage of the process pressure inside airbag has to decrease in order to compensate increase of the contact area and to maintain force generated by an airbag on a constant level. Decrease of pressure is governed by the equation:

$$p(u) = \frac{(p_x - p_A)A_x}{A_C(u)} + p_A \tag{6.2.6a}$$

Required mass of gas inside airbag can be calculated from adiabatic ideal gas law:

$$m(u) = \left(\frac{p(u)}{p_x}\right)^{1/\kappa}\left(\frac{V(u)}{V_x}\right)m_x = \left(\frac{(p_x - p_A)A_x}{A_C(u)} + p_A\right)^{1/\kappa}\left(\frac{V(u)}{V_x}\right)m_x \tag{6.2.6b}$$

and total mass flow rate of the gas is equal to time derivative of the above function:

$$\begin{aligned}\dot{m}_{tot}(t) = -\left[\frac{1}{\kappa}\left(\frac{(p_x - p_A)A_x}{A_C(u)} + p_A\right)^{1/\kappa - 1}\frac{(p_x - p_A)A_x}{A_C(u)^2}\frac{dA_C(u)}{du}\dot{u}\right]\left(\frac{V(u)}{V_x}\right)m_x + \\ + \left(\frac{(p_x - p_A)A_x}{A_C(u)} + p_A\right)^{1/\kappa}\left(\frac{1}{V_x}\right)\frac{dV(u)}{du}\dot{u}m_x\end{aligned} \tag{6.2.6c}$$

In case of active pressure minimisation assumption $p(u) = p_x$ leads to the simple formulae defining required mass of the gas inside airbag and required total mass flow rate of the fluid:

$$m(u) = \left(\frac{V(u)}{V_x}\right)m_x, \qquad \dot{m}_{tot}(t) = \frac{1}{V_x}\frac{dV(u)}{du}\dot{u}m_x \tag{6.2.7a,b}$$

Similarly as in case of single-chamber adaptive pneumatic cylinder, the calculated mass flow rate is decreasing during the major part of the process and decrease is faster when constant deceleration is maintained. Calculation of the optimal mass flow rate of gas through

the valve requires preliminary determination of the leakage through the airbag fabric. For the problem of acceleration minimisation and pressure minimisation we obtain, respectively:

$$\dot{m}_A(u) = -C_A A_A(u) \frac{\sqrt{2(p(u)-p_A)p(u)}}{\sqrt{RT(u)}} = \tag{6.2.8}$$

$$= -C_A A_A(u) \frac{\sqrt{2\left(\frac{(p_x - p_A)A_x}{A_C(u)}\right)\left(\frac{(p_x - p_A)A_x}{A_C(u)} + p_A\right)}}{\sqrt{RT_x (p_x)^{1/\kappa - 1}\left(\frac{(p_x - p_A)A_x}{A_C(u)} + p_A\right)^{-(1/\kappa - 1)}}}$$

and

$$\dot{m}_A(u) = -C_A A_A(u) \frac{\sqrt{2(p(u)-p_A)p(u)}}{\sqrt{RT(u)}} = -C_A A_A(u) \frac{\sqrt{2(p_x - p_A)p_x}}{\sqrt{RT_x}} \tag{6.2.9}$$

where T_x denotes temperature of gas at time instant when the valve becomes opened.

Optimal adaptation of the pneumatic structure (i.e. obtaining constant value of pneumatic force or constant pressure in the second stage of impact) is possible under condition that during the whole process the mass flow rate of gas caused by fabric leakage $|\dot{m}_A(t)|$ is smaller than total required mass flow rate of gas $|\dot{m}_{tot}(t)|$. In such a situation required flow of the gas through controllable valve $\dot{m}_V(t)$ can be calculated as:

$$\dot{m}_V(t) = \dot{m}_{tot}(t) - \dot{m}_A(t) \tag{6.2.10}$$

Corresponding change of the flow resistance coefficient of the controllable valve, which allows to maintain constant level of generated pneumatic force (and landing object decelerations) or constant level of pressure can be determined from the formula:

$$C_V(t) = -\frac{p(u) - p_A}{\dot{m}_V(t)} \tag{6.2.11}$$

Let us note that during the second stage of impact total required mass flow rate of gas, as well as mass flow rate of gas caused by fabric leakage are decreasing. The first one is decreasing due to reduction of the velocity of airbag compression, while the second one due to reduction of airbag surface where the leakage occurs. At certain time instant of the process, expected mass flow rate of the fabric leakage $|\dot{m}_A|$ may exceed total required mass flow rate of the gas $|\dot{m}_{tot}|$, which indicates that the effect of force reduction caused by fabric leakage prevails over the effect of force increase caused by airbag compression. In such a situation maintaining constant level of pneumatic force by means of controllable exhaust valve is not possible. Application of the proposed strategy of adaptation (with full closing of the valve when coefficient C_V determined from Eq. 6.2.11 achieves negative values) would lead to a situation in which an airbag is not able to stop the landing object and the object directly hits the ground.

Alternative adaptation strategy dedicated to the above situation assumes opening of the valve at later time instant than the one defined by conditions (3.2.46) or (6.2.5a) indicating optimality of the previous strategy. Consequently, generated force (or pressure) is maintained

on the higher level at the beginning of the second stage of impact in order to compensate decrease of pneumatic force at the end of the process. The complete form of the proposed algorithm of valve opening reads:

$$C_V(t) \to \infty \quad \text{for} \quad t < t_x \tag{6.2.12}$$

$$C_V(t) = \frac{p(u) - p_A}{\dot{m}_V(t)} \quad \text{for} \quad t > t_x \text{ and } \left|\dot{m}_{tot}(t)\right| - \left|\dot{m}_A(t)\right| > 0$$

$$C_V(t) \to \infty \quad \text{for} \quad t > t_x \text{ and } \left|\dot{m}_{tot}(t)\right| - \left|\dot{m}_A(t)\right| < 0$$

Optimal time of valve opening t_x can be found by solving one of the following simple optimisation problem:

$$\text{Find } t_x \text{ such that } J_2 = \max_t \left|\ddot{u}(t)\right| \text{ is minimal} \tag{6.2.13a}$$

$$\text{Find } t_x \text{ such that } J_3 = \max_t p(t) \text{ is minimal} \tag{6.2.13b}$$

Let us note that optimal solutions of the considered problems (i.e. minimal value of falling object deceleration and minimal value of pressure inside airbag) are expected to be obtained for the case when whole available stroke of an airbag is utilised.

Corresponding numerical examples concern both minimisation of falling object deceleration and minimisation of internal pressure. In order to simplify the formulae governing the control strategy, it was assumed that the area of fabric leakage remains constant during the process. Optimal change of the flow resistance coefficient of the valve as well as resulting mass flow rate of the gas, resulting internal pressure and resulting total force are presented in Fig. 6.2.7-I and 6.2.7-II.

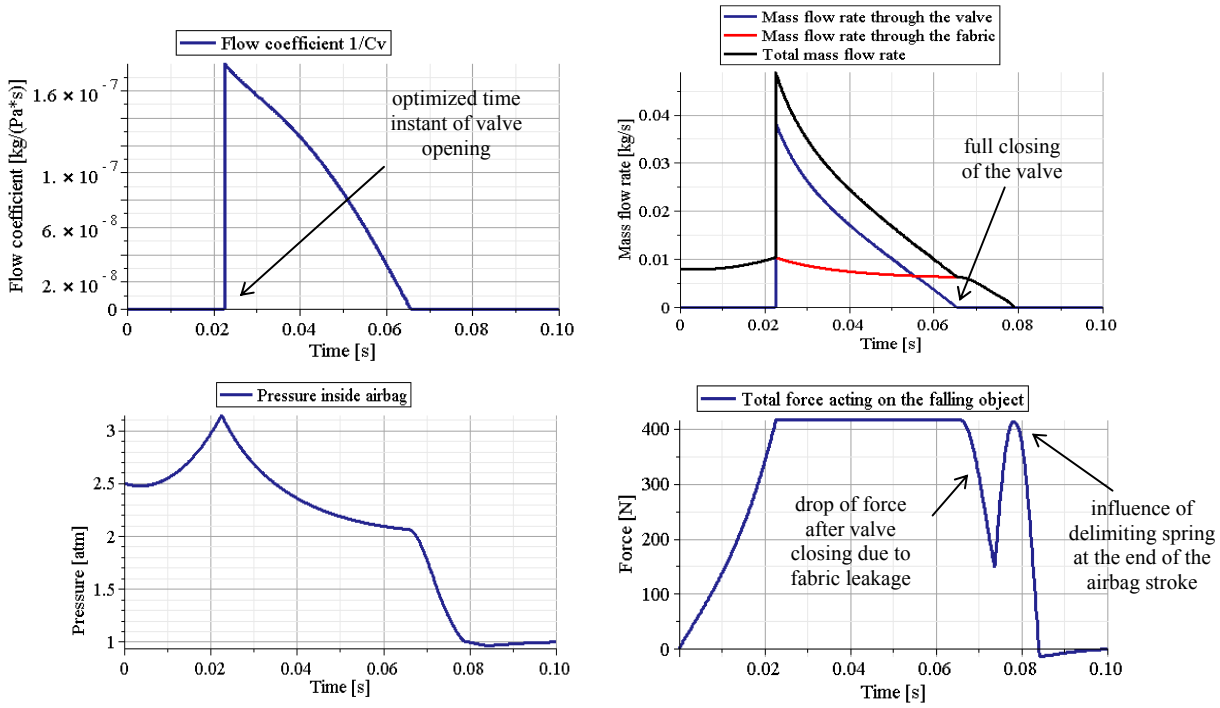

Fig.6.2.7-I. Adaptation aimed at minimisation of falling object deceleration: a) valve opening represented by flow resistance coefficient, b) mass flow rate of the outflow, c) pressure inside airbag, d) total force acting on falling object

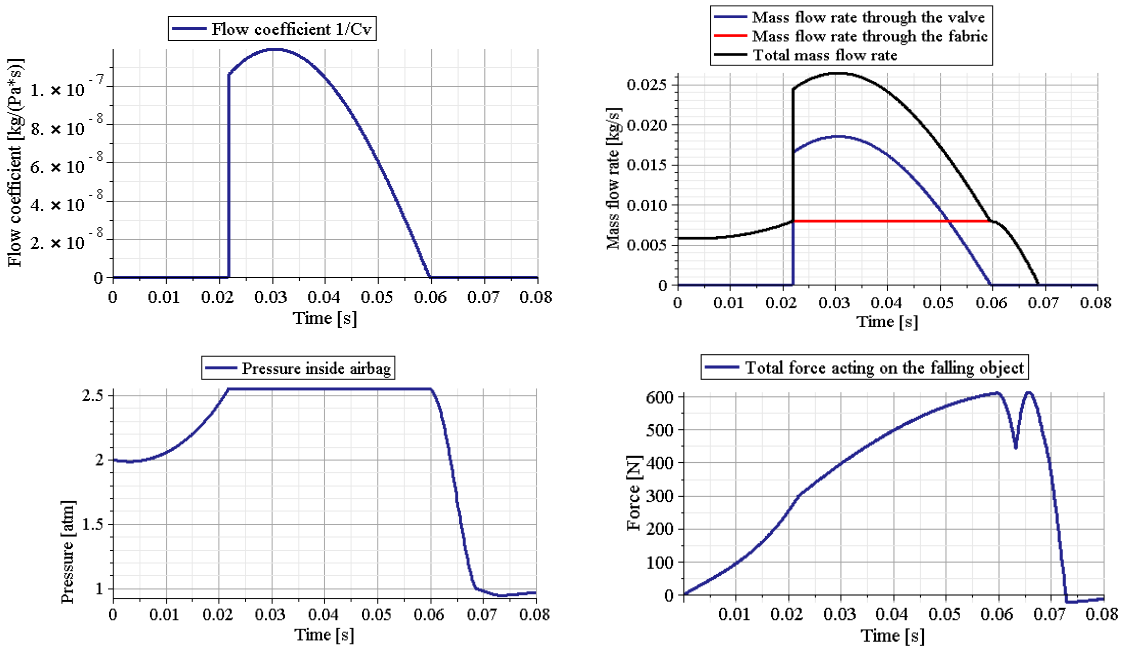

Fig.6.2.7-II. Adaptation aimed at minimisation of internal pressure: a) flow resistance coefficient, b) mass flow rate of the outflow, c) pressure inside airbag, b) total force acting on falling object

Model based on full Uniform Pressure Method

In the following examples 'full Uniform Pressure Method' will be applied for airbag simulation, i.e. the airbag fabric will be modelled by membrane elements and the assumption of uniform distribution of gas inside airbag will be adopted. The whole problem will be solved by means of finite element method complemented with equations describing internal gas and its controlled release (cf. Eqs. 6.2.3 and Sect. 2.3). 'Full UPM approach' allows for precise modelling of the airbag deformation during the landing process, what is achieved at the expense of increasing the number of degrees of freedom in the model and longer computation time. Particular advantages of the method include:

- accurate modelling of the contact between the airbag and the ground including modelling of generated friction forces,
- possibility of accounting for airbag wrinkling in regions were compression occurs,
- exact modelling of force transferred from the airbags to the platform,
- precise modelling of change of fabric leakage area (the leakage may be totally or partially blocked if contact with the ground occurs).

The most basic finite element model of the landing object equipped with single adaptive airbag is reduced into two spatial dimensions, Fig. 6.2.8. The upper longitudinal part of the model is composed of beam elements of a relatively large stiffness and predefined total mass. The airbag itself is modelled by beam elements of small thickness which can be treated as two-dimensional equivalent of the membrane elements typically used for airbag modelling. For the purpose of simulation of the touchdown process the contact conditions between the airbag and the ground and between the airbag and the upper longitudinal element were defined.

Thermodynamic part of the model consists of ideal gas law, energy conservation law and balance of mass inside the airbag. The model involves fabric leakage and outflow through controllable valve. The difference, in comparison to the model described by Eq. 6.2.3, is that airbag volume V as well as contact surface A_C and lateral surface A_A are not defined as functions of horizontal displacement, but they are obtained from finite element analysis.

The simulation of the landing process is performed by using explicit finite element method which provides efficient solution for considered problem with large deformation (i.e. full compression) of the airbag and changing contact conditions. The following, basic numerical examples are aimed at implementation of adaptation strategies for minimisation of internal pressure inside airbag and minimisation of a total force acting on the falling object.

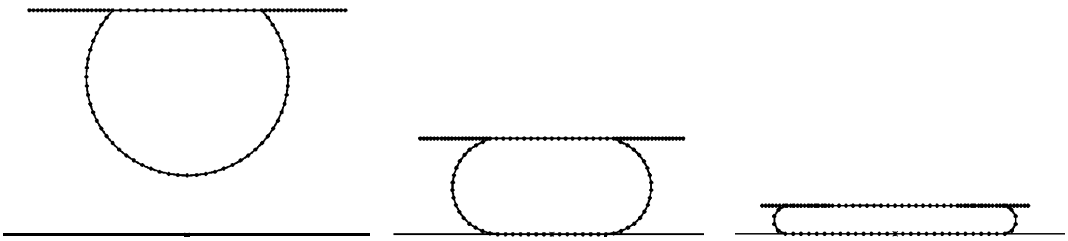

Fig. 6.2.8: Finite element simulation of landing of the object equipped with a single airbag: a) airbag inflated before landing, b) intermediate stage of the process c) final stage of the process.

Adaptation strategies

The strategy of pressure minimisation and strategy of force minimisation (and in particular methodologies for maintaining their constant values during the second stage of the process) are exactly the same as in case of 'reduced UPM' model (cf. Eq. 6.2.4 - 6.2.13). The intrinsic difference is that the whole procedure has to be incorporated into transient dynamic analysis conducted with the use of finite element model of the airbag. The following methodologies of maintaining constant level of controlled quantity were applied:

- Change of the flow resistance coefficient of the valve $C_V(t)$ was determined from the Eq.6.2.11 and derivatives of airbag volume and contact area over time (dV/dt and dA_C/dt) required for calculation of the mass flow rate $\dot{m}_V$ were obtained directly from finite element simulation.
- Change of the flow resistance coefficient of the valve $C_V(t)$ was determined from the Eq.6.2.11 and derivatives of airbag volume and contact area over time were calculated as $\frac{dV(u)}{du}\dot{u}$ and $\frac{dA_C(u)}{du}\dot{u}$, with the use of analytical formulae defining change of airbag volume and contact area in terms of displacement $V(u)$, $A_C(u)$ and velocity $\dot{u}$ obtained from finite element analysis.
- Pressure inside the airbag was used as a control variable and it was changed directly during finite element simulation of the landing process. Results obtained from the simulation (airbag volume and area of the fabric leakage) were used to calculate parameters of gas inside airbag, mass flow rate of

fabric leakage and finally required mass flow rate through the valve and required flow resistance coefficient.

Each of the proposed methods was implemented with the use of coupling of the ABAQUS and MATLAB. With the use of developed software the finite element analysis was repeatedly stopped at the predefined time instants, the analysis results were read, the required values of the control variables (flow resistance coefficient or pressure) were calculated and, finally, the finite element analysis was restarted with new input data.

Exemplary results of the adaptation aimed at minimization of pressure obtained by three described methods are presented in Fig. 6.2.9. In no case pressure remains exactly constant because of strong nonlinearity of the problem, artificial vibration of the structure caused by explicit method of solution and resulting inaccuracy in calculation of required time derivative of landing object displacement.

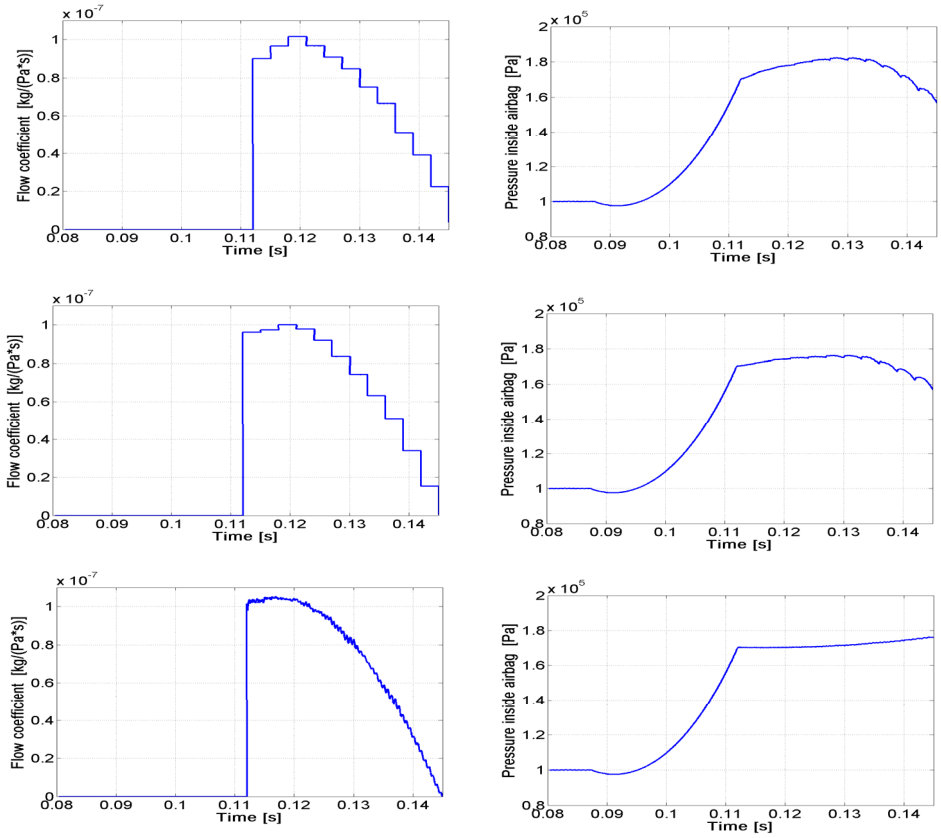

Fig.6.2.9. Adaptation aimed at minimisation of pressure inside airbag: a) flow coefficient representing valve opening, b) obtained change of pressure inside airbag

The best results of the adaptation aimed at minimisation of force acting on the falling object were obtained with the use of the last of described methods (see Fig. 6.2.10). Within this approach optimal value of pressure during each time step can be calculated by using two alternative methods:

$$p^{opt}(t) = \frac{(p_x - p_A)A_x}{A_C(t)} + p_A \quad \text{and} \quad p^{opt}(t) = p(t) + \frac{(F_x - F(t))}{A_C(t)} \tag{6.2.14}$$

The first of the above formulae defines optimal value of pressure p^{opt} in terms of pressure and area of contact with the ground at the beginning of the second stage of impact (p_x and A_x) and

utilises one parameter (actual area of contact $A_C(t)$) which has to be updated during conducted finite element simulation. By contrast, the second formula defines optimal value of pressure in terms of contact force at the beginning of active stage of impact (F_x), but instead it utilises two parameters (actual value of force $F(t)$ and contact area $A_C(t)$) which have to be modified online. Both formulae are theoretically equivalent and lead to a similar change of force during the process. The difference is that in the second case change of pressure level occurs more frequently since it is caused by change of two independent factors.

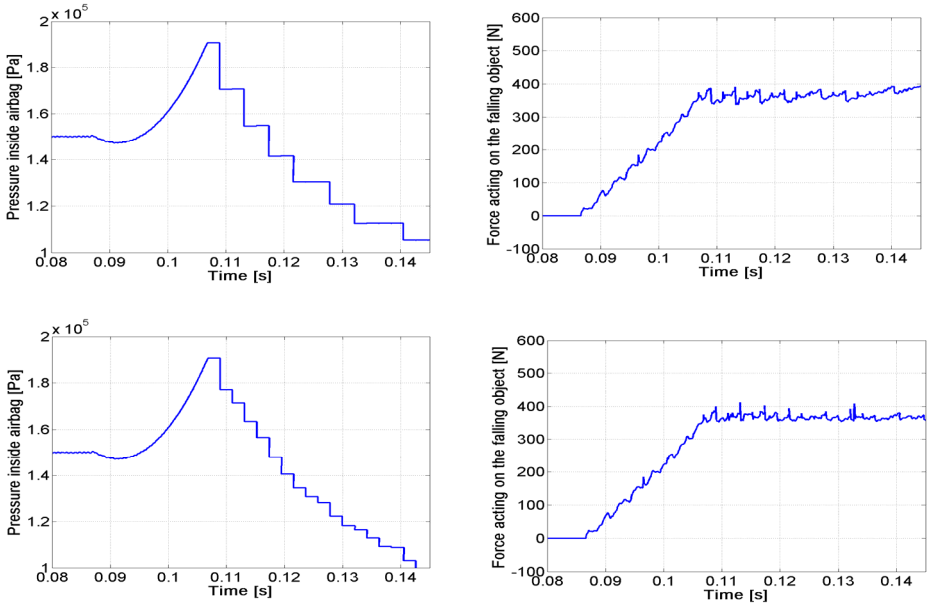

Fig.6.2.10. Adaptation aimed at minimisation of falling object acceleration: a) pressure inside airbag, b) total force acting on falling object (no filtering applied)

In case of force minimisation, the first method of adaptation (which utilises flow resistance coefficient and direct calculation of time derivatives) is difficult for numerical implementation because of non-smooth change of the contact area which results from finite element discretisation of the airbag. Therefore, the second method of adaptation, which utilizes analytical definition of the airbag volume and contact area in terms object displacement, is recommended to be applied.

6.2.2. Adaptive landing platform

This section is aimed at development of control strategies for a landing platform equipped with adaptive airbags. Considered landing object is two dimensional and consists of longitudinal rigid element with predefined mass distribution (rod with unequal point masses) and two airbags attached at both ends, Fig. 6.2.11. The airbags are assumed to be located vertically, regardless of position of the landing object. In general, initial rotation angle of the landing object and its initial angular velocity are assumed to be non-zero. The problem will be approached with ‘reduced UPM’ method.

The introduced model can be treated as preliminary, the most simplified model of the emergency landing system based on adaptive airbags.

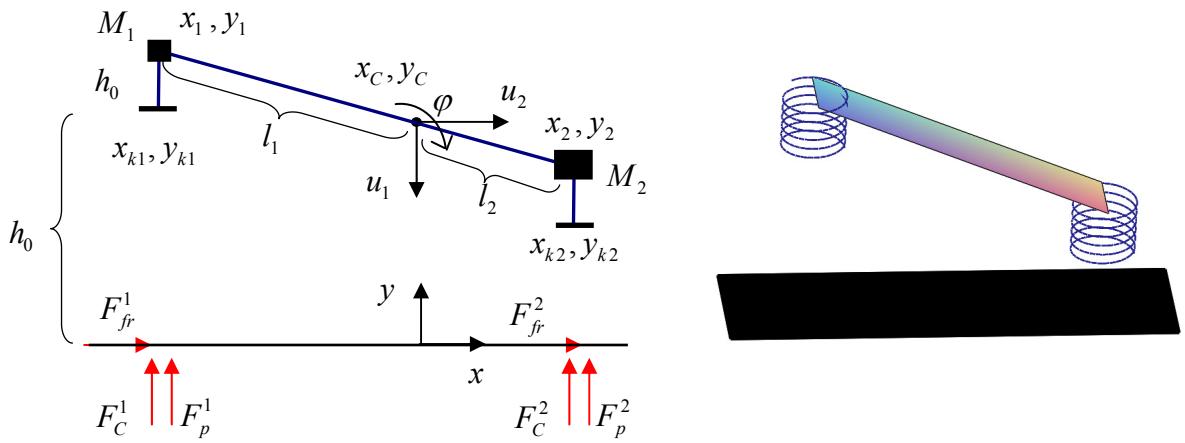

Fig. 6.2.11. Scheme of a landing platform equipped with adaptive airbags.

The mathematical model of a landing platform is based on reduction of system inertia to the centre of mass and setting equations of vertical, horizontal and rotational equilibrium. The governing equations take into account pneumatic forces generated by airbags (F_p^1 and F_p^2), contact forces between the platform and the ground (F_C^1 and F_C^2) and friction forces between airbag and the ground (F_{fr}^1 and F_{fr}^2). System of equilibrium equations read:

$$(M_1+M_2)\frac{d^2u_1}{dt^2}-(M_1+M_2)g+F_p^1+F_p^2+F_C^1+F_C^2=0 \tag{6.2.15a}$$

$$(M_1+M_2)\frac{d^2u_2}{dt^2}-F_{fr}^1-F_{fr}^2=0 \tag{6.2.15b}$$

$$I_\omega\frac{d^2\varphi}{dt^2}-F_p^1(x_C-x_{k1})+F_p^2(x_{k2}-x_C)+F_{fr}^1y_C+F_{fr}^2y_C=0 \tag{6.2.15c}$$

Pneumatic forces F_p^1 and F_p^2 are active when bottom of the airbag remains in contact with the ground and internal pressure is positive:

$$F_p^{1/2}=(p_{1/2}-p_A)A_C^{1/2}(s_{1/2}) \quad \text{if} \quad s_{1/2}<h_0 \quad \text{and} \quad p_{1/2}-p_A>0 \tag{6.2.16}$$

$$F_p^{1/2}=0 \quad \text{otherwise}$$

where $s_{1/2}$ denotes actual stroke of each airbag. Contact forces F_C^1 and F_C^2 arise when one of the airbags becomes totally compressed and the landing platform comes into a direct contact with the ground:

$$F_C^{1/2}=ky_{1/2} \quad \text{if} \quad y_{1/2}\le 0{,}001h_0\ , \quad F_C^{1/2}=0 \quad \text{otherwise} \tag{6.2.17}$$

Friction forces F_{fr}^1 and F_{fr}^2 are defined either as proportional to vertical forces generated by the absorbers or according to below definition which takes into account smooth transition in case of change of sliding direction and critical velocity v_{fr} at which friction force occurs:

$$F_{fr}^{1/2}=\mu_{1/2}\left|\tanh\left(c\frac{dx_{k1/k2}}{dt}\right)+cv_{fr}\right|\left(F_p^{1/2}+F_C^{1/2}\right) \quad \text{if} \quad \frac{dx_{k1/k2}}{dt}<-v_{fr} \tag{6.2.18}$$

$$F_{fr}^{1/2}=-\mu_{1/2}\left|\tanh\left(c\frac{dx_{k1/k2}}{dt}\right)-cv_{fr}\right|\left(F_p^{1/2}+F_C^{1/2}\right) \quad \text{if} \quad \frac{dx_{k1/k2}}{dt}>v_{fr}$$

$$F_{fr}^{1/2} = 0 \quad \text{otherwise} \tag{6.2.19}$$

Moreover, actual location of the centre of inertia (x_C, y_C) and location of the edges of the structure (x_1, y_1), (x_2, y_2) can be expressed in terms of displacement of centre of inertia, rotation angle and object dimensions:

$$x_C = u_2\,,\ y_C = h - u_1 \tag{6.2.20}$$

$$x_1 = u_2 - l_1 \cos\varphi\,, \quad y_1 = h - u_1 + l_1 \sin\varphi$$

$$x_2 = u_2 + l_2 \cos\varphi\,, \quad y_2 = h - u_1 - l_2 \sin\varphi$$

Locations of the airbags' bottoms $(x_{k1/k2}, y_{k1/k2})$ and actual strokes of airbags (s_1, s_2) are expressed as:

$$x_{k1} = x_1\,, \quad x_{k2} = x_2\,, \tag{6.2.21}$$

$$y_{k1/k2} = y_{1/2} - h_0 \quad \text{if} \quad y_{1/2} \geq h_0\,, \qquad y_{k1/k2} = 0 \quad \text{otherwise}\,,$$

$$s_{1/2} = y_{1/2} - y_{k1/k2}$$

Moreover, inertial properties of the system are defined as:

$$l_1 = \frac{M_2}{M_1 + M_2} l\,, \qquad l_2 = \frac{M_1}{M_1 + M_2} l\,, \quad I_\omega = M_1 l_1^{\,2} + M_2 l_2^{\,2} \tag{6.2.22}$$

The simple form of definition of centre of mass and moment of inertia is the consequence of initial assumption that mass of the falling object is concentrated on its left and right sides.

In order to simplify thermodynamic part of the problem, it will be assumed that no leakage through the airbag fabric occurs and that system operates under isothermal conditions. Consequently, two equations being combination of definition of mass flow rate of gas through the valve and ideal gas law read:

$$p_1 - p_A = -\frac{C_V^{\,1}(t)}{RT_0}\left[\frac{dp_1}{dt} V_1(s_1) + p_1 \frac{dV_1(s_1)}{dt}\right] \tag{6.2.23}$$

$$p_2 - p_A = -\frac{C_V^{\,2}(t)}{RT_0}\left[\frac{dp_2}{dt} V_2(s_2) + p_2 \frac{dV_2(s_2)}{dt}\right]$$

Initial conditions for the landing platform include its initial position and two components of the platform velocity, initial rotation angle and angular velocity:

$$u_1(0) = u_{10}\,, \quad u_2(0) = u_{20}\,, \quad \dot{u}_1(0) = v_{10}\,, \quad \dot{u}_2(0) = v_{20}\,, \tag{6.2.24}$$

$$\varphi(0) = \varphi_0\,, \quad \dot{\varphi}(0) = \omega_0\,,$$

The initial conditions for the gas are defined by the initial gas pressure (volume of the airbag is defined by its stroke and temperature of gas remains constant) :

$$p_1(0) = p_{10}\,, \quad p_2(0) = p_{20} \tag{6.2.24}$$

The exemplary simulations of the landing process were conducted for the platform of fixed total mass and initial vertical velocity, i.e. kinetic energy and mass/velocity ratios remained unchanged in all cases. Initially, simulation of typical symmetric landing with uniform mass distribution, zero rotation angle and zero angular velocity was conducted. Initial pressures in both airbags and constant in time valves openings were adjusted to provide compression of the whole airbag stroke and minimal value of force exerted on the landing object, Fig. 6.2.12a.

In further simulations non-uniform mass distribution (Fig. 6.2.12b), initial rotation of the platform (Fig. 6.2.12c) and initial angular velocity (Fig. 6.2.12c) were introduced and the same adaptation strategy was applied. As expected, the dynamic response of the system (linear and angular acceleration and total forces generated by airbags) appeared to be strongly dependent on considered landing scenario. Application of the strategy developed for symmetric landing resulted in significantly non-optimal response with high level of forces and accelerations, which clearly indicates that adaptive system has to be precisely tuned not only for total mass and velocity but also for all other parameters of landing scenario.

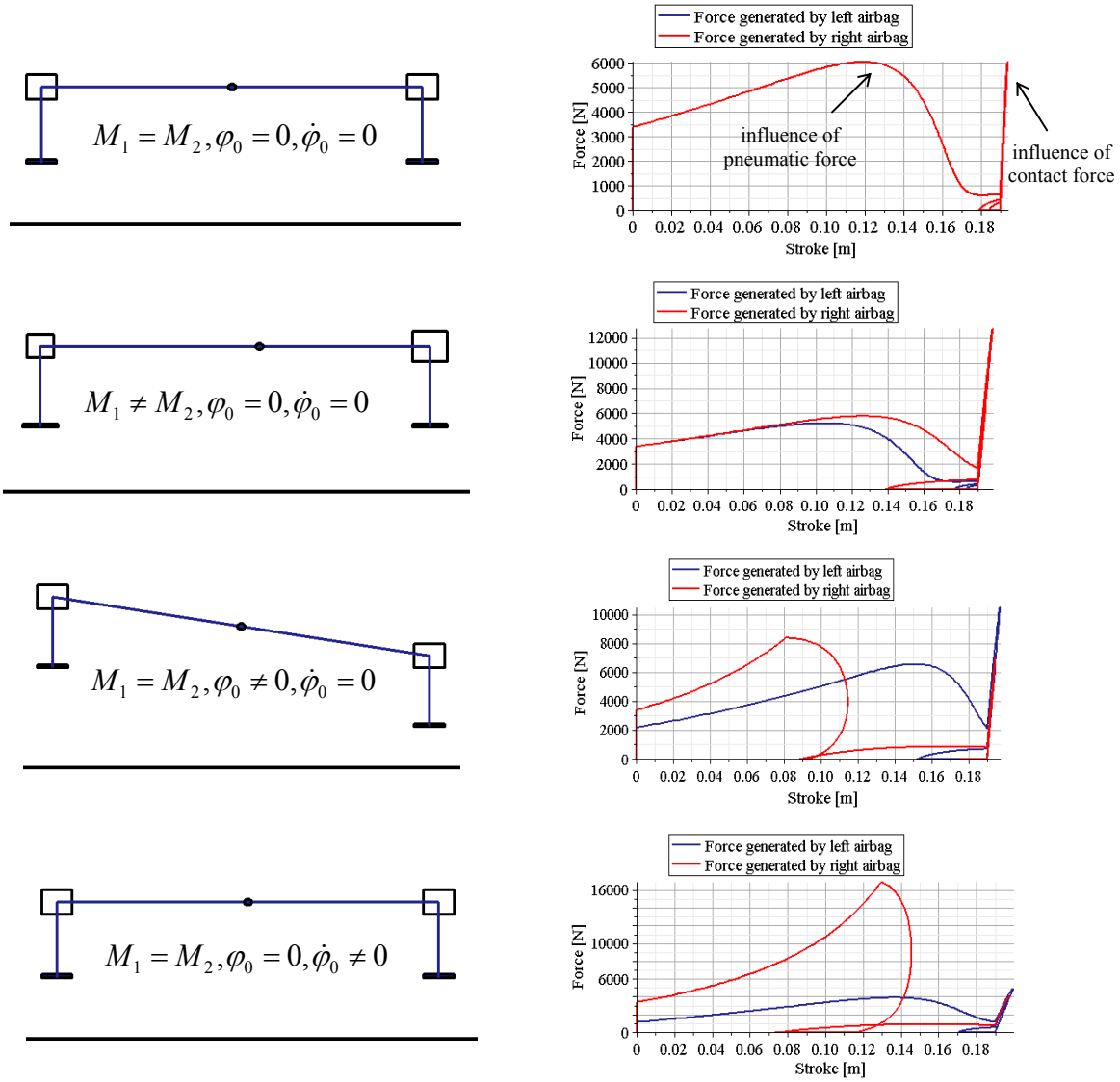

Fig.6.2.12. Simulation of landing with passive airbags: a) 'symmetric landing', b) non-uniform mass distribution, c) initial rotation, d) initial angular velocity

Adaptation strategies for deceleration minimisation

Development of control strategies for considered two-dimensional landing scenario will be confined to minimisation of deceleration of the landing object. Since the problem is two-dimensional formulation of the control objective is not as obvious as in one-dimensional case and the controlled quantity should involve both linear and angular components of deceleration. Three possible approaches include:

- strategy in which sum of maximal vertical decelerations in selected points of the platform (for instance its edges) is minimised,
- strategy in which weighted sum of maximal vertical acceleration and maximal angular acceleration is minimised,
- strategy which assumes the priority of minimisation of maximal vertical deceleration and angular acceleration is minimised incidentally.

The first of the mentioned strategies represents the most typical and general approach. For minimisation of vertical deceleration of left and right platform edge the mathematical formulation of the optimisation problem reads:

$$\text{Find } C_V{}^1(t), C_V{}^2(t) \quad \text{such that } \mathrm{J} = \max_t \left[\ddot{u}_L(t)\right]^2 + \max_t \left[\ddot{u}_R(t)\right]^2 \quad \text{is minimal} \tag{6.2.25}$$

Since vertical deceleration of an arbitrary point of the platform can be expressed by vertical deceleration of centre of inertia and angular deceleration, the objective function can be rearranged to the form:

$$\mathrm{J} = \max_t \left[\ddot{u}(t) - l_1\ddot{\varphi}(t)\right]^2 + \max_t \left[\ddot{u}(t) + l_2\ddot{\varphi}(t)\right]^2 \tag{6.2.26}$$

Mathematical formulation of the optimisation problem corresponding to the second strategy of adaptation is straightforward and reads:

$$\text{Find } C_V{}^1(t), C_V{}^2(t) \quad \text{such that } \mathrm{J} = a\max_t \left|\ddot{u}(t)\right| + b\max_t \left|\ddot{\varphi}(t)\right| \quad \text{is minimal} \tag{6.2.27}$$

The above formulation simplifies to minimisation of linear or angular acceleration when appropriate values of weighting coefficients are imposed.

In the following examples the third, regarded as more original, approach will be applied. The strategy of 'priority of minimisation of vertical deceleration' assumes that minimisation of linear deceleration is conducted at the first step of the procedure. Since maintaining constant level of vertical deceleration requires constant sum of forces from both pneumatic absorbers $F_p(t) = F_p^1 + F_p^2 = const.$, it can be performed in various manners. In proposed control method, the division of total pneumatic force between the left and right absorber is chosen in a way that minimises angular acceleration.

The problem of acceleration minimisation can be formulated either in terms of pressures (with pressures values being main control variables) or in terms of valves openings. In the first formulation both increase and decrease of pressure can be performed immediately. Moreover, applied pressure directly influences total value of force and torque exerted on the falling object. On the contrary, in the second formulation change of pressure is executed only by opening the exhaust valves. Therefore, pressure can be only decreased and moreover, change of total force and change of torque can not be performed instantaneously.

Consequently, pressure formulation can be treated as an initial stage before solving more complicated problem involving valves openings. Mathematical formulation of the pressure-based control problem reads:

1. Find $F_p(t)$ such that $\mathrm{J}_1 = \max_t \left|\ddot{u}(t)\right|$ is minimal (6.2.28)
2. Find $p_1(t)$ such that $\mathrm{J}_2 = \max_t \left|\ddot{\varphi}(t)\right|$ is minimal

In turn, mathematical formulation of the control problem which utilises valves openings (and corresponding valve resistance coefficients) can be defined as follows:

1. Find $F_p(t)$ which can be obtained by $C_V{}^1 > 0$ and $C_V{}^2 > 0$ (6.2.29)
   such that $\mathrm{J}_1 = \max_t \left|\ddot{u}(t)\right|$ is minimal
2. Find $C_V^1(t) > 0$ such that $\mathrm{J}_2 = \max_t \left|\ddot{\varphi}(t)\right|$ is minimal

The above optimisation problems require formulation of additional conditions related to final state of the system. Although minimisation of vertical deceleration automatically results in full compression of the absorber and zero final vertical velocity, it is not the case for the angular deceleration since rotation angle is not arbitrarily confined. Therefore, angle of rotation and angular velocity at time instant t_{stop} when vertical movement of the platform is stopped will be defined explicitly:

$$\varphi(t_{stop}) = 0, \quad \dot{\varphi}(t_{stop}) = 0 \tag{6.2.30}$$

The above requirement is justified both in case of system of adaptive airbags for emergency landing and, even more, in case of adaptive pneumatic landing gear where horizontal velocity of considered object after landing is non-zero.

The strategy of adaptation to particular landing scenario depends on relation between initial parameters of the landing, i.e. initial rotation angle and initial angular velocity. Possible landing scenarios are presented in Fig. 6.2.13.

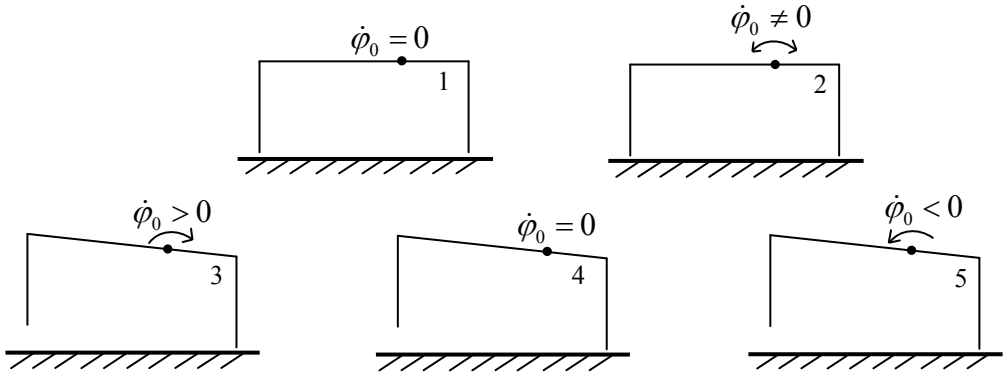

Fig.6.2.13. Possible scenarios of landing considered in a control problem.

Direct pressure control

The analysis will begin with development of the simpler strategies of adaptation which are based on direct change of pressure inside airbags. Considered process of landing can be divided into the following stages:

- stage 1: landing platform is in the air (none of the airbags touches the ground)
- stage 2: only one airbag is in contact with the ground
- stage 3: both airbags are in contact with the ground

During the second stage of landing the strategy of adaptation of pneumatic absorbers is fully determined by the objective of vertical deceleration minimization and angular deceleration is not controlled. The complete control is performed only in stage 3 when both absorbers are in contact with the ground. Possible configurations of the system at the beginning of third stage of landing resulting from scenarios 1-5 (Fig. 6.2.13) are presented in Fig. 6.2.14.

Each configuration has to be considered separately due to different strategy of minimisation of angular deceleration. Scenario 1 and Scenario 2 (Fig.6.2.14) where initial torque and rotation angle has the same sign $(M<0,\varphi>0)$, but which differ by the sign of angular velocity will be further precisely analysed.

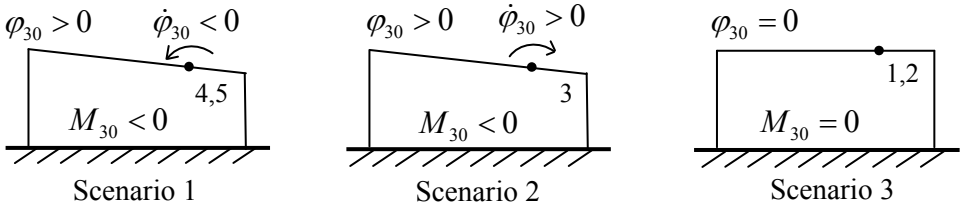

Fig.6.2.14. Possible configurations of the system at time instant when both airbags reach the ground.

Development of control strategy for 'Scenario 1'

1. Optimal value of total pneumatic force F_{opt}^{tot} which has to be exerted on the platform to diminish its vertical velocity to zero before total compression of the absorbers is determined under assumption that force can be maintained constant during the whole process of landing:

$$F_{opt}^{tot}=\frac{(M_1+M_2)V_{20}^{\ 2}}{2(h_0+l_2\sin\varphi_{20})}+(M_1+M_2)g \tag{6.2.31}$$

In the above formula initial velocity and angle of rotation (V_{20},φ_{20}) correspond to time instant t_{20} when right wheel becomes in contact with the ground (beginning of the second stage).

During the second stage of landing, when only right wheel is in contact with the ground, total pneumatic force has to be generated by the right absorber. Solution of the differential equations governing motion of the platform during the second stage of landing (Eq. 6.2.15a,c with introduced force 6.2.31) allows to determine parameters of the system at time instant t_{30} when both wheels reach the ground (beginning of the third stage of impact). In turn, these quantities enable to calculate the remaining time period of vertical velocity reduction:

$$t_{end}^{vel}=V_{30}^{\ 2}/2(h_0-l_1\sin\varphi_{30}) \tag{6.2.32}$$

Moreover, obtained results allow to compute value of constant positive torque required to simultaneously diminish the angle of platform rotation and its angular velocity to zero M_{opt}^{rot}, as well as duration of the corresponding period of time t_{end}^{rot} :

$$M_{opt}^{rot}=\frac{I_\omega\omega_{30}^{\ 2}}{2\varphi_{30}},\quad t_{end}^{rot}=-\frac{2\varphi_{30}}{\omega_{30}} \tag{6.2.33}$$

For two alternative situations which may arise, namely $t_{end}^{rot} \geq t_{end}^{vel}$ and $t_{end}^{rot} < t_{end}^{vel}$, different strategy of adaptation will be adopted.

2. In case, $t_{end}^{rot} \geq t_{end}^{vel}$, which corresponds to large angles of rotation and small angular velocities application of torque M_{opt}^{rot} defined by Eq. 6.2.33a leads to undesired landing scenario in which neither rotation angle nor angular velocity reaches zero at time instant when vertical movement of platform centre of inertia is stopped. Therefore, proposed alternative adaptation strategy assumes:

- continuation of negative torque which allows to decrease rotation angle and to obtain situation when condition $t_{end}^{rot} = t_{end}^{vel}$ is satisfied,
- change of torque into positive one which allows to stop rotation of the platform,
- reduction of total pneumatic force to the value equal to weight of the platform and reduction of torque to zero in order to obtain state of static equilibrium.

3. In order to minimise absolute value of angular acceleration during the third stage of landing the absolute values of both torques are assumed to be equal, i.e.: $M_3 = -M_4$. Absolute value of torque and time instant of change of torque sign t_3 are determined from the set of equations enforcing zero angular velocity and rotation angle at the end of the process:

$$\frac{M_4(t_{end} - t_x)}{I_\omega} + \frac{M_3(t_x - t_{30})}{I_\omega} + \omega_{30} = 0 \tag{6.2.34}$$

$$\frac{1}{2}\frac{M_4(t_{end} - t_x)^2}{I_\omega} + \left(\frac{M_3(t_x - t_{30})}{I_\omega} + \omega_{30}\right)\left(t_{end} - t_3\right) + \frac{1}{2}\frac{M_3(t_x - t_{30})^2}{I_\omega} + \omega_{30}\left(t_x - t_{30}\right) + \varphi_{30} = 0$$

Let us note that immediate increase of the absolute value of initial negative torque with conservation of the total value of pneumatic force F_{opt}^{tot} can not be achieved. If such a result is obtained, value of negative torque has to be assumed as equal to initial negative torque $M_3 = M_2$ and the remaining quantities have to be determined from the Eq. 6.2.34.

4. The next step relies on calculation of pressures in both absorbers which result in generation of the previously calculated torques. The corresponding system of equations reads:

$$\left(p_1^{opt} - p_A\right)A_1 + \left(p_2^{opt} - p_A\right)A_2 = F_{opt}^{tot} \tag{6.2.35a}$$

$$\left(p_1^{opt} - p_A\right)A_1 l_1 \cos\varphi - \left(p_2^{opt} - p_A\right)A_2 l_2 \cos\varphi = M_{3/4}$$

and results in values of pressure dependant on actual rotation of the platform:

$$p_1^{opt} = \frac{M_{3/4} + F_{opt}^{tot} l_2 \cos\varphi + p_A\left(A_1 l_1 \cos\varphi + A_1 l_1 \cos\varphi\right)}{A_1(l_1 + l_2)\cos\varphi} \tag{6.2.35b}$$

$$p_2^{opt} = \frac{-M_{3/4} + F_{opt}^{tot} l_1 \cos\varphi + p_A\left(A_2 l_1 \cos\varphi + A_2 l_2 \cos\varphi\right)}{A_2(l_1 + l_2)\cos\varphi}$$

The contact areas between each airbag and the ground A_1,A_2 depend on airbag compression and they are functions of actual displacement of centre of inertia and actual rotation angle. Since angles of platform rotation can be considered as relatively small, the formulae defining optimal pressures can be linearised by neglecting trigonometric function in Eq. 6.2.35b.

Finally, at the end of the process, pressures are reduced to values corresponding to static equilibrium of the platform. The numerical example below presents application of the above control strategy to basic scenario 4 (Fig. 6.2.13) together with obtained results of adaptation (Fig. 6.2.15, 16).

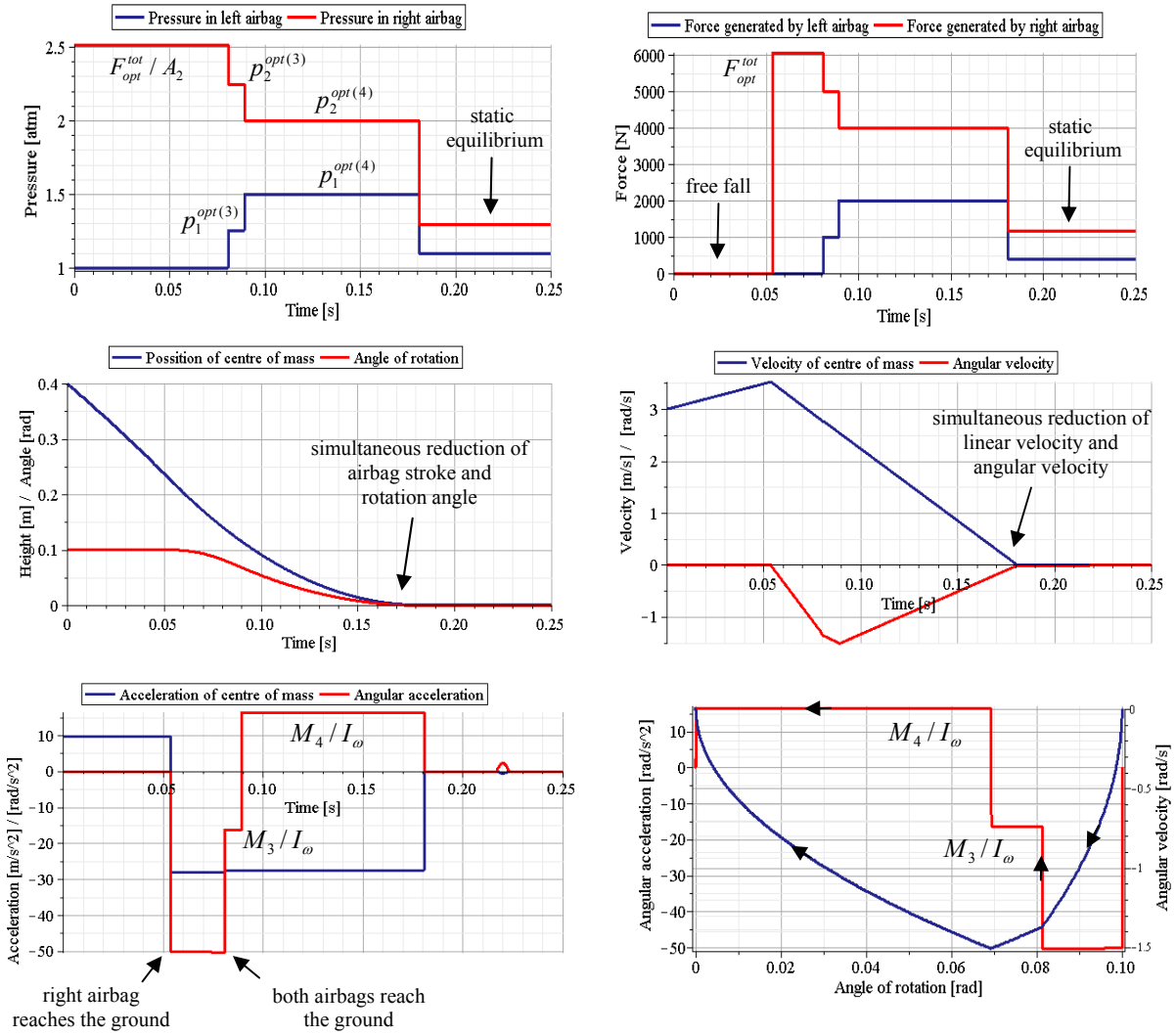

Fig.6.2.15. a, b) Change of pressure and change of force generated by both airbags, c, d, e) kinematics of the system in terms of time, f) angular velocity and acceleration in terms of angle of rotation.

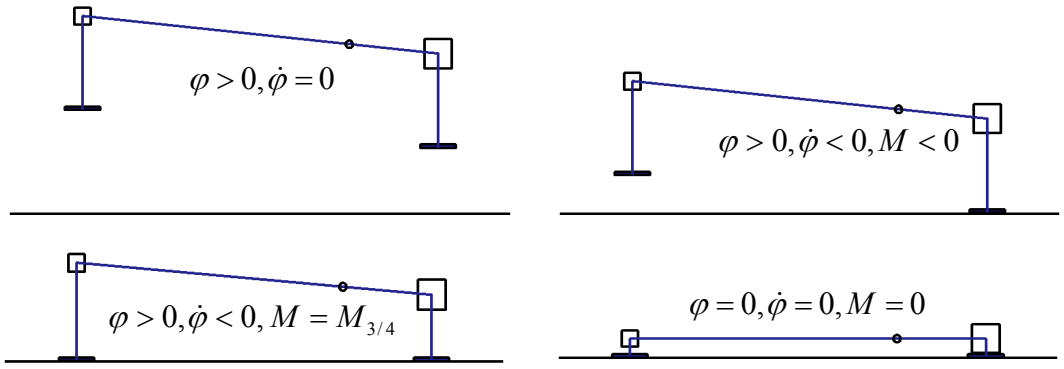

Fig.6.2.16. Simulation of the landing with adaptive landing gear: a) initial situation, b) the second stage of landing, c) third stage of landing, d) final state of the system.

In case of 'Scenario 1' with $t_{end}^{rot} < t_{end}^{vel}$, which corresponds to small angles of rotation and large angular velocities, application of constant positive torque M_{opt}^{rot}, defined by Eq. 6.2.33a, leads to reduction of angular velocity and rotation angle at early stage of the process before time instant when vertical movement of platform centre of inertia is stopped. Therefore, the easiest adaptation strategy applied at third stage of landing simply assumes:

- application of positive torque M_{opt}^{rot} until platform rotation is stopped,
- reduction of torque to zero and maintaining zero value until the end of the process.

Let us note that the above strategy does not provide minimisation of the angular deceleration. Therefore, an alternative, more advanced strategy is based on the following steps:

- application of positive torque (of a value smaller than M_{opt}^{rot}) which is continued when sign of the rotation angle and sign of the angular velocity changes, until the condition $t_{end}^{rot} = t_{end}^{vel}$ is reached,
- switch of the torque sign into negative in order to stop clockwise rotation of the platform.

The values of torques M_3 and M_4 and time instant of change of momentum sign are determined from set of equations (6.2.34). Since assumption $M_3 = -M_4$ results in obtaining infeasible solution $M_4 > M_2$, the strategy with $M_4 = M_2$ is applied. Results of the above control strategy applied to basic scenario 5 (Fig. 6.2.13) are presented in Fig. 6.2.17.

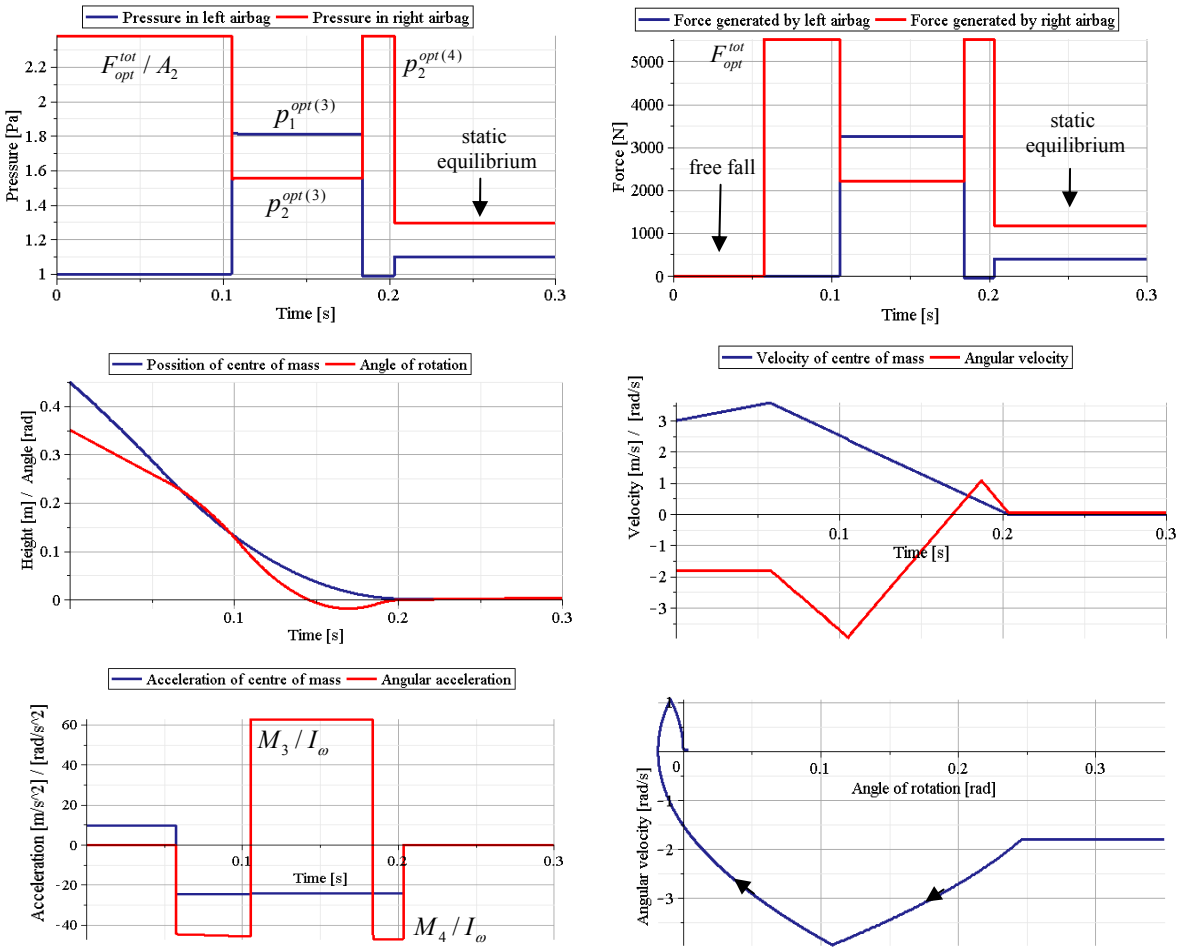

Fig.6.2.17. a, b) Change of pressure and change of force generated in both airbags, c, d, e) kinematics of the system in terms of time, f) angular velocity in terms of angle of rotation.

In case of 'Scenario 2' (Fig. 6.2.14) the first step of adaptation strategy also relies on calculation of optimal value of total pneumatic force F_{opt}^{tot} required to reduce vertical velocity of centre of inertia to zero, with minimal deceleration. The main difference between this example and the ones considered previously are possible strategies of bringing the system to the equilibrium position. Due to conforming sign of angle of rotation and angular velocity, the desired final state of the system defined by Eq. 6.2.30 can not be obtained by applying constant torque and adaptation strategy has to involve change of the torque during the process. Proposed strategy of adaptation contains the following steps:

- maintaining the negative torque which is continued also when angular velocity of the platform changes sign into negative until the condition $t_{end}^{rot} = t_{end}$ is reached,
- change of torque sign in order to stop rotation of the platform.

Similarly as in previous cases, values of torques are assumed to be equal in order to minimise absolute value of angular acceleration in third stage of impact. Absolute values of torques and time instant of change of torque sign are determined from the set of equations (6.2.34). When $|M_3| > |M_2|$ the solution is not feasible and calculation of adaptation parameters has to be repeated with the assumption $M_3 = M_2$. Results of the above strategy applied to basic scenario 3 (Fig. 6.2.13) are depicted in Fig. 6.2.18.

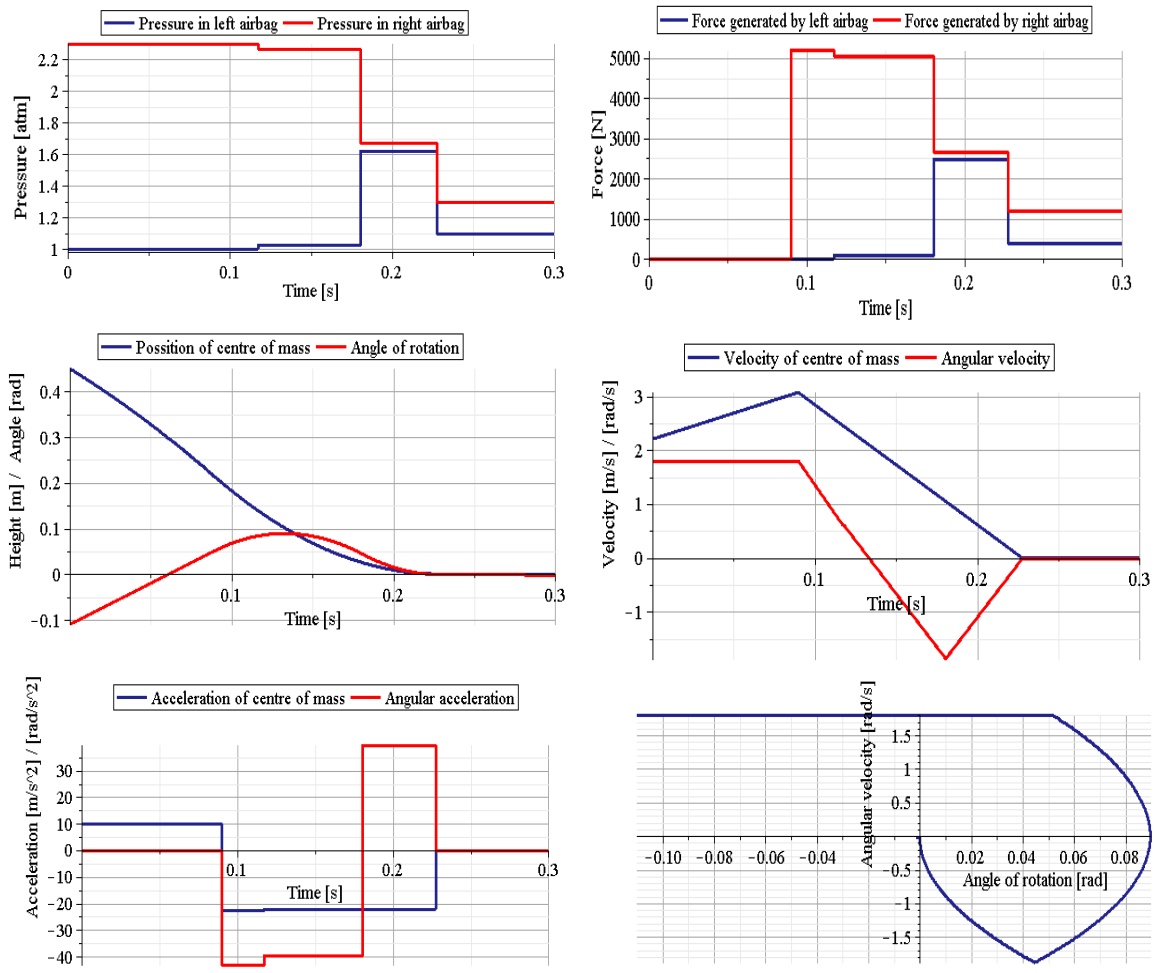

Fig.6.2.18. a, b) Change of pressure and change of force generated in both airbags, c, d, e) kinematics of the system in terms of time, f) angular velocity and acceleration in terms of angle of rotation

Control of valve opening

The adaptation based on control of resistance coefficients of exhaust valves (Eq. 6.2.29) is more complex than the adaptation based on control of internal pressure since sudden change of force and torque acting on the platform can not be obtained. Reduction of pneumatic force occurs with a certain delay to valve opening and increase of pneumatic force can be achieved only by airbag compression. Consequently, after complete reduction of pressure in one of the airbag, the value of torque can be altered only by gradual increase of pressure in the other airbag caused by change of platform position and airbag volume.

Above facts cause that obtaining desired final state of the system may be difficult or even impossible. Therefore, the requirements imposed on ultimate platform position have to be weakened. The condition that final angle of rotation is zero will be either neglected or superseded by the requirement of minimisation of platform rotation angle at the end of the process. Modified conditions defining desired final configuration read:

$$\dot{\varphi}(t_{stop}) = 0 \ , \qquad \varphi(t_{stop}) \text{ is minimal} \tag{6.2.36}$$

Dependencies between the problem of minimisation of torque and minimisation of final rotation angle will be discussed in the following parts of the sequel.

Similarly as previously, the landing process can be divided into three main stages. After the first stage when contact with the ground does not occur, in the second stage adaptation strategy assumes increase of total pneumatic force generated by the absorbers. The third stage of impact, when full control is executed, begins when two conditions are fulfilled:

i) both absorbers are in contact with the ground,
ii) total pneumatic force reaches the level required to stop the object by using remaining stroke of the airbags.

Although various configurations of the system at the beginning of third stage of impact may arise (as a result of various combinations of torque, rotation angle and angular velocity), three the most common configurations presented in Fig. 6.2.19 will be considered precisely.

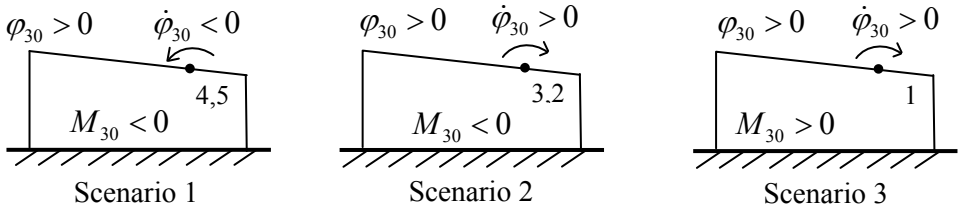

Fig.6.2.19. Considered configurations of the system at the beginning of third stage of impact.

Development of control strategy for 'Scenario 1'

1. In the second stage of landing both valves remain closed in order to increase total value of pneumatic force. Initially, only right airbag is in contact with the ground which causes fast increase of negative torque. At certain time instant left airbag also comes into contact with the ground which results in faster increase of vertical deceleration but simultaneous slower increase of negative angular acceleration. The stage lasts until the condition (3.2.46) is satisfied, i.e. until total pneumatic force reaches the level which can be maintained constant in order to stop the platform by using remaining stroke of the airbags.

The solution of the differential equation governing the problem (6.2.15a,c) allows to determine the state of the system at the end of the second stage of landing $(V_{30}, \varphi_{30}, \omega_{30})$ and further to calculate time required to diminish vertical velocity of the platform to zero:

$$t_{end}^{vel} = V_{30}{}^2 / 2(h_R(t_{30}) + l_2 \sin\varphi_{30}) \tag{6.2.37a}$$

where $h_R(t_{30})$ denotes stroke of the right airbag at the end of the second stage. The value of constant torque which is required to simultaneously diminish angle of rotation and angular velocity to zero, and duration of corresponding period of time are given by the formulae:

$$M_{opt}^{rot} = \frac{I\omega_{30}{}^2}{2\varphi_{30}}, \quad t_{end}^{rot} = -\frac{2\varphi_{30}}{\omega_{30}} \tag{6.2.37b}$$

2. Considered scenario of landing which results from basic scenarios 4 and 5 (Fig. 6.2.13) fulfils the condition $t_{end}^{rot} > t_{end}^{vel}$ which is the consequence of longer duration of the second stage of landing and decrease of absolute value of angular velocity by pneumatic force from the left airbag. Therefore by the analogy to previously described pressure-driven adaptation, proposed strategy will be composed of the following steps:

- stage 3: fast increase of negative torque to optimal level,
- stage 4: maintaining constant negative value of torque in order to decrease the angle of platform rotation,
- stage 5: possibly fast change of torque sign into a positive one,
- stage 6: maintaining constant positive torque in order to stop anticlockwise rotation of the platform,
- stage 7: reduction of torque to zero to maintain system in position of equilibrium.

3. Further, we will derive the formulae defining change of resistance coefficients of valves in both absorbers which are required to realise subsequent stages of the process.

Increase of the absolute value of the negative torque while maintaining constant pneumatic force (stage 3) relies on gradual increase of force generated by the right airbag and simultaneous decrease of force generated by the left airbag. Therefore, during the whole stage exhaust valve of the right airbag remains closed. Pressure in the right absorber can be expressed in terms of kinematics of the system $p_2^{opt} = f(u, \varphi)$, while pressure in the left absorber can be determined from the condition that total vertical force acting on the platform remains constant:

$$p_1^{opt}(u, \varphi) = \frac{F_{opt}^{tot} - \left(p_2^{opt} - p_A\right)A_2}{A_1} + p_A \tag{6.2.38}$$

Resistance coefficients which have to be introduced into the system of governing equation are calculated according to general definition:

$$C_V{}^1(u, \varphi) = \frac{p_1^{opt} - p_A}{\dot{m}} = \frac{\left(p_1^{opt} - p_A\right)RT_0}{\dot{p}_1^{opt}V_1 + p_1^{opt}\dot{V}_1}, \qquad C_V{}^2(u, \varphi) \to \infty \tag{6.2.39}$$

Resistance coefficient of the left valve is here expressed in terms of platform displacement and its angle of rotation. Solution of the basic system of equations governing platform motion (Eq. 6.2.15a, c) allows to find change of resistance coefficient in terms of time.

Pressures inside pneumatic absorbers which allow for maintaining constant value of torque (stage 4) can be determined from the set of equations:

$$\left(p_1^{opt} - p_A\right)A_1 + \left(p_2^{opt} - p_A\right)A_2 = F_{opt}^{tot} \tag{6.2.40}$$

$$\left(p_1^{opt} - p_A\right)A_1 l_1 \cos\varphi - \left(p_1^{opt} - p_A\right)A_2 l_2 \cos\varphi = M_3$$

and therefore they are defined in terms of platform kinematics. Since change of angles of rotation is small, required pressures are almost constant and realisation of assumed adaptation strategy is always possible. Change of flow resistance coefficient in both absorbers is calculated according to formulae:

$$C_V{}^1(u,\varphi) = \frac{\left(p_1^{opt} - p_A\right)RT_0}{\dot{p}_1^{opt}V_1 + p_1^{opt}\dot{V}_1}, \qquad C_V{}^2(u,\varphi) = \frac{\left(p_2^{opt} - p_A\right)RT_0}{\dot{p}_2^{opt}V_2 + p_2^{opt}\dot{V}_2} \tag{6.2.41}$$

For the considered stage both resistance coefficients are expressed in terms of platform displacement and its angle of rotation.

Change of value of torque into the positive one (stage 5) takes place with closed left valve. In this stage, the pressure in the left absorber is defined in terms of platform displacement and rotation. Pressure in the right absorber can be determined from the condition that total pneumatic force remains constant:

$$p_2^{opt}(u,\varphi) = \frac{F_{opt}^{tot} - \left(p_1^{opt} - p_A\right)A_1}{A_2} + p_A \tag{6.2.42}$$

Finally, definitions of flow resistance coefficients which have to be introduced into the system of governing equation are the following:

$$C_V{}^1(u,\varphi) \to \infty, \qquad C_V{}^2(u,\varphi) = \frac{\left(p_2^{opt} - p_A\right)RT_0}{\dot{p}_2^{opt}V_2 + p_2^{opt}\dot{V}_2} \tag{6.2.43}$$

Maintaining constant value of torque in stage 6 is realised in exactly the same way as in stage 4. Determination of resistance coefficients of the valves is preceded by solving the set of equations (6.2.40) in which different value of torque is used. Reduction of the positive torque to zero (stage 7) is performed with the closed right valve. The stage is performed in exactly the same manner as stage 3 where negative value of torque was increased and therefore Eq. 6.2.38 and Eq. 6.2.39 defining change of pressure and change of resistance coefficients hold.

4. The final step of control strategy development is determination of optimal duration of subsequent stages of the process. For stages 3 and 5, the length of the stage determines the subsequent value of applied torque. Corresponding optimisation problem is aimed at finding durations of stages which minimise angular acceleration of the platform:

$$\text{Find } t_3, t_4, t_5, t_6 \quad \text{such that} \quad \mathrm{J}_2 = \max_t \ddot{\varphi}(t) \quad \text{is minimal} \tag{6.2.44}$$

Instead of finding numerical solution of the above problem, let us analyse the influence of the subsequent time parameters on the process of adaptive landing. Increase of duration of the third stage of impact (parameter t_3) increases value of negative angular acceleration which helps to reduce angle of platform rotation but, on the other hand, increases its angular velocity.

Increase of period of fourth stage when torque remains negative (parameter t_4) gives similar effect and, moreover, it automatically determines increase of positive torque (parameter t_5) which has to be used to obtain full reduction of angular velocity at the end of the process. Eventually, duration of the last stage of landing (parameter t_6) has to be adjusted to obtain full reduction of torque.

Presented numerical example of adaptation assumes the priority of minimisation of angular momentum over minimisation of final angle of rotation, cf. Eq. 6.2.29 and Eq. 6.2.36. Consequently, stage 3 is totally omitted. In turn, duration of stage 4 and stage 5 is chosen in a way that absolute value of angular acceleration in stage 6 equals acceleration in stage 4 and, moreover, final angular velocity is reduced to zero. As a result, value of angular acceleration is optimally diminished, i.e. it does not exceed level obtained during the second stage of landing. The cost of optimal minimisation of angular acceleration is only a partial reduction of angle of platform rotation at the end of the process. Applied resistance coefficients representing opening of the valves, resulting pressures as well as kinematics of the platform corresponding to basic scenario 4 (Fig. 6.3.13) are presented in Fig. 6.2.20.

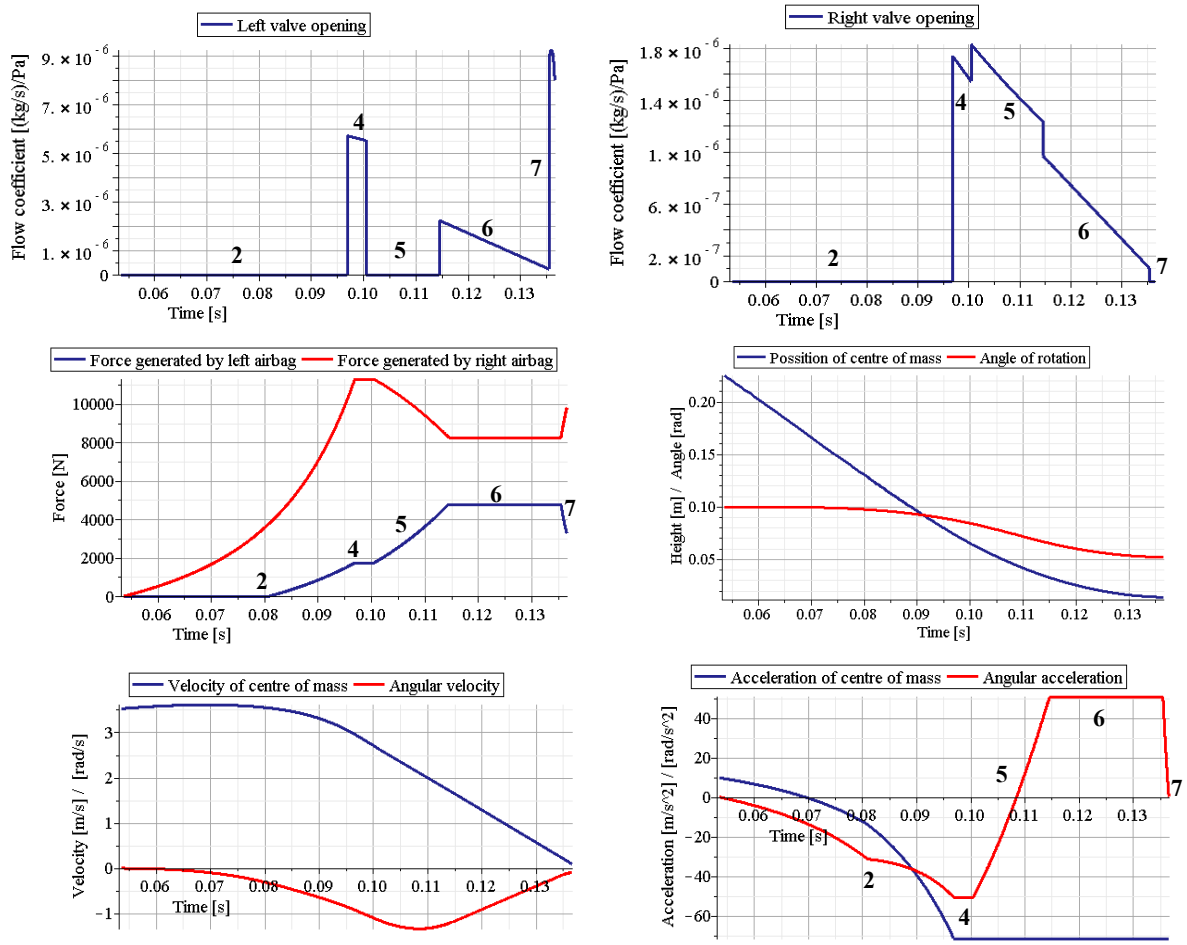

Fig.6.2.20. Strategy aimed at minimisation of angular acceleration: a, b) applied change of flow coefficients in both airbags, c) change of force generated by airbags, d, e, f) kinematics of the system.

An alternative approach to problem of adaptive landing assumes minimisation of acceleration under the requirement that zero rotation angle is obtained at the end of the process. In such an adaptation strategy, stage 4 of landing is typically elongated in order to

enhance reduction of the platform rotation angle. Duration of stage 4 and duration of stage 5 are determined by the requirements of reduction of platform angular velocity and platform rotation angle to zero at the end of the process. The desired final state of the platform can be obtained only at the expense of higher level of angular acceleration during the sixth stage of landing.

The strategy is demonstrated in the following numerical example where basic scenario 4 is considered, Fig. 6.2.21. In this case the condition of final rotation angle and final angular velocity being zero requires slightly higher initial pressure in right absorber, elongation of fourth and fifth stage of impact which results in higher level of positive angular acceleration.

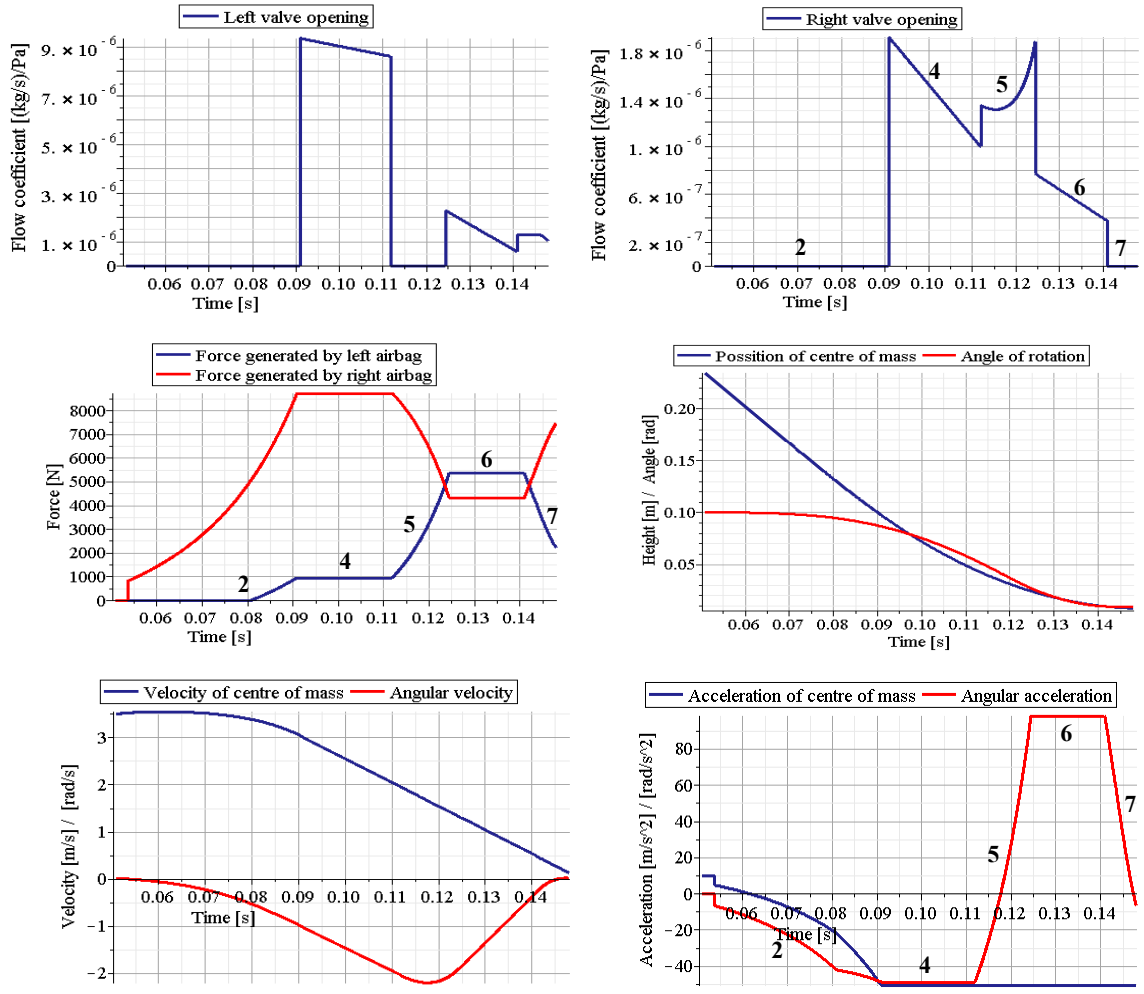

Fig.6.2.21. Strategy aimed at obtaining desired final configuration of the platform: a, b) change of flow coefficients in both airbags, c) force generated by both airbags, d , e, f) kinematics of the system.

In case of 'Scenario 2' (where angular velocity at the beginning of the third stage of impact is positive, see Fig. 6.2.19) the strategy of adaptation also depends on whether the requirement of reduction of final rotation angle remains active. In case when final rotation of the platform can be neglected, simplified adaptation strategy consists of the following steps:

- stage 3: possibly fast increase of torque to optimal level,
- stage 4: maintaining negative value of torque in order to stop rotation of the platform,

- stage 5: reduction of torque to zero to maintain system in position of static equilibrium.

Although the proposed above strategy is relatively simple, its realisation is almost always possible and it often leads to optimal reduction of angular acceleration. On the other hand, the strategy results in increase of final rotation angle in comparison to the initial one (increase of rotation angle occurs during the entire landing process).

When the requirement for minimisation of the final rotation angle (Eq. 6.2.36b) is active, the strategy of adaptation follows the scheme proposed for scenario 1. However, negative torque has to be maintained constant for a longer period of time in order to change angular velocity into the negative one and to decrease angle of platform rotation. In certain time instant torque has to be changed into the positive one in order to reduce anticlockwise platform rotation. In numerical example related to the basic scenario 2 (Fig. 6.2.13), the implementation of the method and additional adjustment of initial pressure allow to obtain equal absolute value of angular acceleration in two main stages of the process (stage 4 and stage 6) and to achieve desired final configuration of the system, Fig. 6.2.22.

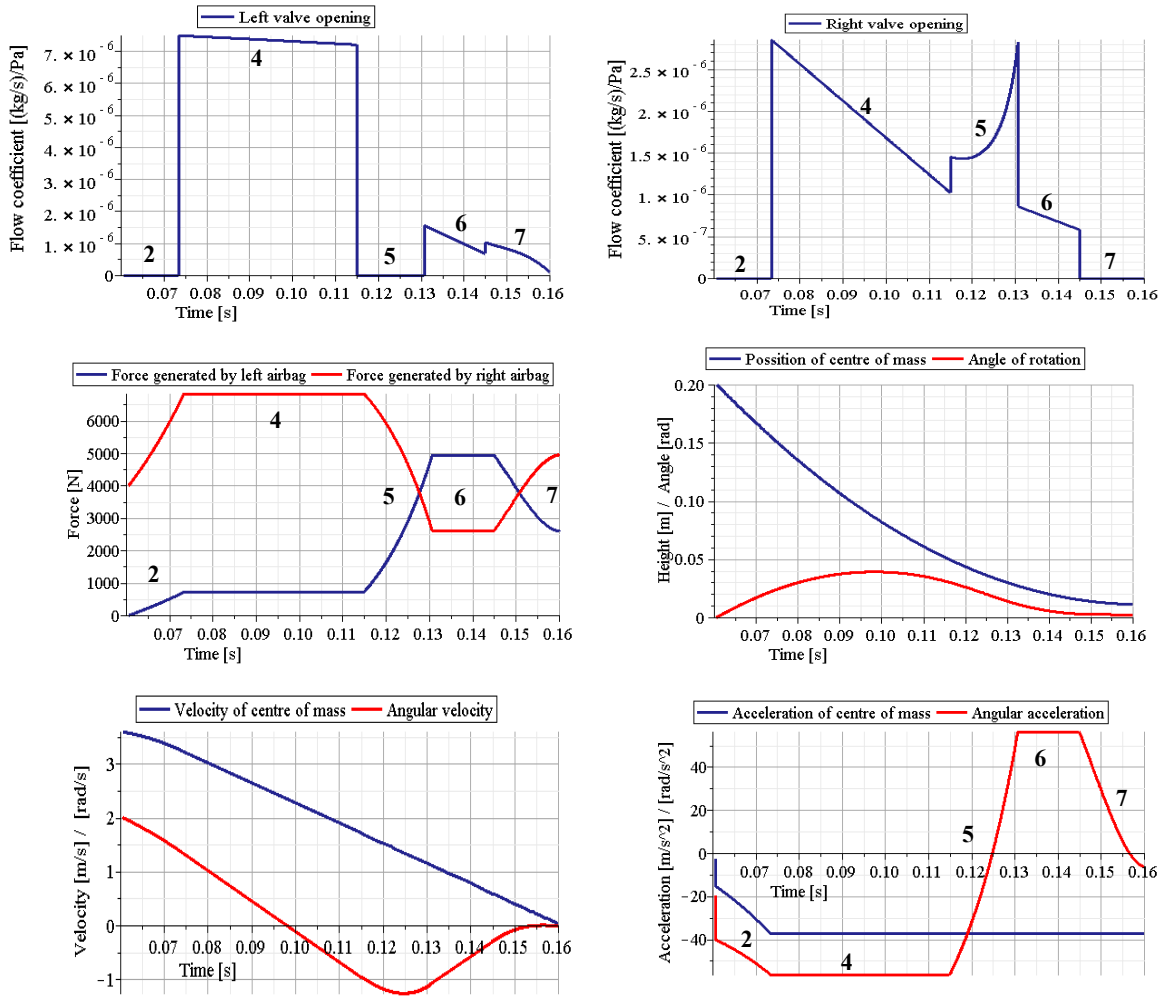

Fig.6.2.22. Strategy aimed at obtaining desired final position of the platform:
a, b) applied change of flow resistance coefficients in both airbags, c) change of force generated by both airbags, d, e, f) kinematics of the system

Finally, in case of 'Scenario 3' (where initial torque is positive) the strategy of leading the system to equilibrium position is the most complex. When final rotation can be neglected the adaptation strategy is composed of the following stages:

- stage 3: change of sign of torque into the negative one,
- stage 4: maintaining constant value of negative torque in order to decrease angular velocity of the platform,
- stage 5: reduction of torque to zero before the end of the process in order to obtain zero angular velocity of the platform.

In the above strategy duration of stage 3 can be determined from the condition that angular velocity has to be equal to zero at the end of the process. The disadvantage is resulting increase of platform rotation angle.

In case when final angle of rotation has to be decreased to zero, the adaptation strategy has to contain the subsequent steps:

- stage 3: change of sign of torque into the negative one,
- stage 4: maintaining negative torque for longer period in order to obtain negative angular velocity and to reduce platform angle of rotation,
- stage 5: change of sign back to a positive one ,
- stage 6: maintaining constant value of torque in order to decrease negative angular velocity,
- stage 7: reduction of torque to zero at time instant when both angular velocity and angle of rotation are equal to zero.

The value of torque at the end of stage 3 has to be subjected to optimisation and length of stages 4 and 5 is determined by assumed final state of the system. In practise, the proposed strategy appears to be too complex since it involves many steps and can not be implemented due to delays in changes of the sign of torque. Therefore, typically, previously proposed strategy, which results in non-zero final rotation angle has to be applied.

6.2.3. Two-dimensional model of compliant landing object

In this section the process of landing of the compliant object equipped with cylindrical airbags will be considered. Two simple two-dimensional models being lateral and frontal projection will be analysed, Fig. 6.2.23. Both models are composed of beam elements and point mass located in the middle of the landing object. Simulation of landing will be conducted with the use of 'full UPM approach', i.e. the structural part will be modelled by the Finite Element Method and gas filling the airbags will be modelled by the Uniform Pressure Method.

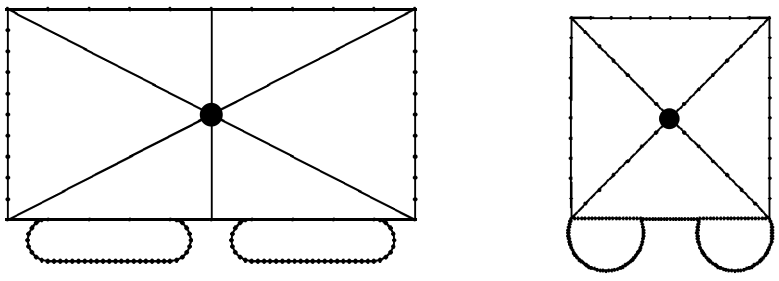

Fig.6.2.23. Models of the landing object considered in further numerical examples

The main goal of this section is to develop strategies of optimal pressure release during landing and to investigate the beneficial influence of airbags adaptability on dynamic response of the landing object.

Basic parameters used in further numerical simulations correspond to a situation of emergency landing of the helicopter. Total mass of the object equals 5000-7000kg, its dimensions are 5m x 2m x 2,5m (length x width x height) and assumed velocity of the emergency landing is up to 10m/s. In case of ideal landing parallel to the ground, basic parameters of the airbags can be determined from the 'reduced UPM' model developed in Sect. 6.2.1, which allows to avoid conducting multiple FEM analyses with various airbags geometry. The process of system design involves the following steps:

1. assumption of airbag geometry and initial pressure,
2. implementation of strategy aimed at minimisation of landing object deceleration (stage of force increase and stage when force is maintained constant, cf. Sec. 6.2.1.,
3. comparison of obtained and maximal allowable deceleration level and appropriate change of airbags geometry and initial pressure.

According to the above analysis, the system of emergency landing considered in further numerical simulations will consist of four cylindrical airbags of diameter 0,65m and length 2m which extend 0,5m below the lower deck of the landing object. Required initial airbag pressure is estimated as 2atm. Proposed airbag system provides that considered landing object is expected to be subjected to decelerations not larger than 12-15g.

Lateral projection of the landing object

Two-dimensional model being lateral projection of the landing object consists of external chassis, four skews and two vertical longitudinal elements which keep the point mass in central position. Total mass of the landing object is 6800kg and its initial velocity in considered landing scenario equals 10m/s. Due to the fact that analysed model is two dimensional, out of plane dimension and mass of the landing object are appropriately reduced (exactly 1/20 of the width and mass, i.e. 0,1m and 340kg are considered). Stiffness of the lower beam of the landing object is intentionally attuned to obtain its significant deformation during landing.

Two airbags are located below the object. Similarly as in case of 2D UPM model of a single airbag in Sect. 6.2.1, the airbags are modelled by thin beam elements of a small thickness. The outflow of the gas from the airbags is described by Saint-Venant-Wantzel formula (Eq. 2.3.28). For the purpose of simulation of the touchdown process proper contact conditions between the landing object, the airbags and the ground are defined.

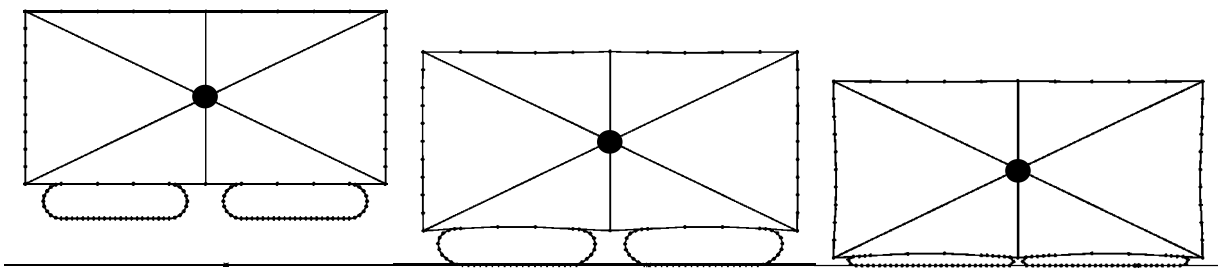

Fig.6.2.24. Simulation of landing: a) initial situation, b) middle stage, c) landing accomplished.

The clear drawback of the considered two-dimensional model with lateral projection of the cylindrical airbags is that after inflation the shape of airbags substantially changes. The above phenomenon occurs only in 2D model of cylindrical airbags and does not arise in full 3D model. The reason is that position of equilibrium of considered 2D airbags under action of internal pressure is substantially different than assumed initial configuration and, moreover, change of shape occurs relatively easily since it does not require elongation of airbag fabric. The above drawback can be omitted by appropriately late triggering of airbags inflation or, alternatively, by using 2D model with frontal projection of airbags.

In general, introduced 2D model allows to analyse the result of application of previously developed standard control strategies to the compliant landing object and, in turn, the influence of landing object compliance on optimal control strategies. In particular, three basic aspects can be distinguished: i) the influence of deformation of the lower beam of the landing object on developed control strategies, ii) the influence of structure compliance on the forces transferred to the point mass and its deceleration, iii) the possibility of observing bending moment and stresses in the lower beam of the landing object. The analysis will be performed in the following order:

- basic simulation of emergency landing with airbags will be compared against simulation of landing without airbags;
- basic strategies used previously for minimisation of deceleration and pressure (Sec. 3.2.2, 3.2.4, 6.2.1) will be examined for reduction of stresses in lower beam of landing object and decceleration of the point mass located in its centre and further precisely tuned to provide optimal reduction of these quantities.

In a basic simulation of the emergency landing the falling object is in horizontal position (zero rotation angle and angular velocity) and has non-zero vertical and horizontal initial velocity. Just before touchdown, when the object is located at height 0,7m, the airbags are inflated to 1,75atm (0,75atm overpressure, Fig. 6.2.25a). The inflation results in increase of the airbags volume and their contact with the ground (Fig. 6.2.24). After the inflation the valves in both airbags are opened and their opening remains constant during the whole landing process. Constant valve opening is chosen in a way that airbags are almost fully compressed but direct contact of the falling object with the ground does not occur. Release of gas is continued when helicopter vertical velocity drops to zero (Fig. 6.2.25b) which results in sudden decrease of pressure.

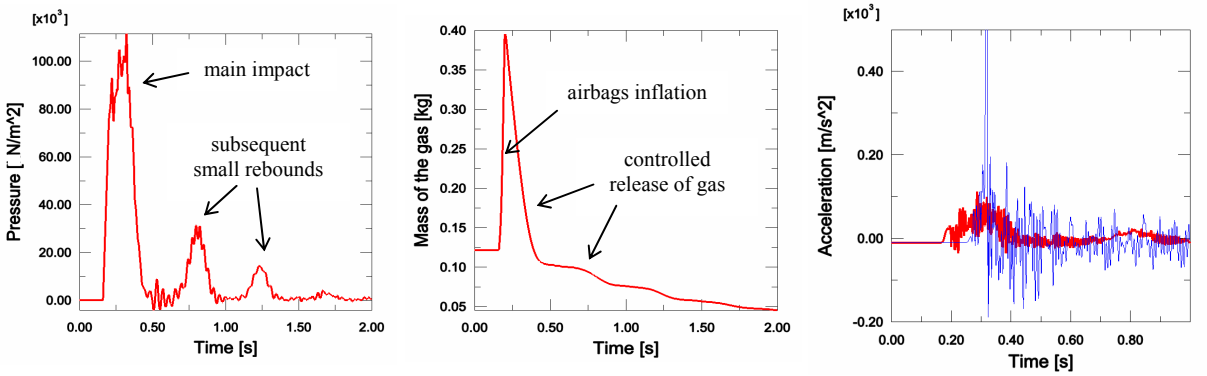

Fig.6.2.25. Basic simulation of emergency landing: a) change of pressure inside airbag, b) mass of the gas inside airbag, c) obtained reduction of accelerations.

Nonetheless, small rebounds of the landing object occur which is the consequence of nonzero exergy of the airbags at time instant when the object is stopped. The subsequent rebounds of the helicopter are reflected by subsequent peaks on the pressure plot. The obtained numerical results indicate that acceleration of the mass located in the middle of the considered structure is reduced several times in comparison to the case when airbags are not applied, Fig. 6.2.25c.

The following analyses were aimed at implementation of the selected pressure control strategies and investigation of their influence on the acceleration of the point mass and stresses generated in the lower beam. The parameters of the landing object and landing scenario were exactly the same as in case of basic simulation of the emergency landing. However, the important difference is that inflation of the airbags was started exactly when the airbags touched the ground (at time instant 0,15s, Fig. 6.2.26) in order to avoid their artificial initial deformation. Three adaptation strategies were implemented:

- semi-active strategy with adjustment of inflation pressure only,
- semi-active strategy with adjustment of inflation pressure and constant in time valve opening,
- active strategy with constant level of pressure during the whole impact period.

The main guidelines for adjustment of parameters of each adaptation strategy were conditions of utilisation of the largest part of airbag stroke and minimisation of internal airbag pressure (here almost equivalent to minimisation of total force acting on the falling object). Since none of the above conditions is exactly equivalent to assumed control objectives, corresponding optimal parameters were used as starting point for optimisation procedures aimed directly at minimisation of stress in the lower beam and acceleration of the point mass.

As it was expected, the type of applied adaptation strategy has significant influence on value of longitudinal stresses generated in the lower beam of the falling object during landing. Application of optimally tuned adaptation strategies leads to the following results: i) adjustment of inflation pressure only (red): $\sigma^{\max} = 397MPa$, ii) adjustment of inflation pressure and constant valve opening (blue): $\sigma^{\max} = 290MPa$, iii) continuous control of valve opening providing constant pressure level (green): $\sigma^{\max} = 252MPa$, Fig. 6.2.26. In case of semi-active adaptation, which involves adjustment of two parameters, similar values of stress can be obtained by applying various initial pressures and corresponding constant valve openings.

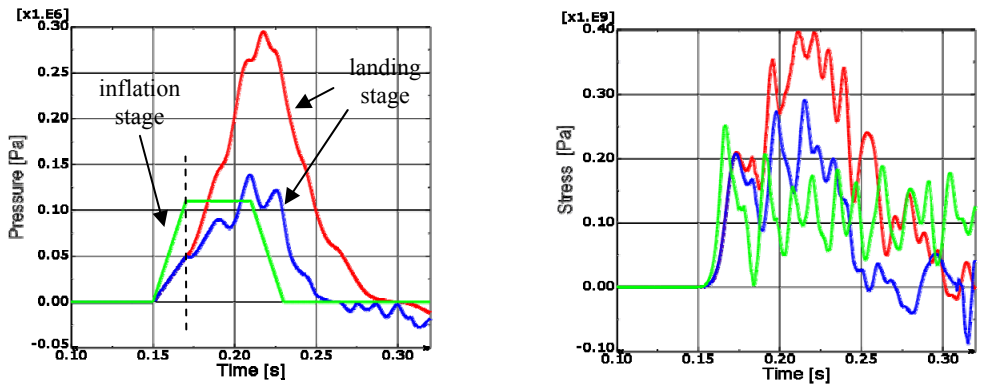

Fig. 6.2.26: Minimisation of stress in the lower beam of the falling object: a) applied pressure control strategy, b) resulting change of longitudinal stress resultant

The problem of minimisation of central mass acceleration results in slightly different optimal values of parameters of considered adaptation strategies, Fig. 6.2.27a. The following results were obtained: i) adjustment of inflation pressure only (red line): $a^{\max} = 508 m/s^2$, ii) adjustment of inflation pressure and constant valve opening (blue line): $a^{\max} = 276 m/s^2$, iii) continuous control of valve opening maintaining assumed constant pressure level (green line): $a^{\max} = 275 m/s^2$, Fig. 6.2.27b.

Although release of pressure caused by constant valve opening leads to significant reduction of point mass acceleration, application of real time adaptation strategy with constant pressure level does not cause additional improvements of results. Both strategies cause similar level of internal pressure and total generated force which is the consequence of relatively large deformation and vibrations of the lower beam of landing object. Despite this fact, in both strategies average force acting on the falling object (which results from pressure 1,1atm) equals approximately 45kN and average acceleration of the object is 120m/s^2, acceleration of the central mass highly exceeds this value due to vibrations of the adjacent beam elements.

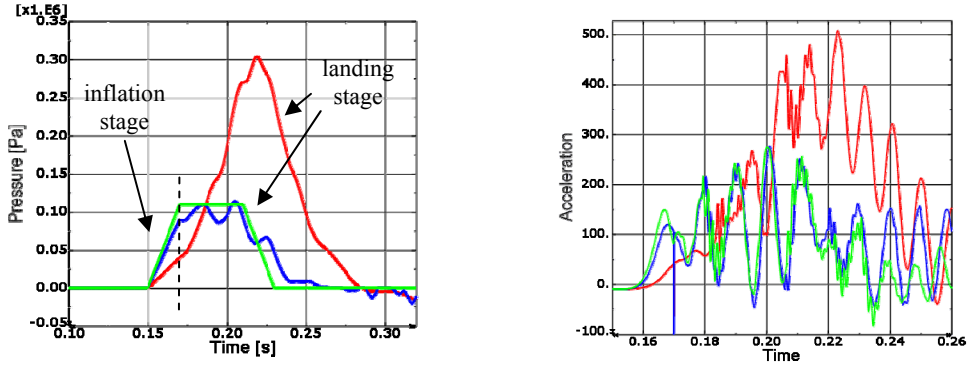

Fig. 6.2.27: Minimisation of acceleration of the point mass: a) applied pressure variation, b) resulting change of the falling mass acceleration.

Frontal projection of the landing object

The simulation of the emergency landing was also performed with the use of two-dimensional model being frontal projection of the landing object. The main difference between two considered models is that in a frontal model the increase of internal pressure does not cause significant change of initially assumed shape of the airbag. Slight change of initial shape of inflated airbag can occur only due to elongation of the airbag fabric. Therefore, the main advantage of the frontal model is the possibility of inflating the airbags to appropriate initial pressure before the beginning of the landing process.

The parameters of the landing object and the landing scenario are similar as in case of previously analysed lateral model. Since mass of the examined object equals 5000kg and 1/50 of the object length is considered, total mass of the two-dimensional model (central mass and all beams) and its out-of-plane dimensions are equal to 100kg and 0,1m, respectively. According to the fact that lateral and frontal model differs substantially in shape and dimensions, minimal accelerations and stresses obtained from numerical simulation of both models can not be directly compared. Typical stages of the landing scenario are presented in Fig. 6.2.28.

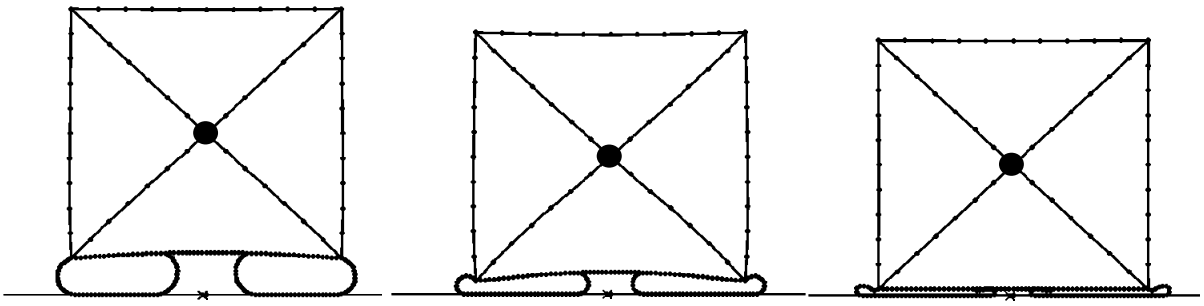

Fig.6.2.28. Simulation of landing: a) initial state of landing b) intermediate stage of landing, c) landing accomplished.

Basic methods of adaptation of the emergency landing system involved:

- adjustment of pressure of initial inflation of the airbags,
- adjustment of initial inflation pressure and constant valve opening activated at time instant when airbags contact the ground.

For each adaptation strategy, the observed response of the system included acceleration acting on the point mass and maximal longitudinal stress generated in its lower beam.

In case of closed valve, adjustment of initial pressure (p=0,1-0,2MPa) changes not only airbags compression, but also their shape of deformation. As a result, value of initial pressure does not substantially alter maximal pressure obtained during the process (Fig. 6.2.29a). Accordingly, the value of maximal deceleration appears to be almost independent of the applied initial pressure, Fig. 6.2.29b. By contrast, the value of the longitudinal stress in the lower beam is significantly changed by adjustment of initial pressure and it achieves its minimal value for the highest initial pressure (Fig. 6.2.29c) which is the consequence of the favourable deformation of the airbag. Further increase of initial pressure causes reduction of the maximal value of stress in the lower beam during landing, however it simultaneously causes the adverse increase of the initial stress caused exclusively by airbag inflation.

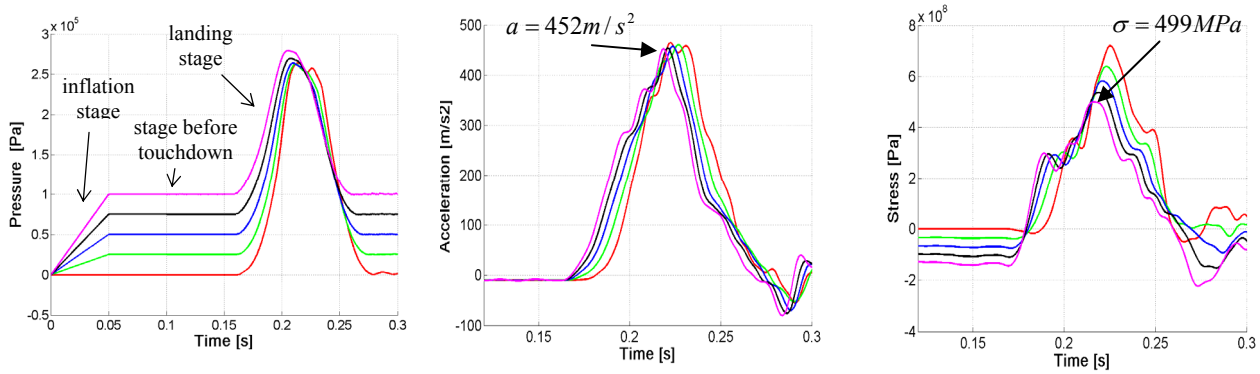

Fig.6.2.29. Adjustment of initial pressure: a) change of airbag gauge pressure during landing, b) corresponding change of mass acceleration, c) corresponding change of stress in lower beam.

The influence of the constant valve opening will be presented for an arbitrary initial total pressure of 2atm for which the largest decrease of stress and mass acceleration was obtained. The opening of the valve (described by SVW model) was gradually increased in the subsequent numerical analyses, Fig. 6.2.30a. The increase of the valve opening caused reduction of maximal value of internal pressure inside airbag (Fig. 6.2.30b) and, consequently,

decrease of central mass deceleration and decrease of stress generated in the lower beam (Fig. 6.2.30c,d). For largest valve opening, pressure inside airbag decreases during the initial stage of impact since the effect of pressure release outperforms the effect of airbag compression. As a result, pressure value oscillates around the initial level during the process. In this case, acceleration and stress achieve minimal value, however, the direct contact of the falling object with the ground occurs (cf. increase of acceleration and stress in Fig. 6.2.30c, d), which clearly indicates the limit of the allowable valve opening.

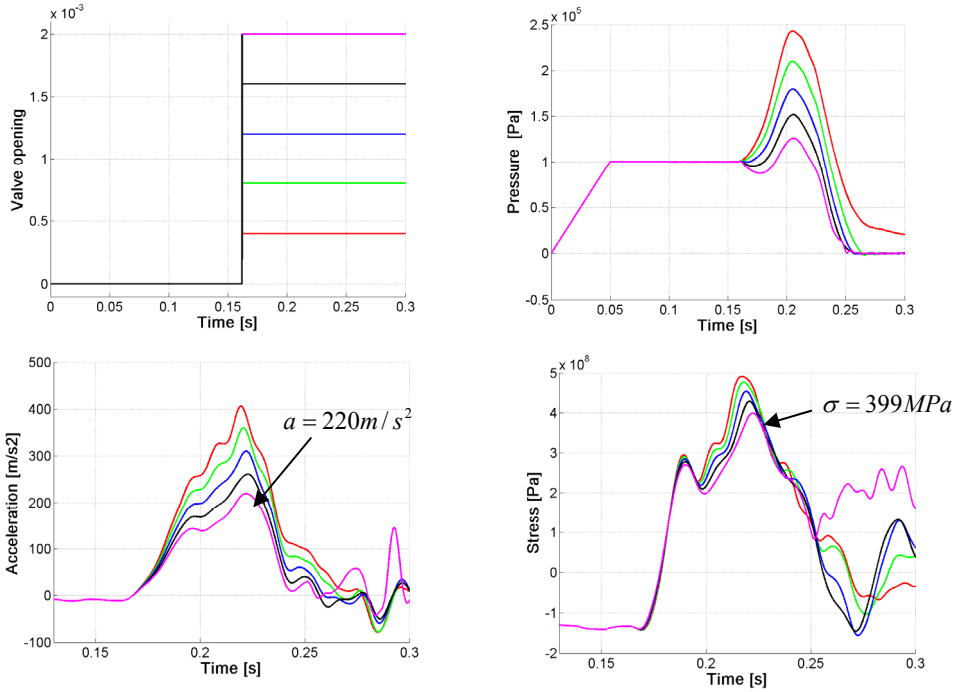

Fig.6.2.30. Adjustment of constant valve opening: a) applied valve opening, b) corresponding change of airbag pressure, c) change of mass acceleration, d) change of stress in lower beam.

Advanced strategies of adaptation (based on real-time change of valve opening) involved the following methods:

1. maintaining constant possibly low value of pressure (initial pressure assumed),
2. maintaining constant possibly low value of pressure during the whole landing period,
3. maintaining constant possibly low global value of the force acting on the landing object during impact.

Elementary considerations regarding the dynamics of the landing object indicate that the third strategy based on minimisation of total force acting on the falling object is expected to lead to a minimal value of mass acceleration and lower beam stress. Nevertheless, all strategies will be tested and compared with each other.

Ad. 1. In the first of the considered strategies the level of initial pressure was arbitrarily assumed and the following part of the process was composed of three stages:

- increase of pressure to a certain level,
- maintaining constant value of pressure until velocity of the falling object drops below assumed threshold,
- reduction of pressure to the value which provides static equilibrium of the landing object, Fig. 6.2.31a.

Realisation of the above adaptation strategy requires adjustment of three parameters: level of pressure which is maintained constant (or corresponding time instant when pressure control is started), time instant when release of pressure begins and duration of time period of pressure release. In presented numerical simulations, reduction of pressure was started when velocity of the object achieved 1m/s and was executed during period of 0,015s. Therefore, performed analysis was focused on the investigation of the influence of assumed value of constant pressure on the acceleration of point mass and stress in the lower beam.

The lowest applied initial pressure was found to be insufficient for stopping the landing object and resulted in its direct contact with the ground, Fig. 6.2.31a, b (red line). Optimal reduction of mass acceleration was obtained for slightly higher value of pressure when direct collision with the ground is prevented, but almost whole stroke of the airbag is utilised, Fig. 6.2.31a,b (green line). Collision with the ground during the last stage of the process (after reduction of pressure) also affects stresses in the lower beam of the landing object Fig. 6.2.31c. However, for the lowest value of applied constant pressure collision with the ground occurs at low velocity and, eventually, for this strategy minimal value of stress is obtained.

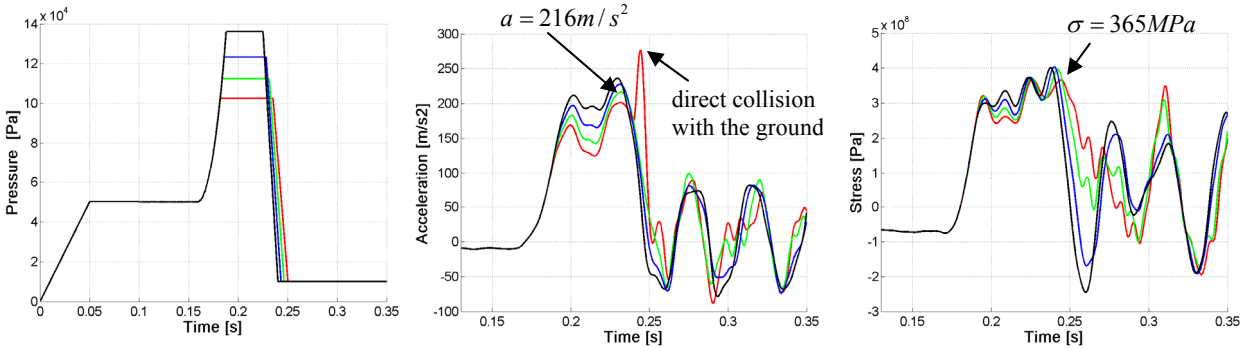

Fig.6.2.31. Adjustment of constant pressure: a) change of airbag pressure during landing, b) corresponding change of mass acceleration, c) corresponding change of stress in lower beam.

Ad. 2. Improvement of the above adaptation strategy can be obtained by avoiding the initial stage of pressure increase, i.e. by maintaining constant level of pressure during the whole landing process. In current strategy the best results are obtained when collision with the ground does not occur. Application of the proposed strategy with appropriate level of pressure allows enables only slight reduction of acceleration and stress, cf. Fig. 6.2.32.

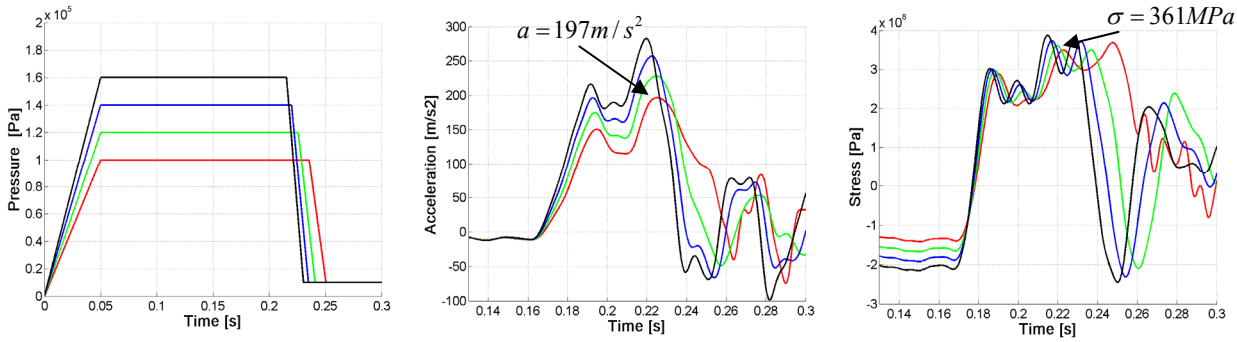

Fig.6.2.32. Adjustment of constant pressure: a) change of airbag pressure during landing, b) corresponding change of mass acceleration, c) corresponding change of stress in lower beam.

Ad. 3. Finally, the last of the proposed approaches utilises the strategy of maintaining constant level of force acting on the landing object. This goal is obtained by direct reduction of pressure according to Eq. 6.2.14. In the second step of the procedure the constant level of force is optimised in order to minimise deceleration of the point mass and stress in the lower beam of the falling object. Similarly, as in previous approaches the value of initial pressure, the condition triggering final pressure reduction and time period of final pressure reduction are arbitrarily assumed.

The presented results of numerical simulations correspond to various time instants of actuation of real-time control of the valve opening and thus various level of maintained constant force. Minimal values of mass acceleration and stress are obtained for the lowest value of force, for which soft contact of the landing object with the ground occurs. The strategy of adaptation based on sustaining constant level of the force provides the smallest values of both minimised quantities, and therefore, it is superior to other proposed strategies.

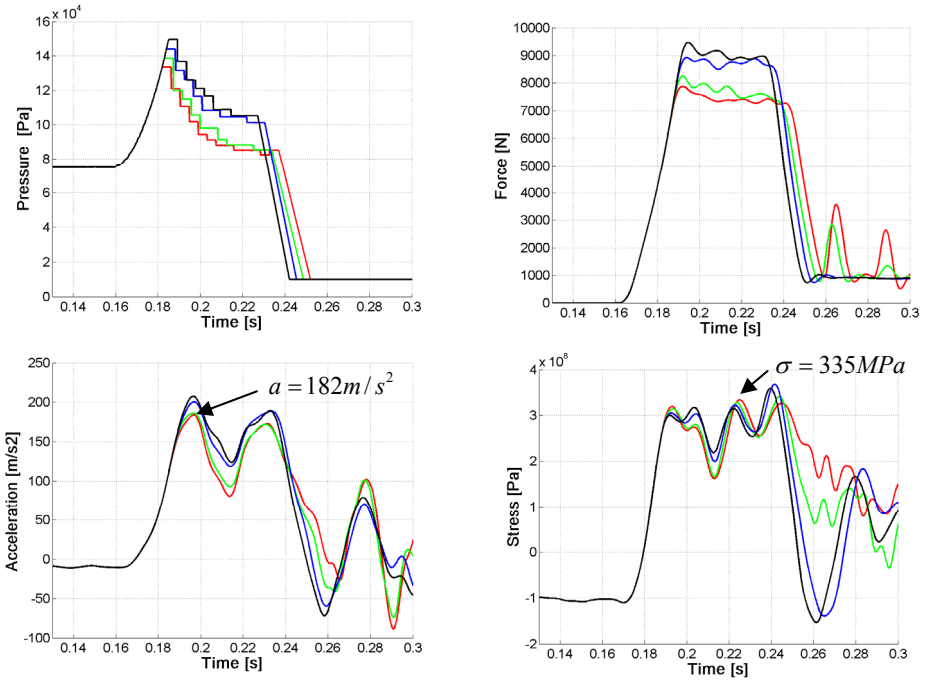

Fig.6.2.33. Adjustment of constant level of force: a) change of pressure, b) change of contact force, c) corresponding change of mass acceleration, d) corresponding change of stress in lower beam.

The developed software tools allow not only for systematic inspection of the space of adaptation parameters, as presented, but also for application of optimisation procedures to find optimal values of these parameters. The corresponding optimisation problem reads:

$$\text{Find } \{p_0, t_x, t_{end}\} \text{ such that } J = \max_t a(t) \text{ or } J = \max_t \sigma(t) \text{ is minimal} \qquad (6.2.45)$$
$$\text{subject to: } p_0 \in \langle p_{\min}, p_{\max} \rangle, \quad t_x \in \langle t_{\min}, t_{\max} \rangle, \quad t_{end} \in \langle t_{\min}, t_{\max} \rangle$$

where p_0 denotes initial pressure, t_x - time instant when pressure/force begins to be maintained constant and t_{end} - time instant when final reduction of pressure starts. Since objective function is expected to have a local minima, various starting points indicating maximal airbags compression should be used. The developed software allows for elaboration of the adaptation strategies not only for the proposed basic model composed of beams and point mass, but for arbitrary landing object equipped with airbag system.

An alternative approach is based on development of valve opening strategies which are not related to maintaining constant level of total force or pressure, as presented, but which correspond directly to minimised quantities, i.e. deceleration of the point mass and stresses generated in the lower beam. The difficulty is that the dependence of the minimised quantities on valve opening is complex since it is influenced by dynamics of the landing object and it can not be expressed analytically. Therefore, development of the adaptation strategies related directly to minimised quantities remains in general an open problem.

In case of arbitrary landing scenario (when initial rotation of the falling object and its initial angular velocity are non-zero or when centre of inertia is not located in the middle of the structure) development of optimal adaptation strategy consists of two steps:

1. assumption of the adaptation strategy developed previously for the reduced UPM approach (cf. Sect. 6.2.2),
2. adjustment of the parameters of the adaptation strategy by optimisation algorithm.

The whole procedure can be treated as semi-heuristic approach. The first step is purely heuristic while the second one precisely tunes assumed adaptation strategy. The second step of the procedure is required since 'reduced UPM' approach does not provide precise prediction of the airbags deformation during landing scenarios, which additionally depends on deformation of the bottom part of the landing object.

6.2.4. Three-dimensional simulations of adaptive emergency landing

The last section of this chapter presents three-dimensional simulation of the process of emergency landing and the development of corresponding control strategies. Consecutively, simplified 'reduced UPM model' and 'full UPM model' of the system will be considered.

Three-dimensional reduced UPM model

Three-dimensional ‘reduced UPM model’ of a landing platform consists of rigid deck equipped with four airbags located vertically during the entire landing process, Fig. 6.2.34. Mass of the platform is uniformly distributed in its four corners. The landing scenario is defined by vertical velocity, two components of horizontal velocity, three angles of rotation and three components of angular velocity.

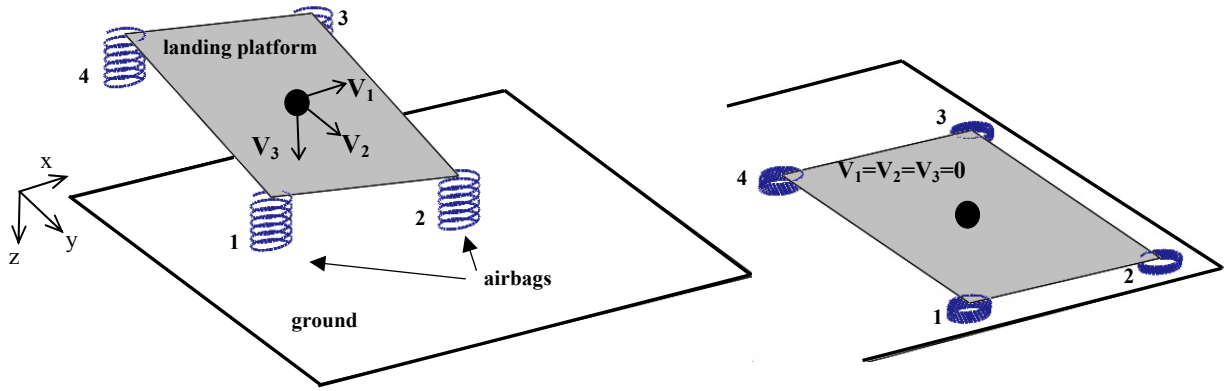

Fig. 6.2.34: Simplified 3D simulation of landing: a) initial configuration, b) final stage of landing.

Since the platform is assumed to be rigid, numerical model of the system is based on equations of equilibrium of a rigid body with six mechanical degrees of freedom. Because of equal value of mass in each corner, centre of system inertia is located in the middle of the platform. Motion of the platform can be decomposed into motion of its centre of inertia $\mathbf{u} = \{u, v, w\}$ and rotations $\boldsymbol{\varphi} = \{\varphi_1, \varphi_2, \varphi_3\}$ with respect to reference frame whose centre coincides with centre of inertia. Positions of the corners of the plate (x_n, y_n, z_n) can be expressed in terms of principal unknowns of the problem, i.e.:

$$x_n = f_{xn}(u, v, w, \varphi_1, \varphi_2, \varphi_3), \quad y_n = f_{yn}(u, v, w, \varphi_1, \varphi_2, \varphi_3), \quad z_n = f_{zn}(u, v, w, \varphi_1, \varphi_2, \varphi_3) \tag{6.2.46}$$

Further, components of the tensor of moments of system inertia **I** with respect to fixed coordinate system are defined by the classical formulae:

$$I_{xx} = \sum_{n=1}^{4} m_n \left[(y_C - y_n)^2 + (z_C - z_n)^2 \right], \qquad I_{yy} = \sum_{n=1}^{4} m_n \left[(x_C - x_n)^2 + (y_C - y_n)^2 \right] \tag{6.2.47}$$

$$I_{zz} = \sum_{n=1}^{4} m_n \left[(x_C - x_n)^2 + (y_C - y_n)^2 \right], \qquad I_{xy} = I_{xy} = -\sum_{n=1}^{4} m_n \left[(x_C - x_n)(y_C - y_n) \right]$$

$$I_{xz} = I_{zx} = -\sum_{n=1}^{4} m_n \left[(x_C - x_n)(z_C - z_n) \right], \quad I_{yz} = I_{zy} = -\sum_{n=1}^{4} m_n \left[(y_C - y_n)(z_C - z_n) \right]$$

where x_C, y_C, z_C are coordinates of centre of inertia. Let us note that tensor of moments of inertia is changing during the process of landing as the platform rotates. Equations of system equilibrium can be derived in most concise way by using the principle of virtual work and they are known as the Newton-Euler equations [310]:

$$M \frac{d^2 \mathbf{u}}{dt^2} = \mathbf{F} \tag{6.2.48}$$

$$\frac{d(\mathbf{I}\boldsymbol{\omega})}{dt} = \mathbf{T} \quad \text{or} \quad \mathbf{I} \cdot \frac{d^2 \boldsymbol{\varphi}}{dt^2} + \frac{d\mathbf{I}}{dt} \cdot \frac{d\boldsymbol{\varphi}}{dt} = \mathbf{T} \quad \text{or} \quad \mathbf{I} \cdot \frac{d^2 \boldsymbol{\varphi}}{dt^2} + \frac{d\boldsymbol{\varphi}}{dt} \times \mathbf{I} \cdot \frac{d\boldsymbol{\varphi}}{dt} = \mathbf{T} \tag{6.2.49}$$

where M denotes total mass of the platform, **F** and **T** denote force and torque acting on the object, respectively. The full form of the above equations read:

$$M \frac{d^2 u}{dt^2} = F_{x1} + F_{x2} + F_{x3} + F_{x4}, \qquad M \frac{d^2 v}{dt^2} = F_{y1} + F_{y2} + F_{y3} + F_{y4} \tag{6.2.50}$$

$$M \frac{d^2 w}{dt^2} - Mg = F_{p1} + F_{p2} + F_{p3} + F_{p4}$$

and

$$I_{xx} \frac{d^2 \varphi_1}{dt^2} + \frac{dI_{xx}}{dt} \frac{d\varphi_1}{dt} + I_{xy} \frac{d^2 \varphi_2}{dt^2} + \frac{dI_{xy}}{dt} \frac{d\varphi_2}{dt} + \ldots = T_x(F_{pn}, F_{yn}, x_n, z_n) \tag{6.2.51}$$

$$I_{yx} \frac{d^2 \varphi_1}{dt^2} + \frac{dI_{yx}}{dt} \frac{d\varphi_1}{dt} + I_{yy} \frac{d^2 \varphi_2}{dt^2} + \frac{dI_{yy}}{dt} \frac{d\varphi_2}{dt} + \ldots = T_y(F_{pn}, F_{xn}, y_n, z_n)$$

$$I_{zx}\frac{d^2\varphi_1}{dt^2}+\frac{dI_{zx}}{dt}\frac{d\varphi_1}{dt}+I_{zy}\frac{d^2\varphi_2}{dt^2}+\frac{dI_{zy}}{dt}\frac{d\varphi_2}{dt}+\ldots=T_z(F_{xn},F_{yn},y_n,x_n)$$

In the above equations F_{pn} denotes vertical pneumatic forces generated by each absorber and F_{xn}, F_{yn} indicate friction forces acting in horizontal directions *x* and *y*, respectively. Moreover the quantities T_x, T_y, T_z denote torques corresponding to rotations about subsequent axes of the coordinate system. Each torque is expressed in terms of forces perpendicular to considered axis and their distance from the axis.

The equations of rotational equilibrium can be transformed into rotating coordinate system which coincides with principal axis of inertia of the platform. The corresponding equilibrium equations known as the Euler equations take the form:

$$I_{x'}\frac{d\omega_{x'}}{dt}+\left(I_{z'}-I_{y'}\right)\omega_{y'}\omega_{z'}=T_{x'}\ ,\qquad I_{y'}\frac{d\omega_{y'}}{dt}+\left(I_{z'}-I_{x'}\right)\omega_{x'}\omega_{z'}=T_{y'} \tag{6.2.52}$$

$$I_{z'}\frac{d\omega_{z'}}{dt}+\left(I_{y'}-I_{x'}\right)\omega_{x'}\omega_{y'}=T_{z'}$$

Now, tensor of inertia contains only diagonal terms $I_{x'}, I_{y'}, I_{z'}$ which remain constant during rotation of the platform. The quantities $\omega_1, \omega_2, \omega_3$ describe changes of angular velocity in rotating non-inertial coordinate system. Consequently, torques $T_{x'}, T_{y'}, T_{z'}$ are expressed with respect to rotating coordinate system.

The pneumatic force is expressed in terms of actual pressure inside airbags and its actual area of contact of each airbag with the ground A_C^n which in general is a function of actual airbag stroke s_n :

$$F_{pn}=(p_n-p_A)A_C^n(s_n)\quad\text{if}\quad s_n<h_0\quad\text{and}\quad p\ -p_A>0 \tag{6.2.53}$$

$$F_{pn}=0\quad\text{otherwise}$$

The friction forces in both horizontal directions are defined as proportional to forces generated by pneumatic absorbers:

$$F_{xn}=\mu F_{pn}\ ,\qquad F_{yn}=\mu F_{pn} \tag{6.2.54}$$

In order to simplify thermodynamic part of the problem, isothermal conditions and absence of leakage through the airbag fabric will be assumed. In such a case change of pressure in each airbag depends on actual airbag compression and opening of the valve; and it is expressed by a single differential equation (cf. Sec. 6.2.2):

$$p_n-p_A=\frac{C_V{}^n(t)}{RT_{n0}}\left[\frac{dp_n}{dt}V_n(s_n)+p_n\frac{dV_n(s_n)}{dt}\right] \tag{6.2.55}$$

Eventually, the system is composed of three differential equations governing vertical and horizontal movement, three equations governing rotation of the platform and four equations governing change of airbags pressure. The initial conditions for the whole system of equations read:

$$u(0)=u_0,\quad v(0)=v_0,\quad w(0)=w_0 \tag{6.2.56}$$
$$\dot{u}(0)=V_1,\quad \dot{v}(0)=V_2,\quad \dot{w}(0)=V_3$$
$$\varphi_n(0)=\varphi_{n0},\quad \dot{\varphi}_n(0)=\omega_{n0},\quad \mathrm{n}=1..3$$

The initial conditions for the gas define initial pressure inside each airbag:

$$p_1(0)=p_{10},\quad p_2(0)=p_{20},\quad p_3(0)=p_{30},\quad p_4(0)=p_{40} \tag{6.2.57}$$

The resulting system of governing equations was implemented in Maple software and solved by Runge-Kutta method. The initial simulations were conducted with the use of passive airbags which were not adjusted to particular landing conditions. Dynamic response during exemplary landing scenario with two initial rotation angles ($\varphi_1=-\varphi_2=0{,}1\mathrm{rad}$) and three non-zero components of initial velocity (Fig. 6.2.34) is presented in Fig. 6.2.35. Application of passive airbags leads to adverse landing process with non-equal distribution of linear (especially vertical) and angular accelerations, Fig. 6.2.35b,c.

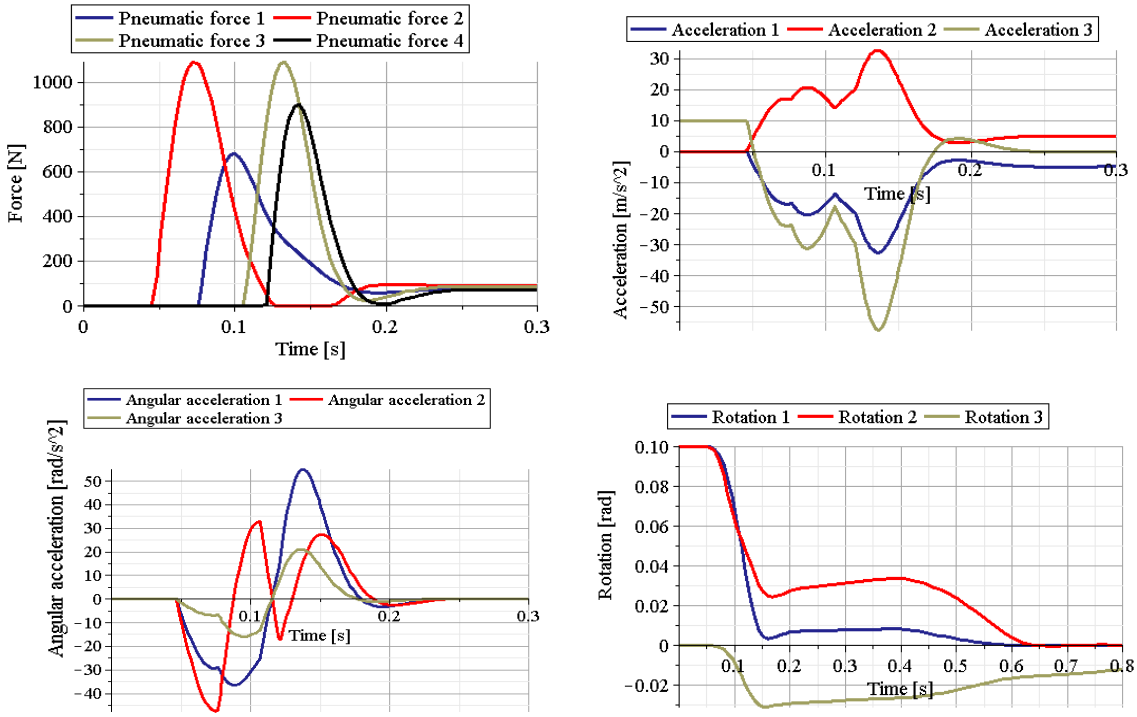

Fig.6.2.35. Results of conducted simulation of 3D landing of the platform (passive absorbers): a) pneumatic forces generated by the absorbers, b) three components of linear acceleration, c) three components of angular acceleration, d) rotation of the platform.

The main purpose of implementation of the above 3D model of the landing platform with adaptive airbags is development and testing of the control strategies aimed at minimisation of the platform acceleration. Proposed adaptation strategies are generalisation of the methods developed previously for 2D model of the landing platform (Sec. 6.2.2). The adaptation strategies were implemented for a simplified model of the system where horizontal friction forces and, consequently, torque relative to z-axis are equal to zero. As a result, two equations governing equilibrium in horizontal direction and rotational equilibrium with

respect to vertical axis can be omitted and motion of the system is described by one displacement and two angles of rotation governed by Eq. 6.2.50c and 6.2.51a,b. For considered 3D model two adaptation strategies were developed: semi-active with constant opening of valves and active with real-time control of valve opening during the landing process.

In case of semi-active adaptation the control problem was to find optimal, but fixed during landing opening of each valve for which landing scenario runs possibly smoothly, i.e. the direct contact of the stiff plate with the ground does not occur and both linear and angular accelerations are minimised. The objective function in optimisation problem was formulated as sum of maximal linear and angular accelerations scaled by weigh coefficients. Each of the valves was activated exactly at time instant when corresponding absorber touches the ground so the only variables in the optimisation problem were values of resistance coefficients of the valves.

It was found that optimal constant in time, but different for each airbag, valves opening (Fig. 6.2.36a) allows to obtain advantageous change of system kinematics with almost constant level of vertical acceleration maintained during the second part of the process, Fig. 6.2.36c. Moreover, the plots of both angular accelerations are composed of two intervals with opposite sign of acceleration (Fig. 6.2.36d) which reveals clear resemblance to adaptation strategies proposed in Sect 6.2.2 for 2D model of landing. Discontinuities of vertical and angular acceleration result from the occurrence of contact of subsequent airbag with the ground and assumed non-zero initial area of contact.

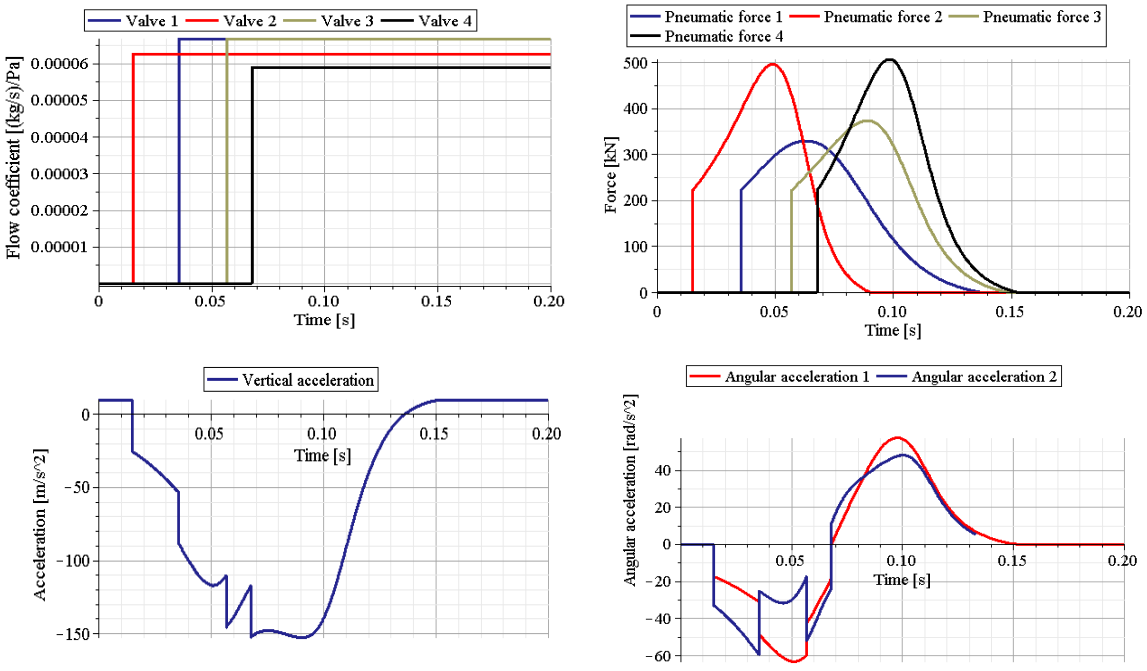

Fig. 6.2.36: Semi-active adaptation of the airbags: a) applied valve opening, b) force generated by the absorbers, c) resulting vertical acceleration of centre of mass, d) resulting angular acceleration.

Active adaptation technique will be based on the 'strategy of priority of minimisation of linear acceleration' which was previously applied for two-dimensional model. Therefore, the objective of the applied control strategy is to lead the system to the final configuration

where vertical velocity, both rotation angles and both angular velocities are equal to zero by the use of method which provides:

- at first, minimal value of vertical deceleration and,
- at second, minimal values of angular accelerations in both directions.

The main difference which occurs in considered 3D model is that maintaining constant possibly low level of pneumatic force (which minimises linear deceleration) is executed with the use of four absorbers which gives wide range of possibilities for controlling both angular accelerations.

The preliminary, strongly simplified control approach, assumes that in considered model without vertical forces and with small angles of rotation the process of controlling angular accelerations relative to the fixed coordinate system is approximately equivalent to controlling angular accelerations relative to principal axes of inertia of the platform. The corresponding simplification of the governing equations relies on assumption of constant values of diagonal terms and zero values of deviatoric terms in the tensor of inertia in Eq. (6.2.51a,b) or assuming $\omega_{z'} = 0$ in Eq. (6.2.52a,b) to obtain:

$$I_{x'} \frac{d^2\varphi_{x'}}{d^2t} = T_{x'} \ , \quad I_{y'} \frac{d^2\varphi_{y'}}{d^2t} = T_{y'} \tag{6.2.58}$$

According to the above equations angles of rotations in both directions are uncoupled and can be controlled separately by two pairs of forces located on opposite sides of the plate (e.g., forces 1, 2 and 3, 4 for rotation around axis 1). Let us stress the fact that simplified equations (6.2.58) are intended to be used only for the purpose of system control, not for governing its dynamics.

As it was described in case of 2D model of the landing platform (Sec. 6.2.2.) the strategy of adaptation depends on the relation of the initial rotation angle, angular velocity and torque at the beginning of the controlled stage of landing. Due to the fact that two rotation angles, two angular velocities and two torques are considered a huge variety of combinations can be encountered during the analysis of the 3D landing system.

Let us consider the exemplary landing scenario characterised by two initial rotation angles $(\varphi_1 > 0, \varphi_2 < 0)$, zero initial angular velocity and non-zero initial vertical velocity, Fig. 6.2.34. The order in which absorbers come in contact with the ground partially depends on applied adaptation strategy, however, it typically occurs in the sequence 2,1,3,4. Further, we will consider the adaptation strategy based on direct control of pressure inside absorbers which involves fewer limitations due to possibility of immediate change of the value of torque. The proposed procedure of control of the landing process contains the following steps:

1. Free falling when none of the absorbers is in contact with the ground.
2. Only absorber 2 is in contact with the ground. The value of pneumatic force generated by absorber 2 is determined by the objective of minimisation of vertical deceleration. Required value of force F^{opt} and corresponding period of time t_{opt}^{vel} are computed with the use of initial velocity and distance of centre of platform inertia to the ground (equations similar to Eq. 6.2.31, 6.2.32).
3. Absorbers 2 and 1 are in contact with the ground. Contact of the second absorber with the ground allows to control angle of rotation φ_2 and corresponding angular

acceleration $\ddot{\varphi}_2$. The stage commences with identification of actual angle of rotation, angular velocity and calculation of constant value of torque M_2^{opt} which allows to simultaneously reduce angle of platform rotation φ_1 and its angular velocity $\ddot{\varphi}_1$ to zero and at time period t_{opt}^{rot-1}, cf. Sec. 6.2.2. Depending on mutual relation of the parameters at the beginning of the stage and ratio of t_{opt}^{vel} and t_{opt}^{rot-2} the appropriate strategy for controlling rotation and acceleration in direction φ_2 is assumed. The formulae for calculation of optimal values of torques $M_{3/4}^2$ and corresponding values of internal pressure take similar form as Eq.6.2.34 and Eq. 6.2.35, respectively.

4. Absorbers 2, 1 and 3 are in contact with the ground. Contact of the second absorber with the ground allows to control angle of rotation φ_1 and corresponding angular acceleration $\ddot{\varphi}_1$. Similarly as previously, the stage commences with identification of actual angle of rotation, angular velocity and calculation of constant value of torque M_1^{opt} and corresponding time period t_{opt}^{rot-1}. The above quantities allow to assume optimal strategy of controlling rotations φ_1 and accelerations $\ddot{\varphi}_1$. The values of optimal torques $M_{3/4}^1$ corresponding to rotation φ_1 can be computed independently from previously determined optimal values of torques $M_{3/4}^2$. The corresponding values of pressures in three absorbers can be determined from the following set of equations:

$$\left(p_1^{opt} - p_A\right)A_1 + \left(p_2^{opt} - p_A\right)A_2 + \left(p_3^{opt} - p_A\right)A_3 = F^{opt} \tag{6.2.59}$$

$$\left(p_1^{opt} - p_A\right)A_1 l_{1\_2} - \left[\left(p_2^{opt} - p_A\right)A_2 + \left(p_3^{opt} - p_A\right)A_3\right]l_{3\_2} = M_{3/4}^2$$

$$\left[\left(p_1^{opt} - p_A\right)A_1 + \left(p_2^{opt} - p_A\right)A_2\right]l_{2\_1} - \left(p_2^{opt} - p_A\right)A_2 l_{2\_1} = M_{3/4}^1$$

In the above equations where the quantity l_{n_m} indicates distance of the absorber number *n* from the rotation axis number *m*. Moreover, $M_{3/4}^1$ and $M_{3/4}^2$ indicate torques relative to axis 1 and 2, respectively, in subsequent stages of the landing process.

5. Absorbers 2, 1, 3 and 4 are in contact with the ground and strategy of maintaining appropriate values of torques is continued. Contact of absorber 4 with the ground causes that required values of torques can be obtained with various combinations of forces in particular absorbers. Therefore, the redundant absorber allows to avoid infeasible situation when required value of pressure in one of the absorbers drops below the level of ambient pressure. Finally, at the end of the landing process, when vertical velocity of the object and both rotational velocities are diminished to zero and the platform is located in parallel to the ground, pressures in each absorber are reduced to provide conditions of static equilibrium.

Presented strategy of adaptation based on direct control of pressure inside pneumatic absorbers should be treated as an initial step before developing adaptation strategy based on changing the resistance coefficients of valves located in each absorber. The delays in changes of pressure and delays in changes of torques are expected to enforce application of simplified adaptation schemes, similarly as it occurred in case of 2D system.

Three-dimensional full UPM model

Finally, as a last stage of the research, the most complex three-dimensional 'full UPM' model of the landing object was developed. The model is composed of compliant (not totally rigid) platform with uniform weight distribution and emergency airbags attached below. Two design options of emergency landing system were considered: simple system with a single cylindrical airbag covering the whole bottom surface of the landing platform and a more complex system comprising four airbags located at its corners, Fig. 6.2.37 a,b.

In both considered cases the platform has dimensions 2m x 4m and mass of 6240kg and it is modelled by shell elements of thickness 0,1m. The airbags are modelled by membrane elements of thickness 0,001m and isotropic elastic material with the Young modulus equal to 4GPa. Assumed properties of the airbags provide that maximal stress in airbag fabric during landing does not exceed allowable tensile strength for typical airbag fabrics (~100MPa). The simulation of landing is conducted by using contact conditions defined between the airbags and the ground, and between airbags and a landing platform.

One of the important features of the proposed model is that centre of inertia of the platform is located relatively low in comparison to real landing object (e.g. helicopter). Since location of the centre of inertia strongly influences rotation of the object during landing, the global response of the platform and helicopter may vary substantially. Moreover, in case of non-zero horizontal velocity, the landing scenario is strongly influenced by friction forces between the airbags and the ground which in real situation depend on landing terrain, while in numerical analysis has to be assumed arbitrarily. Therefore, presented simulations should be treated as idealised test examples and with the awareness of the discrepancies in response which may result from the landing object and the ground type.

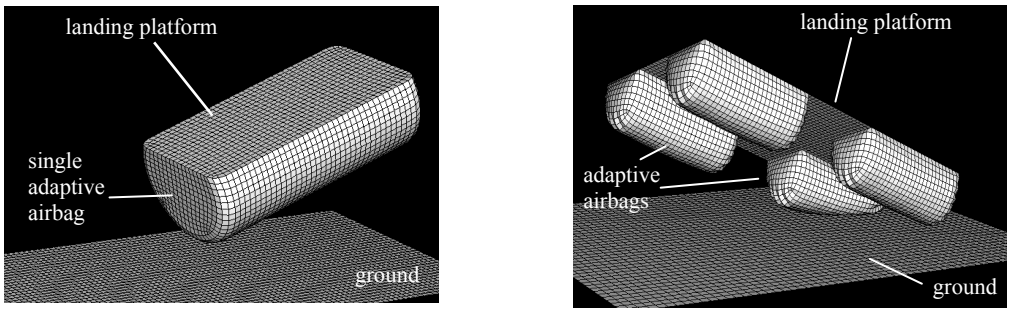

Fig. 6.2.37 Three-dimensional model of emergency landing: a) single adaptive airbag, b) system composed of four adaptive airbags located in the corners of the landing platform.

The goal of applying the control strategy was to provide possibly smooth landing conditions, i.e. to avoid direct contact of the platform with the ground with a large velocity and, at the same time, to prevent its strong rebound or rotation during landing. In an optimal situation, the above objectives are obtained with the use of the whole stroke of an airbag and with possibly low value of the pneumatic force. The secondary, minor goal of adaptation was to avoid small bouncing and rotations of the plate during the final stage of landing which are typical features of landing with large horizontal velocities and small friction forces. In general, the mentioned objectives can be considered as the stabilisation of the object during landing. At this stage, the objective function was not formulated mathematically (e.g. as a mean

measure of vertical and angular acceleration or final velocity after rebounds) but instead the response of the system was observed qualitatively.

The simulation of the emergency landing of the platform equipped with a single airbag was conducted for three scenarios involving zero horizontal velocity and non-zero initial rotation angles in both direction, see Fig. 6.2.38. Although the system is characterised by large airbag volume and large area of contact with the ground, it offers limited possibilities of adaptation to various landing conditions since only one value of pressure can be controlled. For each landing scenario two adaptation strategies were tested: i) semi-active strategy where initial pressure and constant valve opening were adjusted and ii) real-time strategy where pressure inside airbag was maintained on a constant level during major part of the landing period (pressure level and time instant of final pressure release were adjusted).

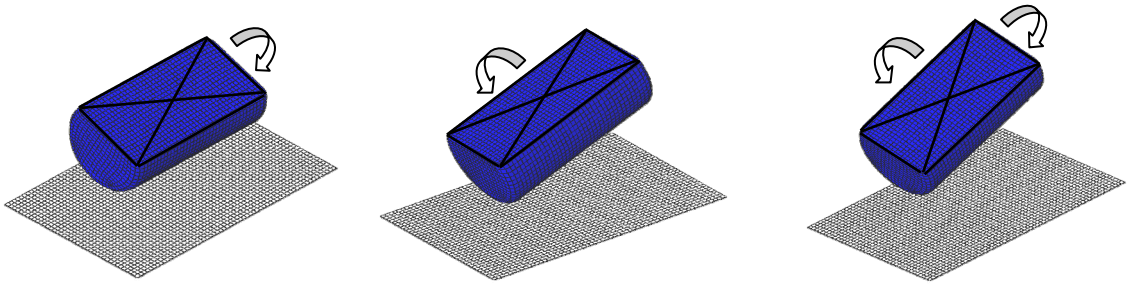

Fig. 6.2.38. Analysed landing scenarios: a) lateral inclination, b) longitudinal inclination of the platform, c) both-directional inclination.

The conducted simulations indicate that properly tuned parameters of a single airbag system provide desired response only for initial horizontal position of the platform, Fig. 6.2.39a, and for small initial inclination angles. In case of landing with lateral inclination, proper adaptation strategy also leads to acceptable response of the system. However, in case when landing platform was rotated longitudinally (Fig. 6.2.39b) or both-directionally, none of tested adaptation strategies assured satisfactory smooth process of the landing.

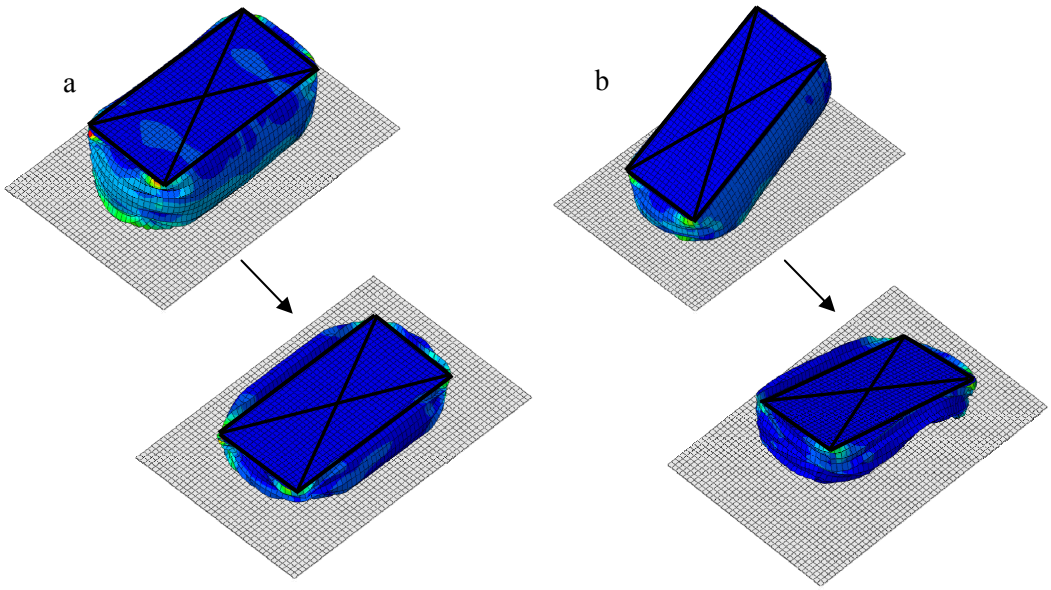

Fig. 6.2.39. Emergency landing with a single airbag: a) desired response in case of initial horizontal position of the platform, b) adverse response with partial rebound in case of initial longitudinal rotation of the platform.

High pressure which is required to avoid collision of the bottom edge/corner with the ground causes large torque and rotation of the plate during the second stage of the process. As a result, either front or rear part of the plate bounces from the ground. The example confirms that optimal adaptation to diverse landing conditions requires non-uniform distribution of supporting forces in different parts of the plate (cf. part of this section concerning 3D 'reduced UPM' model) which can not be realised by means of a single airbag.

The simulations were also conducted for the case of non-zero initial horizontal velocity of the landing object. Both longitudinal and lateral components of velocity were imposed. In such a landing scenario, especially the one with lateral velocity, the landing object appeared to be more unstable due to the action of friction forces causing platform rotation. As a result, development of control strategies providing acceptable response of the system was difficult or even impossible, which proves the necessity of applying the system equipped with four airbags which ensures better adaptation capabilities.

The system equipped with four airbags located in the corners of the plate was tested primarily for the landing scenarios for which single airbag did not provide appropriate response , i.e. the scenarios with longitudinal and both-directional initial rotation angles (with and without horizontal velocity), cf. Fig. 6.2.40.

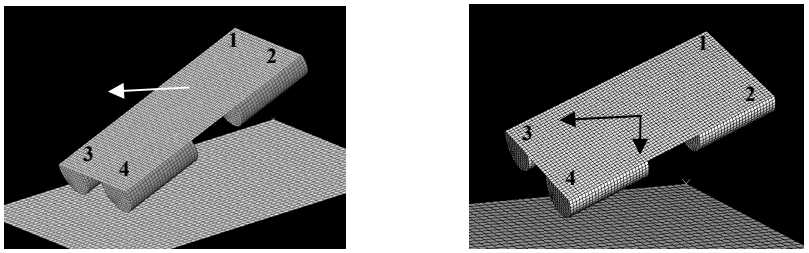

Fig.6.2.40. Considered landing scenarios

Initially heuristic adaptation strategies were developed for landing scenarios with zero horizontal velocities. Further, some of these strategies were tuned to the situation when the landing object has also vertical velocity. For each of landing scenario two types of adaptation strategies were developed:

- semi-active strategy based on adjustment of initial pressure, time instant of valve activation and constant opening of the valve in each airbag,
- real-time adaptation strategy based on adjustment of constant value of pressure inside each airbag and time instant when final reduction of pressure begins.

In case of initial longitudinal rotation of the landing object, heuristic semi-active strategy of adaptation comprises the following steps:

1. strong initial inflation of the frontal airbags 3 and 4 with initial pressure which prevents direct collision of the plate and the ground,
2. opening of the valves in airbags 3 and 4 at time instant when vertical movement of the front platform edge is nearly stopped (valve opening adjusted to minimise rebound of the front part of the platform in the following stages of landing),
3. inflation of the rear airbags 1 and 2 with pressure adjusted to vertical velocity of the rear part of the landing object which results from both initial vertical velocity and rotation caused by contact of the frontal airbags with the ground,

4. adjustment of constant valve opening which provides full compression of both rear airbags.

The above strategy utilises the fact that airbags located in front and rear part of the platform are used almost independently, i.e. during the first stage of the process only frontal airbags are employed while during the second stage of landing only rear airbags are utilised Fig. 6.2.41. The strategy of adaptation of the rear airbags is influenced by the strategy of adaptation of the front airbags, however, it can be developed independently during the second stage of impact. The coadjuvancy of the front and rear airbags takes place at the final stage of the process.

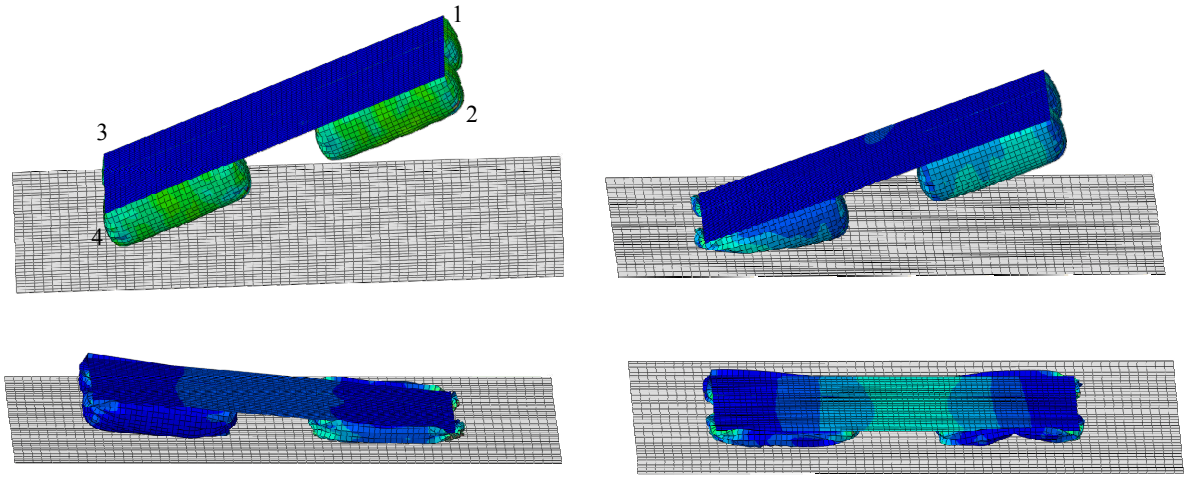

Fig. 6.2.41. Simulation of the emergency landing with four airbags and initial longitudinal rotation: a) the landing scenario, b) the first stage of landing , c) the second stage of landing, d) landing accomplished.

The semi-active strategy of adaptation can be relatively easily applied in case of initial lateral rotation of the landing platform. The main difference is that not front and rear, but left and right airbags are sequentially adapted (inflated and deflated by applying constant valve opening). Moreover, due to smaller inertia of the platform in the lateral direction and smaller offset between airbags and platform centre, the rotation of the system occurs when left airbags (3 and 1) are already in contact with the ground and the whole process occurs more smoothly.

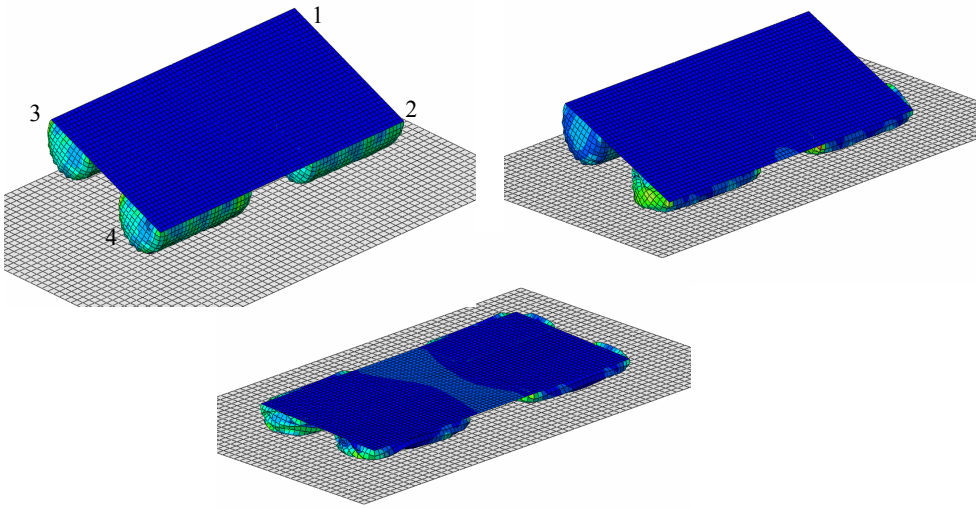

Fig. 6.2.42. Simulation of the emergency landing with initial lateral rotation: a) the first stage of landing, b) intermediate stage of landing, c) landing accomplished with full airbags compression

In case of two-directional initial rotation of the landing platform, the application of the semi-active adaptation strategy also results in acceptable landing process without direct contact of the plate with the ground and almost with no rebound. However, obtaining optimal course of landing requires very precise adjustment of pressure in particular airbags during the subsequent stages of the process. Therefore, for the landing scenario with initial rotations in two directions the heuristic real-time control strategy was developed. The strategy is composed of the following steps (Fig. 6.2.43, 6.2.44):

1. strong initial inflation of the 'airbag 4' which contacts the ground as a first one (inflation pressure adjusted to prevent direct contact of the adjacent corner of the plate with the ground), weaker inflation of the adjacent 'airbag 3';
2. reduction of pressure in 'airbag 4' at time instant when vertical velocity of the neighbouring corner of the plate is almost reduced to zero;
3. strong inflation of the 'airbag 1' (which approaches the ground with larger velocity due to strong diagonal rotation of the platform) adjusted to its actual vertical velocity; weaker inflation of the adjacent 'airbag 2';
4. reduction of pressure in 'airbag 3' when velocity of the neighbouring corner approaches zero;
5. simultaneous reduction of pressure in 'airbag 1' and 'airbag 2' to the level required for static equilibrium of the platform.

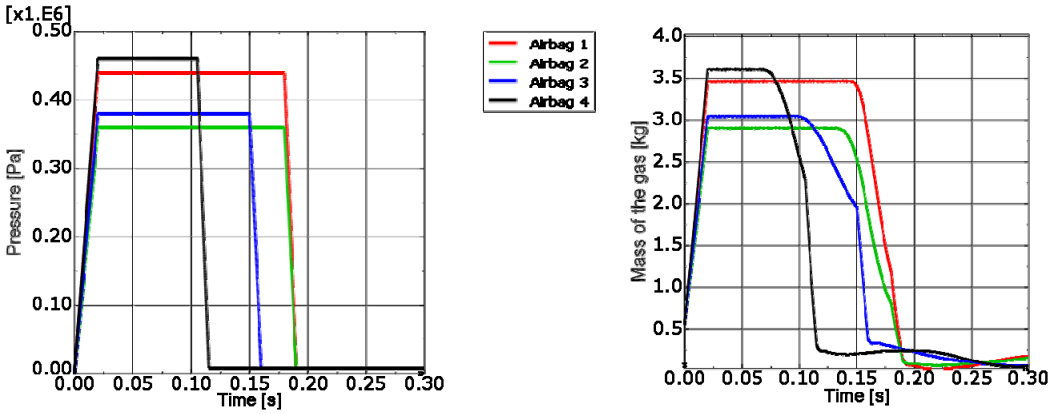

Fig. 6.2.43 Adaptation of the system for the landing with initial two-directional rotation: a) applied change of pressure in each airbag, b) corresponding mass of gas

The numerical simulation was performed for the landing object comprised of a totally rigid (not deformable) platform. The development of the adaptation strategy for the rigid platform is easier than for deformable one since a rigid plate does not gather elastic energy which often magnifies landing object rebound. The applied optimal change of pressure in each airbag together with corresponding change of gas mass inside each airbag are presented in Fig. 6.2.43a and Fig. 6.2.43b, respectively, while the corresponding main stages of the landing process are depicted in Fig. 6.2.44. Proposed adaptation strategy results in desired, smooth process of landing without direct contact of the plate with the ground, but with almost full compression of all airbags and total mitigation of rebound.

The comparison between the semi-active and active (real-time) adaptation strategies reveals that although the semi-active adaptation does not usually provide fully optimal

response of the system, it appears to be relatively robust, i.e. it works properly when landing scenario or the values of adjusted parameters (initial pressure and valve opening) are slightly modified. By contrast, the real-time adaptation has to be very precisely tuned to actual landing scenario. Slight change of the landing conditions or change of the parameters of the adaptation strategy often leads to a significant adverse change of the whole process of landing. Therefore, the choice of a proper adaptation strategy depends on particular landing conditions, on the precision of their identification and the possibilities of precise realisation of the control strategy.

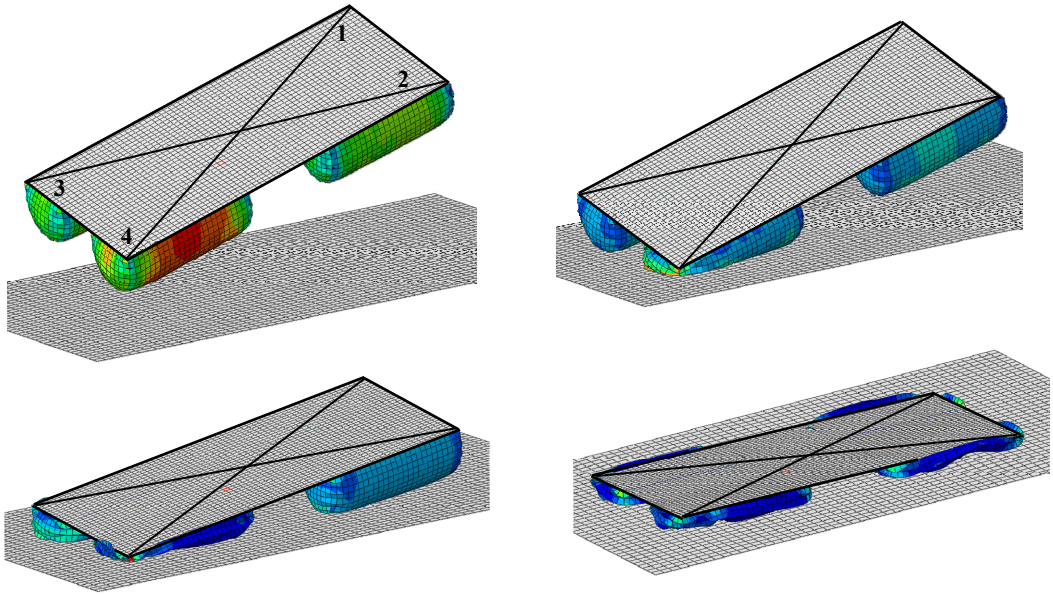

Fig. 6.2.44. Simulation of the emergency landing with four airbags and longitudinal inclination: a) initial stage of landing, b,c) intermediate stage of landing, d) final stage of landing.

The next steps of the adaptation involve optimisation-based tuning of the heuristic strategy aimed at:

- obtaining minimal value of a certain objective function(s), typically: linear or angular accelerations in certain points of the plate, rebound velocity or maximal stresses in certain locations of the plate;
- altering generic heuristic strategy in order to take into account the elastic/plastic deformation of the platform deck,
- altering the heuristic strategy in order to account for friction forces arising as a result of horizontal movement of the landing object during a touch-down.

The above methodology of tuning the initially assumed heuristic strategy is justified when the additional conditions do not significantly change the process of landing, i.e. when the influence of the plate compliance and influence of friction force between airbags and the ground are relatively small. Otherwise, the generic heuristic strategy of adaptation, which originally takes into account all system properties and landing conditions, should be elaborated.

Although the proposed strategies do not provide a totally optimal response of the adaptive landing system, they significantly improve overall process of emergency landing and may substantially contribute to increase of safety of the passengers.

Summary of Section 6.2

The section introduces the concept of adaptive 'flow control - based' airbags and analyzes their application for enhancement of the emergency landing of flying or falling objects. Basic simulations of the landing process are conducted and development of the control strategies for various landing objects and landing conditions is thoroughly discussed.

In the introductory part, two models of an object equipped with a single adaptive airbag are developed: 'reduced UPM' model based on analytical description of airbag deformation and 'full UPM' model based on FEM modelling of airbag deformation. Both models include changing area of contact between airbag and the ground, fabric leakage and the controllable valve. The 'reduced UPM' model is proved to provide adequately precise dynamic response with smaller corresponding numerical cost. For both models the strategies of real-time control of the valve opening aimed at minimisation of generated force and minimisation of internal pressure are elaborated.

The following part of the section concerns 2D model of adaptive landing platform equipped with two adaptive airbags. The proposed adaptation strategy is aimed at common minimisation of vertical and angular acceleration with additional conditions enforcing desired final configuration of the structure. Corresponding numerical simulations reveal that realisation of the above strategies is possible, however it requires nontrivial multi-stage change of valves openings. The analysis of 2D systems equipped with two airbags is continued for the compliant landing objects composed of beams and point masses. For these objects heuristic control strategies are applied and further precisely tuned to achieve optimal reduction of dynamic response. It is shown that the system with advanced real-time control strategy outperforms systems without or with basic pressure control.

In the last section 3D model of the emergency landing of the platform equipped with adaptive airbags is analyzed. Initially the problem is considered with reduced UPM model for which semi-active and active adaptation aimed at minimisation of accelerations is proposed. In turn, full UPM model is used to present effectiveness of heuristic control strategies which provide soft process of landing and rebound mitigation for various initial inclination angles.

Presented consideration and numerical examples confirm that adaptive airbags equipped with controllable valves can be effectively used to improve safety of emergency landing. The use of adaptive airbags allows to adjust the system to initial conditions and to provide smooth scenario of the landing with optimal mitigation of accelerations and rebound, which is unattainable by the classical passive airbags.

CHAPTER 7 - CONTROLLABLE HIGH PERFORMANCE VALVES

The chapter describes two types of high performance valves which can be used to control release of gas from Adaptive Inflatable Structures: piezoelectric valve and self-closing membrane valve. The first type of valve utilises controlled unidirectional movement of the valve head with the use of piezoelectric stack, while the second one exploits controlled expansion of the membrane evoked by pressure of the flowing gas. The main goal of this chapter is to develop various methodologies for modelling of two above types of valves and to propose algorithms aimed at controlling rate of the gas through these valves.

Modelling of the controllable valves requires precise simulation of the fluid flow and its interaction with movement or deformation of the solid part of the valve. Consequently, precise distribution of gas velocity, gas pressure and resulting forces exerted on the mechanical parts of the valve have to be determined. This goal can not be obtained by using Uniform Pressure Method, but instead it requires solving coupled problem of fluid and solid mechanics. Additionally, the proposed numerical model has to contain a mechanism providing controllability of the analysed valve. It can be realized in straightforward way by introducing functional material, e.g. with piezoelectric properties or, alternatively, by implementation of analytical model of controllable part of the valve. The developed control algorithms are relatively simple due to the complexity of the considered models, however, they provide basic insight on possibilities and range of controllability of the analysed valves.

The problem of modelling and simulation of the valve flow is considered in the literature mainly in the context of mechanical engineering and biomechanical devices. A typical mechanical problem is modelling of the flow through the valve during exhaust stroke of the internal combustion engine. In such a case, the movement of the piston and the valves is typically predefined and the problem solved can be simplified to a purely CFD problem with changing geometry of the fluid domain [311 312]. Modelling of other types of valves such as butterfly valves or tilting-disc valves require interaction of the fluid flow with rotation of the rigid body [313]. In turn, modelling of typical suction and discharge valves in linear compressors used for instance in refrigerators requires FSI models to handle interaction of the deforming parts of the valve and the fluid flow [314]. Both of the above types of problems can be approached with moving and fixed grid methods, with monolithic and partitioned coupling schemes. Practical applications of CFD simulations of the valve flow include investigation of the characteristics of control valves and improvement of their design e.g. by reduction of aeration or cavitations effects [315]. Another example is the application of the simplified fluid-solid analysis to optimise disc-spring valve system in a shock absorber [268]. Regarding biomechanical applications, the most well known problem is modelling of the flow of blood through bileaflet mechanical heart valves in order to optimise blood flow patterns. A detailed review of state of the art numerical methods developed for this problem is presented in [316].

7.1. Piezoelectric valves

Piezoelectric valves are based on actuators which utilise an inverse piezoelectric effect, i.e. deformation of the material caused by applied electric field [48]. Such valves are applied in

devices where high precision and operating speeds are required, for instance in diesel engines to control injection of the fuel. The piezoelectric valves analysed in this section utilise the piezoelectric stack which is constructed as a pile of piezoelectric plates separated by the electrodes. This type of actuator utilises the so-called 'd33 effect', i.e. deformation in the direction parallel to the direction of applied electric field. The main feature of the considered piezoelectric valves is high operating speed (up to ~1000Hz) contradicted to a relatively small poppet displacement (up to ~1mm) depending on type and size of the piezoelectric stack [317].

The problem of modelling of the piezoelectric valves is approached by both analytical and numerical methods. Simple fully analytical model of a piezoelectric valve coupling poppet displacement with applied electric excitation and pressure difference is described in [318]. In turn, the authors of [240] utilise FSI approach (ALE method) to model the flow developed inside damper controlled by piezoelectric valve. New design concepts and applications of fast piezoelectric hydraulic valves are presented in paper [319].

7.1.1 Construction of the piezoelectric valves

Two examples of valves based on piezoelectric stacks are the following: i) the valve equipped with mechanical displacement amplifier [317 241 245] (Fig. 7.1.1) and ii) the valve without amplifier with straightforward operating principle (Fig. 7.1.2). In the second case, a small displacement of the valve head can be compensated for instance by its special design providing large mass flow rate of gas [246]. Both valves are designed in a way that they remain closed when electric voltage is not applied to the piezoelectric stack. The main external parameters which influence the response of the valves are:

- initial force pressing the valve head to the wall of the pressure tank which provides initial air-tightness of the valve,
- stiffness of the pre-stressing device (displacement amplifier or elastic spring) which determines resistance force generated during valve head displacement,
- pre-stress of the piezoelectric stack which provides that the stack is not tensioned when voltage is applied.

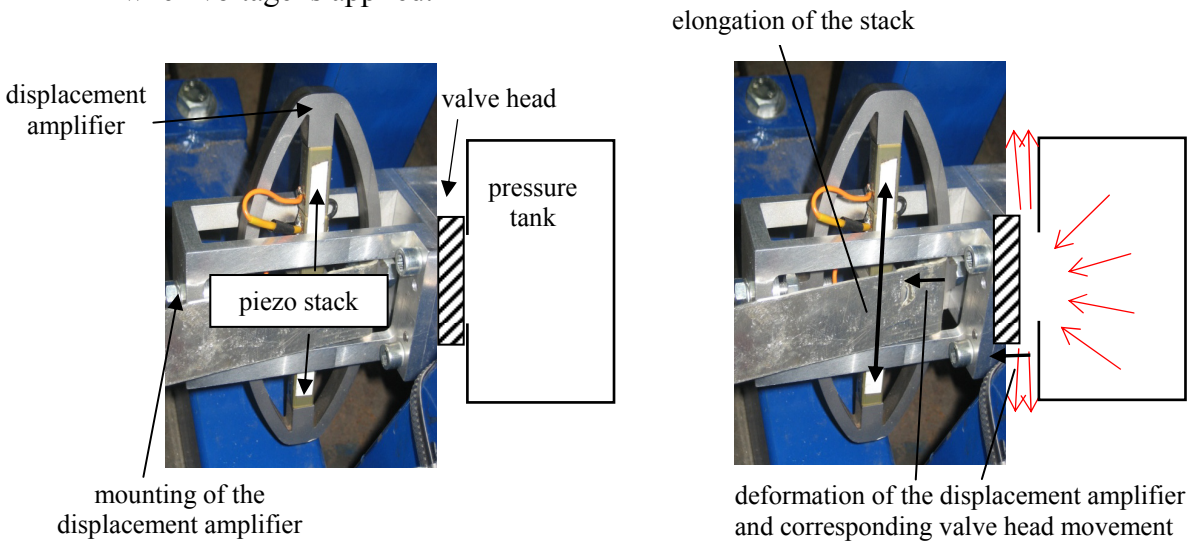

Fig.7.1.1. Operating principle of the valve with displacement amplifier: a) valve closed, b) activation of the piezoelectric stack which causes displacement of the valve head and valve opening.

The valve with the amplifier is typically located outside the pressure chamber due to its large dimensions (Fig. 7.1.1a). When the piezoelectric stack is activated it expands and the whole displacement amplifier elongates in vertical direction and shortens in the horizontal one. As a result, the valve head recoils from wall of the tank allowing for the fluid outflow, Fig. 7.1.1b. The valve with amplifier is characterised by increased displacement of the valve head but also longer response times resulting from large dimensions and total mass.

In the second type of the piezoelectric valve, the movement of the valve head is driven directly by the piezoelectric stack without any amplification. When piezoelectric stack is activated, it elongates and acting against the pre-stressed spring shifts the valve head from the wall of the tank. In two basic configurations of the system the valve head is moved outside or towards the pressure tank, Fig.7.1.2. In the first configuration (Fig. 7.1.2a), pressure of the fluid inside the tank contributes to the process of valve opening. Consequently, the pre-stress of the external elastic spring has to be relatively large in order to provide air-tightness of the valve in initial closed position and the possibility of closing the valve when piezoelectric stack is deactivated. By contrast, in the second configuration (Fig. 7.1.2a) the pressure of the fluid contributes to the process of valve closing and thus the required pre-stress of the external elastic spring can be smaller.

In both considered cases the elastic spring can be located at the same side of the valve head as the piezo-stack without causing a significant influence on behaviour of the system (the only difference is that the spring has to be initially elongated not contracted). The valve without displacement amplifier has simpler construction and smaller mass which results in shorter response times but, on the other hand, a smaller displacement of the valve head.

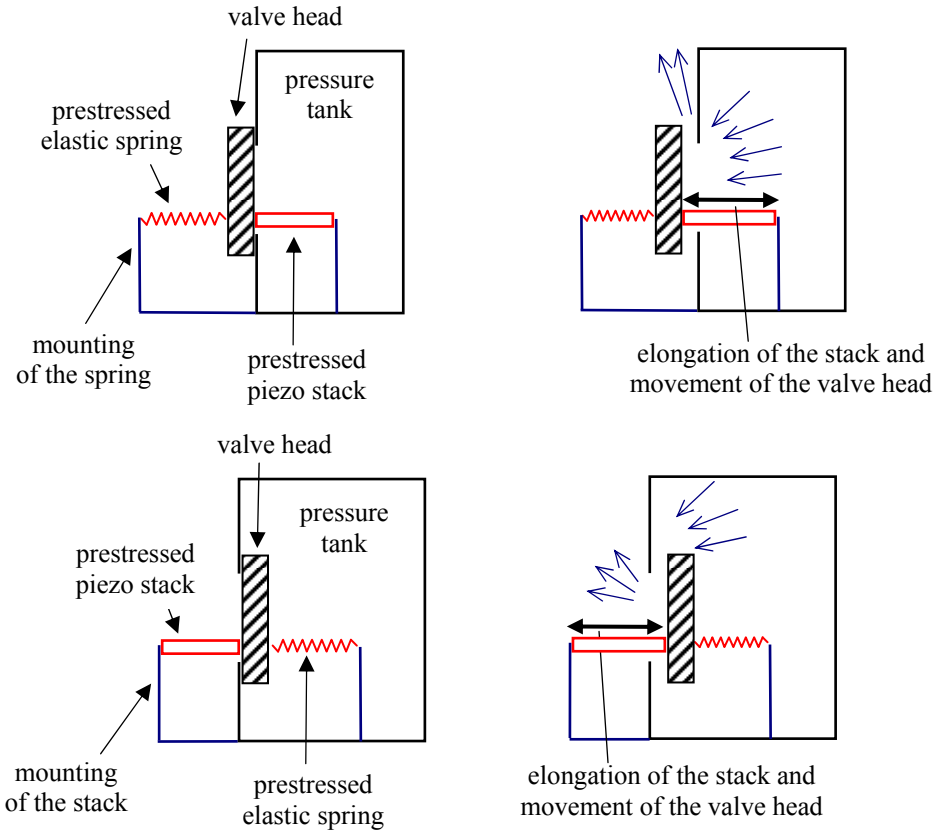

Fig.7.1.2. Operating principle of two types of the valves driven directly by piezoelectric stacks

7.1.2. Coupled analysis of piezoelectric valves

The core of the simulation of the flow through controllable valve is the solution of the fluid mechanics problem and therefore it has to be incorporated into each modelling method. Solid part of the problem and its coupling with the fluid part can be approached in various ways by precise and simplified methods. Three proposed procedures for simulation of the flow through piezoelectric valve are the following:

1. separation of the piezoelectric problem and fluid mechanics problem with pre-calculated displacement of the valve head - 'decomposition method',
2. solution of the fluid mechanics problem with analytical description of the mechanics of the piezoelectric stack - 'semi-analytical method',
3. full coupling of the fluid mechanics problem and piezoelectric problem (being itself coupling of the solid mechanics and electricity) - 'fully coupled method'.

'Decomposition method'

The simplest of the proposed methods, the 'decomposition method', separates the problem of modelling deformation of the piezoelectric stack and valve head movement from the problem of modelling fluid flow through controllable piezoelectric valve. The procedure of numerical analysis consists of two basic steps:

- computation of the response of the valve head to applied electric excitation conducted with the use of mechanical and electrical properties of the piezoelectric stack, mass of the valve head, value of initial pre-stress of the external spring and stiffness of this spring;
- steady-state or dynamic analysis of the flow through the valve conducted for previously determined extreme position of the valve head or for the whole time-history of the valve head movement.

In the above procedure the dynamics of the valve head is determined without considering forces generated by the flowing fluid. Therefore, the proposed method is precise only when displacement of the piezoelectric stack does not depend on forces exerted by the flow of the fluid, i.e. when piezoelectric stack has relatively large operating power. The method completely neglects 'force coupling' of piezoelectric and fluid problems. It accounts for 'displacement coupling' which, however, should be treated as approximate due to a disregard of the force coupling. In other words, the above method provides 'one-way coupling': valve head displacement affects flow of the fluid but not vice-versa.

Let us further consider the simple design of the piezoelectric valve where the valve head is moved directly by the piezoelectric stack and mechanical amplifier is not applied. The piezoelectric part of the model consists of piezoelectric stack (a pile of piezoelectric plates separated by the electrodes, Fig. 7.1.3a (bottom) which is clamped on the right side, the elastic spring and rigid object (the valve head) located between them, Fig. 7.1.3b (top). The fluid part of the model consists of a fluid domain of an arbitrary size and located inside moving void region, which models the valve head, Fig. 7.1.3b.

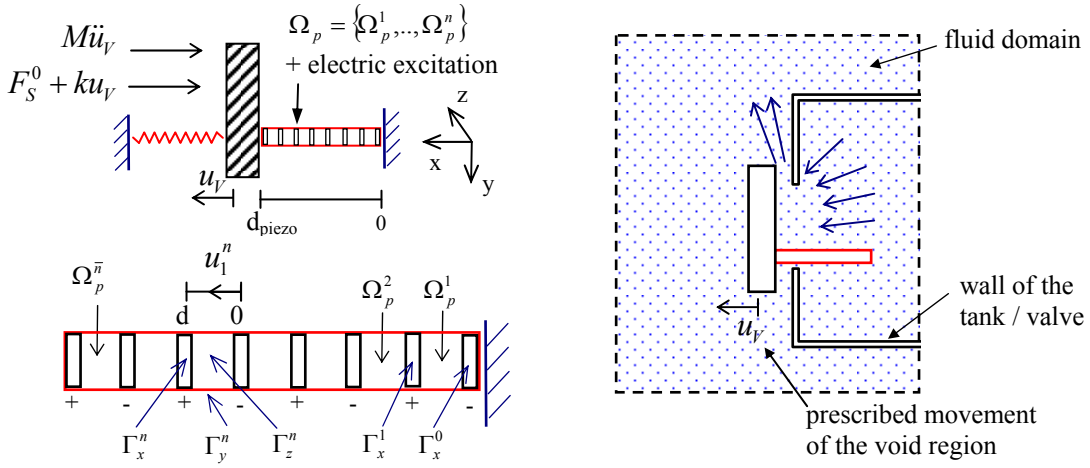

Fig.7.1.3. 'Decomposition method', decomposition of the problem considered into: a) piezoelectric part of the model (with zoom of the piezo-stack), b) fluid part of the model

The '<u>mechanical part</u>' of the piezoelectric system can be analysed under an assumption of small displacements and it is described by the classical equations of motion and kinematic relations:

$$\sigma_{ij,j} + f_i = \rho \ddot{u}_i\,, \qquad \varepsilon_{ij} = \tfrac{1}{2}(u_{i,j} + u_{j,i}) \tag{7.1.1}$$

where σ_{ij}, ε_{ij}, u_i, denote respectively stress, strain and displacement of the piezoelectric material; ρ is density of the piezoelectric material and f_i is vector of surface forces (here equal to zero). The electric part of the problem is described by the Gauss and Maxwell laws:

$$D_{i,i} - q = 0\,, \qquad E_i = -\varphi_{,i} \tag{7.1.2}$$

where D_i is electric displacement, q is electric charge, E_i is electric field vector and φ is electric field potential. Piezoelectric constitutive relations couple stress in the piezoelectric material σ_{ij} with electric field vector E_i and moreover, electric displacement D_i with stress in the piezoelectric material σ_{ij}:

$$\sigma_{ij} = c_{ijkl}\varepsilon_{kl} - e_{kij}E_k\,, \qquad D_k = e_{kij}\sigma_{ij} + \in_{ki} E_i \tag{7.1.3}$$

where c_{ijkl} is a fourth order tensor of the elastic material constants, e_{kij} is a third order tensor of piezoelectric constants and $\in_{ki}$ is a second order tensor of the dielectric constants. When combined, the above equations give full system of equations governing the piezoelectric problem with primary variables u_i and φ:

$$\begin{aligned} -\rho\ddot{u}_i + c_{ijkl}u_{k,lj} + e_{kij}\varphi_{,kj} + f_i = 0 \\ e_{kij}u_{i,kj} - \in_{kj} \varphi_{,kj} - q = 0 \end{aligned} \tag{7.1.4}$$

which has to be complemented with Dirichlet or Neumann boundary conditions for both solid and electric part:

$$\begin{aligned} u_i = \widetilde{u}_i \quad \text{or} \quad \sigma_{ij}n_j = \widetilde{F}_i\,; \\ \varphi = \widetilde{\varphi} \quad \text{or} \quad D_i n_i = -\widetilde{Q} \end{aligned} \tag{7.1.5}$$

where $\widetilde{F}_i$ are specified surface forces and $\widetilde{Q}$ are specified surface charges.

Since the piezoelectric stack is composed of separate piezoelectric plates, in the most straightforward approach the coupled system of piezoelectric equations can be formulated independently for each piezoelectric domain Ω_p^n separated by the electrodes Γ_x^{n-1} and Γ_x^n, Eq. 7.1.6a. The electrodes itself are not modelled as a separate regions (as being relatively thin) but they serve for applying electric boundary conditions and they constitute interfaces between the domains. Mechanical boundary conditions for the system (Eq. 7.1.6a, $\mathrm{BC_{mech}}$) involve zero longitudinal displacement of the right end of the stack and zero loading at free edges of the stack. Electric excitation of the stack is modelled by electric boundary conditions of Dirichlet type (voltages $\widetilde{\varphi}$) imposed to subsequent piezoelectric domains at the location of electrodes (Eq. 7.1.6a, $\mathrm{BC_{electric}}$). The coupling conditions (Eq. 7.1.6a, $\mathrm{CC_1}$) provide continuity of the mechanical quantities, i.e. displacements and stresses, between considered piezoelectric domains.

Moreover, coupling of motion of the valve head and motion of the piezoelectric stack has to be provided. The corresponding equilibrium equation involves inertia of the valve head $M\ddot{u}_V$, force generated by pre-stressed external spring $F_s^0 + k_s u_V$, delimiting force F_D resulting from contact with the tank wall and, finally, force generated by the piezoelectric stack. In turn, the equation of kinematic continuity couples displacement of the valve head with displacement of the left end of the piezoelectric stack and takes into account initial longitudinal displacement of the left end of the stack $\widetilde{u}_{01}^{\bar{n}}(d)$ resulting from its pre-stress, (Eq. 7.1.6a, $\mathrm{CC_2}$). The system of equations governing piezoelectric part of the problem reads:

$$-\rho\ddot{u}_i^n + c_{ijkl}u_{k,lj}^n + e_{kij}\varphi_{,kj}^n = 0 \quad \text{in} \quad \Omega_p^n,\ n = 1...\bar{n} \tag{7.1.6a}$$

$$e_{kij}u_{i,kj}^n - \in_{kj}\varphi_{,kj}^n = 0 \quad \text{in} \quad \Omega_p^n,\ n = 1...\bar{n}$$

$$\mathrm{BC_{mech.}}:\ u_1^1 = 0 \ \text{ on } \ \Gamma_x^0, \quad \sigma_{ij}^n n_j = 0 \ \text{ on } \ \Gamma_y^n \cup \Gamma_z^n \quad \text{for } \ n = 1...\bar{n}$$

$$\mathrm{BC_{electric}}:\ \varphi^n = \pm\widetilde{\varphi} \ \text{ on } \ \Gamma_x^{n-1} \cup \Gamma_x^n, \quad D_i n_i = 0 \ \text{ on } \ \Gamma_y^n \cup \Gamma_z^n \quad \text{for } \ n = 1...\bar{n}$$

$$\mathrm{CC_1}:\ u_i^n = u_i^{n+1}, \quad \sigma_{ij}^n n_j = \sigma_{ij}^{n+1} n_j \quad \text{on } \ \Gamma_x^n \quad \text{for } \ n = 1...\bar{n} - 1$$

$$\mathrm{CC_2}:\ M\ddot{u}_V + F_s^0 + k_s u_V = \int (\sigma_{11}^{\bar{n}})\mathrm{d}\Gamma_x^{\bar{n}} + F_D, \quad u_V = u_1^{\bar{n}}(d) - \widetilde{u}_{01}^{\bar{n}}(d)$$

In the above equations the upper indices n denote subsequent piezoelectric domains or electrodes of the stack. In coupling conditions, the scalar values σ_{11} and u_1 indicate stress component and displacement in the longitudinal direction of the piezoelectric stack. The initial conditions for the system correspond to the situation when the valve remains closed:

$$\mathrm{IC}:\ u_i^n(0) = \widetilde{u}_{0i}^n, \ \ v_i^n(0) = 0 \quad \text{for } \ n = 1...\bar{n} \tag{7.1.6b}$$

$$\varphi^n(0) = \widetilde{\varphi}_0^n \quad \text{for } \ n = 1...\bar{n}$$

$$u_V(0) = 0, \ \ v_V(0) = 0$$

The pre-stress of the elastic spring (defined by force F_S^0) and pre-stress of the piezoelectric stack (defined by initial negative displacement $\widetilde{u}_0^n$) are arbitrary. However, pre-stress of the elastic spring has to provide air-tightness of the valve in situation when piezoelectric stack is not excited.

In a simplified model of the piezoelectric system, only the longitudinal deformation of the piezoelectric stack is considered since this phenomenon is dominant and accounts for displacement of the valve head. Simultaneously, the equations governing electrical part of the problem can be reduced to a single dimension due to approximately uniform distribution of the electric field inside each piezoelectric domain. One-dimensional counterpart of the piezoelectric constitutive relations (Eq. 7.1.3) can be expressed in the form:

$$\sigma = \widetilde{E}\varepsilon - eE\,, \quad D = e\sigma + \in E \tag{7.1.7a}$$

where all introduced quantities are 1D equivalents of the corresponding quantities in Eq. 7.1.3. In particular, $\widetilde{E}$ is a Young modulus of the piezoelectric material. Classical equations of piezoelectricity (7.1.4) can be simplified into equations governing longitudinal deformation of the piezoelectric stack and longitudinal propagation of the electric field potential:

$$-\rho\frac{d^2u}{dt^2} + \widetilde{E}\frac{d^2u}{dx^2} + e\frac{d^2\varphi}{dx^2} = 0 \quad \text{in} \quad \Omega_p^n \tag{7.1.7b}$$

$$e\frac{d^2u}{dx^2} - \in\frac{d^2\varphi}{dx^2} = 0 \quad \text{in} \quad \Omega_p^n$$

The above equations have to be applied for all piezoelectric domains of the considered piezoelectric stack. Boundary, coupling and initial conditions for the system are basically similar as in Eq. 7.1.6, however, reduction of the system dimensionality has to be taken into account.

The next step of simplification of the piezoelectric stack modelling is a disregard of the inertia of the piezoelectric material. Under such an assumption the system of governing equations simplifies to the form:

$$\widetilde{E}\frac{d^2u}{dx^2} + e\frac{d^2\varphi}{dx^2} = 0 \quad \text{in } \Omega_p^n \tag{7.1.8}$$

$$e\frac{d^2u}{dx^2} - \in\frac{d^2\varphi}{dx^2} = 0 \quad \text{in } \Omega_p^n$$

which indicates that both electric field E and strain ε are constant in each piezo-electric plate comprising the stack. When voltage excitation is applied, the electric field does not depend on deformation of the considered piezoelectric plate and it is uniform along the stack. Therefore, the stack does not have to be divided into separate piezoelectric domains but instead it can be considered as a whole. According to constitutive relation (7.1.7a) the force F_p generated by piezoelectric stack can be expressed as follows:

$$F_p(u_V, \Delta\varphi) = -(\widetilde{E}A\varepsilon - eAE) = -k_p(u_V + \widetilde{u}_0(l)) + \frac{eA}{l}\Delta\varphi = -k_p u_V + F_p^0 + k_p e E^{-1}\Delta\varphi \tag{7.1.9}$$

where k_p denotes longitudinal stiffness of the piezoelectric stack and F_p^0 denotes initial pre-stressing force. Finally, the mathematical description of the considered system comprising the valve head, piezoelectric stack and the spring simplifies to single ordinary differential equation:

$$M\ddot{u}_V + F_s^0 + k_s u_V = F_p(u_V, \Delta\varphi) + F_D \tag{7.1.10}$$

In the other simplified approach to modelling of the piezoelectric stack (the so-called temperature analogy), the electric displacement D_i is assumed to be independent of stress σ_{ij} generated in piezoelectric material, i.e. the classical relation between electric displacement D_i and electric field vector E_i is assumed. The second constitutive relation for the piezoelectric material can be expressed in the form:

$$\sigma_{ij} = c_{ijkl}(\varepsilon_{kl} - \varepsilon_{kl}^T) = c_{ijkl}(\varepsilon_{kl} - \alpha_{kl}T) \tag{7.1.11}$$

$$\text{where:} \quad \varepsilon_{kl}^T = e_{mij}(c_{ijkl})^{-1}E_m = -e_{mij}(c_{ijkl})^{-1}\varphi_{,m} \ , \quad \alpha_{kl} = \varepsilon_{kl}^T / T \tag{7.1.12}$$

In the considered simplified approach the piezoelectric problem is governed by the following set of equations:

$$-\rho\ddot{u}_i + c_{ijkl}u_{k,lj} + e_{kij}\varphi_{,kj} + f_i = 0 \tag{7.1.13}$$

$$\in_{kj} \varphi_{,kj} - q = 0$$

According to Eq. 7.1.13b electric part of the problem can be solved independently of the mechanical part, while field potential φ and electric field vector E_i depend only on applied electric boundary conditions and distributed charge q. In case of piezoelectric stack, where each piezoelectric plate is subjected to similar voltage excitation, the electric field inside each piezoelectric domain is approximately the same and therefore the whole stack can be considered as a single piezoelectric domain with electrodes at its edges Γ_x^0 and Γ_x^1. The system of equations governing piezoelectric part of the problem reads:

$$-\rho\ddot{u}_i + c_{ijkl}u_{k,lj} + e_{kij}\varphi_{,kj} = 0 \ \text{ in } \Omega_p \tag{7.1.14a}$$

$$\in_{kj} \varphi_{,kj} = 0 \ \text{ in } \Omega_p$$

$$\text{BC}_{\text{mech.}}\text{: } u_1 = 0 \ \text{ on } \ \Gamma_x^0, \ \ \sigma_{ij}^n n_j = 0 \ \text{ on } \ \Gamma_y^n \cup \Gamma_z^n$$

$$\text{BC}_{\text{electric}}\text{: } \varphi = -\widetilde{\varphi} \ \text{ on } \ \Gamma_x^0, \quad \varphi = \widetilde{\varphi} \ \text{ on } \ \Gamma_x^1, \quad D_i n_i = 0 \ \text{ on } \ \Gamma_y^n \cup \Gamma_z^n$$

$$\text{CC: } M\ddot{u}_V + F_s^0 + k_s u_V = \int(\sigma_{11})\mathrm{d}\Gamma_x^1 + F_D, \quad u_V = u_1(d_{piezo}) - \widetilde{u}_{01}(d_{piezo})$$

The corresponding initial conditions for the system are the following:

$$\text{IC: } u_i(0) = \widetilde{u}_0 \ , \ \ v_i(x,0) = 0 \tag{7.1.14b}$$

$$\varphi(x,0) = \widetilde{\varphi}_0(x) \ , \ \ u_V(0) = 0 \ , \ \ v_V(0) = 0$$

When the governing equations are considered only in a single spatial dimension (along the axis of the piezoelectric stack) the constitutive relation takes the form:

$$\sigma = \widetilde{E}(\varepsilon - \varepsilon^T) = \widetilde{E}(\varepsilon - \alpha T) \tag{7.1.15a}$$

$$\varepsilon^T = -eE^{-1}\frac{d\varphi}{dx} \ ; \quad \alpha = \varepsilon^T / T$$

The solution of the equation governing electric part of the problem with zero distributed charge leads to a linear change of electric field potential and a constant value of electric field.

Therefore, the last term of the equation of equilibrium vanishes and the equilibrium of the stack is governed by a simple wave equation:

$$-\rho\frac{d^2u}{dt^2}+\widetilde{E}\frac{d^2u}{dx^2}=0 \quad \text{in} \quad \Omega_p \tag{7.1.15b}$$

and boundary, coupling and initial conditions are formulated in a similar way as in Eq. 7.1.14. In case when dynamics of the piezoelectric stack is neglected, strain and stress inside the piezoelectric stack are constant and force generated by the piezoelectric stack equals:

$$F_p(u_V,\Delta\varphi)=-\widetilde{E}A(\varepsilon-\varepsilon^T)=-k_p(u_V+\widetilde{u}_0(l))+\frac{Ae}{l}\Delta\varphi=-k_pu_V+F_p^0+k_peE^{-1}\Delta\varphi \tag{7.1.16}$$

which is fully to previously derived Eq. 7.1.9. Let us note that since the above model completely neglects inertia of the piezoelectric stack, its application in case of dynamic excitation of high frequency is limited.

The last method of modelling of piezoelectric stack is based on data provided by manufacturers of the stacks which involves plots of force generated by piezoelectric stack F_p in terms of relative displacement of its ends u^* and applied voltage U and which can be approximated by the formula:

$$F_p(U,u^*)=-\frac{F_{\max}}{u_{\max}}u^*+F_p^0+\frac{U}{U_{\max}}F_{\max} \tag{7.1.17}$$

In the above formula the force $F_{\max}$ is the so-called blocking force (maximal force generated by non-prestressed stack with fixed ends), and consequently $u_{\max}$ is maximal displacement which can be obtained by non-prestressed piezoelectric stack. The resemblance of the Eq. 7.1.17 and Eq. 7.1.16 proves the correctness of the proposed modelling methodology.

The '<u>fluid part</u>' of the numerical analysis of the piezoelectric valve is related to determination of the fluid flow and its dynamics caused by changes of the valve head position. The maximal mass flow rate through the valve can be computed by solving steady state CFD problem with maximal displacement of the valve head. In turn, the precise determination of changes of the flow pattern and mass flow rate of gas at outlet during opening or closing of the valve requires more complicated dynamical model which involves changing in time fluid domain with variable position of the valve head.

Since the methodology for determination of the displacement of the valve head caused by arbitrary excitation of the piezoelectric stack was developed in the previous step of the procedure, in the current step the valve head can be treated as rigid body arbitrarily moving inside fluid domain. Consequently, this part of the analysis of the piezoelectric valve can be reduced to a pure fluid mechanics problem which can be solved by the following approaches:

- Arbitrary Lagrangian Eulerian method where movement of the void region causes deformation of the surrounding fluid mesh,
- 'Immersed Solid' method where void region moves through fixed (Eulerian) back-ground fluid mesh (special case of Coupled Eulerian Lagrangian method, cf. Chapt.2)

The first approach can be treated as a problem of fluid flow through a domain with changing geometry, while the second one can be viewed as a problem of fluid flow through

the region with moving obstacle. Consequently, in both approaches various formulations of the boundary conditions can be applied. In ALE approach velocity of the mesh is set to velocity of the valve head $\hat{\mathbf{v}} = \dot{\mathbf{u}}_V$ and, moreover, either velocity of fluid in referential domain is set to zero $\mathbf{w} = \mathbf{0}$ or velocity of fluid in space is set to velocity of the valve head $\mathbf{v}_f = \dot{\mathbf{u}}_V$ and both these conditions are formulated at fluid-solid interface $\Gamma_{f/v-h}$. On the contrary, in the Immersed Solid method the second option is used ($\mathbf{v}_f = \dot{\mathbf{u}}_V$) and the condition is formulated at the boundary which changes (moves) in time $\Gamma_{f/v-h}(t)$. In both methods the conditions of equilibrium between fluid and the valve head are not considered, however forces exerted on the valve head can be calculated after the analysis in order to estimate the correctness of the applied method of simulation.

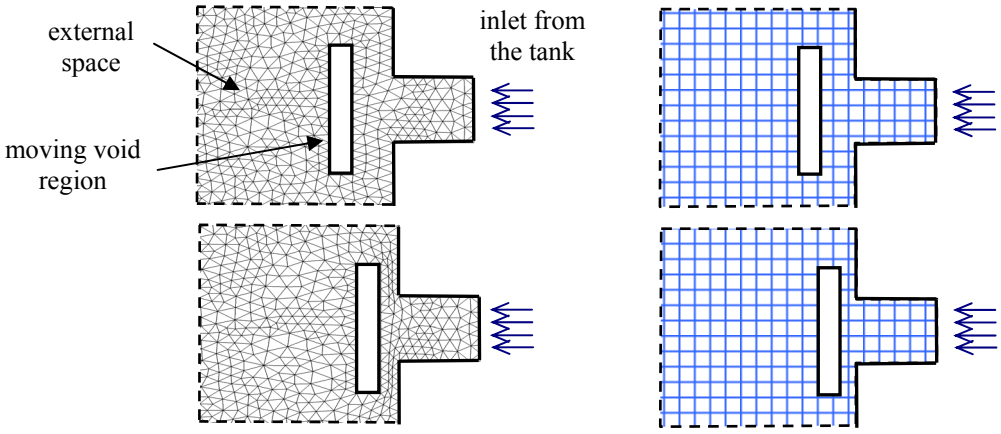

Fig.7.1.4. Comparison of two basic methods which can be used for analysis of the controllable valve: a) Arbitrary Lagrangian Eulerian method, b) Immersed Solid method

The accuracy of both methods strongly depends on the quality of the applied finite volume mesh. In case of ALE approach the valve head should be surrounded by a finer (usually hexagonal) mesh in order to capture the boundary layer. Similarly, in case of Immersed Solid method the mesh in the region of valve head movement should be appropriately fine in order to avoid leakages of the fluid to/through the void domain. Alternatively, special techniques aimed at refinement of the finite volume mesh around moving valve head should be applied. Further analyses of the controllable valve will be performed with the use of ALE method included in commercial CFD software ANSYS CFX.

The exemplary numerical simulation was performed for two-dimensional system where the gas enters and leaves the valve chamber by narrow channels and the inflow of the gas is controlled by position of the valve head (Fig. 7.1.5). The purpose of the analysis was to observe the dynamics of the valve, i.e. subsequent changes of the flow pattern and variation of the mass flow rate at outlet caused by a fast movement of the valve head. The numerical analysis comprises the following steps:

1. assumption of initial condition, pressure boundary conditions at inlet and outlet; conducting dynamic analysis until steady state of the system is obtained, Fig. 7.1.5a,
2. fast closing of the valve executed by moving the valve head in the direction of the wall (2 ms), Fig. 7.1.5b,
3. stopping the valve head in vicinity of the wall and continuation of the dynamic analysis in order to reach steady state of the system (50 ms), Fig. 7.1.5c,

4. fast opening of the valve by backward movement of the valve head (2ms), Fig. 7.1.5d,
5. stopping the valve head at the initial position; solution of the dynamic problem until steady state of the system is reached, Fig. 7.1.5e.

The conducted analysis shows that fast movement of the valve head causes immediate change of the flow pattern only locally (i.e. in the vicinity of inlet), and in other regions of the considered domain the flow remains almost unchanged (Fig.7.1.5a vs. b and Fig.7.1.5c vs. d). Change of the flow pattern in the whole domain occurs after substantial delay (here ~50 ms). The analysis is accomplished with the initial position of the valve head and the steady state of the system which clearly resembles the initial one.

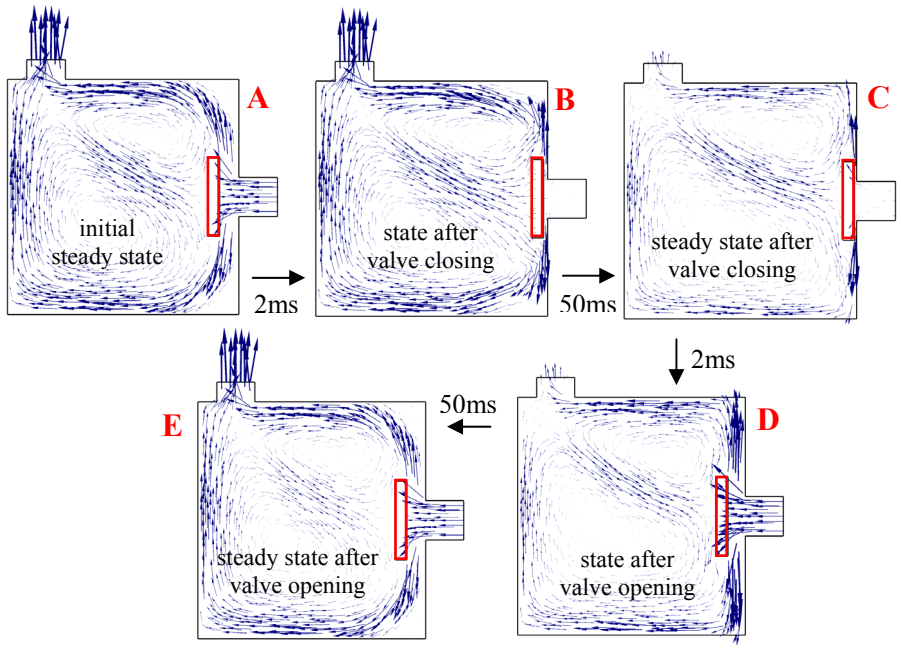

Fig.7.1.5. Change of the flow pattern caused by fast displacement of the valve head (geometric scale of the problem increased in comparison to typical piezoelectric valve)

Change of mass flow rate of gas at outlet during the whole analysis was compared against actual opening of the valve in Fig. 7.1.6. The time-shift between time instant when extreme position of the valve head is reached and time instant when extreme mass flow of gas is obtained, is clearly observable and it is longer in case of valve closing than in case of valve opening. Let us note that in real control system, the inertia of the valve head causes additional time-shift between application of the control signal and movement of the valve head.

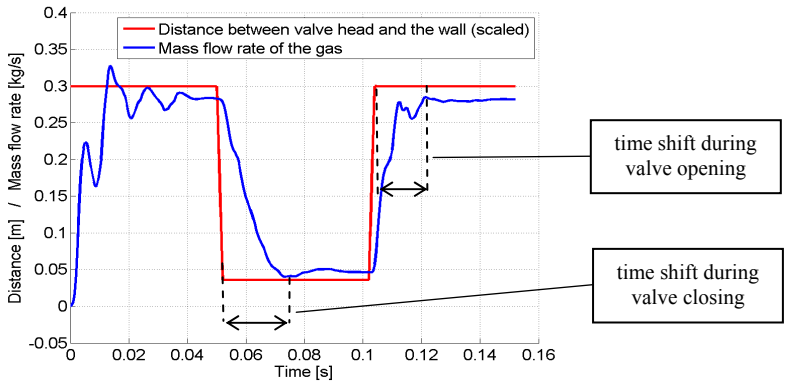

Fig.7.1.6. Change of mass flow rate at outflow caused by movement of the valve head.

The above simple example proves that in case of fast movement of the valve head (corresponding to high frequency of the applied control signal) solution of the dynamic problem with moving valve head can not be replaced by solutions of steady-state problems corresponding to a certain position of the valve head. Instead, the proposed two-step methodology based on preliminary determination of time-history of valve head displacement and further dynamic CFD analysis with changing in time fluid domain has to be applied.

'Semi-analytical method'

'Semi-analytical method' of modelling piezoelectric valve provides two-way coupling of simplified analytical model describing movement of the valve head and finite volume-based computational model of the fluid flow. In this approach, the forces exerted by the flowing fluid influence movement of the valve head which, in turn, changes the shape of the region where the fluid flow occurs.

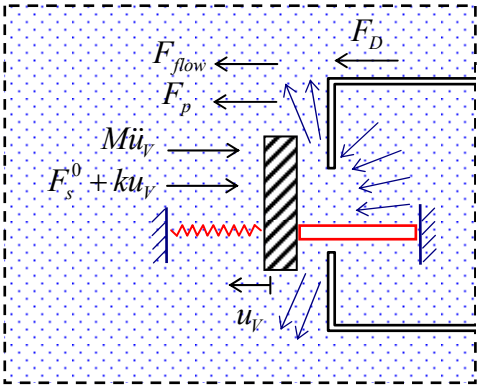

Fig.7.1.7. 'Semi-analytical method': single model of the system which provides two-way coupling of the analytical approximation of the piezoelectric problem and fluid dynamics problem.

Dynamics of the valve head is described by ordinary differential equation analogous to Eq. 7.1.10 which involves inertia of the valve head, force generated by external spring and force generated by piezoelectric stack which depends on applied excitation according to Eq. 7.1.9. The intrinsic difference is that equation of valve dynamics is complemented with the component F_{flow} denoting total force exerted on the valve head by the flowing fluid:

$$M\ddot{u}_V + F_s^0 + k_s u_V = F_p^0 + \frac{U}{U_{\max}} F_{\max} - \frac{F_{\max}}{u_{\max}} u_V + F_D + F_{flow} \tag{7.1.18}$$

The above equation can be applied not only to piezoelectric valves, but also to other types of controllable valves with various types of excitation. The force F_{flow} is determined from the solution of transient fluid mechanics problem in which movement of the internal void region (the valve head) results from solution of the Eq. 7.1.18. The fluid mechanics problem is approached by the ALE method and it is described in moving coordinate system whose deformation is arbitrary, however conforms with a movement of the valve head. Boundary conditions at the edges of the valve head assume no slip of the fluid, i.e. velocity of the fluid in deforming coordinate system equals zero at the edges of the void region.

The general procedure which has to be performed at every time step of the dynamical analysis involves the following steps:

- solution of the fluid dynamics problem and determination of forces exerted on the valve head by the flowing fluid,
- calculation of displacement of the valve head caused by applied external electric excitation, taking into account forces exerted by fluid (procedure based on discretised form of Eq. 7.1.18),
- shift of the valve head to a new, previously determined position and subsequent solution of the fluid dynamics problem.

The complete solution procedure was successfully implemented within ANSYS CFX by means of built-in programming language (CEL). The simple numerical example concerns the valve of geometry presented in Fig. 7.1.5. At the beginning of the analysis the valve head is located at the vicinity of the chamber wall, which in approximate way models the closed valve and the system is maintained in a steady state as in Fig. 7.1.5c. During the numerical analysis active element is subjected to excitation signal U of amplitude depicted in Fig. 7.1.8a. Three methods of the coupled analysis were implemented and compared (Fig. 7.1.8):

- assumption of the constant value of force exerted on the valve head by the fluid (equal to the value in the initial state),
- total neglecting of the fluid force acting on the valve head ('decomposition method'),
- coupling of the fluid flow and valve head displacement by means of 'semi-analytical method' described above.

The results of the analysis strongly depend on initial pre-stress of the spring and active element, stiffness of both elements and maximal excitation force that can be achieved. The above quantities were adjusted to provide equilibrium of the system in the initial state ($F_s^0 = F_{flow}^0$, $F_p^0 = F_D = 0$) and to observe qualitative effects of implemented two-way coupling.

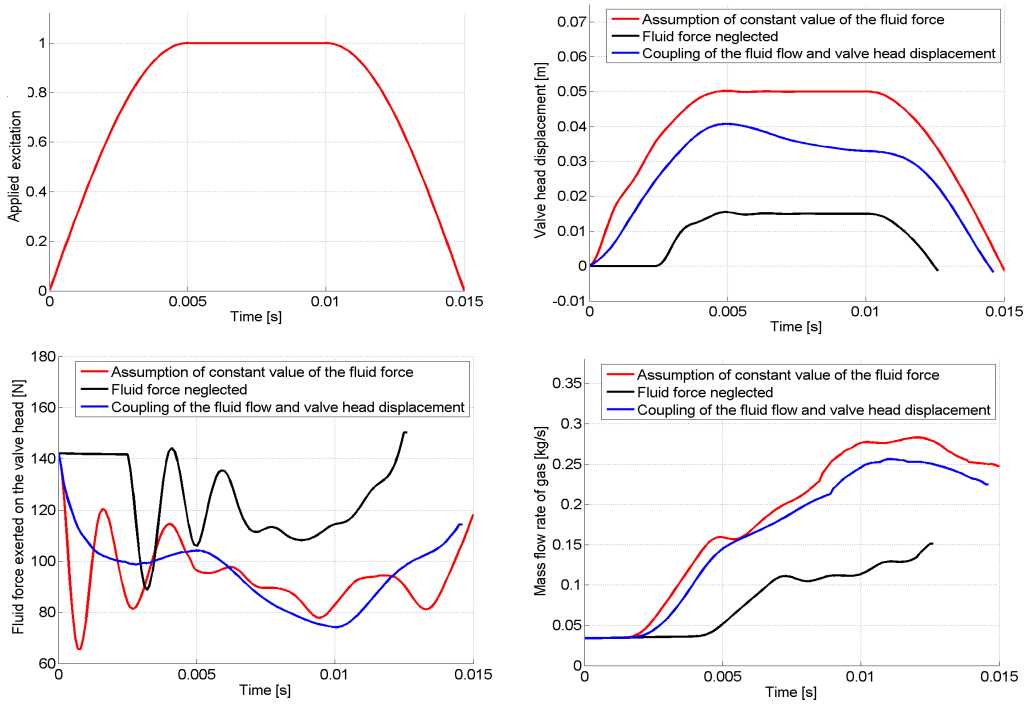

Fig.7.1.8. Comparison of the response of the system obtained by various methods:
a) applied excitation, b) valve head displacement, c) force exerted by fluid on the valve head,
d) mass flow rate of the gas at outlet.

The first coupling effect relies on change of the displacement of the valve head caused by force exerted by the fluid. When the fluid force is assumed to be constant and equal to the initial one, the valve opening is the largest because of permanent support of the active element by a constant force. On the contrary, when the fluid force is totally neglected, the valve does not move until excitation force equilibrates force exerted by external spring and consequently maximal displacement of the valve head is substantially diminished. In case of two-way coupling obtained by 'semi-analytical method' displacement of the valve head is located between two former curves and time-progressing reduction of valve opening correlated with decrease of force exerted by fluid (t=5-10ms) is clearly observed (Fig. 7.1.8b,c).

The second coupling effect relies on influence of the valve head movement on the fluid flow. It is clearly revealed by change of the flow pattern, force exerted by fluid on the valve head and, finally, mass flow rate of the fluid. In cases when zero or constant value of the artificial fluid force is assumed, the real force exerted by the flowing fluid determined from CFD analysis exhibits strong oscillations which are the effect of improper handling of the coupling conditions (Fig. 7.1.8c). By contrast, in case of two-way coupling the force exerted by the fluid is declining when the external excitation is applied due to a development of the fluid flow and corresponding reduction of local pressure. Mass flow rate of the fluid at outlet corresponds to opening of the valve, however, it occurs with a certain delay (Fig. 7.1.8d).

The conducted simulations indicate that 'semi-analytical' method is deprived of limitation resulting from 'one-way coupling' applied in 'decomposition method'. The proposed methodology allows for determination of general properties of controllable valve, its maximal opening and corresponding maximal mass flow rate of gas.

Comparison of two configurations of the valve

The introduced method can be applied to compare two basic designs of the controllable valves, i.e. the configuration where the valve head is moved outside and towards the pressure chamber (Fig. 7.1.2a and Fig. 7.1.2b, respectively). The initial data for the analysis is pre-stress of the active element F_p^0, longitudinal stiffness of the active element k_p and external spring k_s and maximal value of the excitation force $F_{\max}$. An additional parameter is minimal value of the delimiting force $F_D^{\min}$ for which the valve remains air-tight in a closed position.

Let us initially consider the system where the valve head is moved outside the pressure chamber (Fig. 7.1.7). Minimal value of pre-stress of the elastic spring F_s^0 which is required to provide air-tightness of the valve can be expressed in terms of pre-stress of the piezo-stack F_p^0, minimal delimiting force $F_D^{\min}$ and initial pneumatic force acting on the valve head F_{pneu}^0:

$$F_s^0 \geq F_p^0 + F_D^{\min} + F_{pneu}^0 \tag{7.1.19a}$$

Pre-stressing force of the elastic spring should also provide the possibility of closing the valve where the fluid flow occurs. In configuration preceding complete valve closing, when the fluid flow is still partially developed (and force F_{flow}^{0+} is exerted on the valve head) but external excitation is negligible, the pre-stressing force F_s^0 has to satisfy the condition:

$$F_s^0 \geq F_p^0 + F_{flow}^{0+} \tag{7.1.19b}$$

Since according to Bernoulli principle the expression F_{pneu}^{0} is expected to be larger than F_{flow}^{0+}, the condition (7.1.19a) is critical for determination of minimal required pre-stress of the elastic spring. By introducing minimal value of the pre-stressing force $F_s^0 = F_p^0 + F_D^{\min} + F_{pneu}^0$ into equation of valve head motion (7.1.18) we obtain:

$$M\ddot{u}_V + F_D^{\min} + F_{pneu}^0 + k_s u_V = \frac{U}{U_{\max}} F_{\max} - \frac{F_{\max}}{u_{\max}} u_V + F_D + F_{flow}^1 \tag{7.1.19c}$$

where F_{flow}^1 indicates total force acting on a valve head caused by flow of the fluid, which supports action of the active element. Maximal displacement of the valve head is obtained for maximal excitation signal $U_{\max}$ and it can be calculated with the assumption of static equilibrium of the valve head:

$$u_V = \frac{F_{\max} - F_D^{\min} + F_{flow}^1 - F_{pneu}^0}{k_s + k_p} \tag{7.1.19d}$$

The analogous formulae can be derived for the system where the valve head moves towards the pressure chamber (Fig. 7.1.2b). In such a case minimal pre-stress of the elastic spring which provides air-tightness of the valve in initial configuration has to satisfy the condition:

$$F_s^0 \geq F_p^0 + F_D^{\min} - F_{pneu}^0 \tag{7.1.20a}$$

and minimal pre-stressing force which provides the possibility of valve closing is defined as:

$$F_s^0 \geq F_p^0 - F_{flow}^{0+} \tag{7.1.20b}$$

Since the expression $F_D^{\min} - F_{pneu}^0$ is expected to be larger than $-F_{flow}^{0+}$ minimal pre-stress force is defined by initial configuration (Eq. 7.1.20a). The required pre-stress of the elastic spring is now smaller than for the valve with outside movement of the valve head due to supporting influence of gas pressure which seals the valve. The equation of motion of the valve head of analysed valve is similar as in previous case:

$$M\ddot{u}_V + F_s^0 + k_s u_V + F_{flow}^2 = F_p^0 + \frac{U}{U_{\max}} F_{\max} - \frac{F_{\max}}{u_{\max}} u_V + F_D\,, \tag{7.1.20c}$$

However, now the force exerted by fluid F_{flow}^2 counteracts action of the active element. By substituting minimal value of the pre-stressing force $F_s^0 = F_p^0 + F_D^{\min} - F_{pneu}^0$ into Eq. 7.1.20c we obtain:

$$M\ddot{u}_V + F_D^{\min} - F_{pneu}^0 + k_s u_V + F_{flow}^2 = \frac{U}{U_{\max}} F_{\max} - \frac{F_{\max}}{u_{\max}} u_V + F_D \tag{7.1.20d}$$

Maximal displacement of the valve head is achieved for maximal excitation $U_{\max}$ and for conditions of static equilibrium of the valve head:

$$u_V = \frac{F_{\max} - F_D^{\min} - F_{flow}^2 + F_{pneu}^0}{k_s + k_p} \tag{7.1.20e}$$

Approximate comparison of the efficiency of both valves can be based on comparison of maximal displacements of the valve heads which are defined by Eq. 7.1.19d and Eq.7.1.20e.

Since in both cases total force exerted by the flowing fluid is smaller than initial pneumatic force $F_{flow}^{1/2} < F_{pneu}^{0}$, the displacement of the valve head and, consequently, maximal mass flow rate of gas are expected to be larger for the second type of valve.

Nonetheless, the precise comparison of both valves requires computation of forces exerted on the valve heads by the flowing fluid. The complete comparative analysis of two types of valves can be conducted by the proposed 'semi-analytical method' with the use of equations of motion of both valve heads (Eq.7.1.19c and Eq.7.1.20d) coupled with the fluid dynamics problem defined in domain with changing geometry. The evaluation methodology can be based on application of the same excitation to active elements of both valves, comparison of obtained valve head dynamics, flow of the fluid and resulting mass flow rate of gas.

'Fully coupled method'

The most complex and precise method of modelling piezoelectric valves, the 'fully coupled method', involves full modelling of the piezoelectric stack and two-way interaction of the valve head movement with the flow of the gas. In this approach, the piezoelectric stack is modelled by coupling of the equations of solid mechanics and electricity, as in 'decomposition method'. Moreover, interaction of the unidirectional valve head movement and flow of the fluid is provided by transferring the fluid forces to the valve head and by altering geometry of the fluid domain according to valve head displacement.

The fully coupled problem involves coupling of three different fields: solid mechanics, electricity and fluid mechanics. Therefore, the attention should be paid to proper definition of the domains where particular governing equations are defined and determination of regions where the couplings take place, see Fig. 7.1.9. Coupling of the mechanical and piezoelectric equations occurs at the whole domain occupied by the piezoelectric stack. In turn, coupling of the valve head movement, piezoelectric stack deformation and flow of the fluid occurs only at the boundaries of the interacting adjacent regions.

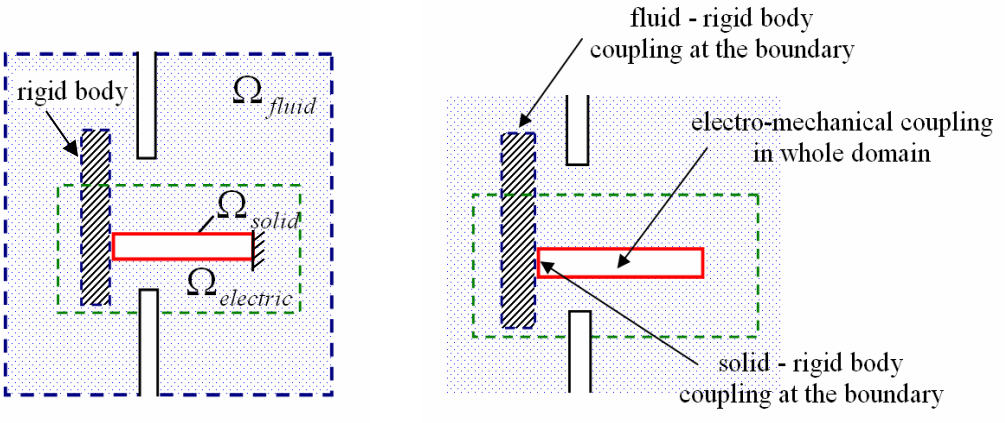

Fig.7.1.9. Fully coupled problem: a) division of the considered domain into sub-domain where mechanical, electrical and fluid flow equations are defined, b) the coupling regions.

Let us briefly summarise the multi-physical model of the system and the set of governing equations. Piezoelectric stack itself is modelled as a pile of thin piezoelectric plates described by coupled set of mechanical and electrical equations with electric boundary

conditions imposing voltages on both sides of the piezo-plates, zero displacement at right end of the stack and conditions providing mechanical coupling between adjacent piezoelectric regions (cf. Eq. 7.1.6.a). The fluid flow is described in classical way by Navier-Stokes equations (balance of mass, momentum and energy) complemented with ideal gas law, definition of internal gas energy and appropriate initial and boundary conditions.

The dynamics of the valve head is governed by the equation of motion which takes into account force exerted by the piezoelectric stack as well as forces exerted by the fluid:

$$M\ddot{u}_V + F_s^0 + k_s u_V = \int_A (\sigma_{11}^p)\mathrm{d}\Gamma_{p/v-h} + \int_A (\sigma_{ij}^f n_j)\mathrm{d}\Gamma_{f/v-h} + F_D \tag{7.1.21}$$

In the above equation $\Gamma_{p/v-h}$ denotes boundary between piezoelectric stack and the valve head, while $\Gamma_{f/v-h}$ denotes boundary between fluid and the valve head. The quantities σ_{11}^n and σ_{ij}^f denote components of the stress tensors of the piezoelectric material and the fluid. The following conditions provide kinematic coupling of both mechanical fields. At first, displacement of the valve head in horizontal direction u_V equals displacement of the adjacent free end of the piezoelectric stack u_1^p. Secondly, velocity of the valve head $\dot{\mathbf{u}}_\mathbf{V}$ equals to velocity of the fluid at the boundary of the void region $\mathbf{v_f}$:

$$u_V = u_1^p \quad \text{at} \quad \Gamma_{p/v-h} \tag{7.1.22a}$$

$$\dot{\mathbf{u}}_\mathbf{V} = \mathbf{v_f} \quad \text{at} \quad \Gamma_{f/v-h} \tag{7.1.22b}$$

As mentioned previously, in ALE approach the second condition is imposed by setting mesh movement equal to valve head movement and by setting fluid velocity in moving coordinate system equal to zero.

Let us note that equation of valve head motion (7.1.21) can be treated as force coupling between piezo-stack and fluid which is satisfied in an integral form. Namely, total force exerted on the valve head by piezoelectric stack and total force exerted by fluid in vertical direction are coupled with each other. Consequently, the kinematic coupling between piezoelectric region and fluid is accomplished by the valve head and it occurs only in vertical direction (along axis of the stack). The direct coupling between piezoelectric and fluid domains at 'free' boundaries of the piezoelectric stack is neglected as imperceptible for the considered process of valve opening.

An additional comment has to be made to description of the kinematics and the configuration in which the equilibrium equations are set. Since, the displacement of the piezoelectric stack is small, equations of stack equilibrium (except the coupling condition at the left end) can be established in initial, undeformed configuration. On the other hand, flow of the fluid has to be described in actual configuration which takes into account actual position of the valve head. The above discrepancy in description of both domains, does not affect the consistency of the problem formulation.

Implementation of the 'fully coupled' model requires establishing connection between computational solid mechanics software (with implemented model of piezoelectricity) and fluid dynamics software. Proposed 'fully coupled method' of simulation of the valve flow can be performed by using partitioned approach and a coupling algorithm based on Eq. 7.1.21 and Eq. 7.1.22, which can be implemented by relatively simple in-house code.

7.1.3. Optimisation and control of piezoelectric valves

The problem of **control of the adaptive valve** is aimed at obtaining desired mass flow rate of gas through the valve during the process of adaptive impact absorption. The control of the gas flow can be performed in two manners: by direct control of the valve head position and by control of the excitation of active element which drives the movement of the valve head. The first approach is more general since it can be applied for various types of controllable valves with diverse mechanisms of valve opening. By contrast, the second method refers to a particular type of the valve and particular type of excitation applied to the valve head.

The problem of control of the mass flow rate of gas will be solved for the system introduced in Fig. 7.1.5 where flow of the gas through the valve chamber is considered. Numerical model of the system comprises constant pressure inlet, constant pressure outlet and the mobile valve head which constraints the inlet. The valve head is used to control mass flow rate of gas at the outlet from the chamber. Arbitrarily assumed change of mass flow rate corresponds to typical strategy of optimal control of inflatable structures. It involves initial stage of minimal outflow $q_{\min}$, stage of maximal constant outflow $q_{\max}$ and final stage when gradual reduction of outflow back to minimal value $q_{\min}$ is performed (cf. Fig. 7.1.10b):

$$\begin{aligned} q_{opt} &= q_{\min} \quad \text{for} \quad t \in (0, t_{open}), \\ q_{opt} &= q_{\max} \quad \text{for} \quad t \in (t_{open}, t_x), \\ q_{opt} &= q_{\max} - \frac{q_{\max} - q_{\min}}{t_{end} - t_x}(t - t_x) \quad \text{for} \quad t \in (t_x, t_{end}) \end{aligned} \tag{7.1.23}$$

The first method of controlling mass flow rate of gas is based on direct change of the position of the valve head. The objective of the control problem is to find change of valve head location during the process which results in obtaining desired mass flow rate of gas at outlet. The above task can be formulated as optimisation problem:

$$\text{Find } \Gamma_V(t) \text{ such that } \int_0^{t_{end}} \left(q_{opt} - q\right)^2 dt \quad \text{is minimal} \tag{7.1.24}$$

where $\Gamma_V(t)$ denotes actual distance of the valve head from the chamber wall and the objective function is defined as discrepancy between assumed and obtained mass flow rate of gas through the valve during the whole process.

The simplest approach for controlling mass flow rate of the fluid is based on determination of extreme positions of the valve head which correspond to maximal and minimal mass flow rate of gas ($q_{\max}$ and $q_{\min}$) in a steady state of the flow. Moreover, it is assumed that valve opening is performed instantly and the process of valve closing is linear in time. In such an approach, valve opening is controlled by three parameters (cf. Fig. 7.1.10):

- time t_1 which denotes time instant of valve opening,
- time t_2 which indicates beginning of valve closing,
- time t_3 which denotes time instant when valve becomes fully closed.

In the optimisation problem the subsequent time instants (t_1, t_2, t_3) should be searched in the vicinity of the time instants corresponding to change of mass flow rate of gas (t_{open}, t_x, t_{end}), and they should slightly precede them due to expected delay in system response.

As it stems from conducted numerical simulations, the strategy allows for obtaining acceptable precision of fluid outflow by relatively simple movement of the valve head. The substantial delay between valve opening and corresponding change of mass flow rate is clearly observed, cf. subsequent stages of the process in Fig.7.1.10a and Fig.7.1.10b. A slight disadvantage of the method is insufficient mass flow rate at the final stage of the process ($t = 0{,}18 - 0{,}20s$).

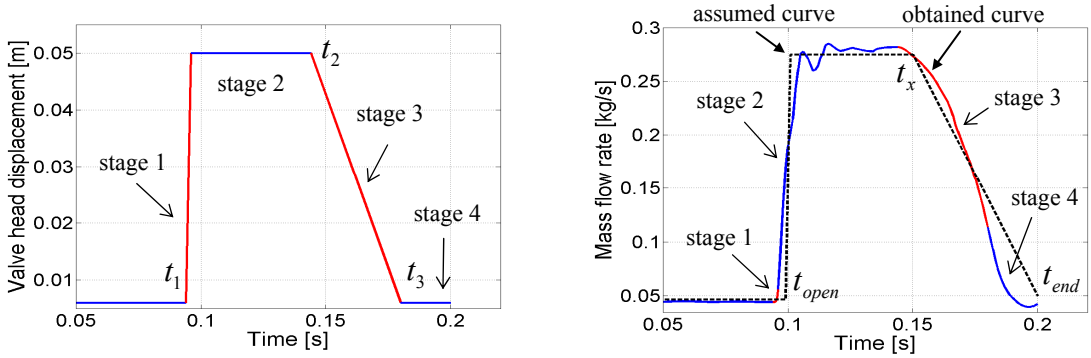

Fig.7.1.10. Control of mass flow rate of the fluid by changing position of the valve head: a) change of valve head position b) resulting mass flow rate of gas.

In a more precise approach, controlling flow of the fluid through the valve is conducted in similar way as controlling pneumatic force exerted on the piston during impact with high initial velocity (cf. Chapter 4, Fig. 4.7). The proposed algorithm utilises subsequent control steps for changing actual velocity of the valve head v_v on the basis of mass flow rate of gas obtained from the numerical simulation. Due to delay between valve opening and corresponding gas outflow, the so-called 'predictive analyses' are used to determine the influence of actual valve opening on mass flow rate of gas obtained after certain time delay (Fig. 7.1.11). The developed control strategy effectively exploits:

- the assumption of constant length of the time-shift between change of the valve head position and steady mass flow rate of gas at outlet (examined in one of previous numerical examples and depicted in Fig. 7.1.6) and
- the assumption that mass flow rate of gas at outlet is approximately proportional to distance of the valve head from the chamber wall before the time-shift.

Since the time-shift is assumed to be equal to 15ms, the length of the control step is chosen as $\Delta t = 10ms$ and the 'predictive analysis' is twice longer. Each predictive analysis starts with calculation of the approximate valve head velocity v_{approx} for which valve opening in the middle of the control step (at time instant $t_0 + 5ms$) is expected to provide required mass flow rate of gas at the end of the predictive step (at time instant $t_0 + 20ms$). Further, predictive analyses for the time period $\langle t_0, t_0 + 20ms \rangle$ are conducted in order to precisely tune previously estimated valve head velocity and to obtain final mass flow rate of gas within assumed range of tolerance $(q_{opt} - tol, q_{opt} + tol)$. At the last stage, the condition of maximal valve head displacement is checked and the algorithm follows to the next control step.

In the numerical example, the control algorithm is applied to the last stage of the process when the valve is gradually closed. The scheme of control procedure is presented in Fig. 7.1.11 and obtained mass flow rate of gas which closely follows assumed curve is depicted in Fig. 7.1.12.

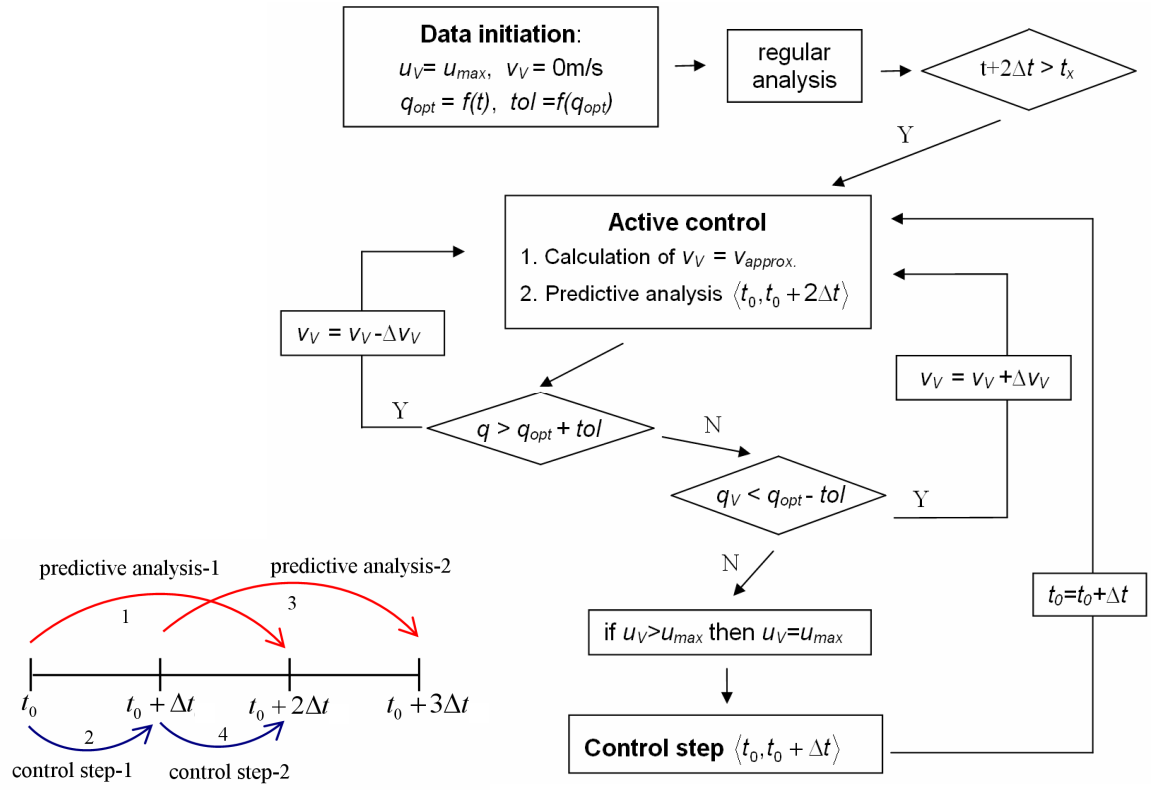

Fig.7.1.11. Scheme of numerical procedure for controlling flow of the fluid through the valve by changing position of the valve head.

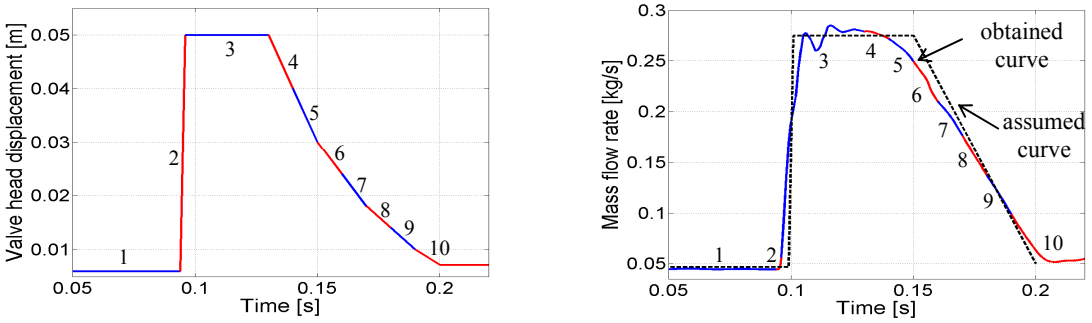

Fig.7.1.12. Control of mass flow rate of the fluid by changing position of the valve head: a) change of valve head position b) resulting mass flow rate of gas.

In the second method, the mass flow rate of the fluid through the valve is controlled by changing excitation applied to active element of the valve, for instance to the piezoelectric stack. In this case, the problem is formulated in the form equivalent to Eq. 7.1.24:

$$\text{Find } F(t) \text{ such that } \int_0^{t_{end}} \left(q_{opt} - q\right)^2 dt \quad \text{is minimal} \tag{7.1.25}$$

however, now the control quantity $F(t)$ denotes applied external excitation. The current formulation of the control problem is, in general, more complicated than the previous one. First of all, it requires numerical model which involves two-way coupling of movement of the valve head and flow of the fluid. The direct consequence is that optimal excitation applied to active element depends not only on desired mass flow rate of gas but also on force exerted on

the valve head by the flowing fluid. The other issue is additional delay time-shift in response of the system which may result from:

- delay in response of the active element on applied excitation,
- delay in movement of the valve head caused by its inertia.

The results obtained by controlling excitation of the active element are expected to be less precise than results obtained from direct control of valve head position since the first control method influences flow of the fluid in more indirect way.

Both above control strategies assume that proportional opening of the valve is possible, i.e. that during the process the valve head can be located in all positions between the chamber wall and the most remote allowable location. An alternative control strategy assumes on/off control of valve opening, in which the valve head is repeatedly switched between the extreme positions. Such a process is difficult for precise numerical simulation due to requirement of numerous fast movement of the valve head, which in ALE approach is associated with large deformation of fluid mesh and aggravated convergence of the solution. Alternatively, the average mass flow rate of gas through the valve controlled by on/off strategy can be estimated by computing mass flow rate corresponding to extreme positions of the valve head and by comparing the lengths of time periods when the valve remains opened and closed.

An important problem in **design of adaptive piezoelectric valve** is optimal shaping of the valve head. At this stage we will assume that properties of the piezoelectric stack are predefined and optimally chosen and we will focus exclusively on the design of the valve head. In general, the valve head should fulfil two basic criteria:

- it should have minimal inertia,
- it should provide maximal mass flow rate of gas at extremely remote position.

The first criterion determines time of the valve response and it is especially important when on/off strategy of valve opening is applied. Maximal mass flow rate through the valve depends on geometry of the main parts of the valve, i.e. geometry of the valve head and geometry of the aperture in adjacent immobile part of the valve. Both geometries determine size of surfaces subjected to internal pressure and therefore predefine value of initial pre-stress of the external spring which provides air-tightness of the valve. This force, in turn, determines maximal displacement of the valve head which can be obtained by means of actuator of given characteristics. Moreover, geometry of the main part of the valve defines shape of the channel where flow of the fluid occurs and the corresponding flow pattern. Both above factors contribute to maximal mass flow rate of gas which can be obtained.

In the proposed approach, the shape of the valve head is subjected to topological optimisation in order to obtain maximal mass flow rate of the fluid. Theoretical formulation of the problem reads:

$$\text{Find } \Omega_V \text{ such that } q_{\max} \text{ is maximal} \tag{7.1.26}$$

where Ω_V denotes geometry of the valve head and $q_{\max}$ indicates maximal mass flow rate through the valve which is obtained for maximal excitation of the active element. In an alternative approach maximisation of the mass flow rate of gas is considered in conjunction with the minimisation of the valve head inertia:

$$\text{Find } \Omega_V \text{ such that } \int \rho d\Omega_V + \left(q_{\max}\right)^{-1} \text{ is minimal} \tag{7.1.27}$$

The solution of the problems (7.1.26) and (7.1.27) requires the following steps:

1. assumption of the initial shape of the valve head,
2. computation of minimal initial pre-stress of external spring which provides air-tightness of the valve and the possibility of valve closing,
3. computation of maximal mass flow rate through the valve obtained at maximally remote position of the valve head,
4. arbitrary change of shape of the valve head (exemplary based on topological derivative) and repeating of the entire procedure.

Let us note that although the initial external pre-stressing force which provides air-tightness and the possibility of valve closing can be estimated analytically, its precise computation requires performing CFD simulation. Moreover, the most remote position of the valve head has to be determined as solution of the FSI problem which involves coupling of the dynamics of the valve head excited by piezo-stack and flow of the fluid ('semi-analytical' method or 'fully coupled' method can be applied).

According to the above facts, formulated topology optimisation problems turns out to be fairly complicated since they require advanced numerical algorithms which combine coupled multi-physical problems and optimisation procedures. The solution of such problems is challenging and requires separate research work.

7.2. Membrane valves

The second considered type of high performance valve for Adaptive Inflatable Structures is a self-closing membrane valve. The valve is composed of two layers of fabric: the external membrane [3] which is open at both sides and forms an external wall of the outflow channel, and the internal membrane [4] which is balloon-shaped and closed on the bottom side, Fig. 7.2.1. At the initial configuration of the system both membranes are clamped by two controlling rings [6,7] and thus the valve remains closed and outflow of the gas is blocked. Opening of the valve is executed by loosening (or detaching) of the external ring [6] which evokes expansion of the external membrane and enables flow of the gas between two layers of fabric. Closing of the valve is executed by slackening (or disconnecting) the internal ring [7] which causes that gas fills closed volume of the internal balloon-shaped membrane, the membrane expands and restricts the outflow of gas. If the internal membrane reaches the external one, the outflow of gas is totally blocked. The concept of membrane valve was proposed by M.Ostrowski and it is protected by Polish and European patents pendings [320 321].

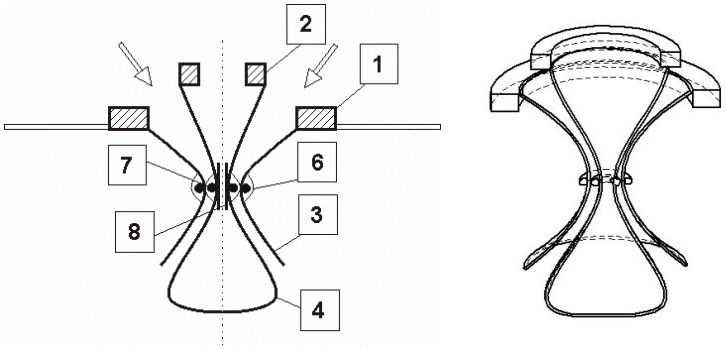

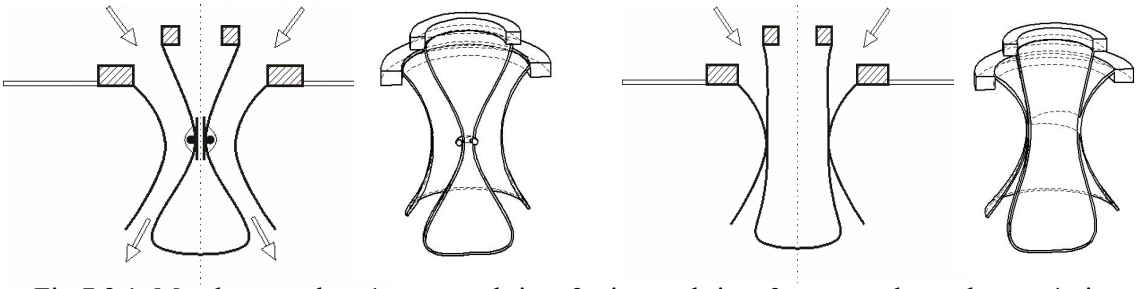

Fig.7.2.1. Membrane valve: 1 - external ring, 2 - internal ring, 3 - external membrane, 4 - internal membrane, 6 - external controlling ring, 7- internal controlling ring, 8 - pressure equalisation pipe: a) initial stage (valve closed) , b) external ring detached (valve fully open), c) internal ring detached (valve again closed) [320 321]

In the simplest design, external controlling rings are detached at certain time instants of the impact process and therefore the valve may be only opened and closed and intermediate valve openings can not be obtained. However, when loosening of the internal ring is precisely controlled, the width of the outflow channel can be precisely altered and intensity of the gas flow can be changed in an arbitrary way. Therefore, self-closing membrane valve can accomplish previously proposed optimal strategy of inflatable structure adaptation which involves initial stage of force increase with the closed valve and a stage of maintaining constant force executed by opening the valve and its gradual closing.

The main advantage of the membrane valve is its simple and lightweight construction which can be easily applied in external airbags and other structures made of fabric. Another important feature is the possibility of controlling large flows of the gas without introducing additional energy to the system (closing of the valve occurs exclusively owing to the forces resulting from gas pressure). The proposed valve can be fully opened and closed without using external energy only once during the impact process. Subsequent opening of the valve is possible; however, it requires tightening of the internal controlling ring which counteracts forces exerted by gas pressure and therefore requires external energy source. Alternatively, controlling actual intensity of gas outflow can be obtained by using several valves of the same construction mounted in other parts of the inflatable structure and their successive opening and closing during the impact process.

The first part of this section focuses on various methods of two- and three-dimensional modelling of the self-closing membrane valves. In the second section, diverse options of controlling gas flow through membrane valve are considered and exemplary control strategies are developed. Practical aspects of constructing membrane valves and their experimental testing constitute separate challenging research topic [322] and thus they will not be covered herein.

7.2.1. ALE and CEL modelling of the membrane valve

Simulation of membrane valves requires precise handling of the interaction between deformation of the membrane and forces exerted by the flowing fluid and therefore it has to be based on a model which involves full coupling of structural mechanics and fluid mechanics (FSI approach). Due to the fact that opening of the membrane valve induced by detaching the external ring is a standard process which does not require numerical verification, the attention

will focused on the process of closing the valve caused by disconnecting the internal controlling ring. Since deformation of the external membrane has only subsidiary function in the process valve closing, it will be considered as immobile (fixed in space) and only deformation of the internal membrane will be analyzed.

The proposed numerical model is composed of internal balloon-shaped membrane located within the outflow channel confined by rigid walls (external boundaries of the fluid domain), Fig. 7.2.2. Inlet and outlet (opening) boundary conditions are defined at the top and bottom edges of the considered fluid domain. At the beginning of the analysis membrane is located in the middle of the outflow channel, the valve remains partially open and outflow of the gas is possible. The internal controlling ring is assumed to be already detached and therefore it is omitted in the numerical model. The purpose of conducting dynamic FSI simulation is to analyze the process of valve closing caused by expansion of the membrane including changes in distribution of fluid pressure and velocity in the considered domain as well as change of mass flow rate of gas through the valve.

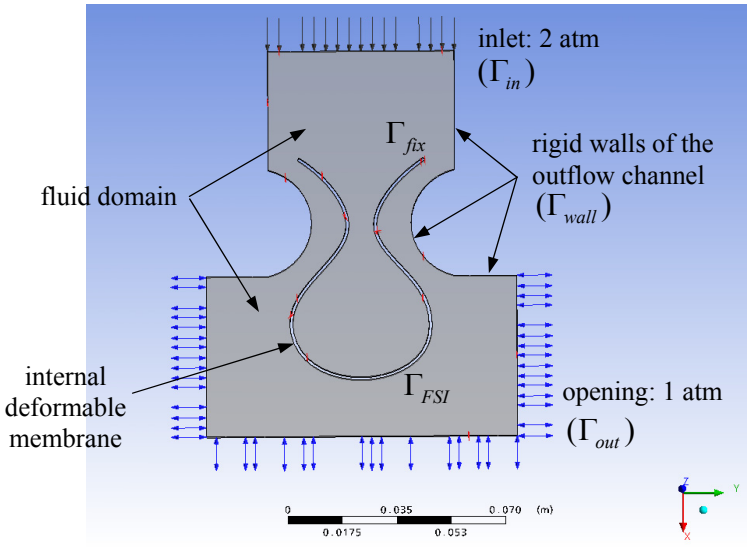

Fig.7.2.2. Self-closing membrane valve: numerical model of the system.

The problem will be approached by two main methods of analysis of FSI problems which were described in Chapter 2: the Arbitrary Lagrangian Eulerian method and the Coupled Eulerian Lagrangian method. Both methods and the obtained qualitative results will be compared against each other and the better-suited method will be selected for modelling of fully controllable membrane valve with internal controlling ring and for developing the corresponding strategies of flow control.

ALE approach

The first approach for simulation of the membrane valve is based on Arbitrary Lagrangian Eulerian (ALE) method which belongs to the class of conforming boundary methods. The method utilizes the Lagrangian description of solid (membrane) kinematics and arbitrary Lagrangian-Eulerian description of fluid kinematics. Deformation of the fluid mesh is determined during numerical analysis and it is based on actual deformation of the membrane. Regarding the solution method, it is based on coupling of two distinct solvers for structural

and fluid part of the problem ('partitioned approach'). The solver used for solid part is commercial software ANSYS Structural, while the solver used for fluid part is commercial software ANSYS CFX. Coupling of both problems is executed by using ANSYS Multi-field Code Coupling (MFX).

The model of the structural part of the problem is based exclusively on equations of mechanical equilibrium and it neglects heat transfer through membrane and the corresponding equation of internal energy balance. Although the most appropriate approach for modelling internal membrane is using membrane elements without compression and bending stiffness, the requirement of using 3D elements imposed by the applied software enforces application of solid elements of a small thickness. Fluid flow is modelled by compressible viscous Navier-Stokes equations involving balance of mass, momentum and internal energy. The complete system of equations governing the problem reads:

$$\frac{D}{Dt}(J\rho_{\mathbf{S}}\mathbf{v}_{\mathbf{S}}) = \nabla\cdot(J\boldsymbol{\sigma}_{\mathbf{S}}{}^{\mathrm{T}}\mathbf{F}^{-\mathrm{T}}) + \rho_{\mathbf{S}}J_{\chi}\mathbf{f} \quad \text{in } \Omega_S \tag{7.2.1}$$

$$\left.\frac{\overline{D}(J_{\chi}\rho_{\mathbf{f}})}{\overline{D}t}\right| + \nabla_{\chi}\cdot\left[\rho_{\mathbf{f}}J_{\chi}\left(\mathbf{v}_{\mathbf{f}} - \frac{\partial\hat{\mathbf{u}}_{\mathbf{f}}}{\partial t}\right)\mathbf{F}_{\chi}^{-\mathrm{T}}\right] = 0 \quad \text{in } \Omega_F \tag{7.2.2a}$$

$$\frac{\overline{D}(\rho_{\mathbf{f}}J_{\chi}\mathbf{v}_{\mathbf{f}})}{\overline{D}t} + \nabla_{\chi}\cdot\left[\rho_{\mathbf{f}}J_{\chi}\mathbf{v}_{\mathbf{f}}\otimes\left(\mathbf{v}_{\mathbf{f}} - \frac{\partial\hat{\mathbf{u}}_{\mathbf{f}}}{\partial t}\right)\mathbf{F}_{\chi}^{-\mathrm{T}}\right] = \nabla_{\chi}\cdot\left[J_{\chi}\boldsymbol{\sigma}_{\mathbf{f}}{}^{\mathrm{T}}\mathbf{F}_{\chi}^{-\mathrm{T}}\right] + \rho_{\mathbf{f}}J_{\chi}\mathbf{f} \quad \text{in } \Omega_F \tag{7.2.2b}$$

$$\frac{\overline{D}(\rho_{\mathbf{f}}J_{\chi}E_f)}{\overline{D}t} + \nabla_{\chi}\cdot\left[\rho_{\mathbf{f}}J_{\chi}E_f\left(\mathbf{v}_{\mathbf{f}} - \frac{\partial\hat{\mathbf{u}}_{\mathbf{f}}}{\partial t}\right)\mathbf{F}_{\chi}^{-\mathrm{T}}\right] = \quad \text{in } \Omega_F \tag{7.2.2c}$$

$$= -\nabla_{\chi}\cdot\left[J_{\chi}\mathbf{q}_{\mathbf{f}}\mathbf{F}_{\chi}^{-\mathrm{T}}\right] + \nabla_{\chi}\cdot\left[J_{\chi}(\boldsymbol{\sigma}_{\mathbf{f}}\mathbf{v}_{\mathbf{f}})\mathbf{F}_{\chi}^{-\mathrm{T}}\right] + \rho_{\mathbf{f}}J_{\chi}\mathbf{f}\cdot\mathbf{v}_{\mathbf{f}} + \rho_{\mathbf{f}}J_{\chi}h$$

$$\frac{\partial\hat{\mathbf{u}}_{\mathbf{f}}}{\partial t} = \mathbf{D}(\hat{\mathbf{u}}_{\mathbf{f}}) \qquad \text{in } \Omega_F \tag{7.2.3}$$

In the above equations the indices 's' and 'f ' denote solid and fluid, respectively. The symbol D/Dt stands for time derivative in the Lagrangian coordinate system, while the symbol $\overline{D}/\overline{D}t$ stands for time derivative in the arbitrary Lagranian-Eulerian coordinate system. The quantity $\hat{\mathbf{u}}_{\mathbf{f}}$ denotes displacement of the fluid mesh and **D** is an arbitrary differential operator. Meaning of the other quantities conforms to the one introduced in Chapter 2.

Coupling conditions concern only mechanical part of the problem and involve fluid and solid velocities and stresses at their common interface:

$$\mathbf{v}_{\mathbf{f}} = \mathbf{v}_{\mathbf{S}} \quad \text{and} \qquad \boldsymbol{\sigma}_{\mathbf{S}}\mathbf{n} = \boldsymbol{\sigma}_{\mathbf{f}}\mathbf{n} \ \text{ on } \ \Gamma_{FSI} \tag{7.2.4}$$

Boundary conditions for the membrane concern only displacements of its upper points:

$$\mathbf{v}_{\mathbf{S}} = 0 \quad \text{on } \ \Gamma_{fix} \tag{7.2.5}$$

Mechanical and thermal boundary conditions for the fluid involve conditions at subsonic inlet and opening:

$$\begin{aligned} \boldsymbol{\sigma}_{\mathbf{f}}\mathbf{n} &= -p_{in}\mathbf{n}, \quad T_{\mathbf{f}} = \widetilde{T}_{in} \quad \text{on } \ \Gamma_{in} \\ \boldsymbol{\sigma}_{\mathbf{f}}\mathbf{n} &= -p_{out}\mathbf{n}, \quad T_{\mathbf{f}} = \widetilde{T}_{out} \quad \text{on } \ \Gamma_{out} \end{aligned} \tag{7.2.6a}$$

zero fluid velocity and heat transfer at the lateral boundaries of the fluid domain:

$$\mathbf{v}_\mathbf{f} = 0 \quad \text{and} \quad \mathbf{q}_\mathbf{f} \cdot \mathbf{n} = 0 \ \text{ on } \ \Gamma_{wall} \tag{7.2.6b}$$

and zero heat transfer at the walls of the membrane balloon:

$$\mathbf{q}_\mathbf{f} \cdot \mathbf{n} = 0 \ \text{ on } \ \Gamma_{FSI} \tag{7.2.6c}$$

Kinematic boundary conditions for mesh deformation (variable $\hat{\mathbf{u}}_\mathbf{f}$) involve conformity with displacement of membrane and zero displacement at external edges of the considered domain:

$$\hat{\mathbf{u}}_\mathbf{f} = \mathbf{u}_\mathbf{S} \quad \text{on } \ \Gamma_{FSI} \quad \text{and} \quad \hat{\mathbf{u}}_\mathbf{f} = 0 \quad \text{on } \ \Gamma_{wall} \cup \Gamma_{ext} \tag{7.2.7}$$

cf. Fig. 7.2.3. Finally, initial conditions are imposed on the velocity of the membrane, parameters of the fluid and mesh deformation:

$$\begin{aligned} &\mathbf{v}_\mathbf{S}(0) = 0, \quad \hat{\mathbf{u}}_\mathbf{f}(0) = \tilde{\mathbf{u}}_\mathbf{f} \\ &\rho_\mathbf{f}(0) = \tilde{\rho}_\mathbf{f}, \quad \mathbf{v}_\mathbf{f}(0) = 0, \quad T_\mathbf{f}(0) = \tilde{T}_\mathbf{f} \end{aligned} \tag{7.2.8}$$

The main features of the implemented numerical solution are the following:

1. solid part: solution of solid mechanics problem by Finite Element Method and an implicit scheme of integration of equations of motion;
2. fluid part: solution of the CFD problem by Finite Volume Method with vertex-centred discretisation and a 'coupled algebraic multigrid' for solving governing equations [323];
3. coupling scheme: strong coupling of the partitioned solvers which requires equilibrium of each point located at the fluid-solid interface at every coupling step.

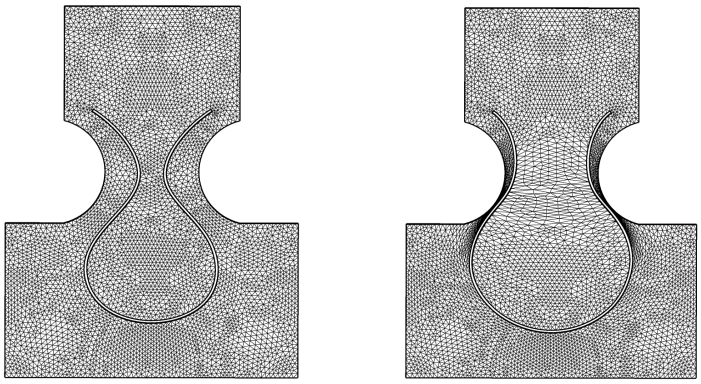

Fig.7.2.3. Numerical model based on Arbitrary Lagrangian Eulerian method: a) initial stage of simulation with generic mesh, b) final stage of simulation with deformed mesh.

The advantages of the method involve: i) application of well-established, verified and efficient CFD solver based on Finite Volume Method and ii) application of strong coupling algorithm providing precise solution of the interaction problem. On the other hand, the main drawbacks of the proposed approach are: i) application of implicit integration scheme which may cause convergence problems, and ii) lack of possibility of simulating full closing of the valve due to the requirement of preserving the initial topology of the system.

The simulation of closing of the valve was initially performed for 2D model. Since the applied software and coupling methodology enforce using three-dimensional elements, the computational model is composed of one layer of 3D solid and fluid elements along 'z'

dimension. Moreover, the 'symmetry' boundary conditions are imposed on the front and rear surfaces, which imitates two-dimensionality of the model. The assumed initial and boundary conditions (cf. Fig. 7.2.1 and Eq. 7.2.1-7.2.8) cause unsteady state at the initial situation and gradual propagation of the pressure wave along the valve region. During the simulation, as the flow develops, pressure inside membrane balloon increases and exceeds pressure between membrane and lateral rigid wall. The process results in progressive expansion of the internal membrane, change of the flow pattern of the fluid and, finally, leads to total blocking of the gas flow, Fig.7.2.4a-c. Despite the simplicity of the assumed model, the conducted simulation clearly confirms assumed operating principle of the valve.

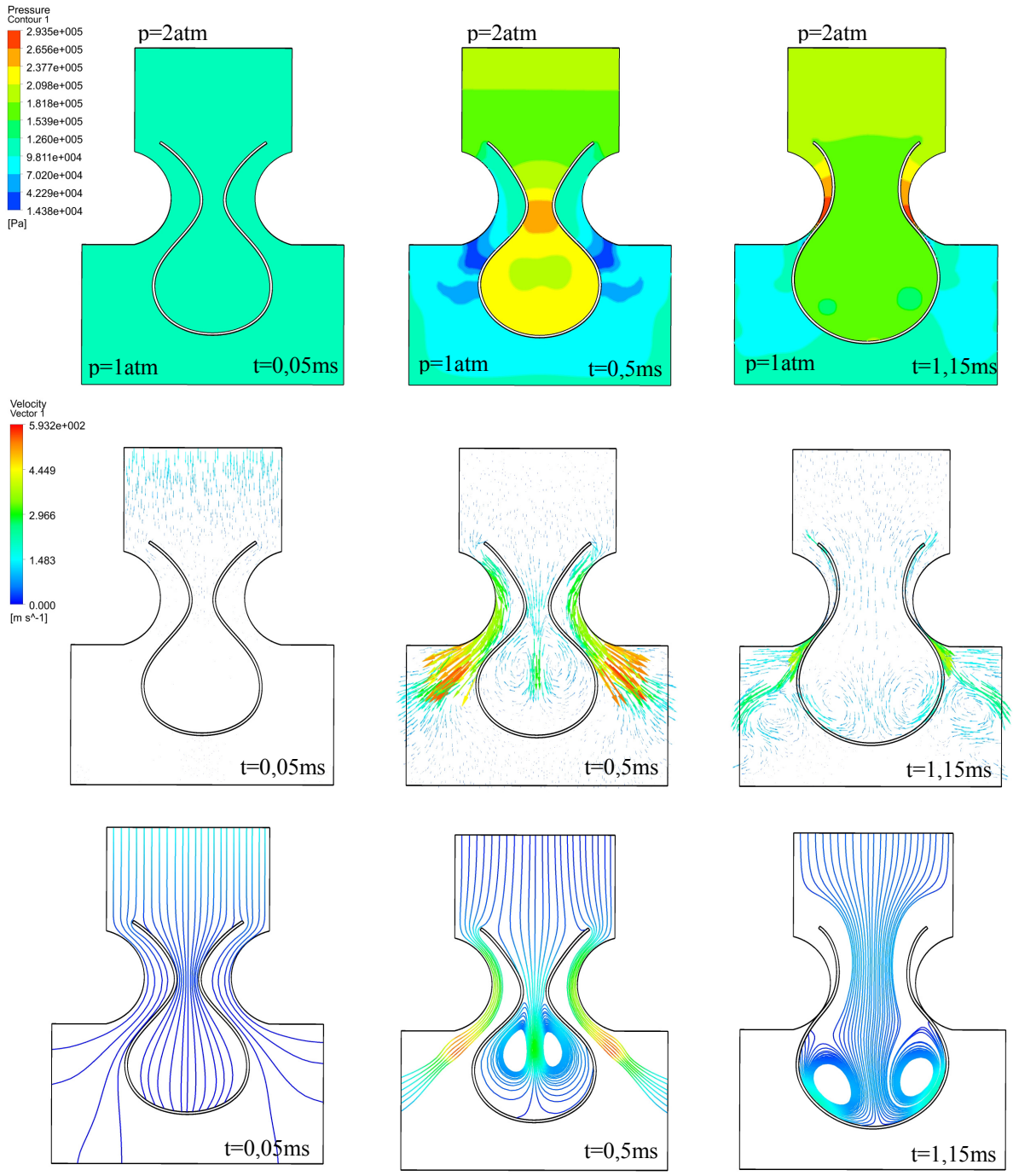

Fig.7.2.4. Two-dimensional simulation of adaptive membrane valve by ALE method:
a) pressure distribution, b) fluid velocity distribution, c) streamlines of the fluid flow.

The simulation of valve closing was also conducted for the case when in the initial situation flow of the fluid through the valve region is fully developed. The simulation consisted of three subsequent steps:

- analysis of gas flow through the valve with immobile membrane located in the middle of the outflow channel until steady state is obtained (Fig. 7.2.5a, t=0-4ms);
- coupled FSI analysis of the interaction between flow of the fluid and deformation of the membrane (Fig. 7.2.5b, t=4-4,95ms);
- continuation of the analysis of fluid flow through the valve with immobile internal membrane until steady state is achieved (Fig. 7.2.5b, t=4.95-6ms).

The obtained response of the system qualitatively resembled the response from previous simulations, i.e. pressure inside membrane gradually increased and membrane gradually expanded in the outer direction. The process of closing the valve was slightly faster (it lasted less than 1ms) and it was reflected by decrease of mass flow rate of gas at the lower boundary of the considered fluid domain. The delay between an expansion of the membrane (and corresponding change of width of the flow channel) and change of mass flow rate at outlet was clearly observed. At the last stage, when deformation of the membrane was arbitrarily stopped at the vicinity of the outer wall, the mass flow rate of gas was stabilized at a low level.

Let us note that since the model is two-dimensional, the results obtained from the above simulations should be treated rather qualitatively than quantitatively.

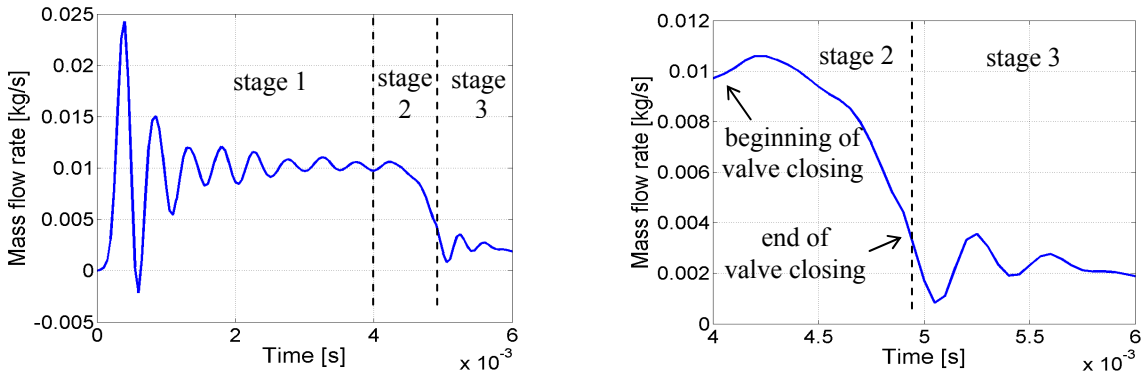

Fig.7.2.5. Change of mass flow rate of gas during valve closing: a) stage 1: obtaining initial steady state, b) stage 2: gradual closing of the valve and stage 3: maintaining the valve almost closed.

In a further step, a three-dimensional model of the membrane valve was developed and three-dimensional simulation of valve closing was conducted. Two initial configurations of the internal membrane were considered:

- the configuration in which the membrane is wrinkled in its middle part;
- the configuration in which membrane is narrowed in its middle part.

Only the first configuration precisely corresponds to an assumed design of the membrane valve. In the second configuration, the operating principle of the valve differs from the initial concept since the process of valve closing requires substantial stretching of the membrane and consequently low value of the Young modulus of the membrane fabric has to be applied. In both cases, a large displacement of the membrane (modelled by solid elements of a small thickness) causes severe convergence problems which strongly aggravate obtaining solution of the coupled system of equations with the use of ALE approach.

Presented results of the numerical simulations correspond to the second modelling option where membrane is narrowed in its middle part (Fig. 7.2.6). Preliminary simulations were performed for the case when membrane is non-deformable and they were aimed at investigation of distribution of gas velocity and pressure inside the valve. Results of the 3D analysis revealed the increase of pressure inside membrane balloon and therefore, qualitatively confirmed the results obtained previously for 2D model (Fig. 7.2.6b). The following simulations utilised full FSI coupling and concerned the initial stage of the membrane deformation, Fig. 7.2.6c. Although only the initial part of the process was analysed, the simulation had shown the tendency of the membrane for outward deformation and confirmed the ability of the valve for restricting the fluid flow.

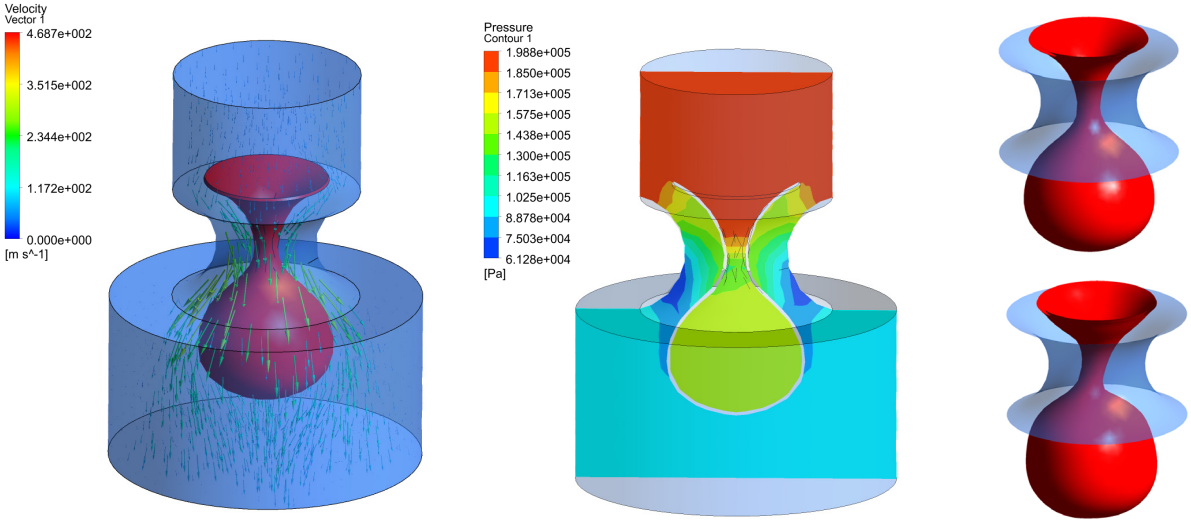

Fig.7.2.6. Three-dimensional simulation of adaptive membrane valve by ALE method: a) fluid velocity distribution, b) pressure distribution, c) deformation of the membrane.

CEL approach

The second approach for simulation of the membrane valve is based on the Coupled Eulerian Lagrangian (CEL) method which belongs to the class of fixed background grid methods, cf. Fig. 7.2.7. This approach utilises the Lagrangian description of deformation of the solid body which moves inside fixed in space Eulerian fluid domain. Similarly as in case of ALE method, the numerical solution is based on coupling of two distinct solvers for solid and fluid part of the problem ('partitioned approach'). Both solvers applied hereinafter are incorporated and automatically coupled inside commercial software ABAQUS Explicit.

The methodologies used for development of two- and three-dimensional models of the membrane valve will be similar as in case of ALE method. Two-dimensional model will be composed of a single layer of three-dimensional elements with appropriate symmetry conditions imposed on front and rear surfaces. In case of 3D model, membrane is modelled by a thin layer of solid elements. Such an approach is recommended in CEL method in order to minimise possible leakages of the fluid through the membrane.

The applied method of fluid modelling accounts for compressibility of the fluid but neglects its viscosity and heat transfer. Accordingly, isothermal or adiabatic conditions of the fluid flow have to be assumed and the energy balance equation is either omitted or reduced to

a simple equation (2.2.117). Due to the above assumptions the model is less precise than the previously developed ALE model and it should be used for qualitative analysis of the valve response. The complete system of equations governing the flow of the fluid through membrane valve reads:

$$\rho_{\mathrm{S}} \frac{D}{Dt}(J\mathbf{v}_{\mathbf{S}}) = \nabla_{\mathrm{X}} \cdot (J\boldsymbol{\sigma}_{\mathbf{S}}{}^{\mathrm{T}}\mathbf{F}^{-\mathrm{T}}) + \rho_{\mathbf{S}} J\mathbf{f} \quad \text{in } \Omega_S \tag{7.2.9a}$$

$$\frac{\partial \rho_f}{\partial t} + \nabla \rho_f \cdot \mathbf{v}_{\mathbf{f}} = -\rho_f (\nabla \cdot \mathbf{v}_{\mathbf{f}}) \quad \text{in } \Omega_F \tag{7.2.9b}$$

$$\rho_F \frac{\partial \mathbf{v}_{\mathbf{f}}}{\partial t} + \rho_f (\nabla \mathbf{v}_{\mathbf{f}}) \mathbf{v}_{\mathbf{f}} = \nabla \cdot \boldsymbol{\sigma}_{\mathbf{f}}{}^{\mathrm{T}} + \rho_f \mathbf{f} \quad \text{in } \Omega_F \tag{7.2.9c}$$

where D/Dt and ∇_{X} denote time and space derivatives in Lagrangian coordinate system, while $\partial/\partial t$ and ∇ denote derivatives in Eulerian coordinate system. The described simplifications of the fluid modelling cause that fluid tensor assumes reduced form containing only a spherical part which corresponds to fluid pressure. Coupling conditions concern fluid and solid stresses and velocities at the interface Γ_{FSI} (cf. Fig. 7.2.2):

$$\mathbf{v}_{\mathbf{f}} = \mathbf{v}_{\mathbf{S}} \quad \text{and} \quad \boldsymbol{\sigma}_{\mathbf{S}}\mathbf{n} = \boldsymbol{\sigma}_{\mathbf{f}}\mathbf{n} \quad \text{on } \Gamma_{FSI} \tag{7.2.10}$$

The second of the above conditions simply indicates that forces applied perpendicularly to the solid body are equal to gas pressure. Boundary conditions for the membrane balloon concern displacement of its upper edges:

$$\mathbf{v}_{\mathbf{f}} = 0 \quad \text{on } \Gamma_{fix} \tag{7.2.11}$$

At inlet and outlet, the pressure boundary conditions are formulated, while at lateral walls perpendicular components of fluid velocity are equal to zero:

$$\rho_{\mathbf{f}} = \widetilde{\rho}_{\mathbf{f}} \quad \text{on } \Gamma_{inlet}, \Gamma_{outlet} \tag{7.2.12}$$

$$\mathbf{v}_{\mathbf{f}\perp} = 0 \quad \text{on } \Gamma_{wall}$$

The initial conditions are imposed on density and velocity of the fluid and on the initial velocity of the membrane:

$$\rho_{\mathbf{f}}(0) = \widetilde{\rho}_{\mathbf{f}}, \quad \mathbf{v}_{\mathbf{f}}(0) = 0, \quad \mathbf{v}_{\mathbf{S}}(0) = 0 \tag{7.2.13}$$

The main features of the numerical solution by CEL method conducted within ABAQUS Explicit are the following:

1. Solution of solid mechanics problem is performed by Finite Element Method and explicit scheme of time integration of equations of motion.
2. Solution of the fluid dynamics problem is also conducted by FEM with explicit scheme of time integration. The applied method consists of Lagrangian phase which is followed by an Eulerian transport phase (the so- called 'Lagrange-plus-remap') [324]. The main unknowns of the problem are fluid displacements, not fluid velocities as in typical CFD methods.

3. Weak coupling of the fluid and solid solvers is used and equilibrium of the interface is not required at each coupling step. The applied coupling scheme is a straightforward consequence of the applied explicit method of integration of equations of motion.
4. Volume of fluid (VOF) method is used as interface tracking technique.
5. Eulerian-Lagrangian contact is performed by means of penalty method.

The most serious drawbacks of the applied method include: i) application of uncertain, untypical and not well-verified fluid solver deprived of possibility of an implementation of precise models of fluids and turbulence modelling, ii) loose coupling algorithm which does not provide precise exchange of data between fluid and solid solver, iii) possibility of 'leakages' of the fluid when coarse fluid mesh is used.

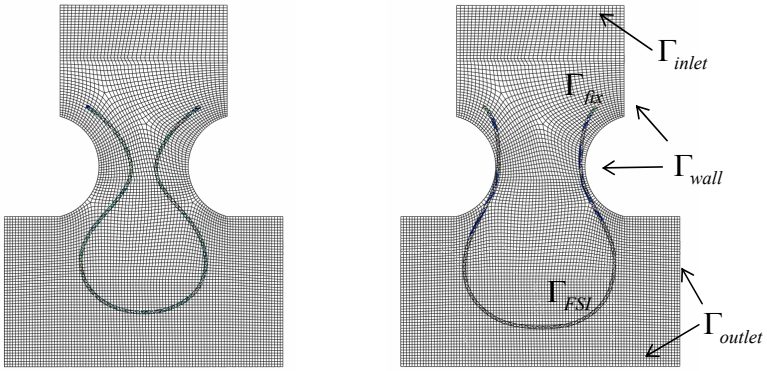

Fig.7.2.7. Numerical model based on Coupled Eulerian Lagrangian method: a) initial stage of simulation with generic mesh, b) final stage of simulation with deformed solid.

The simulation was initially conducted for two-dimensional model of the system. The main purpose of the simulation was to compare the results obtained by using simplified (in terms of fluid viscosity and coupling algorithm) CEL model with the results obtained previously from a more precise ALE model. The geometry of the system, fluid and membrane parameters, boundary and initial conditions were all similar as in case of ALE model, besides differences resulting from type of equations governing the fluid (Euler equations vs. Navier-Stokes equations). The number of elements used for modelling of both fluid and membrane was also comparable as in case of ALE approach (total number of elements was c.a.10000).

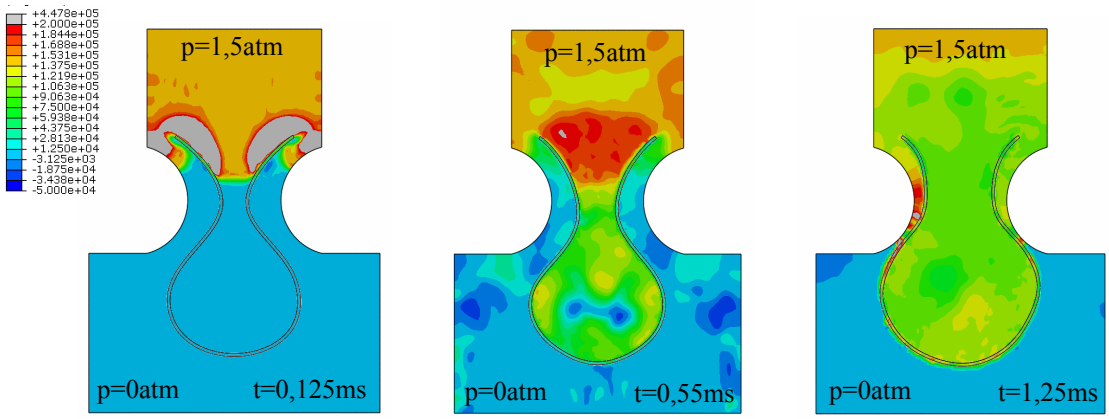

Fig.7.2.8b. Two-dimensional simulation of adaptive membrane valve by CEL method: pressure distribution in subsequent stages of the process (overpressure [Pa]).

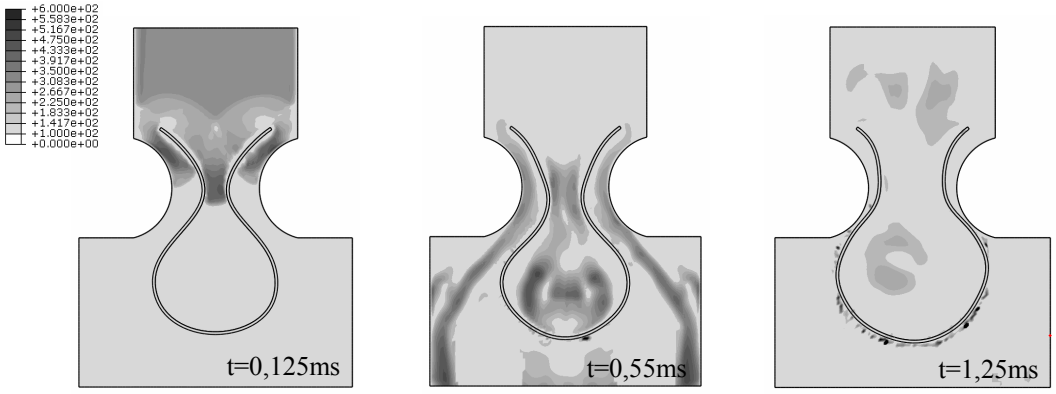

Fig.7.2.8b. Two-dimensional simulation of adaptive membrane valve by CEL method: fluid velocity distribution in subsequent stages of the process [m/s].

The main advantages of application of CEL method for 2D modelling of the membrane valve, revealed during the conducted numerical simulations, is the lack of difficulties with convergence of the solution (due to implicit method of solution) and possibility of modelling full closing of the valve (due to application of CEL method which allows for changes in system topology). The qualitative results of CEL analysis confirm the results obtained by ALE method - pressure inside membrane balloon increases, membrane expands and flow of the fluid is gradually blocked, Fig. 7.2.8a,b. In general, change of distribution of pressure inside considered domain is similar as in ALE method. However, pressures resulting from CEL method undergo larger fluctuations and therefore comparison at certain point of fluid domain does not show precise correspondence. Nevertheless, the time of valve closing, which is one of the most important features characterising the valve, is in both cases comparable and equals approximately 1.2 ms.

In a further step a 3D simulation of closing of the membrane valve was conducted. Application of the CEL method allows to analyse both previously described models of the valve (membrane that is narrowed and wrinkled in the central part), however, only the second modelling option was chosen for the numerical simulation as more equivalent to the assumed design of the valve. In the first step of the simulation, a cylindrical one-sidedly closed membrane was tightened in its central part either by means of internal springs or a kinematic excitation applied at several points along its circumference, Fig. 7.2.9. The procedure was performed for membrane elements, shell elements and solid elements of a small thickness. Although the most appropriate deformation was obtained for membrane elements, solid elements were chosen for further processing as recommended for CEL analysis.

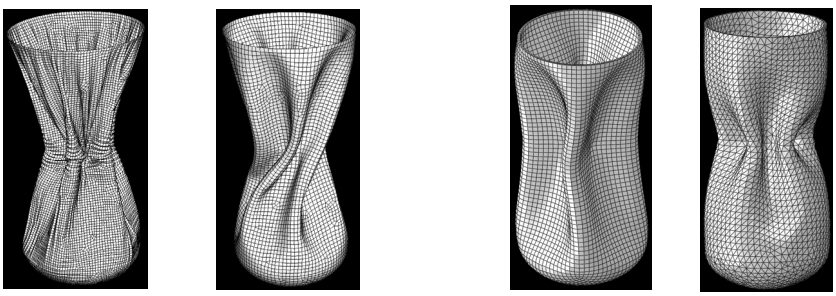

Fig.7.2.9. Various models of wrinkled membrane for CEL analysis: a) membrane elements, b) shell elements, c, d) solid elements of small thickness (4 and 6 imposed boundary conditions).

In the second step, the CEL model of the system composed of a flow channel and located inside deformed membrane balloon was developed, cf. Fig. 7.2.10a. Inlet and outlet were defined at the top and bottom of the considered fluid domain, analogically as in Fig. 7.2.7, while 'wall' boundary condition was defined in its central part. The pressure boundary conditions were imposed at inlet and outlet. Simulation of the response of the system with a relatively complex geometry was possible due to the following features of the CEL method:

- application of fixed ‘background’ Eulerian fluid mesh which substantially simplifies the procedure of meshing the fluid region,
- application of explicit scheme of integration and loose coupling algorithm which eliminates problems with convergence of the numerical solution.

Despite the above advantages, the method requires fine space discretisation which results in a large size of the model. The developed model was composed of 85000 fluid and solid elements due to limitations of applied hardware and computation time. Nevertheless, the applied discretisation still seems too coarse and since some leakages of the fluid through membrane had occurred.

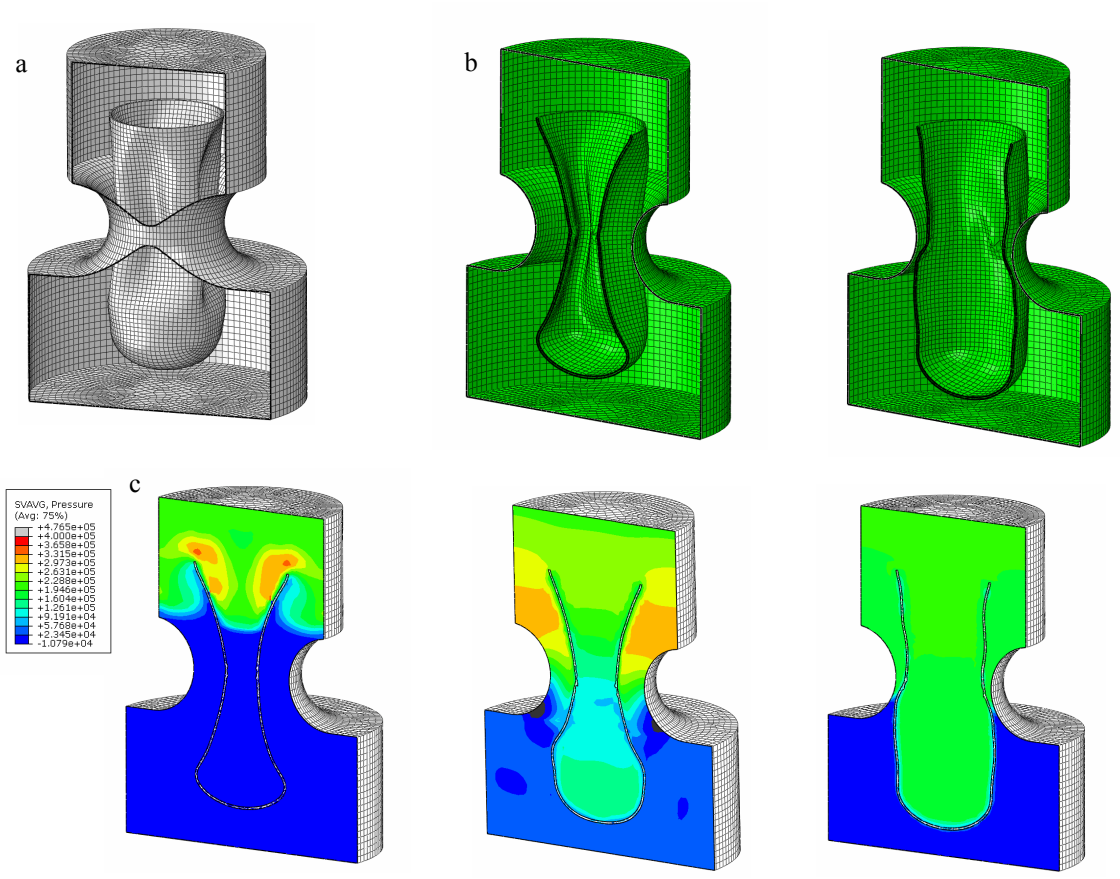

Fig.7.2.10. Three-dimensional simulation of membrane valve by CEL method: a) numerical model of the system, b) deformation of internal membrane, c) change of overpressure during the process [Pa].

The results of the numerical simulation (Fig. 7.2.10) reveal the increase of pressure inside membrane over the pressure between membrane and external wall of the channel, which causes expansion of the membrane and gradual closing of the valve. The performed simulations ultimately confirm the correctness of the concept of the membrane valve and the possibility of restricting the flow in semi-active way without submitting additional energy.

7.2.2. Adaptability and control of membrane valve

The previously presented simulations concerned the case when the membrane valve remains passive and can not be controlled during the process of closing. By contrast, this section is aimed at modelling and simulation of the adaptive membrane valve, i.e. the valve whose characteristics can be altered in real-time in order to control actual conditions of the fluid flow. The undertaken task constitutes a preliminary step before developing control algorithms aimed at obtaining desired mass flow rate of gas through the valve and resulting optimal response of the inflatable structure.

Change of valve characteristics will be executed in two distinct manners, Fig. 7.2.11. The first method corresponds directly to the initial concept of the valve and is based on application of active 'linking element' which ties membrane in its middle part. Mechanical properties of the linking element and, consequently, forces transmitted to membrane can be changed during the numerical analysis, which allows to control deformation of the membrane and actual valve opening. The second method is based on application of active 'covering element' located above the membrane. In this case, altering length or position of the covering element changes conditions of gas inflow into the membrane and enables control of valve opening. The main idea behind using two above methods is that the first one corresponds to change of properties of the solid body (linking element is defined as a solid), while the second one is related to a direct change of geometry of the fluid domain (covering element is defined as internal void inside fluid domain). Thus, change of valve characteristics will be executed by components which belong to solid and fluid part of the problem.

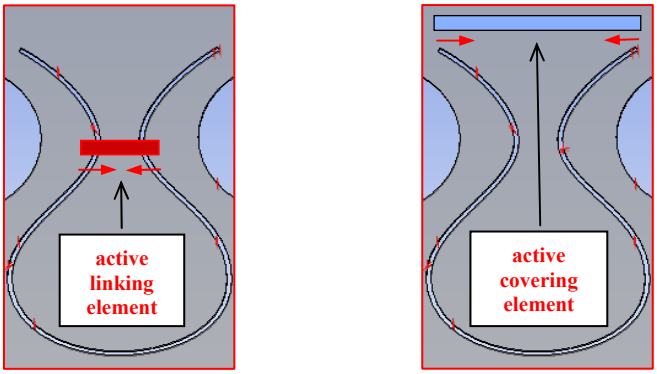

Fig.7.2.11. Two methods of control of the membrane valve: a) active linking element (part of solid domain), b) active covering element (void region inside fluid domain).

The methodology of modelling adaptive membrane valve will be based on Arbitrary Lagrangian Eulerian approach implemented in ANSYS software. This method was chosen among the other possible approaches due to possibility of precise modelling of fluid dynamics and more accurate treatment of fluid-solid interaction which occurs at the interface.

Modelling of adaptive membrane valve is not a trivial task due complex methodology of solving fluid-structure interaction problem which involves two separate numerical solvers. The proposed methodology of modelling of adaptive membrane valve involves both a 'classical coupling' and an additionally introduced 'adaptation coupling' which enables to execute the feedback control. Both types of coupling differ in terms of exchanged variables and methods of implementation:

- 'Classical coupling' is a two-way coupling of quantities at interface of both domains. The 'adaptation coupling' is a one-way coupling of arbitrary results obtained inside each domain with a control variable (input data or excitation) applied in the other domain.
- 'Classical coupling' of fluid and solid solvers is executed at every time step of solid and fluid analysis (the same time discretisation is used) and 'adaptation coupling' is executed more rarely, usually every several time steps.
- 'Classical coupling' is natively implemented in applied commercial software (and executed by MFX commands), while 'adaptation coupling' is not supported and has to be implemented manually.

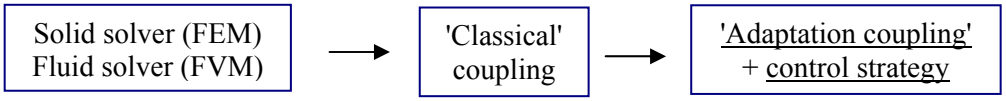

Fig.7.2.12. General scheme of the procedure of simulation of adaptive membrane valve involving 'classical coupling' and 'adaptation coupling'.

Adaptation coupling together with control strategy constitute cross-domain feedback control algorithm. In numerical analysis, this algorithm is executed by a 'software controller' which is repeatedly activated to execute feedback control loop. The software controller comprises of 'sensor' for reading actual results of the analysis and 'actuator' for altering actual properties of the system according to assumed control strategy. Both sensor and actuator may pertain to fluid or solid domains, which results in four possible types of the adaptive system:

- Type 1: CSM-CSM (sensor solid - actuator solid),
- Type 2: CFD-CSM (sensor fluid - actuator solid),
- Type 3: CSM-CFD (sensor solid - actuator fluid),
- Type 4: CFD-CFD (sensor fluid - actuator fluid).

The quantities being a typical input for the sensor as well as quantities being an output from the actuator in the numerical analysis of the adaptive membrane valve are collected in Fig. 7.2.13. The input for the software controller are the results obtained from current or previous time steps, integral and differential quantities related to space and time. The output from the actuator directly defines excitations applied to active elements or particular features of the system at actual time instant, cf. Fig. 7.2.13.

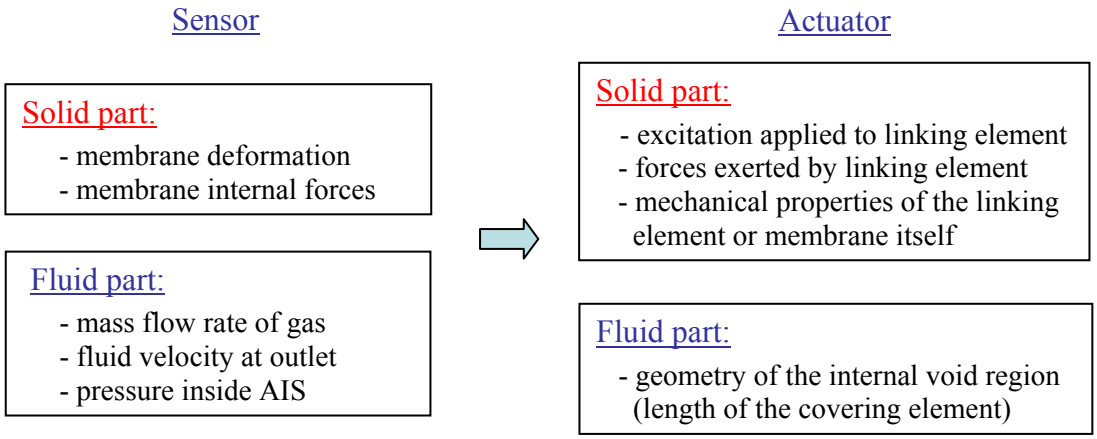

Fig.7.2.13. Typical quantities used for sensors and actuators in feedback coupling algorithm.

The 'software controller' executes feedback control by stopping coupled analysis, reading result files from solid and fluid solvers, performing calculations according to implemented control strategy, processing appropriate input files for solid and fluid solver and finally by restarting the analysis, Fig. 7.2.14. The 'software controller' can be implemented either by internal subroutines of fluid and solid solvers or by external software. The usage of the internal subroutines of applied FEM/FVM solvers is possible only in case when sensor and actuator utilise quantities governed by the same solver (i.e. for solid-solid or fluid-fluid couplings). In other cases, when exchange of data between fluid and solid solvers is required the external software has to be used. For the sake of consistency of all possible types of feedback control, the second method was implemented and MATLAB was used as external software which governs the whole procedure.

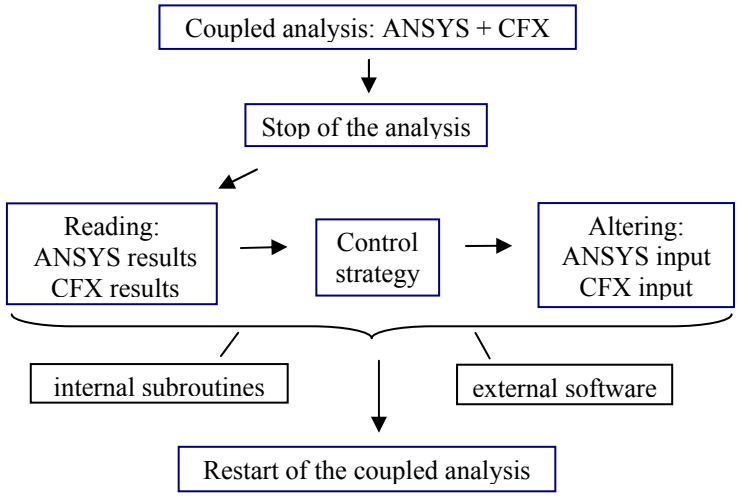

Fig.7.2.14. General operating principle of 'software controller': single step of feedback control.

The numerical examples presented below demonstrate various types of adaptation couplings, their influence on response of adaptive membrane valve and obtained mass flow rate of gas.

Solid-solid control coupling

Basic application of solid-solid adaptation coupling to membrane valve relies on changing the excitation applied to active linking element (Fig. 7.2.11) or its mechanical properties on the basis of actual response of the membrane. Alternatively, it can be assumed that the whole membrane is made of functional material whose mechanical properties can be altered during the process. In a simple feedback control algorithm (Fig. 7.2.15), the Young modulus of the membrane is changed depending on actual vertical displacement of certain point of the membrane u_m measured by sensor. In case when measured displacement exceeds the limit value u_{max} the Young modulus is substantially increased. Checking of membrane displacement, as well as determination and setting of the value of Young modulus is executed at the end of each adaptation coupling step of a constant length t=0,1ms.

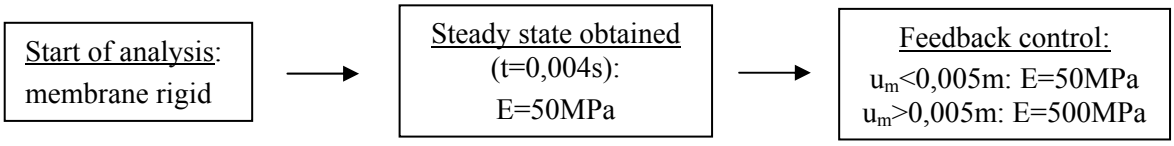

Fig.7.2.15. Solid-solid control coupling: scheme of the applied procedure.

During the initial stage of the process (t=4-4.7 ms), internal membrane is gradually expanded by pressure of the flowing fluid. Consequently, total mass flow rate of the fluid at outlet is decreasing. Exceed of critical displacement of the membrane u_{max}, determined by the sensor at time t=4.7 ms, causes activation of control. The applied increase of Young modulus results in a sudden increase of membrane internal forces, stopping of membrane expansion, and its fast gradual tightening (Fig. 7.2.16, 7.2.17b). Since displacement of the tracked node quickly drops below assumed limit, the Young modulus is decreased back to the initial value which causes decrease of internal forces and gradual increase of deformation caused by gas.

At the beginning of membrane compression caused by activation of control the total mass flow rate of the fluid at outlet was observed to temporarily decrease (probably as a result of imposed sudden change of the system state). However, in a further stage it substantially increases, as expected, due to larger width of the channel where fluid flow occurs, Fig. 7.2.17.

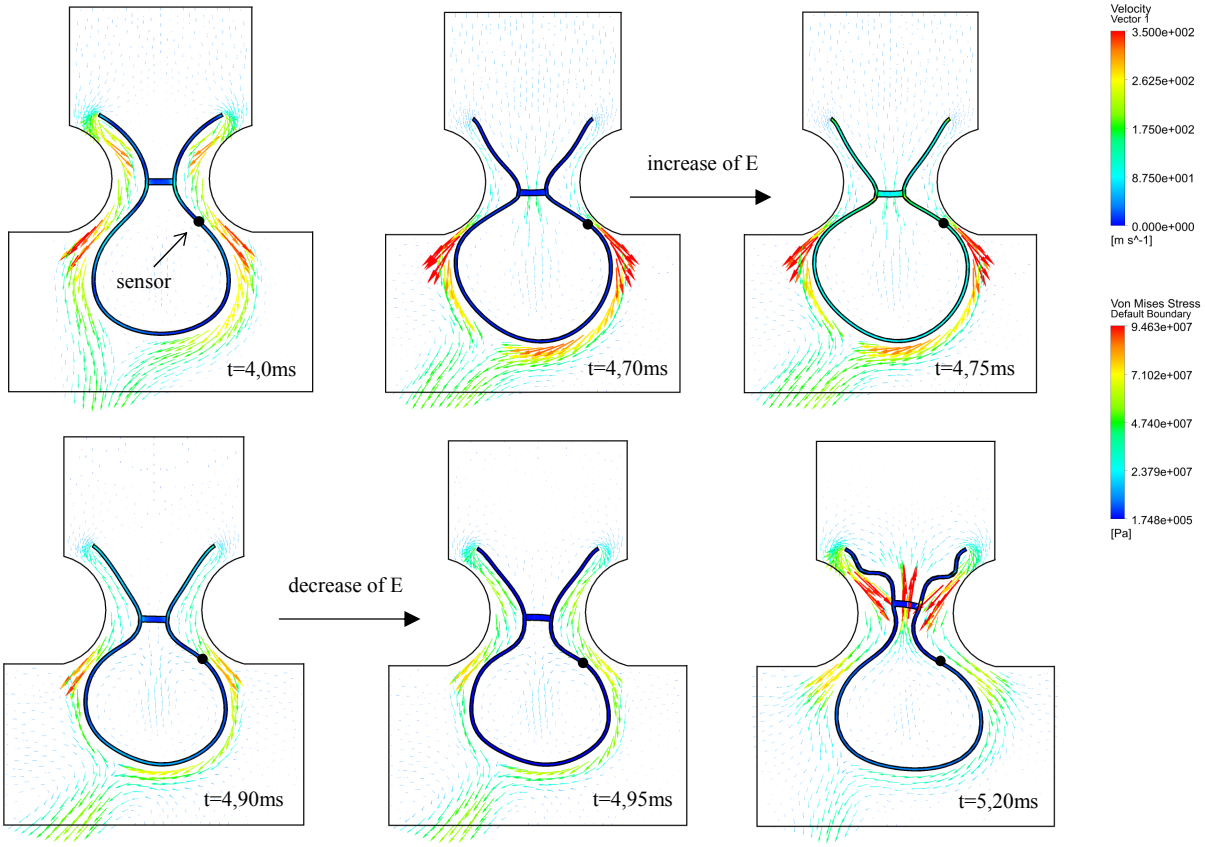

Fig.7.2.16. Subsequent stages of simulation of membrane valve with solid-solid control coupling (linking element is invisible for the fluid flow).

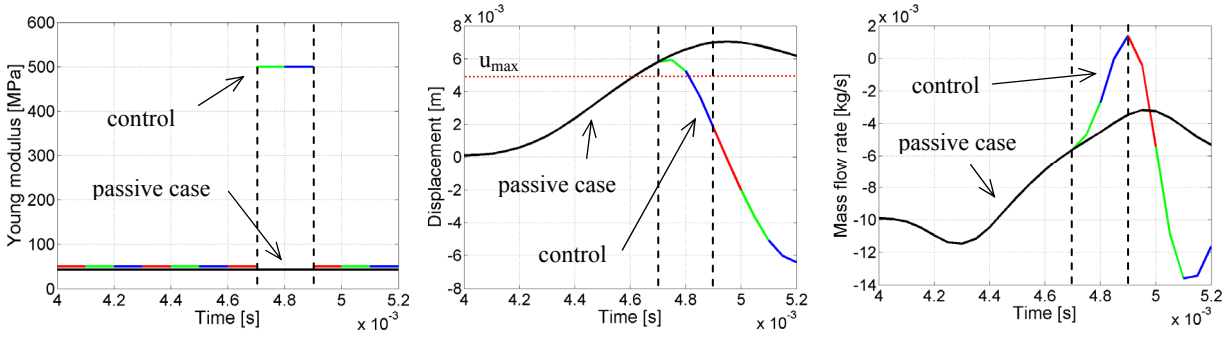

Fig.7.2.17. Solid-solid control coupling: a) applied change of Young modulus, b) vertical displacement measured by sensor, c) resulting mass flow rate of the fluid at outlet.

Another application of solid-solid adaptation coupling is not related to control of the mass flow rate of the fluid through the membrane valve but to modelling of its total closing. Typically, in situation when membrane approaches external wall of the flow channel, ALE analysis is stopped due to local total compression of the fluid mesh and change of system topology. In the proposed approach, just before contact with external wall the membrane is 'frozen', i.e.:

- strains at each element of the membrane are decreased to zero and its stiffness is substantially increased, or
- membrane is removed from the analysis and fluid mesh is set as immobile.

The method allows for stopping deformation of membrane in configuration when the valve is almost closed and prevents termination of the numerical analysis. Although fluid flow is nearly blocked, the numerical analysis proceeds and forces exerted by the fluid on membrane balloon can be still computed. When fluid forces tend to separate membrane from the external wall of the flow channel, membrane becomes 'un-frozen', i.e. original state of the membrane in terms of strains and Young modulus is retrieved and typical FSI analysis is continued.

An alternative for the above proposed procedure is application of the standard contact algorithm (application of additional contact force to the membrane) which should be activated slightly before time instant when membrane approaches the external wall. Both proposed methods allow for partial overcoming of the requirement of preserving system topology which is one of the most intrinsic drawbacks of the ALE approach.

Fluid-solid control coupling

Fluid-solid adaptation coupling is based on changing mechanical properties of the linking element (or the whole membrane) according to data obtained from the fluid part of the simulation, i.e. mass flow rate of gas, gas velocity at certain location or pressure inside inflatable structure. The method can be considered as more direct since mass flow rate of gas which is the quantity used as a sensor is also the main quantity controlled during the process.

In a simple numerical example, the Young modulus of the whole membrane is changed depending on actual total mass flow rate of the fluid at outlet according to scheme presented in Fig. 7.2.18. In case when mass flow rate drops below a certain level certain level, the Young modulus of the membrane is increased. The above control condition is checked at the end of each adaptation coupling step, every 0.1 ms.

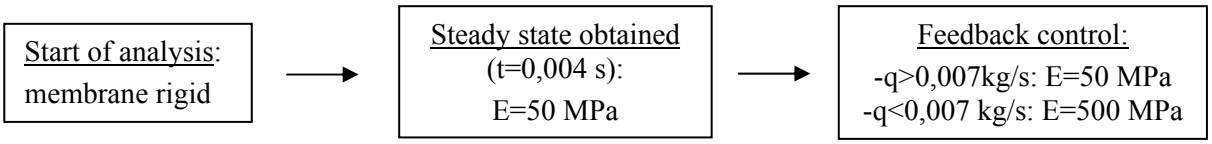

Fig.7.2.18. Fluid-solid control coupling: scheme of the applied procedure.

Qualitative results of the applied fluid-solid control coupling are similar to results from previously considered solid-solid coupling, Fig. 7.2.19. Increase of the Young modulus prevents further expansion of the membrane, causes its gradual contraction and with a certain delay stops decrease of total mass flow rate of the fluid. Since, at the end of the process, total mass flow rate of gas exceeds the limiting value, the low value of Young modulus is retrieved.

Longer time period when the Young modulus remains increased results in final shape of membrane deformation which is different from the one obtained in solid-solid coupling.

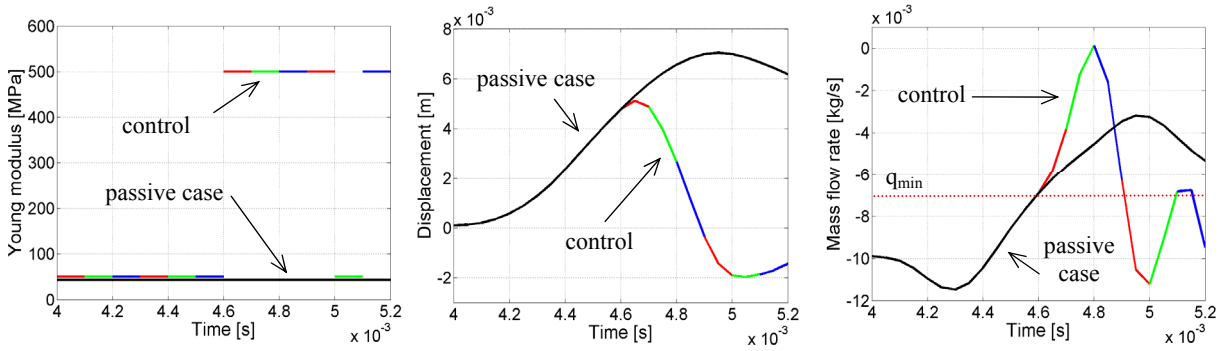

Fig.7.2.19. Fluid-solid control coupling: a) applied change of Young modulus, b) measured vertical displacement, c) resulting mass flow rate of the fluid at outlet.

Solid-fluid control coupling

Solid-fluid adaptation coupling relies on change of properties of the fluid or change of shape of the fluid domain based on actual dynamic response of the membrane.

In the considered adaptive membrane valve, the control will be applied by changing actual length of the additional 'covering element' located above membrane and modelled as a void region inside fluid domain (Fig. 7.2.21). The length of the 'covering element' determines the rate of gas inflow into the membrane balloon, velocity of membrane expansion and corresponding speed of valve closing. Since the covering element of a full length does not totally block the inflow of gas into the membrane, it does not prevent the valve closing but only slows it down (around four times in comparison to generic valve without covering).

The numerical example concerns initial stage of gas outflow when gas flow rate at outlet still remains unsteady. The idea of applying control coupling will be different than in previously considered examples, i.e. the control will be applied in order to increase speed of valve closing and to decrease mass flow rate of fluid through the valve. According to a simple control algorithm (Fig. 7.2.20), the analysis begins with maximal length of the covering element (d_{cov}=0,045 m) which initially remains constant. Shortening of the covering element with velocity v_{cov} is started when vertical displacement of the sensor u_m reaches the limit value u_{max}. In further part of the process, the speed of shortening of the active element is decreased and finally stopped due to a local large deformation of the fluid mesh.

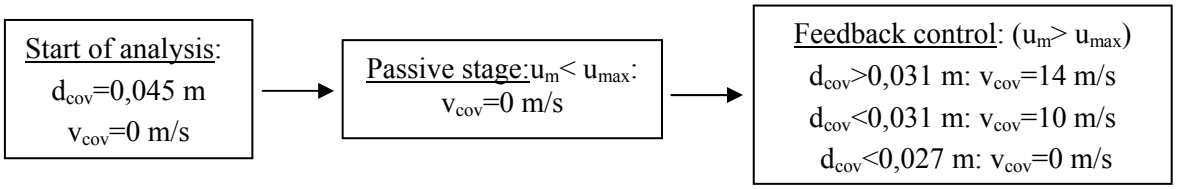

Fig.7.2.20. Solid-fluid control coupling: scheme of applied procedure.

Activation of control causes increase of gas inflow into membrane balloon and increase of pressure inside membrane, Fig. 7.2.21a,b. Observed process of membrane expansion (Fig. 7.2.21b,c) is substantially faster than for membrane valve with immobile covering and it is reflected by larger vertical displacement measured by sensor (Fig. 7.2.22c).

After activation of control, the mass flow rate of gas temporarily raises , but slightly after it is substantially decreased which proves the effectiveness of applied strategy (Fig. 7.2.22d). The delay between applied control and observed response of the system is clearly visible both in displacement of the membrane and in the mass flow rate of gas at outlet, Fig. 7.2.22.

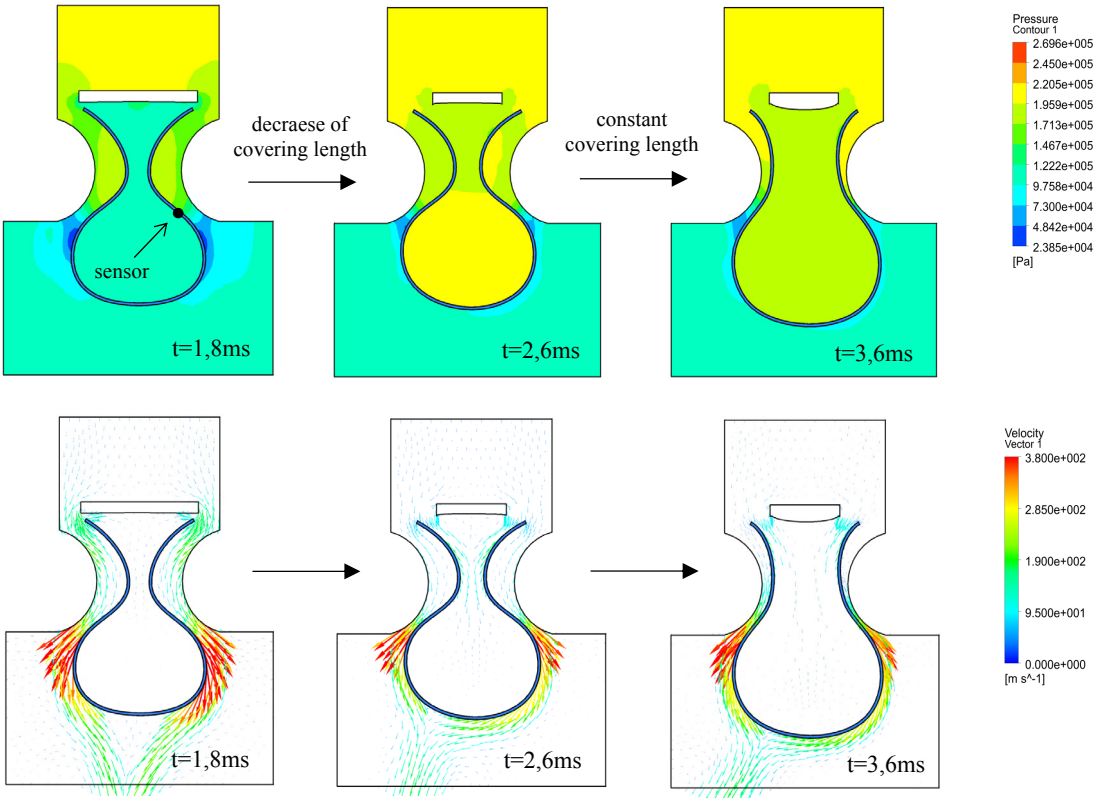

Fig.7.2.21. Subsequent stages of simulation of membrane valve with solid-fluid control coupling.

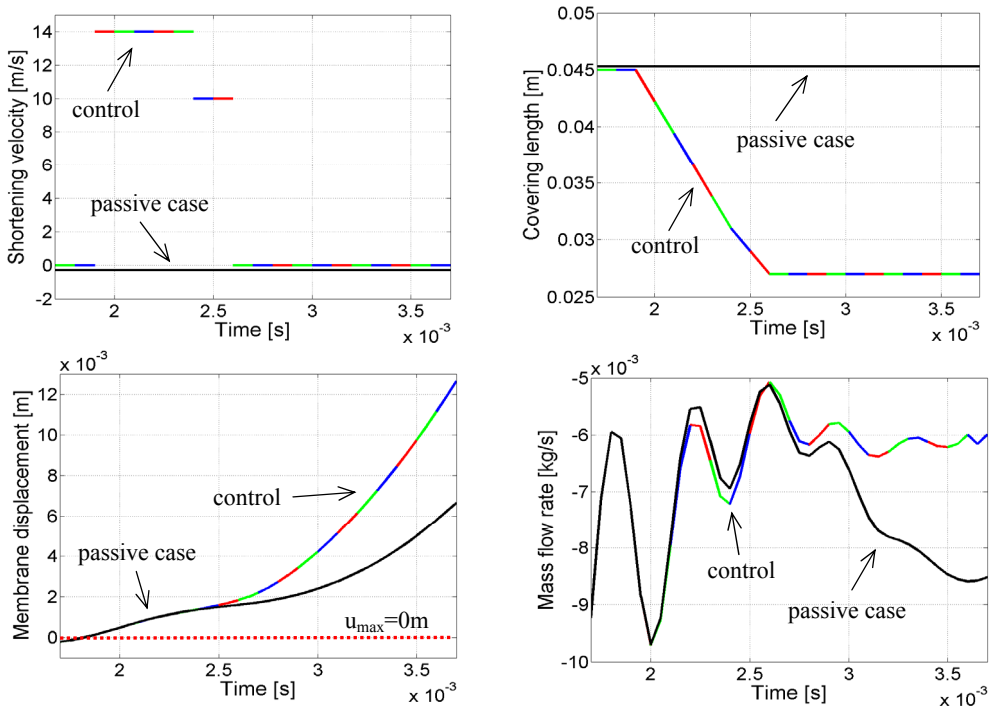

Fig.7.2.22. Solid-fluid control coupling: a), b) imposed change of geometry of the covering, c) vertical displacement measured by sensor, d) resulting mass flow rate of the fluid at outlet.

Fluid-fluid control coupling

Finally, fluid-fluid adaptation coupling concerns the situation when properties of the fluid or shape of the fluid domain are changed depending on results obtained from the fluid part of the analysis. A typical example of such a coupling is change of length of the covering element based on the total mass flow rate of the fluid through the valve.

In the numerical example, the control is aimed at increasing speed of valve closing during the process. Similarly, as in previous case, at the beginning of simulation the covering element has its maximal length. The control starts at time instant of 1ms and relies on decreasing length of the covering element with an arbitrary velocity v_{cov}=10m/s when mass flow rate of fluid through the valve exceeds threshold value q_{max}, Fig. 7.2.23.

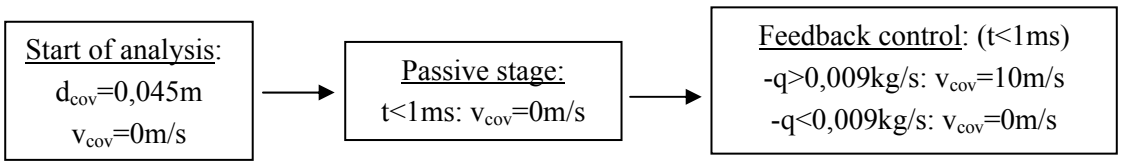

Fig.7.2.23. Fluid-fluid control coupling: scheme of the applied procedure.

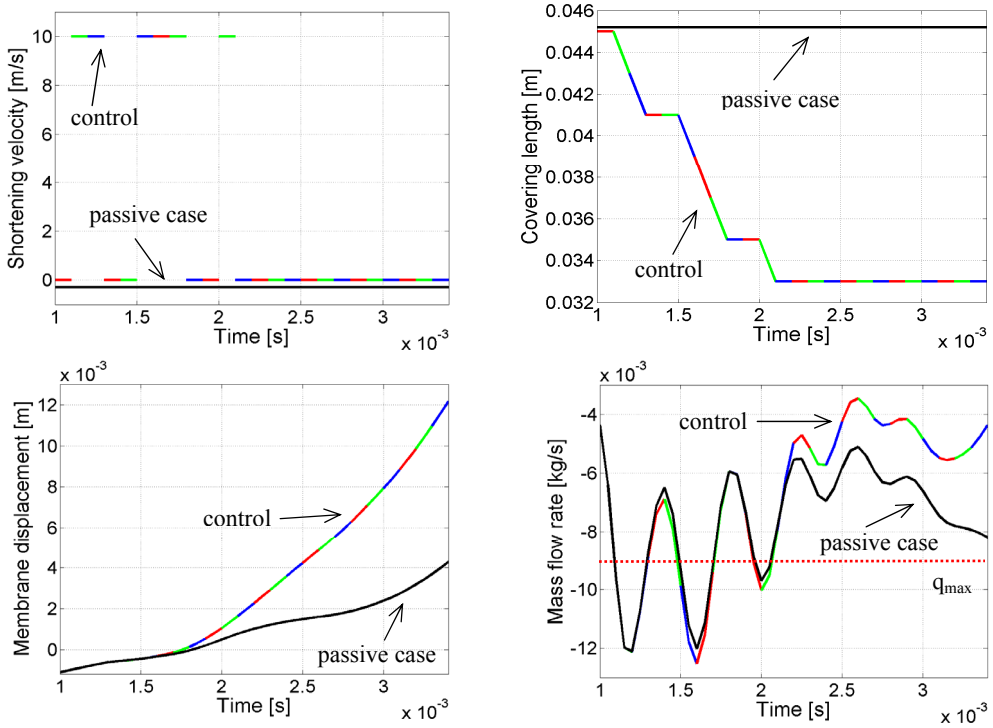

Fig.7.2.24. Fluid-fluid control coupling: a), b) applied change of geometry of the covering, c) measured vertical displacement, d) resulting mass flow rate of the fluid at outlet.

Both in case of passive and adaptive membrane valves, the mass flow rate of gas exceeds threshold value three times during the first half of the process. Therefore, the length of active covering element is decreased in three subsequent stages (Fig. 7.2.24a, b). The effect of applied control becomes transparent after some delay and it is reflected by larger displacement of the membrane and decrease of mass flow rate of fluid at outlet (see Fig. 7.2.24c and 7.2.24d, respectively).

Another application of solid-fluid and fluid-fluid adaptation coupling is controllable change of local fluid properties as for example change of yield stress level of the magneto-rheological fluid caused by magnetic field. In the considered case, gas viscosity can be changed by local increase of temperature of gas flowing through the valve. However, since change of gas viscosity with temperature is small, its influence on the flow through the valve is not expected to be substantial.

Application of 'adaptation coupling' to general model of Adaptive Inflatable Structures

The proposed methodology utilising 'adaptation coupling' can be applied not only to adaptive membrane valve but also to other types of Adaptive Inflatable Structures modelled by the Fluid-Structure Interaction approach.

The methods of control of inflatable structure are collected in Fig. 7.2.25 which is a generalisation of Fig. 7.2.13 related exclusively to membrane valve. Let us note that the right column concerning 'actuators' directly corresponds to general FSI models of Adaptive Inflatable Structure with controllable valve introduced in Section 2.2.3. Recapitulating, the following options of AIS control can be distinguished:

- change of fluid boundary conditions can be used for direct control of outflow of the fluid ('boundary condition control');
- change of solid boundary condition can be used for altering width of the outflow orifice ('orifice width control');
- change of geometry of the fluid domain can be used for controlling position and shape of the valve head ('valve head control', simplified version);
- applied external excitation can be used to change position or shape of the valve head ('valve head control', advanced version).

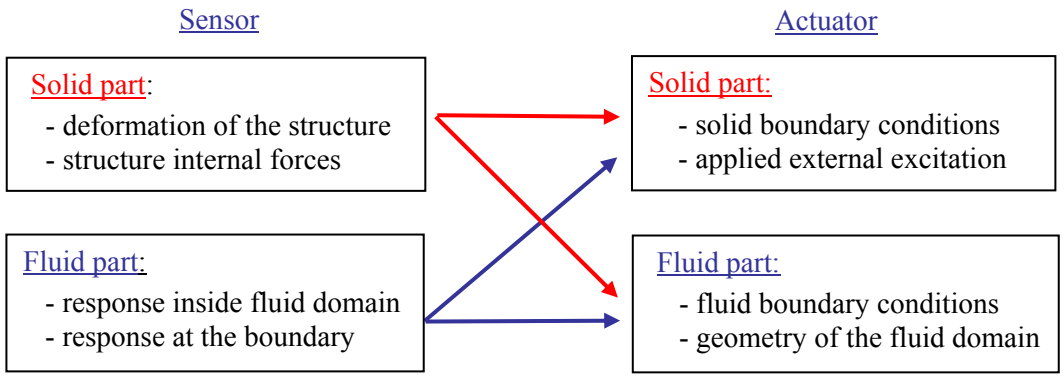

Fig.7.2.25. General scheme of control of Adaptive Inflatable Structure.

According to the presented argumentation, the developed software which is based on 'adaptation coupling' for additional linking solid and fluid solvers and which utilizes cross-domain feedback control algorithms can be effectively used for simulation of arbitrary type of Adaptive Inflatable Structure with internal pressure control.

Summary of Chapter 7

The chapter presents two types of high performance valves for Adaptive Inflatable Structures, proposes various methods of their simulation and examines their adaptability and basic

methods of control.

The first section concerns piezoelectric valve in which unidirectional displacement of the valve head is driven by the piezoelectric stack. Several types of piezoelectric valves are described and three methods of valve modelling are proposed. The first method is based on separation of the problem of movement of the valve head caused by piezo-stack and the problem of fluid flow through the region where position of the valve head changes. Diverse numerical and analytical approaches for modelling piezoelectric part of the problem are proposed. The following methods of modelling piezo-valves are based on coupling of analytical model of the piezoelectric stack and numerical model of the fluid flow, as well as, on full coupling of the problems of solid mechanics, electricity and fluid mechanics. Two methods are demonstrated on simple examples and one of them is used to compare two designs of piezo-valve. Finally, the feedback control algorithm aimed at finding continuous movement of the valve head which provides desired mass flow rate of gas through the valve is proposed and tested numerically.

The second section pertains to the self-closing controllable membrane valve. Initially, valve operating principle is outlined and mathematical model of passive valve based on coupling of structural and fluid mechanics equations is formulated. Further the process of valve closing is simulated with the use of 2D and 3D models, with two competitive approaches (ALE and CEL) and two numerical methods. Although each model has different capability of valve simulation, all models confirm that during gas outflow the pressure inside membrane increases, which causes membrane expansion and valve closing. Further, the model of the passive valve is complemented with active linking element or active covering element and the problem of controlling the response of system modelled by full FSI approach is considered. The concept of ‘adaptation coupling’ is introduced in order to implement cross-domain feedback control algorithms and verify the adaptability of the membrane valve. Corresponding numerical examples prove that membrane expansion and mass flow rate of gas at outlet can be controlled with the use of various sensing and actuation techniques.

Although the chapter slightly diverges from the main topic of research aimed directly at simulation of structures subjected to impact loading, it constitutes essential part of thesis since it proposes methods of simulation and control of high performance valves which are indispensable element of Adaptive Inflatable Structures. From theoretical viewpoint the chapter extends the range of considerations and numerical examples on the systems modelled as a full coupling of structural and fluid mechanics equations.

CHAPTER 8 - FINAL REMARKS

8.1. Summary and conclusions from conducted research

The most general conclusion from the conducted research is that Adaptive Inflatable Structures with controlled release of pressure are effective methodology for Adaptive Impact Absorption. Comprehensive numerical results, as well as basic experimental results obtained within this thesis, indicate that the concept is feasible and can be applied in engineering practice. Both the appropriately adjusted initial inflation of the chambers and precisely controlled release of pressure allow for adaptation to actual dynamic loading of various characteristics and for optimal mitigation of the dynamic response of both the impacting object and impacted structure. Adaptive Inflatable Structures have promising applications for impact absorption in automotive, waterborne and aeronautical industry.

Due to heterogeneous nature of this work each chapter was summarized in the course of the thesis. Nevertheless, the brief summary and the most intrinsic conclusions from each part are recalled below.

Chapter 2, entitled 'The concept and modelling of Adaptive Inflatable Structures', introduces the idea of inflatable structures equipped with sealed air chambers and controllable valves. The first part of the chapter is dedicated to formulation of theoretical model of adaptive inflatable structure based on coupling of PDEs describing the solid walls and internal fluid. The conservation laws are derived in the most general, ALE frame of reference and further transformed into other reference frames. The models of passive inflatable structure, based on 'conforming boundary' and 'fixed grid' methods, are presented and two solution methods, partitioned and monolithic, are discussed. The model of passive inflatable structure is complemented with controllable valve, for which several modelling options are proposed. Further, simplified method of modelling of adaptive inflatable structure based on uniform distribution of gas parameters in each chamber and analytical model of the gas flow is developed and generalized into multi-chamber systems. Moreover, the hybrid method of modelling of inflatable structures is introduced and control problems related to adaptation of inflatable structure to actual impact loading are formulated.

The chapter reveals that simulation of Adaptive Inflatable Structures requires complex modelling which involves various branches of continuum mechanics including nonlinear solid mechanics, fluid dynamics and thermodynamics. Consequently, sophisticated mathematical description is required to analyze dynamic response of inflatable structure subjected to impact loading. The chapter classifies the methods of modelling of inflatable structures and provides theoretical background for further considerations.

Chapter 3, 'Adaptive Pneumatic Cylinders', introduces three types of adaptive pneumatic cylinders equipped with controllable valves. Simplified modelling by Uniform Pressure Method is used to predict response of the pneumatic absorbers to impact loading and to investigate their dynamic characteristics. Special attention is given to the energy dissipation which is analyzed from mechanical, thermodynamic and mathematical viewpoint in order to gain an insight to its complex nature. The problem of impact identification is briefly outlined to prove the possibility of identification of impact parameters at the initial stage of the process. Miscellaneous strategies of impact reception are proposed and verified numerically. The

analysis is focused on the problem of minimization of impacting object deceleration, for which various strategies taking into account diverse constraints and operating principles of the valve are considered. The methodology of optimal design of the adaptive pneumatic cylinders is developed and applied to design landing gear for small aerial vehicle. The chapter finishes with the experiment which confirms the feasibility of real-time control of internal pressure during the impact process.

Chapter 4, entitled 'CFD models of adaptive pneumatic cylinders', proposes separate, more complex methodology based on methods of computational fluid dynamics for modelling and control of the adaptive pneumatic cylinders subjected to impact loading of high initial velocity. The model utilizes coupling of the Navier-Stokes equations with dynamics of the piston and incorporates the procedure for real-time control of the valve opening. Two strategies aimed at maintaining constant level of impacting object deceleration, based on various methods of valve flow control, are proposed and tested numerically. CFD-based modelling of double-chamber cylinders with two options of the gas flow and application of hybrid method of modelling are also described. The final example concerns modelling and control of one-dimensional pneumatic system subjected to impact loading.

Chapter 3 together with Chapter 4 provide the methodology for modelling, control and optimal design of adaptive pneumatic cylinders. The main conclusion from conducted research is that pneumatic cylinders with controllable valves can serve as an efficient impact energy absorbers which outperform passive devices. Diverse control strategies can be proposed depending on the control objective and limitations of the valve. Application of the proper control strategy allows for adjustment of absorber characteristics to actual impact loading in order to provide optimal impact reception.

Chapter 5 entitled 'Crashworthiness of Adaptive Inflatable Structures' is dedicated to investigation of the dynamic characteristics, impact durability and energy dissipation capabilities of the inflatable thin-walled steel structures. The chapter begins with the simple experiment which confirms the beneficial influence of internal pressure on buckling of the aluminium can. Further, FEM is used to show the effect of internal pressure on stress distribution, vibration frequencies, buckling and bursting of the inflated cylindrical structures. The following numerical examples related to inflatable hull compartments, door of the car and traffic barriers demonstrate change of structure deformation and durability caused by appropriate inflation. A simple 2D model of the multi-chamber barrier is used to develop algorithms for adjustment of pressure in particular chambers aimed at maximization of structure load capacity under constraints imposed on its limiting deformation. The following control strategies are oriented towards optimal adaptation to actual impact loading.

The outcome of the chapter is the analysis of the influence of internal pressure on dynamic characteristics of thin-walled structures. As it was proved, application of internal pressure profitably influences load-bearing capacity and energy dissipation capabilities. When multi-chamber system is used and pressure is precisely adjusted and controlled during impact, the gain in structure load capacity might be significant.

Chapter 6, 'Adaptive flow control - based airbags' presents the concept of adaptive airbags which, in contrast to classical ones, are equipped with controllable valves activated during the impact process. The first considered application is pneumatic torus-shaped fender

for protecting offshore wind turbine tower during ship docking. Numerical simulation of the adaptive system proves that developed control strategies effectively mitigate dynamic response of both the impacting ship (deceleration and rebound) and impacted wind turbine tower (local stresses and vibrations). The second proposed system are adaptive airbags for the emergency landing. Conducted numerical simulations exploit both analytical and numerical modelling of the airbag deformation. Adaptation strategies are elaborated for a single airbag, 2D model of the landing platform, 2D model of compliant landing object and finally for 3D object. Inflation and pressure release from the particular airbags are precisely adjusted to actual scenario of the landing and they provide minimisation of the landing object rebound, minimisation of its linear and angular decelerations, and stabilisation during landing.

The main conclusion arising from conducted numerical simulations is that classical design of the airbag can be significantly improved by application of the controllable valve. The concept of introducing controllable gas exhaust was found to be effective both in case of pneumatic fenders for maritime applications and in case of system of adaptive airbags for an emergency landing.

Chapter 7, 'Controllable high performance valves' concerns modelling and control of high speed and stroke valves for inflatable structures. In the first part, piezoelectric valve of a simple design is analyzed. Three methods of valve modelling based on coupling of the piezoelectric problem and fluid dynamics problem are proposed. Moreover, the strategy of controlling valve head position aimed at obtaining desired mass flow rate of the fluid is developed. In the following part, the operation of self-closing membrane valve is examined by means of two- and three- dimensional models and two FSI methods based on various types of coupling of solid and fluid mechanics equations. Control of the valve is obtained by implementation of the feedback control algorithm which requires supplementary coupling of the arbitrary quantities of solid and fluid analysis. Proposed methodology allows for controlling deformation of the membrane and the process of valve closing depending on actual results of the numerical analysis.

The outcome of the chapter are the methods of modelling and control of valves for inflatable structures, which utilize solution of the coupled problem of solid and fluid dynamics and additional coupling for execution of the control algorithm. Conducted simulations initially confirm the possibility of controlling mass flow rate of gas during the impact process and thus the possibility of realization of previously proposed pressure control strategies.

8.2. Original achievements of the thesis

The objectives of the thesis were divided into three separate groups concerning modelling of inflatable structures, development of control strategies and elaboration of concepts of engineering structures utilizing the above paradigm. Therefore, original achievements of the thesis are related to three above groups of problems.

<u>Achievements concerning modelling of Adaptive Inflatable Structures:</u>

- Formulation of theoretical model of single-chamber Adaptive Inflatable Structure based on coupling of conservation equations describing solid wall and Navier-Stokes

equations describing internal fluid (FSI models), which take into account diverse methodologies of modelling controllable valves

- Formulation of simplified models of Adaptive Inflatable Structure based on uniform pressure method (UPM model) with various options for modelling of heat transfer through the walls and various models of the gas flow through the valve; generalisation of the above models for multi-chamber systems
- Formulation of the hybrid model of Adaptive Inflatable Structures which utilizes division of the considered structure into regions modelled by means of FSI- and UPM-based approach with appropriate inter-domain coupling conditions
- Implementation of FSI-based model by using coupled commercial CSM and CFD software by introducing additional coupling to provide structure adaptability
- Implementation of UPM-based model of AIS by using commercial solid mechanics software and by applying either internal subroutines or coupling to external software
- Implementation of models of adaptive pneumatic cylinders of various design and simplified analytical models of airbags by own-developed codes.

Achievements concerning development of control strategies for AIS:

- Development and implementation of miscellaneous valve opening strategies for single- and double-chamber pneumatic cylinders (aimed at minimisation of deceleration and internal pressure and maximisation of the load capacity), which take into account diverse operating principles of the valve and various constraints
- Development of two strategies of valve flow control aimed at maintaining constant deceleration of the object impacting pneumatic cylinder with high initial velocity; their implementation with the use of CFD-based model of pneumatic cylinder
- Elaboration of the pressure adjustment strategies providing maximisation of the load capacity of inflatable road barrier and its adaptation to actual impact loading
- Elaboration of strategies of adaptation of torus-shaped pneumatic fender, which provide mitigation of the dynamic response of the wind turbine tower and the ship during offshore docking
- Development of control strategies intended to mitigate the process of emergency landing; their implementation for 2D model of the landing platform, 2D model of the landing object, 3D model of the landing platform with full modelling of airbags
- Elaboration of the procedures aimed at controlling mass flow rate of gas through controllable valves; development and implementation of the feedback control algorithm for membrane valve based on additional coupling of non-boundary quantities of solid and fluid domain (feedback control of the FSI problem).

Achievements concerning development of concepts of engineering structures utilising introduced paradigm and numerical simulation of their effectiveness:

- Numerical simulation of the three types of adaptive pneumatic cylinders with implemented control strategies for optimal impact reception, comparison of various

adaptation strategies and various pneumatic cylinders against each other; development of methodology for design of adaptive cylinders; estimation of efficiency of the pneumatic landing gear

- Development of the concept of adaptive inflatable multi-chamber thin-walled barrier, simulation of the response of the barrier to the impact loading, analysis of the influence of pressure release strategy on increase of the structure load capacity, deceleration of the impacting object and final structure deformation
- Elaboration of the concept of torus-shaped adaptive pneumatic fender for protecting offshore wind turbine tower during ship docking, optimal design of the system, comparison of the system effectiveness in terms of ship and tower protection for various types of adaptation strategies
- Development of concept of adaptive 'flow control - based' airbags for emergency landing; verification of the system efficiency for various landing scenarios and with the use of diverse numerical models
- Elaboration of the methodology for estimation of the performance of valves for inflatable structures; verification of the operating principle of the self-closing membrane valve by two numerical methods and basic analysis of its controllability

8.3. Further challenges in a field of adaptive inflatable structures

Several important topics related to modelling and control of inflatable structures has not been considered and discussed herein. The most intrinsic general lines of research which are planned to be undertaken include:

- Application of the most precise FSI model based on full coupling of fluid and solid mechanics problems for simulation of Adaptive Inflatable Structures subjected to impact loading; development of control strategies with the use of the above model
- Further development of hybrid model of Adaptive Inflatable Structure composed of FSI- and UPM-based parts and its application for numerical simulations
- Experimental testing of the valve control strategies developed for pneumatic cylinders; experimental verification of the proposed concepts of engineering structures: adaptive inflatable thin-walled barriers, pneumatic tours-shaped fenders and adaptive airbags;
- Development of complete methodology for optimal design and control of complex adaptive pneumatic structures subjected to multiple impact load cases involving simultaneous processes of topological optimisation (choice of structure shape and division into pressure chambers), optimal placement of the controllable valves and development of pressure control strategy.

The author cherish hope that the thesis will be helpful for the engineers involved in design of inflatable structures for impact absorption and that the concepts presented in this thesis will contribute to development and widespread application of adaptive systems of impact absorption.

9. BIBLIOGRAPHY:

[1] Holnicki-Szulc J. (ed.), Smart Technologies for safety engineering, Willey, 2008

[2] Holnicki-Szulc J., Graczykowski C., Mikułowski G., Mróz A., Pawłowski P., (2009), Smart Technologies for Adaptive Impact Absorption, *Solid State Phenomena*, vol. 154, pp. 187-194

[3] Holnicki-Szulc J., Graczykowski C., Mikułowski G., Pawłowski P., Adaptive Impact Absorption, the concept, innovative solutions, applications, *Proceeding of the International Conference on Smart Materials and Structures*, Porto, Portugal, 2009

[4] Holnicki-Szulc J., Mikułowski G., Mróz A, Pawłowski P., Adaptive Impact Absorption, *Proceeding of the Fifth International Conference on Engineering Computational Technology*, Las Palmas, Spain, 2006

[5] Holnicki-Szulc J., Mota-Soares C.A. (Eds.), Advances in Smart Technologies in Structural Engineering, Springer, 2004

[6] Janocha H. (ed.) Adaptronics and smart structures : basic, materials, design and applications. Springer, Berlin, 1999.

[7] Worden K., Bullough W.A., Haywood J., Smart Technologies, World Scientific, New Jersey, 2003.

[8] Srinivasan A.V., McFarland, Smart Structures. Analysis and Design, Cambridge, 2001

[9] Banks H.T., Smith R.C., Wang Y., Smart material structures: modeling, estimation and control, Wiley, 1996

[10] Proceedings of the International Conference on Adaptive Structures and Technologies (International Conference on Smart Structures and Materials), 1990-2011

[11] Proceedings International Conference on Smart Materials and Structures (SMART), 2003-2011

[12] Gryboś R., Teoria uderzenia w dyskretnych układach mechanicznych, PWN, 1969 (in polish)

[13] Stronge W.J., Impact Mechanics, Cambridge, 2000

[14] Kaliski S., Drgania i fale, PWN, 1986

[15] Alexander J.M., (1960), An approximate analysis of the collapse of thin cylindrical shells under axial Loading. *Q. J. Mech. Appl. Math.*, 4(13), pp.10–15

[16] Jones N. Structural Impact. Cambridge Univ. Press, 1989.

[17] Jones N. and Wierzbicki T. (eds.), Structural crashworthiness, London, Butterworths, 1983.

[18] Jones N. and Wierzbicki T. (eds.), Structural failure, John Wiley & Sons New York, 1989.

[19] Jones N. and Wierzbicki T. (eds.), Structural crashworthiness and failure, Elsevier Applied Science, 1993.

[20] Ambrosio J.A.C. (ed.), Crashworthiness of transportation system: structural impact and occupant protection, Kluwer Academic, 1997

[21] Bangash M., Impact and Explosion, Blackwell, 1993

[22] Clough R.W., Penzien J., Dynamics of Structures. McGraw-Hill, 1975.

[23] Chopra A.K., Dynamics of structures. Theory and Applications to Earthquake Engineering, Prentice Hall, 2007

[24] Chmielewski T., Zembaty Z., Dynamika konstrukcji, Arkady, 1998 (in polish)

[25] Bathe K.J., Finite Element Procedures in Engineering Analysis, Prentice Hall, 1981.

[26] Cook R.D., Malkus D.S., Plesha M.E., Concepts and Applications of Finite Element Analysis, John Wiley & Sons, New York, 1989.

[27] Zienkiewicz O.C., The Finite Element Method, McGraw-Hill, 1997

[28] Kleiber M., Metoda elementów skończonych w nieliniowej mechanice kontinuum, PWN, 1985

[29] Reddy J.N., Introduction to nonlinear finite element methods, Oxford, 2004

[30] Belytschko T., Liu W. K., and Moran B. Nonlinear Finite Elements for Continua and Structures, John Wiley & Sons, 2000.

[31] Abramowicz W., Macro element method on crashworthiness of vehicles. In: Ambrosio J. (ed.), Crashworthiness - energy management and occupant protection. Springer; Wien, New York, 2001.

[32] Laursen T.A., Computational impact and contact mechanics. Fundamentals of modeling interfacial phenomena in nonlinear finite element analysis, Springer, 2002

[33] Meirovitch L., Dynamics and control of structures, John Wiley, 1990

[34] Dorf R.C., Bishop R.H., Modern control theory, Prentice Hall, 2001

[35] Athans M., Falb F.L., Optimal control, McGraw-Hill, New York, 1976.

[36] Ioannou P.A., Sun J., Robust adaptive control, Prentice-Hall, 1996.

[37] Sastry S. and Bodson M., Adaptive Control: Stability, Convergence, and Robustness, Prentice-Hall, 1994

[38] Preumont A., Vibration control of active structures: an introduction, Chapter 12, Springer, 2002

[39] Gaul L., Albrecht H., Wirnitzer J., Semi-Active Friction Damping of Flexible Lightweight Structures, *Proceeding of the Workshop on Smart Materials and Structures*, Jadwisin, Poland, 2003

[40] Green J.F, Howell W.E., (1973), A technique for design active control systems for aeronautical telescope mirrors. NASA TN D-7090, 973

[41] Balas M.J., (1979), Direct Velocity Feedback Control Of Large Space Structures, *AIAA J. Of Guidance,* Vol. 2(3), pp. 252-253

[42] Fujino Y., Warnitchai P., Pacheco B.M., (1993), Active stiffness control of cable structures, *ASME J. of Applied Mechanics*, vol. 60, pp. 948-953
[43] Suhardjo J., Spencer B. F. Jr., Kareem A., (1992), Frequency domain optimal control of wind-excited buildings, *Journal of Engineering Mechanics*, vol. 118, no.12.
[44] Błachowski B.D, Optymalne sterowanie drganiami masztów z odciągami, rozprawa doktorska, IPPT PAN, 2004
[45] Bossens F., Preumont A., (2001), Active Tendon Control of Cable-Stayed Bridges: a large-scale demonstration, *Earthquake Engineering and Structural Dynamics*, 30, 961-979
[46] Cheng F.Y., Jiang H., Lou J.K., Smart Structures: Innovative Systems for Seismic Response Control, CRC Press, 2008
[47] Wang Z. L., Kang Z.C., Functional and smart materials: structural evolution and structure analysis, Springer, 1998
[48] Yang J., The Mechanics of Piezoelectric Structures, Danvers, 2006
[49] Gautschi G., Piezoelectric sensorics : force, strain, pressure, acceleration and acoustic emission sensors, materials and amplifiers, Springer, Berlin, 2002
[50] Smith R.C., Smart Material Systems. Model Development, Philadelphia, 2005
[51] Pasierbiński J., Zbysiński P., Układy programowalne w praktyce, WKiŁ, 2002, (in polish)
[52] Bender E.K., Berkman E.F., Bieber M., A feasibility study of active landing gear. Affdl-tr-70-126, U.S. Air Force, 1971.
[53] McGehee J.R., Carden H.D., Analytical investigation of the landing dynamics of a large airplane with a load-control system in the main landing gear, Technical Report 1555, NASA, 1979.
[54] McGehee J.R., Dreher R.C., Experimental investigation of active loads control for aircraft landing gear. NASA Technical Paper 2042, Langley Research Centre, 1982.
[55] Horta L.G., Daugherty R.H., Martinson V.J., Modeling and validation of a Navy A6-Intruder actively controlled landing gear system. Technical Report TP-1999-209124, NASA, 1999
[56] Lou Z., Erwin R.D., Winkler C.B., Filisko F.E., An electro- rheologically controlled semi-active landing gear. SAE paper 931403, Langley Research Centre, 1993
[57] Gavin H., Hoagg J. and Dobossy M., Optimal design of MR dampers. In Optimal design of M Dampers, *Proc.of U.S.-Japan Workshop on Smart Structures for Improved Seismic Performance*, Seattle WA, 2001.
[58] Ghiringhelli G.L., (2000), Testing of semi-active landing gear control for a general aviation aircraft, *AIAA Journal of Aircraft*, 37(4), pp. 606-616
[59] Adaptive Landing Gears for Improved Impact Absorption, ADLAND, EU FP6 project IST-FP6-2002-Aero-1-502793-STREP. http://smart.ippt.gov.pl/adland.
[60] Mikułowski G., Holnicki-Szulc (2007), Adaptive landing gear concept - feedback control validation, *Smart Materials and Structures*, 16, pp. 2146-2158
[61] Jankowski Ł., Mikułowski G., Adaptive landing gear: optimum control strategy and improvement potential. *Proceeding of the International Conference on Noise and Vibration Engineering*, Leuven, Belgium, 2006
[62] Mikułowski G., Adaptive aircraft Shock absorbers, Ph.D. Thesis, IPPT PAN, 2008
[63] Pawłowski P., Systemy adaptacyjnej absorpcji obciążeń udarowych: identyfikacja udaru, sterowanie absorberów, dyssypacja energii (in polish), PhD Thesis, IPPT PAN, 2011.
[64] ADLAND, EU FP6 project. Final report.
[65] Kikuchi N., Bendsoe M.P., (1988), Generating optimal topologies in structural design using homogenization method. *Comp. Meth. in Applied Mech. and Eng.*, 71, 197–224.
[66] Mayer R.R., Kikuchi N. and Scott R.A. (1996), Applications of topology optimization techniques to structural crashworthiness, *Int. J. Numer. Methods Eng.*, 39, 1383–1403
[67] Maute K., Schwartz S. and Ramm E., (1998), Adaptive topology optimization of elasto-plastic structures, *Structural and Multidisciplinary Optimization*, 5, 81–89.
[68] Neves M.M., Rodrigues H. and Guedes J.M., (1995), Generalized topology design of structures with a buckling load criterion, *Structural and Multidisciplinary Optimization*, 10, 71–78
[69] Yuge K., Iwai N. and Kikuchi N., Topology optimization algorithm for plates and shells subjected to plastic deformations, *Proceeding of the ASME Design Engineering Tech. Conf.*, 1998
[70] Arora J.S., Kim C.H. and Mijar A.R., Simplified models for automotive crash simulation and design optimization, *Proceeding of 3rd World Congress of Structural and Multidisciplinary Optimization,* Buffalo, NY, 1999
[71] Yamakawa H., Tsutsui Z., Takemae K., Ujita Y. and Suzuki Y., Structural optimization for improvement of train crashworthiness in conceptual and preliminary design, *Proc. 3rd World Congress on Structural and Multidisciplinary Optimization,* Buffalo, NY, 1999
[72] Soto C.A., Application of structural topology optimization in the automotive industry: Past, present and future,

Proc. of 5th World Congress of Computational Mechanics, Vienna, Austria, 2002

[73] Soto C.A., (2001), Structural Topology Optimization: from Minimizing Compliance to Maximizing Energy Absorption, *International Journal of Vehicle Design*, Vol. 25, No. 1-2, pp. 142-163

[74] Pedersen C.B.W., On Topology Design of Frame Structures for Crashworthiness, Ph.D. Thesis, Technical University of Denmark, 2002.

[75] Holnicki-Szulc J., Maćkiewicz A., Kołakowski P., (1998), Design of Adaptive Structures for Improved Load Capacity, *AIAA Journal*, Vol.36, No.3, pp. 471-476.

[76] Marzec Z., Holnicki-Szulc J., Optimal Design of Adaptive Barriers, *Proc. 2nd European Conference on Structural Control*, Champs-sur-Marne, France, 2000

[77] Marzec Z., Holnicki-Szulc J., Adaptive barriers with maximal impact energy absorption, *Proc. 3rd World Congress of Structural and Multidisciplinary Optimization*, New York, US, 1999.

[78] Holnicki-Szulc J., Bielecki T., Structures with Highest Ability of Adaptation to Overloading, *Proc. of IUTAM Symposium on Smart Structures and Structronics Systems,*Magdeburg, Germany, 2000

[79] Bielecki T., Holnicki-Szulc J., Jezequel L., Knap L., Deployable Adaptive Car Buffer, *Proc. VI French-Polish Conference on Modelling and Simulation of the Frictions Phenomena in the Physical and Technical Systems*, Warsaw, Poland, 2000

[80] Holnicki-Szulc J., Wikło M., Adaptive Impact Absorbers, the Concept, Design Tools and Applications, *Proc. 3rd World Conference on Structural Control*, Como, Italy, 2000

[81] Holnicki-Szulc J., Knap L., Optimal design of adaptive structures for the best crashworthiness. *Proc. of 3rd World Congres of Structural and Multidisciplinary Optimization*, Buffalo, USA, 2000

[82] Holnicki J., Knap L., (2004), Adaptive Crashworthiness Concept, *International Journal of Impact Engineering,* vol. 30, no. 6, pp. 639-663

[83] Kołakowski P., Wikło M., Holnicki-Szulc J., (2008), The virtual distortion method - a versatile reanalysis tool for structures and systems, *Structural and Multidisciplinary Optimization*, vol. 36, no. 3, pp. 217-234

[84] Wikło M., Holnicki-Szulc J., Remodelling of adaptive structures designed for impact load, *Proceeding of 4th European Congress on Computational Methods in Applied Sciences and Engineering*, Jyvaskyla, Finland, 2004

[85] Wikło M., Holnicki-Szulc J., (2008), Optimal design of adaptive structures: Part I. Remodeling for impact reception *Structural and Multidisciplinary Optimization,* vol. 37, no. 3, pp. 305-318

[86] Wikło M., Holnicki-Szulc J., (2008), Optimal design of adaptive structures: Part II. Adaptation to impact loads *Structural and Multidisciplinary Optimization,* vol. 37, no. 4, pp. 351-366

[87] Holnicki-Szulc J., Pawlowski P., Wikło M., (2003), High-performance impact absorbing materials - the concept, design tools and applications, *Smart Materials and Structures*, No. 12, pp. 461-467

[88] Pawłowski P., Wikło M., (2004), Design of adaptive structures under random impact conditions, In: Advances in Smart Technologies in Structural Engineering, J.Holnicki-Szulc, C.A. Mota-Soares (Eds.), Springer, 2004

[89] Pawlowski P., Holnicki-Szulc J., Adaptive structures under extreme loads - impact detection, self-adaptation, self-repairing, *Proc. of 3rd European Conference on Structural Control, 3ECSC,* Vienna, Austria, 2004

[90] Ostrowski M., Griskevicius P., Holnicki-Szulc J., Feasibility study of an adaptive energy absorbing system for passenger vehicles, *Proc. of Int. Conf. on Computer Methods in Mechanics*, Częstochowa, Poland, 2005

[91] Ostrowski M., Griskevicius P, Holnicki-Szulc J., Adaptive Crashworthiness of Front-End Structure of Motor Vehicles, *Proc. of the SAE 2007 World Congress*, Detroit, USA, 2007

[92] Ostrowski M., Holnicki-Szulc J., Adaptive Impact Absorption Controlled via Pyrotechnic Devices, *Proc. of the 4th European Conference on Structural Control*, Petersburg, Russia, 2008

[93] Mróz A., Holnicki-Szulc J., Karna T., (2006), Mitigation of Ice Loading on Off-shore Wind Turbines, *Computers and Structures*, vol. 86, no. 3-5, pp. 217-226

[94] Grzędziński J., Mróz A., (2010), Gust load reduction concept in wind turbines, *Wind Energy*, vol. 13, no. 2-3, pp. 267-274

[95] Lee D.W., An innovative inflatable morphing body structure for crashworthiness of military and commercial vehicles, PhD Thesis, University of Michigan, 2009

[96] Jawad, S.A.W., (1996), Intelligent hydraulic bumper for frontal collision mitigation. ASME Applied Mechanics Division*,* 218, pp. 181-189.

[97] Witteman W.J., Improved Vehicle Crashworthiness Design by Control of the Energy Absorption for Different Collision Situations, PhD thesis, Eindhoven University of Technology, 1999.

[98] Woo D., Choi S.B., Choi Y.T., Wereley N.M, (2007), Frontal Crash Mitigation using MR Impact Damper for Controllable Bumper, *Journal of Intelligent Material Systems and Structures,* 18: 1211-1215,

[99] Wågström L., Thomson R., Pipkorn B., (2004), Structural adaptivity for acceleration level reduction in

passenger car frontal collisions, *International Journal of Crashworthiness*, Vol. 9, No. 2, pp.121-127

[100] Deshmukh S.S., McKinley G.H., (2007), Adaptive energy-absorbing materials using field-responsive fluid-impregnated cellular solids, *Smart Materials and Structures*; No. 6 pp. 106–113

[101] Zhang X., Conceptual Study of Adaptive Energy Absorbers. PhD thesis, The Hong Kong University of Science and Technology, 2009.

[102] Balandin D.V., Bolotnik N.N., Pilkey W.D., (2005), Pre-acting control for shock and impact isolation systems. *Shock and Vibration*, vol. 12, pp. 49-65.

[103] Pawłowski P., ADLAND Project, Deliverable 9: Hardware Controller.

[104] Sekuła K., Mikułowski G., Holnicki-Szulc J., Real time dynamic mass identification, *Proc. of the Third European Workshop on Structural Health Monitoring*, Grenada, Spain, 2006

[105] Sekuła K., Holnicki-Szulc J., Comparison of real time impact load identification procedures, *Proc. of the III ECCOMAS thematic conference on smart structures and materials*, Gdansk, Poland, 2007

[106] Topham S., Blow Up: Inflatable Art, Architecture and Design, Prestel Verlag, Munchen, 2002

[107] Proceedings of the 1st International Colloquium on Pneumatic Structures, University of Stuttgart, Germany, 1967

[108] Sharp D., Twentieth century architecture: a visual history, Images Publishing, 2002

[109] American Patent No.3744191, Author: Bird W.W, Birdair Structures, 1971

[110] Tensinet Association: www.tensinet.com

[111] Firt V., Statics, formfinding and dynamics of air-supported membrane structures, Academia, Praque, 1982

[112] Yoshikatsu T., Recommendations for air-supported structures, Madrid, IASS, 1985

[113] Herzog T., Pneumatic structures : a handbook of inflatable architecture, Oxford University Press, New York, 1976

[114] Build Air Company: www.buildair.com

[115] Performance Survey of Inflatable Dams in Ice-Affected Waters, U.S. Army Cold Regions Research and Engineering Laboratory, Hanover, New Hampshire, *Ice Engineering*, Number 30, 2001

[116] Bogart A., Mechanical behavior of vacuum (deflated) supported membrane structures, *Proceedings of 2nd International Conference on Textile Composites and Inflatable Structures*, Stuttgart, Germany, 2005

[117] Airlight Company: www.airlight.biz

[118] Luchsinger R.H., Pedretti M., Reinhard A. (2004), Pressure induced stability. From pneumatic structures to Tensairity, *Journal of Bionics Engineering,* Vol.1 No.3, 141–148

[119] Plagianakos T.S, Teutsch U., Crettol R., Luchsinger R.H., (2009), Static response of a spindle-shaped tenairity column to axial compressions, *Engineering structures*, Vol. 31, Issue 8, pp. 1822-1833

[120] Luchsinger R.H., Crettol R., Plagianakos T.S, Temporary Structures With Tensairity*, Proceeding of the 3rd Latin American Symposium On Tensile-Structures*, Acapulco, Mexico, 2008

[121] Chi J.Y., Pauletti R.M.O, An outline of the evolution of pneumatic structures, *Proceeding of the 2nd Latin American Symposium On Tensile-Structures, Caracas, Venezuela,* 2005

[122] Proceedings of 2nd International Conference on Textile Composites and Inflatable Structures, Stuttgart 2005, E.Onate, B.Kroplin (eds.)

[123] Proceedings of 3rd International Conference on Textile Composites and Inflatable Structures, Barcelona 2007, E.Onate, B.Kroplin (eds.)

[124] Gillispie C.C., The Montgolfier brothers and the invention of aviation, 1783-1784 : with a word on the importance of ballooning for the science of heat and the art of building railroads, Princeton, 1983

[125] Dick H.G, Robinson D.H., The Golden Age of the Great Passenger Airships, Graf Zeppelin & Hindenburg, Smithsonian Institution Press, 1992

[126] Bain A., Van Horst W. D, (1999) The Hindenburg tragedy revisited: the fatal flaw fund, *International Journal of Hydrogen Energy*, *Volume 24, Issue 5*, 1 May 1999, pp. 399-403

[127] Winchester J., The World's Worst Aircraft: From Pioneering Failures to Multimillion Dollar Disasters. Amber Books Ltd., London, 2005.

[128] Model Ga-468 Single-Place Inflatoplane. Marine Corps Landing Force Development Center Quantico Va, Summary report, Jun 1961

[129] Modification And Testing of A One-Place Inflatoplane GA-468, Goodyear Aerospace Corp Akron OH, Final Engineering Report, Sept. 1961

[130] Prospective Concepts Company: http://www.prospective-concepts.ch

[131] Jacob J.D., Smith S.W, Cadogan D., Scarborough S., Expanding the Small UAV Design Space with Inflatable Wings, *Proceeding of the SAE AeroTech Congress and Exhibition*, Los Angeles, CA, 2007

[132] Cadogan D., Smith T., Uhelsky, F., MacKusick, M., Morphing Inflatable Wing Development for Compact Package Unmanned Aerial Vehicles, *Proceeding of 45th AIAA/ASME/ASCE/AHS/ASC Structures, Structural Dynamics and Materials Conference*, Palm Springs, California, 2004

[133] Simpson, A., Jacob, J. D., and Smith, S., Flight Control of a UAV with Inflatable Wings with Wing

Warping, *Proceeding of 24th AIAA Applied Aerodynamics Conference*, San Francisco, CA, 2006

[134] Simpson A., Coulombe N., Jacob J., Smith S., Morphing of Inflatable Wings, *Proceeding of the 46th AIAA/ASME/ASCE/AHS/ASC Structures, Structural Dynamics & Materials Conference*, Austin, Texas, 2005

[135] Cassapakis C., Thomas M., Inflatable Structures Technology Development Overview, AIAA Technical Papper 953738

[136] L'Garde company: www.lgarde.com

[137] Bell L., Pressurized membrane structures in space: examples and special design considerations, In: *Proceedings of 3rd International Conference on Textile Composites and Inflatable Structures*, Barcelona, Spain, 2007

[138] Sasakawa International Center for Space Architecture: www.sicsa.uh.edu

[139] Kafloat Company: www.kafloat.com

[140] Majumdar S.J., Pneumatic systems: principles and maintenance, McGraw-Hill, 2001

[141] TRW Company: www.trw.com

[142] Systemy poduszek powietrznych SRS, Raport firmy TRW

[143] Clark C.C., Young W.A., Car Crash Theory and Tests of Airbag Bumper System, SAE Technical Paper Number 951056, 1995

[144] Train Crash Airbags, Smash Lab, Discovery Science, 2008

[145] American Patent No: 540253513, Restraining inflatable neck guard, 13 Dec 1993, J. C. Green, CONAP, Inc.

[146] Van Meel F., Biesalski A. Blattner C, (2002), Audi adaptive air suspension - the Audi A8's new air suspension. *ATZ Automobiltechnische Zeitschrift.* Vol. 104, pp. 37-40

[147] Polskie Zakłady Lotnicze Świdnik: www.pzl.swidnik.pl

[148] Rotorcraft External Airbag Protection System (REAPS), *Defense Update*, *International Online Defense Magazine*, Issue 3, 2005

[149] Yosuf V., BenMoshe A., Noyman,Y., Gansman B., Bradney C., (2006), Rotorcraft External Airbag Protection System, *American Helicopter Society Annual Form 62 Proceedings*, Phoenix, AZ

[150] NASA webpage: http://mars.jpl.nasa.gov/MPF/

[151] Fasanella E.L., (2009), Multiterrain Earth Landing Systems Applicable for Manned Space Capsules, *Journal of Aerospace Engineering*, vol. 22:3(201)

[152] Ishimura K., Higuchi K., Fundamental characteristics of multi-cellular inflatable space structures, *Proc. of 3rd International Conference on Textile Composites and Inflatable Structures*, Barcelona, Spain, 2007

[153] Instytut Technologii Bezpieczeństwa Moratex: www.moratex.eu

[154] Juntikka R., Hallström S., (2004), Weight-balanced drop test method for characterization of dynamic properties of cellular materials, *International Journal of Impact Engineering* No. 30, pp.541-554.

[155] Graczykowski C., Holnicki-Szulc J., Inflatable Structures with Controlled Release of Pressure for Adaptive Impact Absorption, *Proceeding of 19th International Conference on Adaptive Structures and Technologies*, Ascona, Switzerland, 2008

[156] Bungartz H.J., Schafer M. (eds), Fluid - Structure Interaction: Modelling, Simulation, Optimization, Springer, Berlin, 2006.

[157] Bungartz H.J., Mehl M., Schafer M. (eds), Fluid - Structure Interaction II: Modelling, Simulation, Optimization, Springer, Berlin, 2010.

[158] Hartmann S., Meister A., Schafer M., Turek S. (eds), *Proceeding of International Workshop on Fluid-Structure Interaction: Theory, numerics and applications,* Kassel University Press, 2009

[159] *Computational Mechanics*, Volume 43, Number 1, 2008, Special issue: Fluid-Structure Interaction

[160] Marklund P.O., Nilsson L., (2009), Simulation of airbag inflation processes using a coupled fluid structure approach, *Computational Mechanics,* 29, pp.289–297

[161] Wuchner R., Kupzok A., Bletzinger K.-U., (2007), A Framework for Stabilized Partitioned Analysis of Thin Membrane-Wind Interaction, *Int. J. Numer. Meth. Fluids* 54, pp. 945–963

[162] Kupzok A.M, Modeling the Interaction of Wind and Membrane Structures by Numerical Simulation, PhD thesis, Technischen Universität München, 2009

[163] Cheng Y., Oertel H., Schenkel T., (2005), Fluid-Structure Coupled CFD Simulation of the Left Ventricular, *Annals of Biomedical Engineering*, Vol. 33, No. 5,

[164] Morsi Y.S., Yang W.W, Wong C.S., Das S., (2007), Transient fluid–structure coupling for simulation of a trileaflet heart valve using weak coupling, *J Artif Organs,* 10, pp.96–103

[165] Malvè M., Pérez del Palomar A., López-Villalobos J. L., Ginel A., Doblaré M., (2010), FSI Analysis of the Coughing Mechanism in a Human Trachea, *Annals of Biomedical Engineering*, Vol. 38, No 4, pp.1556-1565

[166] Ostrowska-Maciejewska, Mechanika ciał odkształcalnych, PWN, Warszawa 1994 (in polish)

[167] T. Belytschko, W. K. Liu, and B. Moran. Nonlinear Finite Elements for Continua and Structures. John Wiley & Sons, 2000.

[168] Ogden R.W., Nonlinear Elasticity with applications to material modeling (Lecture notes), AMAS, Centre of excellence for Advanced Materials and Structure, IPPT PAN, 2003
[169] Martinec Z. Continuum Mechanics (Lecture notes), Faculty of Mathematics and Physics, Prague
[170] Donea J., Huerta A., Ponthot J.-Ph., Rodriguez-Ferran A., Chapter 14: Arbitrary Lagrangian-Eulerian methods, In Encyclopedia of Computational Mechanics, E.Stein, de Borst R and Hughes T.J.R. (eds) Volume 1: Fundamentals
[171] Hron J., Turek S., (2006), A monolithic FEM/multigrid solver for ALE formulation of fluid-structure interaction with application in biomechanics. In: *Fluid–Structure Interaction – Modelling, Simulation, Optimisation*, Springer-Verlag, Berlin, 2006
[172] Novotny A., Straskraba I., Introduction to mathematical theory of compressible flow, Oxford university Press, 2004
[173] Simo J.C, Hughes T.J.R., Computational inelasticity, Springer-Verlag, 1998
[174] J.Necas, I.Hlavacek, Mathematical Theory of elastic and elasto-plastic bodies, Elsevier, 1981
[175] Anderson J.D., Computational Fluid Dynamics. The Basics with Applications, McGraw-Hill, 1995
[176] D.J. Acheson, Elementary fluid dynamics, Oxford University Press, 2000
[177] Ali A.H., (1999), Statistical mechanical derivation of Cattaneo's heat flux law, *J. Thermophys. Heat Trans.* 13, 4, pp. 544-546
[178] Evans L.C., Równania różniczkowe cząstkowe, PWN, 2002 (in polish)
[179] Van Loon R., Anderson P.D., van de Vosse F.N., Sherwin S.J., Comparison of various fluid–structure interaction methods for deformable bodies, *Computers and Structures* 85, pp. 833-843
[180] Wall W., Gerstenberger A., Gamnitzer P., Förster C., Ramm E., Large Deformation Fluid-Structure Interaction – Advances in ALE Methods and New Fixed Grid Approaches. In: *Fluid–Structure Interaction – Modelling, Simulation, Optimisation*. Springer-Verlag, Berlin, 2006
[181] Guilkey J.E., Harman T., Xia A., Kashiwa B., McMurtry P., (2007), An Eulerian-Lagrangian approach for large deformation fluid structure interaction problems, Part 1 : algorithm development, *Computers and Structures*, Volume 85, Issue 11-14
[182] Hughes T.J.R., Liu W.K., Zimmermann T.K. (1981), Lagrangian–Eulerian finite element formulation for incompressible viscous flows, *Comput Methods Appl Mech Eng*, 29:329–349
[183] Wall W.A., Gerstenberger A., Mayer U.M., (2009), Advances in Fixed-Grid Fluid Structure Interaction, *Proceeding of the ECCOMAS Multidisciplinary Jubilee Symposium Computational Methods in Applied Sciences*, Vol.14
[184] Bungartz H.J., Benk J., Gatzhammer B., Mehl M, Neckel T., Partitioned Simulation of Fluid-Structure Interaction on Cartesian Grids. In: *Fluid - Structure Interaction II: Modelling, Simulation, Optimization*, Springer, Berlin, 2010.
[185] Peskin C.S, (1972), Flow patterns around heart valves: a numerical method, *J. Comp Phys,* 10, pp. 252–271.
[186] Wang X, Liu W.K., (2004), Extended immersed boundary method using fem and rkpm. *Comput Method Appl Mech Eng,* 93, pp. 1305–21.
[187] Zhang L., Gerstenberger A., Wang X., Liu W.K., (2004), Immersed finite element method. *Comput Method Appl.Mech Eng,* 193, pp. 2015–67.
[188] Glowinski R., Pan T.W., Periaux J., (1997), A lagrange multiplier/fictitious domain method for the numerical simulation of incompressible viscous flow around moving rigid bodies: (i) case where the rigid body motions are known a priori. *CR Acad Sci*, Paris 25(5), pp. 361–9.
[189] Wang X., (2006), From immersed boundary method to immersed continuum method, *Int J Multiscale Comp Eng*, 4, pp. 127–45.
[190] Wall W.A., Gamnitzer P., Gerstenberger A., (2008), Fluid-structure interaction approaches on fixed grids based on two different domain decomposition ideas, *International Journal of Computational Fluid Dynamics*, 22, 6, pp. 411- 427
[191] Wall W.A., Gerstenberger A., Kuttler U., Mayer U.M., An XFEM Based Fixed-Grid Approach for 3D Fluid-Structure Interaction. In: *Fluid - Structure Interaction II: Modelling, Simulation, Optimization,* Springer, Berlin, 2010.
[192] Hirt C.W., Nicholls B.D., (1981), Volume of fluid (VOF) method for the dynamics of free boundaries, *J. Comput. Phys.* 39, 201
[193] Rannacher R., Richter T., An Adaptive Finite Element Method for Fluid-Structure Interaction Problems Based on a Fully Eulerian Formulation. In: *Fluid - Structure Interaction II: Modelling, Simulation, Optimization*, Springer, Berlin, 2010.
[194] Mehl M., Brenk M, Bungartz H.-J., Daubner K., Muntean I.L, Neckel T., (2008), An Eulerian approach for partitioned fluid–structure simulations on Cartesian grids, *Comput Mechanics* 43, pp. 115–124
[195] Heil M., Hazel A., Boyle J., (2008), Solvers for large-displacement fluid-structure interaction problems, segregated vs. monolithic approaches. *Comput Mechanics*, 43, pp. 91–10

[196] Degroote J., Bathe K.-J., Vierendeels J., (2009), Performance of a new partitioned procedure versus a monolithic procedure in fluid-structure interaction, *Computers and Structures* 87**,** pp. 793.
[197] Zilian A., Dinkler D., Vehre A., (2009), Projection-based reduction of fluid-structure interaction systems using monolithic space-time modes. *Computer Methods in Applied Mechanics and Engineering*, 198 (47-48), pp. 3795-3805.
[198] Heil M., (2004), An efficient solver for the fully coupled solution of large-displacement fluid-structure interaction problems, *Computer Methods in Applied Mechanics and Engineering* 193, 1-23
[199] Tezduyar T.E., Sathe S., (2007), Modelling of fluid–structure interactions with the space–time finite elements: Solution techniques, *International Journal for Numerical Methods in Fluids*, Volume 54, Issue 6, pp. 855-900
[200] Matthies H., Steindorf J., (2003), Partitioned strong coupling algorithms for fluid-structure interaction, *Computers and Structures*, 81, pp. 805–812.
[201] Sternel D.C., Schäfer M., Heck M., Yigit S., (2008), Efficiency and accuracy of fluid-structure interaction simulations using an implicit partitioned approach, *Comput Mech*, 43, pp. 103–113.
[202] Doerffer P., Ochrymiuk T., Rządkowski R., Rachwalski J., Kubitz L., Modelowanie sprzężeń aeromechanicznych z uwzględnieniem charakterystyk materiałowych, Gdańsk, 2008 (in polish)
[203] Fernandez M., Moubachir M., (2005), A Newton method using exact jacobians for solving fuid-structure coupling, *Comput. Struct.* 83, pp. 127-142
[204] Gerbeau J.-F., Vidrascu M., (2003), A quasi-Newton algorithm based on a reduced model for fluid-structure interaction problems in blood flows. *ESAIM: Mathematical Modelling and Numerical Analysis* 37 (4), pp. 631–648.
[205] Vierendeels J., Implicit Coupling of Partitioned Fluid-Structure Interaction Solvers using Reduced-Order Models. In *Fluid - Structure Interaction: Modelling, Simulation, Optimization*, Springer, Berlin, 2006.
[206] Küttler U., Wall W., (2008), Fixed-point fluid-structure interaction solvers with dynamic relaxation, *Computational Mechanics*, 43 (1), pp. 61–72.
[207] Prosnak W.J., Równania klasycznej mechaniki płynów, PWN, 2006.
[208] Fahy F.J., Fundamentals of engineering acoustics, 2006
[209] Van Wylen G. J., Sonntag R. E., Fundamentals of Classical Thermodynamics. John Wiley & Sons, 1978.
[210] Gumiński K., Termodynamika, PWN, 1955
[211] Werle J., Termodynamika fenomenologiczna, PWN, 1957
[212] Wrzesiński Z., Termodynamika, OW PW, 2002
[213] Sado J., Wybrane zagadnienia termodynamiki, OW PW, 1997
[214] Poniewski M.E., Sado J., Staniszewski B., Termodynamika procesów nierównowagowych, OW PW, 2008
[215] Nefske D.J., (1988), A Basic Airbag Model, SAE Technical Paper Number 720426
[216] Wang J.T., Nefske D.J., (1988), A New CAL3D Airbag Inflation Model, SAE Technical Paper Number 880654
[217] Bird R.B., Stewart W. E., Lightfoot E. N, Transport Phenomena, Wiley, New York, 2002.
[218] Mitosek M., Mechanika płynów w inżynierii środowiska*,* OW PW, Warszawa, 1997.
[219] Atkins P.W., Chemia fizyczna, PWN, 2007
[220] Szargut J., Termodynamika, PWN, 1985
[221] Doubova A., Cara E.F., (2005), Some Control Results for Simplified One-Dimensional Models of Fluid-Solid Interaction. Mathematical Models and Methods in Applied Sciences. Vol. 5., pp. 783-824
[222] Sobieszczanski-Sobieski J., Haftka R.T., (1997), Multidisciplinary aerospace design optimisation: survey of recent developments, *Struct Multidisc Optim,* 14, 1-23
[223] Lund E., Mřller H., Jakobsen L.A., (2003), Shape design optimization of stationary fluid-structure interaction problems with large displacements and turbulence, *Struct Multidisc Optim* 25, pp. 383–392
[224] Bruyneel M., Jetteur P., Granville D., Langlois S., Fleur C., (2006), An augmented Lagrangian optimization method for inflatable structures analysis problems, *Struct Multidisc Optim*, 32
[225] Messac A., Van Dessel S., Mullur A.A., Maria A., (2004), Optimization of large-scale rigidified inflatable structures for housing using physical programming, *Struct Multidisc Optim* 26, 139–151
[226] Craig K. J., Kingsley T.C., (2007), Design optimization of containers for sloshing and impact, *Struct Multidisc Optim*, 33, pp. 71–87
[227] Schafer M., Sternel D.C., Becker G., Pironkov P., Efficient Numerical Simulation and Optimization of Fluid-Structure Interaction. In: *Fluid - Structure Interaction II: Modelling, Simulation, Optimization*, Springer, Berlin, 2010.
[228] Baecker G., Falk U., Schafer M., Shape Optimisation with Higher Order Surfaces in Consideration of Fluid Structure Interaction, *Proceeding of International Workshop on Fluid-Structure Interaction: Theory, numerics and applications*, Kassel University Press, 2009
[229] Hojjat M., Stavropoulou E., Gallinger T., Israel U., Wuchner R., Bletzinger K.-U., Fluid-Structure

Interaction in the Context of Shape Optimization and Computational Wind Engineering, In *Fluid - Structure Interaction II: Modelling, Simulation, Optimization*, Springer, Berlin, 2010.

[230] Israel U., Stavropoulou E., Barcelos M., Gallinger T., Bletzinger K.-U., Wüchner R., (2009), Shape Optimization in Partioned Analysis for Fluid-Structure Interaction, *Proceeding of International Workshop on Fluid- Structure Interaction: Theory, numerics and applications,* Kassel University Press, 2009

[231] Nocedal J., Wright S.J., Numerical Optimisation, Springer, 2006

[232] Bubnicki Z., Teoria i algorytmy sterowania, PWN, Warszawa, 2005.

[233] US Patent 4030715, Pneumatic shock absorber for suspension of cars and/or similar vehicles, 1977

[234] US Patent 5884734, Air damper, 1999

[235] Polish Patent 187957, Amortyzator pneumatyczny, zwłaszcza do roweru (in polish)

[236] Roebuck R.L., Jones A.R. and Cebon D., (2010), An investigation of air damping for heavy goods vehicles, *International Journal of Heavy Vehicle Systems*, 17, in print

[237] Khamitov R.N., Aver'yanov G.S., Korchagin A.B., (2009), Pneumatic Shock Absorber with an Active Damping System, *Russian Engineering Research*, Vol. 29, No. 9, pp. 871–873

[238] Khamitov R.N, Aver'yanov G.S., Korchagin A.B., (2009), Operational Processes in a Dual-Chamber Pneumatic Shock Absorber with Rapid Switching, *Russian Engineering Research*, Vol. 29, No.10, pp. 974–978

[239] Khamitov R.N, Aver'yanov G.S., Zubarev A.V., (2008), Dynamics of Oscillatory Systems with Controllable Shock Absorbers, *Russian Engineering Research*, Vol. 28, No. 6, pp. 543–547.

[240] Teixeira R.L., Neto F.P., Ribeiro J.F., (2006), Modelling and experimental investigation of an active damper, *Shock and Vibration*, Volume 13, Number 4-5

[241] Mróz A., Holnicki-Szulc J., Semi-active control of wind impact effects by means of pneumatic system, *Proc. of the 2nd Int. Conf. on Nonsmooth Nonconvex Mechanics,* Greece, 2006

[242] Polish patent pending P.387534, Sposób dyssypacji energii uderzeń i absorber pneumatyczny. Autorzy: Graczykowski C., Mikułowski G., Mróz A., Sekuła K. (in polish)

[243] Graczykowski C., Mikułowski G., Mróz A., Pawłowski P., Sekuła K., A feasibility study of adaptive pneumatic impact absorber, *Proceeding of 3rd European Conference on Structural Control*, Petersburg, Russia, 2008

[244] Graczykowski C., Mikułowski G., Pawłowski P., Holnicki-Szulc J., (2009), Koncepcja absorbera pneumatycznego do zastosowania w podwoziach aparatów latających z wykorzystaniem układu rozpoznania energii uderzenia, *Journal of Aeronautica Integra*, vol 5, pp.25-31

[245] Mikułowski G., Pawłowski P., Graczykowski C., Wiszowaty R., Holnicki-Szulc J., On a pneumatic adaptive landing gear system for a small aerial vehicle, *Proceeding of International Conference on Smart Materials and Structures*, Porto, Portugal, 2009

[246] Wiszowaty R., Biczyk J., Graczykowski C., Mikułowski G., Method of impact energy dissipation by the use of the pneumatic impact absorber with a piezo-valve. *Proceeding of International Conference on Smart Materials and Structures*, Saarbrucken, Germany, 2011

[247] Khamitov R.N, Aver'yanov G.S., Korchagin A.B., (2009), Operational Processes in a Dual-Chamber Pneumatic Shock Absorber with Rapid Switching, *Russian Engineering Research*, Vol. 29, No.10, pp.974–978

[248] Lee J.H., Kim K.J., (2007), Modeling of nonlinear complex stiffness of dual-chamber pneumatic spring for precision vibration isolations, *Journal of Sound and Vibration*, 301, pp. 909–926

[249] Erin C., Wilson B., (1998), An improved model of a pneumatic vibration isolator theory and experiment, *Journal of Sound and Vibration*, 218(1), pp. 81-101

[250] Ilchmann A., Sawodny O, Trenn S., (2006), Pneumatic cylinders: modelling and feedback force control, International journal of control, 79, 6, pp. 650-661

[251] Shen X., Goldfarb M., (2007), Energy Saving in Pneumatic Servo Control Utilizing Interchamber Cross-Flow, *Journal of dynamical systems, measurement and control*, Volume 129, Issue 3, 303

[252] Wang J., Pu J, Moore P., (1999), A practical control strategy for servo-pneumatic actuator systems, *Control Engineering Practice*, Vol. 7, pp.1483-1488

[253] Kuźniewski B., Dynamika tłokowych urządzeń pneumatycznych, WNT, 2001 (in polish)

[254] Kuźniewski B., (1995), Non-Linearity Compensation in a pneumatic vibration generator with a dual chamber for a variable component, *Mechanical Systems and signal processing* Vol. 9, No.4

[255] Kuźniewski B., (2000), Pneumatic generator of monoharmonic vibrations with nonlinearity and feedback compensation, *Advances in Technology of Machines and mechanical equipment*, Vol. No 3,

[256] Graczykowski C., Heinonen J., Adaptive Inflatable Structures for protecting wind turbines against ship collisions, *VTT Working Pappers*, 59, Espoo, 2006

[257] Martin M.T., Doyle J.F., (1996), Impact force identification from wave propagation responses. *International Journal of Impact Engineering*, 18, pp. 65–77

[258] Inoue H., Harrigan J., Reid S., (2001), Review of inverse analysis for indirect measurement of impact force. *Appl. Mech. Rev*, 54 pp. 503–524

[259] Klinkov M., Fritzen C.P., (2007), An updated comparison of the force reconstruction methods. *Key Engineering Materials*, 347, pp. 461–466

[260] Sekuła K., Real-time dynamic load identification, PhD Thesis, IPPT PAN, 2011

[261] Jankowski Ł., (2009), Off-line identification of dynamic loads, *Structural and Multidisciplinary Optimization*, 37, pp.609–623

[262] Sekuła K., Graczykowski C., Holnicki-Szulc J., (2011), On-line impact load identification, *Shock and vibration*, submitted

[263] Polish patent pending, Sposób identyfikacji prędkości zderzenia, masy oraz energii kinetycznej obiektu uderzającego w przeszkodę i urządzenie do identyfikacji prędkości zderzenia, masy oraz energii kinetycznej obiektu uderzającego w przeszkodę. Autorzy: R.Wiszowaty, C.Graczykowski, K.Sekuła, J.Holnicki-Szulc.

[264] Martins F. P., Siqueira C., Spogis N., Development and validation of a CFD model to investigate the oil flow in a shock absorber, SAE Technical Paper, 2005-01-4030.

[265] Kruger, M., Kessler, M., Ataídes, R., Junior, G. Numerical simulation of fluid flow inside a valve for an automotive shock absorber, SAE Technical Paper, 2008-36-0179

[266] Herr F., Mallin T., Lane J., and Roth S. A Shock Absorber Model Using CFD Analysis and Easy5, SAE Technical Paper*,* 1999-01-1322.

[267] Guzzomi F.G., O'Neill P.L., Tavner A.C.R., Investigation of Damper Valve Dynamics Using Parametric Numerical Methods, *Proceeding of the 16th Australasian Fluid Mechanics Conference*, Queensland, 2007

[268] Czop P., Gąsiorek D, et al., (2011), Optimization of a Disc Spring Valve System with the use of Fluid-Structure Simulations, *Simulation: Transactions of the Society for Modeling and Simulation International,* submitted

[269] Sławik D., Czop P., Król A., Wszołek G., (2010), Optimization of hydraulic dampers with the use of Design For Six Sigma methodology, *Journal of Achievements in Materials and Manufacturing Engineering*, Vol. 43, No.2, pp.676-683.

[270] Kim H.S., Wierzbicki T., (2001), Effect of The Cross-Sectional Shape on Crash Behaviour of a Three Dimensional Space Frame, *International Journal of Vehicle Design*, Vol. 25, No.4, pp. 295-316

[271] Kim H.S., Wierzbicki T., (2001), Effect of The Cross-Sectional Shape of Hat-Type Cross-Sections on Crash Resistance of an S-Frame, *Thin-Walled Structures*, Vol. 39, No. 7, pp. 535-554

[272] Han J., Yamazaki K., (2003), Crashworthiness Optimization of S-Shape Square Tubes*, International Journal of Vehicle Design*, Vol. 31, No.1, pp. 72-85

[273] Alghamdi A., (2001), Collapsible Impact Energy Absorbers: an Overview, Thin-Walled Structures, Vol. 39, No. 2, pp. 189-213

[274] Lu G., Yu T.X. Energy Absorption of Materials and Structures. Woodhead Publishing Limited, Cambridge, 2003

[275] Greń K., (2002), Dissipation of energy in absorber filled with compressed air, 2002 *Warsaw University of* Technology, *Publications of Institute of Vehicles*, 4/47, pp. 19-34.

[276] Pipkorn B., Haland Y., (2005), Proposed variable stiffness of vehicle longitudinal frontal members, *Int. J. Crashworthiness*, No.10, pp. 603-608.

[277] Polish Patent pending, P-357761. Sposób i układ sterowania sztywnością i zdolnością do dyssypacji energii cienkościennej belki wielomodułowej oraz cienkościenna belka wielomodułowa. Autorzy: J.Holnicki-Szulc, R.Chmielewski

[278] Graczykowski C., Chmielewski R., Holnicki-Szulc J., Controlled impact absorption in adaptive pressurized structures, *Proceeding of the 4th European Congress on Computational Methods in Applied Sciences and Engineering*, Jyväskylä, Finland, 2004

[279] Graczykowski C., Holnicki-Szulc J., Optimization of dynamic properties of adaptive pressurized structures subjected to impact loads, *Proceeding of the 2nd ECCOMAS Thematic Conference on Smart Materials and Structures*, Lisbon, Portugal, 2005

[280] Mazurkiewicz Z., Cienkie powłoki sprężyste. Teoria liniowa (in polish), OW PW, Warszawa, 2004

[281] Flugge F., Stresses in shells, Springer-Verlag, Berlin, Heidelberg, New York, 1973

[282] Amabili M., Garziera R., (2000), Vibrations of circular cylindrical shells with nonuniform constraints, elastic bed and added mass; Part II: shells containing or immersed in axial flow. *Journal of Fluids and Structures* 16(1), pp. 31-51

[283] Amabili M., Garziera R., (2000), Vibrations of circular cylindrical shells with nonuniform constraints, elastic bed and added mass; Part I: empty and fluid-filled shells. *Journal of Fluids and Structures* 14, pp.669-690.

[284] Wiśniewski K., Kołakowski P., (2003), The effect of selected parameters on ship collision results by dynamic FE simulations, *Finite Elements in Analysis and Design* 39, pp. 985–1006.

[285] Rastegar S., Adaptive security and protective barriers and traffic security protective bumps, US Patent,

2008/0056818
[286] Gupta R., Kelkar A.D. Nonlinear crash dynamics sumualtion of novel airbag based next generation energy absorbing barrier, *Proc. of the 9th International LS-Dyna Users conference*, Detroit, 2006
[287] Haftka R.T., Gürdal Z., Elements of Structural Optimization, Kluwer Academic Publishers, Dortrecht, Boston and London, 1992
[288] Hasse A., Campanile F., Synthesis of Compliant Mechanisms for Shape Adaptation by means of a Modal Procedure, *Proceeding of the 19th Conference on Adaptive Structures and Technologies*, Ascona, Switzerland, 2008.
[289] Graczykowski C., Holnicki-Szulc J., Adaptive flow controlled based airbags for adaptive impact absorption, *Proceeding of 3rd European Conference on Structural Control,* Petersburg, 2008
[290] Reports of Europen Wind Energy Association: www.ewea.org
[291] Wilson J.F., Dynamics of Offshore Structures, Wiley, New York, USA, 1984.
[292] Kärnä T., Kolari K., Mitigation of dynamic ice actions on offshore wind turbines, *Proceeding of the Third European conference on Structural Control*, Vienna, Austria, 2004
[293] Mróz A., Kärnä T., Mitigation of ice loading. Feasibility study of semi-active solution, *VTT Working Papers* 39, 2005.
[294] Biehl F., Lehmann E., Collisions of ships and offshore wind turbines: Calculation and risk evaluation, *Proceedings of the International Conference on Offshore Mechanics and Arctic Engineering OMAE*, 2006
[295] Biehl F., Collision Safety Analysis of Offshore Wind Turbines, LS-DYNA Forum, Bamberg, 2005.
[296] Graczykowski, C., Heinonen J., Feasibility study of Adaptive Inflatable Structures for protecting wind turbines, *Finnish Journal of Structural Mechanics*, Vol.40, 2007
[297] Graczykowski C., Holnicki-Szulc J., (2009), Protecting offshore wind turbines against ship impacts by means of Adaptive Inflatable Structures, *Shock and Vibration*, vol. 16, no.4, pp. 335-353, IOS Press, Netherlands
[298] Jackson K.E., Boitnott R.L., Fasanella E.L., Jones L.E., Lyle K. H., A History of Full-Scale Aircraft and Rotorcraft Crash Testing and Simulation at NASA Langley Research Center, *Proceeding of the 4th Triennial International Aircraft and Cabin Safety Research Conference*, Lisbon, Portugal, 2004
[299] Taylor A., Gardinier D., Sabberton A., Design Optimization of the Beagle II Mars Lander Airbags through Explicit Finite Element Analysis, *Proceeding of the LS-DYNA Users Conference*, 2002
[300] Northey D., Morgan C., (2006), Improved inflatable landing systems for low cost planetary landers, *Acta Astronautica* vol. 59, pp.726 – 733
[301] Groenenboom P., Lasry D., Subbian T.H., Narwani G., (1993), A diffusive Gas Jet Model in PAM-SAFE for Airbag Inflation. SAE Paper 930228
[302] Marklund P.-O., Nilsson, L., (2002), Simulation of airbag inflation process using coupled fluid-structure approach, *Computational Mechanics*, vol. 29 , pp. 289-297
[303] van der Veen W.A., Simulation of a compartmented airbag deployment using an explicit, coupled Euler-Lagrange method with adaptive Euler domains, *Proceeding of NAFEMS World Congress*, Florida, 2003
[304] Yeh, L.Chai, N.Saha (2006), Application of ALE to airbag deployment simulation, *International Journal of Vehicle Safety,* Vol. 1, No.4 pp. 348 - 365
[305] Beesten B., Hirth A., Reilink R., Remensperger R., Rieger D. and Seer, G., Out of Possition simulation – A tool to design airbags? Current capabilities in numerical simulation. *Proceeding of the 7th International Symposium and Exhibition on sophisticated safety systems*, Karlsruhe, Germany, 2004
[306] Haufe A., Franz U., On the simulation of out-of-position load cases with ALE-method, *Proceeding of the 7th International Symposium and Exhibition on sophisticated safety systems*, Karlsruhe, Germany, 2004
[307] Fokin, D., Dessarud E., Simmulation of curtain airbag with arbitrary Lagrangian-Eulerian method, *LS-DYNA Anwenderforum*, Frankenthal, Germany, 2007
[308] Hirth A., Haufe A., Ollovson L., Airbag simulation with LS-DYNA. Past-present-future, *LS-DYNA Anwenderforum*, Frankenthal, Germany, 2007
[309] Zhang H., Gopal M.M. and Saxena R., Zhang H., Avula X.J. , An Integrated Optimization System for Airbag Design and Modeling by Finite Element Analysis, SAE Technical Paper, 2003-01-0506
[310] Leyko J., Mechanika ogólna, PWN
[311] Ogorevc T., Sekavcnik M., Katrasnik T., Zun I., (2009) , Three-dimensional numerical simulation of the exhaust stroke, *Forsch Ingenieurwes*, Vol. 73, pp. 147–160
[312] Srikanth C, Bhasker C, (2009), Flow analysis in valve with moving grids through CFD techniques, *Advances in Engineering Software*, Vol. 40, pp. 193–201.
[313] Hsu U.-K., Lu P.-J., (2011), Dynamic simulation of a tilting-disc valve with clearance in pulsatile channel flow*, Journal of Vision,* Vol., 14, pp. 23–39
[314] Choi Y., Lee J. , Jeong W., Kim I., (2010), Dynamic behavior of valve system in linear compressor based on fluid-structure interaction, *Journal of Mechanical Science and Technology*, Vol. 24(7), pp. 1371-1377

[315] An Y.J., Kim B.J., Shin B.R., (2008), Numerical analysis of 3-D flow through LNG marine control valves for their advanced design, *Journal of Mechanical Science and Technology*, Vol.22, pp.1998-2005

[316] Sotiropoulos F., Borazjani I., (2009), A review of state-of-the-art numerical methods for simulating flow through mechanical heart valves, *Med Biol Eng Comput*, Vol, 47, pp. 245–256.

[317] Cedrat company: www.cedrat.com

[318] Ouyang X.P., Yang H.Y., Jiang H.Y., Xu B., (2008), Simulation of the piezoelectric high-speed on/off valve, *Chinese Science Bulletin,* Vol. 53, No. 17, pp. 2706-2711.

[319] Reichert M., Murrenhoff H., New concepts and design of high response hydraulic valves using piezo-technology. In: *Power Transmission and Motion Control*, Bath, 2006.

[320] Polish patent pending P-385086 Zawór sterowalny zwłaszcza do poduszki gazowej oraz sposób ograniczania przepływu medium. Autorzy: M.Ostrowski, P.Pawłowski, C.Graczykowski

[321] European patent pending, Drivable valve to be used in gas bags in particular and method for restricting the flow of the fluid, European patent pending EPO9461509,3. Authors: M.Ostrowski, P.Pawłowski, C.Graczykowski

[322] Ostrowski M., Holnicki-Szulc J., High performance valve for adaptive inflatable impact absorbers, *Proc. of the 5nd ECCOMAS Thematic Conference on Smart Materials and Structures*, Saarbrucken, Germany, 2011

[323] ANSYS CFX, Users Manual, ver. 11.0

[324] ABAQUS, Users Manual, ver. 6.9.